



**Identifying and characterizing lysosomal storage
disease phenotypes for utilization in novel
screening and monitoring assays**

Abdullah Alshehri

Ph.D. 2019

Abstract

In the lysosomal storage disease (LSD) field there are very few studies examining large cohorts of LSD samples in order to identify suitable new pan-LSD biomarkers and identify pan-LSD disease mechanisms. This thesis investigated the possibility of using a simple fluorimetric test for lysosomal swelling, simple enzyme assays and the associated accumulation of storage material alongside the presence of unique heavy metal accumulation to identify the majority of LSDs. The results showed that lysosomal swelling is a highly sensitive phenotype and that high-throughput analysis can be achieved using the fluorescent marker lysotracker. This probe can be used to screen LSD cells as both a suitable biomarker and potentially for drug screening to develop new treatments for LSDs. This thesis was also identified that secondary alteration of lysosomal enzymes is a common feature of LSDs. Such secondary lysosomal enzyme alteration could be useful for treatment monitoring and some novel biomarkers for some and potentially all of the LSDs have emerged. I have also conducted the first electron microscopy (EM) study that compares all classes of LSDs. This technique was proven to be useful for characterisation of the lipids and other macromolecules stored both primarily and secondarily in the majority of LSDs. EM also confirmed that alteration of secondary lysosomal enzymes could be the reason behind the accumulation of materials in some LSDs. Divalent cation signalling defects have been reported in several LSDs, I therefore studied Ca^{2+} and trace element (TEs) ion changes across all the LSDs and discovered that lysosomal Ca^{2+} defects are common and that changes in Zn^{2+} and a few other TEs were identified in almost all or specifically altered in some of the LSDs respectively. Our results highlight the possibility of using inductively coupled plasma mass spectrometry (ICP-MS) for monitoring changes in blood TE levels during the course of clinical treatment of CLN5 patients. Finally, evidence points to the NPC1 protein function, in terms of Zn^{2+} efflux from lysosomes, was inhibited by common storage of sphingoid bases and is a common phenotype across the majority of LSDs that explains the occurrence of secondary lipid accumulation across most of the LSDs. Our findings provide new potential biomarkers, new mechanisms of pathogenesis and new therapeutic targets that are common to all of the LSDs validating the power of studying multiple LSDs together.

Acknowledgements

This project was funded by King Fahad Medical City and Royal Embassy of Saudi Arabia Cultural Bureau, London.

First of all, I wish to express my gratitude to a wonderful supervisor Dr. Emyr Lloyd-Evans for his support and advice during my PhD. I am really grateful for his consistent assistance and patience all through my PhD and for his positive encouragement. He made my PhD years enjoyable and fully informative big thanks to you Emyr!!

I would like to thank Dr. Helen Waller-Evans for her advice. I really appreciate her taking the time for a critical reading of my thesis in a short period of time (Thanks a ton, Helen!).

I would also like to thank every single member of the ELE lab; a wonderful group of people, their suggestions were always helpful, especially those that were constantly with me during projects; Emily, Katie, Rafa, Sophie, Brendan and more recently Dr.Hannah. I would like to thank the final year project students, summer and placement year students especially Hiu Tung Shek. I would also like to give a big thanks to Dr. John Milton Lucocq, of St Andrews university for helping me with the electron microscope work, without his experience the electron microscope project would not have been possible! Thanks to our collaborator in Cardiff & Vale University Health Board especially Dr. Duncan Cole, Dr. Stuart Moat and I am also very thankful for Mr. Paul Bramhall for his help with ICP-MS. I am grateful to Dr Peter Watson for reading my previous reports and providing such valuable advice.

I greatly appreciate the support of my wonderful family, especially my parents for their assistance and patience. I wouldn't have been able to achieve this without their support. The special thanks off course will be to my loving and wonderful wife who was very supportive despite the fact that I was always in the lab, leaving her to take care of kids. She was always by my side, trying to help me overcome any difficulties during my degree, Thanks a lot Hanadi!!, I also want to say thanks to my special kids Firas and Sila the shining light of my live. Finally, I wish to extend my gratitude to my brothers, sisters and `friends. As I always say, my success is attributable to Allah firstly and then to my wonderful family for their support.

Abbreviations

4MU	4-methylumbelliferone
AGA	Aspartylglucosaminidase
AM	Acetyoxymethyl ester
AMC	7-amino-4-methylcoumarin
APs	Acid phosphatase
aSMase	Acid sphingomyelinase
BafA1	Bafilomycin A1
BCA	Bicinchoninic acid
B-LCLs	B-lymphoblastoid cell lines
BSA	Bovine serum albumin
CAX	Ca ²⁺ /H ⁺ exchanger
CDE	Clathrin dependent endocytosis
CIE	Clathrin independent endocytosis
Co	Cobalt
CRSL	Cathepsin L
CTR1	copper transporter 1
CTSB	Cathepsin B
CTSD/E	Cathepsin D E
CTxB, CtxB	Cholera toxin B-subunit
Cu	Copper
DMEM	Dulbecco's modified eagle's medium
DMSO	Dimethyl sulfoxide
DMT1	Divalent Metal Transporter 1
DPP	Dipeptidyl peptidase
EM	Electron microscopy
ER	Endoplasmic reticulum
FACS	Fluorescence activated cell sorting
FBS	Fetal Bovine Serum
Fe	Iron
GalCer	Galactosylceramide
GCase	β glucosidase
GDI	Gaucher disease type 1
GDII	Gaucher disease type 2
GSL	Glycosphingolipid
GUSB	β Glucuronidase
HBSS	Hank's balanced salt solution
HexA	β-hexosaminidase A
HexB	β-hexosaminidase B
HF	Human fibroblast
HMU	6-Hexadecanoylamino-4-methylumbelliferone
HPβCD	2-Hydroxypropyl-β-cyclodextrin
Hr	Hour
I cell	Mucopolidosis II
ICP-MS	Inductively coupled plasma mass spectrometry

IDU	α -L-iduronidase
LacCer	Lactosylceramide
LAL	Acid lipase
LAMP 2	Lysosomal-associated membrane protein 2
LAMP1	Lysosomal-associated membrane protein 1
LDL	Low density lipoprotein
LE	Late endosomes
LPDS	Low density lipoprotein
LSD	Lysosomal storage disease
Lys	Lysosome
Lys-SLs	Lysosphingolipids
LTB	Lysotracker blue
LTG	Lysotracker green
LTR	Lysotracker red
M6P	Mannose-6-phosphate
MLIV	Mucopolidosis type IV
Mn	Mangenase
MPS	Mucopolysaccharidosis
MPS I	Mucopolysaccharidosis type I
MPS II	Mucopolysaccharidosis type II
MPS III	Sanfilippo syndrome
MPS IVB	Morquio syndrome
MS/MS	Tandem mass spectrometry
MSD	Multiple Sulfatase Deficiency
Na ₂ CO ₃	Sodium carbonate
NaAz	Sodium azide
NAGLU	α ,N-acetylglucosaminidase
NaOH	Sodium hydroxide
NaTc	Sodium taurochlorate
NCLs	Juvenile neuronal ceroid lipofuscinosis
NEU	Sialidase
NPA	Niemann-pick type A
NPB	Niemann-pick type B
NPC	Niemann-pick type C
PADK	Z-Phe-Ala-diazomethylketone
PBS	Phosphate buffered saline
PFA	Paraformaldehyde
PKC	Protein kinase C
PPT1	Palmitoyl-protein thioesterase 1
rhLAL	Recombinant human lysosomal acid lipase
ROS	Reactive oxygen species
Se	Selenium
SLs	Sphingolipids
TEs	Trace elements
Total Hex	Total β -hexosaminidase
TPP1	Tripeptidyl-peptidase 1

TRPML1	Transient receptor potential mucolipin 1
V-ATPase	Vacuolar ATPase
WT	Wild-type
Zn	Zinc
α -Fuc	α -L-Fucosidase
α Gal A	α -galactosidase A
α -Glu	α glucosidase
α -Man	α mannosidase
β -gal	β galactosidase

List of figures

Figure 1.1 Lysosomal enzyme synthesis pathway.	6
Figure 1.2 Schematic diagram of key lysosomal Ca ²⁺ and other ion channels on the lysosomal membrane.	11
Figure 1.3 Schematic diagram of major trace element transporters and channels on the lysosomal membrane.	13
Figure 1.4 A view of the sphingolipid biosynthetic pathway.	21
Figure 1.5 The sphingolipid degradative pathway in lysosomes and the related sphingolipidoses disease.	23
Figure 3.1 Concentration dependent loading and fluorescence signal of different lysotrackers in control and NPC1 patient fibroblasts.	73
Figure 3.2 Comparison of lysotracker red and green fluorescence in live and fixed conditions.	75
Figure 3.3 Lysotracker red, but not green, photoconverts and emits a lower wavelength green fluorescence after excitation.	78
Figure 3.4 Lysotracker concentration and incubation time alters lysosomal pH.	81
Figure 3.5 Investigating conditions that alter lysotracker loading into LE/Lys compartments.	85
Figure 3.6 Lysotracker detects fusion with autophagic vacuoles but is not increased.	87
Figure 3.7 Comparison of different standardization methods for converting lysotracker into a higher throughput 96 well plate assay.	90
Figure 3.8 Lysotracker fluorescence intensity of healthy controls and one non-LSD patient with cystic fibrosis.	93
Figure 3.9 Lysotracker fluorescence intensity across the sphingolipidoses.	95
Figure 3.10 Localisation and intensity of lysotracker fluorescence across NCL fibroblasts.	97
Figure 3.11 Localisation and intensity of lysotracker fluorescence across mucopolysaccharidoses fibroblasts.	99
Figure 3.12 Lysotracker fluorescence intensity across the lysosomal transmembrane protein associated diseases.	102
Figure 3.13 Lysotracker fluorescence staining in multiple lysosomal enzyme deficiencies.	104
Figure 3.14 Lysotracker fluorescence staining of other lysosomal storage diseases.	107
Figure 3.15 Anti-LAMP2 Immunofluorescent analysis of LSD fibroblasts.	109
Figure 3.16 Changes in lysotracker and LAMP1/2 following treatment with miglustat.	111
Figure 3.17 Elevation of lysotracker and filipin staining in healthy control and NPC1 B-LCLs.	114
Figure 3.18 Comparison of Lysotracker fluorescence in B-LCLs by FACS and magnetic cell capture.	117
Figure 4.1 Heat map of lysosomal enzyme activity among the majority of LSDs fibroblasts.	135
Figure 4.2 Lysosomal enzyme activities in wild type, <i>Idua</i> ^{-/-} , <i>Sgsh</i> ^{-/-} and <i>Naglu</i> ^{-/-} mouse brain tissue.	140
Figure 4.3 Activity of selected lysosomal enzymes in <i>Npc1</i> ^{-/-} and <i>Npc1</i> ^{+/+} mouse tissues.	142
Figure 4.4 Lysosomal enzyme activities in control and NPC1 patient fibroblasts with a range of different mutations.	144
Figure 4.5 Activity of lysosomal enzymes in the control and NPC1 patient fibroblasts treated with miglustat.	146
Figure 4.6 Activity of lysosomal enzymes in control and CLN5 patient fibroblasts treated with miglustat.	148
Figure 4.7 Activity of lysosomal enzymes in CLN5 patient dried blood spots during miglustat treatment.	151
Figure 4.8 Decrease in lysosomal storage material in LSDs following restoration of lysosomal LAL activity with exogenous recombinant enzyme.	154

Figure 4.9 Radar plot showing multiple lysosomal enzyme activities measured in MPS I patient fibroblast.	164
Figure 5.1 Morphological characterization of control fibroblasts.	171
Figure 5.2 Electron microscopy of primary storage material in LSDs.....	174
Figure 5.3 Electron microscope characterisation of lysosomal storage material ultrastructure in the sphingolipidoses	176
Figure 5.4 Electron microscopy characterisation of the storage material in NPC1.	179
Figure 5.5 Electron microscopy characterisation of storage material in Mucopolysaccharidosis.	181
Figure 5.6 Morphological characterization of lysosomal storage in the NCLs.....	183
Figure 5.7 Globoside Gb3 storage, and the reduction in storage effected by miglustat, in CLN5 fibroblasts.	186
Figure 5.8 Morphological characterization of members of the oligosaccharidoses.	189
Figure 5.9 Morphological characterization of MLIV.	192
Figure 5.10 Morphological characterization of Wolman disease fibroblasts.....	193
Figure 5.11 Morphological characterization of lipid storage in I cell disease patient fibroblasts.	195
Figure 5.12 Whorls and zebra bodies are the same structure, whose differing appearance is the result of the plane of sectioning.....	197
Figure 6.1 Lysosomal Ca ²⁺ levels are altered in over half of the LSDs tested.	218
Figure 6.2 Measurement of lysosomal Zn ²⁺ accumulation using different intracellular probes.	222
Figure 6.3 Presence of lysosomal Zn ²⁺ accumulation in LSD patient fibroblasts.	224
Figure 6.4 Phen Green SK staining is quenched by heavy metals in LSD fibroblast lysosomes.....	227
Figure 6.5 Lysosomal Fe ²⁺ accumulates within lysosomes of some LSD fibroblasts	228
Figure 6.6 Lysosomal Cu ⁺ accumulation is observed in some LSD fibroblasts.....	229
Figure 6.7 Zn ²⁺ accumulates in patient fibroblast lysosomes from all forms of NPC disease	232
Figure 6.8 Lysosomal Zn ²⁺ accumulates in NPC B-LCL.	235
Figure 6.9 Alterations in metal ion homeostasis in LSD patient fibroblasts by ICP-MS.	236
Figure 6.10 Alterations in metal ion levels in the culture medium of NPC fibroblasts.	237
Figure 6.11 The effect of miglustat on the TE levels in control fibroblasts.	239
Figure 6.12 Altered metal ion homeostasis in NPC patient CSF measured by ICP-MS	241
Figure 6.13 Altered heavy metal homeostasis in CLN5 patient blood samples during a miglustat treatment timecourse of 22 months.....	243
Figure 7.1 Subcellular distribution of free cholesterol and ganglioside GM1 in LSD fibroblasts.	257
Figure 7.2 Activation of TRPML1 with MLSA1 treatment does not correct lysosomal Zn ²⁺ storage in NPC.	258
Figure 7.3 Miglustat unable to rescue lysosomal Zn ²⁺ accumulation in NPC fibroblasts.....	259
Figure 7.4 Effects of Baf A1 on control and NPC fibroblasts.....	261
Figure 7.5 Cholesterol depletion reduces Zn ²⁺ levels in LSDs human fibroblasts.....	263
Figure 7.6 Inhibition of GCase with CBE modulates cellular lipid storage, which induces NPC-like phenotypes in control, but not Farber, fibroblasts.	265
Figure 7.7 Exogenous lyso-SLs elevate lysosomal Zn ²⁺ levels in control fibroblasts.	268
Figure 7.8 U18666A treatment induces lysosomal Zn ²⁺ accumulation in control and Krabbe fibroblasts.	271
Figure 7.9 Psychosine induces lysosomal Zn ²⁺ accumulation in control and Krabbe fibroblasts.	272
Figure 7.10 Inhibition of lyso-Gb3 formation rescues lysosomal Zn ²⁺ accumulation.	273
Figure 7.11 Inhibition of acid ceramidase reduces lysosomal Zn ²⁺ storage.....	274
Figure 7.12 Miglustat treatment improves NPC disease-like phenotypes in Fabry fibroblasts.	276

Figure 7.13 Diagram illustrating prospective disruption to NPC1 function and subsequent lysosomal Zn²⁺ storage in LSDs. 281

List of tables

Table 1.1 Summary of key features of some LSDs with respect to protein deficiency, storage of compounds, tests and genes.....	16
Table 1.2 The most promising biomarkers for the analysis of various LSDs.....	32
Table 2.1 Primary antibodies used in the immunocytochemistry staining.....	43
Table 2.2 Secondary antibodies used in the immunocytochemistry staining.....	43
Table 2.3 Assay conditions.....	51
Table 2.4 Primary and secondary antibodies used in immuno electron microscope cryosection labelling.	61
Table 3.1 The weaknesses of fluorescent probes commonly used for late endosomal and lysosomal compartments.....	66
Table 4.1 Summary of lysosomal enzyme changes amongst LSD groups taken from the figure of this thesis (Figure 4.1).	163
Table 5.1 Summary of the morphological findings of primary lipids under EM examination.	200
Table 5.2 Summary of the primary and secondary storage material in LSDs using EM morphological findings.....	201
Table 5.3 Correlation between the level of activity of lysosomal and the presence of secondary storage.....	206

Table of Contents

1.	CHAPTER 1: GENERAL INTRODUCTION.....	1
1.1	THE LYSOSOME	1
1.1.1	Overview	1
1.1.2	Lysosomal pH.....	3
1.1.3	Lysosome biogenesis and the transport of lysosomal enzymes.....	4
1.1.4	The intracellular role of the lysosome in the endocytic system	7
1.1.5	The role of lysosomes in Ca ²⁺ signal regulation	8
1.1.6	The role of lysosomes in homeostasis.....	12
1.2	LYSOSOMAL STORAGE DISEASES.....	14
1.2.1	Overview	14
1.2.2	Classification.....	15
1.2.3	The cell biology of LSDs	19
1.2.4	Diagnosis	26
1.2.5	Therapy.....	35
1.3	AIMS OF THIS PROJECT.....	38
2	CHAPTER 2: MATERIALS AND METHODS.....	40
2.1	MATERIALS	40
2.2	CELL CULTURE	40
2.2.1	Cell culture conditions.....	40
2.2.2	Cellular cholesterol depletion	41
2.2.3	Starvation protocol to induce autophagy.....	41
2.3	BUFFERS.....	41
2.3.1	Complete Hank's Balanced Salt solution (HBSS).....	41
2.3.2	Blocking buffer	42
2.3.3	Immunocytochemistry fixatives	42
2.4	MICROSCOPY	43
2.5	IMMUNOCYTOCHEMISTRY STAINING	43
2.6	LIVE IMAGING.....	44
2.6.1	Lysotracker staining protocols in adherent patient fibroblasts.....	44
2.6.2	Lysotracker staining protocols for non-adherent B lymphoblasts.....	45
2.6.3	Measurement of lysosomal pH by fluorescence microscopy.....	46
2.6.4	Measurement of autophagy by live cell fluorescence microscopy	47
2.6.5	Whole cell intracellular organelle Ca ²⁺ measurements	47
2.6.6	Live intracellular free Zn ²⁺ imaging methods.....	47
2.6.7	Live intracellular free Cu ⁺ /Cu ²⁺ and Fe ²⁺ /Fe ³⁺ imaging methods.....	48
2.6.8	Intracellular ganglioside GM1 trafficking assay.....	49
2.7	BIOCHEMISTRY	49
2.7.1	Preparation of human fibroblast homogenate.....	49
2.7.2	Bicinchoninic acid assay	49
2.7.3	Fluorometric assays for enzyme activities.....	50
2.7.4	Mouse tissue preparation	54
2.7.5	Assay of lysosomal enzyme activity in human dried blood spots.....	54
2.8	DRUG TREATMENTS	54
2.8.1	Conduritol-β-epoxide, inhibitor of lysosomal GBA1.....	54
2.8.2	MLSA1 drug treatment.....	55
2.8.3	U18666A, an NPC1 inhibitor.....	55
2.8.4	1-(1-naphthylmethyl)-piperazine, a new inhibitor of NPC1	55
2.8.5	Sucrose, an osmotic modulator of lysosomal ion content and volume	55
2.8.6	Bafilomycin, vATPase inhibitor	56
2.8.7	Monensin and nigericin, Na ⁺ and K ⁺ ionophores	56
2.8.8	Gly-Phe β-naphthylamide, lysosomal cathepsin C substrate	56
2.8.9	N-butyl-deoxyojirimycin (Miglustat), inhibitor of GlcCer synthase	56
2.8.10	(1R,2R)-2-N-myristoylamino-1-(4-nitrophenyl)-1,3-propandiol (D-NMAPPD).....	56

2.8.11	TPEN, heavy metal chelator.....	57
2.9	EXOGENOUS SUPPLEMENTS.....	57
2.9.1	Incubation of cells with exogenous sphingolipid.....	57
2.9.2	Incubation of cells in exogenous lyso-lipid.....	57
2.10	FIXED STAINING.....	57
2.10.1	Ganglioside GM1 staining using FITC-CtxB.....	57
2.10.2	Cholesterol.....	58
2.10.3	Nuclear staining.....	58
2.10.4	Autofluorescence assessment.....	58
2.10.5	Mounting of coverslips.....	58
2.11	INDUCTIVELY-COUPLED PLASMA MASS SPECTROMETRY FOR TRACE METAL ANALYSIS.....	58
2.11.1	Sample preparation.....	58
2.11.2	Trace element analysis.....	59
2.12	ELECTRON MICROSCOPY ANALYSIS OF PATIENT FIBROBLASTS.....	59
2.12.1	Conventional method (Epoxy resin embedding).....	59
2.12.2	Cryo sectioning technique for immuno-EM.....	60
2.13	BIOLOGICAL SAMPLES.....	61
2.14	STATISTICAL ANALYSIS.....	61
2.15	MEASURING CELL FLUORESCENCE.....	61
2.15.1	Thresholding and distributional analyses of images.....	61
2.15.2	Corrected total cell fluorescence (CTCF).....	62
2.15.3	Co-localisation analysis.....	62

3 CHAPTER 3: A SIMPLE FLUORIMETRIC TEST FOR LATE ENDOSOMAL AND LYSOSOMAL SWELLING AS A MEANS TO IDENTIFY, MONITOR THE EFFECTIVENESS THERAPIES FOR ALL LYSOSOMAL STORAGE DISEASES. 63

3.1	INTRODUCTION.....	63
3.1.1	Expansion of late endosomal and lysosomal compartments is a common feature across LSDs..	63
3.1.2	Targeting and visualising the late endosomal and lysosomal compartments with fluorescent probes	64
3.1.3	Lysotracker use in diagnosis and monitoring.....	67
3.1.4	Appropriateness of cell lines commonly used in LSD research.....	69
3.1.5	Aims.....	70
3.1.6	A brief summary of the methods used.....	70
3.2	RESULTS.....	72
3.2.1	Lysotracker loading into cellular lysosomes is dependent upon lysotracker concentration.....	72
3.2.2	Neither lysotracker green nor lysotracker red can survive fixation.....	74
3.2.3	Photostability of the lysotracker fluorescence probes.....	77
3.2.4	Lysotracker concentration and incubation time alters intralysosomal pH.....	79
3.2.5	Lysotracker accumulation in acidic endolysosomes is swelling dependent.....	83
3.2.6	Lysotracker fluorescence is not elevated following autophagy.....	86
3.2.7	Developing the lysotracker plate assay for use in high throughput methods.....	88
3.2.8	Lysotracker can be used to detect LE/Lys enlargement in fibroblasts isolated from the majority of LSD patients.....	92
3.2.9	Absence of increase in lysotracker fluorescence in certain LSDs correlates with an absence of expansion in LAMP2 immunocytochemistry.....	108
3.2.10	Lysotracker is capable of faithfully representing reduction in lysosomal lipid storage during drug treatment.....	109
3.2.11	Further validation of the use of lysotracker to detect lysosomal storage in lymphoblastoid cell lines	112
3.2.12	Comparison of flow cytometry and magnetic cell capture as methods to determine lysosomal storage across multiple lysosomal diseases.....	116
3.3	DISCUSSION.....	119
3.3.1	Investigating the fundamental properties of lysotracker as a lysosomal marker in cells.....	119
3.3.2	Lysotracker can identify lysosomal storage across the majority of LSD patient fibroblasts, but not all, and can be used to follow treatment.....	122
3.3.3	Development of a simple high throughput lysotracker assay based on magnetic capture of circulating CD19+ B lymphocytes.....	125

3.4	CONCLUSION	126
4	CHAPTER 4: DEVELOPING NEW ENZYMATIC BIOCHEMICAL MARKERS FOR LYSOSOMAL STORAGE DISEASES.....	127
4.1	INTRODUCTION	127
4.1.1	Use of lysosomal enzymes in diagnosis and monitoring	127
4.1.2	Secondary changes in lysosomal enzymes activities	128
4.1.3	Lysosomal enzyme measurement techniques.....	130
4.1.4	Aims.....	131
4.1.5	Summary of methods	132
4.2	RESULTS	133
4.2.1	Extent of secondary lysosomal enzyme alteration across LSD fibroblasts	133
4.2.2	Identification of secondary enzyme activity defects among the sphingolipidoses	134
4.2.3	Identification of secondary enzyme activities altered in the mucopolysaccharidoses	137
4.2.4	Identification of altered secondary enzyme activities among the transmembrane protein associated lysosomal storage diseases.....	137
4.2.5	Identification of secondary enzyme activities altered in multiple enzyme deficiency diseases.....	138
4.2.6	Lysosomal enzyme alterations in the neuronal ceroid lipofuscinoses	138
4.2.7	Altered lysosomal enzyme activities across the other LSDs (Wolman, Oligosaccharidoses and Glycogenoses).....	139
4.2.8	Confirmation of changes in human patient fibroblast lysosomal enzyme activities in mucopolysaccharidoses knock-out mouse tissues	139
4.2.9	Validation of key lysosomal enzyme changes in NPC1 fibroblasts using Npc1 ^{-/-} mouse tissues.....	141
4.2.10	Comparison of key lysosomal enzyme changes in NPC1 fibroblasts against patient fibroblasts harbouring different NPC1 mutations	143
4.2.11	Evaluation of the effect of miglustat treatment on lysosomal enzyme activities	145
4.2.12	Lysosomal enzyme activities in clinical samples from CLN5 patients undergoing miglustat treatment	149
4.2.13	Determining whether restoration of secondary enzyme activity defects in LSDs can correct storage of associated lysosomal substrates.	153
4.3	DISCUSSION	155
4.3.1	There are multiple lysosomal enzymes altered across LSDs	155
4.3.2	HexA, HexB and Total Hex are elevated and are a possible biochemical marker for the mucopolysaccharidoses.....	155
4.3.3	NPC1 different tissues and mutations exhibit different enzyme activity.....	157
4.3.4	Miglustat changes several lysosomal enzyme activities.....	159
4.3.5	A new biomarker for CLN5 treatment.....	160
4.3.6	Highlighting the importance of lysosomal enzyme alteration in disease mechanism and the correlation between LSDs and other neurodegenerative disease.....	160
4.3.7	An enzyme fingerprint for individual or group of lysosomal storage disease	162
4.3.8	The possibility of the secondary enzymes defect in LSDs becoming a therapeutic target.....	165
4.4	CONCLUSION.....	165
5	CHAPTER 5: A COMPARISON OF LYSOSOMAL LIPID STORAGE ACROSS LYSOSOMAL STORAGE DISEASES BY ELECTRON MICROSCOPY	166
5.1	INTRODUCTION	166
5.1.1	Overview of the use of electron microscopy for LSD diagnosis.....	166
5.1.2	Usefulness of electron microscopy for studying ultrastructural alterations in LSDs.....	167
5.1.3	Aims.....	169
5.1.4	A brief summary of the various methods I used	169
5.2	RESULTS	170
5.2.1	The ultrastructure appearance of lysosomes in control fibroblasts and the localization of lysosome markers.....	170
5.2.2	Morphologies of primary storage molecules accumulating in the LSDs.	173
5.2.3	Morphological characterization of the sphingolipidosis family of diseases by electron microscopy.....	175
5.2.4	The ultrastructural appearance of storage material in the mucopolysaccharidoses	180

5.2.5	Morphological characterization of lysosomal storage in the neuronal ceroid lipofuscinoses. ...	182
5.2.6	Confirmation of globoside storage, and the ability of miglustat to remove storage material, in CLN5 disease.....	185
5.2.7	Morphological characterization of Oligosaccharidosis disease.....	188
5.2.8	Morphological characterization of other LSDs.....	191
5.3	DISCUSSION.....	196
5.3.1	Identifying the ultrastructure of the major storage material in LSDs.....	196
5.3.2	Identifying secondary storage material by EM.....	200
5.3.3	Conclusions.....	208
6	CHAPTER 6: MEASUREMENT OF INTRACELLULAR CA²⁺ AND TRACE ELEMENTS ALTERATION AMONG LSDS	209
6.1	INTRODUCTION.....	209
6.1.1	Ca ²⁺ homeostasis defects associated with lysosomal storage diseases.....	209
6.1.2	The involvement of the lysosome in essential TE metabolism.....	211
6.1.3	Previous studies have demonstrated altered TE homeostasis in LSDs.....	213
6.1.4	Aims:.....	214
6.1.5	A brief description of the methods used.....	215
6.2	RESULTS:.....	216
6.2.1	Lysosomal Ca ²⁺ levels are altered in several LSDs.	216
6.2.2	Determination of suitable probes for Zn ²⁺ intracellular distribution.....	220
6.2.3	Zn ²⁺ alteration is common across the LSDs.....	223
6.2.4	Alterations in intracellular Fe and Cu among the LSDs.....	226
6.2.5	Investigating Fe ²⁺ and Cu ⁺ accumulation in LSDs.....	227
6.2.6	Elevated lysosomal Zn ²⁺ is a possible new biomarker present in NPC cells carrying classical and variant disease causing mutations.....	229
6.2.7	Use of inductively-coupled plasma mass spectrometry to evaluate TEs in LSD cells.....	234
6.2.8	Trace elements could be useful for monitoring treatment of LSDs.	238
6.3	DISCUSSION.....	244
6.3.1	Lysosomal Ca ²⁺ defects are common in LSDs, but is not an appropriate measure for clinical diagnostic use.	244
6.3.2	Lysosomal Zn ²⁺ accumulation is a common phenotype in the LSDs.....	246
6.3.3	Zn ²⁺ has promise as a potential biomarker for NPC.....	247
6.3.4	Feasibility of Inductively-Coupled Plasma Mass Spectrometry in the diagnosis and monitoring of LSDs	249
6.4	CONCLUSION.....	251
7	CHAPTER 7: NPC1 LOSS OF FUNCTION IS OBSERVED ACROSS THE MAJORITY OF LYSOSOMAL STORAGE DISEASES, EXPLAINING THE LYSOSOMAL ACCUMULATION OF ZN²⁺ AND THE PRESENCE OF SECONDARY LIPID STORAGE AND LYSOSOMAL CA²⁺ DEFECTS.	252
7.1	INTRODUCTION.....	252
7.1.1	An overview of the complexity of NPC1 protein function.....	252
7.1.2	Lysosphingolipids (Lyso-SLs) accumulate in most LSDs.....	254
7.1.3	Aims:.....	255
7.1.4	Brief methods:.....	255
7.2	RESULTS.....	257
7.2.1	NPC1 phenotypes overlap with other LSDs.....	257
7.2.2	Neither TRPML1 upregulation nor miglustat treatment normalizes lysosomal Zn ²⁺ accumulation in NPC fibroblasts.....	258
7.2.3	Bafilomycin A1 (Baf A1) treatment induced lysosomal Zn ²⁺ accumulation.	260
7.2.4	Reducing cholesterol storage normalises NPC phenotypes.	262
7.2.5	Inhibition of GCase modulates cellular lipid storage and induces an NPC-like phenotype in control, but not Farber, fibroblasts.	264
7.2.6	The effects of exogenous Lyso-SLs on lysosomal Zn ²⁺ levels in control fibroblasts.....	267
7.2.7	Both inhibiting NPC1 function, or adding psychosine leads to Zn ²⁺ and lipid accumulation in Krabbe	270
7.2.8	Inhibition of lyso-SL formation reduced lysosomal Zn ²⁺ accumulation.....	273

7.2.9	Miglustat treatment corrects lysosomal Zn ²⁺ storage and NPC1 levels.	275
7.3	DISCUSSION	277
7.3.1	Lysosomal Zn ²⁺ accumulation is mainly NPC1 dependent.....	277
7.3.2	Accumulating lyso-SLs have a greater effect on NPC function than SLs.....	279
7.3.3	Blocking GSL biosynthesis is beneficial to Fabry disease.....	281
7.4	CONCLUSION.....	282
8	CHAPTER 8: GENERAL DISCUSSION	283
8.1	SUMMARY	283
8.2	INVESTIGATING THE OPTIMUM CONDITIONS OF LYSOTRACKER BECOMING A SUITABLE BIOMARKER FOR MAJORITY OF LSDs	283
8.3	SECONDARY LYSOSOMAL ENZYME ALTERATIONS ARE A COMMON FEATURE OF LSDs	284
8.4	ELECTRON MICROSCOPY IS ONE OF THE MOST USEFUL TOOLS FOR IDENTIFYING SECONDARY STORAGE MATERIALS AMONG LSDs	286
8.5	TRACE ELEMENTS ARE PROMISING, BUT UNTESTED, BIOMARKERS FOR LSDs.	287
8.6	COMBINATION OF BIOMARKERS SHOWED THE SUCCESS OF MIGLUSTAT THERAPY ON CLN5 PATIENTS	288
8.7	NPC1 PROTEIN DEFECT IS ASSOCIATED WITH THE PRESENCE OF SECONDARY ZN ²⁺ AND STORAGE PHENOTYPES ACROSS THE MAJORITY OF LSDs AND MAY CONSTITUTE A COMMON THERAPEUTIC TARGET FOR THE LSD FAMILY.	289
8.8	CONCLUDING REMARKS	290
9	CHAPTER 9: REFERENCES	291
10	CHAPTER 10: SUPPLEMENTARY	333

Chapter 1: General introduction

1.1 The lysosome

1.1.1 Overview

De Duve, who first described the lysosome as an organelle, postulated that “this particle acts as the digestive tract of the living cell. Its enzymes dissolve the substances ingested by the cell and under certain circumstances can dissolve the cell itself” (de Duve 1959, 1963). The lysosome is an intracellular organelle found throughout the cytoplasm of eukaryotic cells, characterised by a single-layer membrane with an acidic internal environment of pH 4.5–5.0 (Graves et al. 2008; Mellman et al. 1986), whose morphology, number and size (which is estimated to be 0.1–1.2µm) are all highly variable depending on the cell type (Lüllmann-Rauch 2005). Electron microscopy reveals that lysosomes are mainly heterogeneous in size and shape, often displaying electron-dense content and, occasionally, multi-lamellar membrane structures (Klumperman and Raposo 2014). Lysosomes can be distinguished from endosomes by the higher degree of acidification, the presence of transmembrane lysosome-associated membrane proteins (LAMPs) and the lack of mannose-6-phosphate receptor (M6PR) which is recycled back to the Golgi from late endosomes (Huizing et al. 2008; Platt et al. 2012). The main feature of the lysosomal membrane is that it has a high carbohydrate content, due to the presence of highly glycosylated lysosomal membrane proteins of which 50% are composed of LAMP1 and LAMP2 (Lübke et al. 2009).

The primary function of the lysosome is to digest substances, including nucleic acids, proteins, glycosaminoglycans (GAGs), carbohydrates and sphingolipids (SLs), amongst others. Extracellular substances are taken into the lysosome through phagocytosis or endocytosis, whereas the metabolites found inside the cells are delivered to the lysosome by autophagy (Cooper et al. 2000; Kolter and Sandhoff 2006). Biomacromolecules are digested by more than 50 soluble enzymes found in the lysosomal lumen (Braulke and Bonifacino 2009). These enzymes work optimally at an acidic pH. These hydrolases include nucleases, proteases, glycosidases, sulphatases, phosphatases and lipases (Platt et al. 2012). The digested materials exit the lysosome through special protein transporters found in the organelle’s membrane, for example SLC38A9 is a Na⁺ dependent neutral amino acid transporter that mediates the efflux of leucine, tyrosine and phenylalanine (Rebsamen et al. 2015). This catabolic activity makes the lysosome a fundamental part of the cell that is involved in the regulation of cellular homeostasis by controlling cellular recycling of macromolecules, clearance of defective organelles (autophagy) and energy production, in response to the

external environment (Settembre et al. 2012). Lysosomal function is related to the breaking down and recycling of complex macromolecules, the downregulation of cell surface molecules and receptors, the inactivation of pathogenic microorganisms, initiation of apoptotic cell death, and membrane repair, amongst others (Schwake et al. 2013).

Besides digestive enzymes, the limiting membrane of the lysosome contains around 120 membrane proteins (Braulke and Bonifacino 2009). The integral proteins and membrane-associated proteins are involved in controlling the fundamental functions of the organelle, such as the transport and sorting of substrates, the digestion of products, the establishment of pH gradients and the maintenance of the organelle's structure (Bagshaw et al. 2005). The main lysosomal membrane proteins are as follows: (i) LAMP1 and LAMP2; (ii) the enzyme trafficking receptor lysosomal integral membrane protein 2 (LIMP2) and the structural tetraspanin CD63 protein (aka LIMP1 or LAMP3) (Fukuda 1991; Kobayashi et al. 2000). Structurally, LAMP proteins possess a luminal N-terminal domain, a single transmembrane domain and a short C-terminal cytoplasmic tail. They are highly glycosylated proteins with N-linked glycans and O-linked glycans, which make up more than 50% of their total molecular mass. LAMP1 and LAMP2 constitute more than half of the lysosomal membrane protein content, and both proteins have common functions that they perform together including roles in cholesterol mobilisation (Eskelinen 2006). Moreover, the highly glycosylated LAMP proteins make an ~8 nm thick glycocalyx, a gel like coat which protects the lysosomal membrane from degradation by lysosomal hydrolases (Neiss 1984; Neiss 2013; Wilke et al. 2012). They maintain the structural integrity of the lysosome as well as facilitate cholesterol trafficking (Schneede et al. 2011). This is demonstrated by the fact that mutations in the LAMP2 gene cause the lysosomal glycogen storage disease, called Danon disease, in humans. These patients possess accumulated autophagic vacuoles and un-esterified cholesterol in their heart and skeletal muscles (Eskelinen 2006).

LIMP1 and LIMP2 proteins are comparatively less abundant than LAMPs (Fukuda et al. 1988), but also play an important role in maintaining the structural integrity of the lysosome. Structurally, both their N and C terminal domains are found in the cytosol. Encoded by the gene *SCARB2*, LIMP2 is involved in the biogenesis and maintenance of lysosomes and endosomes, and also acts as a specific receptor for glucocerebrosidase (GCase), an enzyme whose deficiency is observed in patients suffering from Gaucher disease (GD) (Gonzalez et al. 2014). LIMP2 is, therefore, involved in the re-capture, internalisation and lysosomal transport of GCase that has been secreted from the Golgi apparatus (Zunke et al. 2016). A recent study provides evidence on the involvement of LIMP2 in cholesterol transport from

lysosomes (Heybrock et al. 2019), providing an alternative lysosomal cholesterol efflux pathway.

CD63 was the first characterised tetraspanin found in late endosomes/lysosomes (LE/Lys). Made up of four transmembrane domains, CD63 at the cell membrane is endocytosed by the clathrin-dependent pathway. In late endosomes, CD63 is abundant in intraluminal vesicles and is secreted as exosomes in specialised cells (Kobayashi et al. 2000; Pols and Klumperman 2009).

1.1.2 Lysosomal pH

Lysosomes are acidic, with a luminal pH of 4.5–5.5, and are more acidic (pH 4–4.5) in cells like macrophages (phagocytic cells). This acidic environment is suitable for substrate degradation as compared with the surrounding intracellular cytosolic fluid, which is slightly alkaline (pH 7.2) (Lloyd-Evans et al. 2008; Mellman et al. 1986). In the process of phagolysosome formation, the pH falls rapidly, activating proteolytic enzymes and causing pathogens to be eliminated (Geisow et al. 1981). The pH changes along the endocytic pathway are important for the function of different compartments. It helps in the recycling of receptors by inducing the separation of receptor and ligand, for example M6PR dissociates from its enzyme cargo at a pH of ~5 within late endosomes (Alberts et al. 2002). The maintenance of an optimum pH is important for the progressive activation of enzymes (Claus et al. 1998). Most lysosomal enzymes have a narrow pH range (e.g. cathepsin D pH range ~ 3.1-3.5), and a small shift in pH leads to a reduction in the enzyme activity (Lloyd-Evans and Haslett 2016). As a result, there is a significant accumulation of lipids within the lysosome compartments. Furthermore, lysosomal deacidification leads to lysosomal Ca^{2+} reduction and affiliated defects in autophagic vacuole-lysosome clearance (Lee et al. 2015).

The exact mechanism by which the lysosome maintains its pH homeostasis using the influx and efflux of cations is yet to be fully understood. The role of the lysosomal vacuolar-type H^+ - ATPase (vATPase) and any potential Cl^-/H^+ antiporter is vital, as it offers an environment with the optimum level of acidity for the functioning of the hydrolytic enzymes stored in the lysosome (Finbow and Harrison 1997). The proton pumps involved in the acidification are the vATPase proteins, which serve as endosomal membrane pumps found throughout the different endocytic organelles, that use the free energy released by the hydrolysis of adenosine triphosphate (ATP) to push protons from the cytosol into the organelle lumen, against the electrochemical gradient. This is an important proton channel for lysosomes as it generates and maintains the acidic pH, which is achieved simultaneously with the outflow of

K⁺ ions through either a cation channel or a transporter (Mindell 2012). Unlike the well-studied regulator of lysosomal acidification vATPase, the Cl⁻/H⁺ antiporter CLC-7 is so far known to provide vital contributions with respect to pH regulation in lysosomes (Graves et al. 2008). It has been reported that the CLC Cl⁻/H⁺ antiporter is the protein through which Cl⁻ gets transported through the lysosomal membrane. *In vivo*, a limit on CLC-7 expression due to short interfering RNA, has been shown to inhibit Cl⁻/H⁺ antiport activity and decrease the acidification of lysosomes. Therefore, CLC-7 is a Cl⁻/H⁺ antiporter that allows the Cl⁻ permeability of lysosomes, which is essential for acid loading in the lysosome (Graves et al. 2008). The recent clinical and genetic evaluation study showed that a gain in function of CLC-7 increased acidity of lysosomes (Nicoli et al. 2019).

1.1.3 Lysosome biogenesis and the transport of lysosomal enzymes

Lysosomes matured from the endocytic system now largely started to change. Recent studies have shown the lysosome is a clearly separate organelle with separate markers and is generated by transcription factor EB (TFEB) (Medina et al. 2011; Settembre and Medina 2015). It mediates the expression of many lysosomal proteins. During lysosomal stress or nutrient deficiencies, TFEB present in the cytosol is phosphorylated by the mammalian target of rapamycin complex 1 (mTORC1) kinase and moved to the nucleus, triggering the transcription of genes in the coordinated lysosomal expression and regulation network, and thus lysosomal biogenesis. mTORC1 kinase is known to regulate cell homeostasis and growth, and depends on the availability of amino acids for proper functioning (Bar-Peled and Sabatini 2014). Considerable evidence now supports the notion that TFEB overexpression is capable of both generating new lysosomes and inducing exocytosis of old lysosomes to reduce the accumulation of molecules within diseased cells (Sardiello et al. 2009). There are ~500 TFEB target genes that include the genes responsible for regulating the expression of autophagy and lysosomal biogenesis (Palmieri et al. 2011; Settembre et al. 2011). TFEB is also involved in lysosomal exocytosis and lipid degradation (Medina et al. 2011).

Lysosomal enzymes and membrane proteins are transported to lysosomes via the biosynthetic pathway, that contains the endoplasmic reticulum (ER), the trans-Golgi network (TGN), the plasma membrane and endosomes (Braulke and Bonifacio 2009). Lysosomal proteins are translated and processed in the ER before they are recognised in the TGN as being tagged with mannose-6-phosphate (M6P) (Figure 1.1). The M6P is added to the N-linked oligosaccharides of hydrolytic enzymes. The M6P tag is created through the actions of two enzymes, namely UDP-N-acetylglucosamine 1-phosphotransferase (GlcNAc-1-

phosphotransferase); which is defective in Mucopolysaccharidosis II disease (I cell) and α -N-acetylglucosamine-1-phosphodiester α -N-acetylglucosaminidase enzyme (Coutinho et al. 2012). In TGN membranes, there are two M6P receptors (M6PRs), a cation-independent M6P receptor and a cation-dependent M6P. These are specific to M6P residues that selectively bind to lysosomal proteins. The receptors bind to the lysosomal enzyme and generate clathrin coats on the cytosol. They also help in the packing of the enzymes from TGN to the endosome compartments. Together, the lowering the pH of the endolysosome and the presence of cathepsin lead to the dissociation of proteins from the M6P receptors, which facilitates the conversion of lysosomal proenzymes to mature enzymes. Then, the receptors are transferred back to the Golgi apparatus from the late endosomes by the means of transport vesicles (Figure 1.1) (Coutinho et al. 2012).

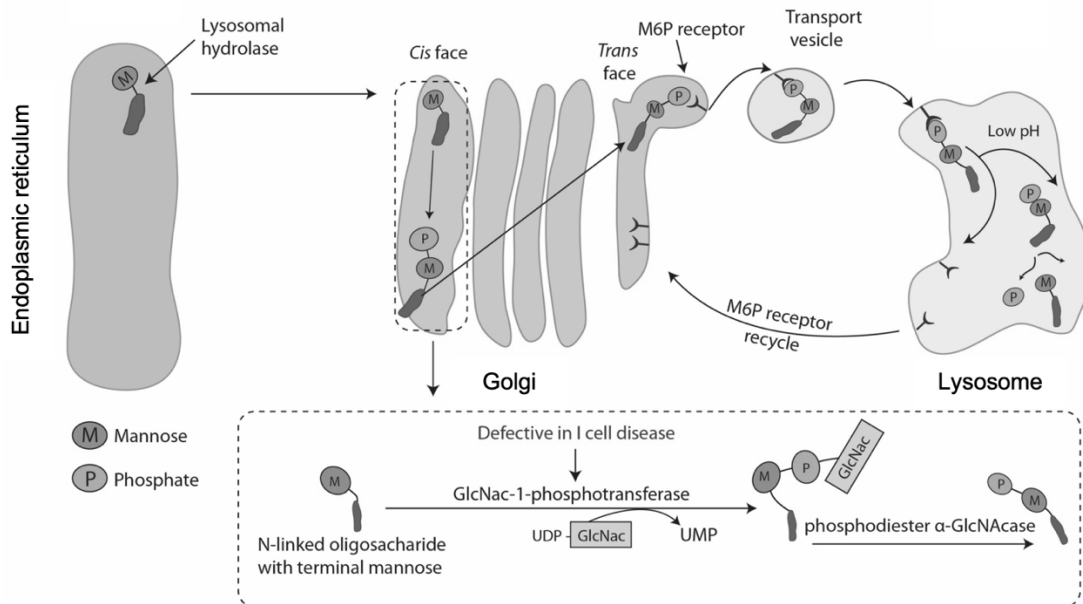


Figure 1.1 Lysosomal enzyme synthesis pathway.

Lysosomal hydrolase is synthesised in the endoplasmic reticulum (ER). The M6P tags are mediated by two enzymes in the *cis*-Golgi. In the first step, GlcNac-1 is phosphorylated by the action of GlcNac-1 phosphotransferase (encoded by *GNPTAB/G*), to produce a molecule of GlcNac-1-phosphate (with phosphorus at the mannose terminal) and UMP. In the second step, the N-acetylglucosamine-1-phosphodiester α -N-acetylglucosamidase (phosphodiester α -GlcNAcase) (encoded by *NAGPA*) cleave the GlcNac residue to generate the M6P recognition marker. This enzyme is transported to the *trans*-Golgi and binds to mannose 6-phosphate receptors. This complex is transported, via the transport vesicle, to the acidic lysosome. The low pH of the lysosome causes the dissociation of the enzyme from the receptor. The phosphate ester is then cleaved to get the mature form of the enzyme while the M6P receptor is recycled back to the *trans*-Golgi. UDP : uridine diphosphate; UMP : uridine monophosphate. Figure adapted from (Coutinho et al. 2012).

The presence of alternative pathways for lysosomal enzymes and membrane protein transportation has been indicated. The study of I cell disease is characterised by defective in GlcNac-1-phosphotransferase activity, involving the formation of M6P, which results in the absence of the M6P tag. As a result, the lysosomal enzymes are unable to bind to MPRs in the TGN; thereafter, these enzymes are secreted. Therefore, the amount of lysosomal enzymes secreted in plasma, serum, cerebrospinal fluid (CSF) etc. increases in I cell patients. Previous studies on I cell found fibroblasts obtained from I cell patients, which showed a

deficiency of the majority of lysosomal enzymes. In contrast, studies on mice lacking M6P receptors showed certain normal lysosomal enzyme activities in the liver, brain and spleen (Dittmer et al. 1999), which means that some soluble lysosomal proteins, cathepsins, GCase and sphingolipid activator proteins (SAPs) are still transported to the lysosomes. More recently, LIMP2 has been identified as a contributor to the M6P-independent pathway, where it is involved in the delivery of GCase to lysosomes in a pH-dependent manner (Blanz et al. 2015). Sortilin, which travels among the TGN and LE/Lys, is capable of binding to numerous molecules. This protein is involved in the transmission of cathepsins (D,H), SAPs and acid sphingomyelinase (ASMase) (Canuel et al. 2008; Lefrancois et al. 2003; Ni and Morales 2006). Therefore, it was suggested that sortilin is another sorting receptor, in addition to the M6PRs, for those soluble enzymes (Canuel et al. 2008).

1.1.4 The intracellular role of the lysosome in the endocytic system

The endocytic pathway is the main pathway by which lysosomes receive proteins from lysosome biogenesis via the TGN, as well as molecules that are unable to cross the plasma membrane for the degradation process. The endocytosis pathway involves the uptake of extracellular materials, mainly via the following two mechanisms: clathrin-dependent endocytosis (CDE) and clathrin-independent endocytosis (CIE) (Grant and Donaldson 2009).

CDE events begin via a concerted assembly of the clathrin coat and adaptor proteins, which interact with the transmembrane proteins (cargo) that are meant to enter cells in endocytotic vesicles. CDE involves the turnover of plasma membrane proteins and lipids, the uptake of low-density lipoproteins (LDL) and iron-saturated transferrin and the endocytosis of growth factor receptors after their activation (Grant and Donaldson 2009). A clathrin-coated vesicle is formed via the sequential action of 50 different proteins, including (1) adaptors, mainly AP-2, which select the transmembrane cargo proteins and link the cargo selection to the polymerisation of the clathrin coat, (2) scission factors, to force endocytic vesicle generating events (Kaksonen and Roux 2018), and (3) the uncoating of endocytotic vesicles (Lee et al. 2006). Clathrin and adaptin from the cytosol bind to the loaded cargo receptor proteins that span the plasma membrane. The plasma membrane invaginates deeper and deeper and encloses the cargo into a vesicle, an action that is aided by the protein dynamin. The clathrin-coated vesicle, then, begins the degradation process. After degradation, the vesicle loses the clathrin coat, approaches an early endosome and fuses with it. The cargo molecules are unbound with regard to the receptors and are released in the endosomal lumen (Kaksonen and Roux 2018). The portion of the endosome containing the cargo receptors breaks off and returns to the plasma membrane (Jovic et al. 2010). H^+ is pumped into the early endosome by the action of the vATPase. The cargo is delivered in annexin A2-positive vesicles that regulate

the multivesicular endosome / late endosomes process (Mayran et al. 2003). Then, the late endosome transporters of cargo to lysosome contain hydrolytic enzymes to digest the cargo content, which is released in the cytosol (Huotari and Helenius 2011).

In the other pathway, CIE, the pathway process involves two dominant mechanisms: the caveolar pathway and fluid-phase endocytosis. Small-scale CIE pathways may or may not require the protein dynamin, or the presence/absence of a coat that marks the internalised patch of a membrane. The dynamin-dependent caveolar endocytotic system involves the detachment of caveolae from the plasma membrane to form an endocytotic caveolar carrier (Mayor and Pagano 2007). Evidence suggests that a build-up of certain lipids involved in protein membrane tethering could trigger membrane budding and form a vesicle in an energy-feasible manner. As such, the caveolar endocytosis mechanism involves the transport of cholesterol, proteins and lipids (Mayor and Pagano 2007). Either CDE or CIE pathways are involved in the gradual increase of the acidity of the endosomal compartments (Mayor and Pagano 2007). In addition to the pH, there are differences between early and late endosomes; the early endosomes contain the effector protein EEA1 and Rab5, a small GTPase belonging to the Rab family (Mayor and Pagano 2007). The conversion from Rab5 to Rab7 occurs in the late endosomes (Rink et al. 2005). Rab7 is a mediator between late-endosomes and lysosomes (Vanlandingham and Ceresa 2009). Rab7 and Rab9 in late endosomes are involved in intracellular transport of glycosphingolipid to Golgi (Choudhury et al. 2002). The late endosomes also contained lysobisphosphatidic acid-rich membranes (LBPA), which is involved in the controlling the cholesterol catabolism through endosomes (Kobayashi et al. 1999).

1.1.5 The role of lysosomes in Ca²⁺ signal regulation

Lysosome-associated organelles are becoming increasingly researched as imperative Ca²⁺ cellular storage organelles that play a major role in intracellular Ca²⁺ signalling (Patel and Cai 2015). Increases in cytosolic Ca²⁺ regulates a lysosome's ability to fuse with the plasma membrane, which results in lysosome exocytosis. The lysosome exocytosis process can be involved in plasma-membrane wound repair (Reddy et al. 2001). The majority of intracellular processes are dependent on Ca²⁺, including the process of transport through the endocytic system, autophagosome-lysosome fusion and membrane recycling (Lloyd-Evans et al. 2010; Pryor et al. 2000). Disturbances in endosomal Ca²⁺ can lead to defects in endocytic and autophagic vacuole-lysosome fusion (Lloyd-Evans and Platt 2011; Lloyd-Evans et al. 2010). Most intracellular Ca²⁺ (~1mM) is stored in the ER and released to the cytoplasm through two kinds of Ca²⁺-release channels that span the ER-membrane: the ryanodine receptor (RyR)

and the inositol 1,4,5-triphosphate-gated (IP₃) Ca²⁺ release channel (IP₃R). Ca²⁺ can be taken from the cytoplasm into the lumen of the ER through the sarcoplasmic/endoplasmic reticulum calcium-ATPase (SERCA) (Berridge et al. 2000). In this vein, lysosomes are acidified Ca²⁺ signalling organelles that contain free Ca²⁺ ions and multiple Ca²⁺ channels (Morgan et al. 2011).

The Ca²⁺ concentration within the lumen of acidic vesicles was found to be in the range of 400–600 μM, indicating that lysosomes are the secondary largest intracellular Ca²⁺ store (Christensen et al. 2002; Lloyd-Evans et al. 2008). However, lysosomes comprise 2–3% of the cellular volume; therefore, Ca²⁺ release from lysosomes does not cause large changes in cytosolic Ca²⁺, as compared to the ER, which volumetrically takes up >10% of the total cellular volume and is the largest Ca²⁺ storage site within the cell (100–1000 μM) (Alberts 2017; Bygrave and Benedetti 1996). Recent findings demonstrate that the Ca²⁺ released from lysosomes affects ER Ca²⁺ release and cellular Ca²⁺ haemostasis (Kilpatrick et al. 2013; Morgan et al. 2013). The pathways responsible for Ca²⁺ uptake and release from lysosomes are not understood completely yet (Höglinger et al. 2015; Lloyd-Evans and Platt 2011). The majority of lysosomal Ca²⁺ is not obtained from endocytosis, as changing extracellular Ca²⁺ only has a slight effect on lysosomal Ca²⁺ content (Christensen et al. 2002). Endocytosed Ca²⁺ ions are mainly transferred from early endosomes to the cytosol in a pH-dependent manner (Lloyd-Evans et al. 2010).

Lysosomal Ca²⁺ filling from the cytoplasm is mainly proton dependent (Christensen et al. 2002). The deacidification of lysosomes by inhibitors of the vATPase leads to the Ca²⁺ release from lysosomes (Christensen et al. 2002). It has been reported that in yeast and plants, Ca²⁺ is taken in by vacuoles using plasma membrane Ca²⁺-ATPases, which breaks down ATP to pump Ca²⁺ into the vacuole (Geisler et al. 2000). A similar homologue of Ca²⁺-ATPase is also found in mammal cells. However, limited knowledge exists on the molecular basis and functional mechanisms of the regulation of H⁺ dependent Ca²⁺ uptake and maintenance in the lysosomes of mammal cells. The Ca²⁺/H⁺ exchanger (CAX) may be involved in the filling of lysosomes by pH-dependent Ca²⁺ uptake (Morgan et al. 2011). There is a possibility that lysosomal Ca²⁺ uptake is dependent on Ca²⁺ coming from the ER (Garrity et al. 2016). Lysosomal Ca²⁺ filling is affected by depleting ER Ca²⁺ and by inhibiting IP₃Rs (Garrity et al. 2016). It is known that Ca²⁺ release from lysosomes is important for organelle acidification. Nicotinic acid adenine dinucleotide phosphate (NAADP) induces Ca²⁺ discharge from lysosomes (Brailoiu et al. 2009; Calcraft et al. 2009; Churchill et al. 2002). The channels involved are, more precisely, two-pore channels (TPCs): TPC 1 and TPC 2, in humans. Structurally, the TPCs contain six transmembrane domains that are similar to those of voltage-

gated Ca^{2+} and Na^+ channels (Calcraft et al. 2009). The mucolipin family of Ca^{2+} -permeable channels found on endolysosomes are Transient Receptor Potential Mucolipins (TRPML1, TRPML2 and TRPML3), all non-selective cation channels. TRPML1 is permeable to multiple ions (e.g. Ca^{2+} , Fe^{2+} , Na^+ , K^+ and Zn^{2+}) (Cuajungco et al. 2014; Dong et al. 2008; LaPlante et al. 2002). TRPML1 is almost only found in lysosomes, whereas TRPML2 is present in endosomes and TRPML3 in the plasma membrane and lysosomes (Cheng et al. 2010). TRPML1 is activated by phosphatidylinositol 3,5-biphosphate ($\text{PI}(3,5)\text{P}_2$) and is involved in lysosome exocytosis (Dong et al. 2010; Pryor et al. 2006). P_2X_4 is another Ca^{2+} -permeable channel found in the central and peripheral nervous systems, mainly located in lysosomes. It remains inactive at lysosomal pH but becomes activated at a neutral pH, upon the presence of a high ATP content (Chuang et al. 2014). This stimulation may lead to Ca^{2+} release from the lysosome in a calmodulin-dependent process (Cao et al. 2015). More channels involved in lysosomal Ca^{2+} are summarised in (Figure 1.2). A recent study showcased the fact that lysosomal Ca^{2+} signals control the process of autophagy via the actions of phosphatase calcineurin and TFEB, which emphasizes the integral function of lysosomes as a central member of the signalling hub and emphasises the significance of having a clear idea about the control of lysosomal Ca^{2+} signalling (Medina et al. 2015; Medina et al. 2011). TFEB stimulates the Ca^{2+} through upregulation of TRML1 to trigger lysosomal exocytosis (Medina et al. 2011).

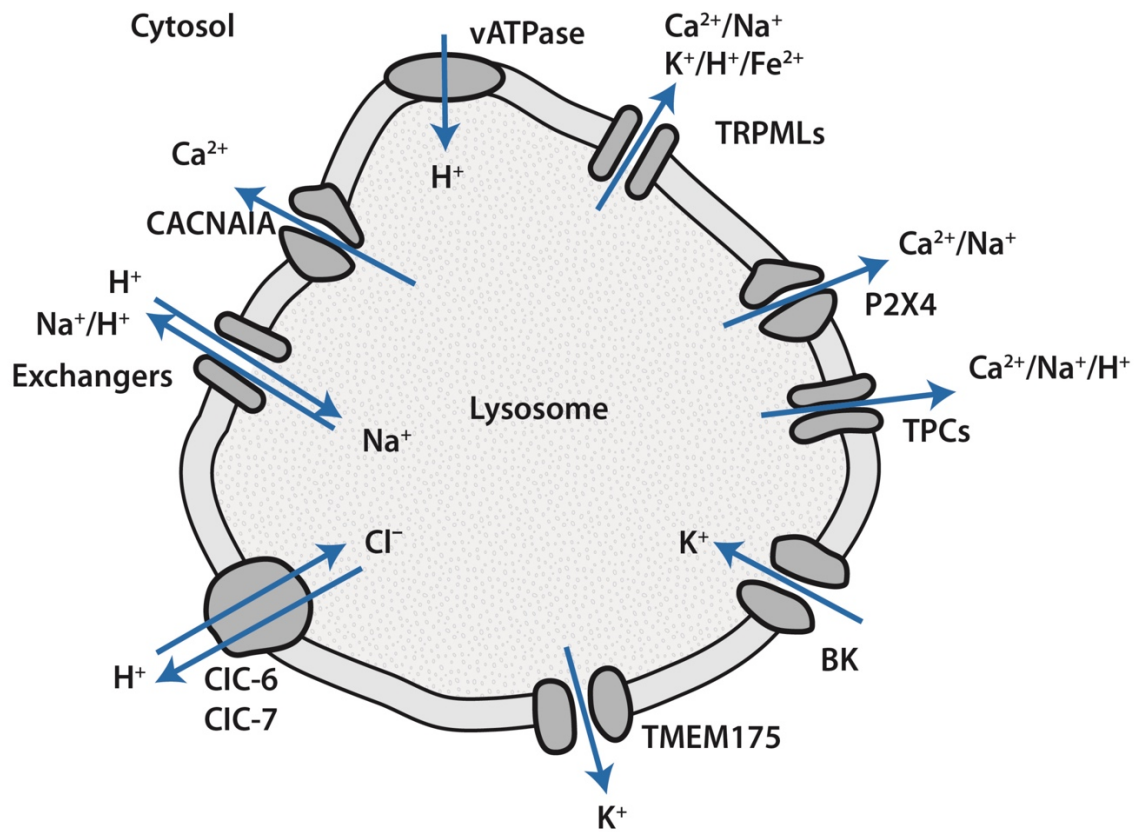


Figure 1.2 Schematic diagram of key lysosomal Ca²⁺ and other ion channels on the lysosomal membrane.

The lysosome lumen contains several channels, such as the proton pumping channel vATPase. The TRPMLs are involved in numerous ion releases. TPCs, P2X4 and the voltage-gated channel (CACNA1A) mainly stimulate lysosome release. K⁺ channel (BK) and TMEM175 constitute the K⁺ channels. The CIC family (CIC-6 and CIC-7) provide the chloride channels. Either NHE3 or Na⁺/H⁺ exchanger regulates the intra-lysosomal H⁺ and Na⁺ (Lawrence et al. 2010; Lloyd-Evans 2016b; Tian et al. 2015; Xiong and Zhu 2016; Zhong et al. 2017).

1.1.6 The role of lysosomes in homeostasis

The homeostasis of metal ions is important for the physiological processes of the body. In the human body, there are essential trace elements (TEs) including zinc (Zn), iron (Fe), copper (Cu), selenium (Se), cobalt (Co) and manganese (Mn). TEs typically work as the co-factors of key antioxidant enzymes and regulate cellular activities. The concentration of TEs is maintained at a low level and is regulated by cellular compartments, which contain metal transporters responsible for loading and unloading metals (Blaby-Haas and Merchant 2014). Over recent years, it has been thought that lysosomes play a role in various aspects of TE metabolism. Metal-containing components, such as metallothioneins (MT), are transported to lysosomes via endocytosis or autophagocytosis. The divalent cation transporter (DTM1), which is involved in cation transporting, has been reported to be localised to endosomes (Tabuchi et al. 2000). Lysosomal metal ions are mainly released via metal-bound proteins. Therefore, lysosomes are considered to be the main intracellular storage sites of TEs in micromolar concentrations (Xu and Ren 2015). The movement of those ions through the lysosomal membrane is mediated by ion channels and transporters (Figure 1.3). Different types of ions move in different amounts, as determined by the permeability of the channels to different ions and their intravesicular concentration. A significant alteration in ion concentrations could lead to a alteration in lysosomal membrane structure and potential impact on lysosomal transporters. For example, the overexpression of ZnT2 leads to an increase in the intracellular Zn^{2+} ; as a result, there is a phospholipid lysobisphosphatidic acid (LBPA) defect and cholesterol storage alongside a sorting/trafficking defect (Kobayashi et al. 1999). The alteration in ion concentrations also has a potential impact on ion channel function alongside possible inhibition of lysosomal enzyme activity (Mindell 2012). The metal pumps and ion transporters play a crucial role in maintaining homeostasis across the lysosomal membrane (Xiong and Zhu 2016).

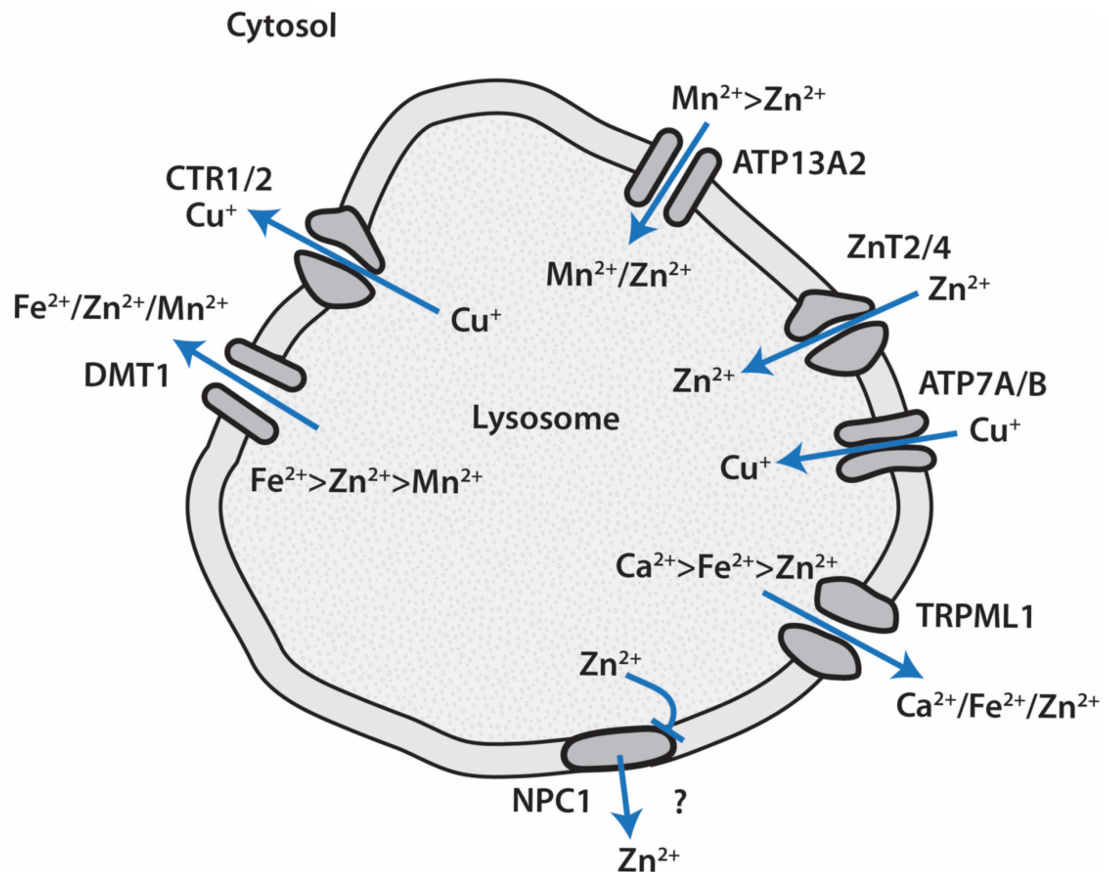


Figure 1.3 Schematic diagram of major trace element transporters and channels on the lysosomal membrane.

The lysosomal lumen contains several trace elements. Arrows indicate the direction of ion fluxes. Confirmed lysosomal channels and transporters include ATP13A2 Mn^{2+} and Zn^{2+} trafficking across the lysosome, with Zn^{2+} getting transported to the lysosome by ZnT2/4. The ATP7A/B channel pumps Cu^{+} to lysosome. TRPML1 is involved in the release of numerous ions including Ca^{2+} , Fe^{2+} and Zn^{2+} . NPC1 binds to Zn^{2+} and is only possibly involved in transportation. The Cu^{2+} transporter Ctr1/2 transports Cu^{+} (Öhrvik and Thiele 2015; Polishchuk and Polishchuk 2016; Tabuchi et al. 2000; van Veen et al. 2014).

1.2 Lysosomal storage diseases

1.2.1 Overview

The lysosomal storage diseases (LSDs) are a group of ~70 rare inherited disorders that usually produce their first symptoms during childhood or adolescence, subsequently shortening life expectancy and leading to varying degrees of disability in affected patients (Gelb et al. 2015). They are predominantly caused by a genetic alteration in, or malfunction of, lysosomal enzymes often associated with defects in lipid transport, which causes the accumulation of different substrates and substances that are not metabolized in the lysosomes, and results in impaired cell function and cell death. LSDs are transmitted genetically as they are autosomal recessive, except for MPS II and Fabry diseases, which are inherited by an X-linked recessive gene. Danon disease is also X-linked, but is dominant (Wilcox 2004). The prevalence of LSDs is approximately one in 5,000–8,000 live births, meaning that the LSDs are the most common cause of childhood neurodegenerative disease (Fuller et al. 2006). This value may be higher, considering the numerical potential for undiagnosed cases (Wassif et al. 2016). For example, Niemann-Pick type C (NPC) has a current clinical prevalence of 1/104,000. However, using bioinformatics tools, the estimated incidences of disease causing mutations in *NPC1* and the closely associated disease gene *NPC2* are 1/92,000 and 1/2,900,000, respectively. Through the evaluation of NPC1 variants and late-onset NPC1 phenotypes, the incidence may increase to 1/19,000–1/39,000 (Wassif et al. 2016). Certain LSDs are highly prevalent in certain geographic regions or among a certain ethnicity. For example, the prevalence of Tay-Sachs disease in the Ashkenazi Jewish population is, for affected people and carriers, 1/3,500 and 1/29, respectively. A carrier screening programme targeting the higher-risk Jewish population has prevented almost 90% of this disease within the population (Rozenberg and Pereira 2001).

Despite the differences in accumulated material in particular LSDs, they contain several overlapping cellular, biochemical and clinical features. LSDs have a wide range of clinical phenotypes such as abnormal craniofacial features, hepatosplenomegaly and skeletal anomalies (Wenger et al. 2003). Most LSD patients are born apparently healthy but subsequently develop symptoms. These diseases affect different systems simultaneously: blood vessels, kidneys, heart and the nervous system (Platt et al. 2012).

1.2.2 Classification

There is no single classification for LSDs. These diseases were previously classified based on the nature of the storage material within the affected tissue (Filocamo and Morrone 2011). Most LSDs belong to the “defects of glycan degradation” category. This group can be further divided into four sub-categories: defects in glycoprotein degradation, glycolipid degradation, glycosaminoglycan degradation and defects in glycogen degradation (Greiner-Tollersrud and Berg 2005). LSDs can be classified based on protein deficiency. Recent classification studies reveal that it is possible to classify them based on their molecular defects (Filocamo and Morrone 2011). Based on our current understanding of LSDs, on a molecular basis the group of LSDs includes the following: (i) sphingolipidoses, due to the accumulation of undegraded sphingolipids, as a result of an enzyme defect or an activator protein defect; (ii) mucopolysaccharidoses, as a result of defect in enzymes that are involved in mucopolysaccharidoses or GAGs degradation; (iii) Transmembrane protein defect, or those diseases which are caused by defects in the transporters of molecules going out of lysosomes; I have included NPC2 (soluble protein) in this group, as it, with NPC1, caused identical disease and both gene products propose function in tandem (Friedland et al. 2003); (iv) glycoproteinoses resulting from single lysosomal enzyme deficiency, that entails the accumulation of oligosaccharides; (v) neuronal ceroid lipofuscinoses (NCLs), which result from defects in lysosomal enzymes or transporters, resulting the storage of subunit c of the mitochondrial ATP synthase (SCMAS) or SAPs A and D; (vi) Glycogenoses, resulting from the defects in enzyme involved in glycogen degradation (Fukuda 1991). Cholesteryl esters and triglycerides storage disease; (viii) multiple enzyme deficiency resulting from the trafficking defects or post-translational processing defects in lysosomal enzymes. Finally, the last group which does not fit with any of the above groups, is diseases caused by the defects in lysosomes and lysosome-related organelles such as Chediak-Higashi syndrome (Mehta and Winchester 2012).

Table 1.1 Summary of key features of some LSDs with respect to protein deficiency, storage of compounds, tests and genes.

(Filocamo and Morrone 2011; Mehta and Winchester 2012; Mole et al. 2018).

Class ^a	Lysosomal storage disease	Genes involved	Protein deficiency	Storage	Initial test	Diagnostic test
Sphingolipidoses	Fabry disease	<i>GLA</i>	α -Galactosidase A	Globotriasylceramide	Glycolipids (U)	Enzyme assay/MGT
	Krabbe disease	<i>GALC</i>	Saposin A	Glucosylceramide	–	Enzyme assay/MGT
	Gaucher disease	<i>GBA</i>	Saposin C	Glucosylceramide	Plasma Chito	Enzyme assay/MGT
	Niemann-Pick disease Type A/B	<i>SMPD1</i>	Sphingomyelinase	Sphingomyelin	Plasma Chito	Enzyme assay/MGT
	GM1-gangliosidosis	<i>GLB1</i>	β -galactosidase	GM1, Keratan sulphate, oligos, glycolipids	Oligos (U)	Enzyme assay/MGT
	GM2-gangliosidosis (Tay-Sachs)	<i>HEXA</i>	β -Hexosaminidase A	GM2, oligos, glycolipids, globoside	–	Enzyme assay/MGT
	GM2-gangliosidosis (Sandhoff)	<i>HEXA, HEXB</i>	β -Hexosaminidase A & B	GM2, Oligos	Oligos (U)	Enzyme assay/MGT
	Gangliosidosis GM2 activator defect	<i>GM2A</i>	GM2 activator protein	GM2, Oligos	GM2 in CSF	MGT
	Farber disease	<i>ASAH1</i>	Acid ceramidase	Ceramide	–	Enzyme assay/MGT
	Metachromatic leucodystrophy	<i>ARSA/ PSAP</i>	Arylsulfatase A / Saposin B	Sulphatides	Sulphatides (U)	Enzyme assay/MGT
Mucopolysaccharidoses	MPS I (Hurler, Scheie, Hurler/Scheie)	<i>IDUA</i>	α -Iduronidase	Dermatan sulphate, heparan sulphate	GAGs (U)	Enzyme assay/MGT
	MPS II (Hunter)	<i>IDS</i>	Iduronate-2-sulphatase	Dermatan sulphate, heparan sulphate	GAGs (U)	Enzyme assay/MGT
	MPS III A (Sanfilippo A)	<i>SGSH</i>	Heparan N-sulphamidase	Heparan sulphate	GAGs (U)	Enzyme assay/MGT
	MPS III B (Sanfilippo B)	<i>NAGLU</i>	Acetyl α -glucosaminidase	Heparan sulphate	GAGs (U)	Enzyme assay/MGT
	MPS III C (Sanfilippo C)	<i>HGSNAT</i>	Acetyl CoA: α -glucosaminide, N-acetyltransferase	Heparan sulphate	GAGs (U)	Enzyme assay/MGT
	MPS III D (Sanfilippo D)	<i>GNS</i>	N-acetyl glucosamine-6-sulphatase	Heparan sulphate	GAGs (U)	Enzyme assay/MGT
	MPS IVA (Morquio A)	<i>GALNS</i>	Acetyl galactosamine-6-sulphatase	Keratan sulphate	GAGs (U)	Enzyme assay/MGT
	MPS IV B (Morquio B)	<i>GLB1</i>	β -Galactosidase	Keratan sulphate	GAGs (U)	Enzyme assay/MGT
	MPS VI (Maroteaux-Lamy)	<i>ARSB</i>	Acetyl galactosamine, 4-sulphatase (arylsulphatase B)	Dermatan sulphate	GAGs (U)	Enzyme assay/MGT
	MPS VII (Sly disease)	<i>GUSB</i>	β -Glucuronidase	Dermatan sulphate, Heparan sulphate, Chondroitin sulfate	GAGs (U)	Enzyme assay/MGT
MPS IX (Prenc and Natowicz)	<i>HYAL1</i>	Hyaluronidase	Hyaluronan	–	MGT	

Class ^a	Lysosomal storage disease	Genes involved	Protein deficiency	Storage	Initial test	Diagnostic test
Transmembrane protein defect	Niemann-Pick disease Type C1	<i>NPC1</i>	Niemann-Pick type 1 (NPC1)	Cholesterol sphingolipids and	Serum Chito	Filipin test, MGT
	Niemann-Pick disease Type C2	<i>NPC2</i>	Niemann-Pick type 2 (NPC2)	Cholesterol sphingolipids and	Serum Chito	Filipin test, MGT
	Mucopolidosis IV	<i>MCOLN1</i>	Mucolipin	Lipids	–	MGT
	Cystinosis	<i>CTNS</i>	Cystinosin	Cystine	–	MGT
	Danon disease	<i>LAMP2</i>	Lysosome-associated membrane protein 2	Cytoplasmatic debris and glycogen	–	MGT
	Sialic acid storage disease	<i>SLC17A5</i>	Sialic acid storage disease; infantile form (ISSD) and adult form (Salla)	Sialin	Free SA (U)	MGT
Glycoproteinoses	Schindler	<i>NAGA</i>	N-acetylgalactosaminidase	Sialylated/asialoglycopeptide, glycolipids	Oligos (U)	BGT, MGT
	α mannosidosis	<i>MAN2B1</i>	–	–	Oligos (U)	Enzyme assay/MGT
	β mannosidosis	<i>MANBA</i>	β-Mannosidase	Man(b1-4)GlnNAc	Oligos (U)	BGT, MGT
	Sialidosis	<i>NEU1</i>	Neuraminidase	Oligos, glycopeptides	Bound SA (U), Oligos (U)	Enzyme assay/MGT
	Aspartylglucosaminuria	<i>AGA</i>	Glycosylasparaginase	Aspartylglucosamine	Oligos (U)	Enzyme assay/MGT
	Fucosidosis	<i>FUCA1</i>	α-Fucosidase	Glycoproteins, glycolipids, Fucoside-rich oligos	Oligos (U)	Enzyme assay/MGT
	Galactosialidosis	<i>CTSA</i>	Protective protein cathepsin A	Sialyloligosaccharides	Oligos (U)	Enzyme assay/MGT
Neuronal ceroid lipofuscinoses	CLN1	<i>PPT1</i>	Palmitoyl protein thioesterase (PPT1)	Saposins A and D	Ultrastructure	Enzyme assay/MGT
	CLN2	<i>TPP1</i>	Tripeptidyl peptidase 1 (TPP1)	Subunit c of ATP synthase	Ultrastructure	Enzyme assay/MGT
	CLN3	<i>CLN3</i>	CLN3, lysosomal transmembrane protein	Subunit c of ATP synthase	Ultrastructure	MGT
	CLN5	<i>CLN5</i>	CLN5, soluble lysosomal protein	Subunit c of ATP synthase	Ultrastructure	MGT
	CLN6	<i>CLN6</i>	CLN6, transmembrane protein of ER	Subunit c of ATP synthase	Ultrastructure	MGT
	CLN7	<i>MFSD8</i>	Lysosomal membrane protein	Subunit c of ATP synthase	Ultrastructure	MGT
	CLN8	<i>CLN8</i>	CLN8, transmembrane protein of ER	Subunit c of ATP synthase	Ultrastructure	MGT
	CLN10	<i>CTSD</i>	Cathepsin D	Saposins A and D / Lipofuscin	Ultrastructure	MGT
	CLN11	<i>GRN</i>	Lysosome enzyme chaperone	–	Ultrastructure	MGT
	CLN 12	<i>ATP13A2</i>	–	–	Ultrastructure	MGT
	CLN13 (Kufs disease Type B)	<i>CTSF</i>	Lysosomal enzyme, cathepsin F		Ultrastructure	MGT

Class ^a	Lysosomal disease	storage	Genes involved	Protein deficiency	Storage	Initial test	Diagnostic test
Glycogenoses Storage disease	Pompe disease		<i>GAA</i>	α -1,4-glucosidase (acid maltase)	Glycogen	Creatinine Kinase/Oligo	Enzyme assay/MGT
	Wolman		<i>LIPA</i>	Acid lipase	Cholesterol esters	Vacuolated lymphocyte	Enzyme assay/MGT
Multiple enzyme deficiency	Galactosialidosis		<i>CTSA</i>	Protective protein cathepsin A	Sialyloligosaccharides	Oligos (U)	Enzyme assay/MGT
	Multiple sulphatase deficiency		<i>SUMF1</i>	Multiple sulphatase	Sulphatides, glycolipids, GAGs	Sulphatides (U), GAGs (U)	Enzyme assay/MGT
	Mucopolidosis II α / β , III α / β		<i>GNPTG</i>	GlcNAc-1-P transferase	Oligos, GAGs, lipids	Oligos (U)/ Sialyl oligo	Enzyme assay/MGT
	Mucopolidosis IIIy		<i>GNPTG</i>	GlcNAc-1-P transferase	Oligos, GAGs, lipids	Oligos (U)	Enzyme assay/MGT
Defects in lysosome- related organelles	Pycnodysostosis		<i>CTSK</i>	Cathepsin K	Bone proteins	X-ray	MGT
	Prosaposin deficiency		<i>PSAP</i>	Prosaposin	Non neuronal glycolipids Ubiquitinated material in neurolysosomes	Urinary Glycosphingolipids	Genetic western blotting
	Kanzaki		<i>NAGA</i>	α -galactosidase B	–	–	Biopsies, MRI, CAT
	Schindler		<i>NAGA</i>	N-acetylgalactosaminidase	Sialylated/ asialoglycopeptide, glycolipids	Oligos (U)	BGT, MGT
	ATP6AP2		<i>ATP6AP2</i>	vATPase assembly factor	–	–	MGT
	Chediak-Higashi syndrome		<i>CHS1/LYST</i>	Lysosome-related organelles	–	Bone marrow examination	MGT
	Hermansky-Pudlak syndrome		<i>HPS1/HPS3, ADTB3A</i>	Lysosome-related organelles	<i>Lipofuscin storage</i>	Bone marrow examination	MGT

MGT: molecular genetic testing; BGT: biochemical genetic testing; CK: creatine kinase; GAG: glucosaminoglycans; MRI; magnetic resonance imaging; CAT: computer-assisted tomography; U; urine. ^a Using a combination of different classification

1.2.3 The cell biology of LSDs

LSDs are mostly caused by the malfunction of lysosomal enzymes coupled with lipid transport defects. The lysosomes with impaired function do not metabolise certain substances, which eventually accumulate and cause cell death, although the exact mechanisms leading to cell death are largely unknown (Vitner et al. 2010). LSDs caused by non-enzymatic protein mutations are usually more complex (Vitner et al. 2010). The storage of primary substrate leads to complicated pathological cascades. This leads to primary defects in lysosome function, secondary defects in the function of other organelles including the endoplasmic reticulum and mitochondria and associated metabolic defects, resulting in the accumulation of secondary storage materials (Futerman and Van Meer 2004; Vitner et al. 2010). There is a similarity in secondary storage materials such as gangliosides and cholesterol that are common across LSDs, despite the differences in the primary accumulated substrates, although the mechanisms causing secondary storage are also largely unknown (Futerman and Van Meer 2004; Walkley and Vanier 2009b).

1.2.3.1 Sphingolipids

Sphingolipids (SLs) belong to a class of lipids that serve as an integral component of the plasma membranes of eukaryotes and are involved in several biological cell processes, such as cell signalling. SLs are made up of ceramide backbones (Figure 1.4) with carbohydrate groups (mono or oligo) at the C-1 position of the sphingosine backbone (Magnusson 1994). They have one polar group (head) and two non-polar groups (tail). The ceramide backbone of sphingolipids is composed of sphingoid bases with long carbon chains and an amine head group instead of a carboxylic acid group. Sphingosine, a long 18-carbon chain amino-alcohol, is the main sphingoid base in mammals as well as a highly active and versatile signalling molecule (Fyrst and Saba 2010; Motyl and Strosznajder 2018). Ceramide is a molecule formed from a combination of sphinganine and fatty acids (Dihydroceramide desaturase adds a double bond on the sphinganine backbone attached to the fatty acid, this creates sphingosine which then is liberated via degradation). The metabolism of SLs involves several pathways that include the synthesis of ceramide, sphingosine (primarily through the breakdown of ceramide) and the addition of sugar head groups to ceramide in order to produce glycosphingolipids (GSLs) (Goñi and Alonso 2006). SL synthesis and recycling are two related processes, as ceramide and glycosphingolipids are predominantly generated via the lysosomal break down and salvage of existing SLs (Goñi and Alonso 2006) or from SLs taken up or recycled from cell membranes into the endocytotic system (Merrill Jr 2011). Ceramide molecules are made in the ER and converted to sphingomyelin or GSLs at the Golgi and then

are transported to the plasma membrane where they function as cell surface receptors and structural components. Their degradation largely happens in lysosomes, which leads to the release and reutilization of sphingosine and product sugars. Sphingosine, a charged molecule, leaves the lysosome via a poorly known route, which involves the lysosomal NPC1 protein (Lloyd-Evans et al. 2008).

In higher organisms, notably vertebrates, the most common class of glycolipids are GSLs (Merrill Jr 2011). GSLs are derived from sphingolipids and are involved in developmental signalling (Hakomori et al. 1998). SL *de novo* biosynthesis begins in the ER. Serine palmitoyltransferase (SPT) catalyses serine and palmitoyl-CoA to produce 3-ketosphinganine. 3-ketosphinganine is then reduced to sphinganine. A fatty acyl chain is added to sphinganine to produce dihydroceramide. Ceramide is created from the action of dihydroceramide desaturase which converts the sphinganine backbone to sphingosine via creation of a double bond (Figure 1.4). In certain specialised cells (e.g. myelinating cells), ceramide is galactosylated in the ER to produce galactosylceramide (GalCer) (Holthuis et al. 2001). Alternatively, ceramide may be transported to the Golgi apparatus via two alternative pathways (Hanada et al. 2003). It can be taken from the ER, via a ceramide-ER transfer protein (CERT), to the outer surface of the trans-Golgi network, where it is used principally for the synthesis of sphingomyelin. Otherwise, ceramide is taken in via vesicular transport to the *cis*-Golgi, where it is glucosylated by the action of the UDP-glucose ceramide glucosyltransferase to produce glucosylceramide (GlcCer) on the cytosolic leaflets of early Golgi membranes (Funakoshi et al. 2000; Gault et al. 2010). GlcCer is then translocated to the lumen of the Golgi apparatus and then glycosylated by β 4-galactosyltransferases V and VI to form lactosylceramide (LacCer) (Kumagai et al. 2010; Miura et al. 1996; Nishie et al. 2010). Since LacCer cannot be moved back to the cytosol, it can be further glycosylated within the Golgi to produce other classes of complex glycosphingolipids, such as gangliosides. The plasma membrane is the main site of action of GSLs and are recycled between the plasma membrane and early endosomes or are transported to lysosomes to be degraded by glycohydrolases and accessory proteins (Van Meer et al. 2008). These proteins break down the glycan moieties in a stepwise manner to ceramide, which is then catabolised by acid ceramidase to produce a fatty acid and sphingosine. Upon exit from lysosomes, sphingosine is metabolized to sphingosine-1-phosphate by a sphingosine kinase, or it may be converted into ceramide in ER.

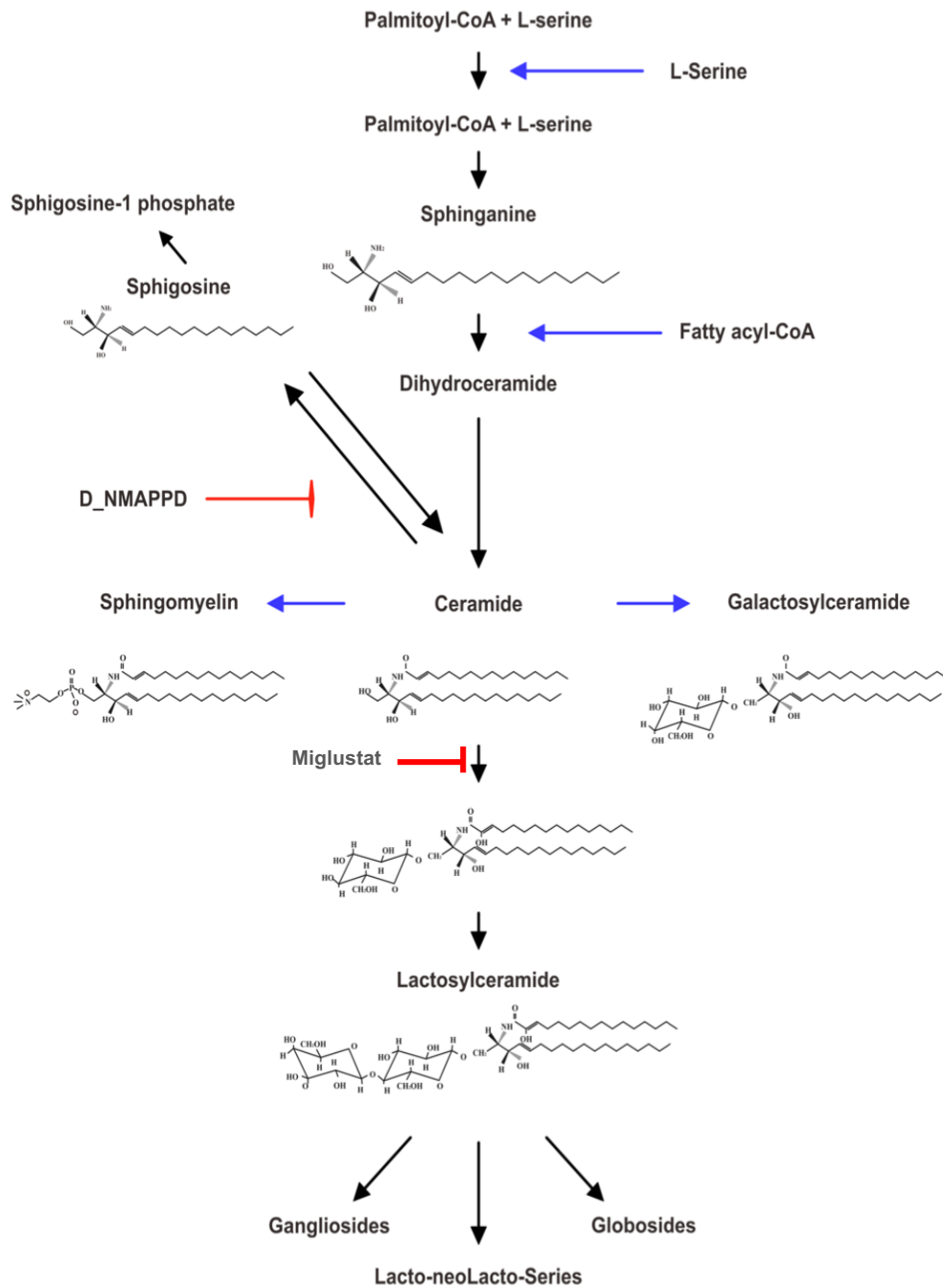


Figure 1.4 A view of the sphingolipid biosynthetic pathway.

The red arrow indicates the enzyme inhibitors; D-NMAPPD inhibits the acid ceramidase enzyme to prevent the synthesis of sphingosine. Miglustat is an inhibitor of ceramide glucosyltransferase, which prevents GlcCer synthesis.

Lysosomal sphingolipidoses are diseases caused by the dysfunction of some of the enzymes that lie in the degradation pathway of sphingolipids (Figure 1.5). Since SLs are hydrophobic in nature, the complexity of these lipids' degradation increases, unlike that of the soluble macromolecules. These lipids are degraded on the intra-lysosomal membrane surface by particular hydrolytic enzymes that require exposure to an activator protein group called saposins (Vellodi 2005). Saposins act to remove the hydrophobic lipid from the internal membranes of lysosomes and present these lipids to their hydrolytic enzyme (Alattia et al. 2006, 2007; Locatelli-Hoops et al. 2006; Remmel et al. 2007). The accumulation of lipids within the lysosome compartments leads to the disturbance of the limiting membrane, resulting in lysosomal membrane destabilisation and proteolytic enzyme escape, which can cleave cellular caspases and prompt cellular apoptosis. Lysosphingolipids (Lyso-SLs) are toxic products arising out of the de-acylation (Kobayashi et al. 1992), or enzymatic removal of the fatty acid group, of the GSL analogues of the primary substrate. These lyso-lipid by-products are primarily elevated in the sphingolipidoses diseases where the pathogenic implications of their accumulation causes an inhibition of protein kinase C signalling (Hannun and Bell 1987). Lyso-SLs storage is correlated with disease severity (Polo et al. 2017).

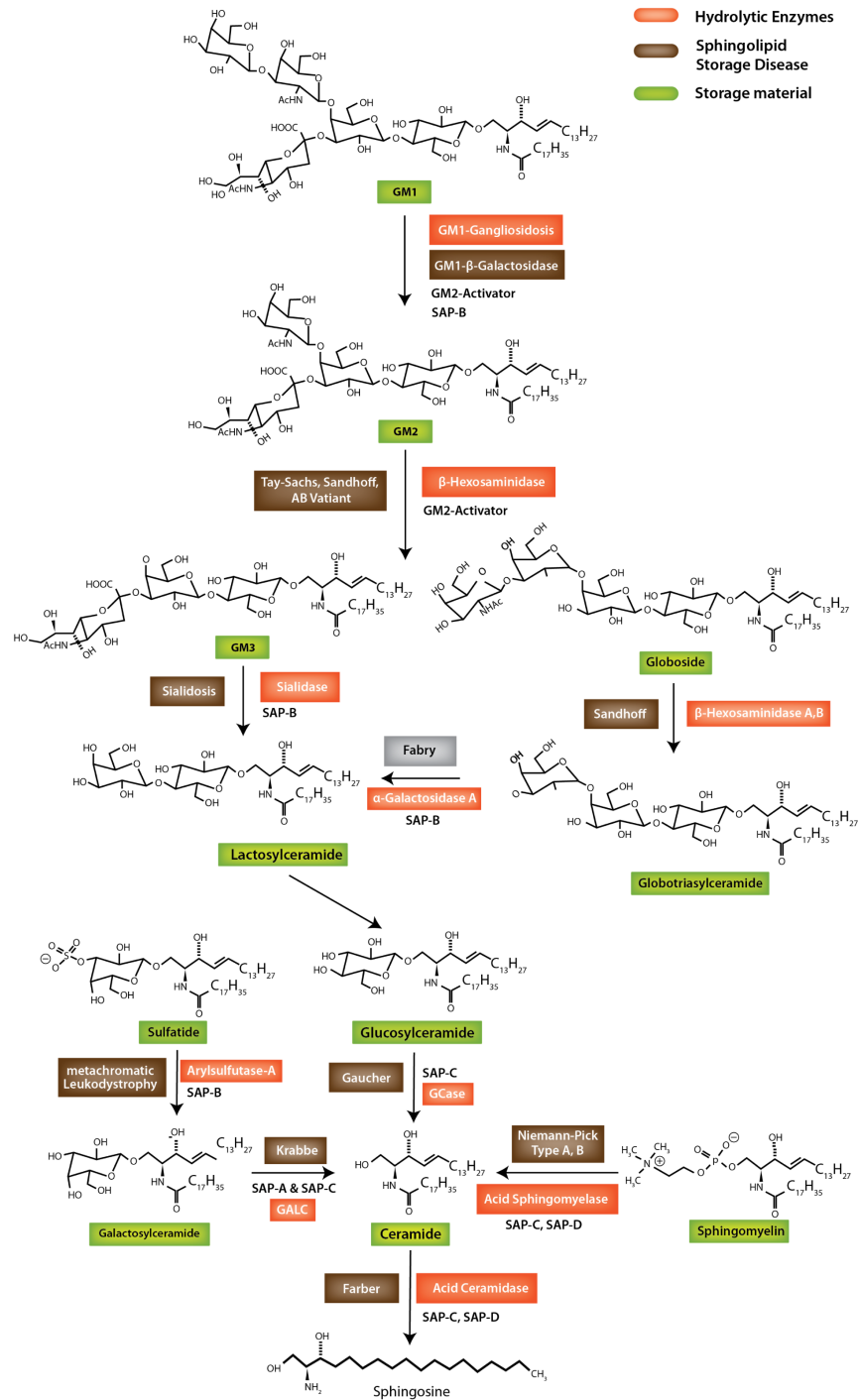


Figure 1.5 The sphingolipid degradative pathway in lysosomes and the related sphingolipidoses disease.

The routes and enzymes required to degrade sphingolipids are described here. Sphingolipids are indicated in green boxes. The required enzyme for the degradation of each individual sphingolipid is indicated in the orange boxes. The associated disease caused by loss of enzyme is indicated in the brown boxes. GM1: ganglioside; GM2, GM2 ganglioside; GM3 ganglioside, sap; saposin. Adapted from (Becker 1999; Mehta and Winchester 2012; Sandhoff 2013).

1.2.3.2 Cholesterol accumulation

Cholesterol is the major sterol in mammalian cells and plays an important role in the maintenance of membrane fluidity and curvature as well as the manufacturing of bile and hormones. Mammals obtain sterols, mainly cholesterol, either from the food they consume or from the cells that synthesise them *de novo* (Ikonen 2008). Cholesterol is made from 3-hydroxy-3-methylglutaryl-coenzyme A (HMG-CoA). The first step is an oxidation reaction involving HMG-CoA reductase to produce mevalonic acid, which eventually makes the first sterol precursor called lanosterol. Lanosterol can be converted into cholesterol via two pathways, namely the Bloch and the Kandutsch–Russell pathways (Mitsche et al. 2015). Cholesterol enters cells mainly packed in lipoproteins, which are picked-up at the cell surface by low-density lipoprotein (LDL) receptors. These LDL-bound receptors are internalised to endocytic vesicles, through which they release their cargo and are returned to the cell surface. The LDL particle itself transports esterified cholesterol to lysosomes, where it is processed into un-esterified ‘free’ cholesterol by the lysosomal enzyme acid lipase (LAL) (Ikonen 2008). Cholesterol from recycled cell membranes are also processed in LE/Lys. The precise molecular mechanisms behind the control of endosomal and lysosomal un-esterified cholesterol are still unknown. However, much has been learned from studies on metabolic diseases including hypercholesterolaemia and NPC (Goldstein and Brown 2009). NPC disease leads to consequences in the storage of exogenous cholesterol and other lipids in LE/Lys, presumably as a result of the activities of the NPC1 and NPC2 proteins, encoded by the *NPC1* and *NPC2* genes respectively. These proteins are found in LE/Lys and are, in some way that remains undefined, involved in the normal exogenous transport of cholesterol and other lipids and cargoes out of the LE/Lys. Numerous studies have shown that NPC2 binds to un-esterified cholesterol and it has been suggested that NPC2 hands cholesterol over to the N-terminal domain of NPC1 (Infante et al. 2008; Kwon et al. 2009; Xu et al. 2007). In most cases of NPC disease, a mutation in the *NPC1* gene is held to be mostly responsible, whereas the *NPC2* gene accounts for only 5% of such cases (Vanier et al. 1996; Vanier 2010; Naureckiene et al. 2000). The NPC1 protein is a transmembrane glycoprotein containing 13 transmembrane segments which is thought to possess a sterol-sensing domain as cholesterol-regulated protein (Ioannou 2000).

LAMP2 may interact with the NPC1 protein to move cholesterol out of lysosomes to be distributed to other organelles (Li and Pfeffer 2016), although the exact mechanisms remain to be identified. SCARB2 as mentioned earlier, has been shown to be capable of transporting cholesterol out of lysosomes (NPC1 has never been shown to be capable of actually doing this), raising questions about the need for a more complicated NPC2 to NPC1 transport

system. The ER is the main pool that regulates cholesterol levels. It contains the acyl-coA cholesterol acyltransferase (ACAT) (Chang et al. 1997; Geisow et al. 1981; Sakashita et al. 2000), which catalyses the esterification of excessive cholesterol, stored together with triacylglycerols in the lipid droplets (Chang et al. 1997; Zhang et al. 2003). Sterol regulatory element binding proteins (SREBPs) and the SREBP cleavage-activating protein (SCAP) are the main cellular cholesterol sensors. Cholesterol is mainly retained in the ER when its level is high leading to alterations in SREBP/SCAP function that prevents activation of cholesterol biosynthesis genes (Radhakrishnan et al. 2008). When cholesterol levels are low, SREBPs are transported from the ER to the Golgi apparatus, the transcription factor SCAP is released following cleavage, where it translocates to the nucleus and upregulates genes for sterol synthesis, such as an HMG-CoA reductase and an LDL receptor (Brown and Goldstein 1997; Goldstein et al. 2006).

1.2.3.3 Other lysosomal storage materials in LSDs

Multiple studies have been conducted in the past to gain a proper understanding of the pathogenic mechanism(s) in the neuronal ceroid lipofuscinoses (NCLs). The main pathological hallmark of NCLs is the accumulation of auto-fluorescent ceroid lipofuscin containing SCMAS in lysosomes. Studies on sheep with ceroid lipofuscinosis, and humans with juvenile and late infantile disease, reveal that unmodified SCMAS builds up in lysosomal-derived organelles in several tissues (Palmer et al. 1992). Sphingolipid activator proteins, (saposins A and D) which appear as distinctive granular osmiophilic deposits (GRODs) (Palmer et al. 1997), also accumulate as part of the storage materials in diseased cells of NCLs (Tyynelä et al. 1993; Tyynelä et al. 1995). SAPs are the major storage body components in CLN1 and CLN10 disease, although the reasons for their accumulation is largely unknown (Tyynelä et al. 1993); (Siintola et al. 2006). As such, SCMAS and SAPs are the main reported pathological hallmarks in NCL cells and tissues (Palmer 2015).

GAGs are a type of polysaccharide, usually disaccharides, formed as a result of the breakdown of proteoglycans, which are present in the extracellular matrix. Eleven lysosomal enzymes are needed to degrade GAGs (Zhang 2010). Dysfunction of any of these enzymes results in the accumulation of GAGs within lysosomes (Table 1.1) (Bobillo Lobato et al. 2016). There are two major types of GAGs, namely sulfatide, which contains dermatan sulphate, heparan sulphate, keratan sulphate and chondroitin sulphate, and non-sulphate, which contains hyaluronic acid (Jackson et al. 1991). The enzymes involved in the degradation of

GAGs therefore include glycosidases, sulfatases and nonhydrolytic transferases. The majority of the MPS diseases share a similar set of symptoms and clinical signs, although varying in severity, including skeletal and joint abnormalities, respiratory complications, facial dysmorphism, hearing loss and mental retardation (Muenzer 2011).

Deficiencies in the enzymes involved in the degradation of glycoconjugates lead to fucosidosis, α -mannosidosis, sialidosis and aspartylglucosaminuria; the names of the diseases refer to the sugar that accumulates within lysosomes, see lysosomal disease table above, table 1.1 (Ferreira and Gahl 2017). Several types of accumulated material are found in Mucopolysaccharidosis II (I cell) /Mucopolysaccharidosis III. They occur due to a defect in lysosomal enzyme trafficking, specifically a defect in GlcNAc-1-phosphotransferase, an enzyme which leads to the loss of M6P modification of lysosomal proteins in the *cis*-Golgi (Reitman et al. 1981). In this disease there is a catastrophic loss of almost all lysosomal enzyme activities and concomitant storage of all types of associated substrates. Defects in lysosomal transmembrane transport of small molecules occur in cystinosis, Salla disease and mucopolysaccharidosis type IV (MLIV). Such defects lead to the ineffective transportation of small molecules across the lysosomal membrane, leading to their accumulation, e.g. cystine amino acid or free sialic acid in the cases of Salla, free ions such as Ca^{2+} and Fe^{2+} in MLIV. Stores of carbohydrates, for example glycogen in Pompe disease, neutral lipids (triglycerides and cholesterol esters) were stored in in Wolman disease, etc. (Ferreira and Gahl 2017).

1.2.4 Diagnosis

Biomarkers are important tools that indicate the occurrence of a biological activity associated with clinical manifestation. They are important for disease follow-up, especially with regard to disease progression, to evaluate treatment response and are increasingly required by regulators in order to approve drugs for new indications (Mayeux 2004). Biomarkers are extremely valuable for the clinical management of LSDs and can support diagnosis and treatment decisions (Aerts et al. 2005). For example, several studies have demonstrated that a prompt diagnosis of an LSD is critical, particularly as patients starting treatment before the onset of substantial symptoms have significant chances of responding positively to treatments (e.g. miglustat for NPC1 treatment) (Patterson et al. 2007). There is considerable phenotypic heterogeneity in LSDs, and genotype–phenotype correlation is not always present in LSDs (Meikle et al. 1999). For example, in Gaucher disease, there are considerable differences in the symptoms of the disease among siblings; one sibling may be nearly normal while the other is severely affected (Amaral et al. 1994). Similar findings have been obtained from twins reported with Gaucher's disease (Lachmann et al. 2004a). In some LSDs, the variation in

disease severity can be loosely correlated to the residual enzyme activity (Platt et al. 2018). In some forms of NCLs, there is a noticeable typical disease phenotype (e.g. ultrastructural features) correlated with disease-causing mutation (Mole et al. 2018; Mole et al. 2005).

There are various kinds of LSDs, such as lipidoses, glycogenoses and oligosaccharidoses, which display similar clinical manifestations in the central nervous and skeletal systems (Meikle et al. 1999). Some of these disorders, milder forms, result in no obvious neurological deficit, such as in Gaucher disease type 1 (GDI). Many LSDs are characterized by different neurologic symptoms either with or without somatic features from birth to adulthood, due to the complexity of accumulated products and their different distributions in tissues (Wenger et al. 2003). NPC is an example of a fairly common disorder, with significant diagnostic problems due to the variable neurological symptoms and variable storage material (Vanier et al. 2016; Wenger et al. 2003). The age at which NPC patients are diagnosed range from birth to adulthood, although there is usually previous evidence of movement problems and ophthalmoplegia in adult patients (Vanier et al. 1988). This is a considerable problem as early diagnosis is essential for improved therapeutic outcome (Wenger et al. 2003). The majority of patients suffering from LSDs show different physical features over time, such as progressive mental retardation, developmental regression or other neurological and skeletal abnormalities. Moreover, LSDs are mostly chronic conditions. Visual loss, seizures, ataxia and dementia are common consequences of LSDs (Pastores and Maegawa 2013). All of these phenotypes make the need for early diagnosis a priority, especially if early phenotypes that have a considerable effect on quality of life, e.g. loss of vision in the NCLs, can be delayed or prevented. Several LSDs may occur at different points in a person's lifetime: infantile stage, juvenile stage and adulthood such as Tay-Sachs, Sandhoff, Pompe, GD, Farber, NCLs etc. The infantile onset forms are all severe, with the occurrence mainly of neurological pathology, whereas skeletal abnormalities and organomegaly from peripheral symptoms are common in LSD occurring during adulthood (Pastores and Maegawa 2013; Vellodi 2005).

The diagnosis of LSDs needs a combination of the expertise of clinicians and laboratory specialists with respect to identification. This represents a challenge, because other metabolic diseases may exhibit similar phenotypes (Filocamo and Morrone 2011) and more often than not the diagnostic old process for a lysosomal disease can take years (Fernández-Marmiesse et al. 2014). However, the development of effective therapies, such as miglustat for Gaucher and NPC diseases has been shown to lead to subsequent improvement in diagnostic and the earlier identification of these diseases for improved therapeutic outcome (Schielen et al. 2017). For example chitotriosidase activity responds during the treatment of GD disease with miglustat (Cox et al. 2000).

1.2.4.1 An overview of current laboratory methods for LSD diagnosis and monitoring

Fluorimetric substrates are tools widely used in the diagnosis of LSDs, they can be used to accurately measure lysosomal enzyme activity in different biological samples and with different instrumentation. This technique is not expensive and can be easily automated in laboratories. As such, it has been efficient in the screening of Pompe and Fabry diseases in asymptomatic infant populations in Taiwan (Chiang et al. 2012); (Chien et al. 2013). However, the possibility for multiplexing is limited in this regard (Yu et al. 2013). A more developed method was designed by Geld in 2006, namely tandem mass spectrometry (MS/MS), that involves the detection of the galactocerebrosidase enzyme (GALC), which is absent in cell lysates from Krabbe disease patients (Gelb et al. 2006). This technique was optimised for wide usage with dried blood spot (DBS) samples, as well as with suitable substrates and internal standards for GD, Fabry, Pompe, and Niemann-Pick diseases as well as mucopolysaccharidosis type 1 (MPS I) (Zhou et al. 2011). This finding encouraged pilot studies in some countries (Orsini et al. 2012; Orsini et al. 2009) and it has been utilised for newborn screening fo Krabbe disease in New York state (Orsini et al. 2016). More recently, Ribas et al. (2017) used the technique to detect six LSDs, namely α -galactosidase (α GalA), acid sphingomyelinase (aSMase), α -glucosidase (α -Glu), GCase, GALC and α -L-iduronidase (IDUA), in large sample sizes. They concluded that the MS/MS method was effective for screening LSDs. However, an accurate diagnosis would mostly be based by combining this method with biochemical or molecular analyses alongside clinical assessment (Ribas et al. 2017). Ultimately, MS/MS techniques are not accessible at all hospitals and restrict diagnoses in countries without access to such instrumentation.

1.2.4.2 Using disease-specific biomarkers

There are two main types of biomarkers used in LSD diagnoses: the first one uses molecules that accumulate during the onset of defective lysosomal action, whereas the second one does not have a direct relationship with the lysosome but instead addresses the consequence of its effect on cells, organs and functions (Bobillo Lobato et al. 2016). Samples of blood, urine or organs and tissues can be tested for the presence of such biomarkers. Biomarkers can also indicate the efficiency of novel therapies used for the treatment of LSDs over time, notably enzyme-replacement therapy, substrate reduction therapy and other molecular-based therapies (Bobillo Lobato et al. 2016). The biomarkers of LSDs are categorised based on the origins of the biomarker itself. Therefore, the study of the use of biomarkers has aroused considerable interest in the fields of disease diagnosis and treatment.

Fabry disease results from the absence of the α GalA enzyme and the lysosomal storage of the neutral glycosphingolipid globotriaosylceramide (Gb3) and other GSLs. However, measuring α GalA enzyme activity can be problematic with respect to diagnosing compound heterozygous female patients, which complicates the use of enzyme-related therapies for treatment (Weidemann et al. 2013); (Kim et al. 2016). This indicates the need to search for alternative early diagnostic biomarkers for such patients. The traditional biomarker used to diagnose the aforesaid disease is the substrate of the deficient enzyme Gb3, which is elevated in the Fabry patients' blood plasma and urine (Matern et al. 2015; Sweeley and Klionsky 1963). Nevertheless, many studies have reported that there are no clear correlations between Gb3 levels and clinical signs and the symptoms or severity of the disease (Thurberg and Politei 2012; Young et al. 2005). Researchers have used the presence of a water-soluble deacylated metabolite of Gb3, known as globotriaosylsphingosine (Lyso-Gb3), as an indicator of the prevalence of Fabry Disease (Aerts et al. 2008). The molecule can be quantified and studied by liquid chromatography and LC/MS/MS techniques to diagnose patients with the disease and follow up their treatment regimes. Lyso-Gb3 is known to be a better marker than Gb3, especially when correlations with the typical clinical signs and symptoms are made (Rombach et al. 2010). Moreover, the use of Lyso-Gb3 is more useful in the diagnosis as it shows elevated in Fabry patient plasma, either hemizygous male or heterozygous female (unlike the elevated plasma Gb3, which was only observed in the affected male while most female Fabry patients were within the normal range) (Rombach et al. 2010).

GD is caused by a limited activity of the lysosomal enzyme GCase, which results in a significant accumulation of GlcCer in macrophages, known as Gaucher cells, that can be seen as a result of May–Grüwald–Giemsa or Hematoxylin–Eosin staining. Although Gaucher cells may serve as one biomarker, they still have some limitations; for instance, these cells are not easily collected (from liver or bone marrow biopsies) and they cannot be used to quantify involvement or show disease progression in a clear manner, and they may overlap in terms of GlcCer concentration (Van Breemen et al. 2007). Chitotriosidase is a secreted lysosomal enzyme that for an unknown reason correlates with the clinical manifestations of GD; hence, it is another biomarker for diagnosis, mainly expressed by phagocytes, that indirectly matches the total body burden of Gaucher cells. The quantification of Chitotriosidase activity is carried out using the production of chromogenic or fluorogenic products (Van Dussen et al. 2014). The use of Chitotriosidase as a diagnostic tool for GD detection is limited in patients with homozygous or heterozygous for a chitotriosidase variant (Boot et al. 1998; Deegan et al. 2005). Also, other polymorphisms affect the levels of Chitotriosidase (Aerts et al. 2011). Hence, the search for alternative biomarkers is necessary. The chemokine CCL18/PARC was found to be between 20- to 50-fold higher in patients suffering from GD; this serves as another

effective biomarker for the disease (Boot et al. 2004). Rolfs *et al.* proposed a better biomarker than Chitotriosidase, stating that GlcSph, the lyso-lipid form of GlcCer, is elevated 100 times higher than levels found in normal healthy individuals (Rolfs et al. 2013). However, it remains unclear whether GlcSph can be used for first-tier analysis in newborns, and liquid chromatography and standardised MS/MS techniques will probably still be needed for accurate identification. More recently, plasma biomarkers for diagnosing GD have been identified 1- α and 1- β macrophage inflammatory proteins, as well as cathepsin and osteopontin (Van Breemen et al. 2007); (Lobato et al. 2015; Vairo et al. 2015).

Krabbe disease is caused by the absence of lysosomal GALC, which cleaves galactosyl moieties from GalCer and the lyso-lipid analogue galactosylsphingosine (psychosine) (Graziano and Cardile 2015). Apart from the different techniques used in disease diagnosis, such as histological analyses and neurophysiological studies, psychosine has more recently been proposed as a biomarker of the disease (Turgeon et al. 2015). Psychosine is a toxic agent that acts on extracellular G protein coupled receptors such as T cell death associated gene 8 (TDAG8) and can kill different neurons and Schwann cells. Psychosine is elevated up to 4-fold in Krabbe patients and can be quantified in blood samples either in dried blood spots (DBS) or CSF (Turgeon et al. 2015). One of the methods used to quantify psychosine is ionization-tandem mass spectrometry (ESI/MS/MS) (Galbiati et al. 2007; Jiang et al. 2009; Whitfield et al. 2001). However, this technique cannot be used to separate psychosine from the related Gaucher disease lyso-lipid glucosylsphingosine (GlcSph), in which case ultra-performance liquid chromatography (LC-MS/MS) needs to be used (Chuang et al. 2013). Newborns with high levels of GALC but low psychosine concentrations are known to have a low risk of suffering from the disease during primary screening. However, it is doubtful whether psychosine analyses can be used as first-tier screening (Chuang et al. 2013).

GAG molecules with specific carbohydrate or sulphated carbohydrate residues accumulated in many tissues of mucopolysaccharidoses patients (Neufeld 2001). The first diagnostic tools to be used are the analyses of GAGs present in urine via spectrophotometry using dimethylmethylene blue. This is a stain that shows sulfated GAGs in biological samples, commonly urine, and lead to changes in the absorption spectrum (De Jong et al. 1989). The diagnosis of GAGs is confirmed by enzyme assay of specific enzyme defects in DBS, leucocytes or cultured cells (Lehman et al. 2011).

Several reports have stated the evaluation of GAGs fragments by MS/MS as a potential biomarker for mucopolysaccharidoses. More recently, a new ultra-performance liquid chromatography-MS-MS method has been made available for the detection of the substrates,

heparan sulfate, dermatan sulfate and chondroitin sulfate in urine and CSF, in order to facilitate the diagnosis of patients with MPS (de Ruijter et al. 2012a; Tomatsu et al. 2013). Langreis *et al.* developed optimised and adapted protocols of GAG quantification by adding the identification of keratan sulfate to provides a multiplex assay for the diagnosis of mucopolysaccharidoses and mucopolipidoses II and III (Langereis et al. 2015). Other proteomic studies have allowed the discovery of further biomarkers, such as β -galactosidase, collagen type I α , fatty-acid binding protein 6, nidogen-1, cartilage oligometric matrix protein, insulin-like growth factor binding protein 7 and Heg1 protein in urine (Heywood et al. 2015). These are lengthy procedures for mucopolysaccharidoses biomarker quantification, it is highly unlikely that glycosaminoglycan fragments can be used for first-tier analyses and to monitor the efficiency of mucopolysaccharidoses therapies (Gelb et al. 2015) .

Niemann-Pick A and B diseases involve an accumulation of sphingomyelin in different organs, due to the lack of aSMase enzymes caused by genetic mutations in the *SMPD1* gene. NPC involves the accumulation of cholesterol in lysosomes, damaging several organs and eventually leading to neurological deterioration. Sphingomyelin is one biomarker that is available for diagnosing Niemann-Pick disease B and has been shown to be raised ~10-fold in a patient's liver and spleen. However, its levels in blood plasma have been shown to overlap with normal controls (He et al. 2001; He et al. 2002; Rodriguez-Lafrasse and Vanier 1999). Lysosphingomyelin, the de-acylated derivative of sphingomyelin, has been proposed to be another biomarker in DBS, with no overlap values. However, its levels do not appear to correlate with aSMase enzyme activity (Chuang et al. 2014).

For NPC patients, the diagnostic tools used involve a series of tests, such as staining of cholesterol using filipin, a UV fluorescent antibiotic that binds cholesterol, in fibroblasts, and measuring chitotriosidase activity in blood samples. However, this technology is not very accurate. The promising biomarkers considered to overcome these limitations are measurements of cholestane-3 β ,5 α ,6 β -triol and 7-ketocholesterol (7-KC) in blood plasma (Porter et al. 2010), for these biomarkers correlate with the disease severity and are shown to be specific to NPC (Tortelli et al. 2014). Another promising biomarker is the presence of neuronal secreted 24(S)-hydroxycholesterol, the concentration of which decreases in the blood plasma of NPC patients, which indicates inefficient cholesterol homeostasis in the central nervous system (Tortelli et al. 2014). Other indicators include the quantification of bile acids (Mazzacuva et al. 2016), calbindin D (Bradbury et al. 2016) and lysosphingomyelin-509 (Giese et al. 2015).

Pompe disease is a rare LSD in which mutations in the *GAA* gene cause deficiencies in the acid α glucosidase (α -Glu) enzyme, leading to the storage of glycogen in the lysosomes of numerous tissues such as cardiac, skeletal and smooth muscle cells (Bembi et al. 2008). The diagnosis of Pompe disease is not always straightforward due to its rarity and the non-specific nature of the clinical phenotypes. The α -Glu enzyme catalyses hydrolysis of the α ,1-4 and α ,1-6 links of glucose polymers, leading to glycogen accumulation. In a typical assay, the various fractions of α -Glu activity can be measured in urine samples, using various techniques such as immunoassays, chromatography affinity using specific antibodies, High-Performance Liquid Chromatography-Ultraviolet (HPLC/UV) etc. (Manwaring et al. 2012; Young et al. 2009). The excretion of urinary Glc₄ can be used as a biomarker, as its response to target tissue has been already demonstrated. Urinary Glc₄ and plasma Hex₄ could be used to monitor the recombinant human α -Glu (An et al. 2005). Other biomarkers that can be used include myostatin and insulin-like growth factor I (Chien et al. 2013). For Pompe disease, glucose tetrasaccharide has been considered to not be specific enough for diagnosis during early development (first-tier newborn screening). Liquid chromatography has recently been developed to monitor glucose tetrasaccharide in urine and has shown that the biomarker is absent in healthy patients but is found in increased levels in confirmed Pompe-affected patients (Manwaring et al. 2012).

Overall, a number of biomarkers have been suggested for the analysis of LSDs. This has been summarised below, in Table 1.2.

Table 1.2 The most promising biomarkers for the analysis of various LSDs.

(An et al., 2000; Rolfs et al., 2013; Chuang et al. 2014; Tomatsu et al. 2013; Lawrence et al., 2014; Mazzacuva et al. 2016).

Disease	Biomarker
Pompe disease	Glucose tetrasaccharide
Gaucher disease	Glucosylsphingosine, Chitotriosidase
Krabbe disease	Psychosine
Niemann-Pick disease	Lysosphingomyelin, 7-ketocholesterol, cholestane-3 β ,5 α ,6 β -triol, Bile acid
Mucopolysaccharidoses	Glucosylaminoglycan fragments

1.2.4.3 “Gold standard” biomarkers and tools

There are no lysosomal disease biomarkers that can be described as “gold standard”. Some of the “global” biomarkers include the following: lysosome-associated membrane proteins and sphingolipid activator proteins, mainly saposins C and D (Chang et al. 2000). Meikle et al. (1997) identified lysosome-associated membrane proteins, or LAMP-1, as a diagnostic biomarker, especially in newborn children and in human skin fibroblasts, and developed a sensitive fluorescence method for the quantification of the protein in blood plasma (Meikle et al. 1997). LAMP-1 and LAMP-2 levels increase in blood plasma during the onset of an LSD. A correlation was observed between the two types of LAMP, precisely a high concentration of LAMP-1 relative to LAMP-2 in plasma, which makes the former a promising biomarker. The diagnosis of a particular LSD, however, depends on the availability of new diagnostic markers (Hua et al. 1998). It is known that approximately 70% of LSD patients have increased LAMP-1 concentrations, which implies that more markers are required for a complete screening. Increased LAMP-1 concentrations appear to be disease-specific, as it has been observed that some LSDs, apart from GD, where sphingolipids or their derivatives are stored do not display increases in LAMP-1. GD shows high concentration of LAMP-1. Some studies on GD with low LAMP-1 concentrations showed no symptoms at the time of detection, except for a 9-year-old infant displaying a severe (type II) presentation. Other neonates are reported to have been above the control range (Meikle et al. 1997). Moreover, Chang et al. (2000) found that saposin A can be used as an LSD biomarker in blood plasma, when used together with LAMP-1 (Chang et al. 2000). However, with respect to determining the potential of LAMPs as a screening marker for LSDs, it still remains unknown why LAMP-1 and LAMP-2 are found to be increased in some disorders but not in others.

In the majority of LSDs, there is not only a deficiency of enzyme activity due to the gene mutation present, there is also a reduction in the amount of the protein. This is either the result of misfolding protein degradation in ER (Brooks 1997), or the instability of protein in the lysosome may be due the RNA instability which leads to insufficient translation (Karageorgos et al. 2004). Therefore, the Immunological assays developed from this view identified multiple LSD. The antibody-based protein detection methods have been developed into 11 different lysosomal proteins on a dry blood spot sample (Meikle et al. 2006). Using these techniques in conjunction with others techniques such as substrate markers by MS/MS may provide a new way to facilitate the screening of newborn children for various diseases (Parkinson-Lawrence et al. 2006).

However, the majority of current methods rely upon on the following: (a) specific tests which only pick up a limited number of disorders (such as enzyme/protein assays specific for each syndrome) (Gelb et al. 2015); (b) many of the current assays do not provide a significantly sensitive level of detection in, for example, assessing elevations in LAMP protein levels (Chang et al. 2000); (c) some of the previous techniques, such as MS/MS, have limitations; for example these instruments are not routinely found in hospitals or the assays themselves are not standardised and as such there are no control ranges and, therefore, are not viable assays for transition into a clinical environment. Furthermore, they are incredibly expensive to purchase and maintain and require specialist technical support to run and analyse data. A simple test that can be used in the first instance to reliably identify lysosomal diseases is clearly needed.

1.2.4.4 Molecular methods

The use of genetic methods for diagnosis of LSDs has been reported to be too slow and expensive for newborn screening, as most patients are complex compound heterozygotes (Gelb et al. 2015). Molecular techniques such as PCR–RFLP (polymerase chain reaction–restriction fragment length polymorphism), PCR–ARMS (polymerase chain reaction–amplification refractory mutation system), Mutations Scanning Methods, DNA sequencing, MLPA (multiplex ligation-dependent probe amplification) and NGS (next generation sequencing) are used to confirm the presence of mutations in specific genes (Mokhtariye et al. 2019). NGS involves the generation of millions of copies of DNA fragments in parallel sequencing. This method was used on Tay-Sachs patients to find point deletions, the conclusion being that it was significantly improved over other genotyping techniques (Hoffman et al. 2013). For instance, in another study, NGS revealed three mutations in a Japanese family with GD, showing two different mutations in the parents without requiring a genetic pedigree (Yoshida et al. 2016). Sequencing of the genes encoding the lysosomal protein, however, is not broadly used, as there exists no complete list of LSD mutations as yet and these techniques remain for the time being quite expensive (Gelb et al. 2015).

1.2.4.5 Prenatal diagnosis

Since most LSDs have no effective treatment, the birth of a child affected with such as disease undoubtedly brings a heavy economic and emotional burden to society and the family, especially in children with early onset, rapidly progressing disease with short survival (Chang et al. 2000). Such families may wish to have more children, but these children would obviously be at high risk of developing the same LSD. How to avoid such risks and provide the necessary

genetic counselling or screening (if available) to families are becoming increasingly urgent topics for families of children with LSDs and clinicians and caregivers (Gelb et al. 2015).

1.2.5 Therapy

1.2.5.1 Enzyme replacement therapy

Enzyme replacement therapy (ERT) is currently one of the most important therapeutic strategies for LSDs. ERT involves an intravenous injection of purified recombinant human lysosomal enzymes. There is a limitation to this approach with respect to the treatment of those LSDs that are characterised by neuronal pathology, as enzymes that are administered intravenously cannot cross the blood brain barrier (BBB) (Barton et al. 1990). ERTs are clinically available in some of the LSDs without neurological involvement. The treatment protocols involve having frequent lifelong infusions, which could either be weekly or monthly (Barton et al. 1990). ERT was not clinically available until 1991, when the Food and Drug Administration (FDA) approved imiglucerase, a recombinant enzyme used to treat non-neuronopathic GDI (Barton et al. 1991; Weinreb et al. 2002). Macrophages constitute the major pathological cell type for this disease (caused by a deficiency in GCCase activity), which makes them essential therapeutic targets. The transport of GCCase is dependent on the binding of mannose terminal residues on the carbohydrate chains of the enzyme. These residues bind to mannose receptors/ LIMP2 on the cell surface of macrophages (Barton et al. 1991; Barton et al. 1990; Reczek et al. 2007). The fact that it is easy to target macrophages with ERT means that this treatment produces remarkable results, improving haematological parameters, reducing pain crises and reducing visceral manifestations, hepatosplenomegaly and skeletal damage (Barton et al. 1991; Grabowski et al. 1995). When it comes to this particular disease, ERT is actually a life-transforming treatment that prevents further progression and reverses the majority of its pathological consequences. ERT's success in the treatment of GD made room for the production of licensed products for other LSDs, including Fabry disease, Pompe disease and different MPSs. These LSDs, in contrast to GD, have an effect on those cells that lack distinct mannose receptors, which are used for the uptake of lysosomal enzymes, e.g. the insulin-like growth factor II/cation-independent mannose 6-phosphate receptor (IGF-II/MP) (Grubb et al. 2010; Kornfeld 1987). There could be possible complications from the circulating antibodies targeting the infused non-self protein. Such immunological reactions are particularly feared in null mutations, since the available immune system remains ignorant of the missing lysosomal enzyme, but are not as much of a concern in the cases with residual enzyme activity, where there is a mutant enzyme involved. The inability of ERT to reach the brain and the central nervous system leads to a lack of storage clearance in those tissues. Recently, to improve this limitation, numerous studies have showed that multiple injection of

high doses of recombinant human β -glucuronidase (hGUS) enzyme lead to a partial reduction of the brain storage materials in the CNS in MPS VII mice (Vogler et al. 2005). Most recently, the intracerebroventricular administration of Tripeptidyl Peptidase 1 (TPP1) in CLN2 disease patients has been shown to delay disease progression (Schultz et al. 2018) and this therapy has now been approved by the NHS in the UK, providing the first evidence in humans of neurological improvement by an ERT.

1.2.5.2 Substrate reduction therapy

Substrate reduction therapy (SRT) aims to reduce the biosynthesis of accumulating substrate (Pastores and Barnett 2003). It then creates a balance between the impaired catabolism rate of the substrate and the rate of synthesis. Inhibitory molecules are employed to restrain the biosynthesis of metabolites feeding into the affected and deficient catabolic pathway. Though there might be certain side effects, as well as parallel metabolic imbalances due to the lack of inhibitor specificity and long-term biosynthetic route disruption, this therapeutic strategy still has a lot of potential. In this regard, the fact that they entail simple oral medication is one of the notable advantages of inhibitor drugs. This approach has been successfully applied to glycosphingolipid storage diseases (primary and secondary) and also miglitol drug for non-insulin diabetes (Coutinho et al. 2016). The most successful therapy is a small imino sugar, *N*-butyldeoxynojirimycin, or miglustat. Miglustat can prevent GSL synthesis through the inhibition of GlcCer synthase (ceramide glucosyltransferase), which is the first step in the biosynthesis of GSLs (Figure 1.4). The drug, therefore, was first developed as a therapy for GSL diseases such as non-neuronopathic Gaucher disease (Cox et al. 2000). Patients suffering from GD exhibit defects in GlcCer degradation, resulting in the storage of these materials, e.g. the GlcCer and GlcSph, in lysosomes (Mehta and Winchester 2012).

The miglustat trial on GD patients demonstrated a reduction in 19% splenomegaly and 12% hepatomegaly after 12 months of treatment. The reductions in organomegaly were improved after 36 months of treatment for those patients who entered an extension in the trial to reach 26.4% and 14.46% reduction in spleen and liver size, respectively (Lachmann 2005).

Furthermore, Zervas et al. (2001) showed that when NPC mice were treated with miglustat, the reduction in GSL accumulation delayed the onset of symptoms and led to an increased lifespan (Zervas et al. 2001). Lachmann et al. (2004) showed that this SRT can improve lipid trafficking defects found in NPC cells from patients and also reduce lysosomal storage and expansion (Lachmann et al. 2004b). In a small clinical trial conducted in the UK and the USA in 2007, it was found that there are beneficial effects of miglustat in terms of reducing NPC

disease pathology, slowing disease progression and in some cases improving certain disease manifestations (Patterson et al. 2007). Thereafter, a number of off-label and small trials in neurological storage disorders have been conducted, the reason being that miglustat can cross the blood-brain barrier. There was no noticeable SRT effect on the neurology of patients suffering from GM2-gangliosidosis, mucopolysaccharidoses or neuropathic Gaucher disease (Maegawa et al., 2009; Schiffmann et al., 2008; Shapiro et al., 2009). Hence, miglustat has been generally accepted everywhere around the globe, except in the USA, as a therapy for NPC patients and, at present, remains the only approved form of therapy for this disease.

2-hydroxypropyl-beta-cyclodextrin (HP- β -CD) is an alternative experimental treatment for NPC1 at present, currently undergoing clinical trial. This is because it has the ability to correct the intracellular accumulation of unesterified cholesterol in NPC mice. Studies in NPC mouse (Davidson et al. 2009; Liu et al. 2009) and cat (Vite et al. 2015) animal models showed a dramatically slowed disease progression. HP- β -CD has been shown to not cross the blood-brain barrier (Camargo et al. 2001). However, the intrathecal HP- β -CD trial showed a reduction of pace in the neurological progression of the disease (Ory et al. 2017). Ototoxicity is an observed side effect of HP- β -CD treatment (Crumling et al. 2012) and is a reason for cyclodextrin treatment being stopped in the UK. In the same manner, there is an ongoing evaluation of genistein, the heparan sulfate synthesis inhibitor, with respect to mucopolysaccharidoses disease (de Ruijter et al. 2012b).

Another treatment option is chaperone therapy. The enzyme deficiency in some patients with Fabry disease can be attributed to an enzyme which is produced but not folded correctly. Molecular chaperones can help by temporarily binding to the enzyme, at non acidic pH, in order to assist with its folding into a more functional form and subsequent delivery to the lysosome where at acidic pH the chaperone dissociates to reveal the partially functional enzyme (Parenti 2009). Research into gene therapy is still being carried out. In animal studies, the adeno-associated virus (AAV) vector has been considered to be safe and provides considerable therapeutic effect. As a result, some gene therapy clinical trials involving MPS type IIIA and MLD are currently at various stages of development (Biffi et al. 2013; Tardieu et al. 2014). There are also some pre-clinical studies using AAV9 in NPC that have shown the ability to cross the brain barrier or in which neurons alone have been targeted and have also shown considerable effectiveness (Chandler et al. 2016; Hughes et al. 2018; Xie et al. 2017). Ultimately, however, small molecule therapy or ERT remains the most likely therapeutic approach for current LSD patients.

Furthermore, other supportive (adjunctive) therapies exist for the treatment of symptoms of LSDs, for example anti-epileptic drugs used in the NCLs to manage seizures. For many LSDs, there are no specific therapies currently available. Existing therapies, however, do not work equally for all symptoms and manifestations. In such cases, supportive symptomatic therapies, such as physiotherapy and occupational therapy, remain indispensable and alleviate some important aspects of patient disease pathology.

1.3 Aims of this project

Recently, treatments for some LSDs have been successfully developed. However, at present the diagnosis of LSDs is complex and there are no single assays that can be used for diagnosis and disease monitoring. The main aim of this project is to conduct a study across most of the LSDs to investigate whether it could be possible to develop novel and simple diagnosis methods for these diseases and to investigate whether they share common phenotypes as a helpful means of understanding the mechanism of disease pathogenesis.

Chapter 2 shows the material and methods that are used throughout most of these chapters. Summaries of the specific methods described in each chapter can be found at the beginning of each chapter.

Chapter 3 investigates the possibility of developing a simple fluorometric assay incorporating lysotracker as a universal biomarker for LSDs by measuring lysosomal expansion.

Chapter 4 investigates 23 lysosomal enzyme activities across the majority of LSDs. The aim is to develop a novel approach to identify common enzymatic changes to assist with diagnosis and monitoring of disease progression involving potentially simple clinical biomarkers, as well as providing insight into the mechanisms of the disease.

Chapter 5 investigates the power of electron microscopy as a tool for LSD diagnosis and disease characterisation.

Chapter 6 determines whether deregulation of trace metal homeostasis is a common feature of multiple LSDs and considers the possibility of developing mass spectrometry methods for detecting heavy metal levels as a potential biomarker for LSDs.

Chapter 7 Discusses the identification of a loss of NPC1 function as a common feature observed across the majority of LSDs which may explain the widespread presence of secondary lipid storage.

Chapter 8 General discussion and conclusion.

Chapter 2: Materials and methods

2.1 Materials

Unless otherwise stated all reagents were obtained from Sigma Aldrich, Poole, Dorset UK; any exceptions to this will be noted.

2.2 Cell Culture

2.2.1 Cell culture conditions

The adherent cell lines used were grown in tissue-culture coated flasks, while suspension cells were grown in untreated flasks (Nunc, ThermoFisher, Waltham, Massachusetts, USA). The optimum cell culture conditions of the various cell lines are mentioned below. Foetal bovine serum (FBS) (Sera Plus – PAN Biotech® Aidenbach, Bavaria, Germany) was heat-inactivated at 60°C for 30 minutes prior to it being used as a supplement.

Foetal bovine serum (FBS) (Sera Plus – PAN Biotech® Aidenbach, Bavaria, Germany) was heat-inactivated at 60°C for 30 minutes prior to it being used as a supplement. This is to deactivate complement proteins in the serum that can interfere with the cell immune response without affecting the growth factors in the medium .

The human fibroblast (HF) and lymphoblast cell lines (B-LCLs) were either purchased from the Coriell Cell Repository or were from collaborators (Supplementary table 1). Human healthy control fibroblast (GM05399); 1year old at sampling, male. NPC1 (GM03123) skin fibroblast, 9 year old at sampling, female, (Heterozygous *NPC1* mutations P237S and I1061T), were mainly used unless otherwise stated. Where possible, cells were passage matched to ensure minimal impact of cellular ageing *in vitro* on the results.

Fibroblast monolayers were grown in Dulbecco's modified Eagle's medium (DMEM) with 10% (v/v) FBS (Sera Plus – PAN Biotech®) in the presence of 1% (v/v) L-Glutamine at a constant temperature of 37°C in a humidified incubator with 5% CO₂.

The lymphoblast cell lines were grown as suspension cultures in Roswell Park Memorial Institute medium (RPMI) with 10% FBS (Sera Plus – PAN Biotech®) in the presence of 1% L-Glutamine and grown as a suspension at 37°C in a humidified incubator with 5% CO₂.

Note that all cells were grown in the absence of antibiotics in order to prevent stop codon readthrough that is triggered by the stabilisation of RNA polymerase by streptomycin. As several LSD mutations incur premature stop codons the presence of antibiotics may inadvertently alleviate some of the cellular phenotypes.

2.2.2 Cellular cholesterol depletion

To achieve the cholesterol depletion conditions, human fibroblast cell lines were grown for 7 days in DMEM with 10% lipoprotein-deficient serum (LPDS) as a substitute for FBS, heat-inactivated at 60°C for 30 minutes before being used as a supplement, in the presence of 1% L-Glutamine.

2.2.3 Starvation protocol to induce autophagy

Two starvation protocols were used: (1) cells were incubated in complete Hank's balanced salt solution (HBSS), which lacks serum and essential amino acids, for 3h before staining; (2) partial amino acid starvation protocol, considered as a "less harsh protocol" (Chen et al. 2014), in which the cells were grown in DMEM with no glutamine and only 1% FBS for 24h before staining with markers of autophagy as outlined below.

2.3 Buffers

2.3.1 Complete Hank's Balanced Salt solution (HBSS)

HBSS functions to maintain cell viability over the course of long experiments, and is used as a substitute for cell medium as it does not have any autofluorescent properties (e.g. from phenol red). The composition of complete HBSS is: 1mM CaCl₂, 1mM MgCl₂, 1mM HEPES pH7.2 (LONZA, Basel, Switzerland) buffer, 1x HBSS solution (LONZA) and MilliQ H₂O.

In the case of Ca²⁺ free HBSS, it was used only for the Ca²⁺ experiments to avoid interference in measuring intracellular Ca²⁺ caused by high extracellular Ca²⁺. The composition is similar to complete HBSS but with only 0.05mM CaCl₂ instead of 1mM CaCl₂.

2.3.2 Blocking buffer

A blocking buffer (Dulbecco's phosphate buffered saline (DPBS) containing 1% bovine serum albumin (BSA) and 0.1% saponin) was used during immunolabelling to eliminate non-specific binding of antibodies and assist with mild permeabilization of cellular membranes to allow entry of antibodies and toxins.

2.3.3 Immunocytochemistry fixatives

Different fixatives were used in this project:

2.3.3.1 4% Paraformaldehyde

This is an aldehyde-based fixative used as a cross-linker between lipids and proteins, which maintains cell structure. Briefly, when the cells reached 80% confluency in flasks, they were washed twice with DPBS and incubated in DPBS containing 0.25% trypsin/EDTA; this was followed by the inactivation of trypsin by the addition of excess complete cell culture medium. Cells were then grown overnight on acid-washed glass coverslips, Ibidi 8 well μ -Slides (Thistle Scientific, Glasgow, UK) or Ibidi black 96 well μ -Plates (Thistle Scientific) for microscopy, or 96 well Collagen I coated plates (Thermofisher) for plate reader assays.

Cells were washed once with DPBS, and fixed in 4% paraformaldehyde in DPBS, pH 7.2, for 10 minutes at room temperature, then washed three times in DPBS, and stored in DPBS at 4°C.

For fixation using cold 4% Paraformaldehyde, samples were placed on ice and washed with ice-cold DPBS. Samples were fixed in 4% Paraformaldehyde for 20 minutes in ice cold conditions, washed in DPBS three times and stored in DPBS at 4°C.

2.3.3.2 Ice-cold methanol

Methanol fixation permeabilises and dehydrates cells. It is widely used to remove lipids from membranes and reveal epitopes during dehydrating, but it also helps proteins to precipitate (Hobro and Smith 2017). In this fixation method, cells were grown on glass coverslips, as in section 2.3.3.1, washed once in DPBS, and fixed in ice-cold methanol for 5 minutes in the freezer, then washed three times in DPBS and stored in DPBS at 4°C.

2.4 Microscopy

Unless otherwise stated, all images were obtained using an inverted Zeiss AxioImager A1 with Colibri LED illumination, a MRm charged-coupled device (CCD) camera and Axiovision 4.7 imaging software. A 40x FLUAR oil immersion objective was used for imaging. Thats images were processed in photoshop and all changes were made equally across all images from the experiment.

2.5 Immunocytochemistry staining

Fixed samples were incubated overnight in blocking buffer containing the appropriate primary antibody (Table 2.1) at 4°C; this was followed by the three washes in blocking buffer and incubation in the appropriate secondary antibody (Table 2.2) for 45 minutes at room temperature. Cells were washed three times in DPBS and either mounted, in the case of coverslips, or left in DPBS in a 96-well plate, and imaged as described above in section 2.4.

Table 2.1 Primary antibodies used in the immunocytochemistry staining.

Immunolabelling	Dilution	Host	Supplier
LAMP1 (mouse) H4A3	1:200	Mouse	Developmental Studies Hybridoma Bank
LAMP2 (human) H4B4	1:200	Mouse	Developmental Studies Hybridoma Bank
Anti-Niemann Pick C1 antibody (ab134113)	1:500	Rabbit	Abcam

Table 2.2 Secondary antibodies used in the immunocytochemistry staining

Immunolabelling	Dilution	Target	Wavelengths (nm)	Supplier
DyLight 488 IgG	1:250	Mouse	488	Vector Laboratories
DyLight 488 IgG	1:250	Rabbit	488	Vector Laboratories
DyLight 594 IgG	1:250	Mouse	594	Vector Laboratories
DyLight 594 IgG	1:250	Rabbit	594	Vector Laboratories

2.6 Live imaging

Different live probes were used in this project:

2.6.1 LysoTracker staining protocols in adherent patient fibroblasts

LysoTracker fluorescence, which stains all late endosomes and lysosomes with a pH below 5.2, was evaluated using a 96-well plate format via a plate reader (detailed below, section 2.6.1.2), or by seeding cells in Ibidi chamber slides (as described above, section 2.3.3.1) for microscopy imaging.

2.6.1.1 LysoTracker quantification by fluorescence microscopy

Primary fibroblasts were grown on Ibidi 8-well micro-slides (Thistle Scientific), as described in section 2.3.3.1. They were then incubated in DPBS containing 200 nM LysoTracker-green DND-26 (Invitrogen, California, USA) for 15 minutes at 37°C. Cells were washed three times using DPBS, were then counterstained with a nuclear marker (see section 2.10.3), and kept in 200 µl DPBS and imaged immediately by microscopy (section 2.4) at 470nm excitation, 520nm emission.

2.6.1.2 LysoTracker quantification by multiwell plate assay using adherent cells

Primary fibroblasts were detached from culture flasks by first washing in DPBS followed by mild enzymatic digestion with 1ml 1X trypsin/EDTA for 5min. Trypsin was deactivated by the addition of 9ml DMEM and cells were counted using FastRead Counting Slides (Immune system, Paignton, UK). 50,000 cells/well were then plated in each well of a Collagen I coated 96 well plate (Thermo Fisher) (to promote cell attachment and reduce the possibility of losing cells during washes) and allowed to adhere overnight. Cells were typically washed once in DPBS, unless stated otherwise in the associated figure legends, then incubated in DPBS containing 200nM LysoTracker-green DND-26 (Invitrogen) for 15 minutes at 37°C, unless stated otherwise. Cells were washed three times with DPBS, and kept in 200µl DPBS for lysoTracker fluorescence evaluation, using two different fluorescence plate readers: a monochromator-based SpectraMAX Gemini EM (Molecular Devices) with SoftMax Pro software or a filter-based FLUOstar (BMG Labtech) with OPTIMA software. Plates were read on both plate readers with excitation set at 485nm and emission at 520nm, unless stated otherwise. It should be noted that some lysoTracker plate reader data was generated as a percentage of the control. This is because the FLUOstar plate reader was out of service in the

middle of this project, and the monochromator-based SpectraMax Gemini EM plate reader was used as an alternative. The fluorescence values are not directly comparable between the two plate readers owing to their different excitation sources and subsequent differences in methods of detection.

2.6.2 Lysotracker staining protocols for non-adherent B lymphoblasts.

2.6.2.1 Lysotracker quantification by fluorescence microscopy

Cells grown as suspension cultures were removed from culture flasks and centrifuged at 800 g for 5 minutes to pellet the cells. The culture medium was removed and the cells rinsed once with sterile HBSS and re-centrifuged. They were then stained with 200 nM Lysotracker-green DND-26 in HBSS for 15 minutes at 37°C. Cells were centrifuged again for 5 minutes at 800 g, and rinsed and re-pelleted twice with sterile HBSS. 200µl cell suspension in HBSS was added to Ibidi 8 well µslide and cells left for 5 minutes to sink to the bottom of the chamber slide so that they could be imaged. Cells were imaged at 470nm excitation, 520nm emission as described in section 2.4.

2.6.2.2 Measurement of lysosomal expansion with lysotracker by flow cytometry

Lymphoblast cell density was counted with a haemocytometer, and cells were centrifuged for 5 minutes at 800 g to pellet them. The culture medium was removed, and the cells rinsed once with HBSS and re-centrifuged. They were then stained in HBSS containing 200nM Lysotracker-green DND-26 (Invitrogen) for 15 minutes at 37°C. The cells were centrifuged for 5 minutes at 800 g, rinsed and re-pelleted twice with sterile HBSS, and centrifuged again a final time for 5 minutes at 800 g. Finally, cells were re-suspended in 0.2ml HBSS, before flow cytometric analysis using a BD Biosciences FACSCanto II flow cytometer. Samples were analysed following gating to remove dead cells and debris and select the whole cell population by Forward Scatter (FSC) versus Side Scatter (SSC) analysis. The selected population is then analysed for single cells (FSC-H vs FSC-A) to discriminate against clumps of cells. The defined population of single cells positive for lysotracker are then selected and ultimately fluorescence intensity per cell is analysed as Mean Fluorescence intensity (MFI) of lysotracker emission (see chapter 3, Figure 3.18 for examples). In total, 10,000 events were collected. All data was analyzed using FlowJo software.

2.6.2.3 B lymphocyte magnetic capture method for lysotracker analysis

Lymphoblast cell density was counted with a haemocytometer, and cells were centrifuged for 5 minutes at 800 g. The culture medium was removed, the cells re-suspended in culture medium and centrifuged for a further 5 minutes at 800 g. Cells were counted again using FastRead Counting Slides (Immune system), and 1,000,000 cells/well were transferred to a 96-well plate. CD19 positive cells were collected using an EasySep CD19 positive collection kit 2 (STEMCELL Technologies, Vancouver, Canada), according to the manufacturer's protocol. Briefly, 100 µl/ml selection cocktail (STEMCELL Technologies) was added to each well, mixed, and incubated for 3 minutes, before 100µl/ml human B lymphocyte specific anti-CD19 conjugated to dextran-coated magnetic particles (STEMCELL Technologies) were added, mixed and incubated for 3 minutes. Each well was made up to a final volume of 0.25ml in separation buffer, placed directly on top of a 96-Well magnet stand (EasySep™ Magnet, STEMCELL Technologies) and incubated for 5 minutes. The supernatant was carefully removed, and the plate containing the isolated cells removed from the magnet stand. This step was repeated once to wash the cells and remove unbound material. The cells were then stained with HBSS containing 200nM LysoTracker-green DND-26 (Invitrogen) and 2µg/ml Hoechst 33342 for 15 minutes at 37°C followed by two washes whilst placed on the magnet as described above, bound and stained cells were then resuspended in 200µl HBSS and lysotracker fluorescence measured using a fluorescence plate reader at excitation/emission 485/525 nm and 360/460 for Hoechst 33342.

2.6.3 Measurement of lysosomal pH by fluorescence microscopy.

In order to measure lysosomal pH, minor modifications of previously published methods using fluorescence-labelled dextrans was done (Bach et al. 1999; Lloyd-Evans et al. 2008). Fluorescein isothiocyanate (FITC) dextran is a pH-dependent fluorescence probe that becomes brighter at higher pH and will be co-localised with a Texas Red dextran loading control, whose fluorescence intensity does not change with pH alteration. Cells growing on Ibidi 8 well µslides were incubated overnight with both 0.25mg/ml FITC dextran 10,000MW and 0.25mg/ml Texas Red dextran 10,000MW (Thermo Fisher) in the cell culture medium for 24 hours, to allow endocytosis of the dextrans to occur. Cells were then washed in complete medium once and incubated in unlabelled medium for 24 hours to ensure that the dextrans were only present in lysosomes as a result of prolonged endocytosis (Bach et al. 1999). This was followed by three washes in DPBS and imaging at 470nm excitation, 520nm emission (FITC) and 565 excitation, 620nm emission (Texas Red) as described above.

2.6.4 Measurement of autophagy by live cell fluorescence microscopy

Autophagic vacuoles were detected in cells using the live cell autophagosome specific labelling dye CYTO-ID® according to the Autophagy Detection Kit 2.0 protocol (Enzo Life Sciences, Exeter, UK). Briefly, cells, grown on Ibidi 8 well μ slides were stained with 1:1,000 CYTO-ID® Green in 1X assay buffer for 30 minutes at 37°C, washed three times with DPBS and imaged live in DPBS at 470nm excitation, 520nm emission by fluorescence microscopy as described in section 2.4.

2.6.5 Whole cell intracellular organelle Ca²⁺ measurements

This method was adapted from Lloyd-Evans (2008). Cells were plated on Ibidi 8 well μ slides and allowed to adhere for at least 12 hours. Cells were washed in chilled culture medium supplement with 1% BSA, and loaded with 5 μ M Fura-2AM mixed with 0.0025% Pluronic F-127 in chilled culture medium supplemented with 1% BSA for 1 hour at 16°C in the dark. Cells were washed in Ca²⁺ free HBSS (see section 2.3.1) and incubated in Ca²⁺ free HBSS for 10 minutes to allow de-esterification of the acetoxymethyl (AM) group of Fura2. Cells were then imaged in Ca²⁺ free HBSS. Intracellular Ca²⁺ responses to ionomycin (Merck, Darmstadt, Germany), and Gly-Phe β -naphthylamide (GPN) (Alfa Aesar, VWR, Lutterworth, UK) were recorded and analysed using a Zeiss Axiovert 35 microscope fitted with a dimmable X-cite HXP lamp, Optospin excitation and emission filter wheels (Carin Research, Faversham, UK) for double excitation/single emission imaging of Fura 2 fluorescence (340/380nm excitation, 520 emission), a Hamamatsu Orca Flash 4.0LT sCMOS camera, Zeiss Fluor objectives optimised for Fura 2, and Metafluor software (Molecular devices, Wokingham, UK).

2.6.6 Live intracellular free Zn²⁺ imaging methods

2.6.6.1 FluoZin-3, AM

Cells were plated on Ibidi 8 well μ slides at a density of 10,000 cells/well and allowed to adhere overnight at 37°C and 5% CO₂. After this overnight incubation, cells were loaded with 1 μ M FluoZin-3, AM (Ex 494nm/ Em 516 nm) (ThermoFisher) in medium containing 0.025% Pluronic F-127 for 37°C for 30 minutes. Cells were washed twice with DPBS and imaged by fluorescence microscopy at 470nm excitation, 520nm emission as described (Section 2.4).

2.6.6.2 Zinquin ethyl ester

Cells were plated on Ibidi 8 well μ slides at a density of 10,000 cells/well and allowed to adhere overnight at 37°C and 5% CO₂. Cells were washed once, and incubated in complete HBSS containing 25 μ M Zinquin ethyl ester (excitation at 370 nm/ emission at 490 nm) (ThermoFisher) at 37°C for 30 minutes. Cells were washed twice in complete HBSS and imaged at 380nm excitation, 460nm emission as described (Section 2.4).

2.6.6.3 Newport Green DCF

Cells were plated on to Ibidi 8 well μ slides at a density of 10,000 cells/well and allowed to adhere overnight at 37°C and 5% CO₂. Cells were incubated with DPBS containing 5 μ M Newport Green DCF (excitation at 494 nm/ emission at 516 nm) (ThermoFisher), at 37°C for 1 hour, washed twice with DPBS and imaged at 470nm excitation, 520nm emission as described (Section 2.4).

2.6.7 Live intracellular free Cu⁺/Cu²⁺ and Fe²⁺/Fe³⁺ imaging methods.

2.6.7.1 Phen Green SK

Cells were plated on to Ibidi 8 well μ slides at a density of 10,000 cells/well and allowed to adhere overnight at 37°C and 5% CO₂. Cells were loaded with 25 μ M Phen Green SK (excitation at 506nm/ emission at 520nm) (ThermoFisher) in complete medium containing 0.025% Pluronic F-127 at 37°C for 1 hour, washed twice with DPBS and imaged at 470nm excitation, 520nm emission as described (Section 2.4).

2.6.7.2 CopperGreen

CopperGreen is a new cell-permeable Cu⁺-specific fluorescent probe (Taki et al. 2010). Cells were plated on to Ibidi 8 well μ slides at a density of 10,000 cells/well and allowed to adhere overnight at 37°C and 5% CO₂. Cells were incubated with 5 μ M CopperGREEN (GORYO Chemical, Inc. Sapporo, Japan) (Ex 480nm/ Em 510nm) in complete medium in for 3 hours at 37°C and 5% CO₂. Cells were washed three times in complete HBSS and imaged at 470nm excitation, 520nm emission as described (Section 2.4).

2.6.7.3 FeRhoNox™-1

FeRhoNox™-1 is a highly specific cell permeable fluorescent probe for Fe²⁺ (Hirayama et al. 2013). Cells were plated on Ibidi 8 well μ slides at a density of 10,000 cells/well and allowed to

adhere overnight at 37°C and 5% CO₂. Cells were stained with 5 µM FeRhoNox™-1 (GORYO Chemical, Inc.) (excitation at 540nm/ emission at 570nm) in complete medium for 1 hour at 37°C and 5% CO₂. Cells were washed three times in HBSS and imaged at 470nm excitation, 520nm emission as described (Section 2.4).

2.6.8 Intracellular ganglioside GM1 trafficking assay

FITC conjugated cholera toxin subunit B (FITC-CtxB) was utilized to assay the endocytosis and intracellular trafficking of plasma membrane ganglioside GM1 (Sugimoto et al. 2001). GM1 at the plasma membrane is the molecular target of FITC-CtxB and is bound by incubation of live cells in cold complete medium containing 1µg/ml FITC-CtxB for 30 minutes at 16°C (to minimize endocytosis). Cells were then washed with pre-warmed medium, and restored to the normal culture medium conditions (37°C, 5% CO₂) for the trafficking 'chase' period of 90 minutes. Once the trafficking was complete, cells underwent three 10 minute back-exchange washes in cold complete medium with 1% BSA to remove non-internalised FITC-CtxB. Cells were then imaged live, or following paraformaldehyde fixation, by fluorescence microscopy at 470nm excitation, 520nm emission as described (Section 2.4).

2.7 Biochemistry

2.7.1 Preparation of human fibroblast homogenate

Homogenate was prepared from human fibroblasts harvested at 90% confluency. Medium was removed, and cells washed twice in DPBS before incubation in 0.25% trypsin/EDTA to detach cells from their flasks. Trypsin was inactivated by adding DMEM, and cells pelleted by centrifugation at 102 g for 5 minutes. Medium was removed, and cells were resuspended in DPBS. The centrifugation and DPBS wash steps were repeated twice, and cells were stored as dry pellets at -80°C. To minimise the effect of thawing on enzyme activity, multiple single-use aliquots were prepared following determination of protein concentration, and these were stored at -80°C.

2.7.2 Bicinchoninic acid assay

Bicinchoninic acid assay (BCA) assays were used to obtain the protein concentration of cellular samples (Walker 2009). BCA Protein Assay (Sigma Aldrich) was conducted according to the manufacturers' instructions. Briefly, cell pellets were resuspended in MilliQ water (Barnstead purifier, ThermoFisher), and cells fractured by three freeze-thaw cycles, followed by 20 passages through a 26-gauge needle. 50µl of homogenate was then taken and

centrifuged at ~13,000 g for 30 minutes at 4°C to pellet insoluble material. The supernatant containing predominantly cytosolic cell lysate was collected and diluted 1:5, 1:10 and 1:20 for determination of protein concentration, using 0-75µg/ml BSA as the standard curve. Samples were plated onto clear, flat bottomed 96 well microplates (Greiner Bio-one, Austria) and incubated with BCA reagent (0.02% Cu₂SO₄ in bicinchoninic acid solution) for 30 minutes at 37°C to allow the colour to develop. Absorbance at 570nm was measured using a TECAN Infinite F50 absorbance microplate reader (Tecan Group Ltd. Switzerland).

2.7.3 Fluorometric assays for enzyme activities

Fluorometric assays were carried out to assess lysosomal enzyme activities. The assay conditions are outlined in (Table 2.2). Briefly, 10µl cell homogenate at the indicated protein concentration (Table 2.2) and 10µl artificial fluorogenic substrate in a working buffer pH adjusted for each enzyme (Table 2.2) and at the indicated concentration were added to clear, flat bottomed 96 well microplates (Greiner Bio-one), and incubated for the indicated time at 37°C. Standards appropriate for each substrate fluorophore were prepared in the working buffer at concentrations ranging between 0 – 200µM. The reaction was stopped by adding 180µl of the indicated stop buffer (Table 2.2), and the released fluorophore measured using a SpectraMAX Gemini EM fluorescence plate reader (Molecular Devices) in different Excitation/Emission; 4MU: 360/460nm excitation/emission, HMU: 404/460nm excitation/emission, MCA: 320/420nm excitation/emission, AMC: 360/460nm excitation/emission. P-nitroanilide absorbance was read at 405nm using an Infinite F50 absorbance plate reader. In all cases the enzyme activity was calculated using µmol/ g protein/ hour. Heat-inactivated control samples were used to measure background fluorescence in the enzyme activity assays. During this process, samples were heated to 95°C for 15 minutes to achieve protein denaturation.

Table 2.3 Assay conditions

Lysosomal enzyme	Summary of reagents and conditions	Reference
β -glucosidase (GCase)	Standards: 4-methylumbelliferone (4MU) (Sigma) Substrate: 4-methylumbelliferyl- β -D-glucopyranoside (2 mM) (Sigma) Amount of protein: 2 μ g Inhibitor: CBE (500 μ M) Reaction buffer: Sodium acetate, pH 5.6 + 0.1% triton + 0.2% NaTc (Sigma) Incubation: 1 hr @ 37°C Stop buffer: Glycine/NaOH, pH 10.6	(Broadhead and Butterworth 1977; Sawkar et al. 2002)
β -galactosidase (β -gal)	Standards: 4MU Substrate: 4MU- β -galactoside (2 mM) Amount of protein: 2 μ g Inhibitor: 1-deoxygalactonojirimycin (1 mM) Buffer: Sodium acetate, pH 4.5 + 0.1% 5 mM NaCl + 0.2% NaTc Incubation: 1 hr @ 37°C Stop buffer: Glycine/NaOH, pH 10.6	(Nowakowski et al. 1988; Nowroozi et al. 2001)
Acid sphingomyelinase (aSMase)	Standards: HMU (Moscerdam) Substrate: HMU-sphingomyelin (0.5 mM) (Moscerdam) Amount of protein: 2 μ g Inhibitor: Zoledronic acid (1 mM) Buffer: Sodium acetate, pH 4.5 + 0.2% NaTc + 0.02% NaAz Incubation: 1 hr @ 37°C Stop buffer: Na ₂ CO ₃ , pH 10.9 + 2.5% triton	(Van Diggelen et al. 2005)
α -galactosidase A (α Gal A)	Standards: 4MU Substrate: 4MU- α -D-galactopyranoside (2 mM) (Sigma) Amount of protein: 2 μ g Inhibitor: N-butyldeoxygalactonojirimycin (NB-DGJ) (1 mM) Buffer: Phosphate citrate, pH 4.5 Incubation: 1 hr @ 37°C Stop buffer: Glycine/NaOH, pH 10.6	(Caudron et al. 2015; Mayes et al. 1981; Olivova et al. 2009)
Hexosaminidase A (HEXA)	Standards: 4MU Substrate: 4MU-N-acetyl- β -D-glucosamine-6-sulphate (2 mM) (Calbiochem) Amount of protein: 2 μ g Buffer: citrate buffer, pH 4.6 + 0.01% triton Incubation: 1 hr @ 37°C Stop buffer: Na ₂ CO ₃ , pH 10.9	(Bayleran et al. 1987)
Hexosaminidase B (HEXB)	Total Hexosaminidase assay (see below), but with heated cells (50°C for 2hrs) to inactivate Hex A (heat labile).	
Total Hexosaminidase (Total Hex)	Standards: 4MU Substrate: 4MU-N-acetyl- β -D-glucosamine (2 mM) (Sigma) Amount of protein: 2 μ g Buffer: citrate buffer, pH 4.6 + 0.01% triton Incubation: 1 hr @ 37°C Stop buffer: Na ₂ CO ₃ , pH 10.9	(Tropak et al. 2004)
β -glucuronidase (GUSB)	Standards: 4MU Substrate: 4MU- β -D- glucuronide (2 mM) Amount of protein: 2 μ g Inhibitor: Suramin (100 μ M) (Sigma) Buffer: Sodium acetate, pH 4.00 + 0.1% triton Incubation: 1 hr @ 37°C Stop buffer: Na ₂ CO ₃ , pH 10.9	(Bramwell et al. 2014)
α -L-iduronidase (IDU)	Standards: 4MU Substrate: 4MU- α -L-iduronate (1 mM) (Carboynth) Amount of protein: 2 μ g Buffer: Sodium formiate, pH 3.2 Incubation: 1 hr @ 37°C Stop buffer: Na ₂ CO ₃ , pH 10.9	(Hopwood et al. 1979; Kingma et al. 2013)
α -N-acetylglucosaminidase (NAGLU)	Standards: 4MU Substrate: 4MU- α -N-acetylglucosaminide (1 mM) (Sigma) Amount of protein: 2 μ g	(Mauri et al. 2013)

	Buffer: Sodium acetate, pH 4.5 Incubation: 4 hr @ 37°C Stop buffer: Glycine/NaOH, pH 10.6	
Acid α -glucosidase (α -Glu)	Standards: 4MU Substrate: 4MU- α -glucopyranoside (4 mM) (Sigma) Amount of protein: 2 μ g Buffer: Phosphate citrate, pH 4 + 0.1% acarbose Incubation: 4 hr @ 37°C Stop buffer: Glycine/NaOH, pH 10.6	(Broadhead and Butterworth 1978; Jack et al. 2006)
α -fucosidase (α -Fuc)	Standards: 4MU Substrate: 4MU- α -L-fucopyranoside (1 mM) (Sigma) Amount of protein: 2 μ g Inhibitor: Deoxyfuconojirimycin hydrochloride (20nM) (Santa Cruz, Dallas, USA) Buffer: Citrate buffer, pH 5 Incubation: 1 hr @ 37°C Stop buffer: Na ₂ CO ₃ , pH 10.9	(Winchester et al. 1990)
α -mannosidase (α -Man)	Standards: 4MU Substrate: 4MU- α -D- mannopyranoside (2 mM) (Sigma) Amount of protein: 2 μ g Inhibitor: Swainsonine (80 nM) (CarboSynth) Buffer: Sodium acetate, pH 4.5 + 0.1% triton Incubation: 1 hr @ 37°C Stop buffer: Glycine/NaOH, pH 10.6	(Gotoda et al. 1998; Prencz and Natowicz 1992)
Sialidase (NEU)	Standards: 4MU Substrate: 4MU-N-acetyl neuraminic acid (0.2 mM) (Toronto) Amount of protein: 4 μ g Buffer: Sodium acetate, pH 4.5 Incubation: 4 hr @ 37°C Stop buffer: Glycine/NaOH, pH 10.6	(Hayre et al. 2012; Winter et al. 1980; Yamada et al. 1983)
Aspartylglucosaminidase (AGA)	Standards: AMC (CarboSynth) Substrate: L-aspartic acid- β -7-amido-4-methyl coumarin (1 mM) (CarboSynth) Amount of protein: 4 μ g Inhibitor: L-asparagine (1 mM) Buffer: Phosphate citrate, pH 6.5 Incubation: 17 hr @ 37°C Stop buffer: Phosphate citrate, pH 4.5	(Vozyi et al. 1993)
Cathepsin B (CTSB)	Standards: AMC Substrate: Z-Arg-Arg-7-amido-4-methylcoumarin (50 μ M) (Merck) Amount of protein: 4 μ g Inhibitor: Z-Phe-Ala-diazomethylketone (10 μ M). Buffer: Sodium acetate, pH 5.5 +0.8 mM EDTA +8 mM DTT Incubation: 30 mins @ 37°C	(Creasy et al. 2007; Headlam et al. 2006; Viswanathan et al. 2012)
Cathepsin D+E (CTSD/E)	Standards: MCA Substrate: 7-methoxycoumarin-4-acetyl-Gly-Lys-Pro-Ile-Leu-Phe-Phe-Arg-Leu-Lys-dinitrophenyl-D-Arg-amide (50 μ M) (Enzo Life Sciences, NY) Amount of protein: 4 μ g Buffer: Phosphate citrate, pH 4.5 + 2 mM EDTA + 50 mM NaCl Incubation: 1 hr @ 37°C	(Ismael et al. 2016)
Cathepsin L (CTSL)	Standards: AMC Substrate: Z-Phe-Arg-7-amido-4-methylcoumarin (50 μ M) (Bachem) Amount of protein: 4 μ g Inhibitor: Z-Phe-Ala-diazomethylketone (10 μ M). Buffer: Phosphate citrate, pH 5.5 + 0.005% BRIJ + 2.5 mM EDTA + 8 mM DTT Incubation: 30 mins @ 37°C	(Ismael et al. 2016; Creasy et al. 2007; Viswanathan et al. 2012)
Palmitoyl-protein thioesterase 1 (PPT1)	Standards: 4MU Substrate: 4MU-6-thiopalmityl β -D-glucoside (0.5 mM) (CarboSynth) Amount of protein: 2 μ g	(Van Diggelen et al. 1999)

	Inhibitor: ABC44 (200 nM) (Sigma) Buffer: Phosphate citrate, pH 4 + 15 mM DTT + 0.375% triton + 0.1U β -glucosidase Incubation: 4 hr @ 37°C Stop buffer: Na ₂ CO ₃ , pH 10.9 + 0.025% triton	
Tripeptidyl peptidase 1 (TPP1)	Standards: AMC Substrate: Ala-Ala-Phe-7-amido-4-methylcoumarin (0.5 mM) (Bachem) Amount of protein: 2 μ g Buffer: Sodium acetate, pH 4.5 + 0.05% triton +10% EDTA + 0.08% E64 + 0.012% PepstatinA Incubation: 1 hr @ 37°C Stop buffer: Phosphate citrate, pH 4.5	(Di Giacopo et al. 2015)
Dipeptidyl peptidase enzymes (DPP)	Standards: p-nitroanilide (Sigma) Substrate: Gly-pro-p-nitroanilide (2.5 mM) (Santa cruz) Amount of protein: 2 μ g Buffer: Tris HCl, pH 7.4 Incubation: 2 hr @ 37°C Stop buffer: Sodium acetate, pH 4.4	(Beckenkamp et al. 2015)
Acid lipase (LAL)	Standards: 4MU Substrate: 4MU-oleate (0.1 mg/ml) (Carboynth) Amount of protein: 2 μ g Inhibitor: Orlistat (1 μ M) Buffer: Sodium acetate, pH 4 + 1% triton Incubation: 1hr @ 37°C Stop buffer: Na ₂ CO ₃ , pH 10.9	(Moheimani et al. 2012)
Acid phosphatase (APs)	Standards: 4MU Substrate: 4MU-phosphate (150 μ M) (Sigma) Amount of protein: 2 μ g Buffer: Acetate buffer, pH 5 + 0.2% triton Incubation: 1hr @ 37°C Stop buffer: Glycine/NaOH, pH 10.6	(LEAKE et al. 1982)
Sulfamidase	Standards: 4MU Substrate: 4-Methylumbelliferyl 2-deoxy-2-sulfamino-a-D-glucopyranoside (4-MU-GlcN) (1mM) (Carboynth) Amount of protein: 4 μ g Buffer: Sodium acetate, pH 5.5 + 5 mM NaCl Incubation: First incubation: 24 hr @ 37°C; second incubation 24 hr @37 with 10 μ l (0.1 U) of α -glucosidase (Sigma) Stop buffer: Na ₂ CO ₃ , pH 10.9	(Karpova et al. 1996)

2.7.4 Mouse tissue preparation

The mucopolysaccharidoses mouse tissues were generously donated by Prof. Brian Bigger, Manchester University. The NPC1 mouse tissues were from the lab of Prof. Frances Platt, University of Oxford, where they had been kept and their organs harvested under a grant from the National Niemann-Pick Disease Foundation, obtained by Prof. Platt and Dr Emyr Lloyd-Evans. Mouse tissues were homogenised using a dounce homogenizer, followed by multiple passages through a 26-gauge needle. Homogenates were centrifuged for 15 minutes at 10,000 g, and the supernatant used for determination of protein content by BCA (section 2.7.2) and lysosomal enzyme activity (section 2.7.3).

2.7.5 Assay of lysosomal enzyme activity in human dried blood spots

This method is modified from (Shigeto et al. 2011). Briefly, barium hydroxide and zinc sulfate were used to precipitate haemoglobin and improve fluorescence intensity. Firstly, 3.2mm punches were made from DBS cards (see section 2.14 for description of ethics), placed in 1.5 mL microcentrifuge tubes containing 60µl working buffer suitable for the indicated enzyme assay (Table 2.2) and incubated at 37°C for 24 hours. Next, 30µl 150mM barium hydroxide was added and incubated for 5 minutes at room temperature. Following that, 30µl 150mM zinc sulfate was added, mixed and the solution incubated for 10 minutes at room temperature. Tubes were centrifuged for 5 minutes at 10,000 g, at 4°C, and 90µl supernatant transferred to clear flat bottomed 96 well microplates (Greiner Bio-one). 110µl of the suitable stop buffer was added (table 2.2), and the released fluorophore measured using a SpectraMAX Gemini EM fluorescence plate reader (Molecular Devices). 4-methylumbelliferone (4MU) fluorescence standards (0, 1, 2, 5, 10, 15, 25, 30µM) were included in each plate. Enzyme activity was measured as picomoles of liberated 4MU per 24 hours per 3.2mm disc.

2.8 Drug treatments

2.8.1 Conduritol-β-epoxide, inhibitor of lysosomal GBA1

Fibroblasts from Gaucher disease patients do not display any disease phenotypes in culture. Therefore, conduritol-β-epoxide (CBE) (Carbosynth, Compton, UK) was used to completely inhibit the activity of β-glucosidase, which causes the storage of glycosphingolipids, and produces Gaucher disease phenotypes in fibroblasts (Sillence et al. 2002). To achieve this, healthy control fibroblasts were incubated with 500µM CBE in the growth medium for 10 days, with the medium changed every two days.

2.8.2 MLSA1 drug treatment

Mucolipin Synthetic Agonist 1 (MLSA1) acts as selective agonist of TRPML1 (Grimm et al. 2010). Fibroblasts cells were either untreated or treated 4 hours with 50 μ M MLSA1 in complete DMEM before live or fixed staining and subsequent imaging.

2.8.3 U18666A, an NPC1 inhibitor

U18666A (Merck) is a positively charged lysotropic drug that produces an NPC phenotype within 24 hours in healthy cells (Lloyd-Evans et al. 2008) by binding and preventing the action of NPC1 (Lu et al. 2015). Cells were treated overnight with 2 μ g/ml U18666A (Lloyd-Evans et al. 2008) before live or fixed staining and subsequent imaging.

2.8.4 1-(1-naphthylmethyl)-piperazine, a new inhibitor of NPC1

1-(1-naphthylmethyl)-piperazine (1NMP), is an inhibitor of resistance-nodulation-division (RND) permeases, a family to which NPC1 belongs. 1NMP is also an analogue of other piperazine drugs shown previously to inhibit NPC1, but which are not commercially available. Preliminary work from the ELE lab has identified that 1NMP may also directly inhibit NPC1, the only mammalian RND permease (Schumacher et al. 2005). Healthy cells grown in presence of 1NMP produce all the cellular phenotypes that resemble NPC disease (ELE lab, unpublished observations). Healthy control cells were treated with 50 μ M 1NMP in complete DMEM for 24 hours in tissue culture conditions before live or fixed staining and subsequent imaging.

2.8.5 Sucrose, an osmotic modulator of lysosomal ion content and volume

Lysosomal storage can be triggered by incubating fibroblasts in medium containing 100mM sucrose. This leads to the rapid uptake and storage of sucrose in lysosomes and causes lysosome expansion by sucrose mediated chelation of free ions and subsequent water entry into lysosomes (Karageorgos et al. 1997). Cells were grown in medium containing 100mM sucrose for 24 hours in cell culture conditions to develop sucrosomes, before live or fixed staining and subsequent imaging.

2.8.6 Bafilomycin, vATPase inhibitor

Bafilomycin A1 is a specific inhibitor of the lysosomal vATPase, which maintains the lysosomal proton gradient (Harada et al. 1997). Fibroblasts were treated with medium containing a low amount (25nM) of bafilomycin A1 for 24 hours, which reduces lysosomal pH (Lee et al. 2010) before live or fixed staining and subsequent imaging.

2.8.7 Monensin and nigericin, Na⁺ and K⁺ ionophores

Lysoosmotic agents cause a disturbance of lysosomes by disrupting Na⁺/H⁺ and K⁺/H⁺ exchanger activity (Lin et al. 2003), which causes the release of H⁺ and Ca²⁺ from the lysosomal lumen. The disrupted pH gradient causes the lysosomal contents to be released and also prevents them from being refilled. The cells were treated with DPBS containing 10 μM monensin or nigericin for 10 minutes before lysotracker staining and lysotracker fluorescence measured using a fluorescence plate reader at excitation/emission 485/525 nm.

2.8.8 Gly-Phe β-naphthylamide, lysosomal cathepsin C substrate

Gly-Phe β-naphthylamide (GPN) (Abcam) is a lysomotropic peptide that is a substrate for cathepsin C. It is widely used to induce lysosomal Ca²⁺ release as the product of GPN hydrolysis induces lysosomal swelling and rupture (Lloyd-Evans et al. 2008; Morgan and Galione 2007). Cells were stained with lysotracker, and incubated in DPBS containing 500μM GPN (Alfa Aesar, VWR, Lutterworth, UK) for 10 minutes before using a fluorescence plate reader at excitation/emission 485/525 nm.

2.8.9 N-butyl-deoxynojirimycin (Miglustat), inhibitor of GlcCer synthase

Miglustat (Toronto Research Chemicals) treatment is a substrate reduction therapy that decreases the levels of glycosphingolipids by inhibiting glucosylceramide synthase. It has been used in the treatment of some LSDs (Platt et al. 1994). Cells were grown in medium containing 50μM miglustat for 5 days, with the medium changed on the third day.

2.8.10 (1R,2R)-2-N-myristoylamino-1-(4-nitrophenyl)- 1,3-propandiol (D-NMAPPD)

D-NMAPPD is a potent inhibitor of acid ceramidase (Raisova et al. 2002). Fibroblasts were grown in medium containing 5μM D-NMAPPD for 48 hours at 37°C in a humidified incubator with 5%CO₂ before being live staining and imaging.

2.8.11 TPEN, heavy metal chelator

TPEN is a membrane-permeable heavy metal chelator with very high affinities for Fe^{2+} and Zn^{2+} (Ollig et al. 2016). Cells were incubated in medium containing $10\mu\text{M}$ TPEN for 3 hours at 37°C before Phengreen staining was undertaken as described (Section 2.4).

2.9 Exogenous supplements

2.9.1 Incubation of cells with exogenous sphingolipid

The ceramide trihexosides (globosides) were purchased from (Matreya LLC, State College, US), and stored as a 2 mM stock in ethanol/DMSO at -20°C . Cells were incubated in medium containing $40\mu\text{M}$ of the indicated sphingolipid for 48 hours at 37°C in a humidified incubator with 5% CO_2 , before live or fixed staining and subsequent imaging. Vehicle treated cells were grown in the same volume of ethanol/DMSO without sphingolipid.

2.9.2 Incubation of cells in exogenous lyso-lipid

The lysolipids Lyso-Monosialoganglioside GM1, psychosine, lyso-ceramide trihexoside (lyso-globoside/lyso-Gb3) and sphingosine were purchased from Matreya LLC and lyso-sphingomyelin was purchased from (Cambridge Bioscience, Cambridge, UK) and stored as a 2 mM stock in ethanol/DMSO at -20°C . Cells were incubated in medium containing $2\mu\text{M}$ of the indicated lysolipid for 48 hours (sphingosine 24 hours) at 37°C in a humidified incubator with 5% CO_2 , before live or fixed staining and subsequent imaging by fluorescence microscopy as described (Section 2.4). Vehicle treated cells were grown in the same volume of ethanol/DMSO without lysolipid.

2.10 Fixed staining

2.10.1 Ganglioside GM1 staining using FITC-CtxB

Ganglioside GM1 was stained in fixed cells using FITC-CtxB (Hansson et al. 1977). Fibroblasts were fixed in 4% paraformaldehyde, incubated in blocking buffer containing $1\mu\text{g/ml}$ CtxB at 4°C overnight, and washed three times in DPBS. Imaging was carried out at 470nm excitation, 520nm emission (FITC channel) as described (Section 2.4).

2.10.2 Cholesterol

Cellular cholesterol was stained using filipin, which is a naturally occurring blue fluorescent polyene antibiotic with high affinity for cholesterol (Bergy and Eble 1968). Cells were fixed in 4% paraformaldehyde, incubated in DMEM containing 187.5 µg/ml filipin for 30 minutes in the dark at room temperature, and washed once in complete medium and then 3 times in DPBS. Filipin was imaged at 380nm excitation, 460nm emission (DAPI channel) as described (Section 2.4).

2.10.3 Nuclear staining

To identify and count cells, nuclei were stained for imaging using Hoescht 33342 (Invitrogen), a membrane permeant blue fluorescent DNA binding probe. Live or fixed cells were incubated in DPBS containing 2µg/ml Hoechst 33342 for 10 minutes in the dark at room temperature and washed before imaging. Hoechst was imaged at 380nm excitation, 460nm emission (DAPI channel) as described (Section 2.4).

2.10.4 Autofluorescence assessment

Fibroblasts were fixed in 4% paraformaldehyde for 10 minutes and imaged at 470nm excitation, 520nm emission (FITC channel) across a range of camera exposures (10ms, 50ms, 100ms, 200ms, 500ms and 1000ms). If autofluorescence was observed, any imaging that required a probe that emits fluorescence in the 490-530nm range was done conducted at exposure times that were substantially lower than those at which I observed autofluorescence as described (Section 2.4).

2.10.5 Mounting of coverslips

A drop of fluoroshield mounting medium (Sigma Aldrich) was added to a microscope slide and the coverslip carefully mounted to avoid trapping air bubbles. Coverslips were left to dry overnight in the dark at room temperature before imaging.

2.11 Inductively-coupled plasma mass spectrometry for trace metal analysis

2.11.1 Sample preparation

Fibroblast cell pellets were prepared as in section 2.7.1, and lymphoblast cell pellets obtained by centrifugation at 800 g for 5 minutes of cell suspensions, rinsing in DPBS twice, and further centrifugation at 800 g at 5 minutes. Dry pellets were kept at -80°C. Serum was collected in

metal-free tubes (BD Vacutainer™) and blood samples were collected in EDTA-containing tubes. CSF samples were kept in clean CSF storage tubes at -80°C.

2.11.2 Trace element analysis

Samples were analysed using inductively-coupled plasma mass spectrometry (ICP-MS) at the Department of Medical Biochemistry and Immunology, University Hospital of Wales. Briefly, serum, CSF and blood samples were diluted in a trace elements diluent containing Triton X-100, Isopropanol, HNO₃, Scandium, Gallium, Germanium, Iridium and Indium as internal standards. The sample was heated at 90°C for 20-60 minutes ensuring that over-heating was avoided to maintain the trace elements content. This was followed by cooling of the sample and measurement of its dry weight. 50% HNO₃ was added to the dry tissue, and microwave digestion used to complete the sample digestion. The samples were then diluted in the trace elements diluent and subjected to analysis using an Agilent 7700 Inductively-Coupled Plasma Mass Spectrometer (ICP-MS), with the ASX 500 Autosampler (Sampson 2004).

2.12 Electron microscopy analysis of patient fibroblasts

2.12.1 Conventional method (Epoxy resin embedding)

Fibroblasts were cultured in 75 cm flasks. At 90% confluency, the medium was removed and cells fixed in electron microscopy fixative (0.5% glutaraldehyde in 0.2 M HEPES buffer, pH 7.2) for 15 minutes at room temperature. Cells were scraped into a microcentrifuge tube and pelleted by centrifugation at ~ 10,000 g for 30 minutes. The fixative was removed, and pellets were washed three times for 10 minutes with 0.1 M sodium cacodylate. Cells were post-fixed in 1% osmium tetroxide in ddH₂O and 0.1 M sodium cacodylate for 30 minutes, before addition of osmium ferrocyanide (1.5% potassium ferrocyanide and 1% osmium tetroxide) for a further 30 minutes, and three 10-minute cycles of 0.1 M sodium cacodylate buffer. Samples were then dehydrated through an ethanol series (30, 50%, 70% and 90%) for 10 minutes each and two 20 minute incubations in 100% ethanol. Samples were then washed twice for 5 minutes in propylene oxide, incubated in 50% Durcupan ACM embedding mixture (Sigma Aldrich, MO, USA), made according to manufacturer's protocol, in propylene oxide for 1 hour, and embedded in 100% Durcupan ACM embedding mixture overnight in a slow rotator. The following day, this was changed to fresh Durcupan for 1 hour. Further fresh Durcupan was added to the labelled capsule for embedding, followed by overnight polymerisation at 60-70°C. Sections 50–80 nm thick were cut on a Reichert OMU4 ultramicrotome (Leica Microsystems (UK) Ltd, Milton Keynes), stained with lead

citrate for 10 minutes, then washed in ddH₂O. Images were recorded (St Andrews, UK) on a JEOL 1200EX transmission electron microscope fitted with an Orius 200 digital camera (Gatan; Abingdon, UK).

2.12.2 Cryo sectioning technique for immuno-EM

This method was modified from (Tokuyasu 1980). Monolayer culture cells were fixed in their culture flasks in 0.2M HEPES, pH 7.2, containing 0.05% glutaraldehyde and 4% paraformaldehyde for 30 minutes. Cells were scraped into a microcentrifuge tube and pelleted by centrifugation at ~ 10,000 g for 30 minutes. Cell pellets were incubated in DPBS for 1 hour, followed by a 2.1M sucrose solution for 20 minutes, transferred to a cryo-EM grid and immediate freezing in liquid nitrogen. Sections were cut on a Leica EM FC7 cryo-ultramicrotome using a diamond knife at low temperatures (-80°C to -110°C). After trimming of the samples, a section was picked up using a wire loop with a droplet of frozen 2.1M sucrose and 2% methyl-cellulose. It was placed on a transmission electron microscope specimen grid (carbon film), and washed four times for 3 minutes with ddH₂O on ice, which is better for removing methyl-cellulose as it is more soluble in cold conditions. Sections were blocked in FSG (0.5% fish skin gelatine) for 10 minutes, and incubated at the indicated concentrations of primary antibody (Table 2.4) in a blocking solution for 20 minutes at room temperature. Sections were washed on droplets of DPBS (3X 5 min), incubated with rabbit anti-mouse immunoglobulin (an intermediate antibody) diluted in a blocking solution for 20 minutes. After a further three washes in DPBS, sections were incubated with Immunogold conjugated protein A, 10nm, (BBI Solutions) (1 in 50 in FSG) for 20 minutes. Sections were washed three times with DPBS (5 min each), followed by further three washes with ddH₂O (1 min each), before staining with 100µl of 3% uranyl-acetate in 90µl of 2% methyl-cellulose for 10 minutes. Sections underwent a final three washes in DPBS (4 min each) and were left to dry before imaging.

Table 2.4 Primary and secondary antibodies used in immuno electron microscope cryosection labelling.

Primary antibody	Dilution	Host	Intermediate antibody
LAMP-1 (mouse) H4A3 (Developmental Studies Hybridoma Bank, Lowa, USA)	Neat	Mouse	Rabbit Anti-Mouse IgG(H+L)- UNLB SouthernBiotech (Alabama, USA)
LAMP-2 (human) H4B4 (Developmental Studies Hybridoma Bank)	Neat	Mouse	
Anti-GM2 Monoclonal Antibody (Clone: MK1-16) (Tokyo Chemical Industry Co, Japan)	1:100	Mouse	
Anti-Gb3 Monoclonal Antibody (Clone:BGR23) (Tokyo Chemical Industry Co)	1:100	Mouse	

2.13 Biological samples

Controls (whole blood EDTA, dry blood spot) were obtained from the Cardiff biobank (Research ethics committee reference number: 18/WA/0089). Age of donors: 27, 37, 55, 56 and 59 years. The CLN5 patient samples (blood, serum, dry blood spot) were obtained from the Nottingham Children's Hospital (ethics approval reference number; NIH NO: 702756409).

2.14 Statistical analysis

Data were analysed using GraphPad Prism to determine statistical significance using one-way ANOVA with Bonferroni post-hoc testing, unless otherwise specified. Fluorescent signals were quantified using Image J unless specified otherwise.

2.15 Measuring cell fluorescence

2.15.1 Thresholding and distributional analyses of images

After fluorescence microscopy imaging, the area of punctate staining was measured using ImageJ analysis software (NIH, Bethesda, USA) (Schneider et al. 2012). A threshold was selected to cover the lysosomal area without selecting the nucleus. Particles below 0.0005 inches² were excluded to remove speckles and noise. The total area value was then divided

by the number of cells in the image to obtain the average. These measurements were repeated for all the different experiments to obtain the final data set for statistical analysis.

2.15.2 Corrected total cell fluorescence (CTCF)

CTCF was analysed using image J. Using selection tools, the cell of interest was selected and, using the set measurements, the area, min & mix gary value, integrated intensity and mean gary value were determined. These measurements were entered in an Excel sheet. The selected background area from the same image as well as intensity measurements were recorded in the Excel sheet. Then, the below formula was used to determine the CTCF.

CTCF= Integrated density – (area of selected cell x mean background fluorescence).

2.15.3 Co-localisation analysis

Co-localisation analysis was carried out using image J. Lines were drawn across the longest axis of the cell and plot profiles were generated displaying fluorescence intensity of puncta across the line. Line selections were copied into the second image of staining, and plot profiles were again generated. Raw data of plot points from both images were entered into an Excel sheet and a graph was generated showing fluorescence signal/intensity of two stains across the same line in the cell. Co-localisation was determined by peaks present in the same plot points in both images.

Chapter 3: A simple fluorimetric test for late endosomal and lysosomal swelling as a means to identify, monitor the effectiveness therapies for all lysosomal storage diseases.

3.1 Introduction

Lysotracker, a fluorescent marker of acidic late endosomes and lysosomes, has been widely used in the LSD research field. In particular, it has been used in clinics for biochemical monitoring of lysosomal volume in isolated circulating B cells from the blood of NPC1 patients treated with miglustat (te Vruchte et al. 2014). It has also been used to show LE/ Lys expansion in 13 LSD patient primary fibroblasts (Xu et al. 2014). There has, however, been several discrepancies in lysotracker optimisation conditions (Cao et al. 2006; Fossale et al. 2004; Xu et al. 2014) and interestingly there has not yet been a study looking at the suitability of lysotracker and similar probes that are applicable across all LSDs. I have therefore decided to 1) investigate the various methods and conditions that can be used to measure LE/Lys expansion with lysotracker and; 2) investigate the possibility of developing the most suitable method into a high throughput approach that can be used in clinical diagnosis, for monitoring or screening, and for developing new drug treatments.

3.1.1 Expansion of late endosomal and lysosomal compartments is a common feature across LSDs.

In recent years, the lysosomal system has emerged as a key component in regulating many cellular functions such as plasma membrane repair, metabolic signalling, cell migration, cell adhesion, etc. (Ballabio 2016; Pu et al. 2016). The biological importance of the lysosomal system is characterized by the occurrence of multiple LSDs (Vitner et al. 2010). There are two well described acidic compartments in the late endocytic system, namely, late endosomes/multi-vesicular bodies and lysosome, there are likely others but not well defined.

Lysosomes are 2-3% of cellular volume with different sizes, shapes, and numbers. They range between 0.1–1.2 μm in diameter (Alberts 2017). Highly active phagocytosing cells, such as macrophages, are composed of a larger volume of lysosomes in comparison to most other cells, which are needed for phago-lysosome clearance of infection (Steinman et al. 1976; Lüllmann-Rauch 2005). The macrophage phagolysosome is a result of late phagosome to lysosome fusion and is characterised by acidic pH (4–4.5) (Lüllmann-Rauch 2005). In case of lysosomal storage of nondegraded material in any cell type, the frequency and size of lysosomes increase (Lüllmann-Rauch 2005). They also increased in conditions of overloading

with non-physiological material such as saccharose, dextran, enzyme inhibitors, or drugs such as lysosomotropic amines that inhibit the lysosomal digestion of certain materials (Lüllmann et al. 1978; Lüllmann-Rauch 2005).

The essential function of the LE/Lys compartment is the catabolism and recycling of cellular substances (Luzio et al. 2007). As previously mentioned in detail in chapter 1, the lysosome's function is typically impaired by an inborn error in metabolism. There is increasing evidence of impairment in diseases of ageing as well, e.g. Parkinson disease (*GBA1* and *ATP13A2*) and Alzheimer disease (Cox and Cachón-González 2012). LSDs are the result of defects in the degradation of either GAGs, sugars, lipids, or proteins. Despite the distinct forms of storage molecules in different LSDs, they nevertheless share several common biochemical and cellular features (Vitner et al. 2010). Lysosomal function is also impaired by defects in transport across the lysosomal membrane, abnormalities in ion signalling or by abnormalities in endosome-lysosome trafficking. These defects in lysosomal degradation, signalling and transportation are common features of LSDs (Platt et al. 2012). Due to all of these features, perturbed lysosomal function can lead to swelling caused by storage of lysosomal substrates, impaired ion homeostasis, or impaired fusion and fission of endo-lysosomes. Expansion in the LE/Lys compartments, that increases either the number or the size of the lysosomes, ranges from >1% to as much as 50% of the total cellular volume (Meikle et al. 1997). As a result, the LE/Lys increase in volume provides a potential universal biomarker of LSDs.

3.1.2 Targeting and visualising the late endosomal and lysosomal compartments with fluorescent probes

The acidic environment in the lysosomes (~pH 4-5) can be stained and tracked after cells have been subjected to various constructs expressing fluorescently stained proteins e.g. GFP-LAMP1 or to low molecular weight fluorescent probes e.g. lysotracker (Pierzyńska-Mach et al. 2014). In fixed cells, antibodies are used against a variety of lysosomal proteins, enabling the lysosomes to be visualised by immunofluorescence. In general, the lysosome protein content is ~50% comprised of LAMP-1 (Igp 120) and LAMP-2 (Igp 110), which are proteins residing in the limiting membrane of lysosomes. LAMPs are ubiquitous to most lysosomes and lysosome related organelles (Fukuda et al. 1988; Mane et al. 1989) and comprise the glycocalyx of the lysosome. With regard to the use of fluorescence techniques, the unique acidic pH of lysosomal compartments has nowadays become of interest for developing sensitive probes to measure lysosome acidification which has been reported in several human diseases including Alzheimer's (Colacurcio and Nixon 2016; Lloyd-Evans and Haslett 2016). There is now a whole variety of commercially available fluorescence probes (Table 3.1) that are

associated with the acidity of organelles (e.g. lysosensor yellow/blue dextran), have the ability to track endocytosis (e.g. Oregon Green–avidin and biotin-dextran for endosome-lysosome fusion (Lloyd-Evans et al. 2008) and lysosomal localization and number (e.g. lysotracker). The various strategies for fluorescence detection that are discussed below have been used to label lysosomes in living cells.

(1) Substrates for lysosomal hydrolytic enzymes: these were predominantly developed as fluorescent reporters which are generated following substrate hydrolysis. Examples of typical lysosomal hydrolytic enzyme substrates are FITC-labelled or BODIPY-labelled casein. Both have only been used to view lysosomal enzyme activity but not for lysosome imaging (Jones et al. 1997; Twining 1984). Also, the Magic red cathepsin substrates are cleaved in the presence of active cathepsins (Pryor 2012). Furthermore, inhibitors of lysosomal enzymes which are fluorescent and bind the active site, thus reporting the localisation of active enzymes, e.g. BODIPY-pepstatin (cathepsin D). An advantage of these probes is that they report lysosomes which are metabolically active, but are not always specific to lysosomes (Chen et al. 2000).

(2) Soluble fluorescent probes, such as dextrans, which are endocytosed to lysosomes, have been used to evaluate the distribution of the lysosomal compartment, intra-lysosomal pH and also intra-lysosomal Ca^{2+} levels (Christensen et al. 2002). Endocytosed fluorescent probes, such as FITC-dextran, have been used to determine the intra-lysosomal pH in living cells. However, since the concentration of the dextran probes accumulating in lysosomes through endocytosis cannot be precisely defined other than via incubation time, it is therefore absolutely necessary to include non-pH or Ca^{2+} sensitive dextrans (e.g. rhodamine dextran) and to subsequently carry out lysosomal labelling using independent verification (e.g. antibodies) to confirm compartment localisation (Brandt 1978).

(3) Acidotropic fluorescent probes are those such as lysotrackers, lysosensors, etc. These basic amine probes have been used as they accumulate in acidic organelles, such as lysosomes, because their pKa value is closer to the lysosomal pH resulting in retention of these molecules within the acidic compartments. The Acidotropic probes have different pKa values, and the low pKa means they are nonfluorescent except when trapped inside the acidic organelles. Therefore, it may decrease the specificity of those fluorescent probes to only active lysosomes (Chen et al. 2015).

Table 3.1 The weaknesses of fluorescent probes commonly used for late endosomal and lysosomal compartments

Fluorescent probe	Weaknesses
Quinacrine	Has a high affinity to incorporate into DNA and RNA. Loading leads to the swelling of lysosome and rupturing was also observed over long incubation times (Caspersson et al. 1970; Comings et al. 1975; Pierzyńska-Mach et al. 2014).
N-(3-[2,4-dinitrophenyl amino] propyl)-N-(3 aminopropyl)methylamine (DAMP)	It is not fluorescent meaning that either fluorophore or antibody must be added to stain the acidic vesicles (Yapici et al. 2015).
Acridine orange	Phototoxic, limited fluorescence. The red signal bleaches quickly and demonstrates phototoxicity when related to the generation of reactive oxygen species (ROS). Also incorporates into DNA (Darzynkiewicz and Kapuscinski 1990; Kapuscinski and Darzynkiewicz 1987).
Neutral red	Less sensitive; it is usually used as a viability screening test (Repetto et al. 2008).
Cresyl violet	It needs to be used in high concentrations ~1 μ M. The protonation of such high concentrations of the probe may alter the luminal pH of lysosomes (Ostrowski et al. 2016).
LysoSensor	Produces a significant pH-dependent increase in fluorescence intensity when acidification occurs, cannot be used to monitor lysosomal swelling under conditions of changes in pH (Ma et al. 2017).
LysoTracker	Photobleaches and LysoTracker red is reported to undergo photoconversion to green (Freundt et al. 2007).

Most studies have utilised lysotracker, probably the most commonly used research probe for selective acidic compartment loading, as a LE/Lys marker to determine endolysosomal structure and for co-localisation studies (Pierzyńska-Mach et al. 2014; Yapici et al. 2015). Furthermore, these lysotracker probes have minimal cell toxicity, and they do not appear to alter cell function (Pierzyńska-Mach et al. 2014). Lysotracker probes, also reveal significantly independent fluorescence from the compartment pH. The underlying mechanism of lysotracker is fairly well understood: lysotracker is freely transmitted into LE/Ly by crossing the lipid bilayers of the plasma membrane and acidic organelles by diffusion. Once there it is trapped as a result of its pKa properties meaning that once protonated in the acidic milieu of the lysosome it remains protonated and cannot exit the lysosome (Duvvuri et al. 2004; Pierzyńska-Mach et al. 2014). It emits fluorescence at a single wavelength, which means any changes in the fluorescence intensity reflects a change in number or size of lysosomes (Guha et al. 2014). Lysotracker has been used as a pH probe (Rahman et al. 2016). However, lysotracker is not sensitive enough to detect small changes in lysosomal pH; it is proposed to only be able to detect large shifts in pH (Avrahami et al. 2013).

3.1.3 Lysotracker use in diagnosis and monitoring

The first clinical study reporting the use of lysotracker was a case report monitoring the first provision of miglustat treatment in one adult onset NPC patient. Across the course of the treatment, peripheral blood B lymphocytes (which are long-lived in the blood) were isolated from the patient using magnetic cell separation, loaded with lysotracker and fluorescence activated cell sorting (FACS) was used for fluorescence measurement (Lachmann et al. 2004b). Following 12 months miglustat treatment, lysotracker green staining was reduced to near-normal levels, representing a decrease in lysosomal lipid storage that mirrored reduced ganglioside GM1 levels that were determined by cholera toxin binding (Lachmann et al. 2004b; te Vrugte et al. 2014). This study was the first to report the use of lysotracker for clinical monitoring purposes. A follow up study by the same group of researchers demonstrated the effectiveness of peripheral blood circulating B cells to quantify lysosomal storage in various lysosomal storage disease mice with a clear increase in lysotracker fluorescence correlating to increasing lipid storage over the lifespan of the *Npc1*^{-/-} mice (te Vrugte et al. 2014). In a further study of 106 NPC patients, 38 patients were analysed before and after miglustat treatment, lysotracker fluorescence in circulating B cells was reduced in response to miglustat therapy. Again, the FACS method was used combining lysotracker with anti-CD19 monoclonal antibody conjugated to PE to determine lysosomal volume whilst selecting for the B cell population (te Vrugte et al. 2014). This study also showed that lysotracker fluorescence correlated with NPC disease progression. In the same study, lysotracker fluorescence was

also used to evaluate bone marrow transplantation efficacy on peripheral lysosomal storage in an NPC2 patient; lysotracker fluorescence in circulating B cells was reduced 1 month after BMT and was within the normal reference range 3 months after BMT. These data raised the possibility of using this biomarker in the clinical monitoring of NPC (te Vruchte et al. 2014). The clinical value of using lysotracker as a monitoring tool became evident in NPC patient samples analysed post 2-hydroxypropyl- β -cyclodextrin (HP β CD) treatment. The B cells of patients treated with HP β CD showed a higher level of lysotracker fluorescence (lysosomal storage) when compared to pre-treatment (te Vruchte et al. 2014), suggesting that HP β CD only serves to move stored lipids from the central nervous system (CNS) to the periphery. In addition, the circulating B cells of two Tay-Sachs disease patients also showed an elevation of lysotracker compared to the age matched control range (te Vruchte et al. 2014).

Xu *et al.* (2014) used lysotracker red to measure lysosomal storage in patient skin fibroblasts derived from a range (but not all) of the LSDs. They demonstrated the use of lysotracker as a simple LSD drug screening platform validated by reduction in lysosomal storage in NPC1 fibroblast cells using methyl- β -cyclodextrin treatment (Xu et al. 2014). However, a note of caution as in this study not only do they focus on the rapidly photobleached lysotracker red but it is also unclear as to whether they fixed the cells prior to fluorescence measurement. In other studies where lysotracker red has reportedly been fixed a much higher concentration of lysotracker has been necessary in order to see residual fluorescence after fixation (Cao et al. 2006; Fossale et al. 2004). Of further concern to the outcomes of this study is the study reporting that lysotracker red photoconverts to green (Freundt et al. 2007). The Xu *et al.* (2014) study also showed a discrepancy in the number of patient cells positive for elevated lysotracker staining between the plate reader quantification and fluorescence microscopy imaging, potentially caused by a lack of accurate optimisation or standardisation. In addition, the study only used 17 LSD primary patient fibroblasts and no associated age range for the controls, with >60 LSDs it is clear that a greater range of patient fibroblast should be studied in order to optimise lysotracker as a broad screening and/or monitoring tool for these diseases.

With regard to the previous studies, it can be said that the lysotracker probe was not fully optimized and the mechanism by which lysotracker loads into lysosomes remains to be fully understood. As is always the case with rare diseases, large cohorts of patient biological samples do not always exist, and, as a result, the role of the lysotracker in diagnosis and disease/therapy monitoring for a broad spectrum of LSDs has not been fully defined.

3.1.4 Appropriateness of cell lines commonly used in LSD research

3.1.4.1 Primary LSD patient skin fibroblasts

The diagnostic examination of LSDs invariably involves fibroblasts to investigate certain accumulated macromolecules, sometimes even being directly used to diagnose LSDs, as was the case with the filipin test for NPC (Vanier and Millat 2003; Wenger et al. 2003). Primary fibroblast cells have been used to characterise particular enzyme deficiencies in single LSDs (Otomo et al. 2011; Wenger et al. 2003). Fibroblast cells from patients have been invaluable in studying underlying fundamental cellular dysfunction, such as impaired Ca^{2+} or organelle function, as the cell size, signalling machinery and membrane potential are highly regulated in fibroblasts. However, skin fibroblast cells do not model everything; they are unsuitable to study a variety of physiological signals associated with excitable cells, e.g. neuronal excitotoxicity (Auburger et al. 2012; Connolly 1998; Kálmán et al. 2016).

The metabolism of skin fibroblasts in cultures is different from that of affected tissues *in vivo*. A decrease in GCCase enzyme activity has been observed in Gaucher disease patient fibroblasts and macrophages. However, in these two cell lines, GlcCer the substrate of GCCase, only accumulates in macrophages. The residual enzyme activity in fibroblasts, coupled with lower levels of synthesis of GlcCer, appears to maintain normal intracellular lipid homeostasis (Sillence et al. 2002). Another example is the mucopolysaccharidoses, it has been shown that there is no such production in large amounts, and hence no storage, of keratan sulphate in fibroblasts, which is considered to be the main stored substrate in MPS IVA (Hollister et al. 1975). It can be assumed that skin fibroblasts may not always provide a perfect model for certain LSDs. Therefore, even with the presence of some limitations in patient primary skin fibroblast cell lines, they remain one of the most powerful models for LSD characterization.

3.1.4.2 B-lymphoblastoid cell lines

It is extremely challenging when carrying out any biomedical research to get the required cells or DNA just from a single source. The use of B-lymphoblastoid cell lines (B-LCLs) has resulted in an acceleration of clinically related biological research, which has resulted in considerable success in recent decades. These B-LCLs have now replaced peripheral blood mononuclear cells (PBMCs) that were used before in biological investigations resulting in a considerable increase in biomedical research, especially as they are the starting point for creating induced pluripotent stem cells. The transfection of peripheral blood B lymphocytes with the Epstein Barr virus (EBV) is used to transform primary patient B cells into immortalised B-LCLs (Neitzel 1986).

The validity of B-LCLs as an experimental model has been shown for several LSDs such as Niemann-Pick disease, Tay Sachs, Sandhoff and MPS I (Levade et al. 1985; Maret et al. 1985; Minami et al. 1977). B-LCLs have several benefits compared to fibroblasts. They have fast proliferation capability, growth in suspension, and as such more cell material can be obtained. B-LCLs have been used to study lysosomal enzymatic activity such as β -gal, GCase, α Gal A, α -Glu and α -L-iduronidase (IDU), and they were used to show there are no changes in enzyme activities cryopreserved for 1 year compared to freshly prepared B-LCLs (de Mello et al. 2011; De Mello et al. 2010; Mello et al. 2006)

3.1.5 Aims

- 1- Due to the high number of discrepancies in the use of lysotracker in the literature, therefore the research was carried out I decided to investigate the mechanisms by which they load into lysosomes. This was achieved by investigating in depth the factors that may affect the efficacy of these probes.
- 2- Using this knowledge, I aimed to develop a high throughput 96-well lysotracker-based fluorimetric test to investigate lysosomal storage across a large panel of patient fibroblasts spanning almost all of the LSDs.
- 3- I aimed to study the ability of lysotracker as a tool to monitor responses to treatment to see if it could be further used for either drug screening or clinical monitoring.
- 4- I also investigated whether it was possible to adapt the assay for 96 well plates in a clinical setting based on magnetic capture of circulating CD19+ B cells and whether this would be suitable in any clinical laboratory for LSD monitoring.

3.1.6 A brief summary of the methods used

In Sections 3.2.1 I used primary fibroblast obtained from healthy control and NPC1 patients to optimise the different lysotracker probes (blue, green, and red) by using different versions and concentrations of lysotracker (see chapter 2 section 2.6.1.1).

In Sections 3.2.2 the chosen lysotracker probes (green and red) were investigated further to determine if fixed or live conditions are more appropriate for those probes.

In Sections 3.2.3 were study the photostability of lysotracker probes (green and red).

In Sections 3.2.4 I decided to study the effect of the incubation time and concentration of lysotracker on intralysosomal pH. I used a combination of Texas Red-Dextran and FITC-Dextran for the pH measurement (see chapter 2, section 2.6.3).

In Sections 3.2.5 I investigated how lysotracker loads into and fluorescently labels the lysosome. I used healthy control fibroblasts that had been treated with different drugs (see chapter 2 section 2.8) to modify lysosomal function so as to determine how lysotracker loads into LE/Lys. LAMP2 was used here as an LE/Lys marker to confirm the lysotracker findings and filipin was also used to confirm cholesterol accumulation.

In Sections 3.2.6 I induced autophagy in healthy control fibroblast and studied the effect of autophagy on lysotracker signal. Cyto ID (see chapter 2, section 2.6.4) was used here to monitor autophagy.

In Sections 3.2.7 the conditions for miniaturizing lysotracker into a 96 well format is described (chapter 2, section 2.6.1.2). I used healthy control and NPC1 patient fibroblasts to investigate the appropriate cell count so as to measure the greatest differences between healthy control and the disease cells. I compared cell counts, BCA protein assay, or Hoechst as ways to standardise the experiments.

In Sections 3.2.8 I went on to test the chosen conditions on almost all the LSD fibroblasts to evaluate lysosomal expansion. Furthermore, to determine the potential power of this method, I compared the ease and reliability of the plate reader methods against fluorescence microscopy imaging.

In Sections 3.2.9, I have used a LAMP2 lysosomal marker (chapter 2 section 2.5) to show the correlation between the lysotracker and lysosome expansion in some LSDs.

In Sections 3.2.10 I treated healthy control fibroblast and NPC1 with miglustat and compared the lysotracker output in order to monitor the drug treatment and compare against the lysosomal markers (LAMP1 and LAMP2).

In Sections 3.2.11 I investigated lysotracker across B-LCLs healthy controls and NPC1 patients treated with 2% DMSO and untreated. In this investigation I used microscopy for imaging, FACS (see chapter 2, section 2.6.2.2) and 96 well plates for the magnetic capture of circulating CD19+ B cells (see chapter 2, section 2.6.2.3).

In Section 3.2.12, I have used B-LCL healthy controls and a few LSDs to compare the FACS and magnetic cell capture as a method to determine the lysosomal storage.

3.2 Results

3.2.1 Lyotracker loading into cellular lysosomes is dependent upon lyotracker concentration.

Lyotracker probes are suitable for multicolour applications because of their presence in various fluorescent colours with differing fluorescence spectra (422 nm, 511 nm, 535 nm, 590 nm) and different structures. Lyotrackers typically contain numerous aromatic rings with positively charged nitrogen at acidic pH (Figure 3.1 A & C & E) (Zhitomirsky et al. 2018). I thus began to investigate further the properties of these different types of lyotracker. There are four lyotracker probes commercially available, namely, blue, green, yellow and red. This study excluded the yellow one due to its spectral overlap with lyotracker green and the need for specific YFP filters on the microscope. It was found that these dyes exhibit different sensitivities when staining healthy control fibroblast compared to when staining large lysosomes in NPC patient fibroblasts. The cells were stained with lyotracker probes in the indicated concentration for 15 min at 37°C and imaged on the Zeiss Colibri LED microscope. Lyotracker blue fluorescence is extremely weak and required a higher than 1 µM concentration and potentially longer incubation time to be observed (Figure 3.1 B). However, the green and red lyotracker stained punctate structures within the cells at lower concentrations (50-200 nM) with clearly visible fluorescence (Figure 3.1 D & F). Lyotracker green seemed to be most suitable for use with visible punctate fluorescence at the lowest concentration range (100 nM – 500 nM) (Figure 3.1 D). However, with 100 nM the lysosomes were only weakly stained and such a concentration would not have been capable of detecting a slight decrease in lysosome enlargement, for example in response to experimental therapies or treatments in patient (Figure 3.1 D). On the other hand, at 500 nM the lysosomes were highly saturated, and such a saturating concentration would not indicate any worsening of the disease process in patients (Figure 3.1 D). Furthermore, the red lyotracker, unlike the green, showed differences between control and NPC1 fibroblasts at 50nM (Figure 3.1 F). However, 200 nM is a suitable concentration as well for lyotracker red because it does not saturate within the enlarged lysosomes and the healthy control cells can be clearly seen (Figure 3.1 F). Hence, it was concluded that lyotracker green and the lyotracker red dyes were the most suitable for detecting and staining control lysosomes and the enlarged lysosomes in NPC fibroblasts at a concentration of 200 nM. I therefore used this concentration for our further investigations.

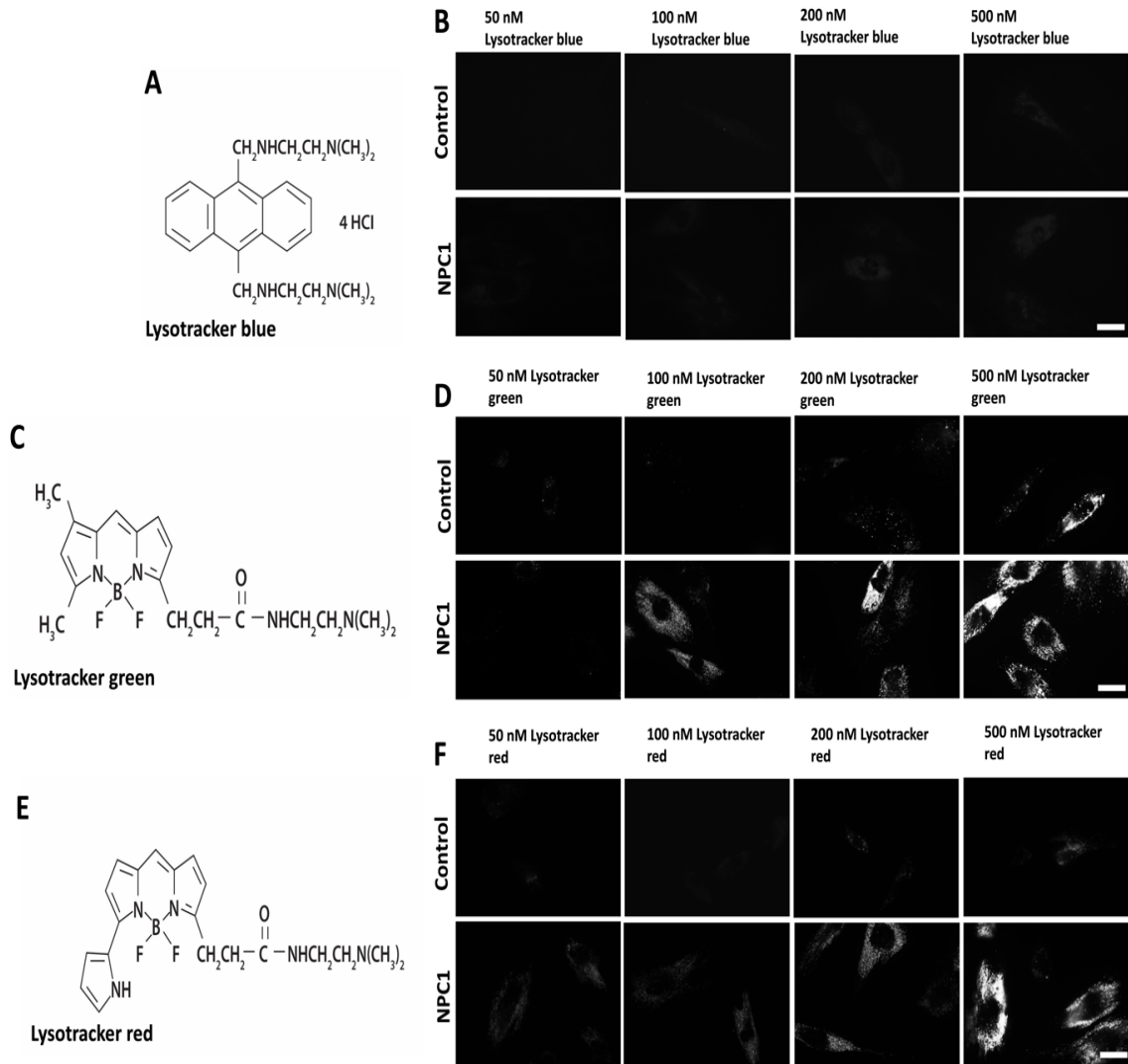


Figure 3.1 Concentration dependent loading and fluorescence signal of different lysotrackers in control and NPC1 patient fibroblasts.

(A) The molecular structure of lysotracker blue, (C) green and (E) red. (B, D & F) Healthy control fibroblasts (GM05399) and NPC1 patient fibroblasts (GM03123) loaded with the indicated concentrations of lysotracker blue, lysotracker green or lysotracker red at 37°C for 15 min, with scale bars of 10 µm, n=3.

3.2.2 Neither lysotracker green nor lysotracker red can survive fixation

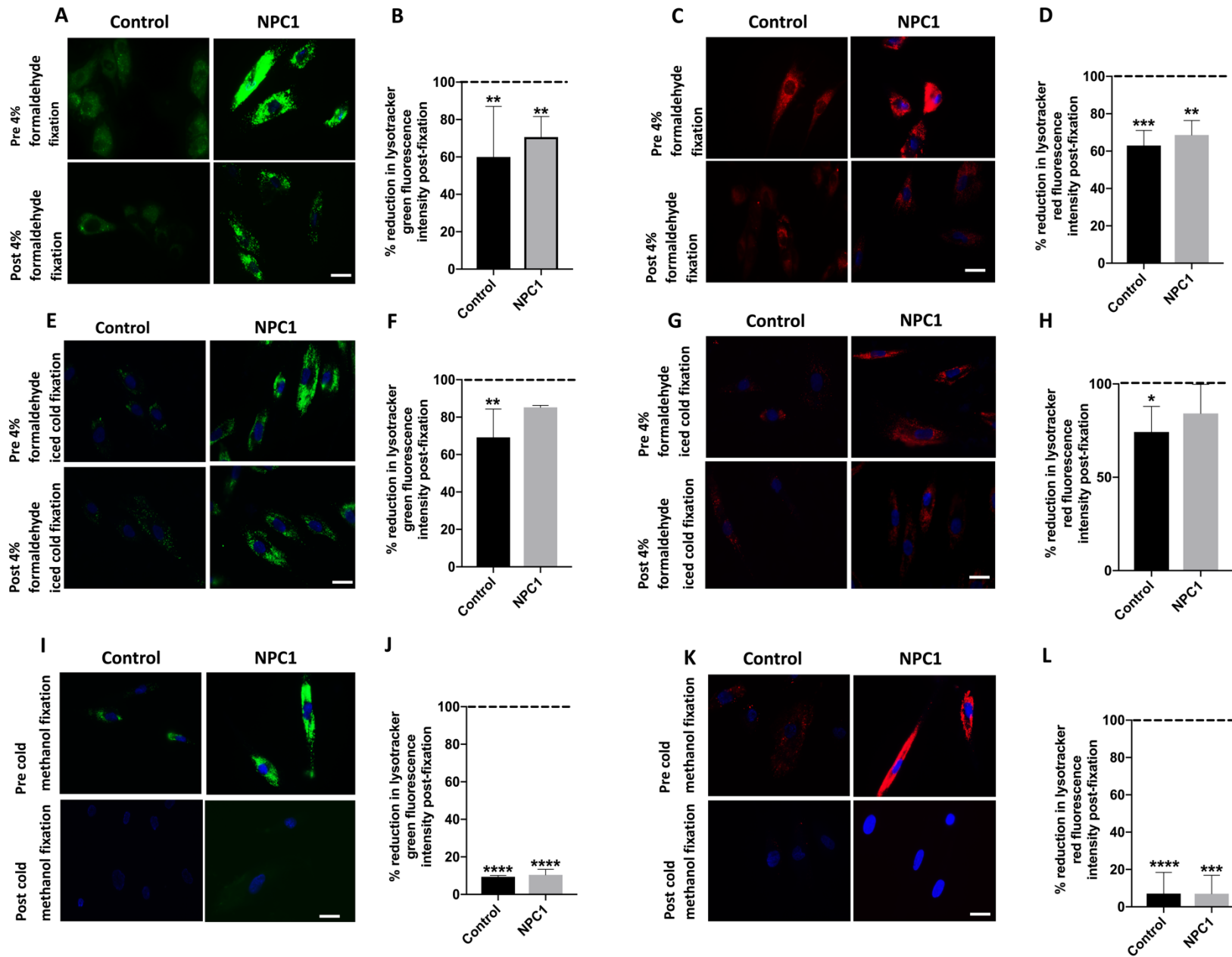
In order to optimize the method and improve our understanding about the appropriate conditions for loading lysotracker into the LE/Lys compartments, I evaluated the fixation steps that have been widely used for lysotracker imaging in research (Cao et al. 2006; Fossale et al. 2004; Xu et al. 2014). The ability to visualise lysosomal staining with lysotracker in fixed cells has been reported by various laboratories (Miyagawa et al. 2016; Otomo et al. 2011) allowing these researchers to use additional specific probes, such as antibodies, to label lysosomes and other structures to study colocalization or in the case of drug screening allow plates to be re-measured.

The effect of various fixatives and conditions on lysotracker fluorescence and localisation has been investigated. Paraformaldehyde (4%, room temperature or ice cold) and ice cold methanol are the most common fixatives being used in research. I first tested the impact of 4% paraformaldehyde at room temperature and observed a loss of about ~30-40% of the lysotracker fluorescent signals from either green or red probes (Figure 3.2 A-D). In contrast, 4% ice cold paraformaldehyde minimizes the significant loss of the fluorescent signal with a smaller 10-35% reduction in either the lysotracker green or the red signals (Figure 3.2 E-H). However, with cold-fixation, there appears to be a difference in lysotracker retention, especially with lysotracker green, when comparing pre and post-fixation between control (35% reduced compared to untreated) and NPC1 (20% reduced), suggesting the potential that cold-fixation could incur artefactual increases in differences between control and LSD cells (Figure 3.2 E-H). Finally, one of the most common fixatives is ice cold methanol. However, fixation with ice cold methanol led to a 90-95% signal loss in cells loaded with either the lysotracker green or red (Figure 3.2 I-L), presumably as a direct result of methanol permeabilization of the lysosomal membrane.

In general, based on our findings, cellular lysosomal staining and imaging post-fixation with lysotracker dyes is not feasible. Only ice cold 4% paraformaldehyde showed promise, but caused artefactual differences when comparing healthy and lysosomal disease cells. Overall, fixation is not considered an appropriate step for accurate measurement of lysotracker fluorescence and all subsequent data is from live cells

Figure 3.2 Comparison of lysotracker red and green fluorescence in live and fixed conditions.

Human healthy control (GM05399) and NPC1 disease (GM03123) skin fibroblasts were loaded with 200 nM of the indicated (see below) lysotracker at 37°C for 15 min prior to nuclear counterstain with Hoechst and either imaging live or fixation (10 min 4% paraformaldehyde room temperature, 20 min 4% paraformaldehyde Ice cold, 5 min for ice cold methanol) and then immediate imaging. All images were taken under the same conditions on the Zeiss Colibri imaging system. (A-B) Lysotracker green, emission pre- and post-fixation with 4% paraformaldehyde.(Cermak et al.)Lysotracker red, emission pre- and post- fixation with 4% paraformaldehyde. (E-F) Lysotracker green, emission pre- and post-fixation with ice cold 4% paraformaldehyde.(Nordestgaard et al.) Lysotracker red, emission pre- and post-fixation with ice cold 4% paraformaldehyde. (I-J) Lysotracker green, emission pre- and post-fixation with methanol. (K-L) Lysotracker red, emission pre- and post-fixation with methanol. The graphs were generated by fluorescence microplate reader. All experiments were analysed using a t test; *p ≤ 0.05;**p ≤ 0.01;***p ≤ 0.001;****p ≤ 0.0001, scale bars: 10 µm. n=3. Data are shown as mean ± SD.



3.2.3 Photostability of the lysotracker fluorescence probes

Based on the previous data, the lysotracker green and lysotracker red dyes are the most sensitive probes, appearing to selectively stain LE/Lys at a low concentration and over a short incubation period. Xu *et al.* (2014) have previously reported that lysotracker red would be a useful probe for lysosome staining as an assay for drug discovery. However, it has previously been suggested that lysotracker red can rapidly photoconvert into a green fluorescent small molecule (Freundt *et al.* 2007). I tested this with both lysotracker green and lysotracker red in human healthy control skin fibroblasts under live imaging conditions and NPC1 cells post-fixation. In control live cells lysotracker green was stable against photoconversion when excited by the 470 nm LED (FITC emission) and then again at the 380 nm LED excitation channel (DAPI emission) (Figure 3.3 A & B). In contrast, lysotracker red does rapidly photoconvert with a reduction in the 565 nm LED excitation channel (TRITC emission) and concomitant appearance of a 470 nm LED excitation signal (FITC emission) occurring within less than 5 seconds (Figure 3.3 C&D). Having confirmed the previous observation of photoconversion of live lysotracker red (Freundt *et al.* 2007), and as lysotracker red has been used widely in fixed cells for co-localisation, I looked at the stability of lysotracker red post-fixation. For this experiment I used NPC1 patient fibroblasts as our previous findings showed that NPC1 cells preserved more lysotracker signal post-fixation compared to the control (Figure 3.2 C & D). Fixation with 4% paraformaldehyde room temperature condition did not reduce the rate of photoconversion (Figure 3.3 E&F). Finally, both lysotracker red and green photobleached rapidly when using an excitation LED light source set to 100%.

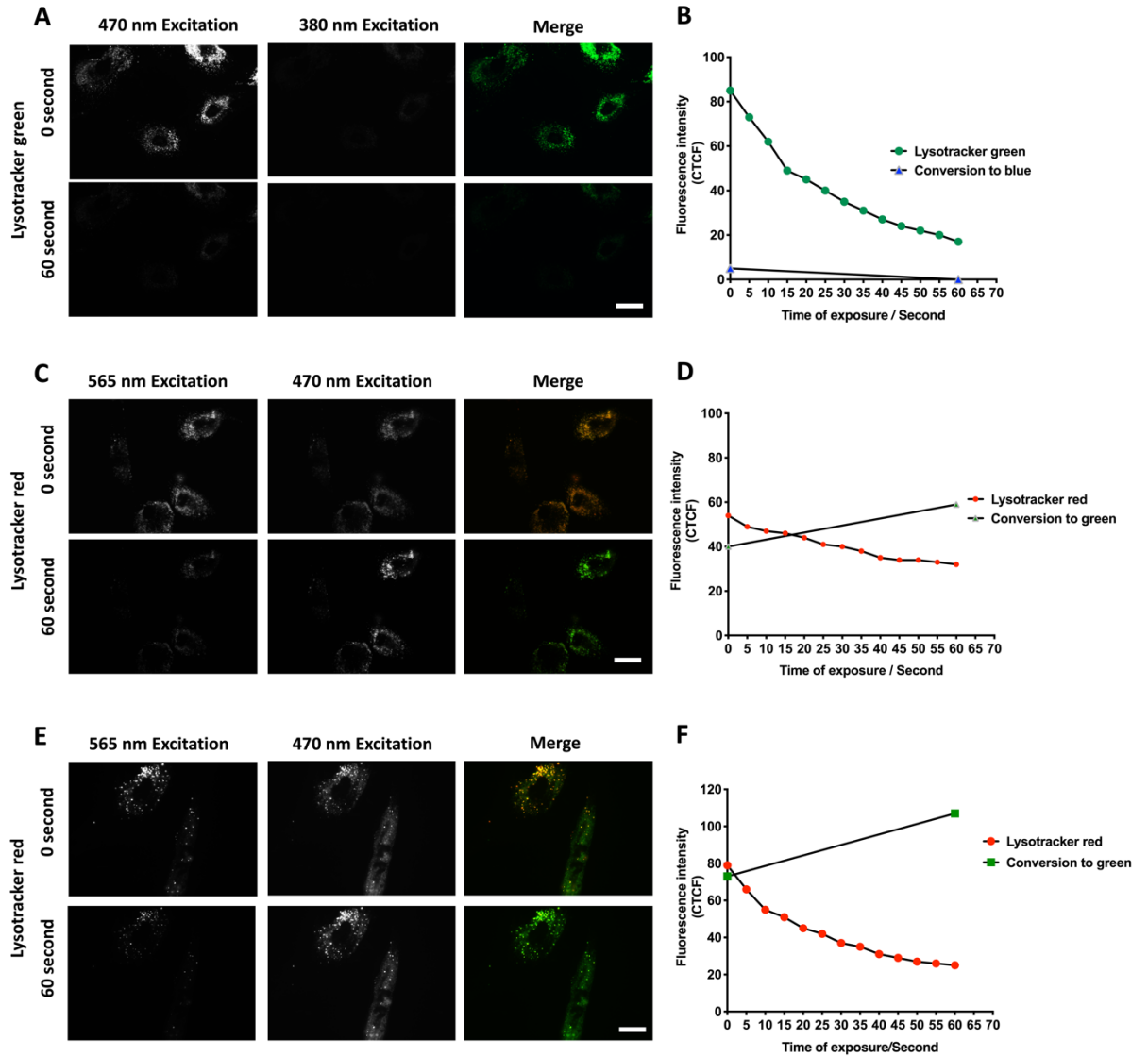


Figure 3.3 Lysotracker red, but not green, photoconverts and emits a lower wavelength green fluorescence after excitation.

(A-B) Human healthy control (GM05399) skin fibroblast stained with Lysotracker green were excited with a 470 nm LED for up to 60 seconds with images captured every 5 seconds on a Zeiss Colibri LED fluorescence microscope. After 60s, potential photoconversion to blue was determined using the 380 nm LED as in (A-B) cells stained with lysotracker red were imaged every 5s up to 60 seconds using the 565 nm LED and photoconversion to green determined using the 470nm LED. (E-F) NPC1 disease (GM03123) skin fibroblasts stained with lysotracker red and then fixed in 4% paraformaldehyde for 10 min were imaged every 5s up to 60 seconds using the 565nm LED and photoconversion to green determined using the 470 nm LED. n=3; the corrected total cell fluorescence (CTCF) was measured using image J. scale bars: 10 μ m.

3.2.4 LysoTracker concentration and incubation time alters intralysosomal pH

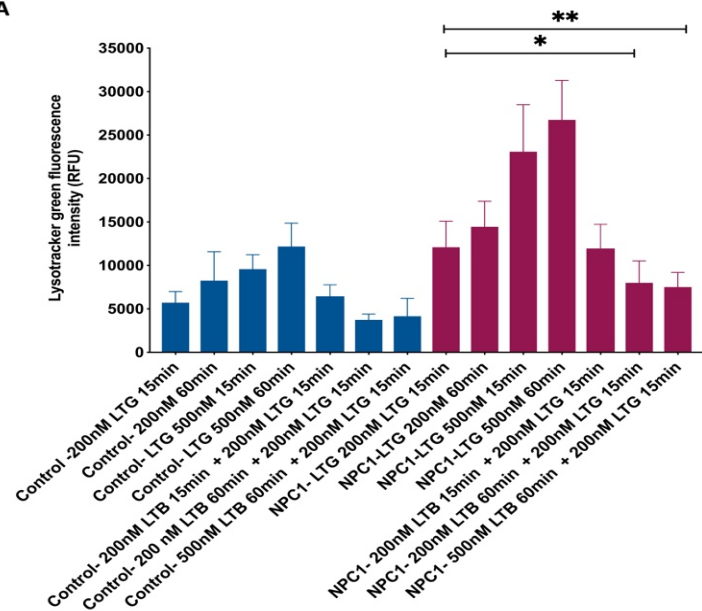
In some previous studies, LysoTracker was used at a high concentration > 500 nM for > 30 minutes (Fossale et al. 2004; Guerra et al. 2019; Rodriguez-Gil et al. 2013). However, long incubations with such high concentrations can theoretically induce the chelation of protons within the lysosomal lumen. To evaluate this, I loaded healthy control fibroblasts and NPC1 patient fibroblasts with different concentrations of LysoTracker green (200 and 500 nM) over a range of incubation times (15 min and 60 min) (Figure 3.4 A). In both control and NPC1 cells there was a clear increase in fluorescence in a concentration dependent manner, with NPC1 cells having 2.5-fold higher LysoTracker green fluorescence compared to control at either 200 or 500 nM. However, there was no big difference in fluorescence intensity when comparing the longer 60 min incubation time to the shorter 15 min incubation (Figure 3.4 A). This raises the possibility that a long incubation time may lead to changes in the internal lysosomal pH. To study this, I first incubated the cells with LysoTracker blue at 200 nM for 15 min followed by staining the same cells with LysoTracker green at 200 nM for 15 min and demonstrated no significant reduction in LysoTracker green fluorescence compared to the 15min 200nM LysoTracker green only incubation measurement (Figure 3.4 A). To study the effect of long incubation time on LysoTracker signal I incubated the cells with LysoTracker blue at either 200 nM or 500 nM for 60 min, followed by staining the same cells with LysoTracker green at 200 nM for 15 min (Figure 3.4 A). This loading of 200 nM and 500 nM LysoTracker blue for a long 60 min period, prior to a shorter loading of LysoTracker green, led to a 20% and 35% reduction in LysoTracker green fluorescence respectively (compared to the 15 min 200 nM LysoTracker green alone measurement) in the NPC1 patient fibroblast (Figure 3.4 A). Representative images are shown in Figure 3.4B, none of the loading conditions affected localisation, only fluorescence intensity. To confirm our findings suggesting that high concentrations of LysoTracker blue is indeed acting as a proton chelator, I decided to load the healthy control fibroblast lysosomes with pH sensitive 10kDa fluorescein isothiocyanate (FITC)-dextran together with a pH insensitive Texas red-labelled dextran as a loading control. Following a pulse/chase detailed in methods (Chapter 2, section 2.6.3) these probes were endocytosed into and trapped in the lysosomal compartment. The cells were incubated with LysoTracker blue for 15 min at 200, and for 60 min at 500 and 1000 nM. As with the LysoTracker blue/LysoTracker green experiment in the control cells (Figure 3.4 A). There was no significant change in lysosomal pH at the lowest 200 nM concentration of LysoTracker for 15 min similar to non-LysoTracker treated (Figure 3.4 C), a slight increase at 500 nM and a considerable increase in FITC-dextran fluorescence/lysosomal pH at 1000 nM (Figure 3.4 D). There is also a noticeable increase in Texas red-labelled dextran at 1000 nM, which means there is a possibility of a long incubation period with such a high concentration of LysoTracker that it may lead to lysosome

expansion (Figure 3.4 D). Based on these findings, a low incubation period (15 min) and a low concentration (200 nM) of lysotracker, in live not fixed cells (Figure 3.2), is the most suitable procedure for monitoring lysosomal expansion without triggering deacidification (which is known to induce abnormalities in lysosomal Ca^{2+} , endocytosis and lipid storage very rapidly).

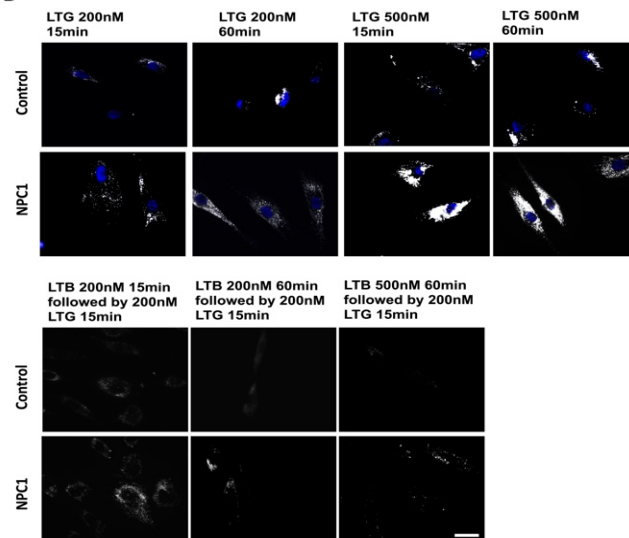
Figure 3.4 Lysotracker concentration and incubation time alters lysosomal pH.

(A) Human healthy control (GM05399) and NPC1 fibroblasts (GM03123) were grown in 96 well plates overnight followed by incubation with Lysotracker green (LTG) at 200 nM or 500 nM for 15 minutes or 1 hour or double loaded with 200 nM, 500 nM of lysotracker blue (LTB) for 1 hour followed with 200 nM Lysotracker green for 15 min. (B) representative fluorescence microscopy images of lysotracker green under all of the conditions shown in (A). control fibroblast cells (GM05399) were incubated overnight with 250 µg/ml of Texas Red-Dextran and FITC-Dextran. Cells were then chased in complete DMEM for 24 hrs followed by loading with lysotracker blue at the indicated concentrations and times and imaged live. Fluorescence intensity and co-localisation plots drawn in ImageJ. Statistical analyses were calculated using one-way anova; * $p \leq 0.05$; ** p . Scale bars, 10 µm. n=2-3. Data are shown as mean ± SD.

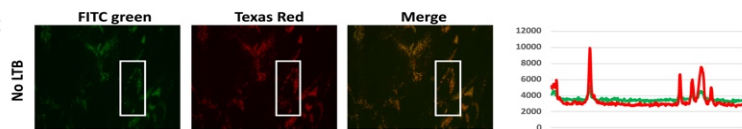
A



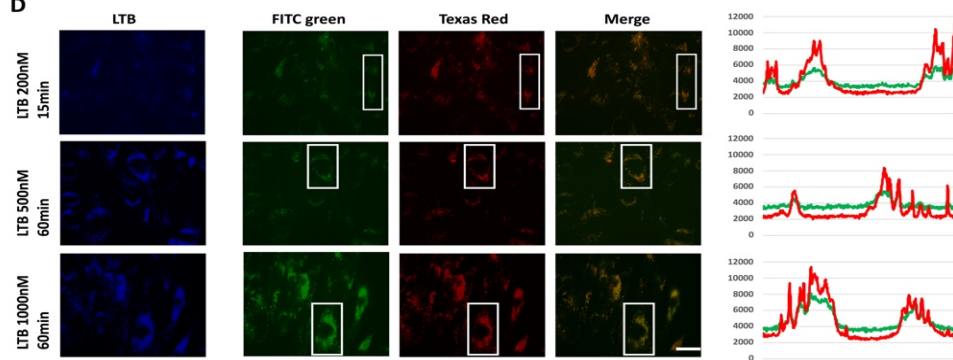
B



C



D



3.2.5 Lysotracker accumulation in acidic endolysosomes is swelling dependent.

I found that lower concentrations of lysotracker are potentially able to have a statistically significant ($p \leq 0.05$) greater effect on the pH of NPC1 disease fibroblast lysosomes compared to control cells (Figure 3.4 A). This suggests that NPC1 lysosomes are either more sensitive to chelation of protons or that lysotracker may load more readily into swollen storage organelles. As NPC1 disease cells do not have a change in lysosomal pH (Lloyd-Evans et al. 2008), it seems most likely that lysotracker therefore not only loads into acidic compartments but also more readily into swollen LE/Lys. In order to test this, I utilised several small molecules that specifically target the acidic LE/Lys compartments altering their pH, osmolarity and causing lipid storage. Bafilomycin A1 is a macrolide antibiotic inhibitor of the vacuolar H^+ -ATPases leading to deacidification of lysosomes. Treatment of human epidermoid carcinoma cells with a low concentration of bafilomycin, shown to alter lysosomal pH from ~ 4.5 to ~ 6.3 (Lee et al. 2015; Yoshimori et al. 1991), led to an $\sim 50\%$ depletion in lysotracker fluorescence (Figure 3.5 A & B). This was accompanied by an increase in punctate lysosomal accumulation of cholesterol stained with filipin as previously reported (Furuchi et al. 1993) and, as a positive control (owing to reduced lysotracker staining), the expansion of lysosomes confirmed using anti-LAMP2 (Figure 3.5 A & D). Furthermore, nigericin and monensin (both of which collapse the proton gradient that normally acidifies the LE/Lys) and GPN (a substrate of cathepsin C, which, when it is cleaved, induces osmotic lysis of the LE/Lys and releases H^+ ions from the lysosome) all depleted lysotracker fluorescence by 70-80% to almost background levels (Figure 3.5 E). These findings confirm that lysotracker is pH dependent, but does not fully explain the loading into lysosomes as even under conditions of abnormal pH there is lysosomal storage and expansion (Figure 3.5 A & C & D).

To determine how lysosomal swelling contributes to lysosomal lysotracker loading I tested the impact of incubation with sucrose, which induces osmotic entry of water into lysosomes by binding free ions in the lysosomal lumen (Karageorgos et al. 1997). To determine the impact of lysosomal expansion, I utilised U18666A which is an inhibitor of lysosomal NPC1 protein function (Lu et al. 2015). This drug has been used extensively to block lysosomal lipid trafficking and efflux, thus inducing a phenocopy of NPC1 disease in healthy cells, and is known to cause an expansion in the lysosomal system (Lloyd-Evans et al. 2008; Lu et al. 2015). Both of these small molecules led to an elevation in lysotracker fluorescence and anti-LAMP2 staining (Figure 3.5 A & D). A clear difference emerges however between the sucrose and the U18666a experiment with respect to cholesterol. The localization (stained with filipin) in U18666a treated cells is punctate and spread throughout the cell (indicative of storage lysosomes) as expected, whereas it is in a more defined finely punctate perinuclear

compartment in the sucrose treated cells (Figure 3.5 A). This staining pattern resembles the endocytic recycling compartment, which is a normal store of cellular cholesterol (Hao et al. 2002) and indicates that vesicular endocytic trafficking is not impaired in sucrose treated cells. I can therefore confirm from the elevated lysotracker and LAMP2 staining with both drugs that one is caused by swelling (sucrose) and the other by a combination of lipid storage, and as previously shown (Lloyd-Evans et al. 2008), increased lysosomal numbers (U18666a). These results imply that lysotracker loading into LE/Lys is dependent not only on acidity but also their volume and number.

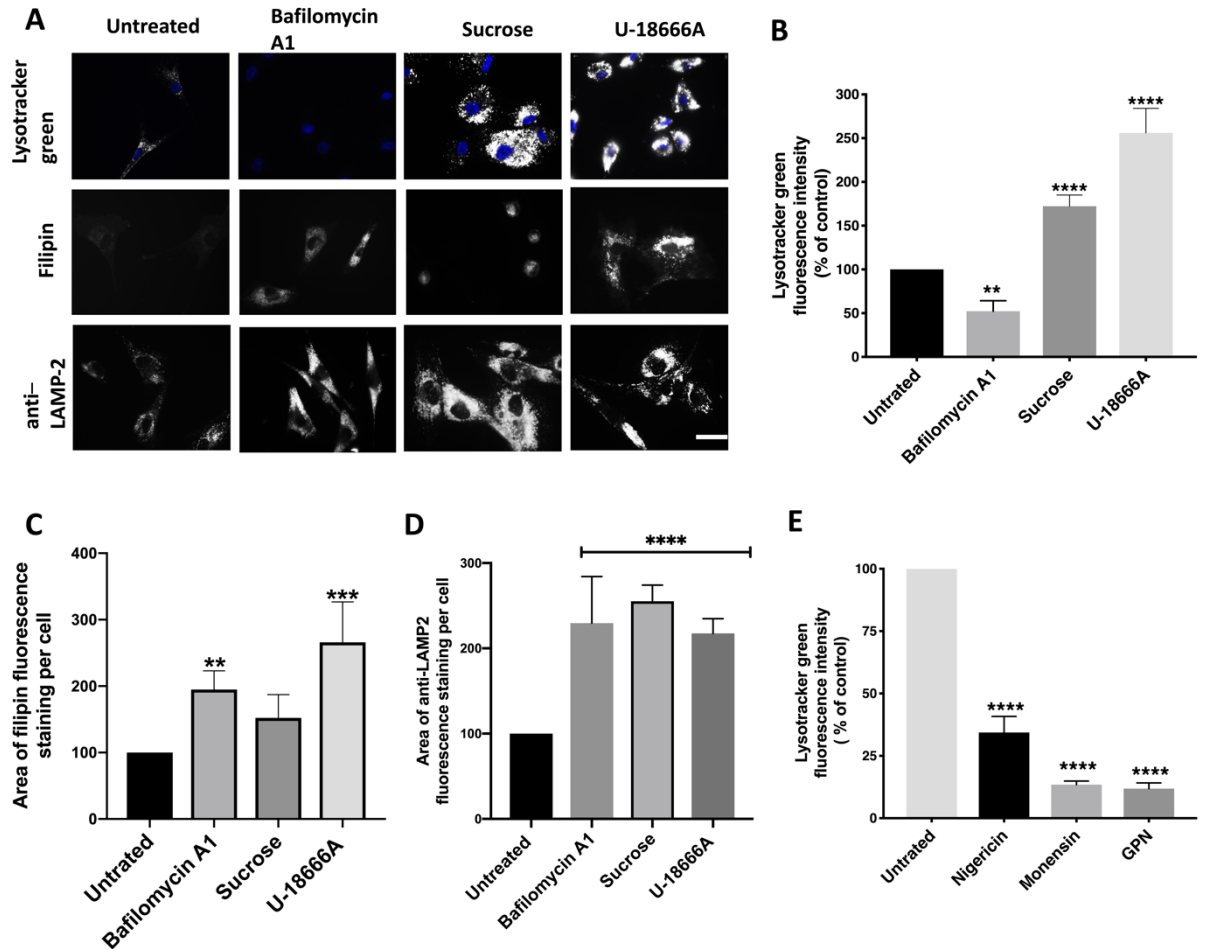


Figure 3.5 Investigating conditions that alter lysotracker loading into LE/Lys compartments.

(A) Human fibroblasts cells were treated with; 25 nM bafilomycin A1 for 24 hr, 100 mM Sucrose for 24 hr, or 2 µg/ml U18666A for 16hr, followed by either lysotracker green staining (200 nM, 15 min) and live visualisation or labelling of fixed cells with filipin or anti-LAMP2, cells were imaged with a Zeiss Colibri LED microscope. (B-D) The fluorescence intensity per cell measured as cellular area of lysotracker, filipin and anti-LAMP2. (E) The human fibroblasts cells were treated by 10 µM nigericin, monensin for 10 min and 500 µM GPN 10 min, followed by lysotracker green staining. Statistical analyses were calculated using one-way anova; **p ≤ 0.01;***p ≤ 0.001;****p ≤ 0.0001.scale bars, 10 µm. n=3 for all experiments. Data are shown as mean ± SD.

3.2.6 Lysotracker fluorescence is not elevated following autophagy

There is a possibility that lysotracker green fluorescence may increase with autophagy, a process that brings defective organelles to the lysosomes for degradation which induces temporary lysosomal swelling (Chikte et al. 2014; Yoshii and Mizushima 2017). Therefore, healthy control fibroblast was either starved for 3 hours with HBSS, starved overnight with an amino acid-free medium, or treated with 700 nM of the autophagy stimulator rapamycin, and were then loaded with lysotracker green or Cyto ID to label autophagic vacuoles (Figure 3.6 A & B). This revealed that while autophagy was increased under all the conditions tested, shown by Cyto ID fluorescence increase, there was no significant elevation in lysotracker green (Figure 3.6 A & B). To study the localisation of lysotracker during the autophagy process, I stained the untreated and 700nM rapamycin-treated fibroblasts with lysotracker red and Cyto ID. I noticed a large degree of overlap between the probes in either treated and the untreated fibroblasts. There was a clear increase in Cyto-ID green, without an increase in lysotracker red, in the 700 nM rapamycin-treated fibroblasts (Figure 3.6 C). Autophagosomes are unlikely to be acidic, and these data indicate that autophagosomes do not load with lysotracker and that the process of autophagy does not cause lysosomes to swell.

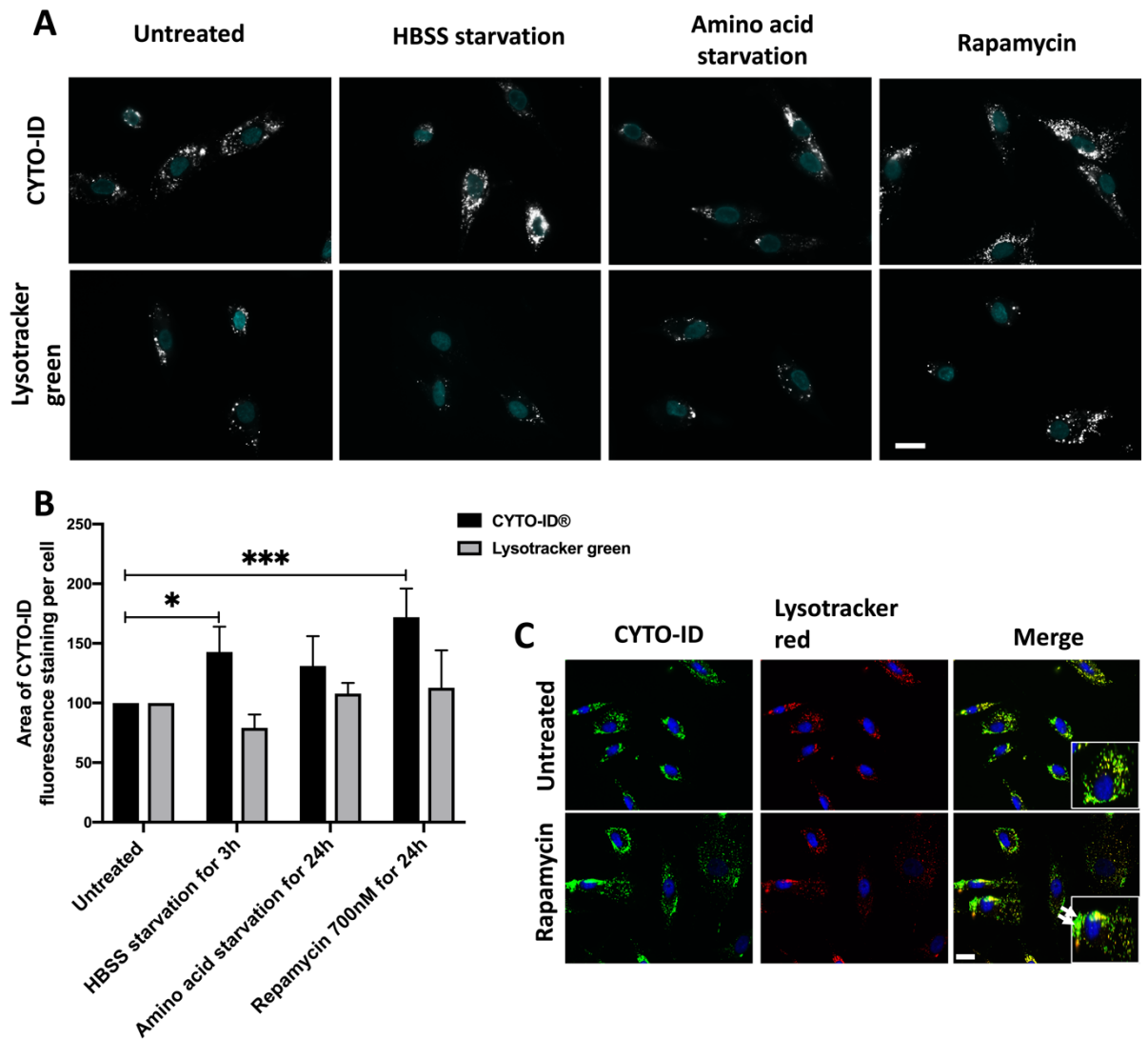


Figure 3.6 Lysotracker detects fusion with autophagic vacuoles but is not increased

(A) Normal human fibroblasts (GM05399) were either starved for 3 hours with HBSS or amino-acid and starved overnight or loaded with 700 nM rapamycin, and then loaded and imaged live with either lysotracker green or Cyto-ID (to label autophagic vacuoles). (B) They were then analysed by ImageJ area measurement to determine lysotracker and Cyto-ID intensity. (C) The fibroblasts (GM05399) untreated or treated with 700 nM rapamycin, then loaded with lysotracker red or Cyto ID, arrows indicated the localization. The significance was calculated using a two way anova $*p \leq 0.05$; $****p \leq 0.0001$. scale bars, 10 μm . $n=3$ for all experiments. Data are shown as mean \pm SD.

3.2.7 Developing the lysotracker plate assay for use in high throughput methods

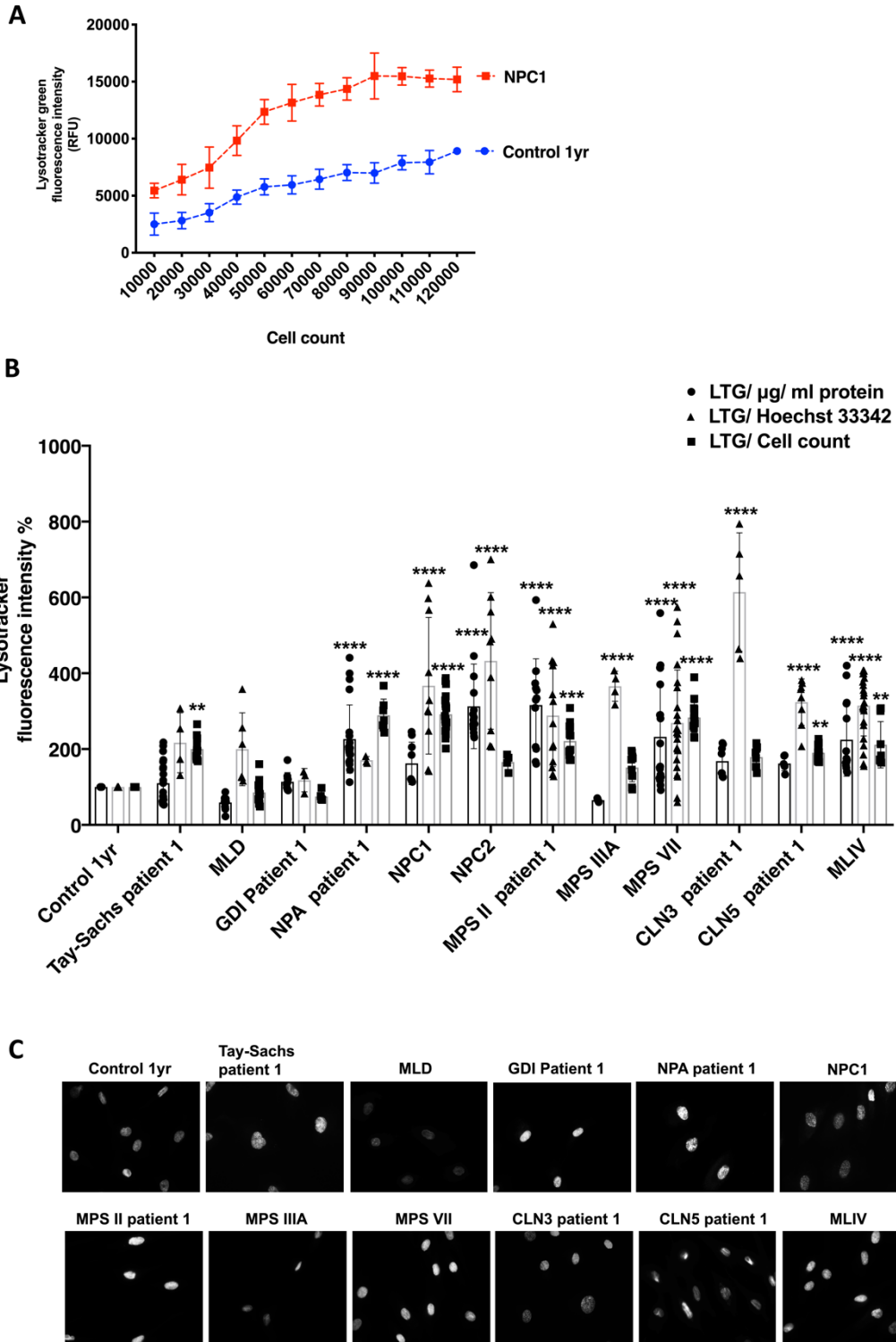
Based on our previous findings, lysotracker could be of use as an indicator for LE/Lys expansion with a high level of sensitivity. In order to develop this fluorescence probe for high throughput methods. First, I investigated the number of fibroblasts that should be seeded in each well. To achieve this, I started by seeding healthy control and NPC1 primary fibroblast from 10,000 to 120,000 cells per well and left overnight to adhere prior to staining with 200 nM lysotracker green for 15 min at 37°C. The appropriate cell number was estimated as 50,000 to 80,000 cells per well, as here I had a ~ 2.5 fold difference between control and NPC1 cells prior to the point of saturation (Figure 3.7 A). Furthermore, using fewer cell numbers would have risked variability due to an observed noisy signal from the plate reader caused by cells not completely covering the bottom of the well (Figure 3.7 A). Fibroblast cells normally grow in monolayers; however, when the fibroblasts reach over-confluency, they can be observed to grow above one another, which artificially enhances the lysotracker fluorescence at these much higher cell numbers and reduces the difference between control and NPC1 cells down to 2 fold (Figure 3.7 A).

Having established the correct number of cells to fill the wells I then tested different strategies to standardise the fluorescent lysotracker emission signal to the number of cells/well. Using BCA to measure the protein concentration in permeabilised cells following lysotracker measurement was considered as perhaps the most accurate method (Figure 3.7 B). However, cellular stress, an often detected LSD phenotype, may cause changes in the protein concentration in some LSD fibroblast. This may account for the absence of a statistical difference when comparing the lysotracker signals between control and NPC1 cells (Figure 3.7 B) despite clear differences by microscopy (Figure 3.2 A). I also investigated using the fluorescence intensity of the nuclear marker Hoechst 33342 dye as a means of controlling against the lysotracker signal with a ratio of lysotracker/Hoechst providing a standardisation to apparent cell number. This provided the highest number of statistically different results across the LSDs compared to the healthy cells (Figure 3.7 B). As a control, I decided to confirm using a fluorescence microscope the degree of nuclear staining in healthy control and LSD fibroblast (Figure 3.7 C). This revealed significant differences in the Hoechst 33342 fluorescence intensity across the LSD fibroblasts. Collectively there were changes in the internalisation and nuclear uptake of Hoechst 33342 in several of the diseases including differences across the different cells in each field of view. For example, NPA patient fibroblasts had one of the highest levels of staining with Hoechst, potentially aligning with changes in membrane fluidity caused by lysosomal accumulation of sphingomyelin, and explaining why no statistical difference was observed versus control cells when using this means of

standardization (Figure 3.7 C). Furthermore, and most worrying considering the widespread use of Hoechst as a standardisation reagent, some of these changes were on a per-cell basis and may represent variation according to cell-size, phase of the cell cycle or metabolic activity, all of which are altered in several LSDs (Brooks 1997; Karageorgos et al. 2004). Frankfurt (1983) found that the uptake of Hoechst 33342 dye increases during the S phase in HeLa cells and in cells exposed to hyperthermia (Frankfurt 1983; Rice et al. 1985). Clearly, the variability of staining means that this approach cannot be utilised. Ultimately, the number of cells seeded per well (50,000 cells/well) appeared to be the least variable standardisation method to adopt and the one with the second highest number of statistically significant differences when comparing LSDs to healthy cells. This method is not affected by fluorescence intensity or cellular metabolism and although there is potential to be affected by cell division, the slow growth of human skin fibroblasts means that seeding overnight and measuring fluorescence in the morning does not signify much of a change in cell number (Lloyd-Evans, unpublished). Clearly all of these factors should be considered when comparing and standardising different types of cells in multi well assays.

Figure 3.7 Comparison of different standardization methods for converting lysotracker into a higher throughput 96 well plate assay.

(A) Healthy control (GM05399) and NPC1 (GM03123) fibroblast counting was done using a haemocytometer prior to being seeded in a 96-well plate overnight and then later loaded using lysotracker and assessed using the plate reader. (B) The indicated human LSD fibroblasts (see supplementary Table 1) were seeded in a 96-well plate and stained with lysotracker, then standardized against; protein concentration $\mu\text{g/ml}$ (circles) measured by BCA, Hoechst 33342 (triangles) was loaded with lysotracker and the 96 well plate scanned at two different wavelengths (460 nm emission for Hoechst and 520 nm emission for lysotracker green) or standardised against the cell count per well (squares). To compare the three different standardizations, I plotted the data as a percentage change from the control. (C) Representative images of Hoechst staining in apparently healthy fibroblasts across and different LSDs fibroblast (see supplementary table 1) .The significance was calculated using a two way anova; * $p \leq 0.05$; ** $p \leq 0.01$; *** $p \leq 0.001$; **** $p \leq 0.0001$. Scale bars, 5 μm . $n=3$ for all experiments. Data are shown as mean \pm SD.



3.2.8 Lysotracker can be used to detect LE/Lys enlargement in fibroblasts isolated from the majority of LSD patients.

Having optimised all components of our lysotracker assay I next surveyed a large panel of LSD fibroblast cells to determine the usefulness of this assay. For the purposes of comparison, I used fluorescence microscopy to confirm the fluorescence microplate assay data.

3.2.8.1 Evaluating lysotracker fluorescence across different healthy control ages and non-LSD patient fibroblasts.

Diagnosing and monitoring LSDs remains a challenge especially when appearance of clinical features is variable (Wenger et al. 2003). LSD phenotype severity has a strong association with age of onset (Pastores and Maegawa 2013; Vellodi 2005). I therefore decided to include healthy controls of various ages (1 yr., 6 yrs., 13 yrs., 26 yrs., 45 yrs., 54 yrs.) and fibroblasts from a non-LSD patient with cystic fibrosis aged 4yrs. A range of age-matched controls spanning the full patient age range is the most appropriate way to standardise such assays, however little is known about the effect of ageing on lysosomal function in humans. Lysotracker has more or less shown an acceptable variability across different age ranges, they differ at most by 20% here (~ 50,000-60,000RFU) as these cell lines are mostly from apparently healthy individuals, possibly unaffected siblings etc. The 26 -year-old was the only seemingly healthy control showing an abnormal increase in lysotracker signals (Figure 3.8 A). There is of course the possibility that some of these individuals may be carriers of a metabolic disorder, therefore, for the purposes of our study I omitted data from this apparent control. Perhaps of greatest importance is that the lysotracker fluorescence of non-LSD cystic fibrosis sufferer was not elevated to any significant level and was within the control range. The control cells all displayed the expected punctate lysotracker fluorescence distribution near the nucleus (Figure 3.8 B).

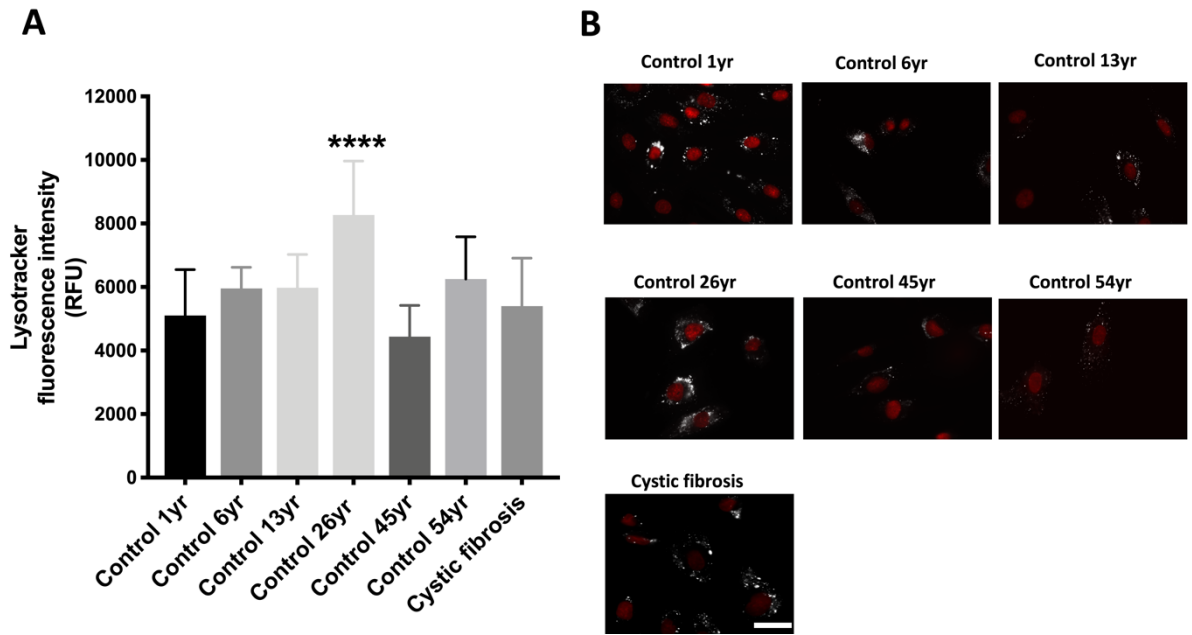


Figure 3.8 Lysotracker fluorescence intensity of healthy controls and one non-LSD patient with cystic fibrosis.

(A) Quantitative measurement of lysotracker green fluorescence across the indicated control fibroblast lines (see supplementary table 1) by fluorescence microplate reader standardised to seeded cell count. (B) Representative images of lysotracker green (white) and Hoechst (red) fluorescence in apparently healthy fibroblasts across the different ages and cystic fibrosis patient line used in the study. $n=3$ for all experiments. The significance was calculated using a one-way anova; **** $p \leq 0.0001$. scale bars, 10 μm . Data are shown as mean \pm SD.

3.2.8.2 Several sphingolipidoses fibroblasts showed elevated lysotracker staining

In the interest of simplifying the dataset I have separated the data out into individual groups of LSDs and included the control data from (Figure 3.8) for comparison purposes. GM1 gangliosidosis showed one of the largest elevations with a 2.5-fold increase in lysotracker fluorescence (Figure 3.9 A). Across the various forms of GM2 gangliosidosis, Tay-Sachs (infantile & adult onset) also showed a 2 fold increase in lysotracker fluorescence as did the AB variant and Sandhoff fibroblasts (Figure 3.9 A). Gaucher disease (GDI & GDII) fibroblasts, as expected, did not show an increase in lysotracker fluorescence (Figure 3.9 A). This may be due to a combination of the residual enzyme activity of the GCase enzyme, and the low levels of its substrate GlcCer in fibroblasts (Sillence et al. 2002). This finding is consistent with previous work both on GD1 and studies utilising Condurotol B-epoxide (CBE), a GCase

inhibitor used widely to generate cellular models of Gaucher disease (Sillence et al. 2002). Krabbe disease phenotypes, characterised by the accumulation of psychosine, like GD do not manifest in some cells including fibroblast. Also, the previous study have shown a lack of galactosylceramide storage in krabbe fibroblast (Takuro et al. 1985; Tanaka and Suzuki 1978). Our result did not show an increase in lysotracker fluorescence in Krabbe fibroblast. MLD, which is characterised by sulfatide accumulation, did not show any significant increase in lysotracker staining this may be due the lack of lysosomal ultrastructural abnormality in MLD fibroblast (Kamensky et al. 1973). However, two different fibroblast samples from Fabry disease patients showed a 1.5-fold increase in lysotracker signals (Figure 3.9 A). Moreover, fibroblasts from two other NPA patients showed a significant increase in lysotracker (~3-2 fold) compared to representative healthy control fibroblasts (Figure 3.9 A). Farber disease showed a ~1.5-fold increase in lysotracker fluorescence compared to the age matched control (Figure 3.9 A). Similar to the plate reader assay results, the GDI, GDII, Krabbe and MLD displayed less than normal lysotracker signals in cell images (Figure 3.9 B). Overall, 7 out of 11 of the sphingolipidoses patient fibroblasts showed an increase in lysotracker fluorescence compared to the representative healthy control fibroblasts covering the whole of the patient age range.

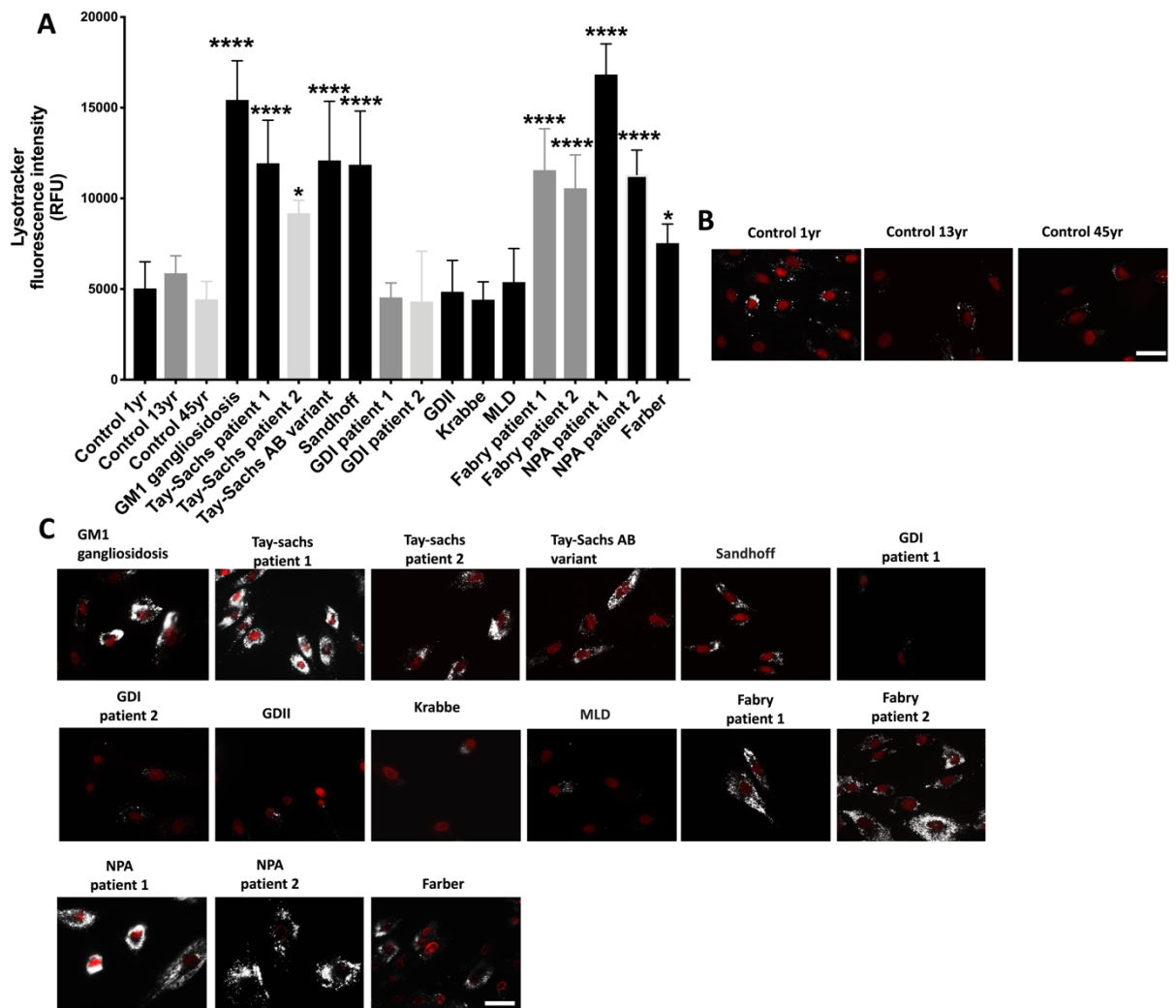


Figure 3.9 Lysotracker fluorescence intensity across the sphingolipidoses.

(A) Quantitative measurement of lysotracker fluorescence across sphingolipidoses patient fibroblast cells (see supplementary table 1) analysed by multiwell fluorescence microplate assay and standardised to cell count (the similarity in colour of columns between LSDs and the control indicate the appropriate age matched control). (B) Representative images of lysotracker staining (white) and nuclei stained with Hoechst (pseudocoloured red) in age matched healthy controls (see supplementary table 1). (C) Representative images of lysotracker staining observed in the indicated range of sphingolipidoses patient fibroblasts. The significance was calculated against the age matched control using a one-way anova; *** $p \leq 0.001$; **** $p \leq 0.0001$. scale bars, 10 μm . $n=3$ for all experiments. Data are shown as mean \pm SD.

3.2.8.3 Expansion of lysosomes is not observed in all neuronal ceroid lipofuscinoses.

Lysosomal storage of lipofuscin, as described earlier consisting of SCMAS and saposins, is a common feature of the NCLs (Mole et al. 2011) and could potentially be detected by lysotracker (see introduction section 1.2.3.3). Fibroblasts from, CLN2, CLN3 and CLN5 (Patient 1, Patient 2 and Patient 3) patients demonstrated 2-2.5-fold increases in lysotracker signals compared to age matched controls (Figure 3.10 A). There was only slightly increased in CLN6 ~ 1.5 fold increased in CLN6. This was confirmed by microscopy (Figure 3.10 B) with lysotracker fluorescence observed in puncta corresponding to lysosomes throughout the cell body in all cases. Some of the NCL patient fibroblasts CLN7, CLN8, and CLN10 (Patient 1 and Patient 2), appear to be normal. Interestingly, there is visibly lower fluorescence signal by microscopy for CLN10, but this is not significant by the plate reader assay (Figure 3.10 A & C). Overall, only 50% of the different NCL disease fibroblasts presented with increased lysotracker fluorescence.

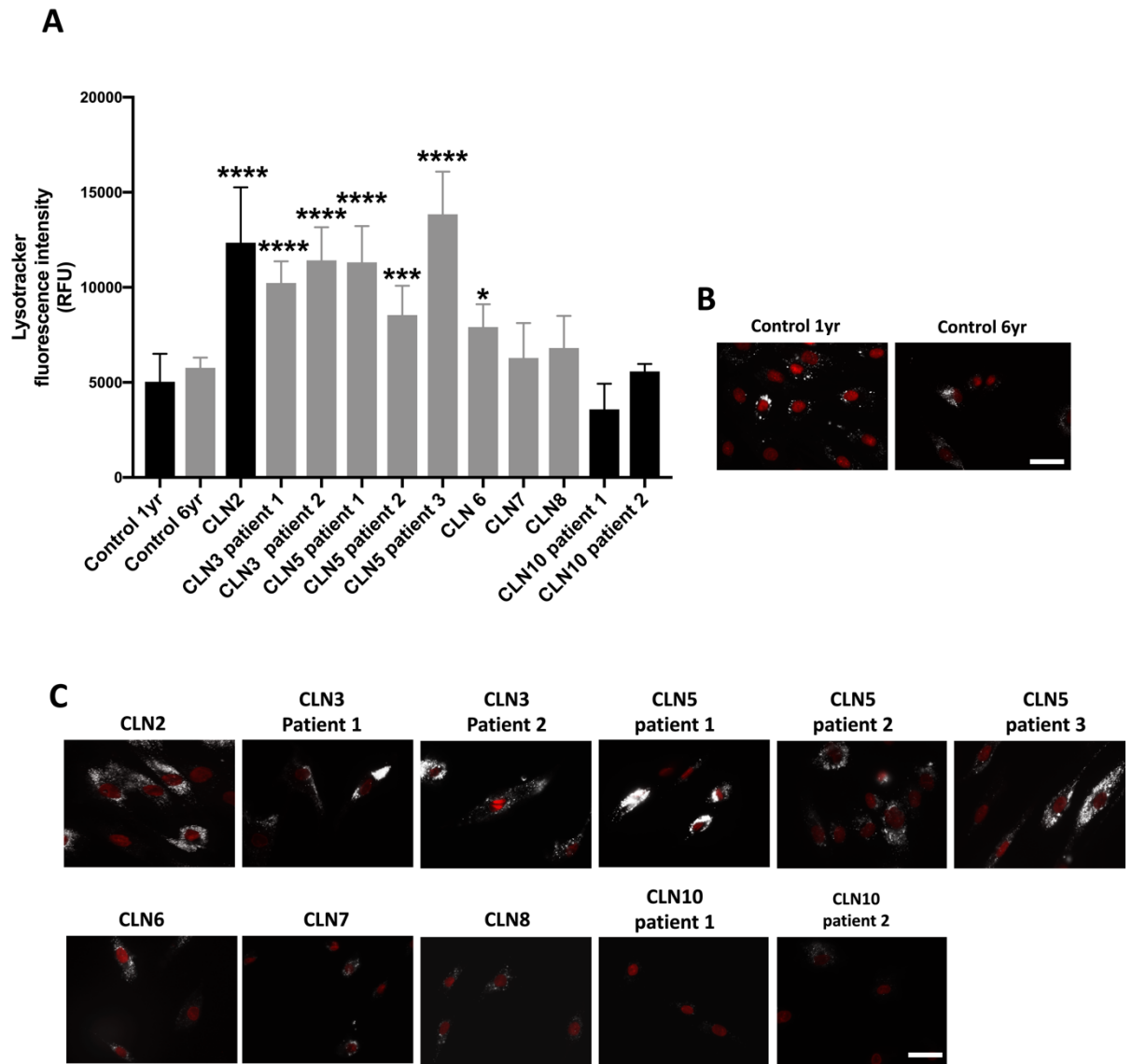


Figure 3.10 Localisation and intensity of lysotracker fluorescence across NCL fibroblasts.

(A) Quantitative multi-well plate measurement of lysotracker fluorescence across the NCL and control cells (see supplementary Table 1), all NCLs fibroblasts here are within the same age range as the controls. Representative images are shown of lysotracker (white) and nuclei stained with Hoescht (pseudocoloured red) fluorescence localisation and intensity observed across (B) age matched 1year and 6 year old healthy control fibroblasts and (C) the indicated different NCL patient fibroblasts. Statistical significance was calculated using a one-way anova against the age matched control; * $p \leq 0.05$; **** $p \leq 0.0001$. scale bars, 10 μm . $n=3$ for all experiments. Data are shown as mean \pm SD.

3.2.8.4 Lysotracker is elevated across almost all the mucopolysaccharidoses

GAG accumulation triggers lysosomal swelling by increasing lysosomal osmolarity which causes water influx in LE/Lys (Oussoren et al. 2011). Lysosomal storage of primary GAGs and secondary lipid storage is a common feature of all the MPS diseases, suggesting that lysotracker could also function as a useful bioassay for this family of diseases. MPSI, MPSII (patient 1 and patient 2) and MPS VII patient fibroblasts demonstrated the most significant, and largest 2-3-fold increases in lysotracker fluorescence versus age matched controls (Figure 3.11 A). Smaller but significant elevations were also observed in lysotracker fluorescence in MPS IIIA and IIIB (Figure 3.11 A). Despite the smaller increases in MPSIIIA and IIIB, LAMP2 immunostaining indicated the enlargement of lysosomes in MPSIIIA and MPSIIIB mouse brain tissue that correlated with microgliosis in different brain areas (Marcó et al. 2016). However, MPS IIID and MPS IVB did not show any significant increase in lysotracker fluorescence (Figure 3.11 A). By microscopy, I observe clear increases in punctate lysotracker staining in all MPSI, MPSII, MPSVII and to a lesser extent MPSIIIA cells. However, imaging of MPS IIIB and IIID shows different populations of cells with different degrees of punctate lysotracker staining (Figure 3.11 C), MPSIIIB cells are occasionally very bright explaining the higher lysotracker signal by plate assay. MPS IVB showed loss of lysotracker signals by microscopy which was not a significant change by plate reader assay, perhaps indicating that quenching by the brighter microscopy light source is affecting our interpretation of this microscopy data (Figure 3.11 C). Overall, 5 out of 7 mucopolysaccharidosis patient fibroblasts demonstrated an increase in lysotracker fluorescence by the plate reader assay.

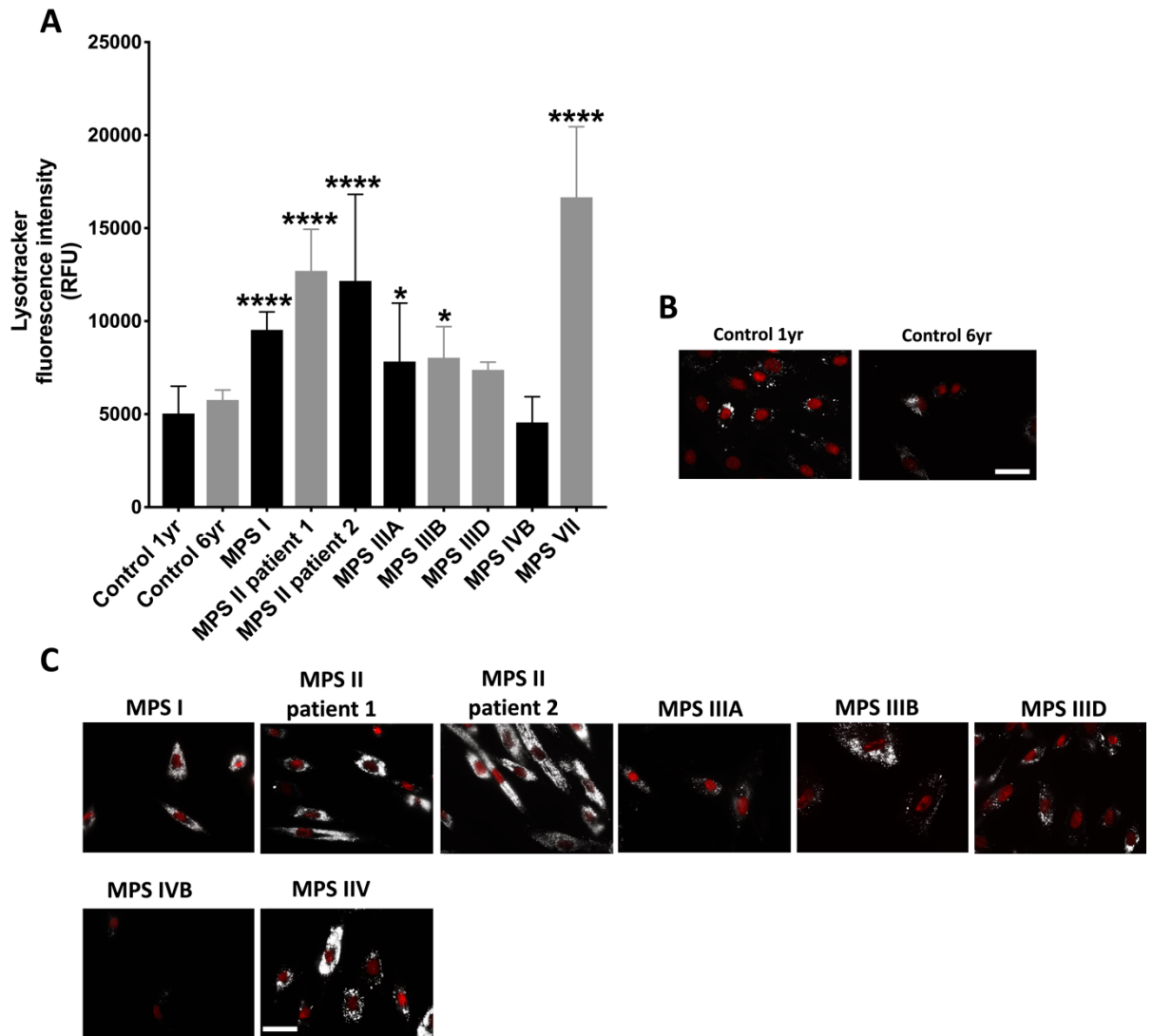


Figure 3.11 Localisation and intensity of lysotracker fluorescence across mucopolysaccharidoses fibroblasts.

(A) Quantitative multi-well plate measurement of lysotracker fluorescence across the mucopolysaccharidoses and control cells (see supplementary Table 1) (the similarity in colour of columns between LSDs and the control indicate the age matched control). Representative images of lysotracker (white) and Hoechst (pseudocoloured red) fluorescence localisation and intensity observed across the indicated different (B) age matched controls and (C) mucopolysaccharidoses patient fibroblasts. The significance was calculated against the indicated age matched controls using a one-way anova; * $p \leq 0.05$; **** $p \leq 0.0001$. scale bars, 10 μm . $n=3$ for all experiments, MPS IIID $n=2$. Data are shown as mean \pm SD.

3.2.8.5 LysoTracker is a powerful biochemical assay for almost all lysosomal transmembrane protein diseases

The presence of lysosomal Ca^{2+} defects leads to complex lipid accumulation, gangliosides GM1, GM2, globoside, sphingomyelin, cholesterol and sphingosine, in the endosomal/lysosomal system in NPC1 patient fibroblasts (Lloyd-Evans et al. 2008; Vitner et al. 2010). I observed a marked increase of ~ 3 fold in lysotracker fluorescence across classical NPC disease fibroblasts harbouring the common NPC1 I1061T mutation, namely NPC1 (P237S/I1061T) and MONPC (I0161T/D948N). In contrast only ~ 2 fold increase in lysotracker fluorescence was observed in the compound heterozygous BSNPC patient line harbouring the (G46V/P691L) mutations (Figure 3.12 A). A NPC patient fibroblast line, KWNPC, harbouring variant disease mutations (I061T/P1007A), which do not manifest with cholesterol accumulation (Sun et al. 2001), also had no significant elevation in lysotracker fluorescence. Further supporting that lysotracker reports the presence of storage or swollen lysosomes. The usefulness of lysotracker as an imaging tool is demonstrated by a visible clustering of lysosomes around the nucleus of some *NPC1*^{+/-} carrier fibroblast cells compared to the wider distribution spread throughout the cytoplasm of the control and NPC1 patient cells (Figure 3.12 B and C), indicating that NPC carrier cells are not completely normal. This is in comparison to a small, non-significant, ~10-20% increase, in overall lysotracker fluorescence (Figure 3.12 A) in its carrier cells when measured by plate reader assay. These data illustrate that by fluorescent plate assay lysotracker can detect storage but not organelle redistribution, microscopy is required for that. However, these data indicate that the plate assay may be useful as a screening tool to discriminate between patient and parent samples in screening assays. As NPC1 and NPC2 are considered to work in tandem to release cholesterol and other lipids out of the lysosome (Ko et al. 2003), I next measured lysotracker fluorescence in NPC2 patient cells and observed ~ 2-fold increase in lysotracker fluorescence signal similar to the NPC1 compound heterozygous BSNPC fibroblasts. MLIV disease, like NPC1, is associated with abnormal lysosomal Ca^{2+} release. In MLIV this is due to genetic deficiency of the *MCOLN1* gene that encodes the lysosomal TRPML1 ion channel; reported to lead to less LE/Lys membrane fusion (Cheng et al. 2010). This is associated with abnormal LE/Lys enlargement (LaPlante et al. 2004), suggesting the potential that lysotracker may also be elevated in these cells. As can be seen (Figure 3.12 A), MLIV patient fibroblasts exhibited a 2-fold increase in lysotracker fluorescence signal with bright punctate staining throughout the cells (Figure 3.12 C).

In addition, I determined the extent of lysosomal expansion in two less commonly researched lysosomal transmembrane diseases, cystinosis and Salla disease. Cystinosis disease is

characterised by intra-lysosomal accumulation of the amino acid cystine. In cystinosis patient fibroblasts lysotracker fluorescence is significantly increased 2-fold above that of the age matched control (Figure 3.12 A and C). This finding is supported by *Ctns*^{-/-} mice skin fibroblast which were shown to have increased lysotracker fluorescence when measured by FACS (Napolitano et al. 2015). Salla disease is characterised by the accumulation of sialic acid in the lysosomal compartment. Previous reports have shown that Salla patients' skin biopsies contain enlarged vacuoles (Aula et al. 1979). Salla disease shows a slight, but significant, ~50% increase in accumulation of lysotracker signals (Figure 3.12 A) and the presence of punctate lysosomal staining throughout the cells (Figure 3.12 C). Collectively, LE/Lys expansion is a common phenotype in these diseases associated with lysosomal transmembrane protein defects indicating the potential usefulness of lysotracker in screening and monitoring of these diseases.

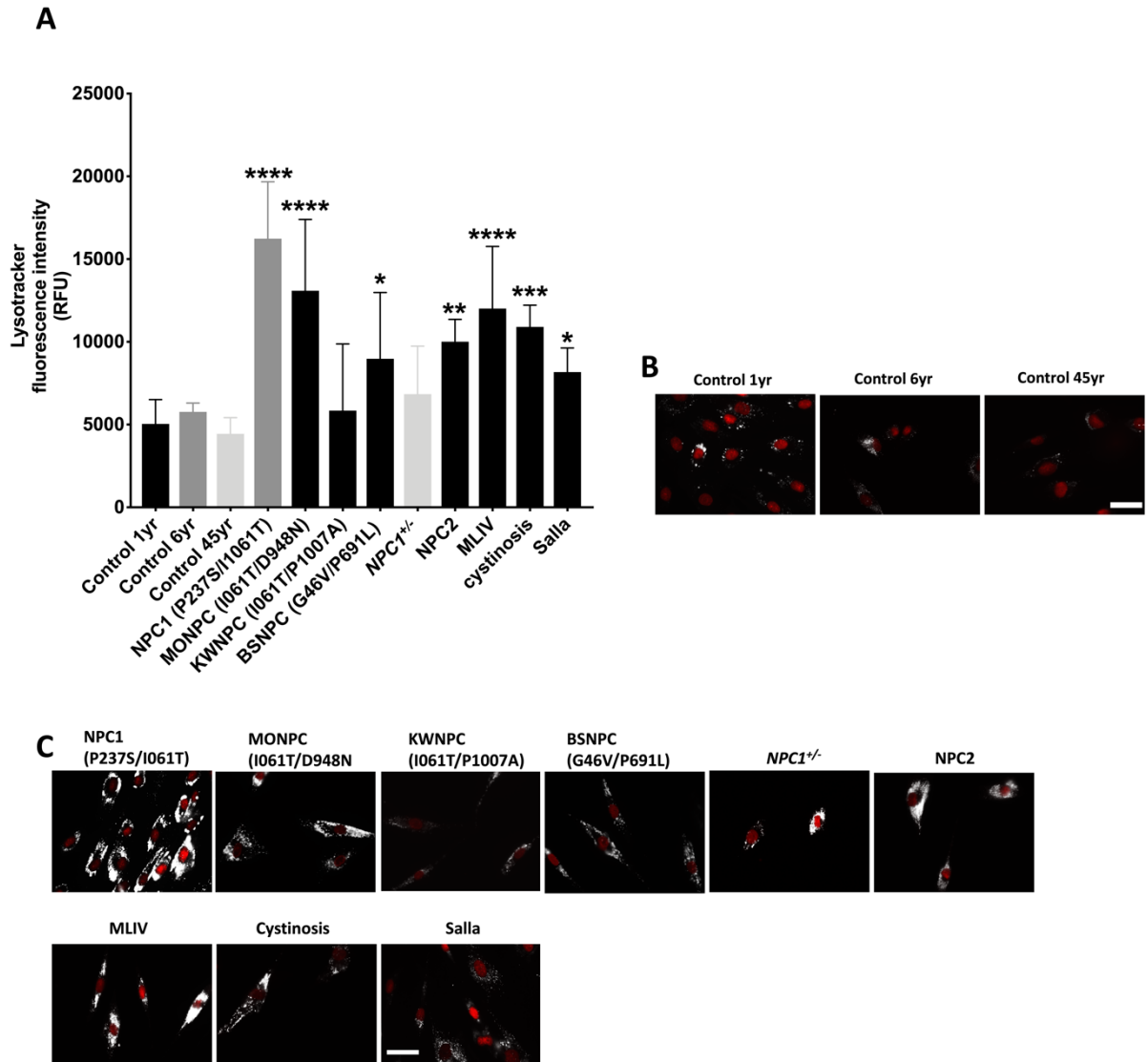


Figure 3.12 Lysotracker fluorescence intensity across the lysosomal transmembrane protein associated diseases.

(A) Lysotracker staining observed in different lysosomal transmembrane diseases (see supplementary Table 1) measured by fluorescence plate reader (similarity in colour of columns between LSDs and the controls indicate the age matched fibroblast lines). Representative images of lysotracker green (white) and Hoechst (red) fluorescence in (B) age matched healthy controls (see supplementary Table 1) and (C) the indicated lysosomal transmembrane diseases (mutations in brackets). $n=3$ for all experiments. Statistical significance was calculated against the indicated age matched controls using a one-way anova; $*=p<0.05$; $**=p<0.01$; $***=p<0.001$; $****=p<0.0001$. scale bars, 10 μm . Data are shown as mean \pm SD.

3.2.8.6 Lysotracker could be a useful assay of multiple lysosomal enzyme deficiency LSD diseases

I cell disease is caused by deficiency of the GlcNAc-1-phosphotransferase enzyme that leads to a general failure of most acid hydrolase enzymes to correctly target the lysosome and, as a result, a variety of enzyme substrates accumulate within the lysosome (Kornfeld 2001; Wang et al. 2018). The skin fibroblasts of I cell possess large vacuoles and lysosomes, containing multiple substrates (Otomo et al. 2011). It was therefore no surprise that I cell patient fibroblasts had a 2-fold increase in lysotracker by the fluorescent plate assay (Figure 3.13 A), and punctate staining visible across the whole cell by microscopy (Figure 3.13 C) compared to the age-matched healthy control fibroblasts (Figure 3.13 B).

Galactosialidosis is caused by a defect in the protective protein/cathepsin A, which is the result of combined deficiency of lysosomal β -galactosidase and neuraminidase (d'Azzo et al. 1982). The Galactosialidosis patients only had a small increase in lysotracker fluorescence by plate assay (Figure 3.13 A), whilst the microscopy images clearly exhibited more lysotracker puncta in the images (Figure 3.12 C). MSD is caused when multiple sulphatase activity is severely reduced resulting in GAGs and sulphatide accumulation. In *Sumf1*^{-/-} mice, GAG storage is associated with the presence of large vacuoles (Settembre et al. 2007), suggesting that lysotracker may be elevated in MSD. MSD fibroblasts (Patient 1 & Patient 2) showed an increase of lysotracker of about 1.6-fold compared to the 13 year old control fibroblast cells (Figure 13 A).

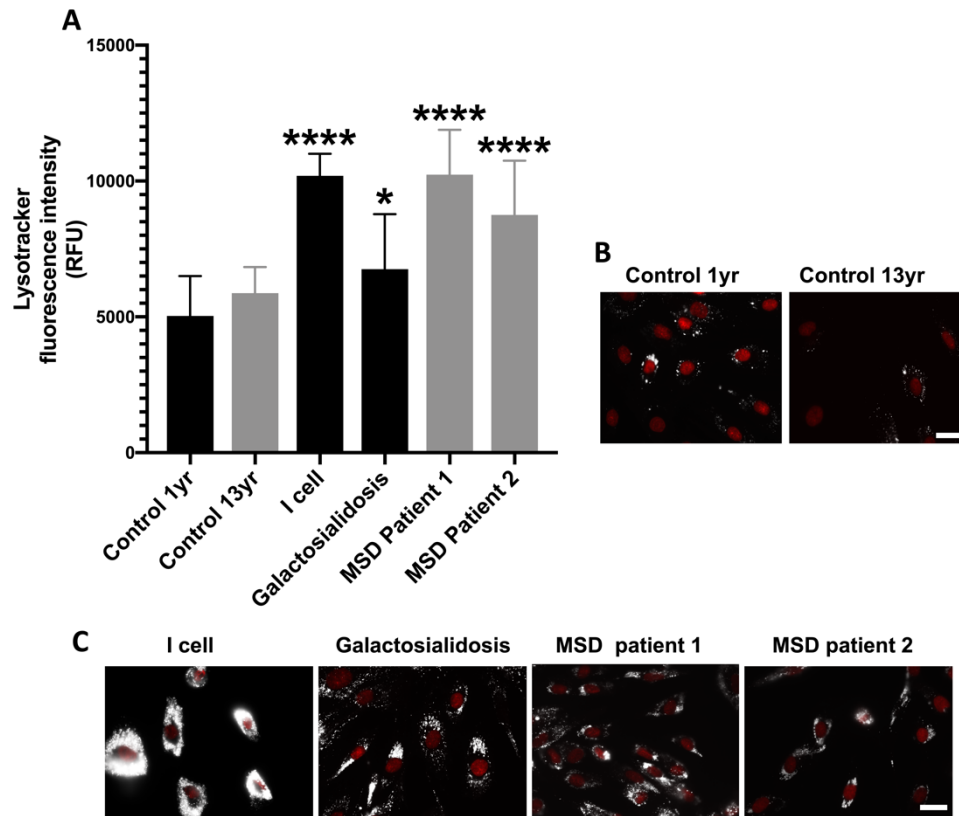


Figure 3.13 Lysotracker fluorescence staining in multiple lysosomal enzyme deficiencies.

(A) Lysotracker staining measured in human fibroblasts from the indicated multiple lysosomal enzyme deficiencies (see supplementary Table 1) using fluorescence plate reader (the similarity in colour of columns between LSDs and the control indicates the associated age matched control). Representative images of lysotracker (white) and Hoescht (red) fluorescent staining in (B) age matched controls (see supplementary Table 1) and (C) different multiple lysosomal enzyme diseases. The significance was calculated against the indicated age matched controls using a one-way anova; *= $p < 0.05$; **= $p < 0.01$; ***= $p < 0.001$; ****= $p < 0.0001$. scale bars, 10 μm . $n=3$ for all experiments. Data are shown as mean \pm SD.

3.2.8.7 Determining the effectiveness of lysotracker as a tool to measure lysosomal expansion in other LSDs

3.2.8.7.1 Wolman disease

The storage of cholesteryl ester and triglycerides occur in Wolman disease, which is caused by loss of lysosomal acid lipase, and it is expected that lysotracker would detect these an increase in lysosomal volume/number caused by these accumulated substrates. Wolman disease presented with a 2-fold increase in lysotracker staining compared to the healthy control (Figure 3.14 A) with punctate staining observed across the cell (Figure 3.14 C). This finding is consistent with previous studies that showed the Wolman neural stem cell derived from patient iPSCs exhibiting an increase in lysotracker staining (Aguisanda et al. 2017).

3.2.8.7.2 Expansion of lysosomes is partially observed in oligosaccharides metabolism diseases.

Lysotracker was unable to detect the majority of glycoprotein derived oligosaccharide catabolism-associated disorders apart from Sialidosis (Figure 3.14 A). These diseases in general lead to an accumulation within the lysosome of partially degraded material, mostly oligosaccharides (Cantz and Ulrich-Bott 1990), in enlarged non-electron dense (“empty looking”) lysosomes (Michalski and Klein 1999; Wolf et al. 2016). These “empty” lysosomes point towards the presence of water soluble storage material including oligomannosides in α -mannosidosis (Michalski and Klein 1999) and fucosylated glycoconjugates in α -fucosidosis. Lysotracker was not significantly increased in α -mannosidosis and α -fucosidosis fibroblasts in lysotracker signal by the plate reader assay (Figure 3.14 A), microscopy images showed a noticeable level of variability in lysotracker signals within the cells (Figure 3.14 C), which could be more effectively detected by FACS. A defect in the catabolism of sialic acid-containing oligosaccharides in sialidosis, caused by deficiency of the *NEU1* gene, leads to the build-up of sialylglycoconjugates in lysosomes of patient fibroblasts and to increased levels of LAMP-1 at the cell surface (Yogalingam et al. 2008). Lysotracker was slightly, but significantly ($p < 0.05$), increased ~ 1.5 -fold by plate assay with concomitant slight elevation in fluorescence intensity and puncta by microscopy imaging (Figure 3.14 A and C). Pompe disease, a lysosomal glycogen storage disease, showed a ~ 1.4 -fold increase in lysotracker fluorescence (Figure 3.14 A) which was reflected by the representative microscopy pictures, albeit with some clumping of lysosomes observed (Figure 3.14 C). This finding supported a previous study by (Karageorgos et al. 1997) that showed Pompe skin fibroblasts had increased LAMP-1 levels, and therefore potentially increased lysosomal numbers, compared to healthy controls.

3.2.8.7.3 Deficiency of the *vATPase* H⁺-transporting lysosomal accessory protein (Atp6ap2)

Lysotracker signal was not significantly increased in a *vATPase* H⁺-transporting lysosomal accessory protein (Atp6ap2) deficient patient fibroblast (Figure 3.14 A). Contrary to our expectations of lower lysotracker, owing to the reduced *vATPase* activity in this disease, I instead observed a normal distribution of lysotracker fluorescent puncta spread across the whole cell (Figure 3.14 C).

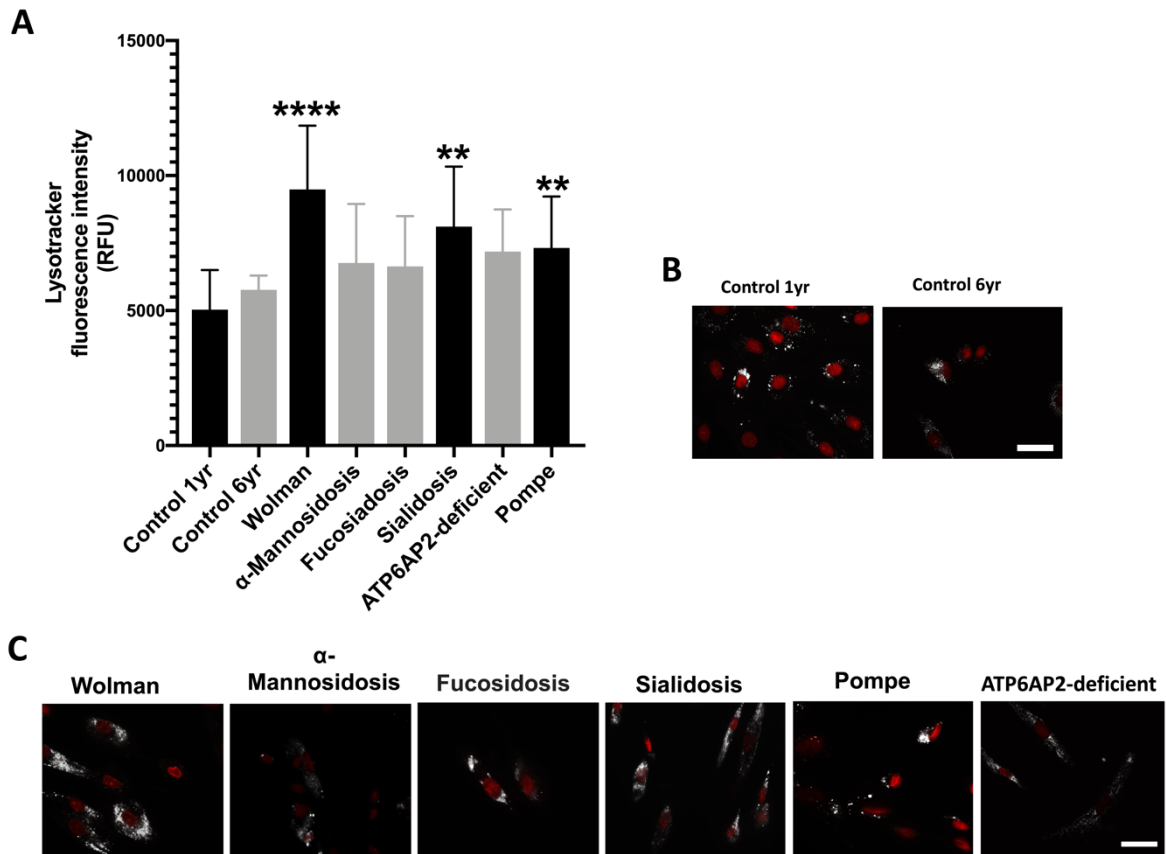


Figure 3.14 Lysotracker fluorescence staining of other lysosomal storage diseases.

(A) Quantitative measurement of lysotracker in oligosaccharide and other lysosomal storage diseases (see supplementary Table 1) was performed by 96-well-plate assay to generate the graph (the similarity in colour of columns between LSDs and the control indicate the associated age matched control). Representative images of lysotracker (white) and Hoechst stained nuclei (red) in (B) age matched healthy controls, (B) other lysosomal storage disease fibroblasts (see supplementary Table 1). Statistical significance was calculated using a one-way anova Compared against their respective age matched controls; **= $p < 0.01$; ***= $p < 0.001$; ****= $p < 0.0001$. scale bars, 10 μm . $n=3$ apart from Sialidosis where $n=2$. Data are shown as mean \pm SD.

3.2.9 Absence of increase in lysotracker fluorescence in certain LSDs correlates with an absence of expansion in LAMP2 immunocytochemistry

Our data has shown that some of the LSDs (Figures 3.9 & 3.10 & 3.11 & 3.12 & 3.14) have normal lysotracker staining. In order to check if this is due to normal lysosome size and numbers in these LSD fibroblasts, the absence of storage, or alternatively due to possible changes in lysosomal pH, I have used LAMP2 staining. LAMP2 is widely used as a lysosome marker and has been published as a potential newborn screening tool (Hua et al. 1998) to identify lysosomal diseases by measuring lysosomal expansion via increased LAMP2 expression.

In NPC1 patient fibroblasts, where there is a clear 3 fold increase in lysotracker fluorescence (Figure 3.12), this correlates with increased lysosomal volume and density as illustrated by both microscopy of lysotracker (Figure 3.12) and also anti-LAMP2 staining (Figure 3.15 A & B) where there is also an ~2.4 fold increase in lysosomal area/cell. In the same manner, GDII and Krabbe were within the normal range for lysotracker staining (Figure 3.9) and also had normal levels of anti-LAMP2 staining (Figure 3.15 A & B).

Although there was no statistical increase in anti-LAMP2 staining in Krabbe fibroblasts (Figure 3.15 A), there was a clear clustering of anti-LAMP2 staining around the nucleus suggestive of altered lysosomal function (Figure 3.15 B). These data above indicate that in the presence of lysosomal lipid storage, lysosomal swelling or expansion in numbers lysotracker is capable of successfully identifying LSD cells.

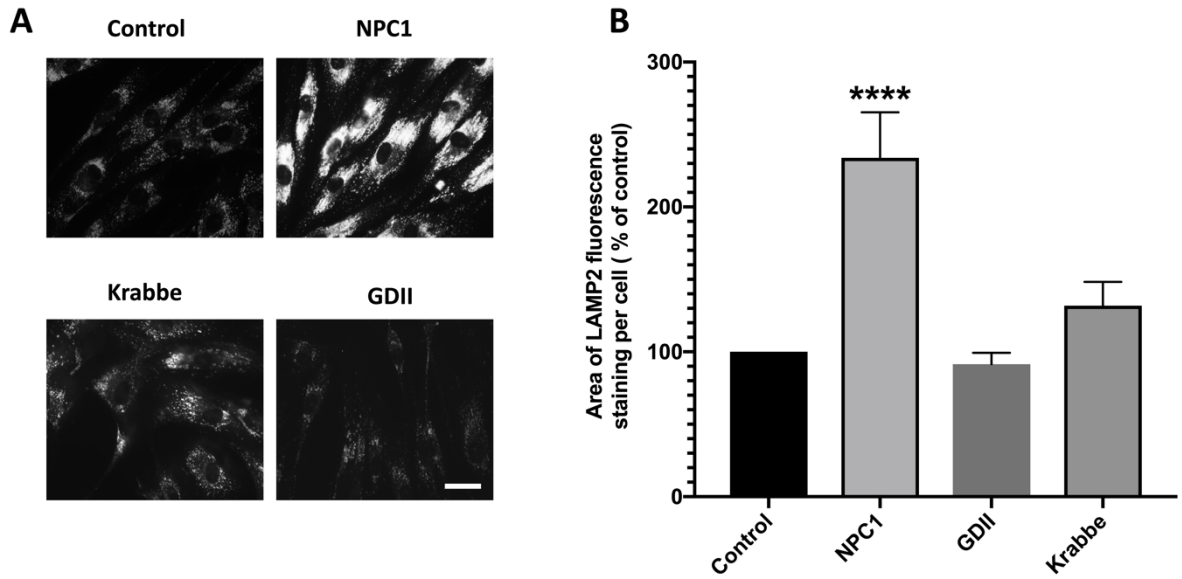


Figure 3.15 Anti-LAMP2 Immunofluorescent analysis of LSD fibroblasts.

(A) Control (GM05399), NPC1 (GM03123), Krabbe (GM06806) and GDII (GM08760) fibroblasts were fixed and stained with anti-LAMP2. (B) Quantitative measurement of LAMP2 fluorescence by analysis of area of LAMP2 staining/cell using Image J software, data is shown as % of control with control set as 100%. Statistical significance was calculated using one-way anova; ****= $p < 0.0001$. scale bars, 10 μ m. $n=3$ for all experiments. Data are shown as mean \pm SD.

3.2.10 Lysotracker is capable of faithfully representing reduction in lysosomal lipid storage during drug treatment

Having shown through our data that the lysotracker assay works to identify LSDs by measuring LE/Lys volume in patient cells compared to healthy controls, I next determined the usefulness of the lysotracker assay to monitor therapeutic improvement. To test the sensitivity of lysotracker, I treated the healthy control and NPC1 fibroblast cells with 50 μ M miglustat for 5 days and then stained them live with lysotracker. After the cells were imaged live I then proceeded to a fixation step, and then the primary fibroblasts were labelled with either anti-LAMP1 or LAMP2. As can be seen (Figure 3.16 A), there is a clear reduction in the density and intensity of staining in the miglustat-treated NPC1 cells loaded with lysotracker (~35% reduction between treated NPC1 and untreated NPC1 cells, Figure 3.16 B), whereas LAMP1 and LAMP2 staining show no decrease apart from the presence of empty vacuoles in the miglustat-treated NPC1 cells. The red arrowheads indicate the presences of these empty vacuoles in the LAMP stained cells and lack of those vacuoles in the lysotracker stained cells

(Figure 3.16 A). In addition to imaging the cells, I also tested the sensitivity of the assay by 96-well plate fluorescence assay; cells were treated with miglustat prior to their transfer to the 96-well plate to be stained by lysotracker (Figure 3.16 B). Despite a ~1.5 fold reduction in lysosomal storage in NPC patient fibroblasts following miglustat treatment compared to pre-treatment levels detected by lysotracker plate assay (Figure 16 3.B), there was no significant decrease in staining with either LAMP1 or LAMP2 (Figure 16 C and D). These data indicate that lysotracker fluorescence correlates with the presence of lysosomal storage to a higher degree than lysosomal volume and provides a more powerful endorsement for the use of lysotracker rather than LAMP protein levels as a therapeutic monitoring tool for LSDs.

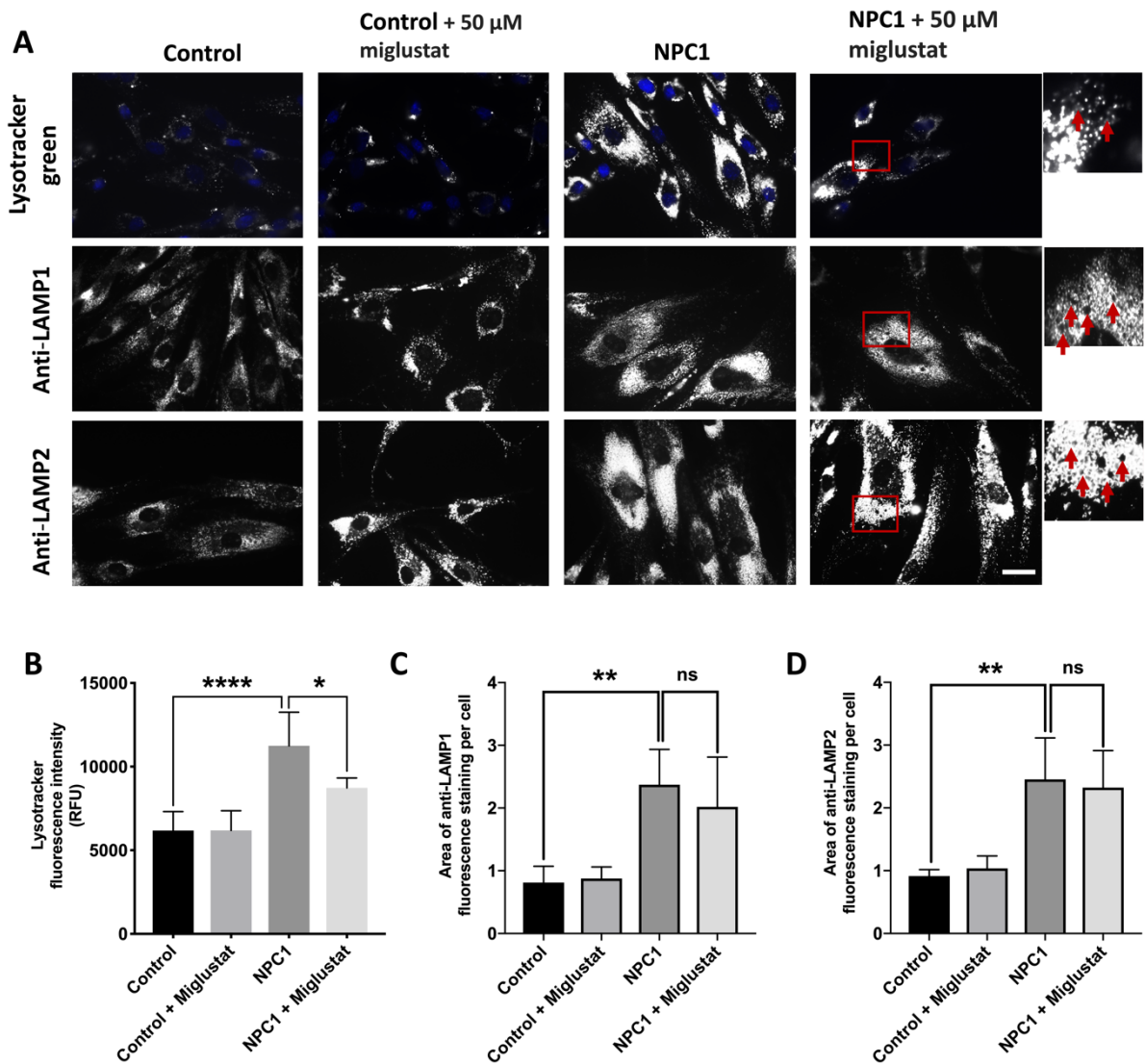


Figure 3.16 Changes in lysotracker and LAMP1/2 following treatment with miglustat.

(A) Control (GM05399) and NPC1 (GM03123) fibroblast cells were treated with 50 μ M miglustat for 5 days, followed by staining with Lysotracker, then fixed with 4% paraformaldehyde and labelled with either LAMP1 or LAMP2. (B) Lysotracker fluorescence intensity using a 96-well plate assay. The graphs generated in (C and D) were based on the fluorescent intensity per cell area of LAMP1 and LAMP2 staining respectively. The arrows indicate the presence (and absence with lysotracker) of vacuole staining. $n=3$ for all experiments. scale bars, 10 μ m. The significance was calculated using a one-way anova; * $p<0.05$, ** $p<0.01$, *** $p<0.001$. Data are shown as mean \pm SD.

3.2.11 Further validation of the use of lysotracker to detect lysosomal storage in lymphoblastoid cell lines

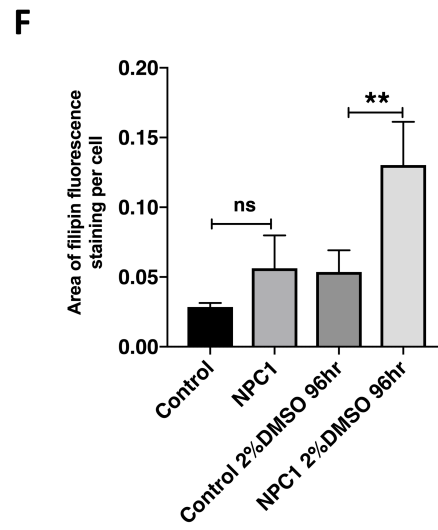
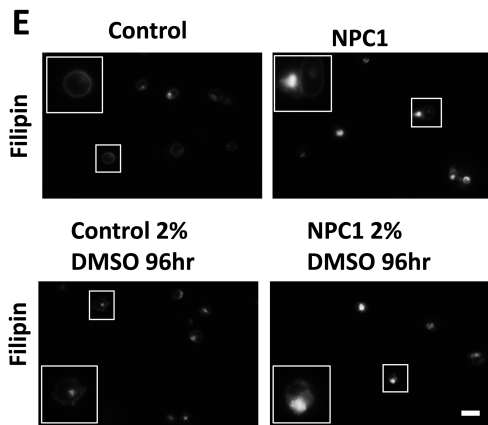
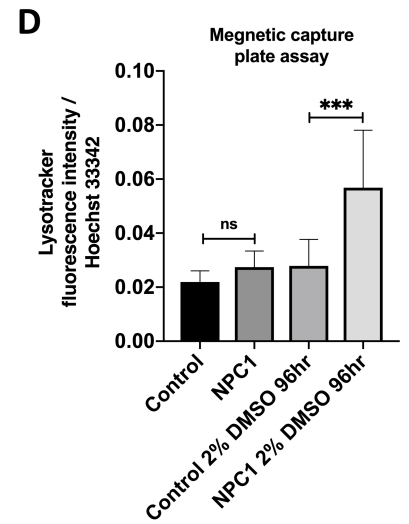
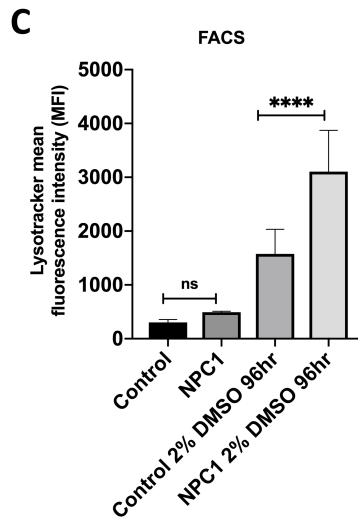
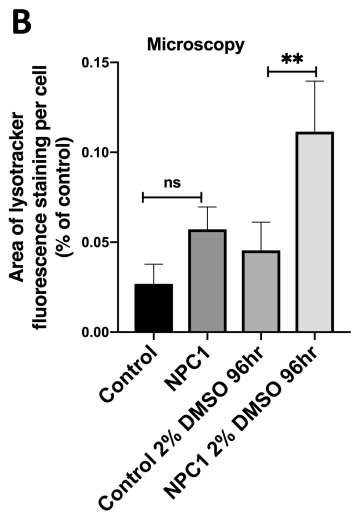
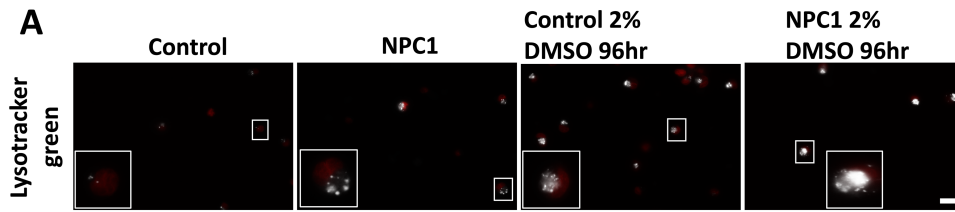
To follow up our previous findings on fibroblast cell lines, I now propose that lysotracker may be a useful diagnostic and therapeutic bioassay/marker for the detection of the majority of LSDs in a single procedure. Some changes are needed to be able to adapt this method for clinical use. For example, taking a fibroblast sample is an invasive procedure and, as such, is not suitable for routine lab diagnosis. However, it is still useful for drug screening (Xu et al. 2014). For the first line of diagnosis, a blood sample is almost always the most appropriate biosample in a clinical setting. There are no lysosomes in erythrocytes; however, all mononuclear cells contain LE/Lys. The precedent is to focus on B cells, as they are long lived and can be recognised as a defined population using the anti-CD19 marker (te Vrugte et al. 2004). To follow up on previous work by others reporting expansion of the lysosomal system in B cells from patients with NPC1, NPC2 and Tay-Sachs, I now go further in this study to validate, using B-LCLs, the possibility that lysotracker could be used as a technique for the diagnosis and monitoring of a broad spectrum of LSDs. Rather than utilise flow cytometry as used in previous lysotracker studies on LSD B cells (Lachmann et al. 2004b; te Vrugte et al. 2014), I instead focused on developing a magnetic 96-well plate capture assay. This has numerous advantages including utilisation of cheaper equipment found in most hospitals, miniaturisation of the assay to reduce costs and sample volumes and no need for an expert user to run and maintain the machine. The characteristics of an ideal biomarker would be a means of measuring that was quick, reliable and inexpensive. Having shown earlier that the lysotracker assay is robust in a high throughput 96-well plate format in patient fibroblasts I determined whether the assay could be modified for direct magnetic capture of circulating CD19+ B cells from whole blood. Anti-CD19 antibodies have been widely used to identify and capture circulating B cells in mononuclear cell fractions of centrifuged whole blood. Our initial aim was therefore to determine whether I could utilise magnetic capture to determine changes in lysotracker fluorescence in a panel of immortalised B lymphoblasts prior to development of the assay towards human patient whole blood samples.

I started by investigating and comparing lysotracker fluorescence intensity in NPC1 B-LCLs by microscopy, FACS, and by 96-well plate magnetic capture by adding the CD19 and dextran-coated magnetic particles to the sample in a 96-well plate prior to separation and retention of CD19+ B cells using a magnetic stand. However, neither microscopy, FACS nor the plate reader assay showed any increase in lysotracker fluorescence in NPC1 B lymphoblasts compared to controls (Figure 3.17 A-D). There were in fact only minimal differences in lysotracker fluorescence between the control and NPC1 (Figure 3.17 A-D). I then tested cholesterol storage (using Filipin) by microscopy, as cholesterol is one of the lipids

stored in NPC1 (Figure 3.17 E-F). The results demonstrated that cholesterol storage measured by filipin staining was not significantly elevated in NPC1 cells leading us to hypothesise that this might be a result of rapid B-LCL cellular turnover (doubling in 16hr) that does not allow time for lysosomal storage to occur. Such a high density of cells also changes the medium pH quickly that can in addition stress the cells. Therefore, in order to minimise cell proliferation, 2% of dimethyl sulfoxide (DMSO) was used to arrest the cell cycle in the G1 phase and to prevent high cellular density (Fiore et al. 2002). I added 2% DMSO to the growth medium tank for 96 hours, and although this method did induce a small degree of cell death (observed by FACS), lysotracker only labels live cells meaning the dead cells could be gated out. In general, using 2% DMSO led to a two fold elevation of lysotracker staining values in NPC1 B lymphoblasts by all methods of analysis (Figure 3.17 A-D). Furthermore, the storage of cholesterol is evident in the NPC1 lymphocytes treated with 2% DMSO, with a ~2.5 fold elevation in the NPC1 B-LCLs (Figure 3.17 E & F). Thus, despite a small degree of cell death, the use of DMSO to arrest the B-LCL cell cycle provided a good model for induction of lysosomal storage and create cells that are more similar, in terms of lysosomal dysfunction, to endemic patient whole blood B cells.

Figure 3.17 Elevation of lysotracker and filipin staining in healthy control and NPC1 B-LCLs.

(A-D) Control (GM13072) and NPC1 (GM03124) B-LCLs grown either with or without 2% DMSO for 96 hours prior to 200 nM lysotracker staining by using either (A-B) fluorescence imaging and area analysis for quantification of lysotracker fluorescence staining per cell, (C) FACS and (D) 96-well plate magnetic capture and quantification by fluorescence plate assay. (E-F) Control (GM13072) and NPC1 (GM03124) B-LCLs treated either with or without 2% DMSO for 96hr prior to being fixed and stained with filipin, images were quantified as above using ImageJ. Statistical significance was calculated using one-way anova; **= $p < 0.01$, ****= $p < 0.0001$. scale bars, 5 μm . n=3 for all experiments. Data are shown as mean \pm SD.



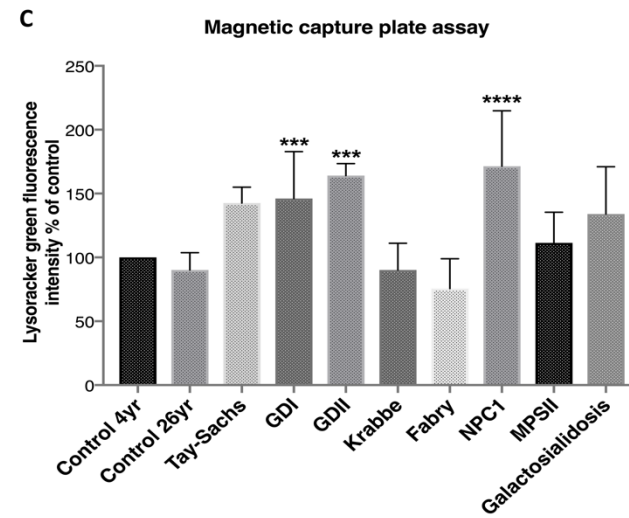
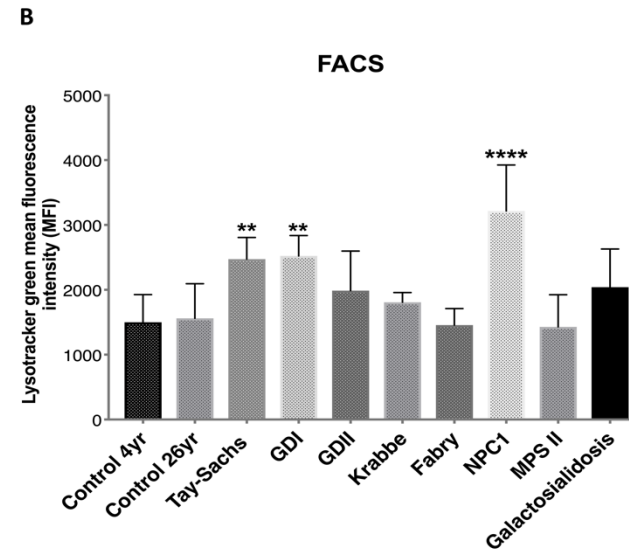
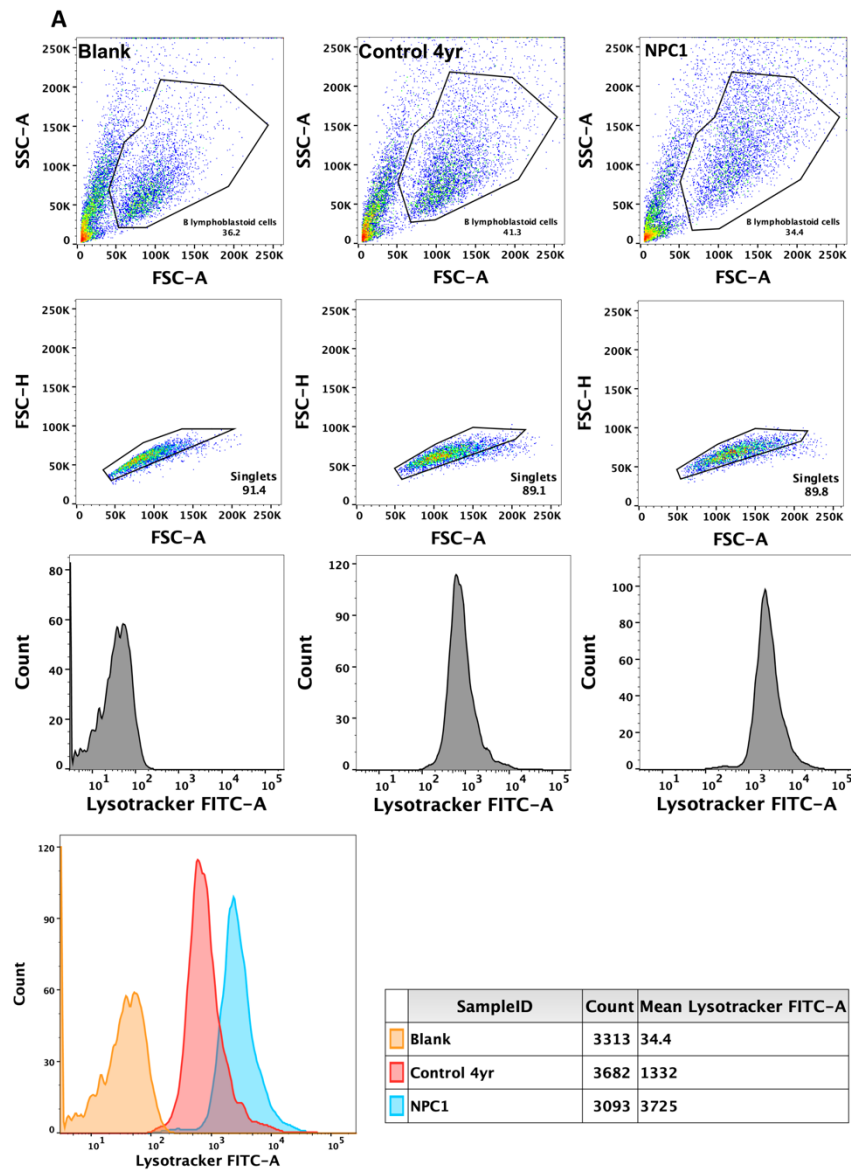
3.2.12 Comparison of flow cytometry and magnetic cell capture as methods to determine lysosomal storage across multiple lysosomal diseases

I next tested a broad spectrum of LSD B-LCLs treated with 2% DMSO for 96h by either FACS or the magnetic capture 96 well plate assay. For FACS I determined the appropriate gating parameters by using particle size to exclude dead cells (Figure 3.18 A). For the plate reader assay I captured the cells following an incubation with anti-CD19 and dextran-coated magnetic particles by placing them on a 96-well plate seated on an EasySep™ magnet stand and washing away non bound B-LCLs. The washing steps resulted in the loss of some cells, and as such it was not possible to standardise the 96-well plate assay against cell count as I had done with the primary fibroblasts (Figure 3.7 A & B). For this reason, I therefore decided to standardise the assay against Hoechst 33342. I am aware that Hoechst 33342 causes issues in the standardisation of fibroblasts as I showed earlier in section 3.2.7. Hence, I will ensure a careful comparison between both methods to discern any differences that may arise not as a difference of the assays used but of the method of standardisation. The possibility of measuring the protein concentration was omitted as I need more washing steps post-lysotracker-measurement to recapture the B-LCL, which may result in the loss of some cells and a further skewing of the data.

I found that the observed lysotracker fluorescence intensities in the LSD B-LCLs were largely similar across both the FACS and the 96-well plate assays (Figure 3.18), presumably as there is no storage in these cells. However, I did observe considerable storage in the NPC1 B-LCLs, with an ~2 fold increase in both cases. Our previous findings on fibroblasts (Figure 3.9) did not show an increase of lysotracker fluorescence in GDI patient fibroblasts, this is due to low levels of endogenous GlcCer and the residual activity of the GCCase enzyme, which degrades the low level of GlcCer storage in the lysosome (Sillence et al. 2002). However, GlcCer is present in higher levels and is known to accumulate in leukocytes, including lymphoblasts, which explains the lysotracker elevation in GDI of ~50% compared to control cells by both FACS and magnetic plate assay (Figure 3.18 B & C). The plate assay was unable to detect the elevations in storage in Tay Sachs compared to the FACS. However, it was able to detect storage in GDII B-LCLs, which flow cytometry could not. These results demonstrate the benefit of using lymphocytes over human fibroblasts in some cases (e.g. GD type I – Figure 3.9), provided the cells are grown in DMSO. Our data also provides a proof of principle that the magnetic capture assay protocol could work as an alternative to FACS for simpler future analysis of patient lysosomal storage in blood samples.

Figure 3.18 Comparison of LysoTracker fluorescence in B-LCLs by FACS and magnetic cell capture

(A) Show the sequential gating strategy used; the control (GM13072) and NPC1 (GM03124) B-LCLs were treated with 2% DMSO for 96 hours, then either unlabelled or labelled with 200 nM lysotracker prior to gating on the basis of size with (FSC-H vs FSC-A), followed by excluded doublets and only count single cells in the analysis. The positive area for lysotracker fluorescence was then selected from this population, followed by generation of the histogram of Mean Fluorescence intensity (MFI) of lysotracker fluorescence per cell. (B) The lysotracker intensity results from FACS assay for B-LCL LSDs and age matched controls. (C) LysoTracker fluorescence intensity from the 96-well magnetic capture method of B-LCL LSDs compared to age matched controls, B-LCLs were isolated using the 96-well plate-based magnetic capture of circulating CD19+ B cells using anti-CD19 magnetic antibodies. In all cases the B-LCLs were untreated or treated with 2% DMSO for 96 hours and then labelled with 200 nM lysotracker green alone (FACS) or combined with Hoechst (magnetic capture). The data is shown as percentage of control, n=3 for all experiments. *= $p < 0.05$; **= $p < 0.01$; ***= $p < 0.001$; ****= $p < 0.0001$. Data are shown as mean \pm SD.



3.3 Discussion

Lysotracker has been extensively used in cell biology to label LE/Lys (Pierzyńska-Mach et al. 2014), despite this, its precise mode(s) of action have largely remained underexplored. As a clinical biomarker, it has been used previously for monitoring NPC1 disease patients on miglustat and for monitoring of an NPC2 patient receiving stem cell treatment (Lachmann et al. 2004b; te Vrugte et al. 2014).

In addition, there has also been another study demonstrating the use of lysotracker as a small molecule screening tool in LSD fibroblasts (Xu et al. 2014). However, there has been considerable inconsistency in the way lysotracker has been used in these and other studies. Although the use of lysotracker is widespread, the aim of this chapter was to determine the precise conditions for appropriate use of lysotracker as a tool for cell biology, identifying and monitoring lysosomal disease treatments and determine whether it could be used for newborn screening. In our experiments I identified that proper use of lysotracker requires live conditions and low concentrations. It only fluoresces at lysosomal pH and loads into swollen and expanded lysosomes, I also identified that it is unaffected by the autophagy process. Our findings show that lysotracker could be a useful, simple and sensitive assay to monitor or identify new treatments (through high throughput screening approaches) for the majority of LSDs.

3.3.1 Investigating the fundamental properties of lysotracker as a lysosomal marker in cells

In order to determine the most suitable conditions for loading cells with lysotracker, I first assessed the suitability of the different types of lysotracker probes. I found that lysotracker green and red both showed a significant difference in fluorescence between a healthy fibroblast cell line and an NPC1 patient's fibroblast at low concentration (Figure 3.1 B-D). I followed this up to determine whether lysotracker was more appropriately used live or in fixed cells as is the suggested utilisation for lysotracker red according to the manufacturer. Our findings revealed that fixation was unsuitable as, by using 4% paraformaldehyde, it led to a partial loss of lysotracker fluorescence signal (Figure 3.2). This is not surprising as fixation leads to loss of protons from lysosomes, which lysotracker fluorescence is chemically dependent upon. I then demonstrated which lysotracker probes are the most photostable; our findings show that lysotracker red and green are not able to resist photobleaching, whilst lysotracker red, as previously reported (Freundt et al. 2007), also photoconverts to emit fluorescence at ~500 nm immediately after stimulation (Figure 3.3 C-F). Lysotracker red photoconversion might indeed be due to the similarity of molecular structures between

lysotracker red and green, with only an additional pyrrole ring in lysotracker red changing the fluorescent. The loss of this pyrrole ring during conjugation has been suggested to lead to a smaller wavelength emission and to conversion to green (Freundt et al. 2007). Therefore, such pseudo-signalling of an observable green signal would have significantly detrimental effects on any co-localisation study and has led to a conflicting interpretation of experiments where two colours were viewed at the same time, especially in high power confocal imaging. According to the literature, lysotracker red for the study of co-localization against brighter fluorophores in the green channel has been widely used (Frese et al. 2008). This finding does not support the use of lysotracker red for any colocalization study. These findings are in contention with a previous study that used lysotracker red in fixed conditions extensively as a small-molecule drug screening tool across LSD human fibroblasts (Xu et al. 2014).

Using a high concentration of lysotracker (>500 nM) for a long incubation time has been a common practice in the lysosomal research field, ensuring a good signal is obtained especially once the fixation step has been accomplished (Fossale et al. 2004). Our findings are the first to indicate that a long incubation period and high concentrations of lysotracker lead to an alteration of the intra-lysosomal pH (Figure 3.4). Lysotracker binds to protons, in doing so it becomes fluorescent and remains so whilst bound to protons, which it most likely retains as not all fluorescence is lost after fixation. This suggests it may act as a proton chelator within the lysosomal lumen, resulting in the increased pH of the LE/Lys compartment (Figure 3.4). Low concentrations of lysotracker, however, do not have the same effect; the amount of weak base captured in the lysosomes does not have any significant effects on osmolality, buffer concentrations or the pH of organelles. Our findings indicate that the high concentrations of lysotracker red used specifically to allow fixation are potentially damaging to the lysosome and have the potential to induce artefactual changes in lysosomal function. Only low concentrations and live staining should be recommended for lysotracker imaging of cellular lysosomes.

The lysotracker loading into LE/Lys is dependent not only on acidity but also their volume and number. Treating fibroblast cells with the Bafilomycin A1, GPN, nigericin and monensin drugs interrupts lysosomal acidification and produces a rise in the pH of the acidified compartment. These drugs lead to a significant decrease in the lysotracker signal, even in the presence of cholesterol accumulation and lysosome expansion (Figure 3.5 A-E). Also, treating fibroblast cells with sucrose (swelling) and U18666a, a chemical inhibitor of NPC1, (causing lipid storage and increase in lysosomal numbers) leads to elevation in lysotracker fluorescence (Figure 3.5 A-D).

In addition to loading into acidic LE/Ly compartments, lysotracker has been suggested as a probe to study the autophagy process. To demonstrate the likelihood of this, I used an autophagy inducer and observed how it affected lysotracker fluorescence. Rapamycin (an inhibitor of mTOR) is an autophagy inducer, it induces autophagy without inhibiting clearance of autophagic vacuoles via lysosomes. Our data demonstrated only a slight increase in lysotracker green fluorescence, indicating that autophagy and autophagosome-lysosome fusion does not significantly increase lysosomal storage or lysotracker fluorescence, despite considerable increase in autophagosomes within the rapamycin treated cells (measured using CytolD). A similar observation was obtained after using HBSS and amino-acid starvation, which are widely used autophagy inducers that again do not impair lysosomal function (Figure 3.6 A-B). The small changes I observe in lysotracker fluorescence may be due to the increase in autophagolysosome and autolysosome numbers but, as these are substantial organelles, are more likely to be the result of elevated pH within these compartments (Maulucci et al. 2015). I also show that there is not considerable overlap between these two separate fluorescent markers, indicating that lysotracker does not act as a marker of the autophagic system (Figure 3.6 C).

Microscopy imaging of lysotracker, although essential for confirming subcellular localisation, is ultimately low-throughput and technically challenging and is therefore not suitable for disease identification, monitoring or small molecule screening. In order to develop lysotracker as a high throughput 96-well plate assay, I firstly looked in-depth at the best method of standardisation for the lysotracker assay. This was identified as a crucial step in achieving optimisation. I decided to compare BCA assays (to determine the protein concentration in each well), Hoechst (a nuclei marker), and a cell count per well and compare the values obtained against microscopy images of lysotracker in the same cell line. Our findings showed that there was some variation when using either BCA or Hoechst (Figure 3.7 B). The level of protein per well was on several occasions too low for the BCA assay, whilst Hoechst staining was shown to be inconsistent in the lysosomal disease cells. Our findings propose for the first time that live cell nuclear markers have increased penetrance into LSD cells, presumably owing to different membrane fluidity, and should therefore not be used as a means of standardisation in LSDs (Figure 3.7 C). Any high throughput assays that have utilised nuclear stains as a means of standardisation in LSD cells must therefore now be questioned. Ultimately, using cell count as a means of standardisation showed the most consistent data when comparing against the microscopy images.

3.3.2 Lysotracker can identify lysosomal storage across the majority of LSD patient fibroblasts, but not all, and can be used to follow treatment.

In contrast to previous studies, this is the first study to look at cells from almost all LSDs (~50 LSDs) to evaluate the usefulness of lysotracker as a new bioassay/marker. The main characteristic of LSD disorders is the build-up and storage of material that is normally cleaved in the lysosome and transported out across the lysosomal membrane (Ballabio and Gieselmann 2009). LSD cells possess large lysosomes and are increased from 2-3% to up to 50% of the total cellular volume (Meikle et al. 1997). In addition, the lysosome is now being targeted for therapy and drug development for the treatment of LSDs. Appropriate assays for compound screening against lysosomes affected by disease have not yet been found, as illustrated by the numerous small molecule screening campaigns for NPC disease that have largely focussed on cholesterol storage and are yet to identify an approved small molecule (Pipalia et al. 2006). Based on our findings, I now know that lysotracker, when used live, can quantify an expansion in or enlargement of lysosomes, irrespective of their storage content, in the diseased cells of patients. I therefore tested whether lysotracker has the potential to be used as a widespread, cheap, high throughput screening tool for lysosomal diseases. Our investigation across LSD fibroblasts found that >60% (29/42) had an elevated lysotracker signal compared to age matched controls, when LSDs where there is no storage in patient fibroblasts are removed (e.g. GDI, GDII, Krabbe), this is then increased to ~75 %. Furthermore, this is the first study to show that lysosome expansion is common across all classes of LSDs. This assay is not specifically designed to identify one particular group of LSDs, but rather it is useful for all LSD groups and as a multi plate assay is considerably easier to conduct and analyse than previously published microscopy or mass spectrometry methods (Tortorelli et al. 2016; Zhang et al. 2008). Positive LSD fibroblasts, as revealed by lysotracker, acts mainly as a mirror, reflecting the build-up and storage of material in the LE/Ly compartments. Storage that can be monitored for any therapeutic change (Lachmann et al. 2004b). In contrast, some LSD fibroblasts do not accumulate storage material and hence have no increase in lysotracker. To investigate the reason behind this, I have compared anti-LAMP2 staining across a few LSDs with normal lysotracker staining (Figure 3.15). Those diseases lacking elevated lysotracker also showed a lack of lysosome expansion as anti-LAMP2 staining was identical to control cells. Some of these diseases have previously been reported as having a lack of accumulated substrates in patient fibroblasts. For example, studies have shown that GDI patient fibroblasts have no accumulation of GlcCer, and an electron microscope study of skin fibroblast failed to show any storage material (Sillence et al. 2002; Vult von Steyern et al. 1996). There is also normal lysotracker in MPS IV most likely due to the lack of keratan sulphate in MPS IV patient fibroblasts as the intracellular storage material

in MPS IV is cell type specific mainly occurring in cartilage derived cells (Hollister et al. 1975). Interestingly, two patients suffering from the same disease (Tay Sachs) exhibited differences in their lysotracker signal (Figure 3.9), that suggests that lysotracker is sensitive enough an assay to reflect the severity of storage level and therefore potentially of disease severity, as has previously been reported in NPC1 disease (te Vruchte et al. 2014). Furthermore, as several of these patient cells harbour mutations that result in the production of a small amount of viable protein, this residual enzyme activity in the fibroblast cells can lead to the elimination or reduction of storage material; one example is galactosialidosis, where minimal storage is detected by lysotracker due to the residual activity of β -galactosidase (β -gal) in the fibroblast (Zhou et al. 1995). From our large screen of lysosomal enzyme activities across the LSDs, in the galactosialidosis cells β -galactosidase activity was ~20% of control (Supplementary Figure 4).

On the other hand, another reason behind some LSDs not showing any elevation in lysotracker is a change in lysosomal pH in some LSDs. Lysotracker illuminates subcellular components with a pH of less than 5.2, particularly LE/Ly (Christine and Ponchel 2017). Our data and others indicate that fluorescence does not change in response to increasing acidity but instead changes in response to the number and volume of compartments that are acidic below pH 5.2. Hence, lysotracker is not pH-sensitive and cannot serve as a linear pH sensor, but it can show the presence of acidic compartments, since it does not fluoresce at pH above 5.2. Therefore, LSDs with increased lysosomal pH will exhibit a reduced lysotracker signal if the pH of the lysosome is 5.2 or above. Toxic lipids in some LSDs lead to the disruption of lysosomal pH regulation, such as psychosine, which is the lipid storage hallmark of Krabbe disease. The previous study have demonstrated the lysosomal pH defect in control cells treated with psychosine (Folts et al. 2016). However, it is unlikely this is the reason behind the lack of lysotracker signal in Krabbe fibroblast as the storage of psychosine was particularly observed in brain tissue (Harzer et al. 2002; Kobayashi et al. 1988). In addition, the elevation of lysosomal pH has been reported across some LSDs including NCLs, mucopolysaccharidosis, MLIV and Gaucher disease (Bach et al. 1999; Golabek et al. 2000; Holopainen et al. 2001; Pereira et al. 2010; Sillence 2013; Soyombo et al. 2006). However, for example, studies on Gaucher disease reported a change of up to 1 pH unit increase in lysosomal pH. So far, GlcCer and GlcSph are the only known accumulated substrates in Gaucher disease (Lloyd-Evans et al. 2003b). With such changes in pH, it would be expected that several more substrates would accumulate in Gaucher disease lysosomes, as has been observed with baf-A1 treatment which changes lysosomal pH by 1 pH unit (Figure 3.5 A-D). Furthermore, cathepsin D is a lysosomal enzyme with an extremely narrow pH optimum of 4.2 (Lloyd-Evans and Haslett 2016), if lysosomal pH was changed by 1 pH unit in all LSD cells

then I would expect to observe lysosomal storage in a similar manner to CLN10 disease where cathepsin D is also deficient, and I do not. With regards to the previous studies, it has been reported that the elevation of lysosomal pH is possibly due to the use of lysosomal pH-detecting probes (e.g. lysosensor, acridine orange), which are not lysosome-specific probes. These probes could be accumulated in all acidic endolysosomes; as long as those probes are not endocytosed, there is no possibility to compare the cellular loading with the probe against a loading control. This may lead to inaccurate lysosome pH measurements (Lloyd-Evans and Haslett 2016). For example, there could be the presence of completely different opposite measurements being reported, as has happened in the literature with for example MLIV (Bach et al. 1999; Soyombo et al. 2006). In this study, it could be that a change in lysosomal pH did not allow the observation of any lysotracker signal in CLN10 patient fibroblasts, this linked to our finding from the ultrastructural study of CLN10, which demonstrated an accumulation of Ganglioside/ Globosides/ triglycerides (see Chapter 6 Figure 5.6 O-S). This suggests the possibility of lysosome de-acidification in CLN10. However, lysotracker is still useful for detecting those diseases with significant pH alternation (reduction in fluorescence compared to control) and for drug screening to identify lysosomal re-acidification drugs (Yang et al. 2014).

Finally, I have confirmed that our high throughput lysotracker assay is capable of monitoring reduction in lysosomal storage in patient fibroblasts using a known approved NPC disease therapeutic, namely, miglustat, a substrate reduction therapy. LAMP immunoquantification by mass spectrometry of dried blood spots has been proposed as an LSD newborn screening test (Hua et al. 1998; Meikle et al. 1999). Of note is that our findings have shown that lysotracker is more sensitive as a monitoring tool for following treatment with miglustat than either of the LAMP antibodies (Figure 3.14). The electron microscope findings showed multiple large empty vacuoles (see Chapter 6, Figure 5.7 D-G). The empty vacuoles not stained with lysotracker suggest they are older ones with a possible higher pH as suggested (Bright et al. 2016). LAMP antibodies, however, still stain these vacuoles (Figure 3.14), so lysotracker is the better fluorescent marker for monitoring substrate reduction therapy. In addition, one direct outcome of this work is the utilisation of the lysotracker assay for small molecule screening to identify analogues of miglustat currently underway in the ELE lab. As cholesterol, the largest material stored by mass in NPC1, does not change with miglustat treatment, it is possible that lysotracker is the best phenotype for indiscriminate small-molecule screening for this and other LSDs.

3.3.3 Development of a simple high throughput lysotracker assay based on magnetic capture of circulating CD19+ B lymphocytes.

Previous studies have used flow cytometry to measure lysotracker intensity in circulating B cells from patient clinical samples (Lachmann et al. 2004b; te Vruchte et al. 2014; te Vruchte et al. 2015). In this chapter I have studied the possibility of developing a 96-well fluorescent plate reader assay, based on the magnetic capture of circulating CD19+ B lymphocyte cells before their loading with lysotracker. There was a limitation to our approach as access to clinical samples was restricted during the project. I therefore decided to use B-LCLs, which are generated by the infection of B lymphocytes *in vitro* with the Epstein Barr Virus resulting in a continuous source of B lymphocytes (Neitzel 1986). B-LCLs specifically express the B lymphocyte marker CD19 resulting in their ability to be captured and separated out of whole blood. Initially I found that fast growing B-LCLs, unlike the B lymphocytes in peripheral blood; had less accumulation of cholesterol in NPC1 and therefore less lysotracker accumulation owing to rapid cell division and turnover. Arresting the cell cycle with 2% DMSO showed the possibility of using these B-LCLs in the development of the lysotracker magnetic capture assay as lysosomal storage was now observed (Figure 3.17).

To develop our fluorescence 96-well plate assay, based on the magnetic capture of circulating CD19+ B-LCLs of LSD patients, I initially investigated the lysotracker assay of healthy control and NPC1 B-LCLs, considering different approaches, namely, microscopy, FACS, and the new CD19+ B-LCLs magnetic capture method (Figure 3.15). An investigation showing significant differences between DMSO treated healthy control and NPC1 B-LCLs encouraged us to test other LSDs using B-LCLs. I found the same trend of lysotracker elevation by FACS analysis and also the new approach of magnetic cell capture and 96-well fluorescent plate reader analysis. Our data also showed that by using B-LCLs Gaucher disease was able to be detected (Figure 3.18 B & C), this was not possible when fibroblasts were used (Figure 3.9). The GDII fibroblast and B-LCLs were from the same patient. Interestingly, in contrast to our findings of elevated lysotracker in Fabry fibroblasts (Figure 3.9), Fabry B-LCLs shows no increase in lysotracker staining (Figure 3.18). This is consistent with a previous study showed the B cells isolated from $\alpha\text{-gal}^{-/-}$ mouse showed normal distribution of BODIPY-LacCer (fluorescent lipid once endocytosed is target the Golgi, it used to the assessment of endocytosis trafficking), and normal cholesterol and lysotracker levels. That was suggested the level of the accumulated lipids in B cells was not sufficient to disrupt endocytosis (Te Vruchte et al. 2010). In the same manner, MPS II B-LCL showed no increase in lysotracker (Figure 3.18 B & C) in contrast to our finding of lysotracker from two MPS II patient fibroblasts, which showed an increase in lysotracker staining (Figure 3.11). That would suggest that B

cells are not always the best model for all LSDs or maybe the variability in lysotracker is a result of disease mutation, stage and clinical severity.

Such a finding opens the door for huge and exciting possibilities: for LSDs, diagnosis by using a simple fluorimetric test for lysosomal swelling. Such a test is available in all hospitals unlike FACS, which is only available in referral hospitals and needs qualified interpreters for the result. I have developed this magnetic capture assay to be used to capture B lymphocytes from a peripheral blood sample, but it could be used for capture of other cell populations as well. This approach allows a straightforward analysis of the blood sample of the patient, one from a family at high risk of LSDs. Furthermore, specific tests can be ordered later for confirmation, enzyme assays for example (see Chapter 4). This simple lysotracker procedure can also be used for LSD patients recruited in clinical trials for new therapies and could be used for monitoring the progress of the patients' treatment.

The downside to using new high throughput lysotracker assay based on magnetic capture of circulating CD19+ B lymphocytes for clinical purposes is that the assay should be done on live cells. There is also a need for healthy control volunteers to be used as a control every time you run the assay. The samples should also be analysed within 3 days to ensure that optimal cell viability is maintained. The loading control used with B-LCLs is not as easy as with fibroblasts. These B-LCLs are growing in suspension and mainly form cell clusters. The washing processes during the magnetic capture method make it impossible to control the cell numbers. Therefore, in our assay I used Hoechst for cell count estimation. Nevertheless, this new 96-well fluorescent plate reader format, using the magnetic capture method, is possible for clinical use as long as cell loading can be controlled. There are factors that still need to be considered with the 96-well-plate-based magnetic capture of circulating CD19+ B lymphocyte cells before this test can become established in clinical and research settings.

3.4 Conclusion

To conclude this chapter, using lysotracker in optimized conditions allows accurate LE/Lys volume measurement. Lysosome expansion is the most common cellular phenotype across LSDs. Lysotracker green offers a sensitive method for identifying, monitoring and developing new therapies for LSDs. Our future work will involve getting access to clinical samples to confirm this approach.

Chapter 4: Developing new enzymatic biochemical markers for lysosomal storage diseases

4.1 Introduction

Multiple lysosomal enzyme activity evaluations across the majority of the LSDs have not previously been achieved. In this study, an analysis of 23 essential lysosomal enzyme activities across the majority of LSDs has been carried out with the aim of developing a potentially simple clinical biomarker, providing an insight of the mechanisms of disease and proposing novel therapeutic approaches.

4.1.1 Use of lysosomal enzymes in diagnosis and monitoring

The majority of LSDs are caused by defects in lysosomal enzyme activity (Desnick et al. 2001). There are also several LSDs that result from loss of accessory protein, transmembrane protein or non-lysosomal enzyme function, such as defects in activator proteins, trafficking proteins or ion channels. LSDs can also result from multiple lysosomal enzyme deficiency resulting from a defect in the processing of enzymes in ER- and Golgi/TGN (Walkley and Vanier 2009a). Since most LSDs are caused by the lack of certain enzymes resulting in the accumulation of their associated substrates, measurement of residual lysosomal enzyme activity provides a useful means of diagnosing LSDs. This can then be confirmed by mutation analysis of the genes encoding the enzyme. The selection of the specific enzyme to be genetically tested is also based on clinical manifestations (Wenger et al. 2002). Enzyme activity could be measured in different biological fluids, such as serum, plasma, urine and CSF. Leukocytes are often used as the most appropriate sample for enzyme assays, but fibroblasts are still considered to be the best sample for diagnosis as they have more optimal enzyme activity. B-LCLs may also be useful but some enzymes such as arylsulphatase A do not exist in B-LCLs (Filocamo and Morrone 2011).

A variety of enzyme assays are used in the diagnosis of LSDs; these are listed in (Chapter 1 Table 1.1). In terms of using the enzymes in disease monitoring, if I use GD, which is caused by a GCCase deficiency, as an example, in GD, the undegraded GlcCer accumulates in the tissues, especially in macrophages. In the 1990's, chitotriosidase, a member of the glycosylhydrolase family, was found in the plasma of GD. It is highly expressed in lipid-laden macrophages (Gaucher cells). The amount of chitotriosidase found in plasma/ serum reflects the total amount in the storage cells and these levels are then used in the clinical management of GD (Czartoryska et al. 1998; Hollak et al. 1994). There have been several studies that have

demonstrated that chitotriosidase activity responds to bone marrow transplantation treatment (Young et al. 1997). Plasma chitotriosidase does not change significantly in enzyme replacement therapy, although it does normalise to some extent if there is a switch to substrate reduction therapy with miglustat (Kuter et al. 2013). The level of chitotriosidase in plasma decreased during the treatment of GD disease with miglustat treatment. Cox et al showed a reduction of 16.4% in elevated GD chitotriosidase at 12 months post treatment (Cox et al. 2000). Another study have shown the reduction of chitotriosidase in plasma was 6.6% at 6 months and it becomes 15.3% at 12 months post miglustat treatment (Heitner et al. 2002). As a result of these properties, chitotriosidase is therefore the best monitoring assay alongside GlcSph measurement in plasma which is one of the primary storage lipids in GD (Rolfs et al. 2013). Another example of an indirect biomarker of lysosomal storage material is the fact that dipeptidyl peptidase IV (DPP-IV) levels increase in the blood plasma of patients with different types of mucopolysaccharidoses. Hence, it has been suggested that DPP-IV enzyme activity could be used as a biomarker for MPS screening (Hetmańczyk et al. 2016). However DPP-IV is not a specific biomarker to mucopolysaccharidoses. It has been proposed as a marker for certain tumors, immunological and viral infections diseases (Lambeir et al. 2003).

4.1.2 Secondary changes in lysosomal enzymes activities

The identified primary storage materials in LSDs typically result from a single enzyme defect. However, the metabolic process in LSDs is much more complicated than simply one enzyme defect and one substrate accumulating in the affected cells. There are in fact multiple storage materials within the affected cells of most of the LSDs (Platt et al. 2012). Such heterogeneity in the accumulated substrates means that there may be more than one affected enzyme. Considering the extent of secondary storage materials across LSDs, it is highly likely to be involved in disease pathogenesis (Walkley and Vanier 2009a). The mechanism behind the accumulation of multiple compounds among LSDs is still not yet fully understood. There is, however, a possible mechanism behind the secondary storage and this may include the inhibition of lysosomal enzyme activity as a result of primary substrate accumulation in the cells. However, there is another possibility that the LE/Lys internal pH may change due to the accumulated materials within the lysosome and this could change the optimum pH conditions for enzyme activity. These expected mechanisms, as well as the storage material itself, could interrupt trafficking and interfere with the fusion of LE/Lys and the induction of autophagy which in turn may impair delivery of enzymes to lysosomes (Walkley and Vanier 2009a).

β -hexosaminidase (comprised of combinations of HexA and HexB subunits) is one of the most studied lysosomal enzymes in LSDs. A lack of the Hex A isozyme, due to mutations in the α -

subunit gene (*HEXA*), causes Tay Sachs disease, whereas mutations in the β -subunit (*HEXB*) cause a deficiency of HexA and HexB, causing Sandhoff disease (Gravel 1995). One indication of a role of β -hexosaminidase in other LSDs is in NPC where mass spectrometry found β -hexoaminidase activity to be increases in serum of NPC mutant animals (Sleat et al. 2012). NPC1 and NPC2 diseases are both characterised by the accumulation of GM2 in lysosomes, as found in 50 day-old mouse models (Vanier 1999). Interestingly, the results from this study are consistent with an increase in β -hexoaminidase as a cellular response to increased levels of GM2, which may at first appear counter-intuitive but is likely a response to enzyme mis-localisation (as occurs with ASMase in NPC disease) or inhibition. In Niemann Pick A/B mutant mice, where ganglioside GM2 storage is also observed, it was found that β -hexoaminidase activity increased two to three times within the brain (Sleat et al. 2012).

Similarly, gangliosidoses (GM2, GM3) are the main secondary storage in mucopolysaccharidoses, which raises the possibility that glycosaminoglycan (GAG) accumulation inhibits the lysosomal enzymes involved in ganglioside degradation (McGlynn et al. 2004). This is supported by a study whereby both subunits of β -hexosaminidase were genetically deleted resulting in primary accumulation of both ganglioside accumulation and GAG storage (Sango et al. 1996). Alternatively, a previous study has demonstrated that β -galactosidase (β -gal) and α -galactosidase A (α Gal A) activities are slightly defective in the livers of patients diagnosed with MPS I, MPS II and MPS III (Kint et al. 1973). Furthermore, the addition of exogenous GAGs *in vitro* to 21 different lysosomal enzymes in leukocytes provoked strong inhibition of those enzymes in a pH-dependent manner (Avila and Convit 1975).

There are several clinical similarities between NPC1, NPA and NPB diseases that are due to defective acid sphingomyelinase (aSMase) activity, as a result of which these diseases are characterised by a build-up of sphingomyelin and cholesterol in the cells (Higaki and Ohno 1998). aSMase's hydrolysis of sphingomyelin produces ceramide and phosphocholine. There is an intracellular relationship between cholesterol and sphingomyelin metabolism. sphingomyelin has a high affinity for cholesterol, resulting in a relatively similar distribution of both lipids (Higaki and Ohno 1998). The involvement of cholesterol in inhibition of the action of the human fibroblast aSMase was identified in 1981 (Maziere et al. 1981). In NPC1 fibroblasts that have a lysosomal accumulation of unesterified cholesterol, the aSMase activity is decreased by 50% when the cells are grown in a medium comprised of 10% FCS or elevated LDL cholesterol (Vanier et al. 1991). Removing lysosomal cholesterol by growth of cells in lipoprotein deficient serum (LPDS) restores the activity of the lysosomal aSMase to normal (Thomas et al. 1989). Hence, it has been proposed that aSMase is affected or regulated by

the concentration of lysosomal cholesterol. The post-translational defect in aSMase have been reported in NPC1 humans and animal model (Harzer et al. 2003; Pentchev et al. 1980). However, other study have shown that there are no changes in the subcellular localisation of lysosomal aSMase in NPC fibroblast (Tamura et al. 2006). This study even suggested that lysosomal cholesterol does not cause reduced aSMase activity (Tamura et al. 2006). This report is however in conflict with earlier work from the *Npc1*^{-/-} mouse model where aSMase activity was not found to be any different in the mouse brain but the enzyme itself was not found in purified lysosomes, indicating a cellular mis-trafficking of the enzyme that explains the presence of sphingomyelin storage (Sakiyama et al. 1987).

Collectively, the effects of storage material may be attributed to a modification in lysosomal enzyme activities either via direct inhibition or mis-localisation. Therefore, secondary lysosomal changes can serve as useful indicators and provide approaches to more substantial investigation. In terms of treatment, notwithstanding the defect in protein responsible for the primary defect, there is the possibility of correcting secondary abnormalities that will in turn lead to the correction of major pathological features of LSDs. For example, aSMase deficiency in NPC1 whereby this defect has become a target for therapeutic treatments. The restoration of aSMase activity by recombinant human aSMase was able to reduce free cholesterol storage (Devlin et al. 2010; Harzer et al. 2003).

4.1.3 Lysosomal enzyme measurement techniques

Enzyme assays are widely used in LSDs for diagnosis and drug-screening to find possible enzyme inhibitors and activators. Many techniques are available and used in LSD lysosomal enzyme measurements (Wenger et al. 2002, 2003). Some of the main techniques are fluorometric assays using 4-methylumbelliferyl (4-MU) substrates, spectrophotometric assays and immune quantification assays (Yu et al. 2013). Over the last decade, however, dried blood spot (DBS) or Guthrie cards have been widely used in enzyme assays as it is cheap, easy to collect and preserves the enzyme activity (Chamoles et al. 2001a; Chamoles et al. 2001b). The 4-MU assay is an essential method for lysosomal enzyme measurement and has been used widely in research. The 4MU fluorophore is based on the natural product umbelliferyl and is chemically attached to a synthetic substrate specific to particular lysosomal enzymes (Yu et al. 2013). The Hopwood group has been developing enzymes and protein content to be used in multiplexed immune quantification assays. The idea here is to capture the enzyme proteins content in DBS by using the antibodies specific to 11 different lysosomal proteins and use fluorometry to immune-quantify the lysosomal protein (Meikle et al. 2006). Li *et al.* (2004) highlighted the usefulness of tandem mass spectrometry via enzyme activity to detect

Gaucher, Pompe, Krabbe, Fabry and Niemann-Pick A/B lysosomal enzymes by DBS (Li et al. 2004). These studies have led to numerous pilot studies. At present, a mass spectrometry-based multiplex assay for measuring lysosomal enzyme activities is being used in many pilot population screenings for Niemann-Pick A/B, Gaucher disease, Pompe disease, Krabbe disease and mucopolysaccharidosis type I (MPS I) disease (Yu et al. 2013).

The main aim of this chapter is to screen a large cohort of lysosomal enzymes across the majority of LSDs. Such large-scale enzyme assays will make use of a 96-well-plate format to save on reagents and expense. Fluorometric enzyme assays are based on the enzymes cleaving to the artificial substrate, which is binding to the fluorophore; when the fluorophore releases it becomes fluorescent, and the fluorescence reflects the relative enzyme activity (Xu et al. 2012a). There are several advantages in using this artificial substrate, namely; (1) high sensitivity of the assay, (2) simple and inexpensive to set up, (3) a high-throughput assay, and (4) it could also be further adapted to enable more advanced techniques to be used (Motabar et al. 2009; Xu et al. 2012a).

4.1.4 Aims

- 1- This study aims to compare the activities of 23 lysosomal enzymes across the majority of LSD fibroblasts (34 LSDs) that could broaden the scope of diagnostic options for LSDs and identify new therapeutic targets.
- 2- To use mouse models of some LSDs to validate the secondary enzymes altered from the fibroblast studies.
- 3- To investigate the effect of miglustat treatment on some lysosomal enzymes and determine the possibility of developing secondarily altered enzyme activities as potential monitoring tools or biomarker for disease progression or treatment.
- 4- To investigate the possibility of rescuing LSD phenotypes by correcting the secondary enzyme defects identified.

4.1.5 Summary of methods

In Section 4.2.1 I measured the lysosomal enzyme activity (see chapter 2 section 2.7) across LSD fibroblasts and compared against age matched controls to identify secondary enzymes defects specific to individual and groups of LSDs.

In Section 4.2.2 I confirmed altered activity of enzymes of interest from the patient fibroblasts in mucopolysaccharidoses mouse tissues

In Section 4.2.3 I validated our findings from NPC1 patient fibroblasts on mouse tissues and other NPC1 patient fibroblasts with less common mutations.

In Section 4.2.4 I showed the effect of miglustat treatment on enzyme activities from the control fibroblasts, NPC1 and CLN5 disease.

In Section 4.2.5 I compared our findings of altered enzymes in CLN5 fibroblasts to CLN5 patient dry blood spots to determine the overall validity of the fibroblast data and to determine usefulness of these assays in monitoring the ongoing effects of miglustat treatment.

In Section 4.2.6 I have tested the possibility of secondary enzymes defect to become a therapeutic target by adding recombinant human acid lipase (rhLAL) enzyme to the culture medium of some LSD fibroblasts.

4.2 Results

4.2.1 Extent of secondary lysosomal enzyme alteration across LSD fibroblasts

First, ~80% confluent fibroblasts cell lines were pelleted and kept at -80°C prior to homogenization and protein determination by BCA (See chapter 2, section 2.7.1 & 2.7.2). The majority of these enzyme assays were modified from previous studies (see table 2.2). Each enzyme assay required a particular substrate, a reaction buffer, a stop buffer, and a standard. The pH effect on the catalytic enzymes was investigated by using different buffers with a range of pH. The use of the optimum pH of each enzyme will enhance the discrimination between the control and the diseased samples (Supplementary figure 1). To confirm the specificity of the substrates I used either the specific disease cell line associated with that particular enzyme deficiency or, if there was no specific disease, I used the specific inhibitor to confirm the accuracy of our developed enzyme assay (Supplementary figure 1). In the absence of any specific assay I developed the suitable conditions to measure the dipeptidyl-peptidase (DPP) enzymes (see table 2.2). In terms of substrates, all the assays were determined by a fluorometric measurement of the liberated fluorophore from the cleaved substrate, apart from the Gly-pro-p-nitroanilide substrate as it is measured by absorbance (see table 2.2). Heat-inactivation was used to deplete all enzymes activity and used as a background only control.

Following optimization of the enzyme condition I measured 23 lysosomal enzymes in skin fibroblast cell lines obtained from 3 controls, 34 LSDs and selected other neurological and neurodegenerative diseases. In all assays I used commercially available inhibitors for each enzyme and heat-inactivated samples to confirm the specificity of the assay and to subtract background. I determined enzyme activity by using the suitable enzyme substrate standard curve to generate enzyme activity as $\mu\text{mol/g}$ of protein/ hr (supplementary figures 3- figure 25). In this project I mainly desired to see if any enzymes could be potential biomarkers for a particular group of LSDs. To simplify the dataset (see supplementary figure 3 – figure 25), I have generated a heat map of the change in enzyme activity as percentage change of the average mean values of the LSDs versus the controls (1yr., 6yrs. and 45yrs.). Interestingly, in the controls, across the enzymes measured I observed an increase in the activity of some enzymes with age (supplementary figure 26) illustrating the importance of having age matched controls over a similar age range to the patient cells.

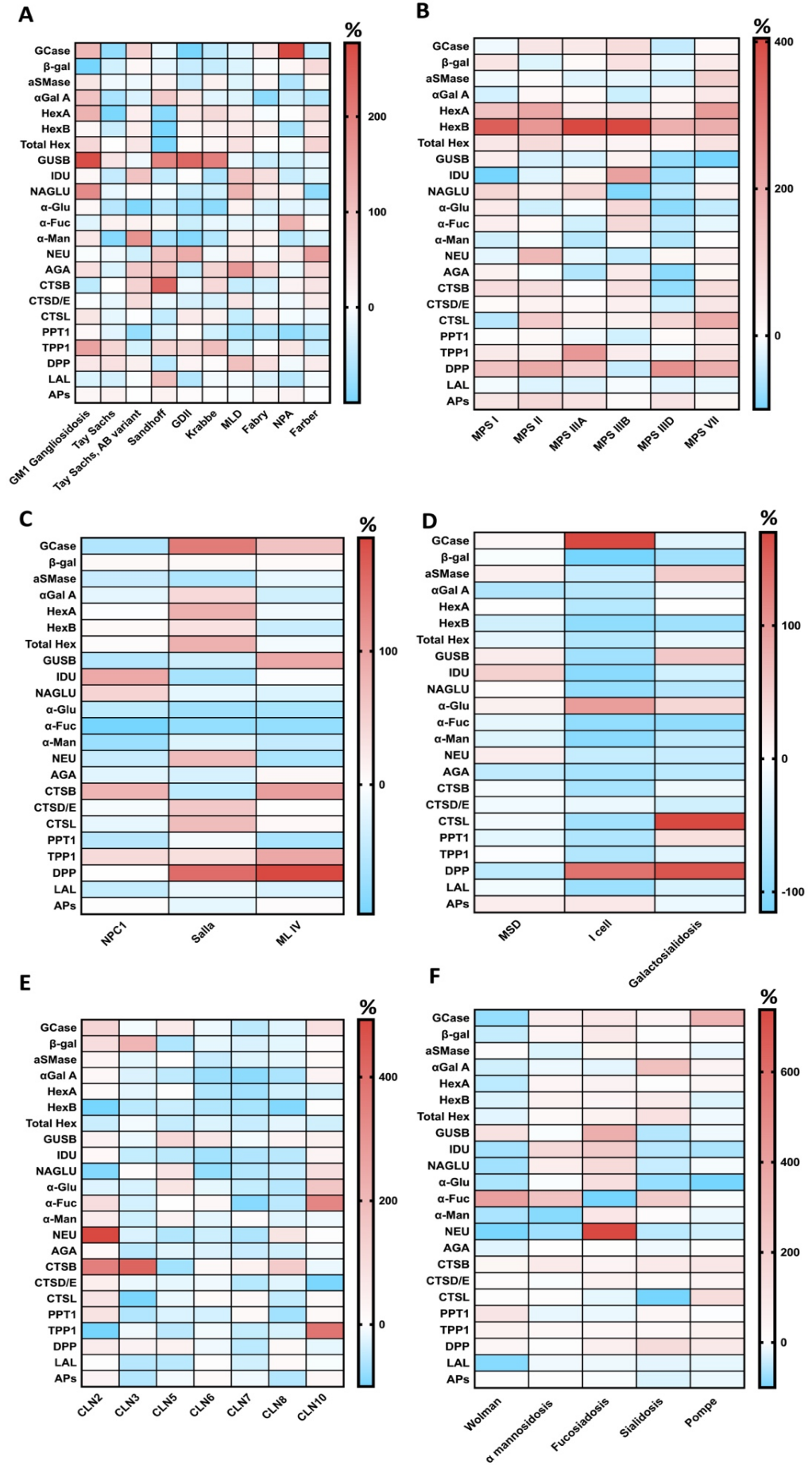
4.2.2 Identification of secondary enzyme activity defects among the sphingolipidoses

In this study I have included one fibroblast line bearing a common mutation representing the majority of sphingolipidoses (Figure 4.1 A). There was no obvious trend of alteration in particular enzymes across the sphingolipidoses. However, there were some significant large differences in some enzymes (Figure 4.1 A). First, an absence of the specific enzyme activity genetically deficient in each disease was confirmed; these were β -gal in GM1 gangliosidosis, GCCase in GDII, HexA in Tay-Sachs, HexA, HexB and Total Hex in Sandhoff, α Gal A in Fabry and aSMase in NPA. The Tay-Sachs AB variant exhibited high HexA activity, due to a deficiency in the HexA activator protein but not at the enzyme level (Hechtman 1977) (Figure 4.1 A). In terms of secondary defects, HexA was found to be increased among 60% of the sphingolipidoses; GM1 gangliosidosis ($p \leq 0.0001$), Tay Sachs AB variant ($p \leq 0.01$), GDII ($p \leq 0.0001$), Krabbe ($p \leq 0.0001$), MLD ($p \leq 0.001$) and Farber ($p \leq 0.0001$). Interestingly, the GUSB enzyme was upregulated the most of all the enzymes in half of the sphingolipidoses; these were GM1 gangliosidosis ($p \leq 0.0001$), Tay Sachs ($p \leq 0.01$), Sandhoff, GDII and Krabbe ($p \leq 0.0001$). α -Glu was decreased in Tay Sachs ($p \leq 0.0001$), Tay Sachs AB variant ($p \leq 0.0001$), Sandhoff ($p \leq 0.0001$), GDII ($p \leq 0.0001$) and Krabbe ($p \leq 0.0001$) and Fabry ($p \leq 0.001$). Of the sphingolipidoses, 70% showed an increase in AGA, which is a glycoprotein catabolism enzyme. There was an increase in the AGA activity in GM1 gangliosidosis ($p \leq 0.01$), Tay Sachs AB variant ($p \leq 0.0001$), Sandhoff ($p \leq 0.0001$), Krabbe ($p \leq 0.0001$), MLD ($p \leq 0.001$), Fabry ($p \leq 0.001$) and Farber ($p \leq 0.001$). There was a reduction in PPT1 activity in $\sim 80\%$ of the sphingolipidoses; Tay Sachs ($p \leq 0.05$), Tay Sachs, AB variant ($p \leq 0.0001$), Sandhoff ($p \leq 0.0001$), Krabbe ($p \leq 0.0001$), MLD ($p \leq 0.001$), Fabry ($p \leq 0.001$), NPA ($p \leq 0.0001$) and Farber ($p \leq 0.0001$). In contrast, TPP1 was increased in GM1 ganglioside ($p \leq 0.0001$), Tay Sachs ($p \leq 0.0001$), Sandhoff ($p \leq 0.0001$), Krabbe ($p \leq 0.0001$) and NPA ($p \leq 0.0001$). LAL activity decreased in only 50% of sphingolipidoses; GM1 gangliosidosis ($p \leq 0.001$), Tay Sachs ($p \leq 0.001$), GDII ($p \leq 0.001$), Fabry ($p \leq 0.0001$) and NPA ($p \leq 0.0001$) (Figure 4.1 A).

Figure 4.1 Heat map of lysosomal enzyme activity among the majority of LSDs fibroblasts.

Heat maps depict the lysosomal enzyme activity in fibroblasts. These heatmaps were generated from the percentage of enzyme activity compared to the controls (1yr., 6yrs, 45yrs old) (see supplementary table 1). Data is separated into different LSD groups comprising (A) sphingolipidoses, (B) mucopolysaccharidoses, (C) transmembrane protein defects, (D) multiple enzyme deficiency, (E) neuronal ceroid lipofuscinoses (NCLs) (F) cholesteryl esters and triglycerides storage disease, oligosaccharidoses and glycogenoses (see supplementary table 1). The rows represent the different lysosomal enzymes assayed (see below) and the columns represent the different LSD fibroblast homogenates used. The scale depicts the percentage change in enzyme activity compared to the controls; the blue gradient represents low activity while the red gradient represents high activity and white means the activity is within the control range. Heat map data was calculated from the mean enzyme activities shown in (appendix figure 3-figure 25).

lysosomal enzymes included: β -glucosidase (GCase), β -galactosidase (β -gal), Acid sphingomyelinase (aSMase), α -galactosidase A (α Gal A), Hexosaminidase A (HEXA), Hexosaminidase B (HEXB), Total Hexosaminidase (Total Hex), β -glucuronidase (GUSB), α -L-iduronidase (IDU), α -N-acetylglucosaminidase (NAGLU), Acid α -glucosidase (α -Glu), α -fucosidase (α -Fuc), α -mannosidase (α -Man), Sialidase (NEU), Aspartylglucosaminidase (AGA), Cathepsin B (CTSB), Cathepsin D+E (CTSD/E), Cathepsin L (CTSL), Palmitoyl-protein thioesterase 1 (PPT1), Tripeptidyl peptidase 1 (TPP1), Dipeptidyl peptidase enzymes (DPP), Acid lipase (LAL), Acid phosphatase (APs).



4.2.3 Identification of secondary enzyme activities altered in the mucopolysaccharidoses

Changes in enzyme activities across the mucopolysaccharidoses disease fibroblasts showed enzyme changes specific for each disease and common across these diseases. As with the sphingolipidoses, the primary enzyme defects in the MPS disorders were initially confirmed, namely; IDU was low in MPS I ($p \leq 0.0001$), NAGLU was low in MPS IIIB ($p \leq 0.0001$) and GUSB was defective in MPS VII ($p \leq 0.0001$). The defective enzymes associated with the other MPS patient fibroblasts could not be confirmed as the assays do not exist or were difficult to replicate. Interestingly, I have found that HexA and HexB were increased across all the mucopolysaccharidoses ($p \leq 0.0001$). Total Hex activity was also increased in most of the mucopolysaccharidoses; MPS I ($p \leq 0.0001$), MPS II ($p \leq 0.0001$), MPS IIIA ($p \leq 0.0001$), MPS IIIB ($p \leq 0.0001$), MPS IIID ($p \leq 0.05$) and MPS VII ($p \leq 0.0001$). The NAGLU enzyme which is involved in the degradation of heparan sulfate were upregulated among the majority of mucopolysaccharidosis; MPS I ($p \leq 0.0001$), MPS II ($p \leq 0.0001$), MPS IIIA ($p \leq 0.0001$) and MPS VII ($p \leq 0.0001$). Across the MPS disease cells, several lysosomal protease enzyme activities were elevated. The CTSB enzyme was upregulated in MPS I ($p \leq 0.001$), MPS II ($p \leq 0.01$), MPS IIIB ($p \leq 0.001$) and MPS VII ($p \leq 0.001$), (Figure 4.1 B). TPP1 activity was increased across 90% of the mucopolysaccharidoses, in MPS I ($p \leq 0.0001$), MPS II ($p \leq 0.0001$), MPS IIIA ($p \leq 0.0001$), MPS IIIB ($p \leq 0.0001$) and MPS VII ($p \leq 0.0001$). Furthermore, DPP was increased significantly, $p \leq 0.0001$, among all mucopolysaccharidosis apart from MPS IIIB. Reduced LAL activity was detected in MPS II ($p \leq 0.0001$), MPS IIIA ($p \leq 0.0001$), MPS IIID ($p \leq 0.0001$) and MPS VII ($p \leq 0.0001$) (Figure 4.1 B). Finally, Aps was upregulated in MPS I ($p \leq 0.0001$), MPS II ($p \leq 0.0001$), MPS IIIA ($p \leq 0.0001$), MPS IIID ($p \leq 0.0001$) and MPS VII ($p \leq 0.01$) (Figure 4.1 B).

4.2.4 Identification of altered secondary enzyme activities among the transmembrane protein associated lysosomal storage diseases

Following regular convention, I grouped together the lysosomal diseases caused by defects in lysosomal transmembrane proteins. There are no specific primary enzyme deficiencies for any individual disease within this group, however, ASMase is known to be reduced in NPC (Vanier et al. 1988) and that is confirmed here ($p \leq 0.0001$) and is also reduced in Salla ($p \leq 0.0001$) and slightly but not statistically significant in MLIV (Figure 4.1 C). I found a remarkable reduction among all of these diseases in α -Glu, α -Fuc, α -Man, LAL activity and an increase in TPP1 activity. α -Glu was decreased ($p \leq 0.0001$) in NPC1, Salla and MLIV. α -Fuc was also decreased in NPC1 ($p \leq 0.001$), Salla ($p \leq 0.0001$) and MLIV ($p \leq 0.05$). A significant decrease

in α -Man was also observed in NPC1 ($p \leq 0.0001$), Salla ($p \leq 0.05$) and MLIV ($p \leq 0.01$). In contrast, TPP1 were remarkably increased in NPC1 ($p \leq 0.0001$), Salla ($p \leq 0.0001$) and MLIV ($p \leq 0.0001$). Finally, LAL was also decreased in NPC1 ($p \leq 0.0001$), Salla ($p \leq 0.01$) and MLIV ($p \leq 0.001$) (Figure 4.1 C).

4.2.5 Identification of secondary enzyme activities altered in multiple enzyme deficiency diseases

The multiple enzyme deficiency diseases MSD, I Cell and galactosialidosis show a lack or lower residual enzyme activities in some lysosomal enzymes or enzymes that impact upon lysosomal transport processes. The prototypical LSD causing multiple enzyme deficiency is I cell (also referred to as mucopolipidosis type II), which shows a decrease in several lysosomal enzymes in fibroblasts but, in contrast, increased amounts of lysosomal enzymes have been recorded in DBS and plasma from I-cell patients, which are the result of enhanced secretion of the mistargeted enzymes (Brooks et al. 2007). I used I cell fibroblasts as an internal control for our enzyme assay analysis, with a considerable intracellular reduction in almost all lysosomal enzyme activities. I did however identify one enzyme whose activity was unchanged (CTSD/E) some enzymes that were elevated in I cell fibroblasts, namely GCCase ($p \leq 0.0001$), α -glu ($p \leq 0.0001$), DPP ($p \leq 0.0001$) and Aps which indicates that these enzymes are retained in lysosomes, or are captured from the extracellular space as is the case for GCCase, even in the case of a lack of mannose 6-phosphate moiety (Reczek et al. 2007). Regarding the other diseases, total Hex was decreased across MSD ($p \leq 0.01$), I cell ($p \leq 0.0001$) and galactosialidosis ($p \leq 0.01$). The AGA enzyme was low in MSD ($p \leq 0.01$), I cell ($p \leq 0.0001$) and galactosialidosis ($p \leq 0.0001$) (Figure 4.2 D).

4.2.6 Lysosomal enzyme alterations in the neuronal ceroid lipofuscinoses

No single enzymes were either increased or decreased across all of the NCLs (Figure 4.1 E). However, one or two of the HexA, HexB or total Hex activities were decreased in all the NCLs. For HexA; CLN6 ($p \leq 0.0001$), CLN7 ($p \leq 0.0001$), CLN8 ($p \leq 0.0001$) and CLN10 ($p \leq 0.0001$). HexB was decreased in CLN2 ($p \leq 0.0001$), CLN3 ($p \leq 0.05$), CLN6 ($p \leq 0.01$), CLN7 ($p \leq 0.001$), CLN8 ($p \leq 0.0001$). Total Hex was decreased in CLN2 ($p \leq 0.000$), CLN5 ($p \leq 0.0001$), CLN6 ($p \leq 0.001$), CLN7 ($p \leq 0.0001$), CLN10 ($p \leq 0.0001$). I found also remarkable reduction in ASMase in CLN3 ($p \leq 0.05$), CLN6 ($p \leq 0.0001$), CLN7 ($p \leq 0.0001$) and CLN8 ($p \leq 0.01$). The reduction in α Gal A enzyme that degrades globoside was decreased in CLN5 ($p \leq 0.01$), CLN6 ($p \leq 0.0001$), CLN7 ($p \leq 0.0001$) and CLN8 ($p \leq 0.0001$). in addition, NAGLU enzyme that degrades heparan sulfate was decreased in CLN2; $p \leq 0.0001$, CLN6 ($p \leq 0.0001$), CLN7

($p \leq 0.0001$), CLN8 ($p \leq 0.05$) and was increased in CLN5 ($p \leq 0.0001$), and CLN10 ($p \leq 0.0001$). Finally, the TPP1 enzyme activity was decreased in CLN2 ($p \leq 0.0001$) as expected and also in CLN5 ($p \leq 0.0001$), CLN7 ($p \leq 0.001$) and CLN8 ($p \leq 0.05$). Interestingly, a reduction in the activities of lysosomal enzymes was a common feature across most of the NCLs apart from CLN2 and CLN10 (Figure 4.1 E).

4.2.7 Altered lysosomal enzyme activities across the other LSDs (Wolman, Oligosaccharidoses and Glycogenoses)

I investigated the possibility of finding an enzyme biomarker for the other LSDs that consisted largely of lysosomal sugar degradative diseases and the acid lipase deficiency Wolman disease. As expected, Wolman disease showed very minimal activity of LAL ($p \leq 0.0001$) (Figure 4.1 F) with an overall reduction in activity of ~50% of lysosomal enzymes in this patient cell line. No obvious pattern or similarity could be discerned between Wolman's and any of the lysosomal sugar hydrolysis diseases. In the sugar diseases, not many trends were observed apart from an increase in the GCCase enzyme in the oligosaccharidoses; α mannosidosis ($p \leq 0.05$), fucosidosis ($p \leq 0.0001$) and sialidosis ($p \leq 0.05$). Total Hex was also somewhat increased in α mannosidosis ($p \leq 0.01$), fucosidosis ($p \leq 0.0001$) and sialidosis ($p \leq 0.0001$). Finally, TPP1 activity was increased in the oligosaccharidosis; α mannosidosis ($p \leq 0.05$), fucosidosis ($p \leq 0.05$) and sialidosis ($p \leq 0.0001$). Pompe disease showed an upregulation of mainly the proteolytic enzymes (e.g. cathepsins) and a downregulation of some sugar and glycolipid degrading enzymes, none of which match the other sugar hydrolytic lysosomal diseases. Interestingly, there was upregulation in all cathepsins; CTSB, CTSD/E, and CTSL ($p \leq 0.0001$). There was also an increase in the TPP1 activity ($p \leq 0.0001$) (Figure 4.1 F).

4.2.8 Confirmation of changes in human patient fibroblast lysosomal enzyme activities in mucopolysaccharidoses knock-out mouse tissues

The metabolism of fibroblasts under tissue culture conditions may be different compared to *in vivo* tissue metabolism. In order to validate the results I have obtained *in vitro* using the fibroblasts, I decided to repeat the enzyme analysis using knock-out mouse tissues. I obtained brain tissue from wild type, MPS I (*Idua*^{-/-}), MPS IIIA (*Sgsh*^{-/-}) and MPS IIIB (*Naglu*^{-/-}) of mouse brain tissue. I first confirmed the specific enzyme defect of each disease. IDU enzyme activity was indeed defective in *Idua*^{-/-}, with a reduction observed in enzyme activity ($p \leq 0.0001$), glucosamine-N-sulfamidase (SGSH) was undetectable in *Sgsh*^{-/-} ($p \leq 0.001$) and NAGLU was decreased in *Naglu*^{-/-} ($p \leq 0.05$) (Figure 4.2). SGSH enzyme activity was not included in our enzyme screening study (Figure 4.1) on fibroblasts as it involves a two-step assay requiring a

long incubation time, which makes it difficult to be adapted for either diagnosis, monitoring or a drug-screening assay (Bhaumik et al. 1999). I next used these knock-out mouse tissues to confirm our observations from the fibroblasts screening (Figure 4.1 B). Similar to the changes observed in patient fibroblasts, the *Idua*^{-/-}, *Sgsh*^{-/-}, *Naglu*^{-/-} brain tissues showed an increase in HexA ($p \leq 0.0001$), HexB ($p \leq 0.0001$) and Total Hex ($p \leq 0.0001$) activity. TPP1 activity, increased in all patient fibroblasts apart from MPSIIID, also increased significantly; $p \leq 0.0001$ across *Idua*^{-/-}, *Sgsh*^{-/-} and *Naglu*^{-/-} mouse brain, compared to the wild type.

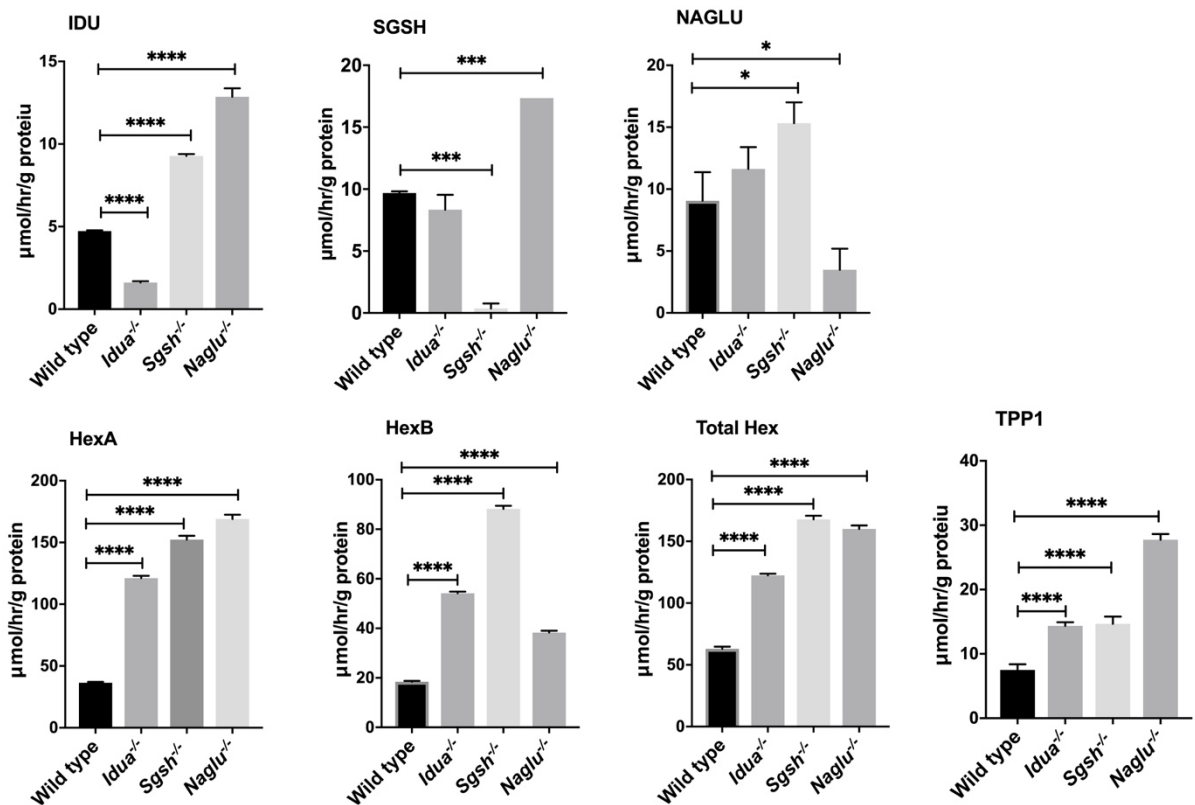


Figure 4.2 Lysosomal enzyme activities in wild type, *Idua*^{-/-}, *Sgsh*^{-/-} and *Naglu*^{-/-} mouse brain tissue.

Mouse brain tissue homogenates were used for enzyme assays which is identified by 4-MU fluorescence (see table 2.2). IDU; α -L-iduronidase, SGSH; Heparan sulfate sulfamidase, NAGLU; α -N-acetylglucosaminidase, HEXA; Hexosaminidase A, HEXB; Hexosaminidase B, Total Hex; Total Hexosaminidase, TPP1; Tripeptidyl peptidase 1. N=3 for all assays apart from SGSH n=2. Statistical analyses were calculated using one-way anova; * $p \leq 0.05$; *** $p \leq 0.001$; **** $p \leq 0.0001$. Data are shown as mean \pm SD. The experiments were performed in conjunction with Ms. Hiu Tung Shek.

4.2.9 Validation of key lysosomal enzyme changes in NPC1 fibroblasts using *Npc1*^{-/-} mouse tissues

I determined whether our observations of altered enzyme activities in NPC1 patient fibroblasts (Figure 4.1 C) were reflected in different tissues and cells from the *Npc1*^{-/-} knock-out mouse (brain, liver and glial cell line). I started by measuring aSMase as it has been reported as being lower in NPC1 (Pentchev et al. 1987; Vanier et al. 1991; Vanier et al. 1988). Surprisingly, I found ASMase activity was normal in the *Npc1*^{-/-} brain but was significantly reduced in the liver ($p \leq 0.0001$) and glial cell line ($p \leq 0.01$) (Figure 4.3). HexA activity was increased in the *Npc1*^{-/-} brain ($p \leq 0.0001$) and in the glia ($p \leq 0.01$) and, in contrast, lower in the liver ($p \leq 0.01$). Similarly, the *Npc1*^{-/-} brain and glia showed an increase in HexB ($p \leq 0.0001$) and also a reduction in the liver ($p \leq 0.01$). Total Hex activity was significantly higher in the brain ($p \leq 0.0001$), normal in the liver and slightly higher in the glia ($p \leq 0.05$). IDU activity was only increased in the *Npc1*^{-/-} liver ($p \leq 0.01$), whereas CTSB activity increased only in the *Npc1*^{-/-} brain ($p \leq 0.0001$) and liver ($p \leq 0.01$). Finally, TPP1 activity increased in all *Npc1*^{-/-} mouse tissues, compared to *Npc1*^{+/+} ($p \leq 0.0001$) (Figure 4.3). Overall, the data from the liver resembles the human fibroblast data, whereas the brain differs. However, this may represent a difference between neuronal and glial enzyme activity as *Npc1*^{-/-} glia accumulate lipids including sphingomyelin and cholesterol, but neurons do not (Vance et al. 2005; Vanier 2010).

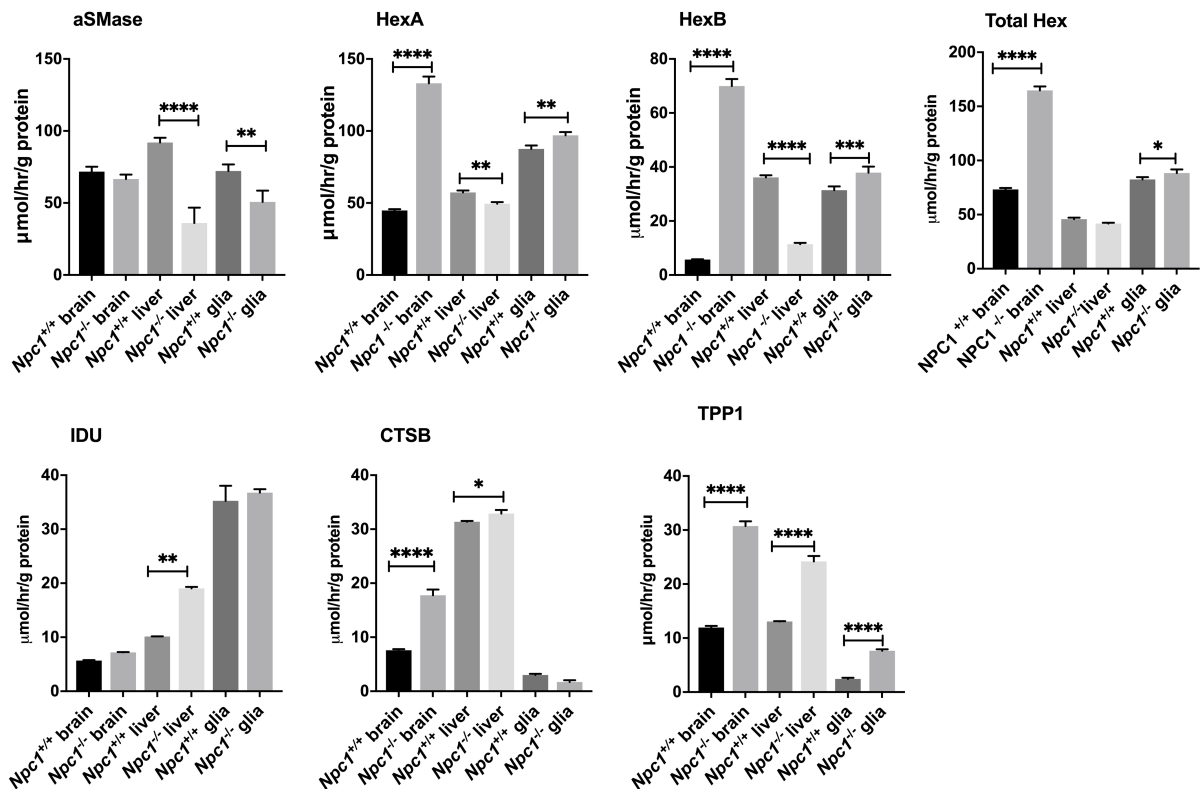


Figure 4.3 Activity of selected lysosomal enzymes in *Npc1*^{-/-} and *Npc1*^{+/+} mouse tissues.

Npc1^{-/-} tissue homogenates (brain, liver and glia) were used for the indicated enzyme 4-MU assay (Table 2.2); aSMase; Acid sphingomyelinase, HEXA; Hexosaminidase A, HEXB; Hexosaminidase B, Total Hex; Total Hexosaminidase, IDU; α -L-iduronidase, CTSB; Cathepsin B, TPP1; Tripeptidyl peptidase 1. N=3 for all assays. Statistical analyses were calculated using one-way anova; *p ≤ 0.05; **p ≤ 0.01; ***p ≤ 0.001; ****p ≤ 0.0001. Data are shown as mean ± SD. These experiments were performed in conjunction with Ms. Hiu Tung Shek.

4.2.10 Comparison of key lysosomal enzyme changes in NPC1 fibroblasts against patient fibroblasts harbouring different NPC1 mutations

NPC1 disease is commonly caused by the NPC I1061T mutation that I used in (Figure 4.1 C) previously to generate the initial enzyme activity map. However, there is a small percentage of patients with mutations referred to as "NPC variants". These variant mutations show the clinical symptoms of NPC but different biochemistry, for example, filipin staining of lysosomal cholesterol storage shows close to normal results (Vanier and Latour 2015), which is also what is reported in *Npc1*^{-/-} mouse neurons and may explain some of the data I obtained in (Figure. 4.3). Therefore, I studied different fibroblast lines harbouring various NPC mutations from patient lines KWNPC (I061T/P1007A), MONPC (I0161T/D948N) and BSNPC (G46V/P691L) in order to compare the differences in lysosomal enzyme activity. Surprisingly, aSMase activity was significantly lower in the classical NPC patient fibroblast line (P237S/I1061T) ($p \leq 0.01$) but, in contrast, was significantly higher in KWNPC (I061T/P1007A) ($p \leq 0.0001$) and there were no noticeable differences in the other mutations (Figure 4.4), potentially explaining the absence of sphingomyelin storage in these patient cells. Classical NPC (P237S/I1061T) ($p \leq 0.05$), MONPC (I0161T/D948N) ($p \leq 0.05$) and BSNPC (G46V/P691L) ($p \leq 0.01$) showed an upregulation in IDU activity. In the same manner, CTSB was increased in NPC (P237S/I1061T) ($p \leq 0.01$) MONPC (I0161T/D948N) ($p \leq 0.0001$) and BSNPC (G46V/P691L) ($p \leq 0.0001$). Finally, TPP1 enzyme activity was significantly increased among all NPC mutations ($p \leq 0.0001$), compared to the control (Figure 4.5). In all cases the NPC1 variant KWNPC line harbouring the I1061T/P1007A compound heterozygous mutations presented with different enzyme activities to all the other patient lines, either considerably greater changes or opposite changes, the significance of this is currently unknown.

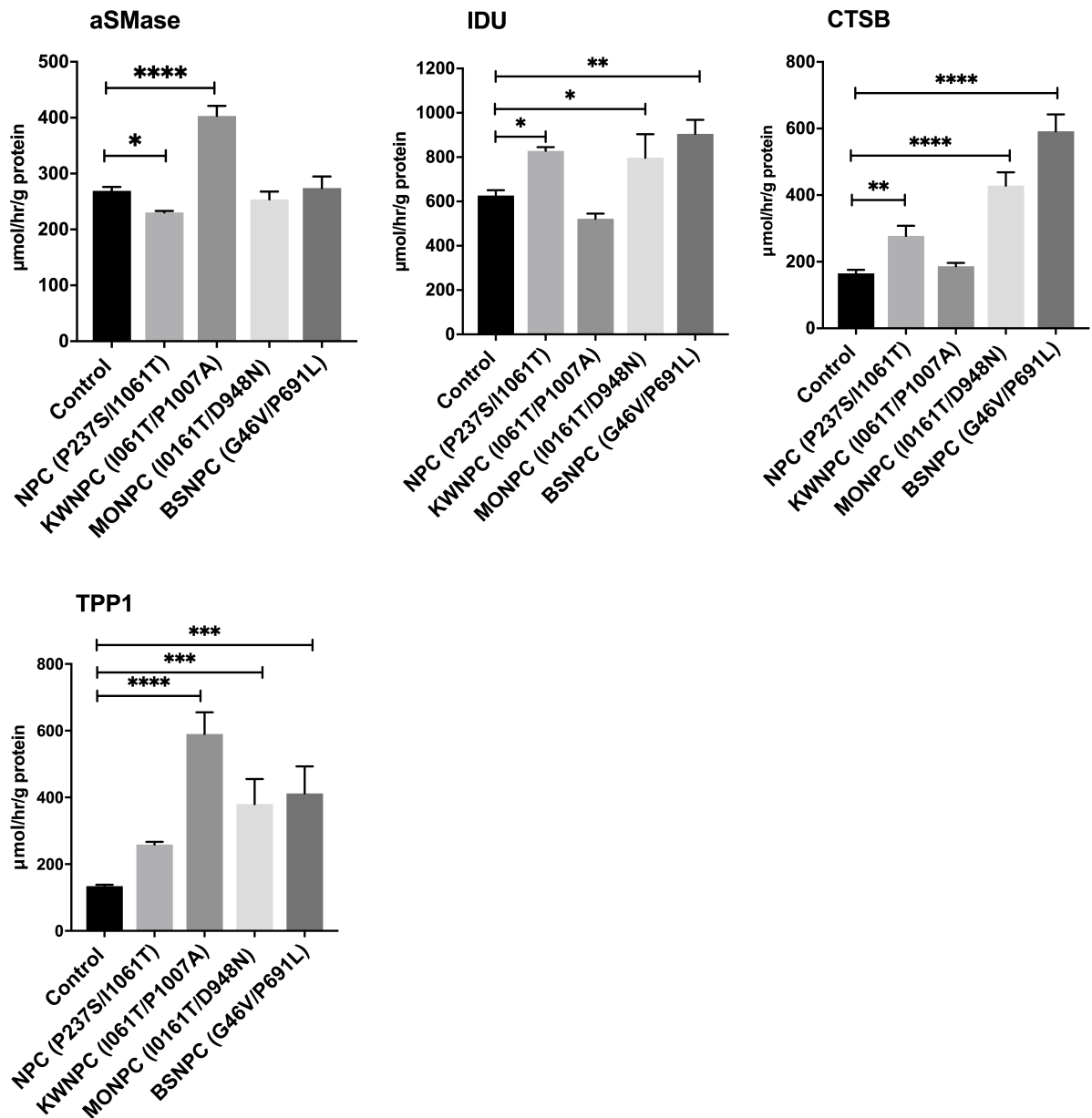


Figure 4.4 Lysosomal enzyme activities in control and NPC1 patient fibroblasts with a range of different mutations.

aSMase, IDU, CT SB and TPP1 enzymes activity by using 4-MU assay (Table 2.2) across NPC (P237S/I1061T), KWNPC (I061T/P1007A), MONPC (I0161T/D948N), BSNPC (G46V/P691L) and control fibroblasts (GM05399). N=3 for all assays. Statistical analyses were calculated using one-way anova; * $p \leq 0.05$; ** $p \leq 0.01$; *** $p \leq 0.001$; **** $p \leq 0.0001$. Data are shown as mean \pm SD. The experiments were performed as teamwork with Ms. Hiu Tung Shek. Abbreviations: aSMase; Acid sphingomyelinase, IDU; α -L-iduronidase, CT SB; Cathepsin B and TPP1; Tripeptidyl peptidase 1.

4.2.11 Evaluation of the effect of miglustat treatment on lysosomal enzyme activities

Miglustat has been shown to reduce neuronal glycosphingolipid storage in NPC animal models, to improve function and survival and delay the onset of neurological symptoms (te Vruchte et al. 2004; Zervas et al. 2001). These studies led to both an off label and eventually a clinical trial of miglustat in NPC patients from which the use of B cells to monitor the improvement in lipid storage and trafficking incurred by miglustat treatment was developed (Lachmann et al. 2004b). However, the exact action of miglustat in terms of how it mediates its benefit is still not fully recognized (Alfonso et al. 2005). Therefore, I decided to examine the impact of miglustat on an NPC1 patient's fibroblast after 5 days of treatment with 50 μ M miglustat. I focused on the most altered NPC1 enzyme activities from the earlier fibroblast data (Figure 4.1 C) and evaluated the possibility of miglustat being able to impact upon the activities of; GCCase, aSMase, α -Glu, CTSB and LAL (Figure 4.5). I observed a significant increase in GCCase activity in the treated controls ($p \leq 0.01$), whereas there were no changes in NPC1. There was also an increase in aSMase activity in the controls treated with miglustat ($p \leq 0.01$), but no difference in NPC1. α -Glu were actually decreased following miglustat treatment in both controls ($p \leq 0.001$) and NPC1 ($p \leq 0.0001$). There were slightly changed in CTSB activity following miglustat treatment, in NPC1 it leads to normalise the activity of CTSB. I did however observe that LAL were increased in the miglustat treated NPC1 fibroblasts ($p \leq 0.05$) to the normal level (Figure 4.5).

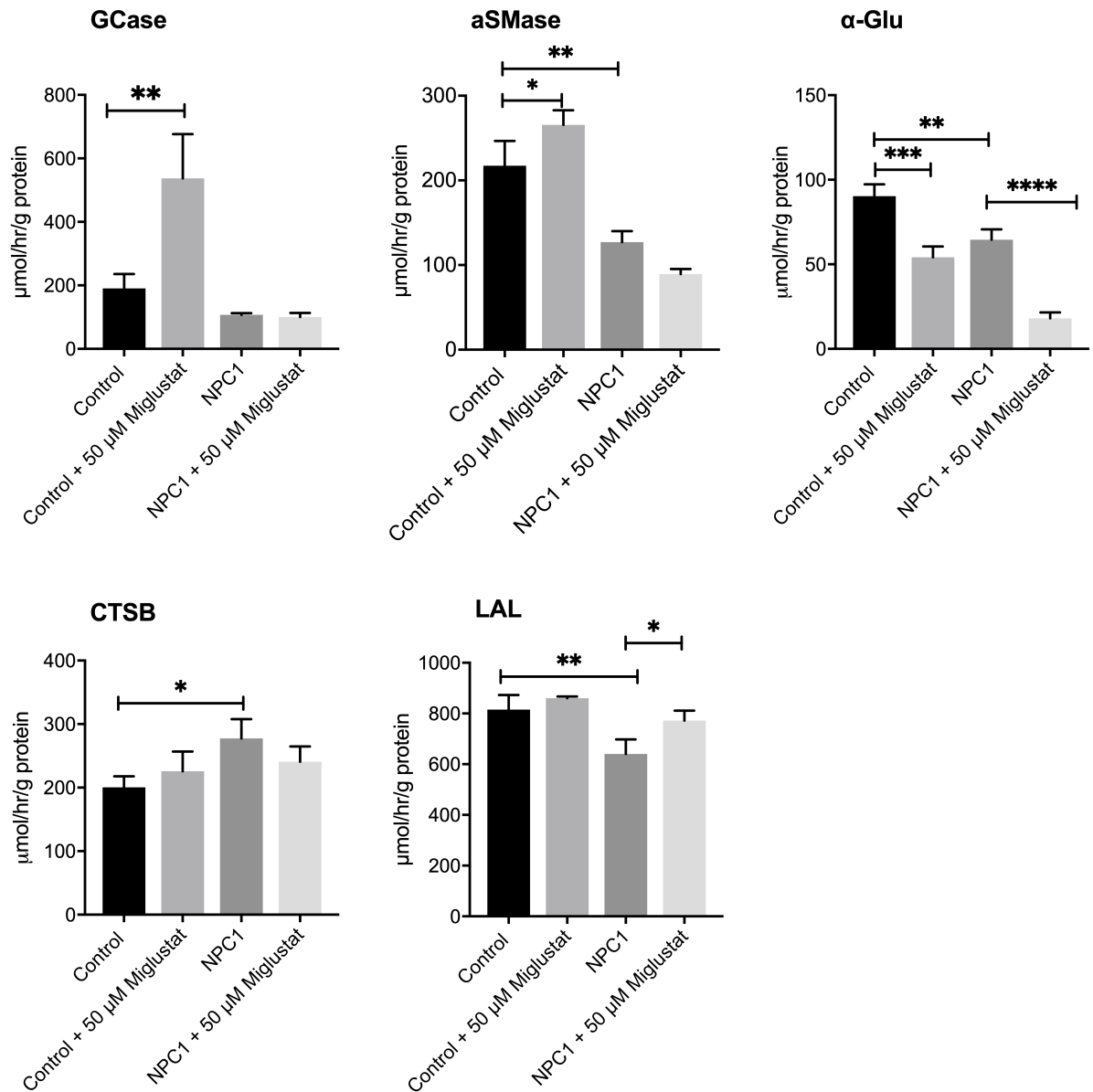


Figure 4.5 Activity of lysosomal enzymes in the control and NPC1 patient fibroblasts treated with miglustat.

GCCase, aSMase, α-Glu, CTSB and LAL activity in fibroblasts from control (GM05399) and NPC1 (GM03123) with miglustat treatment. N=3 for all assays. Statistical analyses were calculated using one-way anova; *p ≤ 0.05; **p ≤ 0.01; ***p ≤ 0.001; ****p ≤ 0.0001. Data are shown as mean ± SD. The experiments were performed in conjunction with Ms. Hiu Tung Shek.

Abbreviations: GCCase; β-glucosidase, aSMase; Acid sphingomyelinase, α-Glu; Acid α-glucosidase, CTSB; Cathepsin B and LAL; Acid lipase.

Having observed only minimal changes in NPC, which is a well characterized lysosomal trafficking disease featuring lysosomal enzyme mis-localisation, I decided to study the effects of miglustat on another LSD. There is currently an ongoing small off label safety study of miglustat treatment on two CLN5 patients (P1/P2) in the UK. I was considering the possibility of utilising enzyme assays from dried blood spots to monitor the effect of this treatment on the patients. I therefore looked for the most altered enzymes in CLN5 fibroblasts (Figure 4.1 E) and found that GCase ($p \leq 0.0001$) was high in CLN5 whereas, β -gal ($p \leq 0.0001$), α Gal A ($p \leq 0.01$) and TPP1 ($p \leq 0.0001$) were lower in CLN5 fibroblasts, compared to the controls. I grew the CLN5 and control fibroblasts in a medium containing 50 μ M miglustat for 5 days prior to the enzyme assays and, as with the NPC1 experiment (Figure 4.4), observed an increase in GCase in the treated controls ($p \leq 0.001$) but not with the CLN5 cells. The β -gal were not changed in either the controls treated with miglustat or in the treated CLN5. There was, however, a trend towards reduction in α Gal A but it was not significant. There was a significant increase in TPP1 enzyme activity in the controls treated with miglustat ($p \leq 0.05$) and CLN5 ($p \leq 0.001$) (Figure 4.6).

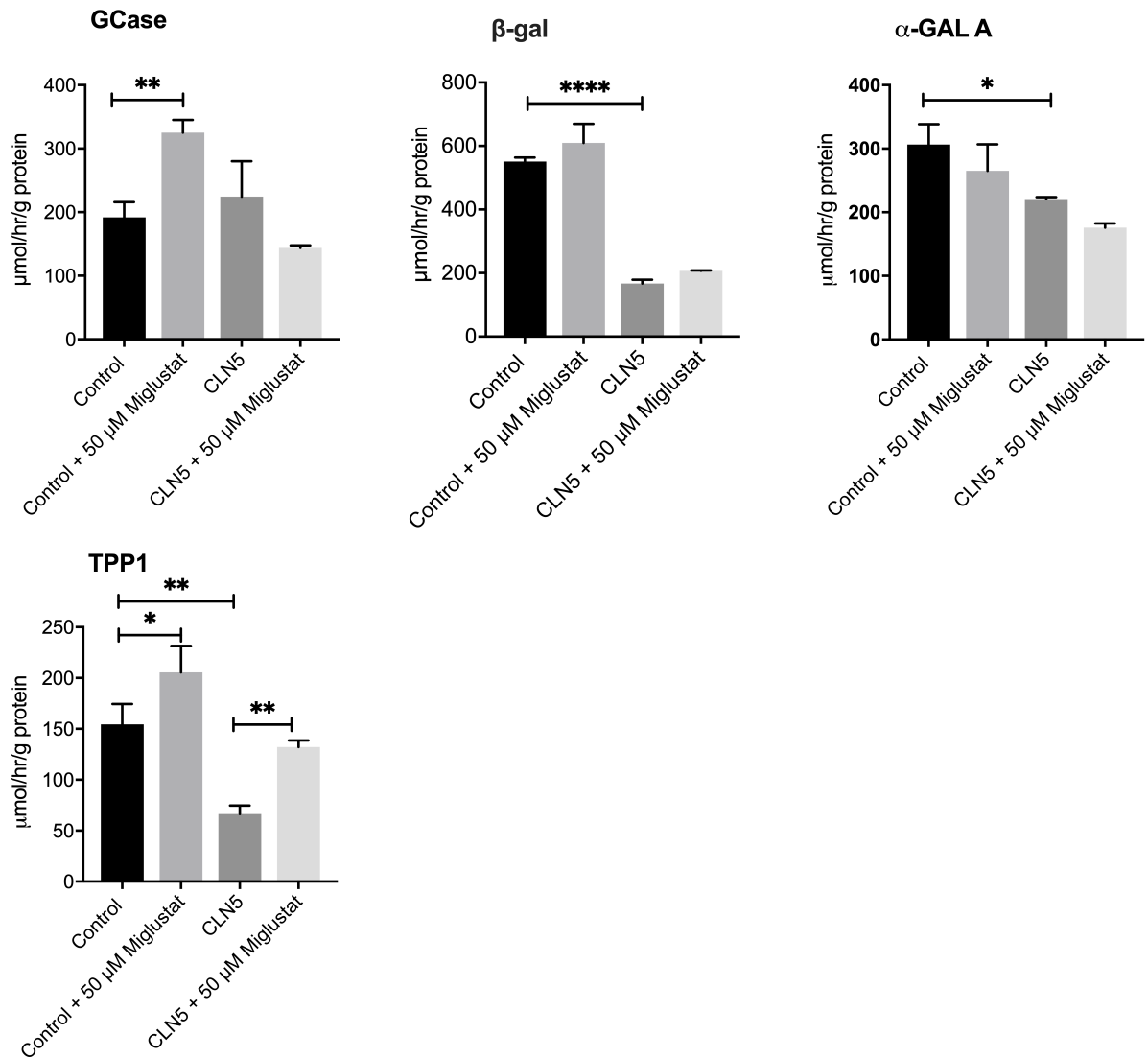


Figure 4.6 Activity of lysosomal enzymes in control and CLN5 patient fibroblasts treated with miglustat.

GCase, β-gal, αGal A and TPP1 activity using the 4-MU substrates (Table 2.2) in hemognised fibroblasts from the control (GM05399) and the CLN5 (P1) patient (See supplementary table 1) with miglustat treatment. N=3 for all assays. Statistical analyses were calculated using one-way anova; *p ≤ 0.05; **p ≤ 0.01; ***p ≤ 0.001; ****p ≤ 0.0001. Data are shown as mean ± SD. The experiments were performed in conjunction with Ms. Hiu Tung Shek.

Abbreviations: GCase; β-glucosidase, β-gal; β-galactosidase, αGal A; galactosidase A, TPP1; Tripeptidyl peptidase 1

4.2.12 Lysosomal enzyme activities in clinical samples from CLN5 patients undergoing miglustat treatment

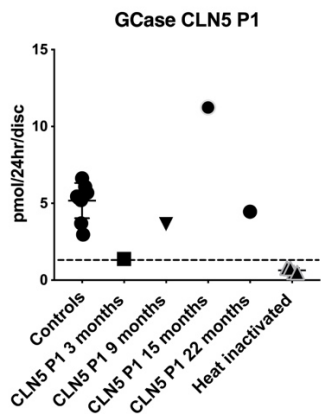
Research in the Emyr Lloyd-Evans lab identified miglustat as a small molecule effector of CLN5 disease cellular dysfunction, work that has led to an off label safety study of miglustat in two childhood CLN5 patients at the Nottingham Children's Hospital. Both patients were given 2 x 100mg of miglustat three times daily, the patients started on miglustat treatment at the age of 11 and the study was conducted for an initial 12 month period followed by a further 12 month extension. Blood samples from CLN5 patients (Nottingham) and controls (Cardiff blood bank) were prepared as described in materials and methods (Section 2.7.5). DBS samples were collected at various times during the miglustat treatment at scheduled clinic visits in months 3, 9, 15 and 22. The enzyme assays measured in (Figure 4.6) were carried out on the DBS by punching 3.2 mm circles from the DBS filter paper and measuring the enzyme activity in those punches by fluorimetry as described (Chapter 2, section 2.7.5). Altered GCCase, β -gal, α Gal A and TPP1 activity were observed in the CLN5 fibroblast (Figure 4.6), I therefore prioritized these enzyme assays in the DBS punches, as I had limited starting material, and compared to enzymes activities in our control DBS punches from an age range of volunteers spanning 27, 37, 55, 56 and 59 years of age.

In contrast to the fibroblasts (Figure 4.6) GCCase activity was lower in the post 3 month treatment samples from both P1 and P2. In P1 GCCase was restored back to the normal range by the 9 month miglustat treatment sample, followed by upregulation of GCCase activity in subsequent samples and a return to the normal range again at the 22 month treatment stage. In P2 GCCase activity was also returned back to the control range at the 9 month treatment stage and remained within this normal range in all subsequent samples (Figure 4.7). Activity of β -gal was below the normal range in the post 3 months samples for both P1 and P2. In P1 there was no recovery in this enzyme activity throughout the treatment course. In P2 β -gal returned back to the normal range in the 9 month sample but returned to below the normal reference range for the rest of the treatment course. α Gal A activities were also below the control reference range in the first sample from P1 and P2 apart from at 9 months during treatment where enzyme activity fell into the normal range, remained low across the course of the treatment. TPP1 activity was initially below the control range in the first sample from both patients. P1 showed an improvement in TPP1 at 9 months during treatment and returned back to a level below the controls in subsequent samples. Similarly, P2 showed improvement in TPP1 activity in the 9 months treated sample, returned to a level below the control range in the 15 month sample and then back to within the normal range in the last sample at 22 months. The fact that I only had access to the biological samples of two patients was a limitation to any

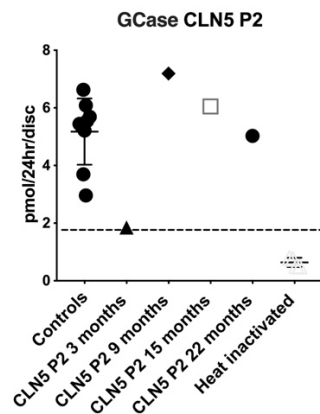
statistical study, further samples may be necessary to determine whether there is a trend for improved TPP1 activity as was observed in the patient fibroblasts (Figure. 4.6).

Figure 4.7 Activity of lysosomal enzymes in CLN5 patient dried blood spots during miglustat treatment.

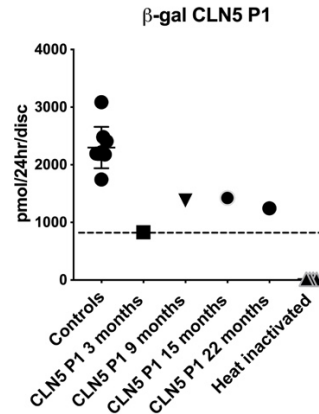
GCcase, β -gal, α Gal A and TPP1 activity in DBS from CLN5 P1 and CLN5 P2 during miglustat treatment. The dash lines indicates the initial value of the patient enzyme from the first sample. Abbreviation: GCcase; β -glucosidase, β -gal; β -galactosidase, α Gal A; α -galactosidase A, TPP1; Tripeptidyl peptidase 1. Control = n 5-6. The experiments were performed in conjunction with Ms. Hiu Tung Shek.



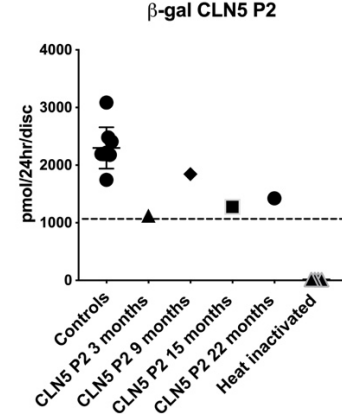
Dry blood spot samples collected during trstment



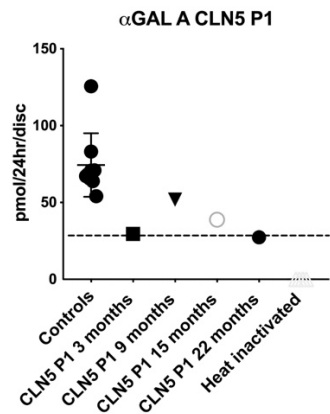
Dry blood spot samples collected during trstment



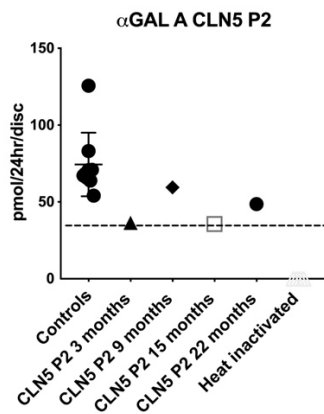
Dry blood spot samples collected during treatment



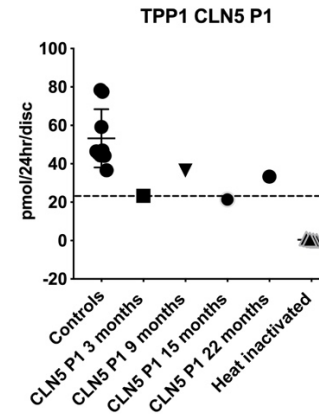
Dry blood spot samples collected during trstment



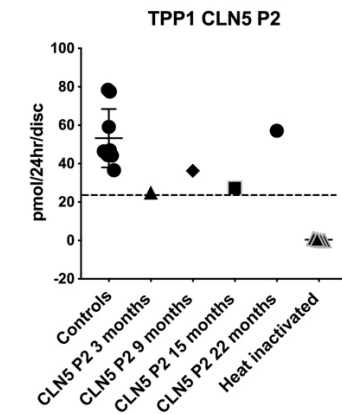
Dry blood spot samples collected during trstment



Dry blood spot samples collected during trstment



Dry blood spot samples collected during treatment



Dry blood spot samples collected during treatment

4.2.13 Determining whether restoration of secondary enzyme activity defects in LSDs can correct storage of associated lysosomal substrates.

I wanted to investigate the possibility of secondary enzyme defects in LSDs becoming a therapeutic target. Our data (Figure 4.1 above and supplementary figure 24) showed defects in the activity of the LAL enzyme in several LSDs. The primary deficiency of LAL activity leads to substantial cholesteryl ester and triglyceride storage in Wolman disease and neutral lipids have been shown to accumulate in both Wolman and NPC disease by Nile red staining (Xu et al. 2012b). I therefore wondered whether I could correct some of the storage materials in NPC1 and also CLN5, which also has reduced LAL activity (Supplementary figure 24), by restoring normal levels of LAL activity. To test this hypothesis, I have treated Wolman, NPC1, and CLN5 fibroblasts with recombinant human LAL (rhLAL) in the culture medium. A change in elevated lysotracker fluorescence, indicative of lysosomal storage (Chapter 3), was used as the outcome assay. Lysotracker was increased in untreated Wolman ($p \leq 0.05$), NPC1 ($p \leq 0.001$), and CLN5 ($p \leq 0.05$). The results, of this preliminary experiment (N=2), showed a correction in lysotracker fluorescence back to control levels in the LAL deficient Wolman fibroblasts, as expected with only the untreated Wolman cells showing a significant difference versus untreated control. For the other two diseases there was a trend of reduction in storage materials (lysotracker) in CLN5 and a significant reduction in NPC1 treated with $0.5\mu\text{g}$ rhLAL ($p \leq 0.05$) compared to untreated fibroblasts (Figure 4.8 A & B).

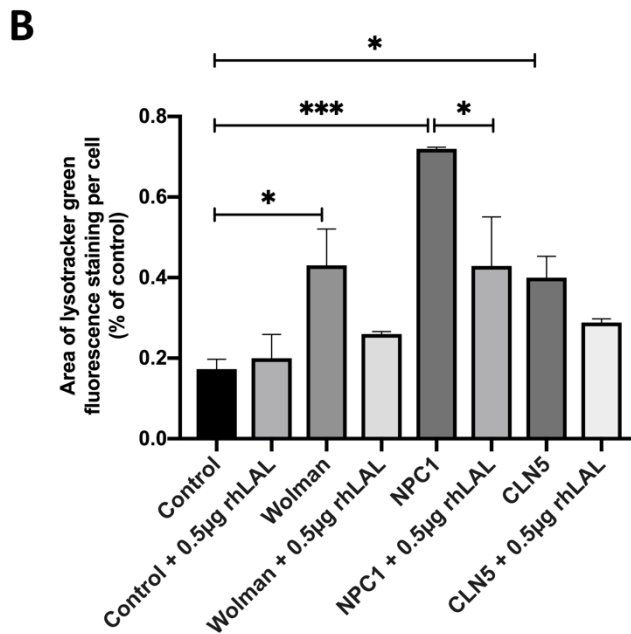
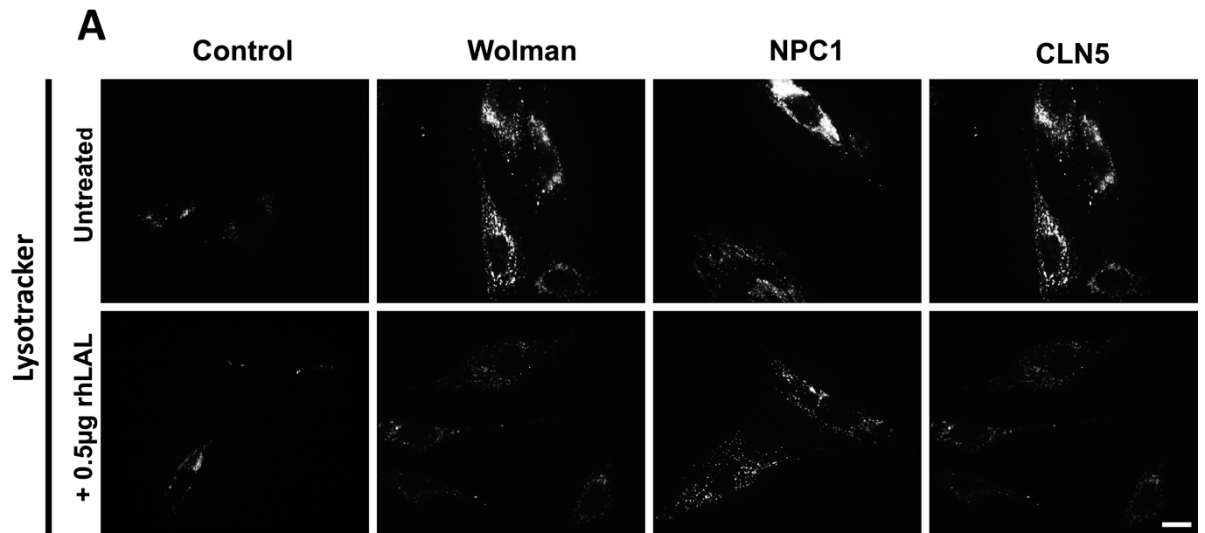


Figure 4.8 Decrease in lysosomal storage material in LSDs following restoration of lysosomal LAL activity with exogenous recombinant enzyme.

Control (GM05399), Wolman (GM01606), NPC1 (GM03123) and CLN5 (P1) fibroblasts were grown in either normal culture medium or culture medium containing 0.5µg rhLAL for 48hr, followed by staining with lysotracker green. n=2, Scale bar: 10µm. *p ≤ 0.05; * * *p ≤ 0.001. Data is shown as mean ± SD.

4.3 Discussion

The primary single enzyme defect associated with LSDs have been studied for many years. However, I hypothesized the presence of more than one enzyme alteration in the LSDs, due to the reported clinical and phenotypic overlap among LSDs for example the accumulation of similar secondary storage molecules such as gangliosides (Vitner et al. 2010; Walkley and Vanier 2009b). Any confirmation of the presence of secondary enzyme defects might help to provide a novel approach to explore; 1) possible diagnosis and monitoring of the LSDs via the altered enzyme activates, 2) potential therapeutic targets either via enzyme inhibition or enzyme replacement and 3) enable greater insight into the underlying mechanism for the diseases.

4.3.1 There are multiple lysosomal enzymes altered across LSDs

In the first part of this study I optimised various lysosomal enzymes by studying the pH optimum (Supplementary figure 1), incubation time (data not shown) and the specificity of the substrate (Supplementary figures 3- figure 25). The pathology, clinical presentation and severity of these diseases can diverge according to patient age (Ballabio and Gieselmann 2009). I therefore included control cells from a range of different ages (1yr., 6yrs., 45yrs.), which covered the majority of LSD patient ages included in this study (see cells table in supplementary table 1). I observed that whenever there was a deficiency of one enzyme or a protein defect associated with single LSDs, it was accompanied by a secondary increase or decrease in other lysosomal enzymes. Predominantly in this study I was looking to see if there was one enzyme altered among the LSDs that could be developed as a unique biomarker. However, there was no single enzyme being uniquely altered in all LSDs (Figure 4.1). Nevertheless, there were some interesting and useful findings, which will be discussed and elaborated on here and in the overall discussion (chapter 8).

4.3.2 HexA, HexB and Total Hex are elevated and are a possible biochemical marker for the mucopolysaccharidoses.

A group of associated enzymes were shown to be outside of the normal range in all the mucopolysaccharidoses cells under investigation (Figure 4.2 B). These were: HexA, HexB, and Total Hex. The mucopolysaccharidoses are caused by deficiencies in enzymes involved in the lysosomal breakdown of GAGs, such as dermatan sulphate. I found that the HexA, HexB and Total Hex activities were significantly increased in several MPS patient fibroblasts. Then this finding was applied to the mucopolysaccharidoses knock-out mouse (Figure 4.2). The

Idua^{-/-}, *Sgsh*^{-/-} and *Naglu*^{-/-} of mouse brain tissue also demonstrated an increase in HexA, HexB and Total Hex activity in the mouse brain, compared to the control (Figure 4.2). A previous study of a knock-out mouse deficient in both subunits of β -hexosaminidase (α and β) exhibited GAG storage (Sango et al. 1996). This finding was consistent with another report that Hexosaminidase S, composed of the β -hexosaminidase α and β subunits, is responsible for the *in vitro* breakdown of dermatan sulphate (Hepbildikler et al. 2002). Upregulation of HexA, HexB and Total Hex, in mucopolysaccharidosis disease cells may therefore be a response to impaired breakdown of GAGs caused by the specific genetic mutation in lysosomal GAG degrading enzymes in each MPS. Alternatively, GAGs could themselves inhibit β -hexosaminidase, leading to an upregulation of the expression of this enzyme, and explaining the presence of secondary ganglioside storage in these diseases (Avila and Convit 1975; McGlynn et al. 2004). Our finding here also raises the possibility of using HexA, HexB and Total Hex in monitoring disease treatment, in no other LSD did I observe as great an increase in activity of HexA/ HexB/ total Hex. Interestingly, TPP1 activity was also elevated among all the MPS diseases including the mouse tissues and patient fibroblast lines, all apart from MPS IIID (Figure 4.2 B). TPP1 is delivered to the lysosome as an immature proenzyme and then lysosomal pH and the presence of Ca^{2+} within the lysosomal compartment required to produce the mature enzyme (Guhaniyogi et al. 2009; Kuizon et al. 2010). GAGs have been shown to interact with TPPI allowing TPP1 autoactivation at a less acidic pH, explaining the elevated activity, and potentially protecting TPP I from changes in intra-lysosomal pH (Golabek et al. 2005). Taken together, these results suggest that lysosomal enzyme changes from either fibroblast or mouse models could be developed further for monitoring and developing new treatments for the mucopolysaccharidosis.

Interestingly, the mucopolysaccharidoses showed an increase in >50% of lysosomal enzymes (Figure 4.1B). Our data is in contrast to the findings of previous studies, which demonstrated inhibition by exogenous glycosaminoglycans of 21 lysosomal enzymes in leucocytes assayed *in vitro*. Heparan sulfate and other glycosaminoglycans may bind to enzymes involved in the degradation of ganglioside, owing to the similarity in terminal sugar residues, and reduce their activity (Avila and Convit 1975; Baumkötter and Michael 1983; Kint et al. 1973). That finding was suggested as an explanation for the secondary ganglioside GM2 and GM3 storage in the mucopolysaccharidoses. However, our findings from studying the majority of lysosomal enzymes across most of the mucopolysaccharidoses, including tissues from some of the animal models, does not show a lack of multiple enzymes activities. Also, from our findings from the EM ultrastructure study of MPS I and MPS IIIA (See chapter 5 figure 5.5), I did not observe multiple secondary storage materials in these diseases which confirms that most enzymes are working *in situ*. Therefore, our study suggests the GAG inhibition of lysosomal

enzymes *in vitro* is either not occurring *in vivo* or is the product of non-physiological effects of exogenous GAGs on lysosomal enzymes.

4.3.3 NPC1 different tissues and mutations exhibit different enzyme activity

A range of lipids, in addition to the cholesterol accumulation within the lysosomes, have been demonstrated as storage molecules in NPC1 (Vanier et al. 1991). However, the cause of this secondary lipid accumulation in NPC1 is not well characterised. Several studies have proposed that, in the absence of NPC1, a secondary alteration in lysosomal function is involved (Lloyd-Evans et al. 2008; Vitner et al. 2010; Walkley and Vanier 2009a). For example, ASMase and GCase enzymes have been shown to be mis-localised and to have reduced enzyme activity in NPC1 cells (Salvioli et al. 2004). Our data, however, showed different changes in lysosomal enzyme activities in different tissues in the *Npc1*^{-/-} mouse and across different NPC1 patient fibroblasts harboring different mutations. Increases of lysosomal enzyme levels were observed in NPC1, such as CTSB, IDU and TPP1, which may not be involved in the catabolism of well-known accumulated material in NPC disease. The accumulation of unesterified cholesterol in liver and spleen tissue from *Npc1*^{-/-} mouse. Livers show an increase in cholesterol concentration in the liver at the age of 35 days (Beltroy et al. 2005). This hepatomegaly is associated with cholesterol accumulation in *Npc1*^{-/-} mouse (Beltroy et al. 2005). The liver is the main tissue to synthesize cholesterol via high degree of uptake of lipoprotein-derived cholesterol (Garver et al. 2007b; Garver et al. 2005), storage of cholesterol in lipid droplets and secretion of excess LDL and high density lipoprotein (HDL) particles as bile acids. Interestingly, our data showed a decrease in aSMase activity in the liver and the glia, which are interconnected as, in a similar manner to the way that the liver deals with peripheral cholesterol, glia are the main source of *de novo* cholesterol biosynthesis within the brain (Petrov et al. 2016). As other studies have shown abnormalities in sphingomyelin degradation in NPC1 disease cells, and a rescue in cholesterol storage by re-addition of recombinant aSMase to these cells, it is highly likely that in cells with a large turnover of cholesterol the loss of aSMase activity clearly contributes to both sphingomyelin and free cholesterol storage in NPC disease. However, the *Npc1*^{-/-} mouse brain showed aSMase to be normal (Figure 4.3). This consistent with an increase of sphingomyelin was reported in the NPC1 liver and spleen in the mouse model of NPC1 (Vanier 1983; Walkley and Vanier 2009a), and, there is a lack of description of biochemical secondary sphingomyelin accumulation in NPC1 brain tissue (Walkley and Vanier 2009a), suggesting the defect in aSMase is the cause of the sphingomyelin storage. However, metabolomic profiling for sphingolipid species on *Npc1*^{-/-} mice of different ages have shown an increase in some sphingomyelin classes in the brain, mainly in 9 weeks (Fan et al. 2013), and some lipids have

been shown to be mis-localised to lysosomes but with no net difference in their levels, suggesting that lipids are stored in lysosomes in neurons but are not elevated by mass. However, another explanation could not be excluded here.

HexA, HexB and Total Hex in the NPC fibroblasts were not significantly different to the controls (Figure 4.1). The *Npc1*^{-/-} mouse brain showed an upregulation in HexA, HexB and Total Hex (Figure 4.3), which may be a compensatory cellular response to the raised GM2 level in the brain (Walkley and Vanier 2009a). This is consistent with a previous study that found the β -hexosaminidase activity was elevated in the *Npc1*^{-/-} mouse brain (Sleat et al. 2012). In the brain, the NPC1 protein is mainly localised in glia in astrocytic development (Patel et al. 1999). NPC1 in glia is believed to mediate lipid trafficking between neurons and glial cells (Ong et al. 2001). The HexA, HexB and Total Hex enzyme activities were also altered in glial cells, similar to the brain tissue. However, the liver exhibited low levels of these enzymes, in particular, HexB. Interestingly, the IDU enzyme activities were only significantly increased in the *Npc1*^{-/-} mouse liver. The previous measurement of sulphatide in NPC1 liver and brain indicated the presence of sulphatide in liver tissue (Brunngraber et al. 1973). Therefore, this upregulation in IDU enzyme is due to the accumulation of one of the glycosaminoglycans, which are known to modulate HexA/B (Sango et al. 1996). CTSB was increased in the brain and liver of the *Npc1*^{-/-} mouse. A previous study demonstrated that CTSB and CTSD are increased in the cerebellum of *Npc1*^{-/-} mice (Amritraj et al. 2009). These results suggest that the increased activity of CTSB may be related to the fundamental cause of neuronal degeneration in NPC disease. Finally, TPP1 activities increased significantly among all *Npc1*^{-/-} mouse tissues, compared to the control (Figure 4.3).

NPC1 mutations mainly show the same trend of upregulation in IDU and CTSB activity, apart from KWNPC (I061T/P1007A), which has a normal level of IDU and CTSB activity (Figure 4.4). This mutation has a normal cholesterol phenotype (Vanier et al. 1991). Also, our previous data from lysotracker showed a normal lysotracker fluorescence (Chapter 3, figure 3.12) in KWNPC (I061T/P1007A). There is a lack of any storage molecules in this NPC mutation. Notably, activity of TPP1 was high among all *Npc1*^{-/-} mouse tissues and all NPC1 mutation fibroblasts, including the KWNPC (I061T/P1007A). It is worth mentioning that TPP1 activity was earlier found to be raised in the brain of NPC1 mice somewhat more in late-stage disease (Sleat et al. 2012). NPC1 is characterized by the presence of Alzheimer like phenotypes, including the accumulation of abnormally processed amyloid fragments β -40-42 and lysosomal c-terminal fragments of the amyloid precursor protein (Kodam et al. 2010; Ohm et al. 2003; Saito et al. 2002; Yamazaki et al. 2001). TPP1 has been shown to be a lysosomal enzyme that processes fibrillar amyloid (Solé-Domènech et al. 2018), whether there is a

connection between the elevated activities of TPP1 and the lysosomal accumulation of amyloid fragments is unknown, but the cellular localization of the enzyme may be worth investigating further. The functional consequence of these lysosomal enzymes alterations in NPC1 is challenging to evaluate but it might provide indications of the mechanistic cause of some of the storage material within the lysosome that has been up until now uncharacterized.

4.3.4 Miglustat changes several lysosomal enzyme activities

The imino sugar family has received a lot of attention over the last few decades due to their ability to inhibit glucosidase enzyme activity (Alfonso et al. 2005; Fan et al. 1999). *N*-butyl-deoxynojirimycin (NB-DNJ, miglustat) as described earlier is currently the only approved small molecule treatment for GD and NPC1 due to its ability to target the ceramide specific glucosyltransferase enzyme, which is the first step of GSLs biosynthesis, with very few off-target effects. In order to have more insight into the mechanism of the actions of miglustat, I investigated the effect of miglustat on a few lysosomal enzymes. I have demonstrated in the present study that miglustat upregulates several enzymes' activity in the control fibroblasts GCase, β -gal, aSMase, TPP1 and LAL (Figure 4.5 & 4.6). Our results agree with those of other authors who demonstrated that Nojirimycin derivatives are capable of working as chemical chaperones for a few lysosomal enzymes (Alfonso et al. 2005; Fan et al. 1999). In addition to Miglustat's effect on substrate synthesis, it also works as a chemical chaperone of GCase (Alfonso et al. 2005; Priestman et al. 2000). Therefore, this might explain the increase of some lysosomal enzyme activity in the control fibroblast. In contrast, however, it was unable to correct the lysosomal enzymes in NPC1 and CLN5 patient fibroblasts. This might be due to the enzymes in affected cells needing more incubation time with miglustat to overcome the misfolding and/or mistrafficking defect in LSDs. It may also indicate a down-regulation of enzyme synthesis in NPC1 and CLN5 rather than a post-translational modification.

Notably, miglustat was able to correct TPP1 and LAL activity in NPC1 and CLN5 respectively. Further investigations are still needed to discover the possible mechanisms by which miglustat affects these enzymes. However, the corrections made in TPP1 and LAL were possibly due the reduction in accumulated substrates within the lysosomes which either themselves inhibit these enzymes or allowed the enzymes to overcome the trafficking defect and reach the lysosome substrates easily.

4.3.5 A new biomarker for CLN5 treatment

It is always challenging to identify and develop biomarkers which permit us to accurately monitor the disease over time, especially the LSDs where rarity limits access to biological samples. During the course of this thesis I had the chance to collaborate on a small safety pilot study of miglustat in two CLN5 patients at the Nottingham Children's Hospital. I utilised DBS, which has been reported to preserve enzymes efficiently for years in samples from patients with Gaucher, NPA/B, GM1 and GM2 diseases (Chamoles et al. 2001a; Chamoles et al. 2002a, b). GCase, β -gal, α Gal A and TPP1, activity were measured from 3.2 mm punches removed from the DBS during the miglustat treatment (Figure 4.7). Over the miglustat time course patients showed an improvement in the GCase, β -gal and TPP1 activity. But there was only a slight improvement in α Gal A activity during this time. The time course of the CLN5 P1 and P2 showed upregulations in the enzymes involved in this study. Miglustat may have acted as a chaperone for some of these enzymes, stabilizing them. Alternatively, the reduction of accumulating substrates could potentially restore the enzyme activity back towards control level. Regardless of the expected mechanism behind the enzyme improvement, a simple lysosomal enzymes assay demonstrated the treatment to be beneficial in this CLN5 patient pilot study. This result raises the possibility of using secondary enzyme defects in monitoring treatment efficacy. It should, however, be borne in mind that more biological samples from patients will still be needed to expand our findings.

4.3.6 Highlighting the importance of lysosomal enzyme alteration in disease mechanism and the correlation between LSDs and other neurodegenerative disease.

It is worth noting a clear reduction in lysosomal enzyme activities among the majority of the NCLs (Figure 4.1 E). This is the second group of LSDs showing low activity of several lysosomal enzymes after the multiple lysosomal enzyme deficiency group (Figure 4.1 D). A recent study has shown that the CLN8 protein is required for lysosomal enzyme transfer from ER-to-Golgi. CLN8 protein deficiency leads to low enzymes activity in lysosome. The study showed that CLN8 interacts with ~65% of lysosomal enzymes (di Ronza et al. 2018). Furthermore, a previous study suggested that CLN5 is localised in lysosomal compartments and involved in lysosomal sorting of receptors recycling back to the Golgi including Cation-independent mannose-6-phosphate receptor (CI-MPR) (Mamo et al. 2012). Several of the NCL proteins interact and connections between all of these diseases likely exist owing to the commonality of SCMAS accumulation across the NCLs forms except CLN1 where the main

component of storage material contains saposin A and D (Tyynelä et al. 1993). Therefore, our finding of low multiple lysosomal enzyme activities across the NCLs provides a second similarity beyond SCMAS storage in the NCLs. This suggests that NCL proteins may be involved in the transport and processing of M6P-containing lysosomal enzymes and more studies need to be carried out to explain the underlying mechanisms.

I have found that the TPP1 enzymes are upregulated among the majority of LSDs and TPP1 activity is also high in Alzheimer's disease patient cells (Supplement Figure 22). There is therefore the possibility of a connection between LSDs and neurodegenerative diseases. Alzheimer's disease is an irreversible and progressive neurodegenerative disorder (Schachter and Davis, 2000). It is characterised by neuritic plaques and neurofibrillary tangles (De-Paula *et al.*, 2012). Neuritic plaques are comprised of amyloid p-peptide (A β) made from the amyloid precursor protein by β -secretase action (Annaert and De Strooper, 2002). TPP1 enzymes are lysosomal serine protease that is involved in the degradation of amyloid-beta (A β) through the proteolysis of the fibrillar A β (Solé-Domènech *et al.* 2018). The accumulation of amyloid-beta (A β) in the brain leads to a neurodegenerative disease (Chartier-Harlin *et al.* 1991).

The cathepsins in lysosomes are known to modify their properties in aging brains by processing the degrading vital neuronal proteins causing harmful effects (Stoka *et al.* 2016). CTSB is elevated across the majority of LSDs. It has been reported that CTSB/L are involved in the degradation of Alzheimer proteins: amyloid- β peptides, C-terminal fragments of the amyloid precursor protein and the degradation of β -secretase (Cermak *et al.* 2016). This further supports the importance of the presence of cathepsins in neurons. When the activity of CTSB/L is inhibited, it causes an accumulation of free cholesterol in late endosomes–lysosomes, which is characteristic of NPC1 (Cermak *et al.* 2016). There is a variety of conditions that can cause the upregulation of cathepsin activity, which is a mediator of inflammation and is used a marker of certain cancers (Levičar *et al.* 2002). More investigation, however, is still needed to find out if this upregulation increases the risk for aging disorders.

Besides LSDs, Alzheimer's disease and Huntington's disease show a reduction in LAL activity (Supplementary figure 24). There have been numerous studies on the cholesterol metabolism involvement in Alzheimer's disease (Kivipelto *et al.* 2001; Lütjohann and Von Bergmann 2003). The LAL polymorphisms result in a risk of Alzheimer's disease (Aslanidis *et al.* 1994; von Trotha *et al.* 2006).

4.3.7 An enzyme fingerprint for individual or group of lysosomal storage disease

Due to the lack of a particular enzyme to be a biomarker for all LSDs, this finding of enzymes studied across LSDs could be useful for developing an enzyme activity 'fingerprint' for a group of LSDs or for single disease. In terms of groups of LSDs, there are potential lysosomal enzymes that could be used to identify particular groups of LSDs (Table 4.1).

Table 4.1 Summary of lysosomal enzyme changes amongst LSD groups taken from the figure of this thesis (Figure 4.1).

Class/Type of LSD	Enzymes involved	Lysosomal storage diseases
Sphingolipodosis	GUSB ↑	GM1 gangliosidosis GDII
	PPT1 ↓	Tay Sachs Tay sachs, AB variant Sandhoff Krabbe MLD Fabry NPA Farber
Mucopolysaccharidoses	HexA & Hexβ & Total Hex ↑	MPS I MPS II MPS IIIA MPS IIIB MPS IIID MPS VII
Transmembrane protein defect	in α-Glu, α-Fuc, α-Man, LAL ↓ TPP1 ↑	NPC Salla MLIV
Multiple enzyme deficiency	AGA & HEXB ↓	MSD I cell Galactosialidosis
Neuronal ceroid lipofuscinosis	HEXB ↓	CLN2 CLN3 CLN5 CLN6 CLN7 CLN8
	Total Hex ↓	CLN2 CLN5 CLN6 CLN7 CLN8 CLN10
Lipodoses, oligosaccharidosis and glycogenoses	TPP1 ↑	Wolman disease α mannosidosis Fucosidosis Sialidosis Pompe disease

In terms of a single LSD, radar plots could be generated to illustrate the enzyme activity pattern for each LSD in order to develop characteristic shapes for each disease that could be used for machine learning (Figure 4.9). For example, MPS I is known to be deficient in IDU, but it is characterised by a range of other different enzyme activities with a notable elevation in hexosaminidase activity (Figure 4.1 B). A robust diagnostic tool could thus be developed.

Machine learning potentially used in future for routine analysis of clinical data (Obermeyer and Emanuel 2016), which would help to identify specific LSDs from their shape/pattern distributions based upon a wide range of basic enzyme assays. The findings from the enzyme assays could also be used to categorise the key 'diagnostic' enzymes for all LSDs that could then be added to multiplex assays in order to develop new options for newborn screening programmes.

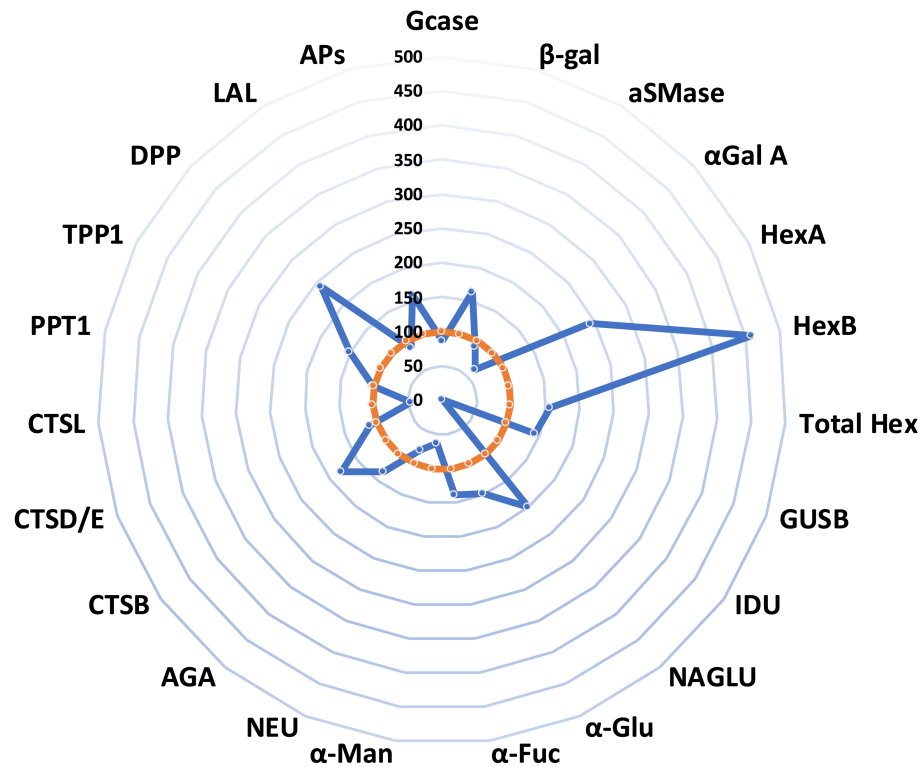


Figure 4.9 Radar plot showing multiple lysosomal enzyme activities measured in MPS I patient fibroblast.

Radar plot or so called “spider diagram” of MPS I enzyme activities generating a unique shape whose pattern can be used to discern the disease (e.g. by machine learning). Data shows the percentage change of the specific disease enzymes (blue) against the control. The red circle is control enzyme activity (100%).

4.3.8 The possibility of the secondary enzymes defect in LSDs becoming a therapeutic target

I considered the possibility that the correction of a secondary enzymes defect in LSDs may lead to overcoming some cellular abnormality in the cells. The LAL enzyme defect was common in several LSDs and neurodegenerative diseases (Supplementary Figure 24). I also observed by electron microscope the presence of lipid droplets in other LSDs, including CLN5 (Chapter 6). The lipid storage phenotype results in a marked enlargement of lysosomes in Wolman, NPC1 and CLN5. I confirmed that defective LAL activity had a role in inducing lipid storage in these diseases as storage was reduced in NPC1 cells by exogenous rhLAL treatment, which presumably leads to correcting the trafficking abnormalities in NPC1. It is also postulated that exogenous rhLAL rescues lysosomal cholesterol ester accumulation which possibly “traps” other lipids within the lysosomal membrane blocking their normal metabolism and cellular movement. The preliminary finding here needs to be investigated further, which may therefore propose new therapeutic opportunities for LSDs even if the primary genetic defect is not corrected. The secondary deficiency in some enzymes, either elevated activity or reduced activities, in LSDs is a more feasible therapeutic target than the primary mutation. Further studies are required to investigate the effect of LAL replacement therapy on the LSDs and neurodegenerative disease phenotypes.

4.4 Conclusion

There are multiple lysosomal enzymes altered among LSDs but there are some enzymes that would be useful for identifying a group of LSDs. I have found that monitoring lysosomal enzyme activity in DBS samples are a useful method for monitoring miglustat treatment. However, further studies are necessary to understand such changes in the lysosomal enzymes and to investigate whether these enzymes are altered by post-translational modification or whether the changes are related to the level of enzyme biosynthesis. This could provide not only valuable insights into LSDs diagnosis but also hypothetically novel objectives for therapeutic intervention.

Chapter 5: A comparison of lysosomal lipid storage across lysosomal storage diseases by electron microscopy

5.1 Introduction

Electron microscopy (EM) is a powerful technique for LSD diagnosis and ultrastructural study. However, apart from case reports (Alroy and Ucci 2006; Boustany et al. 1990; Kamensky et al. 1973; Prasad et al. 1996), there are few studies that carefully characterise intracellular lipid storage in LSDs using EM. Furthermore, from the findings reported in chapters 3 and 4, the presence of lysosomal storage by lysotracker in conjunction with alterations in multiple enzyme activities were observed in the majority of LSDs, which would be expected to result in characteristic secondary storage. Therefore, in this study, EM has been used to observe morphological variations in lysosomal lipid storage across LSDs and to confirm and identify secondary storage lipids that may associate with defective enzyme activities.

5.1.1 Overview of the use of electron microscopy for LSD diagnosis

EM of skin biopsy samples has been used for the diagnosis of LSDs since the 1970s (Belcher 1972; Kamensky et al. 1973). This was followed by use of other tissue biopsies, such as liver, leukocytes, lymph nodes, kidneys etc (Hammel and Alroy 1995). The stored materials in LSDs possess different morphological characteristics in different tissues. Therefore, there is not a single type of tissue that can be used universally for EM diagnosis of LSDs. Optimal results can be obtained using skin and conjunctiva biopsies for LSD diagnosis (Vogler et al. 1987), with use of skin biopsy alone also considered to be a cost-effective, useful and convenient diagnostic tools for LSDs (Prasad et al. 1996). Furthermore, it was also suggested that skin biopsies would be useful not only to understand the mechanisms underlying LSDs, but also to search for novel therapies for these diseases (Prasad et al. 1996; Wenger et al. 2003).

Previously, EM has been used to identify new LSDs. For example, Aula *et al* (1979) reported abundant cytoplasmic inclusion bodies in EM images of skin and leukocytes, coupled with vacuoles in cells from peripheral blood smears, in patients in Northern Finland. No abnormalities were found in the activities of a panel of eight lysosomal hydrolases in lymphocytes or cultured skin fibroblasts. As a result of these observations, it was concluded that these patients were suffering from a genetic LSD, termed "Salla disease", that had not been described before (Aula *et al.*, 1979). EM has now mostly been replaced by more recent techniques, such as molecular

techniques, fluorescence and confocal microscopy. However, a recent study of 74 skin biopsies from patients with neurological abnormalities and developmental delay, confirmed the usefulness of EM for providing clues as to a diagnosis (Zlamy et al. 2019). EM was able to provide a definitive diagnosis that patients in the study (37.8%) included NCLs, NPC1, GM1 gangliosidosis and Aspartylglucosaminuria. For example, the presence of a mixture of curvilinear and fingerprints profiles was used to diagnosis the NCLs (Zlamy et al. 2019). However, the use of fibroblasts will not always detect storage in all LSDs: specific inclusions are not present in Gaucher disease or MLD fibroblasts (Kamensky et al. 1973). Therefore, although skin biopsy EM is a valuable technique for the diagnosis of the majority of LSDs, there may occasionally be some unreliable results due to the accumulation of secondary storage material in LSDs, which makes diagnosis particularly challenging. Further issues that have held back the use of EM for clinical diagnosis are the invasiveness of the tissue biopsies, the fact that randomness of sampling can occasionally lead to false negatives where there is no obvious visible storage in a patient who is otherwise clinically affected and finally the need for specialist equipment and training.

5.1.2 Usefulness of electron microscopy for studying ultrastructural alterations in LSDs

Previous studies utilised EM for the diagnosis of LSDs, based on the wide range of characteristic morphological changes in various cells, or an accumulation of different substrates in the cytosol, that occur in each LSD (Platt et al. 2012). These characteristics render the process of establishing a particular tool for diagnosis complex. The main challenge involved in using EM for LSD diagnosis lies in the fact that a large number of these diseases possess similarities in their stored products (Vitner et al. 2010; Walkley and Vanier 2009b). However, EM remains a useful tool in distinguishing non-lysosomal disorders from lysosomal-based ones through the identification of the nature of stored compounds such as glycolipids, glycoproteins or mucopolysaccharides, which can then undergo further testing. Among LSDs, the overlap between the accumulated primary substrate and secondary storage material should be considered. This building-up of primary storage products in LSD cells activates complex pathological cascades, including events that cause the mounting-up of secondary storage products. Importantly, secondary storage substrates in LSDs can aggressively contribute to the disease pathogenesis (Brunngraber et al. 1973; Walkley and Vanier 2009b).

EM reveals that cytosolic vacuoles are heterogenous, and their appearance differs depending on the cell type. These vacuoles may consist of clear amorphous materials, granular materials, internal debris, internal vesicles, membrane fragments, dense aggregates and multilamellar

structures that form zebra bodies. There are several primary storage products that are linked with similar storage lesions. Many diseases produce similar vesicle features; for example, the presence of zebra bodies is common in many LSDs (Alroy et al. 2013). Typical inclusion bodies have been observed in lysosome-like structures with concentric or parallel lamellae in fibroblasts (Kamensky et al. 1973; Prasad et al. 1996). This structure for example indicates an accumulation of globoside Gb3 within the lysosomes; immunolabeling with anti-Gb3 was localised to multilamellar lysosomal inclusions in patients diagnosed with Fabry disease (Yam et al. 2006).

Previous EM characterisation of storage material in NPC revealed the presence of clear, dark, lamellar structures in different tissues, including fibroblasts (Boustany et al. 1990). The lamellar structures have also been detected in GM1 gangliosidoses (Alroy and Ucci 2006). The most obvious phenotype in NPC cells is the lysosomal accumulation of sphingosine, and of free cholesterol, followed by abnormalities in cellular lipid trafficking, including ganglioside GM1 (te Vrugte et al. 2004). There is a correlation between the presence of lamellar structures and the presence of lipids (Kamensky et al. 1973). Empty vacuoles are mainly found in the mucopolysaccharidoses, and are the result of GAG accumulation (Kamensky et al. 1973). The EM “appearance” of lysosomal material in LSD cells is sometimes unique to particular families of diseases, such as the fingerprint-like structures mainly found in the NCLs (Alroy and Ucci 2006; Nijssen et al. 2003). These structures are the result of lipopigment accumulation in the NLCs, which occur despite the various underlying biochemical aetiologies (Mole et al. 2011). The presence of these characteristic storage materials in specific diseases highlights the possibility of using skin fibroblasts for monitoring disease treatment. It is a less invasive biomarker compared to liver biopsy, which is currently used to evaluate sphingomyelin storage in NPA (Thurberg et al. 2012). Skin biopsies have also been used as a suitable biomarker to monitor the ability of ERT to clear storage material in Fabry disease (Thurberg et al. 2004).

However, there are limited studies in the literature that compare intracellular lipid storage across LSDs and overall the structures of several storage molecules by EM remains undefined. In this study, EM has been used to identify the different accumulated substrates and compare them with each other. The EM technique has been revisited as our findings from our studies of enzyme alteration among LSDs have shown the presence of different secondary enzyme alterations in LSDs (Chapter 4). This has raised the possibility of investigating the morphological structure of these diseases and discovering whether or not the secondary enzymes alteration is linked to morphological changes in the cell.

5.1.3 Aims

1. To investigate the morphology of primary storage lipid containing structures in several LSDs.
2. To study the secondary storage lipids in several LSDs.
3. To examine the localisation of these lipids using immuno-EM.
3. To investigate the ability of miglustat treatment to reduce storage lipids in CLN5.

5.1.4 A brief summary of the various methods I used

In Section 5.2.1 I studied the ultrastructure morphology in control cells using the epoxy resin method (chapter 2, section 2.12.1). I then used the cryofixation method (chapter 2, section 2.13.2) for immunolabelling with anti-LAMP1 and anti-LAMP2.

In Section 5.2.2 I characterised the ultrastructural morphology of primary lipid storage in LSDs.

In Section 5.2.3 I investigated the ultrastructure of storage inclusions in the sphingolipidoses and followed this by using the cryofixed method for immunolabelling NPC patient fibroblasts with anti-GM2.

In Section 5.2.4 I characterised the ultrastructural morphology of the mucopolysaccharidoses.

In Section 5.2.5 I characterised the ultrastructural morphology of the NCLs.

In Section 5.2.6 I studied the localisation of secondary storage in CLN5 using immunolabelling EM, and studied the usefulness of miglustat treatment to normalise the lysosome morphology.

In Section 5.2.7 I investigated the ultrastructure of other LSDs.

5.2 Results

5.2.1 The ultrastructure appearance of lysosomes in control fibroblasts and the localization of lysosome markers

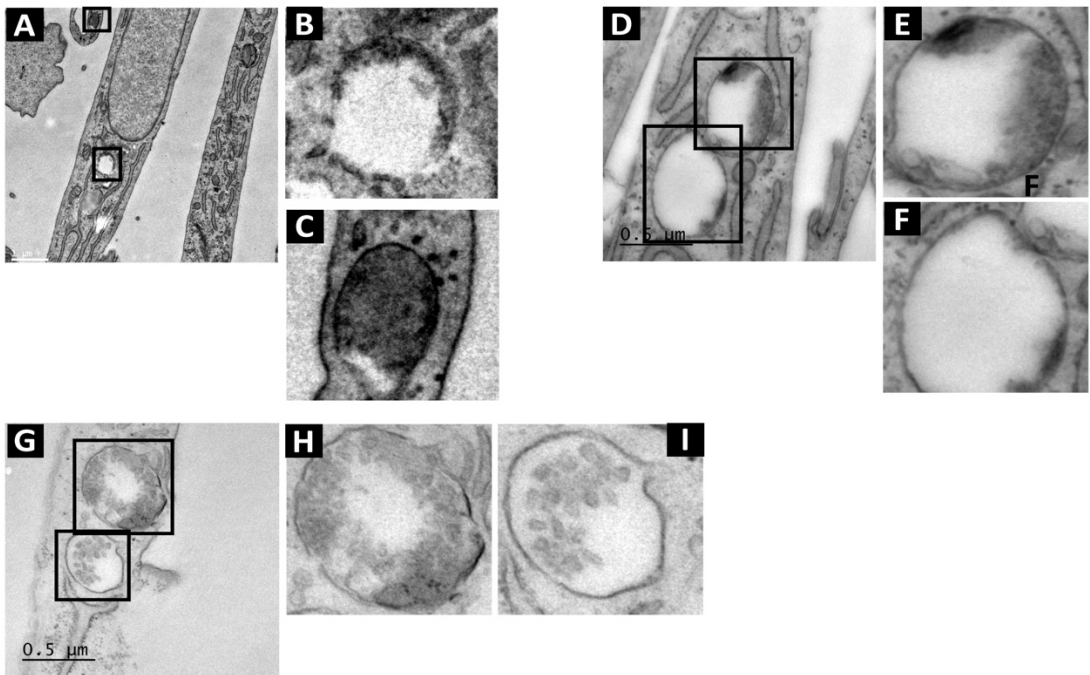
I started by looking at the ultrastructural appearance of lysosomes in control fibroblasts. I used different ages (1yr. and 54yrs.) due to the different ages of onset of different LSDs. This ultrastructural investigation showed that the cytoplasm of 1yr old contains lysosomal vacuoles with either an empty or a light density of materials (Figure 5.1 A-F). The micrograph in Figure 5.1 shows the multivesicular body (MVB) containing small granules.

The 45yr. control had a light density of material in the limiting membrane (Figure 5 J-M). It also showed a few vacuoles with a dark density and a few small zebra-like structure bodies associated with the peripheral membrane (Figure 5.1 N & O). I followed this by investigating the localisation of anti-LAMP1 and anti-LAMP2 in cryofixed fibroblasts. The observed vacuoles in the cytoplasm were organelles with a limiting membrane that appeared either empty, or with a dark density; these are labelled with anti-LAMP1 and anti-LAMP2 antibodies (Figure 5.1 P-S). This finding thus confirmed that these identified vacuoles were mainly lysosomes.

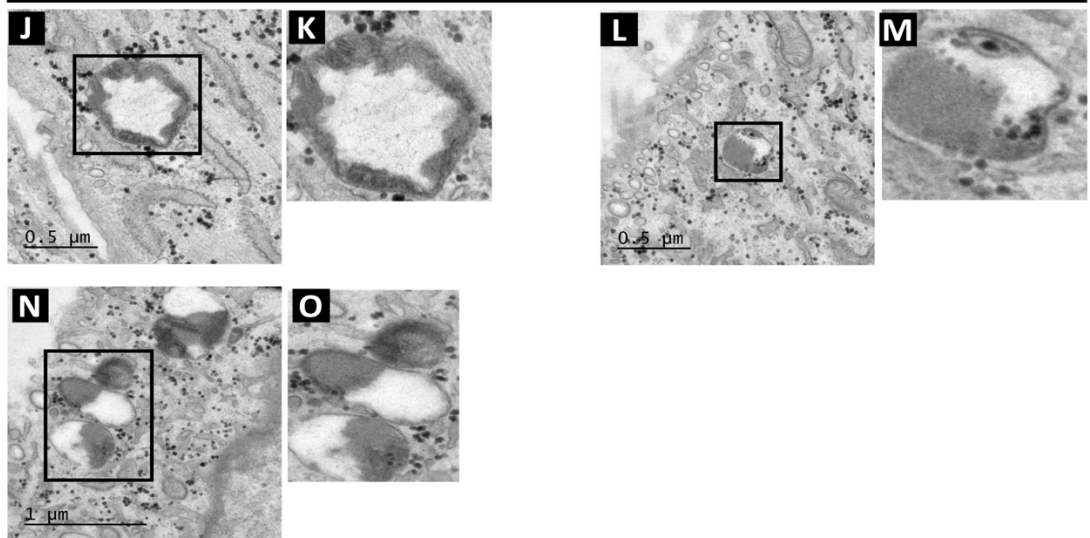
Figure 5.1 Morphological characterization of control fibroblasts.

Fibroblasts from different controls were imaged following conventional (epoxy resin) EM. (A-J) Ultrastructure of the 1yr. control (GM05399). (J-O) Ultrastructure of the 54yrs. control (GM04787). (P-Q) Ultrastructure of control fibroblasts (GM05399) were imaged following cryofixation (immuno-EM) shows the specific localization of anti-LAMP1 (R-S) and anti-LAMP2 (10nm gold). The arrow-heads show the localisation of the antibodies. Representative pictures shown n=1. For all insert images magnification was 7X (B), 10X (C), 2.5X (E-F-HS), 3X (I-M), 2X (K-O-Q).

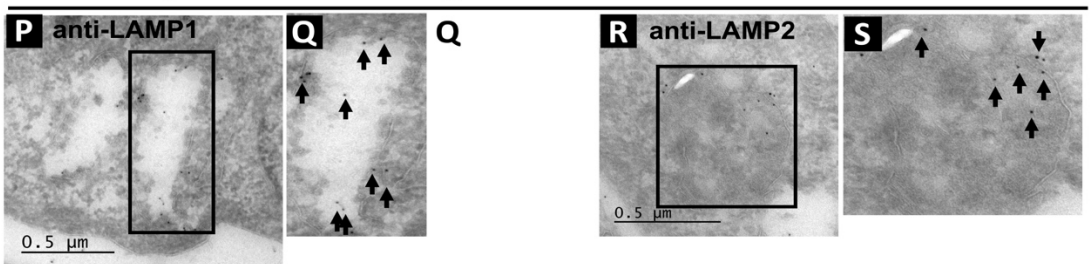
Control 1yr



Control 54yr



Control 1yr immunolabeling



5.2.2 Morphologies of primary storage molecules accumulating in the LSDs.

I followed this by identifying the ultrastructure of the major storage materials across the primary LSDs. Ganglioside GM1 storage appears as dark, thick lamellar whorl structures inside lysosomes (Figure 5.2 A). In Tay Sachs, ganglioside GM2 accumulation appears as grey lamellar, whorl-like structures in the lysosome (Figure 5.2 B). Globoside, in particular globotriosylceramide (Gb3), accumulates in Fabry disease, and appears as a dark membrane associated lamellar structures (Figure 5.2 C). Sphingomyelin storage bodies in NPA appear lighter in colour but are similar to those seen in GM2 gangliosidosis with more repetition (Figure 5.2 D). There are also single lamellar bodies in the lysosomal lumen in NPC, potentially the result of sphingosine storage (Figure 5.2 E) (Lloyd-Evans et al. 2008). The ultrastructural finding in MPS I is the presence of lysosomal vacuoles containing central fine floccular material, which mirrors the storage of GAGs (Figure 5.2 F). Wolman disease fibroblasts accumulate esterified cholesterol, which appears as a crystalline structure (Figure 5.2 G). Furthermore, triglyceride storage appears in the cytoplasm as lipid droplets (Figure 5.2 H). Fingerprint profiles/curvilinear structures were detected in CLN5, characteristic of the storage of lipofuscin-like material, using Cryo-EM (Figure 5.2 I), whilst a more broken down fragmented curvilinear structural profile was identified in cells prepared using conventional epoxy resin (Figure 5.2 J). Oligosaccharide storage in Fucosidosis appears as either empty vacuoles or has a fibrillar structure throughout the vacuole (Figure 5.2 K).

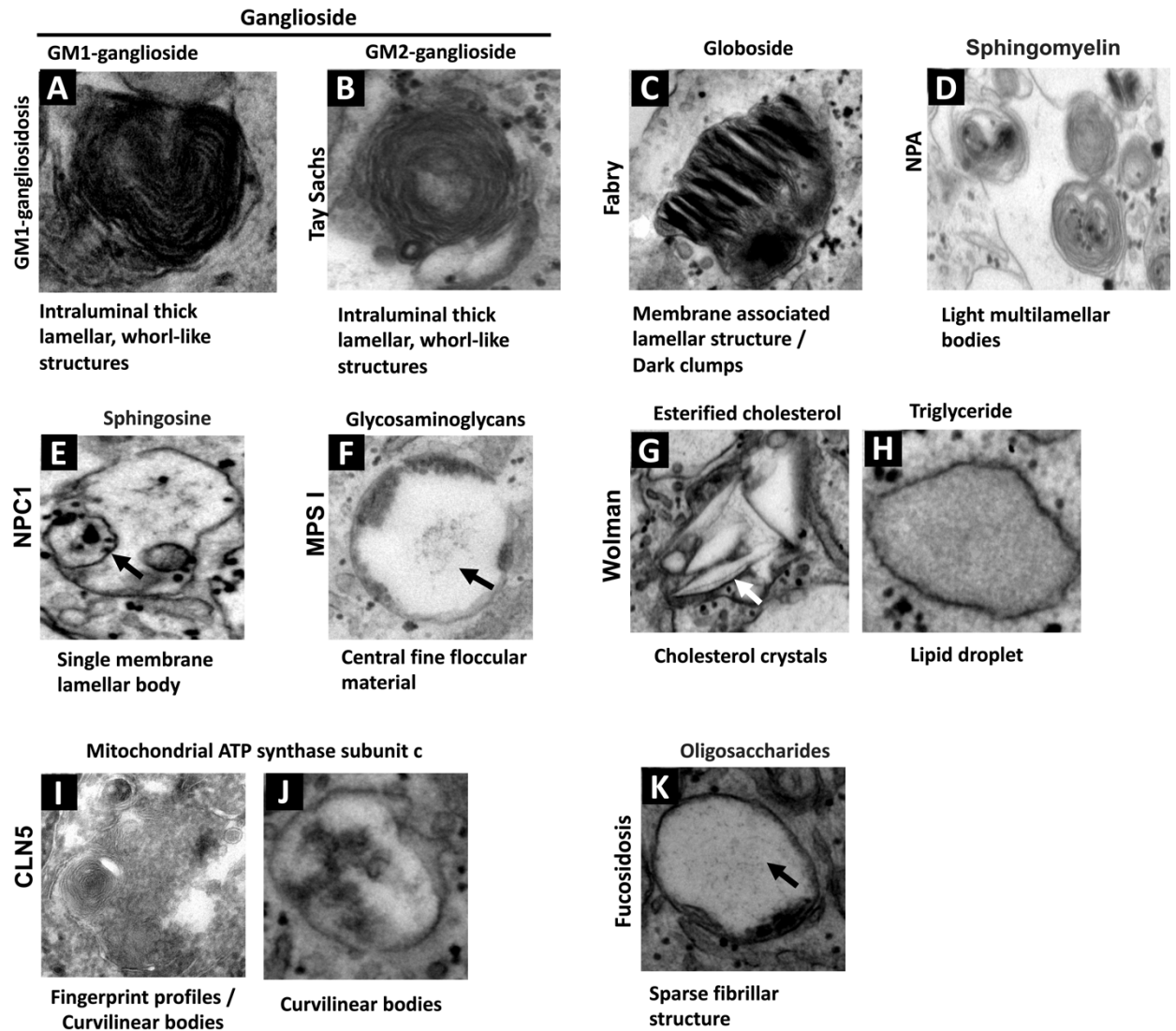


Figure 5.2 Electron microscopy of primary storage material in LSDs.

Fibroblasts from different LSD patients were imaged following conventional (epoxy resin) EM or Cryo-EM. (A) The ultrastructure of ganglioside GM1. (B) The appearance of ganglioside GM2. (C) Globoside Gb3 morphology. (D) The ultrastructure of sphingomyelin. (E) The ultrastructure of sphingosine. (F) Glycosaminoglycan storage morphology in lysosome. (Nordestgaard et al.) The characterisation of esterified cholesterol and triglyceride storage in Wolman disease. (I) CLN5 ultrastructure by Cryo-EM. (J) CLN5 ultrastructure by conventional (epoxy resin) EM. (K) The ultrastructure of oligosaccharides. Representative pictures shown n=1.

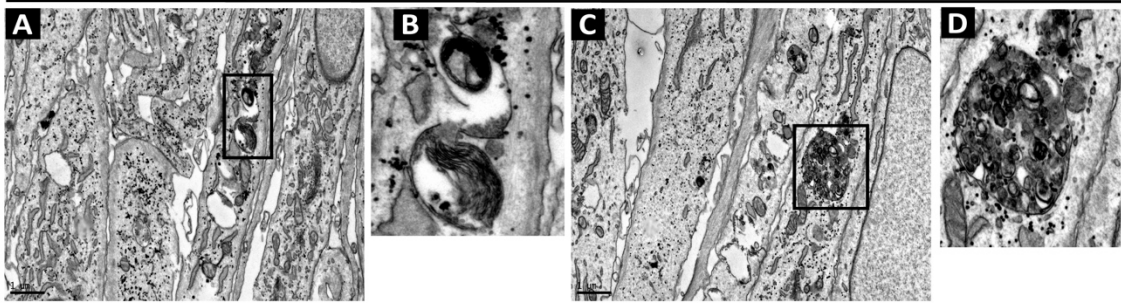
5.2.3 Morphological characterization of the sphingolipidosis family of diseases by electron microscopy

Thick lamellar structures (whorls/zebra bodies) were detected in GM1 gangliosidosis fibroblasts, as were electron dense MVBs (Figure 5.3 A-D). Similarly, the Tay Sachs storage structures appeared as fine lamellar bodies (light whorls/zebra bodies) (Figure 5.3 E & F). Several MVBs are also present (Figure 5.3 G & H). Fabry fibroblasts showed several dark clumps, starting in a circular shape on the intraluminal lysosomal membrane, and developing into whorls then extremely electron dense filled lysosomes, all of which indicate the presence of primary globoside storage (Figure 5.3 I & J). The second identified ultrastructural morphology was the presence of cholesterol crystal (Figure 5.3 K & L). There is only a single case reported that has mentioned the widespread cholesterol crystal in kidney tissues (Shirai et al. 2000). In NPA fibroblasts, sphingomyelin storage typically appears as multiple small, light coloured zebra bodies among the lysosomes (Figure 5.3 M & N). Interestingly, I identified the presence of dark clumps, similar to those that have been detected in Fabry, but these were less dense in NPA (Figure 5.3 O & P). The dark whorl/zebras were also seen in NPA (Figure 5.3 O & Q). There were also larger and denser MVBs, in comparison to control fibroblasts (Figure 5.3 R & S).

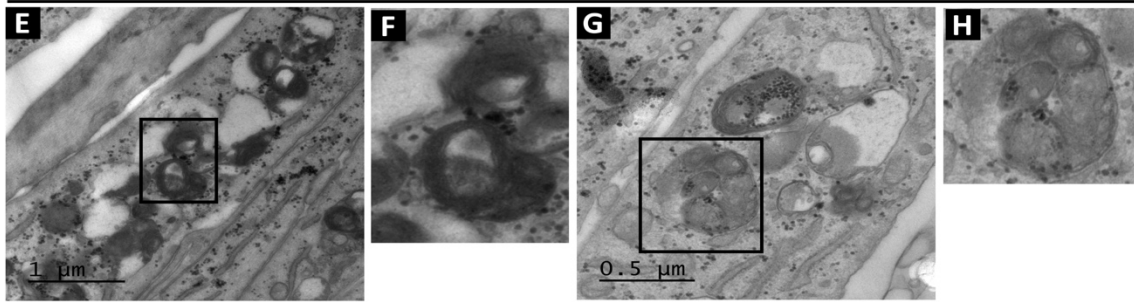
Figure 5.3 Electron microscope characterisation of lysosomal storage material ultrastructure in the sphingolipidoses

Fibroblasts from different LSD patients were imaged following conventional (epoxy resin) EM. (A-D) The morphological structure in GM1 gangliosidosis (GM03589). (E-H) The ultrastructural appearance in Tay Sachs (GM00502). (I-L) The ultrastructural appearance in Fabry (GM00107). (M-S) The ultrastructure of NPA lysosomes (GM00112). Representative pictures shown, N=1. For all insert images magnification was 4X (B-Q), 2.5X (D-F-J), 1.8X (H), 6X (L), 1.5X (N-P), 2X (S).

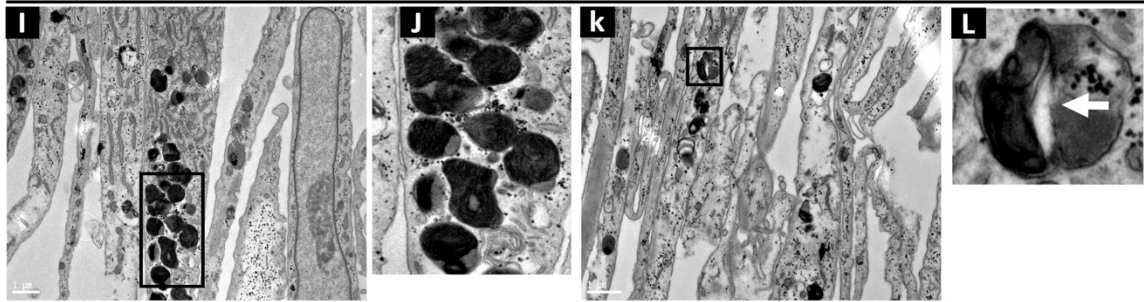
Gm1 gangliosidosis



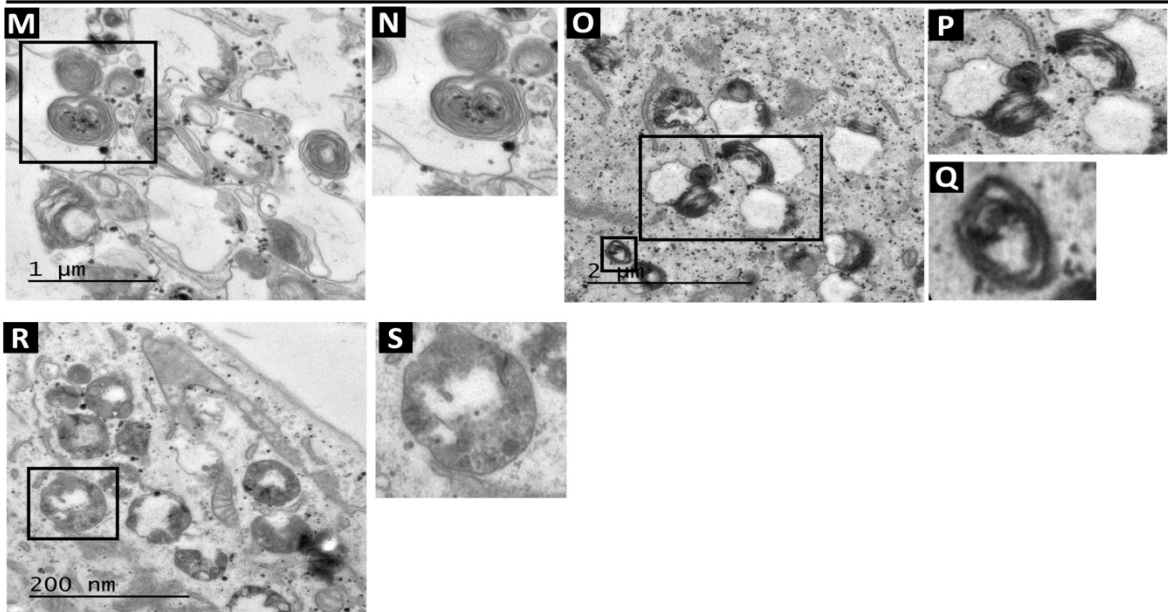
Tay Sachs



Fabry

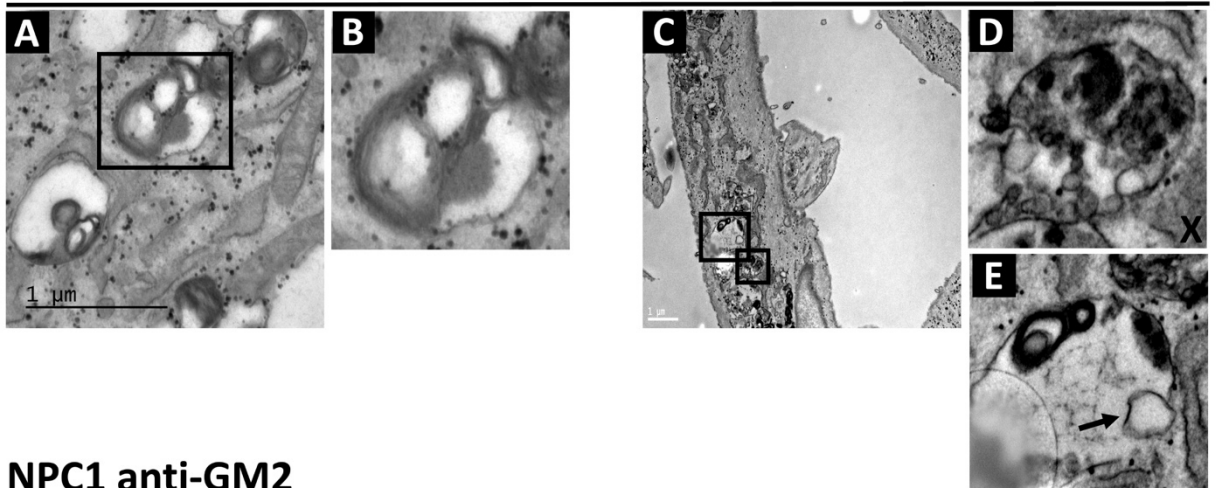


NPA



By looking at the morphological ultrastructure of NPC fibroblasts, I was able to detect the presence of a variety of storage materials, including multilamellar bodies, and both light (B) and dark (E) intralamellar whorls representing the storage of gangliosides (Figure 5.4 A & B), in addition to the presence of large MVBs (Figure 5.4 C & D). I also identified the presence of smaller single circular membrane structures within lysosomes, which are not present in the other LSDs, that I believe to be sphingosine. Furthermore, and have also identified the presence of central fine floccular material similar to that observed in MPSI (Figure 5.4 C & E). In order to determine whether the storage material in NPC contains gangliosides, I stained cryofixed NPC fibroblasts using immuno-EM, and observed the presence of ganglioside GM2 within the storage material in NPC1 lysosomes using an anti-GM2 antibody (Figure 5.4 F).

NPC1



NPC1 anti-GM2

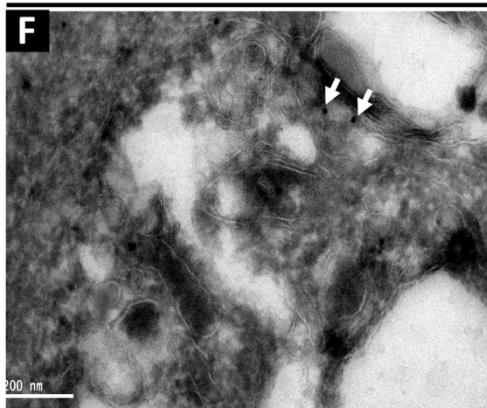


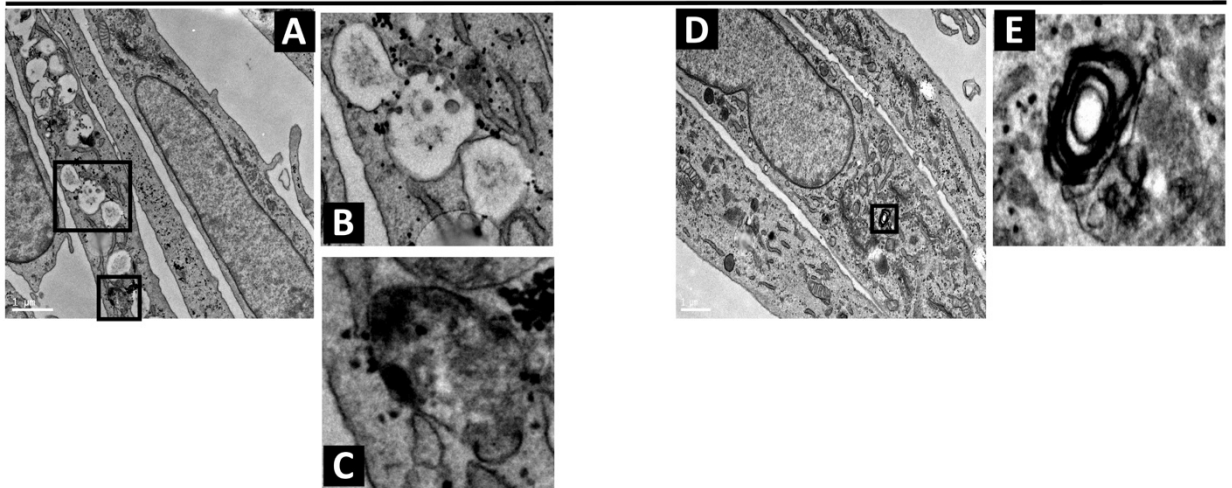
Figure 5.4 Electron microscopy characterisation of the storage material in NPC1.

(A-D) The storage material appearance in NPC1 (GM03123) following conventional (epoxy resin). (F) The immunolabelling of NPC1 (GM03123) with anti-GM2 (10nm gold) in cryofixed sections. The arrowhead shows the localisation of antibodies. Representative pictures shown n=1. For insert images magnification was 2X (B), 5X (D-E).

5.2.4 The ultrastructural appearance of storage material in the mucopolysaccharidoses

Ultrastructural examination was carried out on MPS I and MPS IIIA patient fibroblasts. The MPS I study showed several empty vacuoles, but the majority of vacuoles were filled with floccular material in the centre (Figure 5.5 A & B), indicative of GAGs. The MVBs in MPS I are denser than those observed in control fibroblasts (Figure 5.5 A & C). I also observed the presence of few whorl-like lamellar structures in MPS I (Figure 5.4 D & E). Identical abnormalities were observed in MPS IIIA; the presence of multiple vacuoles with central fine floccular material (Figure 5.5 F & G).

MPS I



MPS III A

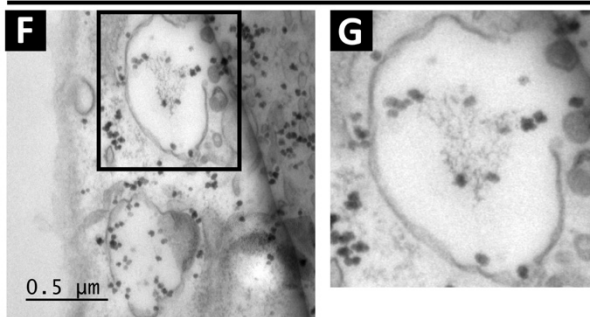


Figure 5.5 Electron microscopy characterisation of storage material in Mucopolysaccharidosis.

MPS I and III A fibroblasts were imaged following conventional (epoxy resin) EM. (A-C) The ultrastructure of lysosomal storage in MPS I (GM00798). (F-G) The ultrastructural appearance of storage material in MPS IIIA (GM01881). Representative pictures shown n=1. For all insert images magnification was 3X(B), 8X(C-E), 2.5X (G).

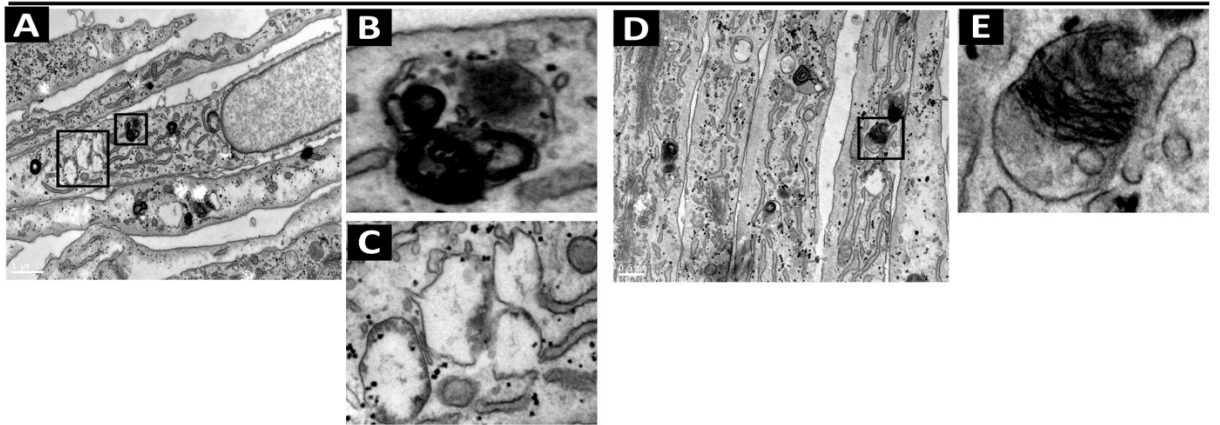
5.2.5 Morphological characterization of lysosomal storage in the neuronal ceroid lipofuscinoses.

The morphological information obtained from our study of NCLs revealed the presence of several types of storage body. Whorl/zebra-like bodies were observed in CLN3, similar to those seen in the gangliosides (Figure 5.6 A & B). There is a possibility of GAGs storage in CLN3 as empty vacuoles were found, with a similar intravesicular floccular structure to those seen in the mucopolysaccharidoses (primary GAGs accumulation diseases) (Figure 5.6 A & C). I have also seen dark zebra body-like structures clumping on the inside of the lysosomal membrane in CLN3 suggestive of globoside storage (Figure 5.6 D & E). The CLN5 lysosomal ultrastructure examination revealed the presence of dark whorls/zebra bodies (Figure 5.6 F & G), and lipid droplets spread throughout the cytoplasm (Figure 5.6 F & H). Dark multilamellar clump structures were also present similar to that seen in Fabry (Figure 5.6 I & J), indicative of globoside storage. Interestingly, multiple vacuoles with central fine floccular material were observed (Figure 5.6 K & L), suggestive of GAGs or sugar accumulation, as were a few curvilinear-like structures (Figure 5.6 M & N). Lamellar, whorl-like structures, membrane-associated dark clump structures presence of curvilinear profile (indicated by arrow) (Figure 5.6 O-Q) were observed in CLN10 fibroblasts, as were lipid droplets in CLN10 (Figure 5.6 R & S).

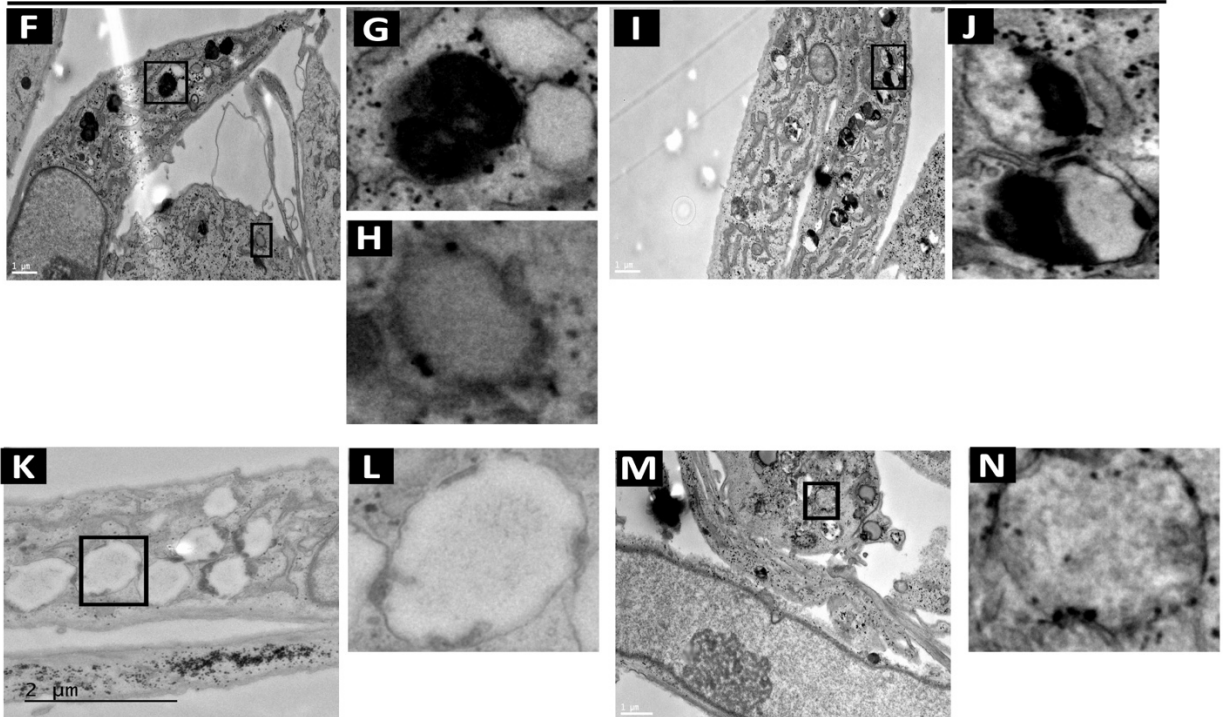
Figure 5.6 Morphological characterization of lysosomal storage in the NCLs.

CLN3, CLN5 and CLN10 fibroblasts were imaged following conventional (epoxy resin) EM. (A-E) The morphological structure of storage materials in CLN3 (CLN3 1KB del). (F-N) The ultrastructural appearance of CLN5 (P1). (O-Q) The morphological structure of CLN10 storage materials, Representative pictures shown, n=1. For all insert images magnification was 8X (B-N), 5X (C), 6X (E-G-S), 10X (H-J), 3X (L), 2.5X (P), 4X (Q).

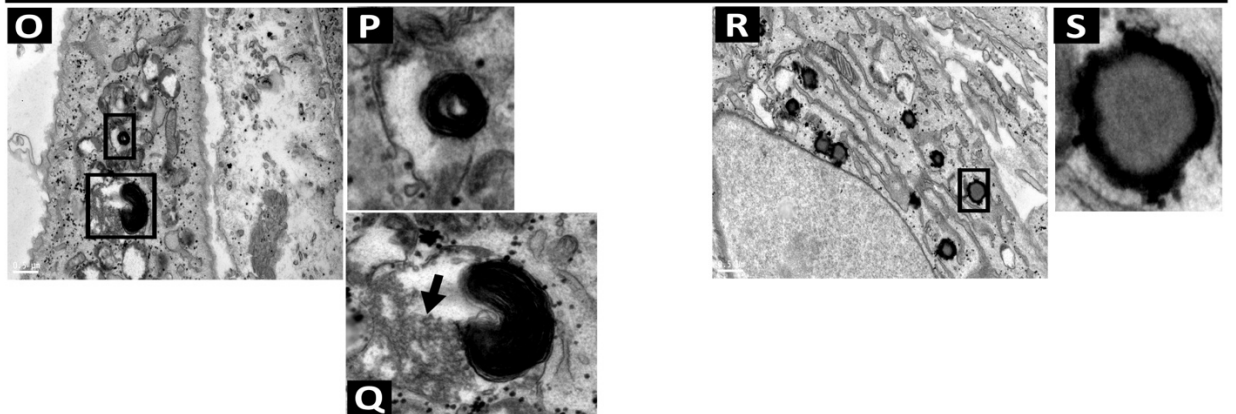
CLN3



CLN5



CLN10



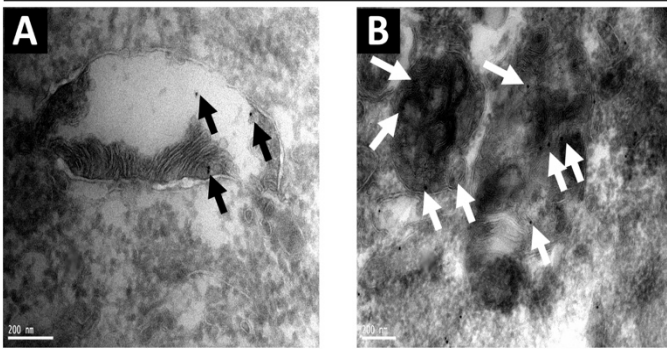
5.2.6 Confirmation of globoside storage, and the ability of miglustat to remove storage material, in CLN5 disease

The dark clump emanating from the inner lysosomal membrane observed in the CLN5 patient fibroblasts (Figure 5.6 I & J) is similar to those seen in Fabry disease, where globoside Gb3 is the primary storage material (Figure 5.6 I & J), and may therefore indicate storage of globoside in CLN5 and also CLN3 where the same structures were observed (Figure 5.6 D & E). In order to determine whether this is the case, CLN5 fibroblasts were cryo-fixed and immunolabelled with anti-Gb3, which confirmed globoside storage within lysosomes containing fingerprint like structures (Figure 5.7 A-B). Following 5 days treatment with 50 μ M miglustat, which reduces glycosphingolipid biosynthesis and therefore globoside Gb3 levels, storage material within the lysosome was reduced in CLN5, resulting in multiple large empty vacuoles or vacuoles with low density contents (Figure 5.7 D & E). Peripheral light whorl/zebra body structures were still present as a result of the reduction in, but not complete elimination of, ganglioside storage but at a dramatically reduced level confirming their identification as gangliosides (Figure 5.7 F & G). Consistent with previous findings (Neises et al. 1997), there is an increase in the density of the plasma membrane which is the presence of miglustat accumulating in the membrane and confirming its effect upon the cells (Figure 5.7 H & I). Furthermore, our data points towards an increased presence of "fingerprint" like structures equating to lysosomal protein/lipofuscin accumulation in the cryofixed sections but no lipids, whereas by regular epoxy TEM processing I see the lipids but dramatically reduced protein structures. This is indicative of a processing issue in terms of identifying all of the components of NCL lysosomal storage.

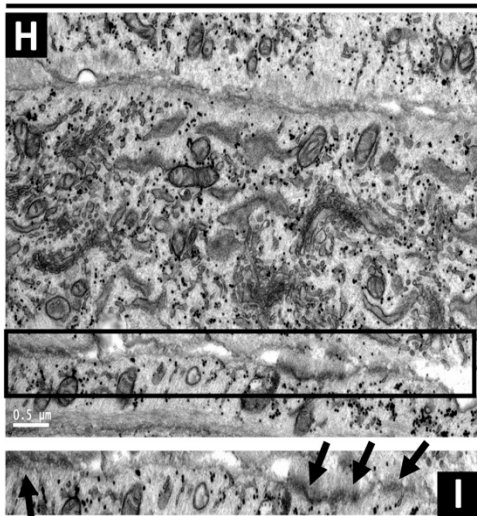
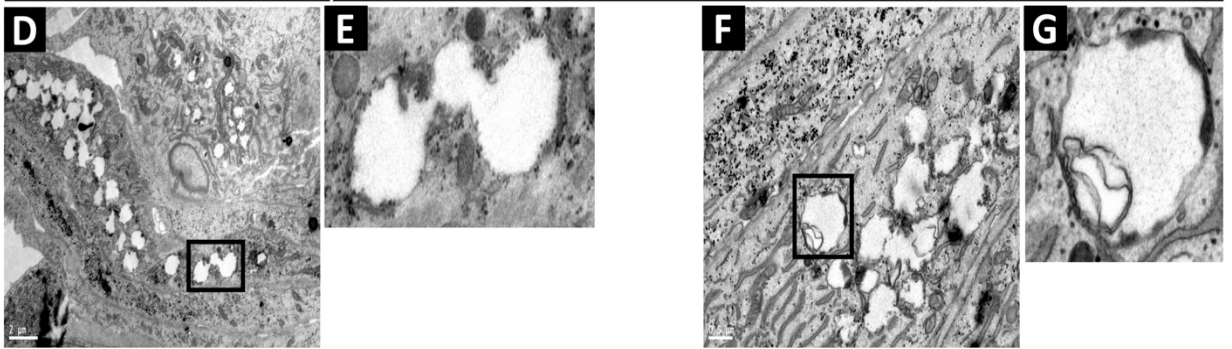
Figure 5.7 Globoside Gb3 storage, and the reduction in storage effected by miglustat, in CLN5 fibroblasts.

CLN5 fibroblasts (untreated or following 5 days treatment with 50 μ M miglustat) were imaged following conventional (epoxy resin) EM or Immuno-EM. (A-B) The ultrastructure of the cryofixed CLN5 (P1) with immuno-EM shows the specific localization of anti-Gb3 (10nm gold). The head of the white arrows shows the presence of the gold labelled secondary antibody. (D-I) Morphological characterization of CLN5 (P1) treated with 50 μ M miglustat. Representative pictures shown, n=1. images magnification was 5X (E), 3X (G), 1.5X (I).

CLN5 anti-GB3



CLN5 + 50 μ M Miglustat



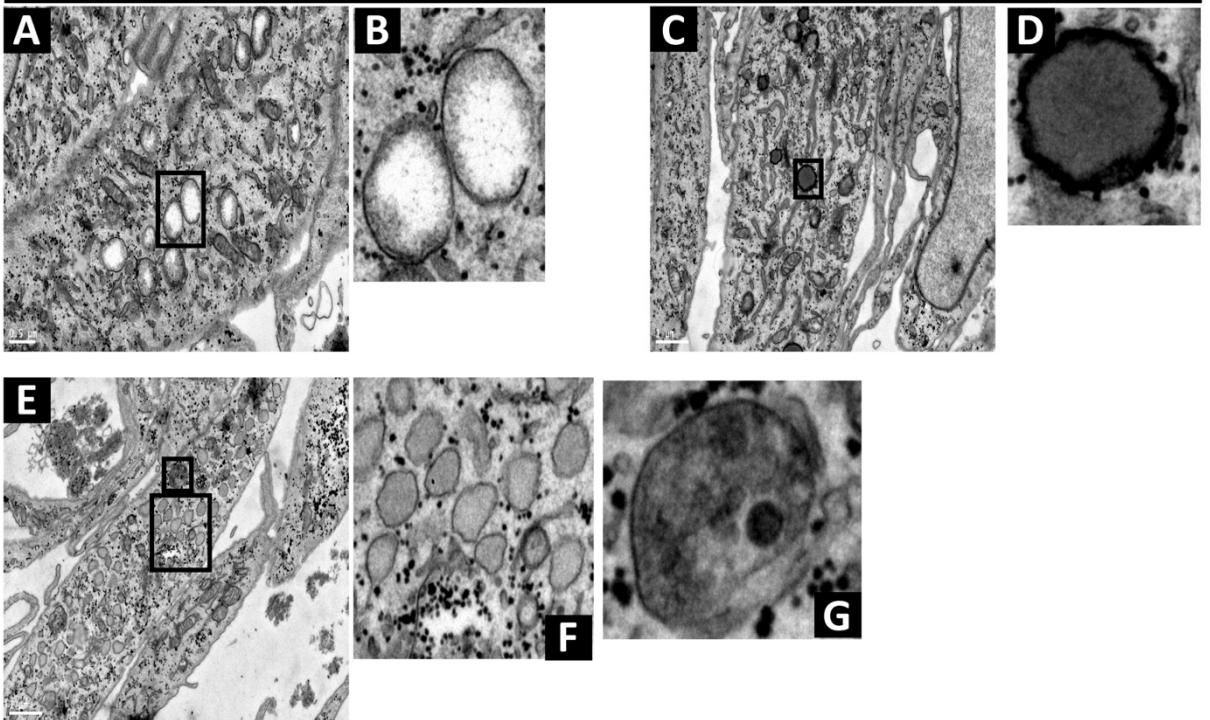
5.2.7 Morphological characterization of Oligosaccharidosis disease

The appearance of storage material in fucosidosis and sialidosis fibroblasts was examined. In fucosidosis fibroblasts, the cytoplasm is filled with numerous enlarged vacuoles that are either empty or contain sparse fibrillar material indicative of sugars (Figure 5.8 A & B), and several lipid droplets (Figure 5.8 C-F), whose identity is confirmed from their presence in the Wolman disease cells where they accumulate as primary storage (Figure 5.2 H). I also observed the presence of large MVBs with dark dense granules (Figure 5.8 E & G). In Sialidosis I saw the presence of large vacuoles with a fibrillar structure were also present (Figure 5.8 H & I), as were lighter whorl/zebra body structures suggestive of ganglioside GM2 or sphingomyelin (Figure 5.8 H & J), and multiple dark structures that appear similar to MVBs (Figure 5.8 K & L). Finally, there was a noticeable presence of lipid droplets (Figure 5.8 M & N).

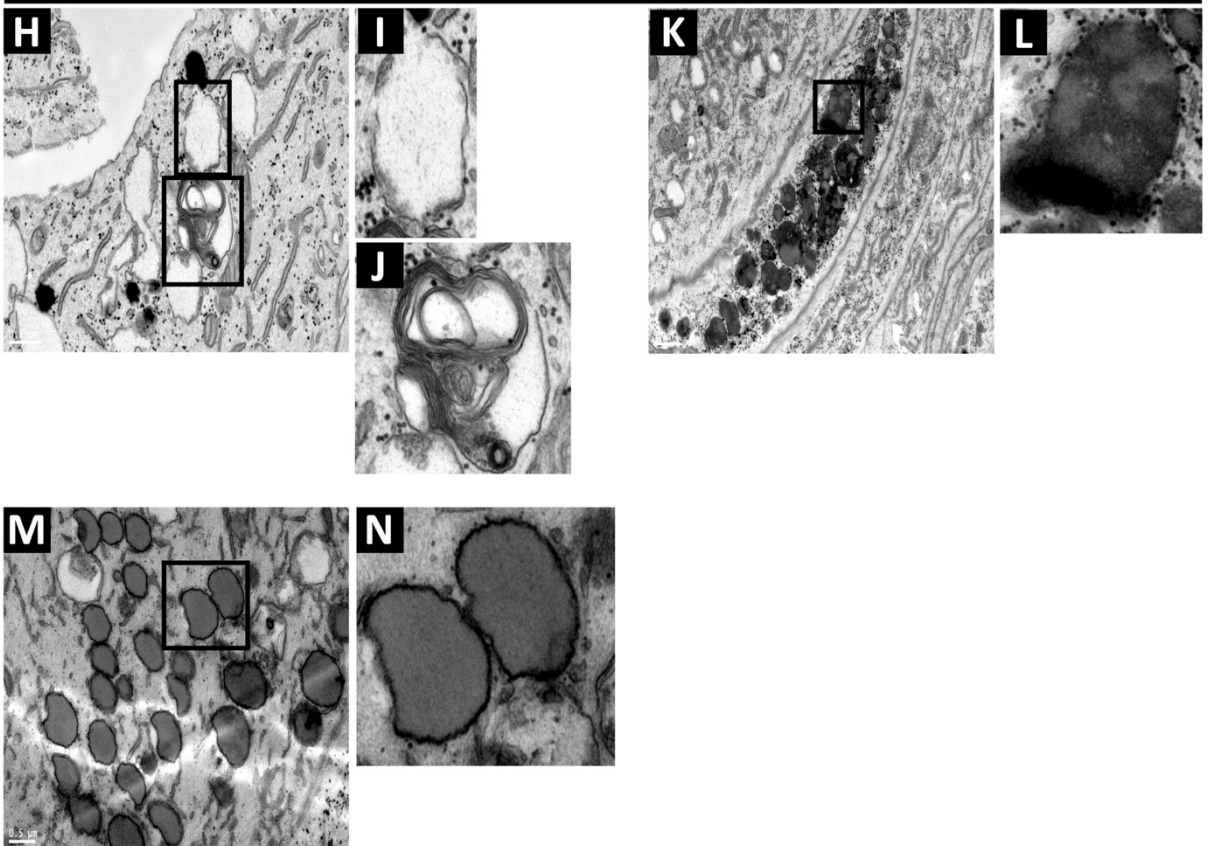
Figure 5.8 Morphological characterization of members of the oligosaccharidoses.

Fucosidosis (GM00291) and sialidosis (GM00654) fibroblasts were imaged following conventional (epoxy resin) EM. (A-G) The morphological structure of storage materials in Fucosidosis. (E-N) The ultrastructure of storage materials in sialidosis. Representative images shown n=1. Images magnification was 4X (B-G), 8X (D-F), 3X (I-N), 2.5X (J), 7X (L).

Fucosidosis



Sialidosis



5.2.8 Morphological characterization of other LSDs

An ultrastructural examination of MLIV fibroblasts revealed multiple storage bodies containing dark whorl/zebra body structures indicative of ganglioside GM1 (Figure 5.9 A & B). There are also lipid droplet-like structures spread throughout the cytoplasm (Figure 5.9 A & C). Vacuoles containing dense material at the periphery of the lysosome as well as floccular material in the centre were observed (Figure 5.9 A & D), as were dark clumps emerging from the lysosomal membrane, indicative of globoside storage (Figure 5.9 E & F) which may comprise some of the thicker whorls (Figure 5.9 B and E). Several MVBs are also present (Figure 5.9 G & H).

MLIV

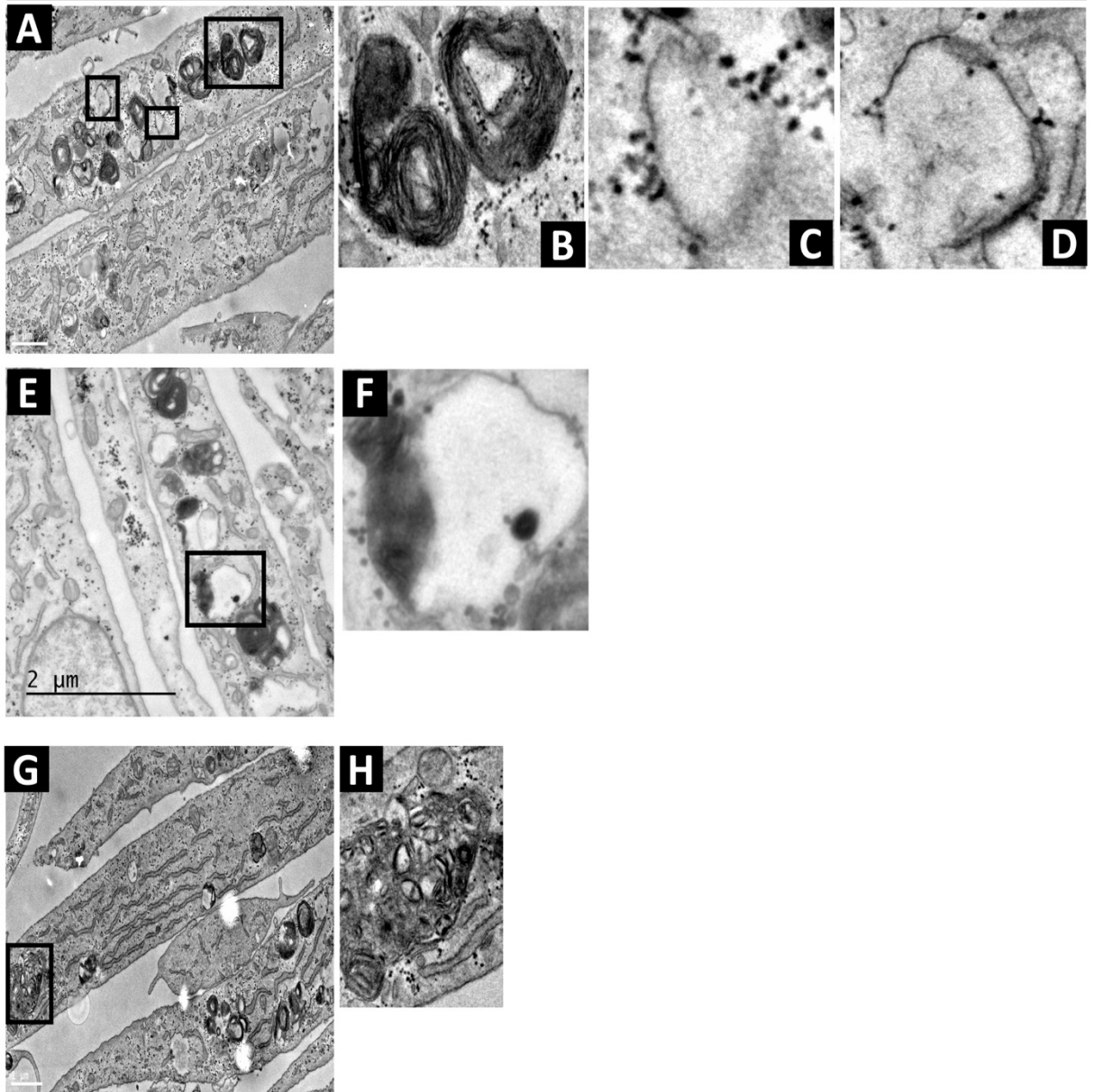


Figure 5.9 Morphological characterization of MLIV.

MLIV (GM02527) fibroblasts were imaged following conventional (epoxy resin) EM. (Tsuboyama et al.) The ultrastructure of lysosomal storage materials in MLIV. Representative images shown n=1. Images magnification was 5X (B), X15 (C), 10X (D), 3X (F), 7X (H).

A morphological study of acid lipase deficient Wolman disease showed the presence of cholesterol crystals (Figure 5.10 A & B) and lipid droplet-like structures in Wolman disease (Figure 5.10 A & C). I also found in the lysosomes zebra body structures containing clear dark whorls that appear anchored to the lysosomal membrane indicative of globoside Gb3 accumulation (Figure 5.10 D & E). Furthermore, enlarged MBVs with dark, dense contents were present (Figure 5.10 F & G).

Wolman

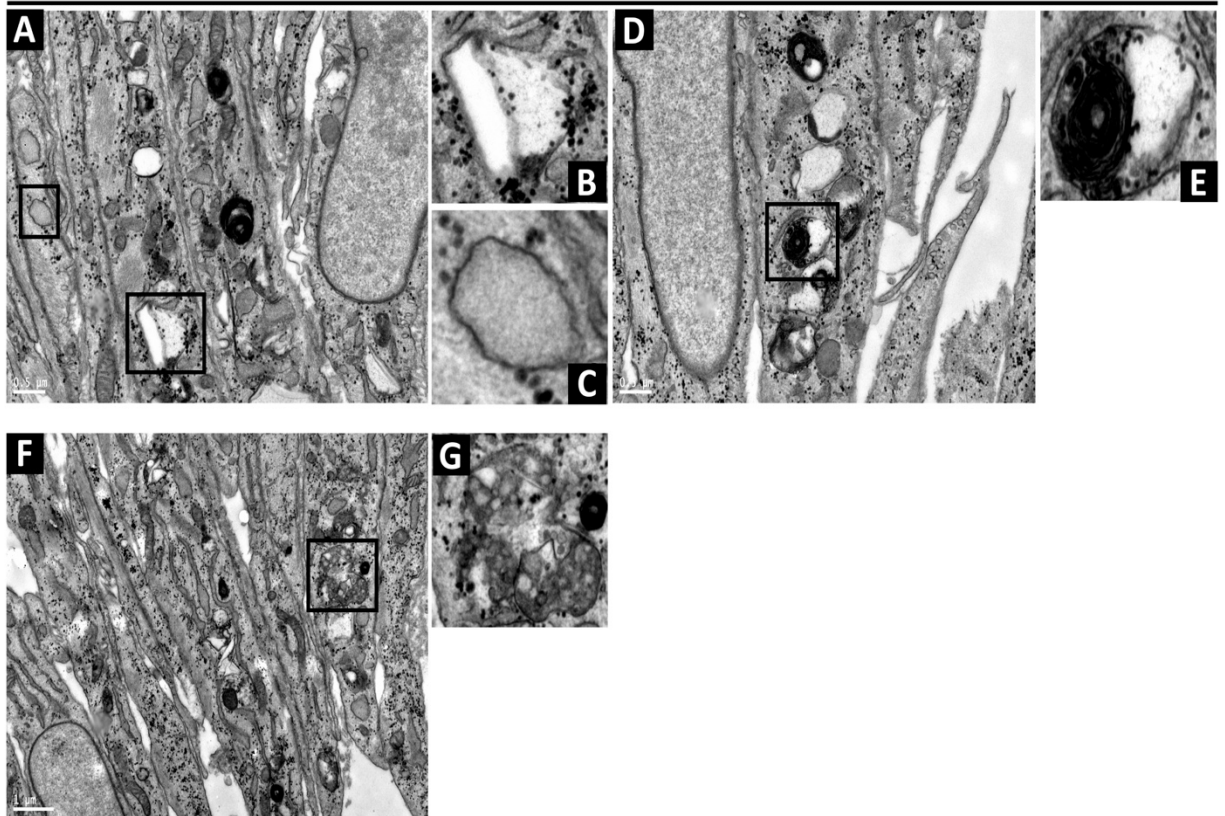


Figure 5.10 Morphological characterization of Wolman disease fibroblasts.

(A-G) Wolman fibroblasts (GM01606) were imaged following conventional (epoxy resin) EM. Representative images shown n=1. For all insert images magnification was 2X (B), 4X (C), 3X (E-G).

The ultrastructural appearance of the storage material in I cell disease fibroblasts included multi-lamellar structures indicative of ganglioside storage (Figure 5.11 A & B), dark zebra bodies, which may indicate either further ganglioside or globoside storage (Figure 5.11 C & D), the white arrow in the same figure indicative the sphingosine structure (Figure 5.11 C & D). The cholesterol crystal cleft was detected in the cytoplasm (Figure 5.11 E & F). Residual curvilinear structures may also be present (Figure 5.11 E & G). Interestingly, multiple caveolae were also observed at the plasma membrane (black arrows), compared to the control (Figure 5.11 H & I). Also in the same Figure I have seen the sphingomyelin structure in the black box (Figure 5.11 H & I). The presence of lipid droplet was identified (Figure 5.11 H & J). The presence of large dark MVBs was also detected (Figure 5.11 K & L). GAGs (floccular) structure were observed in I cell (Figure K & M).

I cell

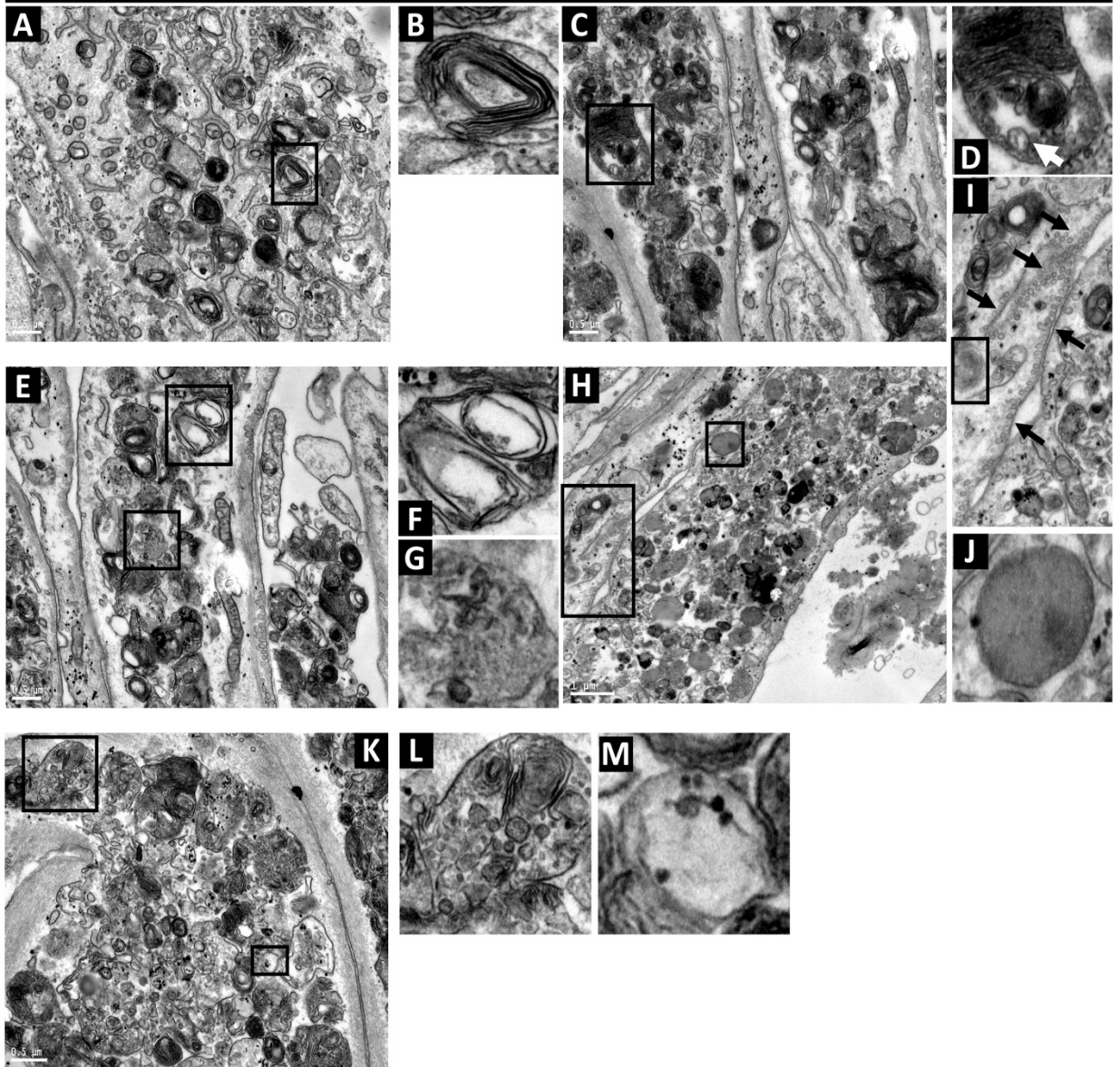


Figure 5.11 Morphological characterization of lipid storage in I cell disease patient fibroblasts.

(A-M) I cell fibroblasts (GM02013) were imaged following conventional (epoxy resin) EM. Representative images shown n=1. For all insert images magnification was 4X (B-G), 2.5X (D-F-I), 3X(C), 2X (I), 3X (J), 5X (M).

5.3 Discussion

Numerous studies have shown that EM still remains a powerful technique for diagnosing LSDs and monitoring responses to therapies (Alroy et al. 2013; Zlamy et al. 2019). EM is often able to aid in the diagnosis of a specific lysosomal disorder by investigating the structure of accumulated materials within the lysosome (Alroy et al. 2013). The complexity of LSDs is evident in the accumulation of different secondary substrates. Evaluation of lysosomal enzyme activities in several LSDs revealed not only primary enzymatic defects but multiple alterations in secondary enzymatic activities as well (Chapter 4). It was possible to confirm that these alterations lead directly to the accumulation of secondary storage material, as storage material identified by EM corresponds to enzyme activity defects in each LSD. For example, I detected secondary storage of globoside in CLN5 disease, where there is a reduction in the activity of α Gal A enzyme, which degrades this substrate.

5.3.1 Identifying the ultrastructure of the major storage material in LSDs

I was aiming to compare the intracellular lipid storage across the LSDs by looking at the morphology of storage bodies. First, I looked at control fibroblasts to identify the normal morphological structure of lysosomes. Examination of control fibroblasts revealed the presence of multiple vacuoles, which were either empty or contained dense storage material adjacent to and in contact with the limiting membrane. MBVs containing granular material were also observed (Figure 5.1 A-I). A few whorl-like lamellar bodies were observed within the lysosomes of the 45yr old control fibroblasts (Figure 5.1 N-O). The 54yr old control fibroblast cells were from an apparently healthy clinically unaffected individual. However, this individual may be a carrier of mutated genes related to LSDs, and some carriers do show alterations in lysosomal localisation and storage as shown with lysotracker staining in NPC1 carriers (chapter 3 figure 3.12). Furthermore, work from the Lloyd-Evans lab (Kirkham *et al*, personal communication) has shown age-dependent changes in lysosomal pH, which may reduce enzyme activity in cells from older individuals and may explain the presence of these whorl-like structures. It was challenging to definitively identify the vacuoles I observed in the control fibroblasts as lysosomes. The majority of publications call them secondary lysosomes, but some describe them as having a lysosome-like structure (Kamensky et al. 1973; Prasad et al. 1996; Zlamy et al. 2019). However, these vacuoles are positive for LAMP1 and LAMP2 by Immuno-EM; I can therefore confidently identify them as lysosomes (Figure 5.1 P-S).

There are common ultrastructural hallmarks observed in the morphology of the storage compartments in LSDs cells (Parkinson-Lawrence et al. 2010). These include lamellar “concentric” whorls and Zebra bodies which appear as stripes within lysosomes. Even now, there is still a lack of three-dimensional (3D) structural information about these lysosomal structures which can cause errors in their classification. I hypothesise that these lamellar and zebra body structures are all the same multilamellar membrane whorls, which can appear as either lamellar or zebra bodies according to the plane of sectioning (Figure 5.12 A & B). As an example, globoside Gb3 staining in Fabry disease can be seen presenting as zebra bodies in Figure 5.2C and then as dark lamellar whorl structures in Figure 5.3J. I have considered this when looking to demonstrate the structure of the major lipid accumulated within the lysosome in LSDs.

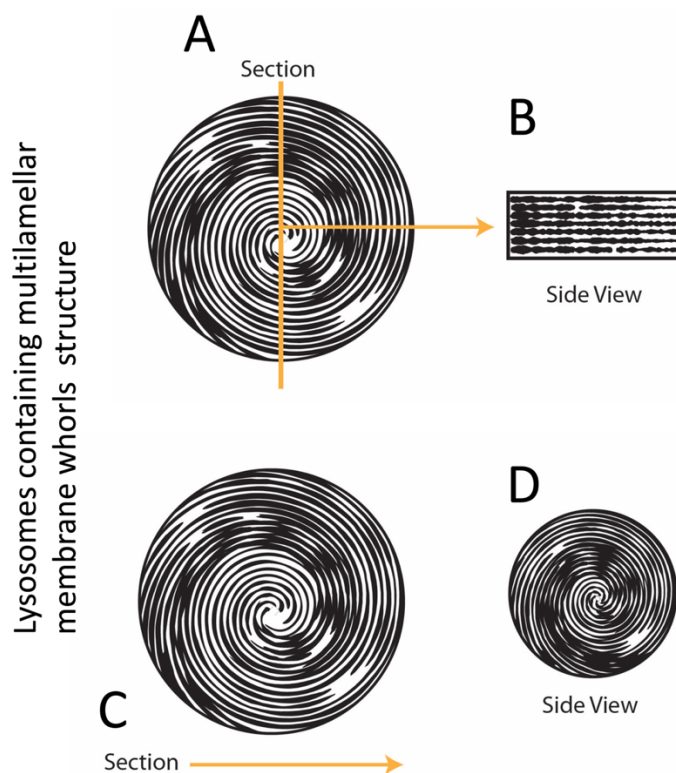


Figure 5.12 Whorls and zebra bodies are the same structure, whose differing appearance is the result of the plane of sectioning.

(A) The lipid whorl structure, with plane of sectioning indicated by yellow arrow. (B) Appearance of the structure after sectioning (zebra bodies (Crossed-lamellar structures)). (C) The lipid whorl structure, with plane of sectioning indicated by yellow arrow. (D) Appearance of the structure after sectioning (lipid whorls).

Ganglioside (GM1 and GM2) storage appears as thin whorl/zebra body-like structures within lysosomes (Figure 5.2 A & B), in agreement with previous report in Tay-sachs disease (Prasad et al. 1996). Furthermore, ganglioside GM1 has a more complex sugar headgroup structure than ganglioside GM2 (see chapter 1 figure 1.5) which therefore appears darker by EM, allowing for some degree of differentiation between the two. Dark, membrane associated lamellae, that correspond to globoside storage, were observed in Fabry (Figure 5.2 C), where they have also been observed *in vivo* (Kamensky et al. 1973). These structures of thicker membrane “sheets” and darker staining than gangliosides appear to emerge from the lysosomal limiting membrane and can eventually fill the lysosome. Sphingomyelin was identified as fine lamellated membranes forming lightly coloured (as here are no sugars on sphingomyelin) whorls within lysosomes, which are smaller than those created by gangliosides, and are more widely spread, creating more wave like lamellae with a clear matrix (Figure 5.2 D). These structures have previously been identified in the skin biopsy of an NPA patient (Alroy and Ucci 2006; Prasad et al. 1996). In summary, I can therefore say that the darkness of an identified lipid structure indeed correlates with the sugar composition. The potassium ferrocyanide/ osmium tetroxide solution used to define cellular ultrastructure in conventional EM has been reported to bind carbohydrates such as glycogen (De Bruijn and Den Breejen 1974) and the sugar mimetic miglustat (Neises et al. 1997) which I also observed in miglustat treated CLN5 cells (Figure 5.7 H& I).

Ultrastructural observations in NPC indicate, in addition to gangliosides and sphingomyelin, an increased presence of small single lamellar membrane structures within lysosomes and associated with the limiting membrane (Figure 5.2 E). Similar structures were observed in cells treated with the sphingosine kinase inhibitor safingol, which leads to increased cellular sphingosine levels (Coward et al. 2009). This observation is the first report of the presence of lysosomal sphingosine in NPC fibroblasts by EM. Increased sphingosine levels are characteristic of NPC and no other lysosomal disease (Lloyd-Evans and Platt 2010), and has been identified as the first intracellular event in the NPC pathogenic cascade (Lloyd-Evans et al. 2008). The cholesterol clefts/crystals I have seen in Wolman represent cholesterol ester storage (Figure 5.2 G) (Prasad et al. 1996). Wolman disease also accumulates triglycerides, leading to the formation of cytoplasmic lipid droplets (Figure 5.2 H).

The accumulation of GAGs in the mucopolysaccharidoses appear as empty vacuoles containing a central fine fibrillar or floccular material (Figure 5.2 F). This central fine fibrillar structure might be due to the GAGs’ hydrophilic quality, which may trap, and lead to the storage of, floccular water-

soluble material (Gitzelmann et al. 1994). Oligosaccharide storage is common in all the glycoproteinoses. Lysosomes accumulating oligosaccharides appear similar to those accumulating GAGs, but with a more sparse fibrillar structure, which is mainly due to oligosaccharides' low molecular weight and solubility in water (Figure 5.2 K).

The ultrastructural lysosomal morphology of the NCLs is mainly reported as showing the presence of fingerprint or curvilinear structures, found in abundance in CLN2, CLN3, CLN5, CLN6, CLN7, CLN8 and CLN9, where they result from lysosomal accumulation of SCMAS (Haltia 2006; Rakheja and Bennett 2018). In our study, I was only able to see the fingerprint profiles by Cryo-EM; they were not observed using conventional epoxy resin EM (Figure 5.2 I). The conventional EM resin embedding method involves chemical fixation of tissues, and dehydration using propylene oxide which is a protein denaturing solvent. As I was unable to observe fingerprint structures using this method, this is consistent with previous study which have shown the lack of SCMAS fingerprints by using the standard EM procedure (Ryazantsev et al. 2007). I can conclude that the fingerprint structures result from lysosomal storage of protein, presumably SCMAS (Figure 5.2 I). Cryo-EM causes less protein denaturation, and allowed these structures to be observed (Figure 5.2 J). Curvilinear like structures were observed using both methods, and are therefore presumably composed of combined lipid and protein aggregates that are more resistant to denaturation. Our data indicate that lysosomal storage in the NCLs is quite complex, comprising of lipids, sugars, proteins and proteolipid and is in agreement with the generally widespread reduction of lysosomal enzyme activities across these diseases (chapter 4, figure 4.1). Our data also indicates that care needs to be taken when preparing NCL material for EM as both methods ultimately affect the material that is visible by EM with lipid storage also being less visible by cryo-EM (Figure 5.7).

Collectively, I was able to identify by EM stored lipids, proteins and polysaccharides in LSD fibroblasts based upon their characteristic appearance within storage bodies of diseases in which these are primary storage materials (Table 5.1).

Table 5.1 Summary of the morphological findings of primary lipids under EM examination.

Lysosomal storage disease	Storage material	EM examination
GM1 gangliosidosis	GM1 ganglioside	Intraluminal thick lamellar, whorl/zebra like structures
Tay-Sachs	GM2 ganglioside	Intraluminal lamellar, whorl-like structures
Fabry	Globosides (Gb3)	Dark clumps, membrane associated thick whorl/zebra like structures
NPA	Sphingomyelin	Light multiple small lamellar bodies
NPC1	Sphingosine	Single lamellar structure
MPS	GAGs	Fine floccular material
Wolman disease	Cholesterol esters and triglycerides	Cleft/crystal-like structure/ lipid droplets
NCLs	Subunit c of mitochondrial ATP synthase or saposins	Fingerprint/ curvilinear profile like structures
Fucosidosis	Oligosaccharides	Sparse fibrillar structure

5.3.2 Identifying secondary storage material by EM

Having demonstrated the nature of the storage structures that accumulated in LSD fibroblasts, I morphologically investigated lysosomal ultrastructural changes in several LSDs. The presence of secondary storage material is known to be a common feature of LSDs (Vitner et al. 2010). Our ultrastructural study of the storage material in LSDs found that gangliosides are highly likely to be the most common secondary storage material in the majority of LSDs, followed by globosides and cholesterol esters/triglycerides (Table. 5.2)

Table 5.2 Summary of the primary and secondary storage material in LSDs using EM morphological findings.

LSDs	Ganglio- side	Globosid- es	Sphingo- myelin	Sphingosine	GAGs	Oligo- saccharide	SCMAS	Cholesterol esters/ triglycerides
GM1 gangliosidosis	P	ND	ND	ND	ND	ND	ND	ND
Tay-Sachs	P	ND	ND	ND	ND	ND	ND	ND
Fabry disease	S	P	ND	ND	ND	ND	ND	S
NPA	S	S	P	ND	ND	ND	ND	ND
NPC1	S	ND	?	P	ND	ND	ND	ND
MPS I	S	ND	ND	ND	P	ND	ND	ND
MPS IIIA	ND	ND	ND	ND	P	ND	ND	ND
CLN3	S	S	ND	ND	S	ND	ND	ND
CLN5	S	S	ND	ND	S	ND	P	S
CLN10	S	S	ND	ND	ND	ND	P	S
Fucosidosis	ND	ND	ND	ND	ND	P	ND	S
Sialidosis	S	ND	ND	ND	ND	P	ND	S
MLIV	S	S	ND	ND	S	ND	ND	S
Wolman	S	ND	ND	ND	ND	ND	ND	P
I cell	P	P	P	P	P	?	P	p

P: Primary storage; S: Secondary storage; ND; non detectable, ? : Possibly but classification of the structure was difficult.

Secondary alterations in brain gangliosides have been reported in several LSDs, either in patients or in animal models (Walkley and Vanier 2009b). Ganglioside storage was observed in NPA (Figure 5.3 O & Q), which may be due to the reduction in activity of the HexB enzyme, which is the lysosomal enzyme that degrades ganglioside GM2, in NPA (Table. 5.3). Lamellar, whorl-like structures were also observed in MPS I (Figure 5.5 D & E), where GM1 storage has been reported in the brains of patients (Constantopoulos and Dekaban 1978; Walkley and Vanier 2009a). Interestingly, our enzyme study findings showed an upregulation of β -gal, HexA, HexB and Total Hex in MPS I fibroblast (Table. 5.3). This would presumably raise questions about the mechanism behind the presence of stored gangliosides in MPS I fibroblasts, although as GAGs have been shown to inhibit ganglioside degradative enzymes (Avila and Convit 1975; Baumkötter and Michael 1983; Kint et al. 1973), the elevation in activity may represent a cellular response to this by attempting to enhance enzyme expression.

Accumulation of gangliosides GM2 and GM3 has previously been observed in the brain of child affected with NPC (Vanier 1999). I observed the presence of whorl-like multilamellar structures in NPC fibroblasts. It was challenging to differentiate these from the sphingomyelin storage structures, which should be present in larger quantity than gangliosides (Vanier 1983), but a few were observed (Figure 5.4 A & B). NPC has a complex lipid storage profile, with sphingosine, cholesterol, gangliosides, sphingomyelin and other GSL stored (Lloyd-Evans et al. 2008). This complexity makes the identification of individual storage products by EM difficult, as each storage body may contain multiple lipid types, which will obviously affect the appearance of the storage bodies. However, I was able to definitively identify GM2 storage within NPC lysosomes by Immuno-EM for the first time (Figure 5.4 F).

The similarity in structure between gangliosides, particularly GM2, with sphingomyelin, makes it difficult to identify the secondary sphingomyelin storage in NPC and other LSDs. Sphingomyelin is known to accumulate in NPC, which is highly likely to be due to a partial defect in aSMase enzyme activity (Vanier et al. 1991). However, proof of sphingomyelin storage in LSDs could be achieved in future through the use of Immuno-EM, using lysenin toxin to stain sphingomyelin (Lloyd-Evans et al. 2008).

However, the observation of secondary storage material by EM does not always correlate with changes in lysosomal enzyme activity. There is secondary ganglioside storage in NPC1 fibroblasts, as shown by the accumulation of whorl-like lamellar bodies (Figure 5.4 A & B). However, the enzymes involved in the degradation of gangliosides (β -gal, HexA, HexB and total hex) were normal in NPC1 fibroblasts (Table. 5.3). This discrepancy could result from the

mislocalisation of enzymes within the cell which has been shown for GCase enzyme in NPC1 disease (Salvioli et al. 2004). The enzyme assays were carried out in cell homogenates, but it is possible that, in intact cells, the enzymes and gangliosides are present in different compartments as a result of endocytic trafficking defects, meaning that the enzyme is unable to break down its substrate even though there is no loss of activity.

This study was the first to confirm the lysosomal accumulation of gangliosides in CLN5, CLN3 and CLN10 (Figure 5.6 A & B, F & G, O & P). Previous studies have demonstrated the possibility of the accumulation of gangliosides or their precursors in various NCLs; indeed, the CLN3 protein has been suggested as the lysosomal galactosylceramide transporter (Persaud-Sawin et al. 2004; Rusyn et al. 2008). More recently, the accumulation of ganglioside GM3 has been observed in CLN3 (Fan et al. 2013). The activity of the HexB enzyme was reduced in CLN3, CLN5 and CLN10 fibroblast and this could be a possible reason for the accumulation of gangliosides. The benefit of EM images are their ability to confirm, almost irrefutably, the visual presence and localisation of lipid storage. In CLN3 a recent report has indicated reduced levels of gangliosides (Somogyi et al. 2018). Whilst this may be the case in terms of total lipid levels, it is clear that gangliosides are indeed accumulating within the lysosomal system, supporting the power of using EM in determining the cell biology of these diseases.

A few lamellar, whorl-like structures were observed in sialidosis fibroblasts (Figure 5.8 H & J). The type 1 neuraminidase enzyme, which is deficient in sialidosis, is minimally involved in the hydrolysis of gangliosides and is more involved in glycoprotein degradation (Oheda et al. 2005). Ganglioside accumulation was also observed in MLIV fibroblasts (Figure 5.9 A & B), which is consistent with several other studies (Bach et al. 1975; Bargal and Bach 1997). The TRPML1 channel is suggested to control lipid trafficking between LE/Lys and reformation of late endosomes and lysosomes from fused LE/Lys intermediates via the release of Ca^{2+} from lysosomal stores. Loss of TRPML1 function could therefore be expected to result in the secondary storage of multiple substrates and the presence of many MVB structures, although few were actually observed (Figure 5.9 G & H). I cell fibroblasts show storage of zebra-like structures, which is highly likely to be due to defects in the activities of the majority of the lysosomal enzymes involved in the degradation of sphingolipids (Figure 5.11 A & B).

Globoside was also identified as a major secondary storage material across several LSDs, particularly the NCLs. Dark membrane associated zebra bodies, indicative of globoside storage, were identified in NPA fibroblasts (Figure 5.3 O & P). The α Gal A activity is reduced in NPA; this reduction is highly likely to cause an accumulation of globoside (Table. 5.3). I also detected globoside accumulation in multiple NCLs (Figure 5.6 D & E, I & J, O & Q), and

confirmed that Gb3 was indeed stored in CLN5 by Immuno-EM with Gb3 antibodies, where it is mostly found in the dark limiting membrane associated clumps within lysosomes (Figure 5.7 A-B). I had previously identified these dark clumps as globoside by morphology in primary globoside storing Fabry disease, which has now been confirmed by the Immuno-EM data in CLN5. Globoside storage in CLN5 can also be explained by reduced α Gal activity (Table 5.3). In a similar manner to the NCLs, secondary globoside storage is found in MLIV fibroblasts (Figure 5.9 E & F), which can again be explained by reduced α Gal activity (Table 5.3). GAG storage and lipid droplets (triglycerides) were also identified in CLN3, CLN5, CLN10 and possibly in MLIV and Wolman (Figure 5.6 A & C, F & H, K & L, R & S, Figure 5.9 A & C, A & D). The possible mechanism behind the GAG accumulation in NCLs and MLIV is unknown, as the activities of the enzymes involved in GAG degradation were either normal or elevated (Table 5.3). This similarity between the NCLs and MLIV in terms of accumulated material (ganglioside, globoside, GAGs, triglycerides) is interesting. The auto fluorescent material, that is the hallmark of the NCLs, has been detected in MLIV fibroblasts (see chapter 6, figure 6.2 G-H) and patient brain samples (Goldin et al. 1995; Tellez-Nagel et al. 1976) and work from the Lloyd-Evans lab has shown the presence of SCMAS accumulation in MLIV patient cells, the hallmark storage material of the NCLs. The presenting clinical features of MLIV include retinal degeneration and blindness, similar to the NCLs (Schulz et al. 2013). These findings suggest that MLIV may be better classified as an NCL.

The presence of ganglioside and globoside storage in CLN5 encouraged us to investigate whether miglustat would be able to reduce the accumulated storage. Ultrastructural examination of CLN5 fibroblasts treated with 50 μ M miglustat for five days revealed that the majority of storage material had been removed (Figure 5.7 D-G), further confirming that this storage material is indeed glycosphingolipid in nature. This finding means that our study is the first to show that miglustat is able to remove the glycolipid storage material in CLN5, and helped facilitate the miglustat safety study in CLN5 patients. This finding was made possible through the power of EM. Lysosomal ganglioside and globoside storage was confirmed by immunocytochemistry using anti-Gb3 and CTxB staining (GM1 gangliosides), where again, miglustat treatment showed a reduction in both lipids (Supplementary figures 27 & 28). Of note was a clear increase in the density of the plasma membrane in CLN5 fibroblasts treated with miglustat (Figure 5.7 H&I). This is consistent with a previous study (Neises et al. 1997), which showed increased plasma membrane staining in myelomonocytic cells treated with miglustat, using potassium ferrocyanide/osmium tetroxide contrast enhancement in conventional epoxy resin EM. This is to be expected, as iminosugars, including miglustat, are known to be stained by the ferrocyanide/osmium tetroxide staining solution (Neises et al. 1997). This increase in plasma membrane density correlates with increases in miglustat concentration in the culture

medium, and can be detected after only 1 hr treatment (Neises et al. 1997). This is far too early for miglustat to reduce glycolipid biosynthesis, and therefore an artefact caused by direct integration of miglustat with the plasma membrane (Neises et al. 1997).

Lipid droplets were seen in some LSDs, mainly in Wolman, CLN5, CLN10, fucosidosis, sialidosis and MLIV. Lipid droplets are highly dynamic structures used by the cell to store lipids, mostly triacylglycerols and sterol esters (Murphy 2012). In Wolman disease, lipid droplets have previously been reported in rat hepatocytes (Kuriwaki and Yoshida 1999). Further research into these lipid droplets might therefore be useful in understanding the pathogenic mechanisms of these diseases. The activity of acid lipase, the enzyme that acts on low density lipoproteins and cholesteryl esters, was low in CLN5, sialidosis and MLIV alone (Table 5.3), which would explain the presence of lipid droplets in these diseases. The reasons for lipid droplet accumulation in CLN10 and fucosidosis are currently unknown. Taking our findings together, the activities of lysosomal enzymes certainly helps to understand why secondary storage of substrates occurs in some LSDs, but it does not always mirror the storage material. Therefore, more specific evidence is required that can lead to a greater understanding of the mechanisms behind secondary storage, which could provide important insights for all LSDs. In particular it would be worthwhile to look at enzyme localisation in some of these diseases where activity does not correlate with presence of storage. Furthermore, the primary storage materials within the LE/Lys may somehow compromise the egress of other substrates from LE/Lys compartments, and this could lead to disturbances in trafficking throughout the endocytosis process, which has been reported in several LSDs (Chen et al. 1999).

Table 5.3 Correlation between the level of activity of lysosomal and the presence of secondary storage.

Lysosomal storage disease	Secondary storage material identified in this chapter	Alteration in the enzymes involved in degradation of secondary storage material (from chapter 4, figure 4.1)
Fabry disease	Ganglioside	Normal (β -gal, HexA, HexB, Total Hex, NEU)
NPA	Ganglioside / Globosides	HexB low / α Gal A low
NPC1	Ganglioside / ASM / GAGs	Normal (β -gal, HexA, HexB, Total Hex, NEU) / α SMase low/ IDU high, GUSB low, NAGLU high
MPS I	Ganglioside	High; (β -gal, HexA, HexB, Total Hex), NEU normal
CLN3	Ganglioside/ Globosides/ GAGs	β -gal high, HexB low/ α Gal normal/ normal; (IDU, GUSB, NAGLU)
CLN5	Ganglioside/ Globosides/ GAGs/ triglycerides/SCMAS	Low (β -gal, Total hex, NEU) / α Gal A low/ GUSB high, NAGLU high/ LAL Low/TPP1 low
CLN10	Ganglioside/ Globosides/ triglycerides/SCMAS	HexB normal, Total hex low/ α Gal A Normal/ LAL Normal/ TPP1 high
Fucosidosis	triglycerides	LAL normal
Sialidosis	Ganglioside/ triglycerides	HexB high, Total hex high, NEU low / LAL low
MLIV	Ganglioside/ Globosides/ GAGs/ triglycerides	Normal (β -gal, HexA, HexB, Total Hex, NEU) / α Gal A low/ GUSB high/ LAL low
Wolman disease	Ganglioside	Low (β -gal, HexA, HexB, Total Hex, NEU)
I cell	Ganglioside/ Globosides/ GAGs/ triglycerides/SMAS	β -gal low/ (HexA, HexB, Total Hex, NEU HexB) low/ α Gal A low// LAL low/ TPP1 low

Our results indicate the presence of enlarged and denser MVBs in several LSDs; GM1 gangliosidosis, Tay Sachs, NPA, NPC1, MPS I, MLIV, Wolman and I cell. Smaller, less dense, MVBs were observed in control fibroblasts (Figure 5.1 G-I). MVBs are part of the endocytic pathway, and the degradation of the intraluminal vesicles found within MVBs occurs when they fuse with lysosomes (Palade 1955; Piper and Katzmann 2007; Urbanowski and Piper

2001). MVBs are differentiated from early endosomes by an increase in acidity, and they contains the two mannose 6-phosphate receptors and lysobisphosphatidic acid (LBPA), which differentiates them from lysosomes (Griffiths et al. 1988); (Griffiths et al. 1990; Piper and Luzio 2001). MVBs are sometimes referred to as late endosomes (Piper and Luzio 2001). Enlargement of MVBs has been demonstrated to be the initial pathological features in Alzheimer's disease. The treatment of neurons with exogenous Amyloid- β peptide was the main cause of MVB enlargement (Willén et al. 2017). This has raised the possibility that MVB enlargement could contribute to neurodegeneration in the LSDs, where Alzheimer like pathology has been widely reported (Lloyd-Evans and Haslett 2016), further investigation is needed.

Ultrastructural observations in I cell fibroblasts showed the storage of multiple lipids. This is assumed to be due to defects in the activities of multiple enzymes in I cell fibroblasts (Table 5.3) (Brooks et al. 2007; Wiesmann et al. 1971). Based on our data I report for the first time the presence of curvilinear structures, similar to those seen in the NCLs, in I cell, which may be due to the lack of TPP1 enzyme activity (Figure 5.11 F & G). Interestingly, an overabundance of caveolae-like vesicles were observed in I cell fibroblasts (Figure 5.11 H& I). The caveolae membrane domain is a major component of the endocytosis process, in lipid metabolism, and in signalling (Kiss and Botos 2009). Caveolae contain sphingolipids and cholesterol (Smart et al. 1999). A recent study has suggested that cholesterol and sphingomyelin accumulation may lead to caveolar dysfunction (Rappaport et al. 2016). Understanding the underlying mechanism behind the accumulation of caveolae-like vesicles in I cell could be key to developing new therapies for the disease.

In this study I have demonstrated the structure of the various lipids accumulated in LSDs, as well as the challenges in identifying these structures. This study has the potential to improve the precision with which storage structures are identified by EM. In this study I used a sample collection method, namely, systematic uniform random (SUR) sampling, which is the most useful method for quantitative analysis of EM images (Howard and Reed 2005; Lucocq 2012). Quantitative analysis could be used to show the relative contributions of primary and secondary materials to the overall storage burden in LSDs. A volume estimate of lysosomes could also be obtained. Together, this could result in a quantitative analysis for diagnostic and disease monitoring purposes, and help to understand the morphological changes that occur at the ultrastructural level in LSD cells, which may enable further insights into the pathogenic mechanisms of these diseases. Our next step is to utilise the methods of our collaborator to quantify the well-characterised lipid morphology from this study across LSDs.

5.3.3 Conclusions

EM remains the best option to investigate the changes in intracellular morphology that occur in the LSDs. I have effectively identified the nature of the primary and secondary storage material in several LSDs, and the appearance of storage bodies containing these materials by EM. This was very useful in investigating the relationship between secondary storage materials present in the majority of LSDs and the enzyme defects identified in chapter 4. Future work should involve using the identified storage structures to develop a simple quantitative method that would be useful not only for understanding the intracellular morphological changes in LSDs, but also for disease monitoring and diagnosis.

Chapter 6: Measurement of intracellular Ca²⁺ and trace elements alteration among LSDs

6.1 Introduction

Reduction in lysosomal Ca²⁺ content and release have been reported to contribute to the pathogenesis of two LSDs, NPC1 (Lloyd-Evans et al. 2008) and CLN3 (Chandrachud et al. 2015). Furthermore, alterations in associated trace elements (TE) homeostasis is also a common pathological feature of numerous neurodegenerative disorders (Bolognin et al. 2009) and certain LSDs (Dong et al. 2008; Grubman et al. 2014b). Here I investigate whether alterations in TE and Ca²⁺ are common across LSDs and evaluate their potential in LSD diagnosis and treatment monitoring.

6.1.1 Ca²⁺ homeostasis defects associated with lysosomal storage diseases

The role of lysosomes in regulation of Ca²⁺ signalling has been mentioned in detail earlier (Chapter 1, section 1.1.5). The exact mechanisms of neuronal cell death in the LSDs remain unknown (Lloyd-Evans 2016a). There is, however, emerging evidence to suggest that defects in intracellular Ca²⁺ homeostasis may cause excitotoxicity and consequent neuronal cell death (Lloyd-Evans et al. 2008);(Lloyd-Evans et al. 2003a); (Pelled et al. 2003; Pereira et al. 2010). Changes in Ca²⁺ haemostasis have been reported in several LSDs (Lloyd-Evans et al. 2010). In terms of ER Ca²⁺ defects, early studies on GD demonstrated that GlcCer, which accumulates in GD, leads to altered neuronal Ca²⁺ homeostasis as GlcCer interacts with, and potentiates release from, ryanodine receptors, Ca²⁺ release channels in the ER (Korkotian et al. 1999; Lloyd-Evans et al. 2003a). In Sandhoff disease, the inhibition of ER Ca²⁺ entry via SERCA occurred due to the accumulation of ganglioside GM2, was associated with neuronal cell death, and could be partially rescued following treatment with miglustat (Pelled et al. 2003). Elevation of cytosolic Ca²⁺ levels have also been reported in the cerebellum of the *Smpd1*^{-/-} mouse model of Niemann-Pick A (Ginzburg and Futerman 2005).

In terms of lysosomal Ca²⁺ defects, NPC is the most characterized LSD. Reduced lysosomal Ca²⁺ content and release is a major factor contributing to the pathogenesis of NPC1 (Lloyd-Evans et al. 2008). NPC is caused by loss of function of the lysosomal proteins NPC1 or NPC2, and is characterised by the accumulation of sphingosine, and other lipids, including cholesterol, SM, and GSLs (te Vrugte et al. 2004). Sphingosine accumulation is a vital discernible primary biochemical alteration occurring as a direct result of the inactivation of NPC1, resulting in persistently lowered levels of Ca²⁺ in the acidic compartment, and also in

secondary lipid storage (Lloyd-Evans et al. 2008). These findings have been confirmed, highlighting the link between sphingosine and lysosomal Ca^{2+} homeostasis. It was speculated that sphingosine is able to activate the lysosomal TPC1 Ca^{2+} release channel to reduce lysosomal Ca^{2+} content (Höglinger et al. 2015). Ca^{2+} release from acidic stores was monitored with the use of a genetically encoded Ca^{2+} indicator, which was directly incorporated into endolysosomes. This showed the lowered Ca^{2+} release from lysosomes in NPC patient cells (Shen et al. 2012), in agreement with previous studies (Lloyd-Evans et al. 2008). However, Shen et al (2012) discovered that the level of Ca^{2+} in the lysosomes showed no alteration, but that Ca^{2+} release was being blocked by the action of the accumulated lipid sphingomyelin (Shen et al. 2012). Although it should be noted that in this study they proposed that activating Ca^{2+} release from the lysosomal TRPML1 channel rescued many NPC1 cellular phenotypes. This is of note as the genetic Ca^{2+} sensor that they used to measure lysosomal Ca^{2+} levels was in fact attached to TRPML1, therefore over-expressing this ion channel and potentially rescuing the very phenotype they were trying to record. This is different from previous findings demonstrating that the alteration in Ca^{2+} levels seen in NPC is attributable to a defect of store filling, based on the observed reduction in intraluminal lysosomal Ca^{2+} levels, measured using a non-genetic intra-lysosomal Ca^{2+} probe (Lloyd-Evans et al. 2008). In contrast to this study, a further report mentioned the presence of elevated lysosomal Ca^{2+} content in sphingosine 1-phosphate lyase null cells, which present with elevated cellular sphingosine inducing phenotypes similar to NPC disease, such as cholesterol accumulation (Vienken et al. 2017). It should be noted that in this study no clamping of Ca^{2+} release from intracellular Ca^{2+} stores was performed, suggesting that their estimation of lysosomal Ca^{2+} levels may be incorrect as lysosomal Ca^{2+} release has been shown to trigger Ca^{2+} release from the ER (Kilpatrick et al. 2013). To our knowledge, there are two studies that have reported increased lysosomal Ca^{2+} in LSDs. There is an increase in the lysosomal Ca^{2+} content of cerebellar granule neuron precursor cells obtained from the CLN3 exon 7/8 1kb deletion mouse (Chandrachud et al. 2015). In a second study, cells from *Idua*^{-/-} mice showed a higher release of lysosomal Ca^{2+} suggesting higher Ca^{2+} content in lysosomes, this was however linked to a defect in proton homeostasis (Pereira et al. 2010), which seems unlikely as the absence of protons in lysosomes would make it impossible to maintain any Ca^{2+} within the store. Intracellular Ca^{2+} , signalling defects are also related to the pathogenesis of other lysosomal diseases, such as Fabry, Pompe etc. (Lloyd-Evans 2016a; Pereira et al. 2010).

6.1.2 The involvement of the lysosome in essential TE metabolism

6.1.2.1 Zinc (Zn^{2+})

Zn^{2+} homeostasis needs to be tightly regulated as any disruption can cause growth defects, impairment in the immune system and neurodegenerative diseases (Szewczyk 2013). Zn^{2+} occurs in cells, tissues and bodily fluids at low concentrations to avoid neurotoxicity. Zn^{2+} binds to approximately 3,000 proteins, and in turn contributes to the activity of enzymes (Xu and Ren 2015). Zn^{2+} chelating proteins and carrier proteins are responsible for maintaining intracellular Zn^{2+} levels (Kukic et al. 2013). Extracellular Zn^{2+} is carried into the cytoplasm by Zip transporters and is then either predominantly bound by Zn^{2+} chelating metallothioneins or is transported into lysosomes by the Zn^{2+} transporters ZnT2 and ZnT4 (see chapter 1 figure 1.3) (Falcón-Pérez and Dell'Angelica 2007; Huang and Gitschier 1997; Palmiter et al. 1996). Zn^{2+} can also be transported to lysosomes by endocytosis or via the autophagy pathway (Kukic et al. 2014; McCormick and Kelleher 2012). Other studies claim that Zn^{2+} can enter the cytoplasm from lysosomes via the lysosomal TRPML1 cation channel (but only when cells are grown in non-physiological 100 μ M extracellular Zn^{2+}), or by active ZIP8 mediated transport as a specific mechanism in T cells (Aydemir et al. 2009; Eichelsdoerfer et al. 2010). In contrast, proteomic analysis of lysosomal membrane proteins was unable to find a possible channel for transporting or pumping Zn^{2+} out of lysosomes (Chapel et al. 2013). Removal of lysosomal Zn^{2+} is an essential process as Zn^{2+} build-up in the lysosomes creates toxic interactions between the ion and membrane lipids, particularly phospholipids. These interactions damage lysosomal membrane and release their content of hydrolytic enzymes into the cell which in turn damages the cell by inducing caspase cleavage via cathepsin activity and ultimately triggering apoptosis (Kukic et al. 2014). Increased levels of Zn^{2+} lead to elevations in reactive oxygen species (ROS) and superoxide, highly toxic molecules that play a role in DNA damage (Wiseman and Halliwell 1996).

6.1.2.2 Iron (Fe^{2+}/Fe^{3+})

Fe is important for a living cell, as it is essential for oxygen transport and energy production. The high reactivity of Fe may lead to ROS creation. Therefore, Fe concentrations are tightly regulated (Kurz et al. 2011; Santana-Codina and Mancias 2018). Excess cellular Fe is stored in ferritin protein, which is an active anti-oxidant, to prevent ROS creation. The lysosome can accumulate Fe as a consequence of degrading iron-rich materials, such as lipofuscin, or via autophagy (Kurz et al. 2011). Extracellular Fe is mainly bound to transferrin (Tf), which binds to transferrin receptor 1 (TfR1) on the plasma membrane, causing internalisation into clathrin-coated pits and endocytosis towards early endosomes. The acidity of early endosomes

interrupts binding between Tf and Fe^{3+} , releasing free Fe^{3+} , which is reduced to Fe^{2+} and transported by the LE/Lys Divalent Metal Transporter 1 (DMT1) to the cytosol in an H^{+} -dependent process (see chapter 1 figure 1.3) (Kurz et al. 2011). Recently, nuclear receptor co-activator 4 (NCOA4), which is enriched in autophagosome has ability to bind Ferritin and deliver it to lysosomes where it is degraded and Fe^{2+} is freed (Mancias et al. 2014). The lysosomal TRPML1 ion channel also releases Fe^{2+} to the cytosol; loss of TRPML1 function causes an accumulation of Fe^{2+} in lysosomes in MLIV disease, and the build-up of Fe^{2+} results in the accumulation of auto-fluorescent lipofuscin (Dong et al. 2008).

6.1.2.3 Copper ($\text{Cu}^{+}/\text{Cu}^{2+}$)

Cu is essential for enzyme activity, but is toxic when present in high concentrations. Hence, the uptake of Cu by cells needs to be highly regulated (Polishchuk and Polishchuk 2016). A lack of, as well as an excess of, Cu can lead to impaired cellular function resulting in severe symptoms. In mammals, copper transporter 1 (CTR1) is the main Cu importer in cells and its intracellular localisation is variable in different cell types (Wang et al. 2011). However, it is possible that CTR1 also transports Cu into the cytoplasm across the lysosomal membrane (Polishchuk, 2016 #127). The link between the Cu transporter, CTR2, in LE/Lys is well known. Cu transport via CTR2 from lysosomes to the cytoplasm drives Cu recycling after degradation of Cu-binding proteins (Wang et al. 2011). Hepatic cells showed overlap of LAMP1 and tagged CTR2, confirming localisation of CTR2 to lysosomes (Polishchuk and Polishchuk 2016). It is presumed that both CTR1 and CTR2 are delivered to the lysosome by endocytosis, where they interact to release the Cu from the lysosome (Liu et al. 2007; Polishchuk and Polishchuk 2016; Van den Berghe et al. 2007). Moreover, metallothioneins play a role in the storage and transport of Cu in lysosomes. Metallothioneins do not transport Cu across the lysosomal membrane, but bind to Cu (and Zn^{2+}) in the cytoplasm and transport it to the lysosome via autophagosome-lysosome fusion (Klein et al. 1998). Lysosome and lysosome-like organelles contain other proteins, such as ATP7A and ATP7B, that use ATP hydrolysis as a mechanism to move Cu ions across the membrane to the lysosome (see chapter 1 figure 1.3) (Van den Berghe et al. 2007; Wang et al. 2011). A slight increase in extracellular Cu levels alters the distribution of ATP7B from the trans-golgi network to LE/Lys. Conversely, a decrease in cytosolic Cu levels causes the release of ATP7B from lysosomes (Wang et al. 2011).

6.1.2.4 Manganese (Mn^{2+}), selenium (Se^{2+}) and cobalt (Co^{2+})

Manganese (Mn^{2+}) is important for maintaining cellular function and in neuronal development. In the immune system, Mn^{2+} acts as a co-factor for several enzymes such as ligases, hydrolases, transferases, and oxidoreductases. However, it is toxic when present in elevated

concentrations (Aschner and Aschner 2005; Roth 2006). Mn^{2+} toxicity can be attributed to environmental overexposure, most commonly in miners and welders, and can be related to a Parkinson's disease-like syndrome (Kwakye et al. 2015). The studies on Mn^{2+} homeostasis in the brain remain controversial, especially with regard to the identification of the exact carriers involved in Mn^{2+} trafficking (Au et al. 2008). The mechanisms identified so far involve high affinity metal transporters, such as Ca^{2+} and Fe transporters (Au et al. 2008). Some of the latter carriers involve DMT1, ZIP-8, transferrin receptor (TfR), voltage-gated and store-operated Ca^{2+} channels, and the ionotropic glutamate receptor (Kannurpatti et al. 2000). The comparative contributions of these transporters to Mn^{2+} homeostasis are largely unknown, but it is highly likely that they are all involved (Au et al. 2008). At the cellular level, DMT1 is found on the plasma membrane, and its precise location depends on the cationic needs of the cell. DMT1 is also known to colocalise with TfR at the plasma membrane and in the endosome recycling compartment (Gruenheid et al. 1999). DMT1 transports Zn^{2+} , Mn^{2+} , and cobalt (Co^{2+}) amongst others (Au et al. 2008; Knöpfel et al. 2005).

Selenium (Se^{2+}) acts as a cofactor for numerous enzymes, including the antioxidant enzyme glutathione peroxidase, and is therefore involved in reducing ROS production (Zhou et al. 2009). ROS are created during oxidative metabolism, which can produce free radicals, superoxide anions (O^{2-}), hydroxyl radicals (HO), hydrogen peroxide (H_2O_2), nitric oxide (NO) etc. Excess ROS or oxidants, in relation to anti-oxidants, causes oxidative stress, a common LSD phenotype. Selenoproteins contain Se^{2+} as a component of the amino acid selenocysteine, which is an essential antioxidant component (Shetty et al. 2014). Cobalt accumulation been reported to enhance ROS production in astrocytes, and causes mitochondrial dysfunction (Karovic et al. 2007).

6.1.3 Previous studies have demonstrated altered TE homeostasis in LSDs

A common feature of neurodegeneration is the dysregulation of bioactive metal homeostasis. Impaired homeostasis of essential redox-active TEs, such as Cu and Fe, can influence physiological changes in ROS (Ucar et al. 2010). Recent studies have demonstrated the association of oxidative damage and pathogenesis in some LSDs such as the NCLs, MPS I, MPS II, MPS IVA, Fabry, Gaucher and NPC (Donida et al. 2017; Fu et al. 2010). An increase in the size and number of lysosomes is the primary outcome of the accumulation of undegraded macromolecules in LSDs. This affects intracellular signalling cascades, such as oxidative stress and Ca^{2+} homeostasis (Donida et al. 2017).

CLN6-affected sheep brains showed increased Zn^{2+} and Mn^{2+} concentrations in six brain regions. Fe, Cu and Co^{2+} homeostasis were also affected in specific brain regions (Kanninen et al. 2013b). The same group has suggested an interaction between CLN6 and Zip7 (Kanninen et al. 2013a). An additional study showed a significant accumulation of the biometals Zn^{2+} , Cu, Mn^{2+} , Co^{2+} and Fe in the brains of CLN1, CLN3, and CLN5 mouse models (Grubman et al. 2014b).

Kalkan *et al* (2010) found reduced Se levels in patients with glycogen storage disease types IA and III, but no differences in Fe, Cu or Zn serum levels, compared to the healthy controls (Ucar et al. 2010). Hung *et al.* (2014) conducted further examinations of transition heavy metals in CSF, blood plasma and tissue samples retrieved from NPC1 patients and *Npc1*^{-/-} mice. This study found a significant increase in Zn^{2+} in both human and mouse NPC1 samples in the cerebrum, when compared to control samples, but a reduction in CSF Zn^{2+} was seen in the majority of patients (Hung et al. 2014).

To our knowledge only one study, following a GD patient treated with Cerezyme as an ERT, has used TEs for monitoring treatment (Zahran et al. 2015). Zn^{2+} , Cu and Se^{2+} had been evaluated in serum from 15 GD patients before and after one year of ERT, and compared to control samples. Zn^{2+} and Cu serum levels were lower in the GD patients, and remained lower following ERT. Se^{2+} was low only in some GD patients, and not increased significantly after 1 year of ERT (Zahran et al. 2015).

6.1.4 Aims:

- 1- Investigate whether reduced lysosomal Ca^{2+} content is a common phenotype across LSDs using the most accurate way to measure lysosomal Ca^{2+} .
- 2- Investigate the most suitable way to measure intracellular Zn^{2+} distribution, and apply this method across several LSDs.
- 3- Use the available live probes for Cu and Fe to discover the differences in their homeostasis amongst LSD fibroblasts.
- 4- Investigate TE levels in LSD cells and clinical samples by ICP-MS.
- 5- Study the possibility of using TEs for either diagnosis or treatment monitoring of LSDs.

6.1.5 A brief description of the methods used

In Section 6.2.1 I measured lysosomal content using GPN to release Ca^{2+} from lysosomes, and Fura-2,AM to monitor cytosolic Ca^{2+} levels (See chapter 2, section 2.6.5) in control and LSD fibroblasts.

In Section 6.2.2 I studied different available live Zn^{2+} probes (Newport green, Zinquin and FluoZin-3, AM) (See chapter 2, section 2.6.6), in control, MLIV and NPC fibroblasts. I followed this up by studying the possible effects of autofluorescence on probe efficacy.

In Section 6.2.3 FluoZin-3,AM was used to investigate Zn^{2+} localization (See chapter 2, section 2.6.6.1) in control and LSD fibroblasts.

In Section 6.2.4 Phen Green SK, a heavy metal probe, (See chapter 2, section 2.6.7.1) was used, in the presence or absence of the heavy metal chelator TPEN (See chapter 2, section 2.8.11), to assess the Cu and Fe homeostasis in control and LSD fibroblasts.

In Section 6.2.5 Coppergreen and FeRhoNox-1 (See chapter 2, section 2.6.7.2 & 2.6.7.3) was used to measure intracellular Cu and Fe^{2+} in control and LSD fibroblasts.

In Section 6.2.6 I compared lysosomal Zn^{2+} accumulation to cholesterol accumulation (See chapter 2, section 2.9.2) and lysotracker fluorescence (See chapter 2, section 2.6.1.1) in fibroblasts from NPC patients with different disease-causing mutations, to gain insight into the function of the NPC1 protein.

In Section 6.2.7 I used ICP-MS to measure TEs (See chapter 2, section 2.11) in control and LSD B-lymphoblasts and fibroblasts.

In Section 6.2.8 I measured TEs in NPC and CLN5 (with and without miglustat treatment) clinical samples (Serum/ blood).

6.2 Results:

6.2.1 Lysosomal Ca²⁺ levels are altered in several LSDs.

There are numerous methods in the literature for measuring lysosomal Ca²⁺ content, most of which utilise Gly-Phe β-naphthylamide (GPN), a cathepsin C substrate that when cleaved induces lysosomal swelling and rupture (Lloyd-Evans et al. 2008; Morgan et al. 2011). However, GPN cannot be used alone to determine lysosomal Ca²⁺ content, as lysosomal Ca²⁺ release can trigger Ca²⁺ release from the ER. As the ER is a much bigger Ca²⁺ store than the lysosome, this ER Ca²⁺ release prevents accurate determination of the initial, small, lysosomal Ca²⁺ release. The accurate way to measure lysosomal Ca²⁺ content is to clamp the other intracellular stores before addition of GPN (Waller-Evans and Alshehri *et al.* manuscript in preparation). Therefore, in order to prevent erroneous measurement of lysosomal Ca²⁺ content, I ensured that, in all cases, cells were first treated with the Ca²⁺ ionophore ionomycin to induce Ca²⁺ release from all intracellular stores except the lysosome (owing to the presence of its glycocalyx) prior to the addition of GPN to then release lysosomal Ca²⁺. Additionally, all experiments were conducted in a low 10 μM CaCl₂ containing buffer to prevent influx of extracellular Ca²⁺. This measurement was then performed in several LSD fibroblasts.

Lysosomal Ca²⁺ levels were measured across a range of control fibroblasts, ranging from 1yr, 6yr and 13yr individuals. This age range was inclusive of the majority of LSD patient fibroblasts used in this study. There was no noticeable difference in lysosomal Ca²⁺ content between these control fibroblasts, which have been reported in fibroblasts from older humans (Kilpatrick et al. 2016). In contrast, among the LSD fibroblasts, I noticed a reduction in lysosomal Ca²⁺ levels in over half of the LSDs (11/20). Across the sphingolipidoses, lysosomal Ca²⁺ was minimally, but significantly, lowered (approximate 30% reduction) in GM1, GD1 and Farber, and an approximate 60% reduction was observed in Fabry (Figure 6.1 A & C). No significant alterations were seen in Krabbe or NPA, although more repeats may yet bring out a significant reduction in the NPA cells as there was a trend towards reduced levels.

In the mucopolysaccharidoses, I noticed an approximate 70% reduction in lysosomal Ca²⁺ in MPS1 compared to controls, which is in contrast to the elevated levels reported previously (Pereira et al. 2010). There were no significant alterations in MPS II, MPS IIIA or MPS VII (Figure 6.1 A & C), although more repeats may yet bring out significance in MPSIIIa where there is a trend towards reduced levels.

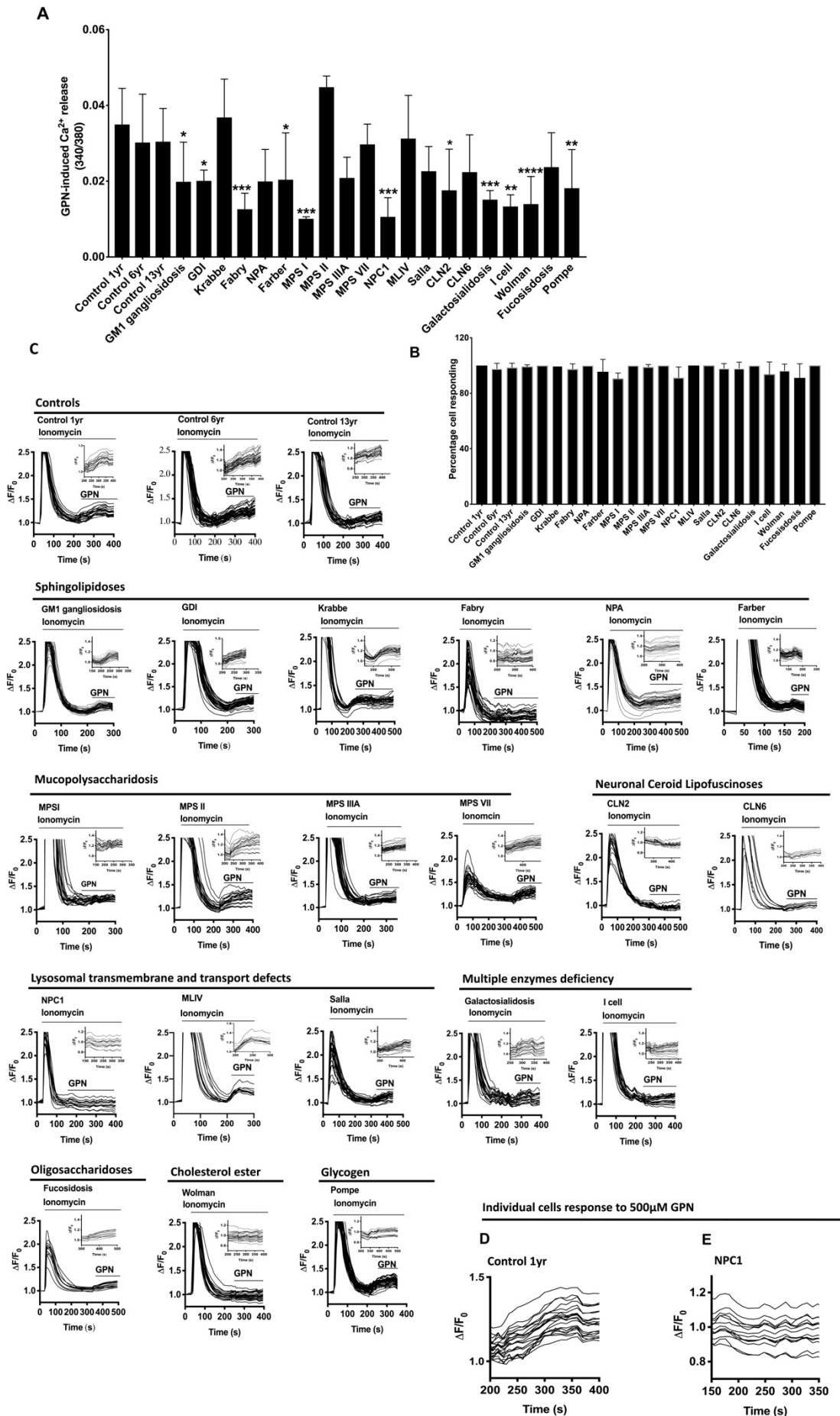
As reported by numerous laboratories, lysosomal Ca^{2+} in NPC patient cells is reduced by approximately 70%. No changes in lysosomal Ca^{2+} content were observed in MLIV, Salla or fucosidosis (Figure 6.1 A & C). Among the NCLs, I recorded an approximate 30% reduction in lysosomal Ca^{2+} in CLN2, but no significant change in CLN6 (Figure 6.1 A & C).

Galactosialidosis is characterised by an approximately 50% reduction in lysosomal Ca^{2+} with a similar reduction in I cell (Figure 6.1 A & C) which is expected as in I cell disease NPC2 cannot get to the lysosome and should phenocopy NPC1. I supported the findings published of Xu, *et al.* (2012), who reported reduced Ca^{2+} in Wolman disease, caused by a loss of acid lipase function (Figure 6.1 A & C) (Xu et al. 2012b). Lastly, there was a less significant approximate 40% reduction in lysosomal Ca^{2+} content in Pompe disease (Figure 6.1 A & C). Almost 100% of cells from all controls and all the LSDs responded to GPN (Figure 6.1 B).

Regarding the utility of lysosomal Ca^{2+} levels as an LSD biomarker, lysosomal Ca^{2+} measurements are technically challenging and are therefore not suitable for clinical use. Additionally, these measurements require specialised equipment, expensive reagents, specialised software and highly skilled workers to interpret the results. Despite the observation that more than half of the LSDs had reduced lysosomal Ca^{2+} , I decided to exclude lysosomal Ca^{2+} measurements from any further investigation of new diagnostics.

Figure 6.1 Lysosomal Ca²⁺ levels are altered in over half of the LSDs tested.

Ca²⁺ was released from lysosomes using GPN following store clamping with ionomycin in control and LSD fibroblasts, and increases in cytosolic Ca²⁺ recorded using Fura-2,AM (A) GPN induced lysosomal Ca²⁺ release in control and LSD fibroblasts (see supplementary table 1). (B) The percentage of cells releasing lysosomal Ca²⁺ in response to 500 μM GPN. (C) Representative traces of the GPN experiments quantified in (A) Insets show a zoom of GPN induced Ca²⁺ release. (D-E) Zoom out on the individual cell response to 500 μM GPN in Control (D) and NPC1 (E). N=3-6, statistical analyses were calculated using one-way anova; *p ≤ 0.05; * * p ≤ 0.01; * * *p ≤ 0.001; * * **p ≤ 0.0001. Data are shown as mean ± SD.



6.2.2 Determination of suitable probes for Zn²⁺ intracellular distribution

Here I investigated suitable probes for the intracellular measurement of Zn²⁺. Commercially available probes tend to interact and interfere with Ca²⁺ ions. These interactions can cause a high false-positive rate, compromising the quantification of free Zn²⁺ ions (Martin et al. 2006; Ollig et al. 2016). The specificity and selectivity of probes are factors to be considered as is the sensitivity of each probe. Each Zn²⁺ probe has a specific property. To study these, I used control fibroblasts and LSD fibroblasts with known accumulation of lysosomal Zn²⁺. These include; MLIV, where loss of TRPML1 function causes accumulation of chelatable Zn²⁺ within enlarged lysosomes and vacuoles (Eichelsdoerfer et al. 2010), and NPC, where previous work in the Lloyd-Evans lab demonstrated that the NPC1 protein binds Zn²⁺, and that lysosomal Zn²⁺ accumulation in NPC contributes to disease pathogenesis (Maguire 2017).

Newport green DCF is a membrane permeant dye with low affinity for Zn²⁺ ($K_d > 1 \mu\text{M}$) (Haugland and Spence 2002), and therefore can bind only high concentrations of intracellular Zn²⁺. It was unable to detect any significant increase in lysosomal Zn²⁺ in either MLIV or NPC fibroblasts. Slight increases in Newport green fluorescence were observed, appearing to stain widespread reticular structures throughout the cells suggestive of the ER, where there is a high concentration of intracellular Zn²⁺ (Figure 6.2 A). However, the localisation of staining was slightly brighter and appeared more punctate in the MLIV cells (Figure 6.2 A). On the other hand, Zinquin ethyl ester (Zinquin) has been used widely as a membrane permeant Zn²⁺ fluorophore. It has more specificity towards Zn²⁺ (Zalewski et al. 1993) and is therefore less likely to stain other divalent cations (Snitsarev et al. 2001). Zinquin usually stains both cytosolic and lysosomal Zn²⁺ (Figure 6.2 C). An approximate 2.5-fold increase in the percentage of cells with punctate staining, indicating lysosomal Zn²⁺ accumulation, was observed in MLIV and NPC fibroblasts compared to controls (Figure 6.2 B).

Another Zn²⁺ probe, FluoZin-3, AM, has a high affinity for Zn²⁺ and is cell permeable, due to the presence of acetoxymethyl (AM) esters. The higher affinity for Zn²⁺ ($K_d = 15 \text{ nM}$), meaning that it is more likely to stain physiological levels of Zn²⁺, particularly within lysosomes where Zn²⁺ is believed to be present at low concentrations (Kaltenberg et al. 2010). FluoZin-3, AM was able to detect a clear difference in Zn²⁺ localisation in MLIV and NPC fibroblasts, compared to controls (Figure 6.2 C), with significant lysosomal accumulation of Zn²⁺ evident in MLIV and NPC, while Zn²⁺ was mostly localised to the Golgi in controls (Figure 6.2 C). As autofluorescence has been reported in both MLIV and NPC (Goldin et al. 1995; Shen et al. 2012), I investigated autofluorescence in our fibroblasts to ensure that this was not interfering with our Zn²⁺ measurements. As expected, MLIV cells showed a high level of autofluorescence

at 490nm excitation, which is consistent with previous studies (Goldin et al. 1995) and may explain the subtle difference in staining with Newport Green DCF (Figure 6.2 A). Ultimately, the fluorescence of both Zinquin and FluoZin was considerably higher than the autofluorescence observed in MLIV, ensuring that images taken at low exposures where no autofluorescence is observed can be used to represent intracellular Zn^{2+} levels alone. No autofluorescence was observed in either NPC or control cells (Figure 6.2 D). Considering all of the above, I decided to use the FluoZin-3, AM probe for further intracellular free Zn^{2+} measurement across the LSDs.

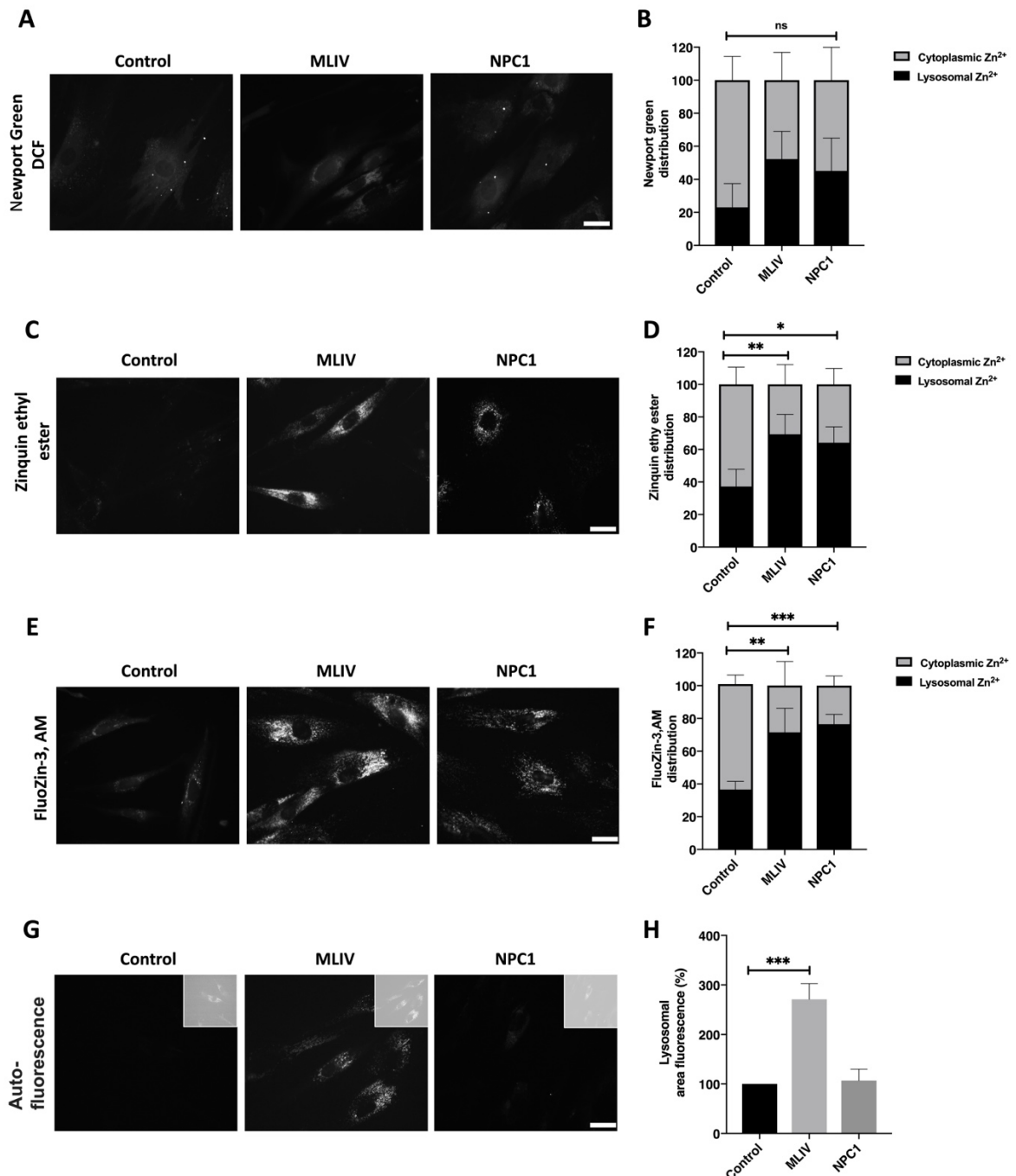


Figure 6.2 Measurement of lysosomal Zn²⁺ accumulation using different intracellular probes.

Control (GM05399), MLIV (GM02527) and NPC1 (GM23151) fibroblasts were stained and imaged live with either Newport green (A), Zinquin ethyl ester (C), or FluoZin-3,AM (E). These pictures were quantified by counting the organellar distribution of the stain per cell to generate the graphs shown in B, D and F. (G) Autofluorescence observed at 490nm excitation, (H) quantification of autofluorescence by lysosomal area analysis in ImageJ. N=3 for all experiments. Representative pictures shown. Scale bar: 10 μ m. Statistical analyses were calculated using one-way anova, ns indicates that it is not significant; ** $p \leq 0.01$; *** $p \leq 0.001$. Data are shown as mean \pm SD.

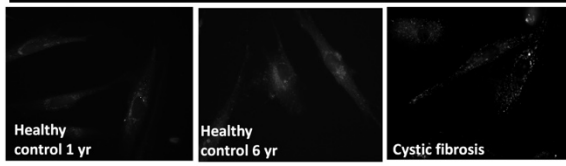
6.2.3 Zn²⁺ alteration is common across the LSDs

Upon staining LSD fibroblasts with FluoZin-3,AM, I found different levels of lysosomal Zn²⁺ accumulation (Figure 6.3). The Lysosomal Zn²⁺ levels were measured in different age controls, namely fibroblasts from an apparently healthy 1 and 6yr old, I also included fibroblasts from a cystic fibrosis patient as a non-LSD disease control. There were no noticeable differences among the healthy controls and the cystic fibrosis patient cell. The FluoZin-3,AM probe in controls mostly stained the Golgi, with a low level of lysosomal punctate staining seen in a low percentage (approximately 35%) of cells (Figure 6.3). In general, I observed punctate lysosomal Zn²⁺ storage in almost all LSD fibroblasts (19/23) (Figure 6.3), with levels of lysosomal Zn²⁺ storage, represented by the fluorescence intensity of FluoZin-3 (Figure 6.3 A), varying across the LSDs. Among the sphingolipidoses, small but significant ($p < 0.05$) approximate 1.5-fold, elevations in lysosomal Zn²⁺ storage were seen in GDI, GDII, Tay-Sachs and Tay-Sachs AB variant patient fibroblasts (Figure 6.3 B). In contrast, there was no lysosomal Zn²⁺ storage in Krabbe and Farber. However, there were highly significant ($p < 0.0001$) approximate 2-fold elevations in presence of punctate Zn²⁺ accumulation in NPA, Fabry and MLD (Figure 6.3 B). Across the mucopolysaccharidoses, lysosomal Zn²⁺ was significantly increased in MPS II ($p < 0.0001$) and MPS VII ($p < 0.001$), whereas no significant lysosomal Zn²⁺ accumulation was seen in MPSI or MPS IIIA. In terms of lysosomal transmembrane, and associated, protein defects, highly significant approximate 2-fold elevations in lysosomal Zn²⁺ storage were observed in NPC1, NPC2 and MLIV. Significant increases ($p < 0.0001$) in lysosomal Zn²⁺ storage was evident in all NCLs tested (CLN1, CLN3, CLN5), I cell disease fibroblasts (characterised by multiple lysosomal enzyme deficiencies), Wolman disease and fucosidosis (characterised by lysosomal oligosaccharide storage).

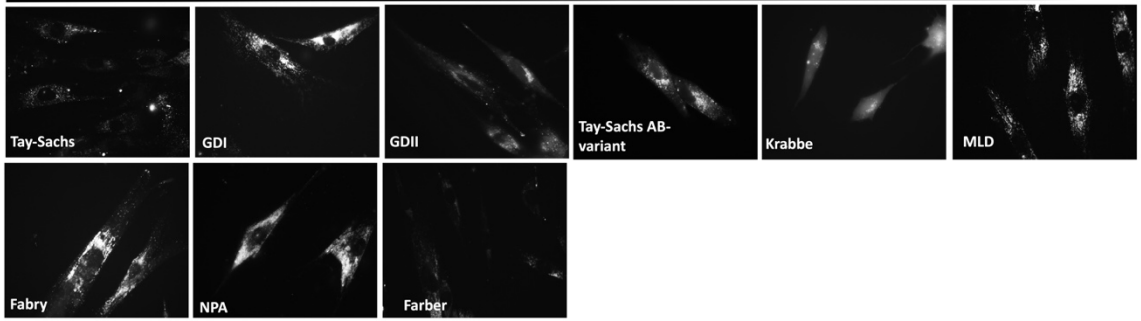
Figure 6.3 Presence of lysosomal Zn²⁺ accumulation in LSD patient fibroblasts.

Alteration of lysosomal Zn²⁺ in LSDs patient fibroblasts: (A) Controls, cystic fibrosis and LSD patient fibroblasts (see supplementary table 1) were stained with FluoZin-3,AM probe. Representative pictures (A) were quantified by counting the percentage of cells with punctate (lysosomal) staining (B). The black line indicates the mean of 1yr control. N=3, Scale bar: 10 μ m. Statistical analyses were calculated using one-way anova against the control 1yr: * p \leq 0.05; ** p \leq 0.01; *** p \leq 0.001; **** p \leq 0.0001. Data are shown as mean \pm SD.

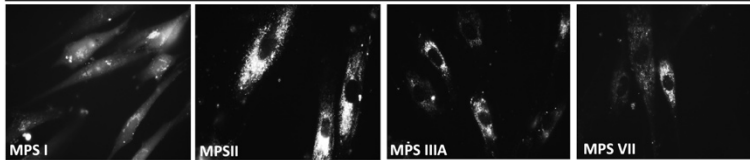
A Controls / Non LSD



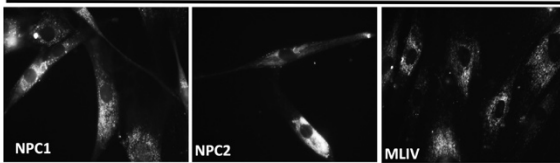
Sphingolipidoses



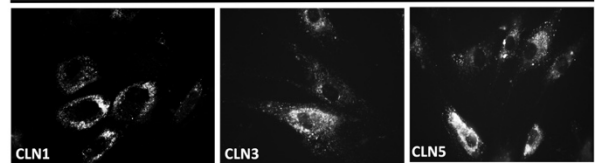
Mucopolysaccharidosis



Lysosomal transmembrane and transport defects



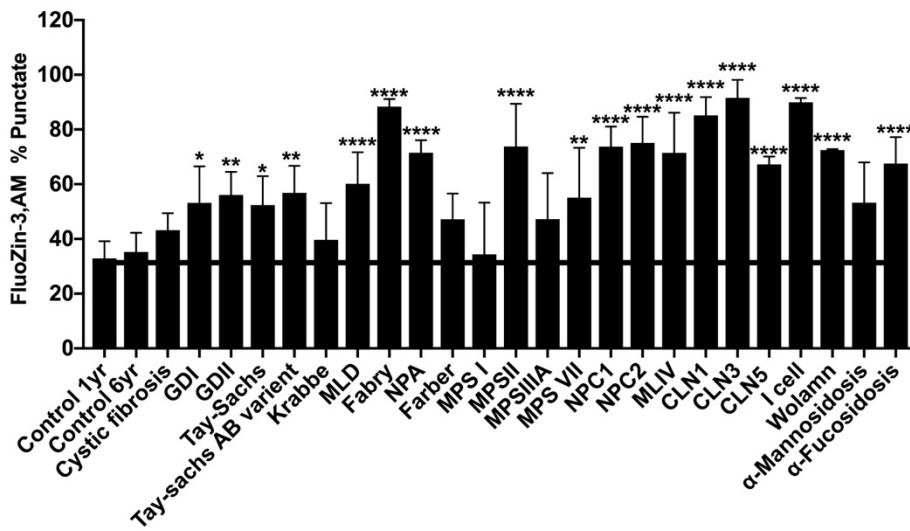
Neuronal ceroid lipofuscinoses



Other LSDs



B



6.2.4 Alterations in intracellular Fe and Cu among the LSDs

To study intracellular Fe and Cu levels, I researched viable probes reported in the literature. The use of turn-on probes, that increase in fluorescence upon ion binding, for imaging of Fe and Cu in live cells to study localisation is limited (Dean et al. 2012; Haugland and Spence 2002). However, numerous turn-off probes, where $\text{Fe}^{2+}/\text{Fe}^{3+}$ or Cu^{2+} binding results in a reduction in the level of fluorescence, have been used for the analysis of cellular ion homeostasis (Dean et al. 2012). Phen Green SK fluorescence is quenched in the presence of Fe but not Ca^{2+} and Zn^{2+} ; however, it is unable to distinguishing between Fe^{2+} and Fe^{3+} (Petrat et al. 1999). In addition, Phen Green SK has been used to measure changes in intracellular Cu by following the quenching of fluorescence upon Cu binding (Chavez-Crooker et al. 2001). Therefore, TPEN, a nonselective heavy-metal chelator, was used here as a control, with chelation of intracellular metals achieved following 3h incubation (Ollig et al. 2016).

In order to study Fe/Cu localisation, control, Tay Sachs, NPC and MLIV fibroblasts were stained with Phen Green SK in the presence and absence of 10 μM TPEN for 3 hours. Phen Green SK fluorescence was quenched by intracellular ions in all fibroblasts. A slight fluorescence signal remained in MLIV, which may be due to autofluorescence, which is observed in these cell, rather than Phen Green SK (Figure 6.4). In cells treated with TPEN, MLIV fibroblasts had the brightest punctate lysosomal Phen Green SK staining, followed by punctate lysosomal staining in NPC then very minimal fluorescence in Tay Sachs and control fibroblasts. This indicates the possibility of lysosomal Fe/Cu storage in MLIV and NPC.

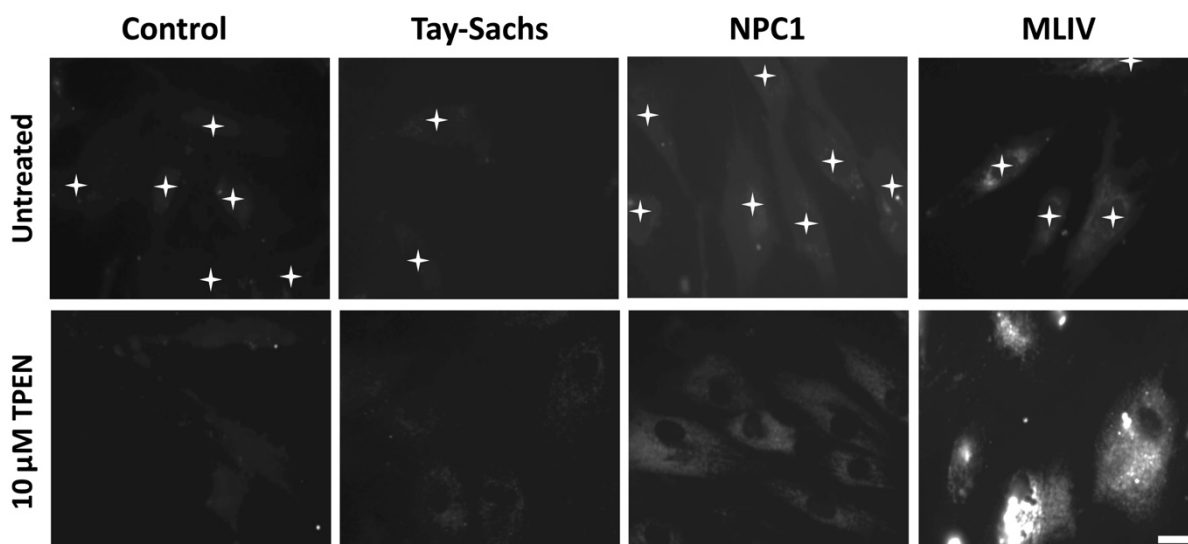


Figure 6.4 Phén Green SK staining is quenched by heavy metals in LSD fibroblast lysosomes.

Control 1yr (GM05399), Tay Sachs (GM00502), NPC1 (GM03123) and MLIV (GM02527) were loaded with Phén Green SK, (quenched upon binding with Fe^{2+} , Fe^{3+} and Cu^{2+}) either with or without treatment with 10 μM TPEN heavy metal chelator for 3 hours prior to staining and live imaging. The stars shape indicates the presences of the cells. $n=3$. Scale bar = 10 μm . Representative pictures shown.

6.2.5 Investigating Fe^{2+} and Cu^{+} accumulation in LSDs

To determine Fe^{2+} accumulation, I used a new membrane permeant turn on probe, FeRhoNoxTM-1, to image labile Fe^{2+} in live cells (Taki et al. 2010). The probe is normally localized in the Golgi as observed in the control fibroblasts (Figure 6.5 A). There was no noticeable increase in Fe^{2+} in Tay Sachs, Fabry or CLN5. Significant alterations in Fe^{2+} were detected in NPC1 (2-fold increase in FeRhoNoxTM-1 fluorescence) and MLIV (3-fold increase in FeRhoNoxTM-1 fluorescence) (Figure 6.5 A). FeRhoNoxTM-1 fluorescence was localised within punctate lysosomes localised throughout the cell in MLIV, NPC1 and CLN5 whereas in the control it was mainly localised to perinuclear crescent shaped Golgi structures (Figure 6.5 A).

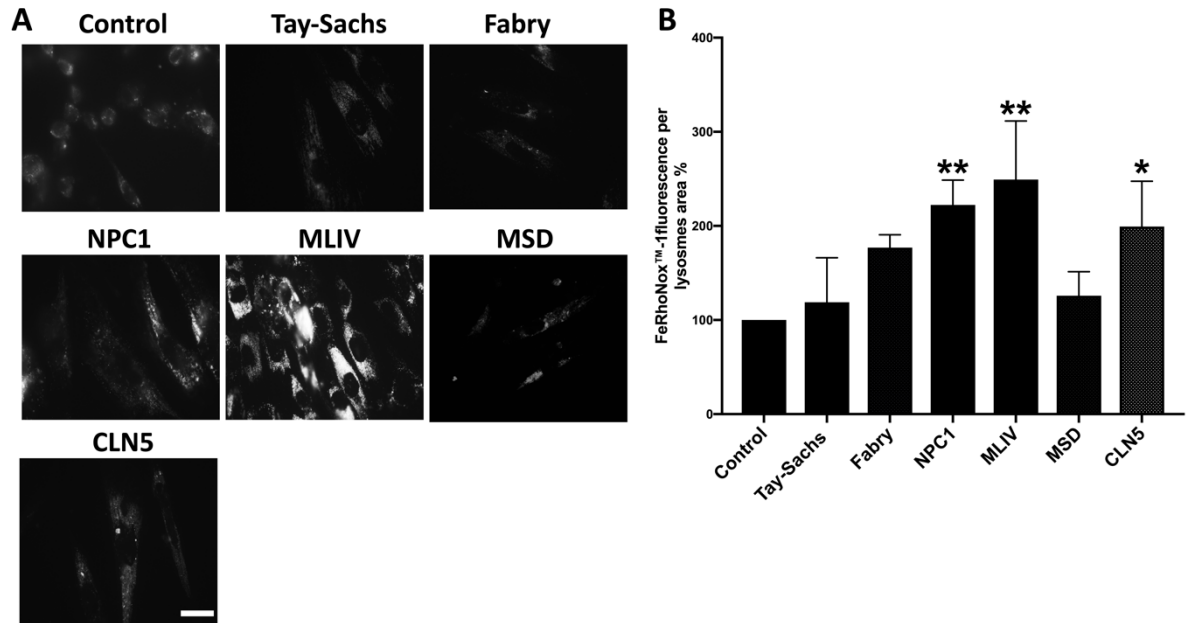


Figure 6.5 Lysosomal Fe²⁺ accumulates within lysosomes of some LSD fibroblasts

Control (GM05399), Tay Sachs (GM00502), Fabry (GM00881), NPC1 (GM03123), MLIV (GM02527), MSD (GM03245) and CLN5 (P1) were stained with FeRhoNox™-1 and imaged live. Representative pictures (A) were quantified by lysosomal area fluorescence to generate graphs (B). N=3. Scale bar: 10µm. Statistical analyses were calculated using one-way anova; *p ≤ 0.05; ** p ≤ 0.01. Data are shown as mean ± SD.

On the other hand, fluorescent probes that are useful in detecting Cu⁺ and Cu²⁺ in living cells are rare. Therefore, I used a new probe, COPPERGreen, for live turn-on imaging of Cu⁺, which is the most dominant form of free Cu in biological systems (Taki et al. 2010). The probe mainly stained punctate structures indicative of lysosomes (Figure 6.6 A). Fluorescence intensity is significantly elevated approximately 2-fold in Tay-Sachs cells, Fabry and MLIV fibroblasts, with a high level of variability in Fabry. Cu⁺ in NPC fibroblasts was elevated approximately 3-fold in punctate lysosomal structures throughout the cells (Figure 6.6 A and B). This is in keeping with reports of elevated copper in *Npc1*^{-/-} mouse tissues (Torres et al. 2019) and defects in transport of the Cu transporting ATPase ATP7B to lysosomes in cells treated with the NPC1 inhibitor U18666a (Yanagimoto et al. 2009). These reports are in keeping with our observations here (Figure 6.6) confirming the validity of using COPPERGreen for intracellular visualisation of Cu⁺. No differences were seen in Cu⁺ levels or localisation in either MSD or CLN5 disease fibroblasts (Figure 6.6 B).

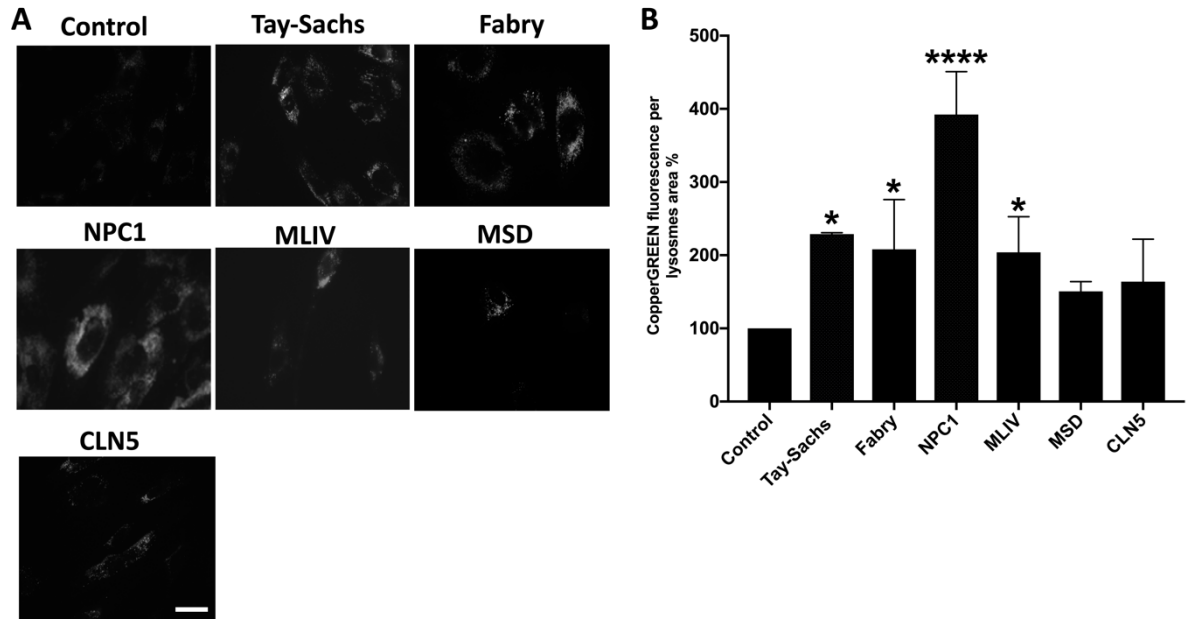


Figure 6.6 Lysosomal Cu⁺ accumulation is observed in some LSD fibroblasts

(A) Control (GM05399), Tay Sachs (GM00502), Fabry (GM00881), NPC1 (GM03123), MLIV (GM02527), MSD (GM03245) and CLN5 (P1) fibroblasts were stained and imaged live with CopperGREEN to compare levels of acidic compartment Cu⁺. (B) Lysosomal fluorescence of COPPERGreen in the pictures were quantified by grey area analysis in ImageJ to generate the graph. n=3. Scale bar: 10µm. Statistical analyses were calculated using one-way anova; *p ≤ 0.05; ****p ≤ 0.0001. Data are shown as mean ± SD.

6.2.6 Elevated lysosomal Zn²⁺ is a possible new biomarker present in NPC cells carrying classical and variant disease causing mutations.

To assess the effectiveness of, and to develop, TEs as potential biomarkers for LSDs, I decided to focus on the lysosomal accumulation of Zn²⁺, as this phenotype is present in the majority of LSDs. I also compared the presence of Zn²⁺ to other NPC bioassays (Figure 6.3). To assess whether lysosomal Zn²⁺ accumulation could be used as an alternative diagnostic method for NPC, I used FluoZin-3, AM (Zn²⁺ storage) and compared against the presence of cholesterol storage by filipin, as well as lysosomal expansion using lysotracker developed in Chapter 3.

1-year-old and 13-year-old control fibroblasts were used in this study as these cover the age range of the NPC patients studied. NPA was included due to the similarity to NPC in terms of ASMase deficiency and filipin accumulation (Vanier and Latour 2015). I used several different

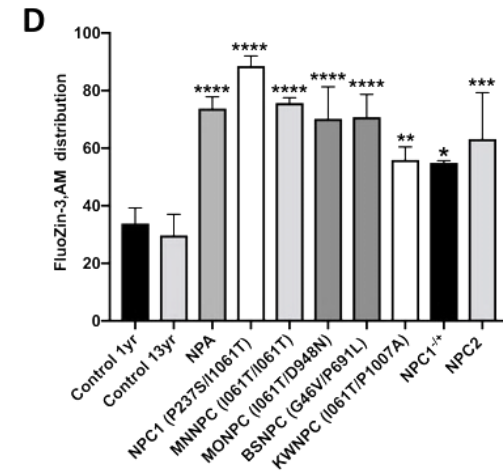
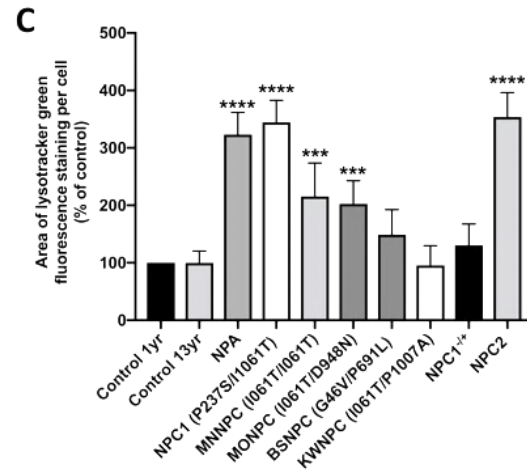
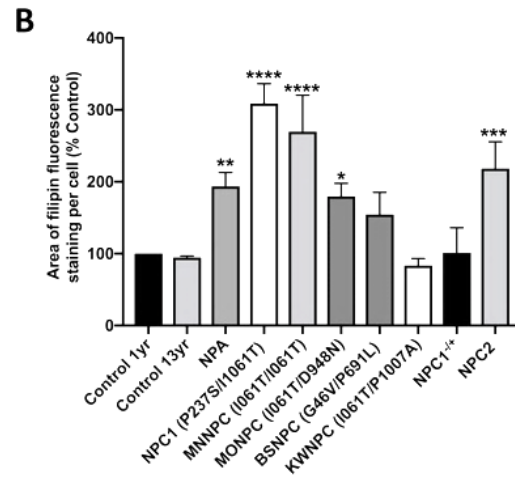
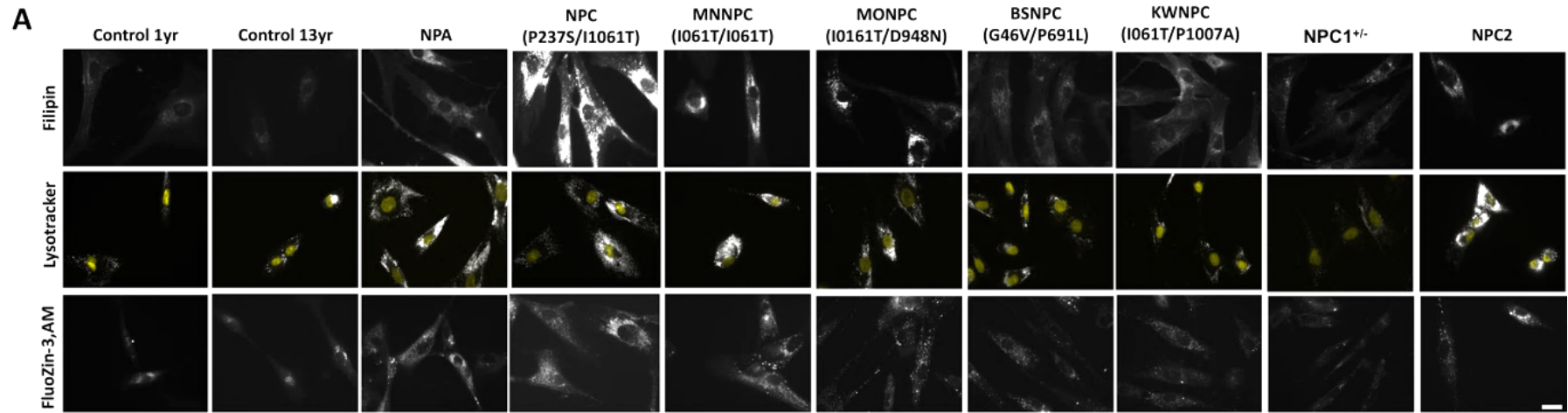
NPC mutations; NPC (P237S/I1061T), MNNPC (I061T/I061T), MONPC (I0161T/D948N), BSNPC (G46V/P691L) and KWNPC (I061T/P1007A). I also included NPC1^{+/-} carrier and NPC2 to broaden our findings and investigate the sensitivity of the developed assay. There is no noticeable difference in either filipin, lysotracker or Zn²⁺ staining among the 1yr and 13yr healthy control fibroblasts (Figure 6.7 A & B & C). NPA cells exhibited an approximate 2-fold increase in filipin fluorescence indicative of the presence of secondary storage of cholesterol in these cells (Figure 6.7 A-B). NPC (P237S/I1061T) and MNNPC (I061T/I061T), harbouring classical NPC mutations, exhibited an approximately 2.5-fold increase in punctate lysosomal filipin fluorescence, whereas with MONPC (I0161T/D948N), which has a combination of classical and variant NPC mutations, there is only a ~ 2-fold increase in filipin fluorescence (Figure 6.7 A and B). No significant increases in filipin fluorescence were observed in BSNPC (G46V/P691L) or KWNPC (I061T/P1007A), which have mild variant mutations or a combination of classical and very mild variant mutations respectively, but there was some clustering of lysosomal puncta (Figure 6.7 A & B). Furthermore, compared to controls, no cholesterol accumulation was observed in terms of filipin fluorescence in the NPC1^{+/-} carrier cells (Figure 6.7 A & B), indicating that 50% of normal levels of NPC1 is sufficient for cellular function. NPC2 patient cells, on the other hand, showed a significant increase in punctate filipin fluorescence as expected. This is due to the hypothesis that the unesterified cholesterol within the lysosome initially binds to the NPC2 protein and is then transferred to NPC1.

In terms of lysotracker fluorescence (lysosomal swelling), NPA and classical NPC (P237S/I1061T) show an approximate 3.5-fold increase in lysotracker fluorescence, compared to control fibroblasts. Classical MNNPC (I061T/I061T) and variant MONPC (I1061T/D948N) show only about a 2-fold increase in lysotracker fluorescence. No significant increases in lysotracker fluorescence were observed in the NPC variant patient fibroblast lines BSNPC (G46V/P691L) or KWNPC (I061T/P1007A) (Figure 6.7 A&C). NPC2 cells exhibit a significant, approximate 3-fold, increase in lysotracker fluorescence, whilst there was no significant increase in NPC1^{+/-} carrier fibroblasts (Figure 6.7 A-C). These data confirm considerable primary storage in the NPA, NPC2 and classical NPC1 (P237S/I1061T) cells, less storage in the variant NPC1 (I1061T/D948N) and homozygous classical NPC1 (I1061T/I1061T) patient cells, where some NPC1 may exit the ER in both cases, and no storage in the variant patient cells. In contrast to these other assays, a change in localization of Zn²⁺ staining (FluoZin-3,AM) was observed across all the NPA and NPC patient fibroblasts, including the NPC^{+/-} carrier fibroblasts (Figure 6.7 A & D). The percentage of cells with lysosomal Zn²⁺ accumulation was increased approximately 2-fold in NPA, MNNPC (I061T/I061T), MONPC (I0161T/D948N) and BSNPC (G46V/P691L). Classical NPC (P237S/I1061T) showed the highest increase in Zn²⁺ puncta with 3 times as many cells

demonstrating punctate lysosomal staining (Figure 6.7 A-D). There is an approximate 1.5-fold increase in the percentage of cells with lysosomal Zn^{2+} accumulation in the mildest variant NPC1 cell line KWNPC (I061T/P1007A) and similar increases in the NPC1^{+/-} carrier and NPC2 patient lines (Figure 6.7 A-D). Taking all of the above data into consideration, our finding of altered cellular Zn^{2+} distribution, and accumulation in the more severe cases, has identified the first ever biomarker for variant NPC disease and highlights the potential for using lysosomal Zn^{2+} accumulation as a powerful bioassay for all forms of NPC disease.

Figure 6.7 Zn²⁺ accumulates in patient fibroblast lysosomes from all forms of NPC disease

Control, NPA and NPC fibroblasts (1-year-old control (GM05399), a 13-year-old control (GM01651), NPA (GM00370), various NPC mutants, NPC1 (P237S/I1061T) (GM03123), MNNPC (I061T/I061T), MONPC (I0161T/D948N), BSNPC (G46V/P691L), KWNPC (I061T/P1007A), NPC1^{+/-} (GM23151) and NPC2 (GM18455)) were individually stained with filipin (for cholesterol), lysotracker (for lysosomal volume), and FluoZin-3 (for lysosomal Zn²⁺). Representative pictures (A) were quantified either by lysosomal fluorescence area analysis by ImageJ for lysotracker (C) and filipin (B) or counted for subcellular distribution of FluoZin-3, AM in either crescent shaped Golgi (control cells) or punctate lysosomes (C). N=3. Scale: 10 μm. Statistical analyses were calculated using one-way anova against the control 1yr; *=p<0.05, **=p<0.01, ***=p<0.00, ****=p<0.0001. Data are shown as mean ± SD.



6.2.7 Use of inductively-coupled plasma mass spectrometry to evaluate TEs in LSD cells.

The data above clearly shows that the use of live probes as tools for imaging the localisation of TEs in living cells is useful. However, this does not seem suitable for clinical use as fluorescence levels were not always elevated (e.g. in NPC1 variants) meaning that a 96 well microplate assay cannot be developed and performing the analyses by fluorescence microscopy is too complex for a clinical setting. I therefore decided, in collaboration with the Department of Metabolic Medicine (University Hospital Wales, Cardiff), to characterise TE levels in LSD cells using inductively-coupled plasma mass spectrometry (ICP-MS), which is available in most hospitals.

I initially utilised B-lymphoblast cell lines (B-LCL) as these are immortalised versions of patient B cells that are themselves easily obtained from patient blood. I first confirmed, using the Zn²⁺ probe FluoZin-3,AM, the presence of lysosomal Zn²⁺ accumulation in NPC1 B-LCLs. As can be seen (Figure 6.8) there is a significant increase in lysosomal Zn²⁺ (green fluorescent puncta) in NPC B-LCL, compared to control B-LCL (Figure 6.8) highlighting that these cells are useful for analysis by ICP-MS.

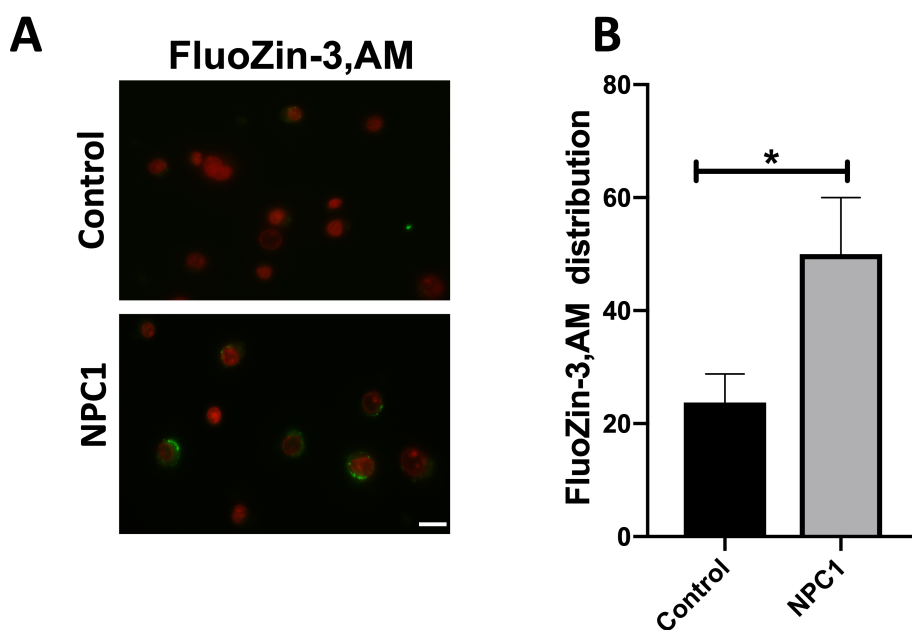


Figure 6.8 Lysosomal Zn^{2+} accumulates in NPC B-LCL.

(A) Control (GM13072) and NPC1 (GM03124) B-LCL were stained with FluoZin-3,AM and Hoechst 33342 and imaged live. (B) Quantification by counting of cells containing punctate lysosomal FluoZin-3 versus cells that were not stained with FluoZin-3. N=3. Scale bar: 5 μ m. Statistical analyses were calculated using t test; * $p \leq 0.05$. Data are shown as mean \pm SD.

Based on this finding, I decided to investigate the levels of TEs (Zn, Fe, Cu, Se, Mn and Co) across a wide range of control and LSD B-LCLs. However, our ICP-MS findings showed a noticeable level of variability, as a result no statistically significant changes in TE levels were observed between LSD and control B-LCL (Supplementary figure 29). This might be because B-LCLs grow very fast, and therefore quickly deplete nutrient in the culture medium, with a subsequent reduction in cell viability.

I therefore decided to investigate TE levels across LSD fibroblasts instead. It is easy to control the growth of fibroblasts compared to that of B-LCLs. The ICP-MS biometal analysis of control, Fabry, NPC and CLN5 fibroblasts showed that Mn and Co are significantly increased compared to control (Figure 6.9). There were other noticeable TE differences in these LSDs compared to the control (e.g. Zn in NPC1) but these were not statistically significant and may require further samples to be analysed. It should be noted that ICP-MS detects the presence of all heavy metals, both free and bound, and as such may not always support the data observed by microscopy which represents free ion content alone.

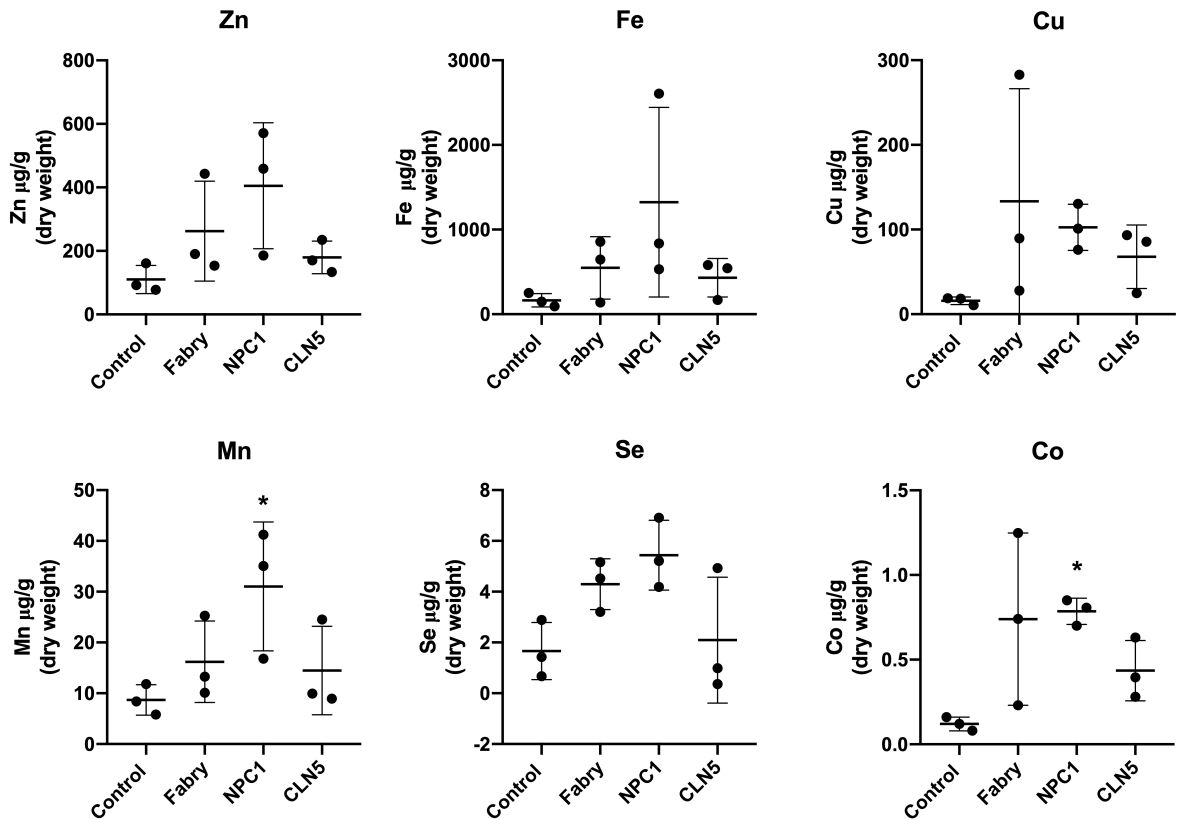


Figure 6.9 Alterations in metal ion homeostasis in LSD patient fibroblasts by ICP-MS.

Zn, Fe, Cu, Se, Mn and Co metal analysis in control (GM05399), Fabry (GM00881), NPC1 (GM03123) and CLN5 (P1) patient fibroblasts by ICP-MS. n=3. Statistical analyses were calculated using one-way anova; * $p < 0.05$. Data are shown as mean \pm SD. The data were obtained from the ICP-MS facilities in collaboration with the University Hospital of Wales.

To gain more insight into possible mechanisms for TE alterations in LSDs, I analysed TEs secreted into the culture medium. Here, I used control and NPC fibroblasts, as the alterations in biometal homeostasis had already been reported in NPC (Hung et al. 2014; Yanagimoto et al. 2009). I grew control and NPC fibroblasts for five days in DMEM supplemented with 10% FBS, which was then analysed for TEs (Zn, Fe, Cu, Se, Mn and Co) by ICP-MS. There was a significant reduction in Se in the NPC culture medium compared to the control (Figure 6.10), which correlates with the trend towards higher levels of Se in NPC fibroblasts above (Figure 6.9). Reductions in Zn and Fe were also noticeable, but were not significant (Figure 6.10).

Collectively the ICP-MS findings from the cells and from the culture medium raise the possibility of a defect in TE secretion, or of a general abnormality in TE homeostasis, in NPC.

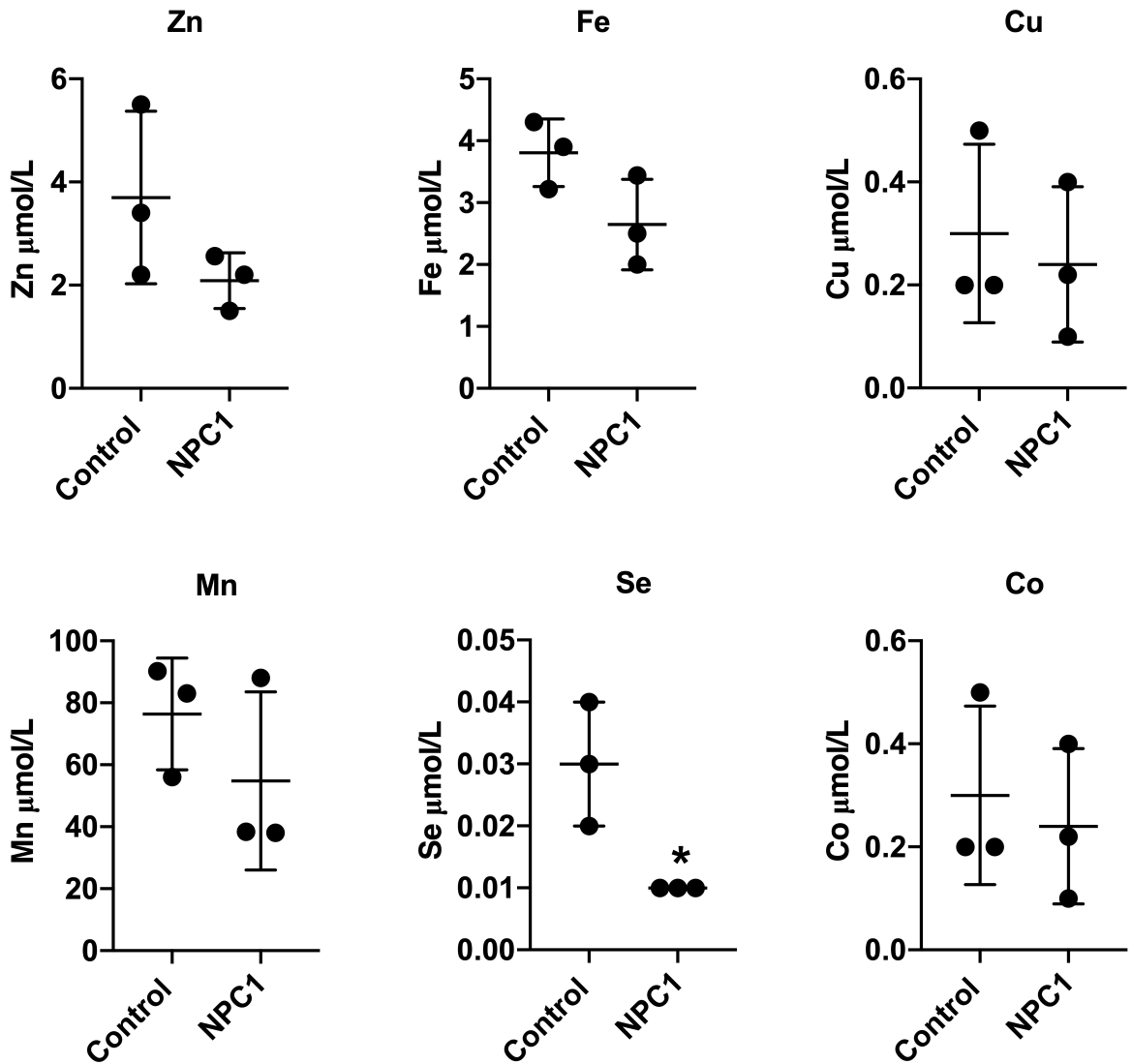


Figure 6.10 Alterations in metal ion levels in the culture medium of NPC fibroblasts.

The culture medium after 5 days from control (GM05399) and NPC (GM03123) fibroblasts was collected and the TEs were measured by ICP-MS. $n=3$. Statistical analyses were calculated using t test; $*p \leq 0.05$. Data are shown as mean \pm SD. The data were obtained from the ICP-MS facility in collaboration with the University Hospital of Wales.

6.2.8 Trace elements could be useful for monitoring treatment of LSDs.

The TE findings so far were encouraging, spurring us on to investigate whether it would be possible to use our findings for monitoring treatment of LSDs. Miglustat is an approved treatment for GD1 and NPC, and is capable of correcting lipid storage and trafficking in NPC patient lymphocytes (Lachmann et al. 2004b). I investigated the effect of miglustat on TE levels in healthy control fibroblasts. Control fibroblasts were grown in DMEM containing 50 μM miglustat for 5 days. Cells were pelleted, and TEs measured by ICP-MS. Of all the heavy metals analysed, there was now only one significant increase, which was of Co, in the miglustat treated cells compared to the untreated control cells (Figure 6.11). Miglustat is therefore not a TE chelator, and any changes in heavy metals in LSD cells following miglustat treatment would likely be due to the reduction in lysosomal storage material and correction of endocytic trafficking in cells.

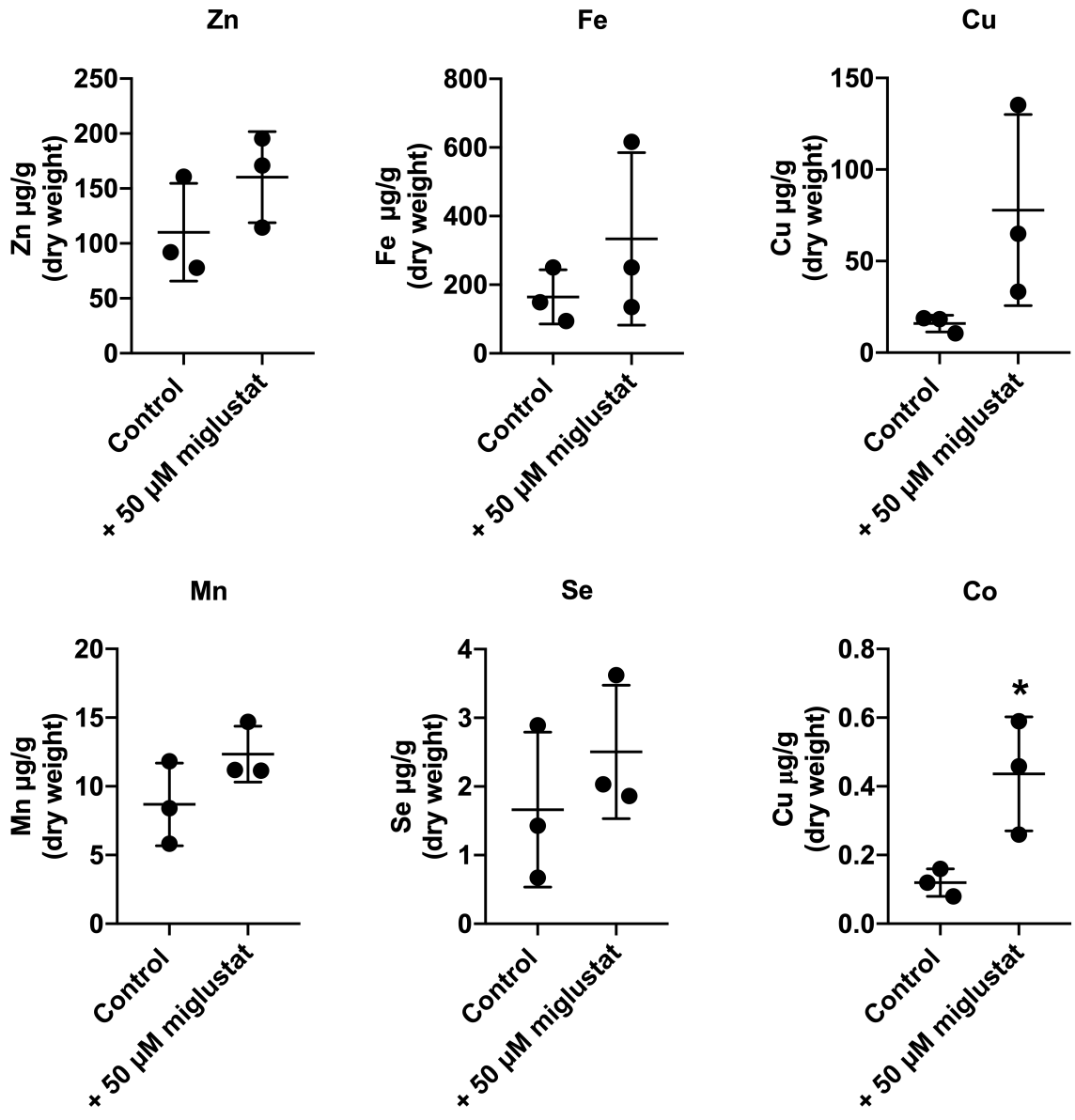


Figure 6.11 The effect of miglustat on the TE levels in control fibroblasts.

Control (GM05399) fibroblasts were either untreated, or treated with 50 µM miglustat for 5 days, followed by pelleting and assessment of TEs using ICP-MS. n=3. Statistical analyses were calculated using t test; *p ≤ 0.05. Data are shown as mean ± SD. The data were obtained from the ICP-MS facilities in collaboration with the University Hospital of Wales.

With regard to the above findings of ICP-MS, I had the opportunity to access historical CSF samples from one control and three NPC patients. The majority of the NPC CSF samples analysed were deficient in TEs (Zn, Fe, Cu, Se, Mn and Co), compared to the control (Figure 6.12). Zn levels in patients 1 and 3 showed about a 50% to 70% reduction, whereas patient 2 had a normal level of Zn. The levels of Cu were markedly decreased ~70% across all the NPC patients. Mn concentration was just below the control level with ~25% reduction in all NPC samples. Fe levels showed a 50% reduction across all the NPC patient CSF, whilst Se levels were not detectable at all in NPC CSF, mirroring what I observed in the tissue culture medium from the patient fibroblasts (Figure 6.10). Finally, Co was also low in NPC CSF, but patient 2 showed only a slight reduction (Figure 6.12). This analysis of human patient CSF is consistent with earlier studies that found deficiencies in Zn, Cu and Se in NPC1 CSF samples, and that Mn concentration was just under the lower reference limit of control (Hung et al. 2014). As I only had access to three patient biological samples, this was a limitation to any statistical analyses.

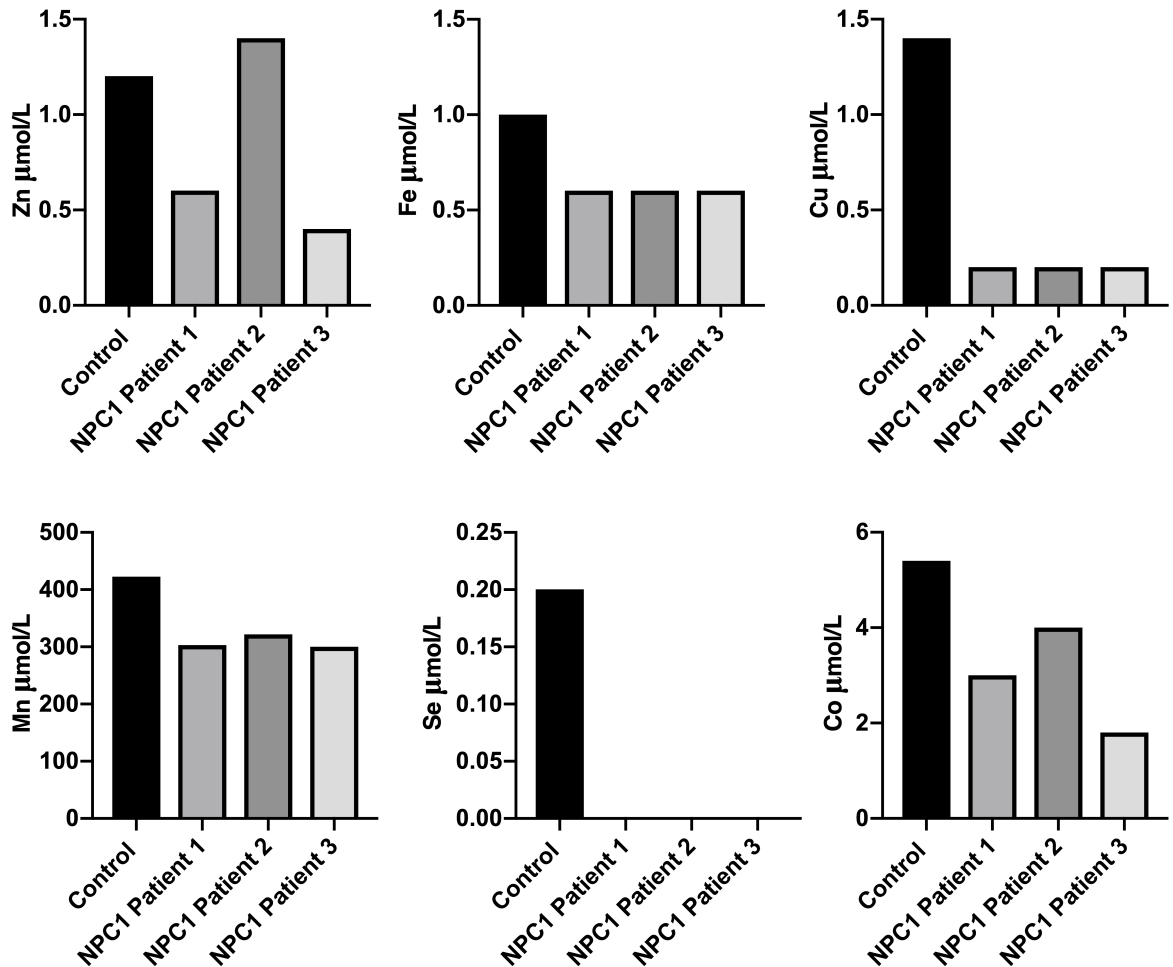


Figure 6.12 Altered metal ion homeostasis in NPC patient CSF measured by ICP-MS

Zn, Fe, Cu, Se, Mn and Co metal analysis of NPC1 patients' CSF by ICP-MS. The data were obtained from the ICP-MS facilities in collaboration with the University Hospital of Wales.

During the course of this thesis work from the Lloyd-Evans lab led to an off label safety and efficacy study of miglustat (3 x200mg miglustat per day) in two CLN5 disease patients at the Nottingham Children's hospital. I used ICP-MS to follow the impact of miglustat treatment on both CLN5 patients (patient 1 (P1) and patient 2 (P2)) across the two year duration of the study. Zn, Fe, Cu and Se were measured in serum, Co levels were measured in serum and blood, and Mn levels were measured in blood. The different samples is based on the TEs concentration in blood and serum. For example the Mn is mainly found in the erythrocyte with about 25 times higher than the concentration of Mn in serum (Paschal and Bailey 1988). These samples were collected from the patients at different times during their miglustat treatment

(post 3 months, post 9 months, post 15 months and post 22 months), were prepared for ICP-MS, analysed and compared against the age-matched control reference range obtained from the University Hospital of Wales. Although I was unable to obtain a pre-treatment sample, the 3 month post miglustat treatment sample in essence acts as a control as miglustat levels measured in other studies at this timepoint are known to be low (Lloyd Evans personal communication). At this 3 month treatment point I observed no differences in the levels of Zn, Fe, Se and blood Co in either CLN5 patient. The most significant difference was a substantial (400-700% fold) increase in Mn levels in CLN5 P1 and P2 respectively (Figure 6.13). The Cu level in CLN5 P2 was within the control reference range but on the low limit, whilst serum Co levels were above the reference range in CLN5 P1. In the post 9-month samples there were no changes in Zn, whilst Fe had moved to above the reference range in CLN5 P1. The Cu level of CLN5 P2 had moved back to the middle of the reference range. Of greatest significance was that Mn was corrected and fell back to within the normal range after 9 months miglustat treatment, as was serum Co in CLN5 P1. All the measured TEs were steadily within the normal range post 15 months, apart from a slight increase in Se in CLN5 P1 (Figure 6.13). In the post 22-month miglustat samples, Mn was still within the normal range, but there was a slight increase in CLN5 P1 blood Co. This data correlates well with the measurement of lysosomal enzyme activities in the CLN5 patient samples as GCase activity, an enzyme that is sensitive to Mn^{2+} , is low at the 3 month timepoint (when Mn is high) and recovers to the normal range at the 9 month timepoint (when Mn is within the normal range) and remains here for the remaining duration of the treatment course (as does Mn). Taking all these findings into consideration, there is strong evidence supporting the use of Mn levels for monitoring CLN5 treatment.

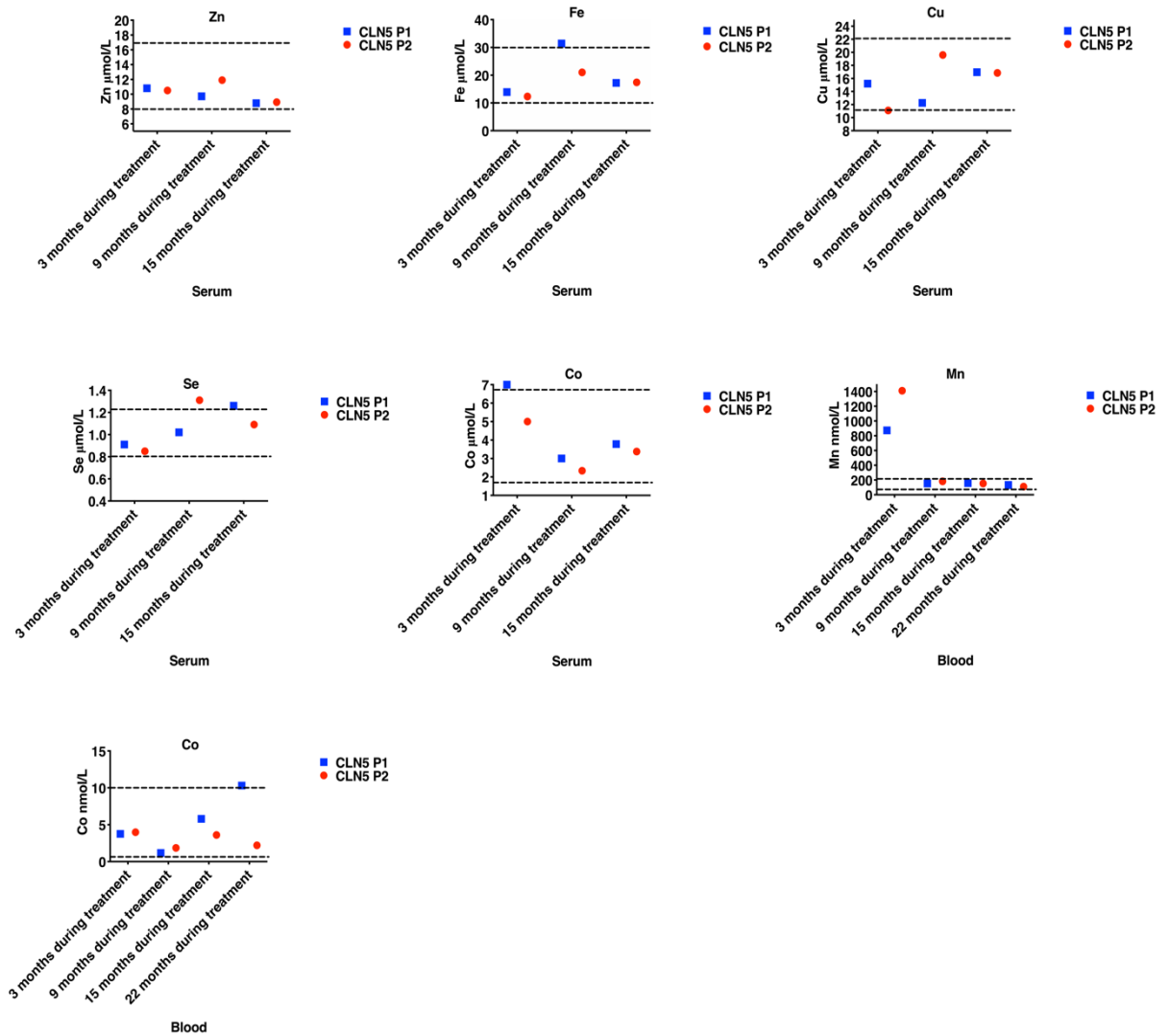


Figure 6.13 Altered heavy metal homeostasis in CLN5 patient blood samples during a miglustat treatment timecourse of 22 months.

Zn, Fe, Cu, Se and Co measurements were performed by ICP-MS using blood and serum from CLN5 Patients 1 and 2 taken at the indicated timepoints. Serum was used for Zn, Fe, Cu, Se and Co, and blood used for Mn and Co. The dash lines represent the reference range of healthy controls established at the University Hospital Wales ICP-MS facility. CLN5 P1 is the red circular point and CLN5 P2 is the blue square point. The data were obtained from the ICP-MS facilities in collaboration with the University Hospital of Wales.

6.3 Discussion

Recently, there has been increased interest in alterations in lysosomal Ca^{2+} homeostasis, which has been linked to defects in lysosomal function, leading to cell death (Lloyd-Evans 2016a). The lysosomal lumen however also contains numerous other ions, including TEs which have been suggested to play a role in the pathogenesis of LSDs (Grubman et al. 2014b; Hung et al. 2014; Kanninen et al. 2013b) including altering lysosomal enzyme activity (Popova and Popov 1998). I therefore decided to investigate Ca^{2+} and TE homeostasis across the LSDs, and to explore the possibility of developing TEs as a useful diagnostic and treatment monitoring tool for LSDs.

6.3.1 Lysosomal Ca^{2+} defects are common in LSDs, but is not an appropriate measure for clinical diagnostic use.

There have been several conflicting reports about lysosomal Ca^{2+} homeostasis in LSDs. Discrepancies in the methods used for the lysosomal Ca^{2+} measurements probably underlie these discrepancies. In our laboratory, I have now developed the most accurate method for lysosomal Ca^{2+} measurement (Waller-Evans and Alshehri *et al*, manuscript in preparation) aimed at addressing numerous discrepancies across multiple publications (Pereira et al. 2010; Shen et al. 2012; Vienken et al. 2017). Although not detailed in this thesis, the method in question, and used in this chapter, relies upon first clamping intracellular stores with ionomycin then releasing lysosomal Ca^{2+} with GPN in the absence of extracellular Ca^{2+} . This method ensures that only lysosomal Ca^{2+} is released and as such controls for off target effects of GPN that have recently been reported (Atakpa et al. 2019). By using this method to measure the lysosomal Ca^{2+} in LSDs, I detected reductions in lysosomal Ca^{2+} in more than half of the LSD fibroblasts that were sampled. In the sphingolipidosis disorders, I found reduced lysosomal Ca^{2+} in GM1, GDI, Farber and Fabry, but not in Krabbe (Figure 6.1). This study contradicts previous studies that showed there was no significant difference in lysosomal Ca^{2+} in GDI and Fabry fibroblasts (Cao et al. 2015; Kilpatrick et al. 2016), which could be the result of different mutations but cannot be tested as the fibroblasts used in those studies are not commercially available. This reduction in lysosomal Ca^{2+} is unlikely to be caused by glucosylceramide, as this does not accumulate in GD fibroblasts, but, is more likely to be caused by mis-folded GCase trapped in the ER, causing ER stress which induces large Ca^{2+} releases from the ER, which may affect intracellular Ca^{2+} homeostasis (Korkotian et al. 1999) or could impair lysosomal Ca^{2+} refilling (Garrity et al. 2016). Another paper has shown normal lysosomal Ca^{2+} content in Fabry, using GPN only (Zhong et al. 2016). However, recent findings in the Lloyd-Evans lab showed that, without clamping of other intracellular stores, the lysosomal Ca^{2+}

release induced by GPN alone can trigger larger Ca^{2+} release from the ER, which can mask changes in lysosomal Ca^{2+} content (Waller-Evans and Alshehri et al, manuscript in preparation) and appears to account for the different measurements observed in this area.

MPS I is the only disease in the mucopolysaccharidoses group tested in this study that showed low lysosomal Ca^{2+} content. In contrast, a previous study showed an increased levels of Ca^{2+} in both the ER and lysosomes from MPS I mice (Pereira et al. 2010). This study, however, used nigericin and Bafilomycin A1 to release lysosomal Ca^{2+} , without first clamping the other intracellular Ca^{2+} stores. It is therefore conceivable that Ca^{2+} release from the ER and even from other cellular compartments may be interfering with the lysosomal Ca^{2+} measurements, as happens with GPN in the absence of store clamping, and explains the discrepancy between our findings here and the previous published results.

Large (approximate 65%) reductions in lysosomal Ca^{2+} content were observed in NPC fibroblasts. This is consistent with previous studies that have demonstrated that the low lysosomal Ca^{2+} level is due to sphingosine accumulation (Lloyd-Evans et al. 2008), acting via an as yet unidentified mechanism. I have also confirmed that there is also a reduction in lysosomal Ca^{2+} in Wolman, another disease where cholesterol is stored, which has previously been reported by the NIH in a study which also confirms lower lysosomal Ca^{2+} in NPC1. Previous studies have demonstrated that incubation with δ -Tocopherol, a small molecule that somehow induces cholesterol efflux from lysosomes, leads to the correction of the lysosomal Ca^{2+} deficiency in Wolman and NPC, with downstream improvements in endocytic trafficking. This and other studies (Lloyd-Evans et al. 2008) have suggested that modulation of lysosomal Ca^{2+} could be a successful therapeutic strategy for NPC and other LSDs (Xu et al. 2012b). Interestingly, in this study, δ -Tocopherol was used to treat and reduce lysosomal storage in Fabry, Farber and CLN2 patient fibroblast cells. Our data indicates that lysosomal Ca^{2+} is reduced in all of these diseases, which was not measured in Xu *et al*, providing a potential explanation for how this small molecule may be mediating its benefit across so many LSDs and suggesting that further diseases could be treated (any disease with lower lysosomal Ca^{2+} from Figure 6.5 above). Lysosomal Ca^{2+} content is unchanged in MLIV, suggesting that TRPML1 is not the NAADP mediated Ca^{2+} release channel of the lysosome (Ruas et al. 2015). Another, more recent, study has reported elevated lysosomal Ca^{2+} content in cerebellar granule neuron precursor cells from a CLN3 mouse model (Chandrachud et al. 2015). This is not common among the NCLs, as here I have found low lysosomal Ca^{2+} content in CLN2 and no significant difference in lysosomal Ca^{2+} content in CLN6 (Figure 6.1). Reductions in lysosomal Ca^{2+} were seen in most, but not all, enzyme deficiency diseases (no reductions

were seen in fucosidosis or Pompe), which might occur as a result of different lipid storage in these diseases.

In general, there is no single explanation for the lysosomal Ca^{2+} reduction in the LSDs. The accumulation of secondary storage materials may have an impact on lysosomal ion channel or transporter activity, leading to reduced lysosomal Ca^{2+} . Intracellular Ca^{2+} is reduced in GM2 gangliosidosis (Walkley and Vanier 2009b) and secondary ganglioside GM2 accumulation is widespread in several LSDs (Walkley and Vanier 2009b), where it may be involved in affecting lysosomal Ca^{2+} content. Further work is nevertheless still needed here. Our Ca^{2+} findings, however, raises the importance of focusing on Ca^{2+} in detail to discover the importance of Ca^{2+} in LSD pathogenesis and, ultimately, to find a suitable treatment. So far, there is no possibility of applying our method of lysosomal Ca^{2+} measurement in the clinic, as highly sensitive imaging systems or expensive microplate readers are needed, along with a high level of expertise to interpret results. Therefore, I instead looked for a trace element that could be detected by ICP-MS.

6.3.2 Lysosomal Zn^{2+} accumulation is a common phenotype in the LSDs.

To our knowledge, this is the first comprehensive study of TE analysis in LSD cells. In order to determine the most appropriate way to measure Zn^{2+} in live cells, I tested the majority of the commercially available Zn^{2+} probes. Autofluorescence within lysosomes is characteristic of MLIV fibroblasts and has been reported in the NCLs (Williams et al. 2006), and, as such, interferes with the reliability of interpreting fluorescent probe data, as the autofluorescence can lead to erroneous assignment of lysosomal probe localisation. This is a particular problem for dim probes, such as Newport green, which is a weak probe for binding Zn^{2+} (Figure 6.2). FluoZin-3,AM is the most suitable fluorescent probe for Zn^{2+} owing to its chemical properties that allowed imaging of Zn^{2+} in multiple subcellular locations. This resulted in the discovery that Zn^{2+} localised to the acidic compartment in almost all LSD fibroblasts and also B-LCLs, but in control cells it is diffuse or localised to the Golgi (Figure 6.2). Previous studies have exhibited the involvement of the Golgi in Zn^{2+} homeostasis due to the presence of Zn^{2+} transporters (ZnTs and ZIPs) on the Golgi membrane (Lu et al. 2016), explaining why I observed a substantial store of Zn^{2+} in this organelle. Interestingly, there is lysosomal Zn^{2+} accumulation apparent in all LSDs, apart from Krabbe, Farber, MPS I and MPS IIIA (Figure 6.3). I have been seeking an explanation for why Zn^{2+} accumulates in lysosomes to different levels across all the LSDs, and I hypothesise that there is an association between the redistribution of Zn^{2+} to lysosomes and the unmetabolised substrate/lysosomal storage material distribution in LSDs (Puri et al. 1999). Considering our finding that Zn^{2+} accumulates

in all of the NPC fibroblasts (discussed below), including the variant patients that otherwise have no discernible storage (Sun et al. 2001), I also hypothesise that the NPC1 protein may itself be involved in lysosomal Zn^{2+} efflux. This theory is tested in more detail in chapter 7.

In addition to measuring Zn^{2+} I have also extended our measurements to other TEs (Fe, Cu, Se, Mn and Co) across the LSDs. However, there is a limitation to TE probes, which are often not completely specific to a single TE. I therefore used the turn-off probe, Phen Green SK, which was used to detect Fe and Cu; fluorescence is turned off when complexed with Fe or Cu, and is de-quenched when the TPEN heavy metal chelator is used (which outcompetes the lower affinity Phen Green for the metal ions). The de-quenching was different in terms of brightness and localisation in different LSDs. With MLIV and NPC1 the de-quenching was more prominent in the lysosomes (Figure 6.4). I have followed this by looking to utilise more specific probes that were only recently commercialised to see whether Fe^{2+} or Cu accumulates to a greater degree in these diseases. These studies with the live staining Fe^{2+} (FeRhoNox) and Cu (COPPERGreen) probes demonstrated an alteration of these TEs in several LSD fibroblasts. As expected, MLIV accumulated more Fe^{2+} compared to the rest of the LSDs (Figure 6.5). As previously discussed, TRPML1 is an ion channel known to release Ca^{2+} and also Fe^{2+} from lysosomes to the cytosol. As TRPML1 is deficient in MLIV, this leads to Fe^{2+} accumulation in the lysosome. In contrast, NPC1 accumulated more Cu compared to the rest of the LSDs (Figure 6.6). NPC1 cells were also found to accumulate lysosomal Fe^{2+} (Figure 6.6). This is in agreement with previous research, which found alterations in metal ion homeostasis in NPC1 (Hung et al. 2014), including of Cu (was increased in liver and lung of *Npc1*^{-/-} and reduced in other tissue). The upregulation of genes involved in metal transport and homeostasis, e.g. the Cu transporters ATP7A/B, the Cu, Fe^{2+} and Zn^{2+} binding and buffering metallothioneins, etc. was observed in *NPC1*^{I1061T} homozygous fibroblasts (Reddy et al. 2006).

6.3.3 Zn^{2+} has promise as a potential biomarker for NPC

It has previously been proposed that the NPC1 protein serves as a cholesterol transporter (Pentchev et al. 1985). 95% of NPC cases are due to deficiencies in the NPC1 transmembrane protein, and this causes a defect in cholesterol transport, resulting in cholesterol accumulation within the LE/Lys system. The “Filipin test”, where cultured fibroblasts are stained with the fluorescent cholesterol probe, filipin, is a technique considered to be the classic method for NPC diagnosis (Wakida et al. 2004). However, following advances in mutation analysis, this view is currently being challenged (Bounford and Gissen 2014). There are small populations presenting clinical symptoms similar to NPC, but their biochemical test results are near-to-normal: this form of the disease is referred to as Variant NPC. The *NPC1* P1007A mutation

associates with variant NPC patients (Millat et al. 2005; Millat et al. 2001; Sun et al. 2001). Variant NPC cells have been found not to store cholesterol with only 10-50% of cells demonstrating filipin positive storage bodies (Vanier and Latour 2015; Vanier et al. 1991). Therefore, the detection of Variant NPC is difficult using existing methods and the phenotypes of these patients potentially argues against a function for NPC1 as a lysosomal cholesterol transporter. As such, a phenotypic screen that can identify all NPC patients may present the ideal biomarker that is more primary in the disease process.

I first studied the feasibility of using lysosomal Zn^{2+} accumulation in human skin fibroblasts to detect NPC caused by different mutations, and compared this to filipin, the original “gold standard” diagnostic method for NPC, and lysotracker, a relatively new biomarker to detect NPC. The I1061T mutation is considered to be the most commonly found NPC1 mutation. The patient fibroblast line NPC (P237S/I1061T) exhibits highly positive Filipin, lysotracker and Zn^{2+} staining. Whereas, the KWNPC (I061T/P1007A) and BSNPC (G46V/P691L) cells exhibit accumulation of Zn^{2+} , but normal filipin and lysotracker (Figure 6.7 A & B). I can therefore conclude that different mutations occurring in NPC (P237S/I1061T), MONPC (I0161T/D948N), and MONPC (I0161T/D948N) cells differentially influence cholesterol trafficking whilst a redistribution of cellular Zn^{2+} to punctate lysosomes can be seen in fibroblasts with all NPC1 mutations (Figure 6.7 C). This shows the benefit of assessing lysosomal Zn^{2+} storage over cholesterol accumulation in any NPC1 diagnosis, and suggests a role for the Zn^{2+} accumulation as a primary event in NPC pathogenesis. Interestingly, emerging evidence demonstrated that carrying a heterozygous mutation in NPC1 may be a risk factor for neurodegeneration, as brains from aged *Npc1*^{+/-} mice exhibited loss of neuronal function (Yu et al. 2005). The Zn^{2+} storage finding in the NPC1^{+/-} carrier fibroblast line may therefore be one of the first events causing this subsequent impaired neuronal function, which could develop with age (Figure 6.7 C). NPC1 and Alzheimer’s disease share phenotypes such as accumulation of cholesterol, A β plaques, and tau accumulation (Malnar et al. 2014). A β plaques bind Zn^{2+} , which promotes plaque expansion, providing a possible mechanism by which heterozygous mutations in NPC1 could lead to neurodegeneration (Bush et al. 1994).

6.3.4 Feasibility of Inductively-Coupled Plasma Mass Spectrometry in the diagnosis and monitoring of LSDs

Estimation of total TE content (free ion and bound ions) in the cell is easily achieved using techniques such as ICP-MS. However, it still remains extremely difficult to establish the exact localization of the TEs in the cell. Also, ICP-MS measures different forms of TEs including the free ion and protein-bound TEs, whereas the live TE fluorescence probes only shows the free TE form. B-LCL is the closest cell line to biological blood samples. However, there is a noticeable variability in TEs across LSDs when B-LCL cell lines are used (Supplementary figure 29). I therefore decided to check TEs in LSD fibroblasts, and here I found TE alterations in NPC, Fabry and CLN5. However, a high level of variability in LSD fibroblasts was also observed. It is always challenging to wash off the FBS from the cell pellet prior to the ICP-MS analysis and failing to do this properly could interfere with the TE analysis.

Despite the inconsistencies in TE measurements in Fabry, NPC1 and CLN5 fibroblasts, I was able to detect significant increases in Mn and Co in NPC fibroblasts (Figure 6.9). The alteration of Mn homeostasis was previously detected in different tissues from the *Npc1*^{-/-} mouse model, supporting the validity of our fibroblast findings (Hung et al. 2014). Previous studies have demonstrated that TE concentration *in vivo* is different from that in the cell culture medium as there are no physiological mechanisms buffering TEs in the cell culture medium (Maret 2015), and cell culture medium does not always reflect metal ion content of interstitial fluid (Ollig et al. 2016). Buffering proteins and, in particular, Zn, Cu etc are all in the FCS supplement (Ollig et al. 2016) and in terms of the protein content these may not always function or interact in exactly the same way with human cell lines.

To understand the involvement of the culture medium in TE measurement, I studied medium supplemented with 10% FBS in which control and LSD fibroblasts had been grown. Our finding showed there was a significant reduction in Se in medium used to culture NPC cells, and slight reductions in Zn and Fe, although these were not statistically significant (Figure 6.10). These changes correspond with increased Se, Zn and Fe in NPC fibroblast, although again, these did not reach statistical significance. The FCS supplement contains transferrin and selenoproteins to transport the Fe and Se to the cell (Helmy et al. 2000; Van der Valk et al. 2010). This would suggest that TE exocytosis into the medium may be defective in some LSDs, and particularly in NPC. This finding is consistent with previous findings that demonstrated Cu accumulation in NPC1 siRNA treated cells, and cells treated with the NPC1 inhibitor U18666A. This correlated with decreased levels of ceruloplasmin (copper carriers) in the medium (Yanagimoto et al. 2009).

Miglustat treatment did not affect the TE content of control fibroblasts, apart from Co, which was elevated (Figure 6.11). I have only a limited knowledge of normal Co metabolism. However, in regard to the finding that miglustat does not change concentrations of heavy metals within cells, it would seem that miglustat neither works as a chelator of heavy metals or alters cellular heavy metal metabolism. However, the glycosphingolipids that are reduced by miglustat may be involved in TE regulation through an as yet unknown mechanism in the regulation.

In terms of biological samples, there was a clear reduction in TEs in CSF from NPC patients, apart from Zn in patient 2 (Figure 6.12). Furthermore selenium being low in culture medium of NPC1 (Figure 6.10) is mirrored by undetectable levels in CSF from all NPC1 patients (Figure 6.12). Our finding is consistent with a previous study that stated the majority of samples from NPC patients and *Npc1*^{-/-} mouse models have disruptions in essential metal homeostasis (Hung et al. 2014). NPC1 regulates ATP7B trafficking, which is involved in Cu metabolism (Yanagimoto et al. 2009). There is a considerable lack of knowledge about the TE metabolism in CSF. In addition, changes in Zn, Cu and Fe levels have been seen in Alzheimer's disease (Lovell et al. 1998), which again suggests a connection between LSDs and other ageing neurodegenerative disorders.

Miglustat treatment was able to correct TE abnormalities in CLN5 patients. Blood Mn levels were corrected in both CLN5 P1 and P2, and serum Co in CLN5 P1 were brought to within normal range following 9 months miglustat treatment. The rest of the TEs were almost within the normal reference range, but changes due to the treatment could nevertheless be detected. For example increased levels of intracellular Zn²⁺ were detected in CLN5 fibroblasts using the FluoZin-3,AM probe. However, there was no noticeable difference in Zn²⁺ level in CLN5 patient serum using ICP-MS. This might be due the protein bound Zn present in serum, the serum contains different forms of Zn (free Zn²⁺, protein bound Zn, mostly complexed with albumin, and Zn bound to low molecular weight ligands such as amino acids) (Lonnerdal 2000; Raffaniello and Wapnir 1989). That may explain why not differences are seen by using the ICP-MS.

NCLs are different from the classic LSDs, as the majority of NCLs are not caused by a specific enzyme defect. The exact functions of the majority of NCL proteins are still unknown. Accumulation of lipofuscin, which contains TEs, is a common feature among the NCLs. The metal homeostasis defect in NCLs is mainly associated with altered localisation of the metal transporter Zip7. This is followed by changes in other Zn transporters including Zip8, Zip4,

ZnT6 and ZnT7 (Grubman et al. 2014a). Lipofuscin accumulation, which triggers ROS formation and subsequent apoptosis, is increased in the presence of Fe and Cu (Höhn et al. 2010). The increase of Co was linked to ROS production and mitochondrial dysfunction (Wang et al. 2000), which is another common NCL phenotype. The upregulation in metallothionein was reported in different forms of NCLs, indicating oxidative stress in these diseases (Grubman et al. 2014b; Kanninen et al. 2013b). Mn is involved in the regulation of inflammatory cytokines, and is increased in the NCLs, providing a possible link between TEs and disease pathogenesis. Mutations in the inorganic cation transporter *ATP13A2* cause CLN12 (Kufor-Rakeb syndrome). Mn^{2+} treatment leads to upregulation of *ATP13A2*, which is suggested to help protect the cell from Mn^{2+} cytotoxicity (Tan et al. 2011). A possible disruption of *ATP13A2* function may explain increased Mn in CLN5, but this remains to be tested. Interestingly, the parkinsonism gene *ATP13A2* may help to provide new insights into Parkinson's disease and its association with NCLs pathogenesis (Bras et al. 2012; Ramirez et al. 2006). Nevertheless, this finding, in connection with previous findings on dysregulation of TE homeostasis in the LSDs (Grubman et al. 2014a; Kanninen et al. 2013b), raises the possibility of using TEs to monitor responses to treatments in the LSDs.

6.4 Conclusion

These findings highlight the importance of assessing metal homeostasis in the diagnosis and monitoring of LSDs. Together, these findings are the very first indication that there is a disruption in lysosomal Ca^{2+} content in multiple LSDs and highlights the importance of additional work in this area, which is urgently needed to decide whether this occurs through a single common or a multiple mechanism. TE profiles might not only be useful biomarkers to monitor therapeutic response but they could also be of use for diagnosis and also improve our understanding of disease mechanisms as I have observed Zn^{2+} storage across all the LSDs. In term of using the TE profiles as a potential biomarkers getting access to the biological samples from LSDs is required.

Chapter 7: NPC1 loss of function is observed across the majority of lysosomal storage diseases, explaining the lysosomal accumulation of Zn²⁺ and the presence of secondary lipid storage and lysosomal Ca²⁺ defects.

7.1 Introduction

In Chapter 6, abnormal Zn²⁺ accumulation was identified at varying levels in several LSD fibroblasts. This raises the possibility of an association between Zn²⁺ accumulation and the presence of lysosomal storage in the LSDs. Previous findings have demonstrated that Zn²⁺ binds to NPC1 (Watari et al. 2000), and previous work in the Lloyd-Evans lab has provided evidence that Zn²⁺ accumulation in NPC contributes to NPC disease pathogenesis and lipid storage (Maguire 2017). Two previous studies have also shown that free cholesterol accumulation (a hallmark of NPC disease) is a secondary storage molecule in almost all LSDs (Puri et al. 1999) and defects in lipid endocytosis (another hallmark of NPC) is also observed across most of the LSDs (Chen et al. 1999). Sphingosine storage in NPC1 leads to lysosomal Ca²⁺ defects (Lloyd-Evans et al. 2008), a phenotype shown in Chapter 6 to be common in several other LSDs. In this Chapter I investigate the hypothesis that reduced NPC1 function is common across the LSDs and may explain the presence of secondary storage, lysosomal Ca²⁺ and endocytosis defects.

7.1.1 An overview of the complexity of NPC1 protein function

The *NPC1* gene is located on chromosome 18q11 (Carstea et al. 1993). It encodes the 1,278 amino acid NPC1 protein, which contains 13-transmembrane domains (Carstea et al. 1997; Davies and Ioannou 2000). NPC1 has a C-terminal di-leucine motif that is necessary for targeting the protein to the late endosomal compartment (Storch and Xu 2009). A further site in the transmembrane domain 3, in the sterol sensing domain (SSD), was found to act as an additional endosomal targeting signal (Scott and Ioannou 2004). NPC1 has also been localised to other subcellular sites, such as the ER, caveolin-1 containing membrane rafts and the Golgi apparatus (Garver et al. 2007a; Garver et al. 2000; Higgins et al. 1999). The function of NPC1 is not yet fully understood.

NPC1 is involved in lipid sorting and vesicular trafficking in direct and indirect ways. It is hypothesised to work together with NPC2 to move cholesterol within the LE/Lys compartments. Cells deficient in NPC1/NPC2 not only accumulate cholesterol, but other sphingolipids (SLs) including; sphingomyelin, glycosphingolipids and sphingosine (Lloyd-

Evans et al. 2008; Vanier 2015). Defective glycolipid metabolism and transport is also implicated in NPC (te Vrugte et al. 2004). Similarly, several of the sphingolipidoses display changes in the distribution of intracellular cholesterol, glycosphingolipids and/or the NPC1 protein (Puri et al. 1999). Reducing cholesterol levels in sphingolipidosis disease cells restores normal trafficking of BODIPY-LacCer to the Golgi in some of these diseases (Puri et al. 1999). These findings show that the regulation of cholesterol is perturbed in many sphingolipidoses diseases, secondary to sphingolipid build-up, and that the movement of sphingolipid from the plasma membrane is restored by normalising cellular cholesterol (Pagano et al. 2000; Puri et al. 1999). It is also interesting to note that reducing cellular uptake of LDL derived cholesterol in NPC cells can also rescue several secondary phenotypes including glycosphingolipid storage and endocytosis defects. Several interactions have been shown between sphingolipids and cholesterol within the LE/Lys system (Pagano et al. 2000), explaining their co-existence and interplay as commonly stored materials. Lloyd-Evans *et al.* were the first to demonstrate that inhibiting NPC1 with U18666A results in sphingosine accumulation prior to lysosomal Ca^{2+} homeostasis defects, and the subsequent accumulation of cholesterol and other SLs (Lloyd-Evans et al. 2008). Hence, it is proposed that sphingosine, directly or indirectly, is implicated in the primary function of the NPC1 protein (Lloyd-Evans and Platt 2010).

Previous biochemical experiments have suggested that NPC1 binds Zn^{2+} (Watari *et al.* 2000). This is considered to be due to the sequence similarity between NPC1 and heavy metal transporting RND permeases in *E. coli* (Scott and Ioannou 2004; Tseng et al. 1999). Work in the Lloyd-Evans lab identified that the NPC1 protein could be a lysosomal Zn^{2+} transporter (Maguire 2017), closely related to the Zn^{2+} transporting bacterial RND permease ZneA. In Chapter 6, I found that Zn^{2+} accumulates in lysosomes, to different levels, across the majority of LSDs. LSDs share several similarities in secondary storage material, despite the difference in the primary accumulated substrates - mainly SLs and cholesterol. As described in chapter 1, the sphingosine base is the backbone of all SLs, and is specifically generated following breakdown of SLs, normally ceramide, by acid ceramidase in lysosomes (Chapter 1 figure 1.4, figure 1.5). This breakdown leads to the generation of lyso-derivatives of the primary SL substrates and fatty acids. So far, only NPC1 is known to accumulate high levels of sphingosine (Lloyd-Evans et al. 2008). Previous studies also shown that the NPC1 protein acts to regulate the lysosomal efflux of endogenous amines, which may include sphingosine. NPC1-deficiency is also shown to cause a decrease in the cellular clearance of amines (Kaufmann and Krise 2008). It has been speculated that NPC1 is therefore needed for the export of sphingosine, trapped by protonation in acidic compartments, from lysosomes (Lloyd-

Evans and Platt 2010). This is essential as it has been estimated by radiolabeling studies that >70% of endogenous SL biosynthesis is reliant on the recycling of sphingosine back into ceramide biosynthesis at the ER (Tettamanti et al. 2003).

7.1.2 Lysosphingolipids (Lyso-SLs) accumulate in most LSDs

SLs possess a long-chain amino alcohol group, known as sphingosine, bonded with a fatty acid to form complex lipids called ceramides. If sugar is added to a ceramide, a cerebroside or glycosphingolipid is formed; if a sulphate group is added to the sphingolipid it is known as a sulfatide; if neutral polysaccharides are added the product is called a globoside and the addition of one or more molecules of N-acetylneuraminic acid to the latter makes it a ganglioside (Ferreira and Gahl 2017) (Chapter 1 Figure 1.3). Most LSDs involve the accumulation of more than one type of substrate (Walkley and Vanier 2009b). Lyso-SLs are derivatives of sphingolipids devoid of the amide-linked acyl chain (Hannun and Bell 1989). In healthy tissues, they are present at low levels in lysosomes (Ito et al. 2000). Many lysosomal disorders are caused by defects in the degradation of SLs, leading to the accumulation of the corresponding Lyso-SLs alongside, and occasionally to a greater extent than, the primary storage molecule (Ballabio and Gieselmann 2009; Kanazawa et al. 2000). For example, in lysosomes, the GCCase enzyme degrades GlcCer. A GCCase deficiency causes an accumulation of GlcCer in lysosomes, which is the main feature of Gaucher disease. Patients suffering from Fabry disease where acid α Gal A is deficient present with lysosomal accumulation of globoside (Gb3) (Aerts et al. 2008). An alternative enzyme capable of catabolising the accumulating GlcCer and Gb3 is acid ceramidase, coded by the *ASAH1* gene. Acid ceramidase is able to process SLs in an alternative catabolic pathway that appears to mainly occur when normal catabolism of the primary SL degrading enzyme is impaired. Acid ceramidase deacylates SLs to form their lyso-derivatives (Ferraz et al. 2016), which are in part secreted from cells (Aerts et al. 2008), therefore reducing the overall lipid storage burden. In Gaucher disease, there is an accumulation of glucosylsphingosine (GlcSph), while lyso-sulfatide accumulates in MLD, globotriaosylsphingosine (Lyso-Gb3) in Fabry, and lysoganglioside GM1 in GM1 gangliosidosis etc. (Folts et al. 2016). In Krabbe disease, galactosylceramide (GalCer) can be converted to psychosine (galactosylsphingosine) by acid ceramidase mediated deacylation due to the genetic deficiency in Galactosylceramidase (GALC) activity (Svennerholm et al. 1980).

Sphingosine, and numerous other Lyso-SLs, are very toxic bioactive lipids, which play crucial roles in central cellular processes, such as apoptosis, cell growth, differentiation and senescence (Bartke and Hannun 2009; Hannun and Obeid 2008). This small sphingolipid

compound is the potent inhibitor for Protein kinase C (PKC). PKC is activated by diacylglycerol generated from phosphatidylinositol tris-phosphate during the signal transduction pathways driven by phospholipase C. It has been suggested that SL derivatives interfere with the interaction between PKC and diacylglycerol (Hannun and Bell 1989), perturbing neuronal activity by interrupting signal transduction. In support of this, PKC activity is indeed reduced in NPC1 as a result of sphingosine storage (RODRIGUEZ-LAFRASSE et al. 1997). As PKC has been shown to be inhibited across multiple LSDs by the presence of lyso-sphingoid bases, I therefore hypothesized whether the lyso-lipids may also inhibit NPC1 and in doing so incur the secondary storage of cholesterol and gangliosides across all LSDs where these lyso-lipids are present.

7.1.3 Aims:

Due to the emerging data about the NPC1 protein being involved in many lysosomal processes, including Zn^{2+} and sphingosine transport, there is a need for the following:

- (1) additional investigation to demonstrate NPC1 involvement in Zn^{2+} homeostasis.
- (2) Investigation into the possibility of NPC1 loss of function across the LSDs.
- (3) Identification of possible mechanism(s) by which NPC1 becomes defective in other LSDs.

7.1.4 Brief methods:

In Section 7.2.1 I identify the phenotypes that overlap between NPC1 and some LSDs.

In Section 7.2.2 I identify the effect of MLSA1 and miglustat (See chapter 2, section 2.8.2 and section 2.8.9) on lysosomal Zn^{2+} accumulation in NPC.

In Section 7.2.3 I use Bafilomycin A1 to induce lipid storage in control fibroblasts (See chapter 2, section 2.8.6) and compare this with NPC fibroblasts.

In Section 7.2.4 I identify associations between cholesterol distribution (See chapter 2, section 2.2.2) and the alteration of Zn^{2+} in multiple LSDs.

In Section 7.2.5 I investigated the effect of CBE (See chapter 2, section 2.8.1) on control and Farber fibroblasts.

In Section 7.2.6 I investigated the effect of Lyso-SLs, sphingosine and SLs (See chapter 2, section 2.9) on lysosomal Zn^{2+} levels.

In Section 7.2.7 I investigated the effects of inhibiting NPC function using U18666A (See chapter 2, section 2.8.3), and addition of psychosine (See chapter 2, section 2.9.2) on control and Krabbe fibroblasts.

In Section 7.2.8 I studied the effect of inhibition of Lyso-SL formation on lysosomal Zn²⁺ storage.

In Section 7.2.9 I investigated the use of miglustat as a substrate reduction therapy to normalise Zn²⁺ distribution and other phenotypes in Fabry disease.

7.2 Results

7.2.1 NPC1 phenotypes overlap with other LSDs.

As our data from Chapter 6 demonstrated, the hallmark NPC phenotypes of a reduction in lysosomal Ca^{2+} and a lysosomal increase in Zn^{2+} were observed across the majority of other investigated LSDs. Here, I decided to look at other NPC phenotypes in several LSD fibroblasts. I first investigated the localization of free cholesterol and ganglioside GM1, which are known to accumulate in NPC (Sugimoto et al. 2001; te Vrugte et al. 2004). Filipin was used to visualise cholesterol, and GM1 ganglioside staining was carried out using fluorescently tagged cholera toxin subunit B (CtxB), which binds ganglioside GM1, which is mainly localized to its site of synthesis in the Golgi in control cells (Figure 7.1). As expected, in NPC there is strong lysosomal filipin staining and a mislocalisation of CtxB to punctate lysosomes. Increased punctate filipin and CtxB staining was observed in GM1 gangliosidosis, NPA and I cell (Figure 7.1). Farber disease, in contrast, exhibits normal filipin staining and normal GM1 distribution. Filipin staining is slightly higher in Wolman where only a few CtxB positive punctae are seen (Figure 7.1).

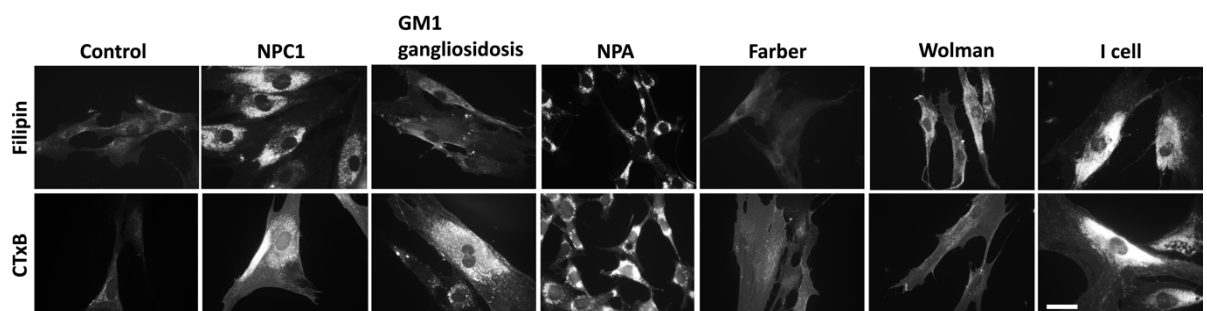


Figure 7.1 Subcellular distribution of free cholesterol and ganglioside GM1 in LSD fibroblasts.

The Control (GM05399), NPC1(GM03123), GM1 gangliosides (GM03589), NPA (GM00370), Farber (GM05752), Wolman (GM01606) and I cell (GM02013) fibroblasts were fixed and stained with either filipin, for free cholesterol, or CtxB for ganglioside GM1. Representative pictures shown. N = 3. Scale bar =10 μm .

7.2.2 Neither TRPML1 upregulation nor miglustat treatment normalizes lysosomal Zn²⁺ accumulation in NPC fibroblasts

TRPML1 is one Ca²⁺ channel of the lysosome. The accumulated lipids in LSDs, particularly sphingomyelin, may work as a negative regulator of TRPML1 (Shen et al. 2012). A previous study claimed that TRPML1 is directly involved in Zn²⁺ transportation from the lysosome (Eichelsdoerfer et al. 2010). Therefore, I activated TRPML1 with its synthetic agonist MLSA1, to see if this would correct the Zn²⁺ accumulation observed in NPC. Cells were incubated in culture medium containing 50 μM MLSA1 for 4 hours prior to Zn²⁺ staining. Untreated NPC fibroblasts demonstrated clear Zn²⁺ accumulation within lysosomes, and there was no reduction in Zn²⁺ accumulation following MLSA1 treatment (Figure 7.2).

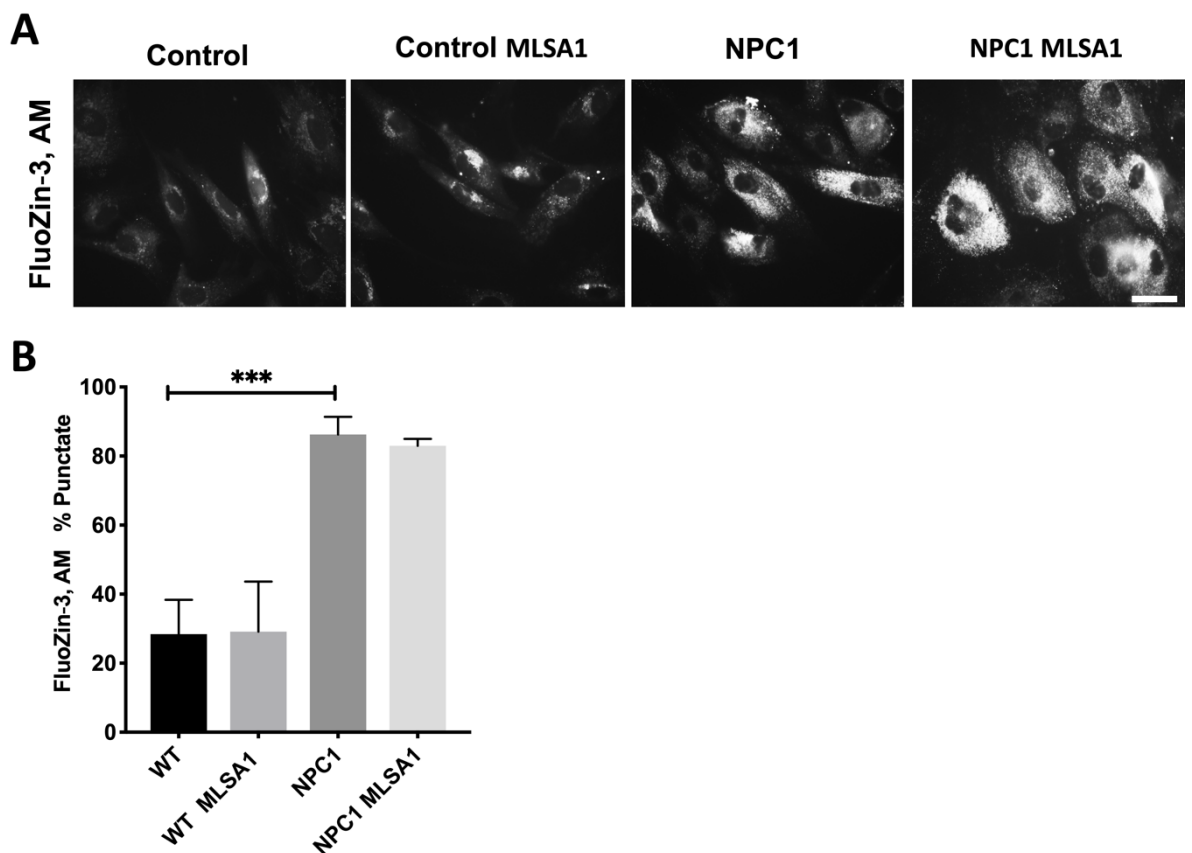


Figure 7.2 Activation of TRPML1 with MLSA1 treatment does not correct lysosomal Zn²⁺ storage in NPC.

(A) Control (GM05399) and NPC (GM03123) fibroblasts were treated with 50 μM MLSA1 for 4 hours prior to staining with FlouZin,3AM. (B) Images were quantified by counting the percentage of cells with punctate staining. N=3, scale bar =10 μm. Representative pictures shown. Statistical analyses were calculated using one-way anova;***p ≤ 0.001, Data are shown as mean ± SD.

I also looked to see if depleting SL accumulation in NPC would help to normalise lysosomal Zn^{2+} storage. Glycosphingolipid synthesis was blocked using miglustat, a small molecule inhibitor of the enzyme glucosylceramide synthase, essential for glycosphingolipid synthesis. Lysosomal Zn^{2+} accumulation was not significantly changed in the NPC patient fibroblasts (Figure 7.3). This confirms that glycolipids, and defective endocytosis (corrected by miglustat treatment (Lachmann et al. 2004b) are not the cause of the Zn^{2+} relocalisation and appears to be another confirmation for the involvement of NPC1 in Zn^{2+} transport. Miglustat also had no effect on the Golgi localisation of Zn^{2+} in the control cells (Figure 7.3).

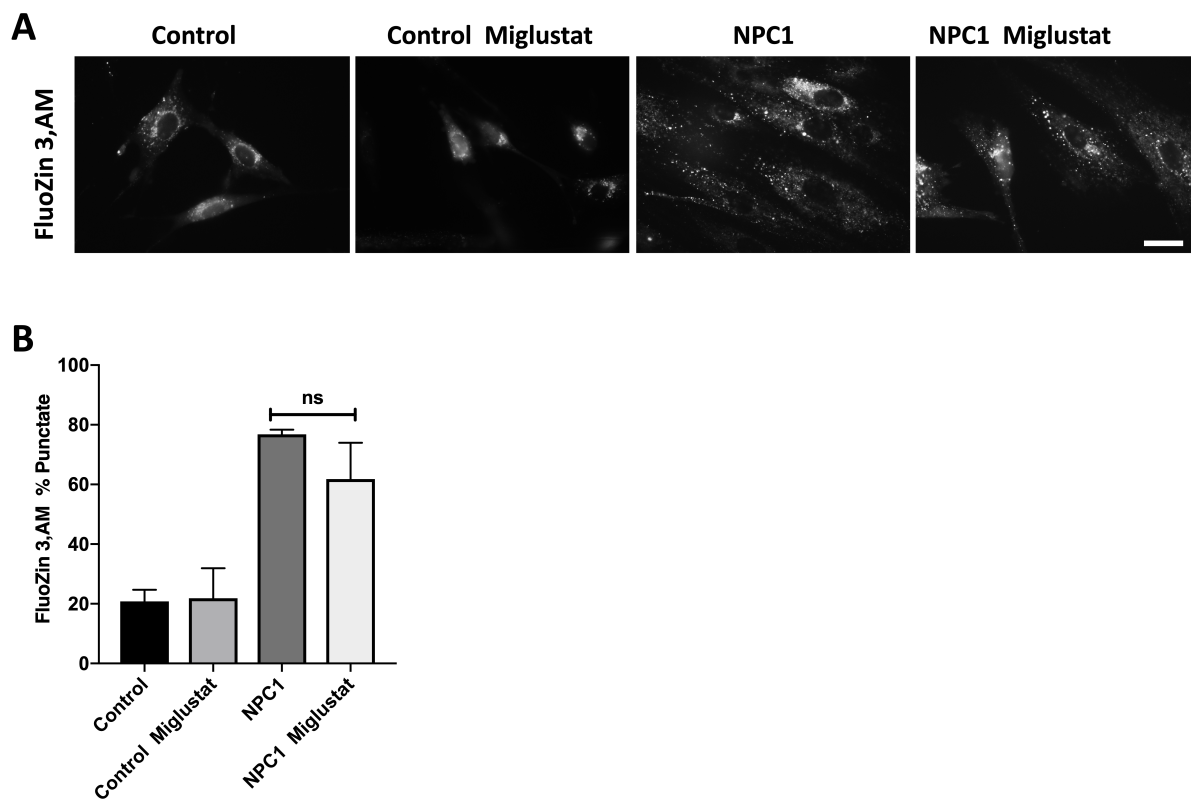


Figure 7.3 Miglustat unable to rescue lysosomal Zn^{2+} accumulation in NPC fibroblasts.

Control and NPC1 human fibroblasts were treated for five days with 50 μ M Miglustat prior to staining with FluoZin3, AM. Images (A) were quantified by counting the percentage of cells with punctate staining. N=3. Scale bar =10 μ M. Representative pictures shown. Statistical analyses were calculated using one-way anova; ns indicates that it is not significant. Data are shown as mean \pm SD.

7.2.3 Bafilomycin A1 (Baf A1) treatment induced lysosomal Zn²⁺ accumulation.

In order to investigate the effect of lipid storage and pH on NPC1 function, Baf A1 was used to deacidify lysosomes via inhibition of the vATPase (Yoshimori et al. 1991). Following vATPase inhibition, changes in intralysosomal pH disturb the optimum conditions for enzyme activity and induce a lysosomal lipid storage phenotype. Lysosomal deacidification also affects NPC1 function, which is dependent on proton motive force (Tseng et al. 1999). Control and NPC fibroblasts were treated with 25nM Baf A1 overnight to partially de-acidify lysosomes (Lee et al. 2015). I noticed an approximate 2.5-fold increase in lysosomal Zn²⁺ accumulation (FluoZin3, AM) in control cells treated with Baf A1, but no noticeable changes in NPC1 patient fibroblast lysosomal Zn²⁺ content (Figure 7.4 A & B). There was an increase in NPC1 staining in control fibroblasts treated with Baf A1 (Figure 7.4 A & C). Similar to NPC1 staining, filipin was also increased significantly in controls treated with Baf A1 (Figure 7.4 A & D). Baf A1-mediated lysosomal pH reduction was confirmed using the lysosomal pH dependent probe, lysotracker (Figure 7.4 A & E). As lipid storage has earlier been shown to not impact on lysosomal Zn²⁺ accumulation in NPC cells (Figure 7.3) it would appear most likely that the Zn²⁺ relocalisation observed in the control cells is due to NPC1 loss of function caused by the reduced proton motive force in deacidified lysosomes.

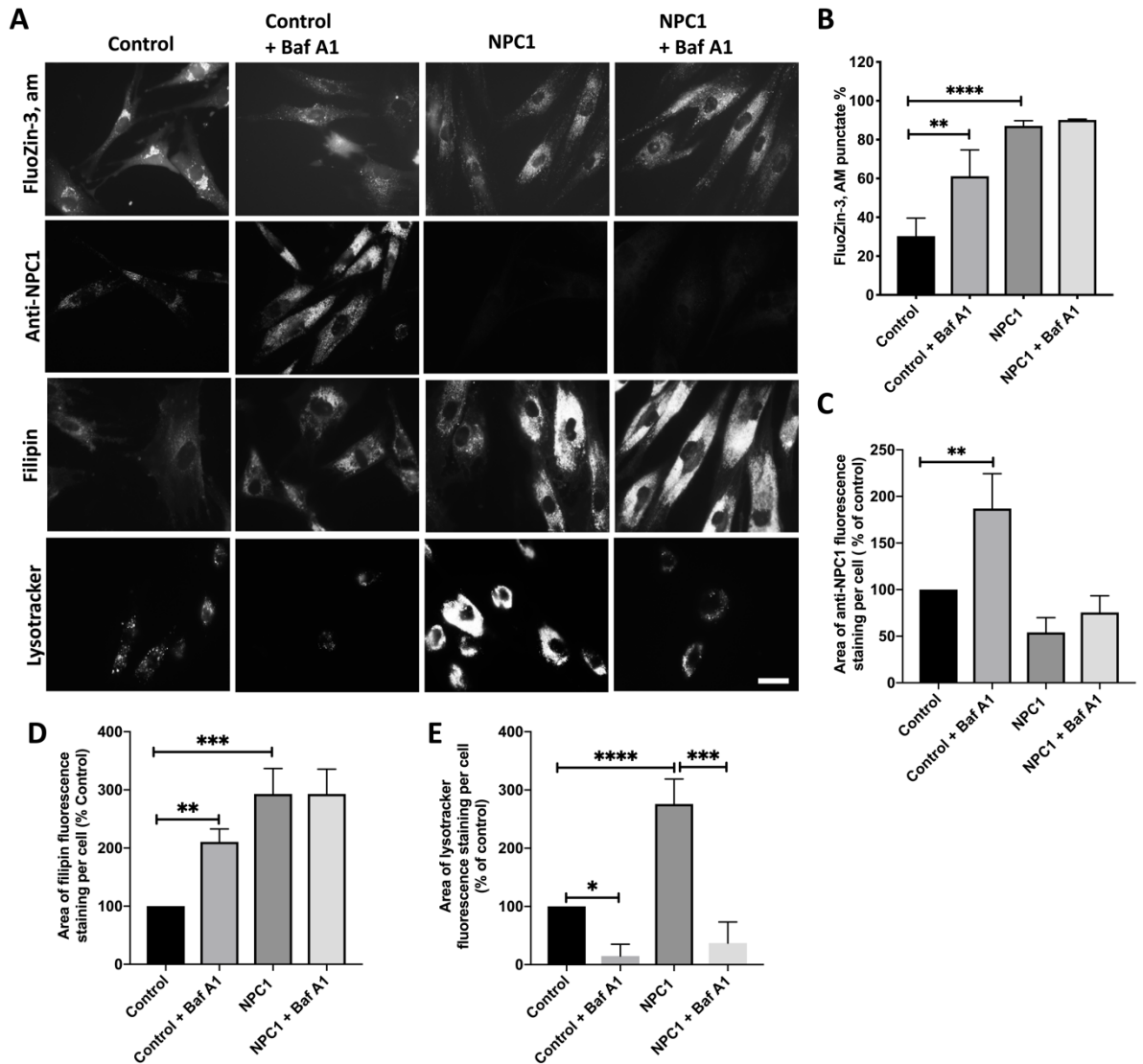


Figure 7.4 Effects of Baf A1 on control and NPC fibroblasts.

Control and NPC1 fibroblasts were treated with 25nM Baf A1 overnight. This was followed by staining the cell with either FluoZin3, AM, anti-NPC1, filipin or Lysotracker. Images (A) were quantified either from the probe distribution (FluoZin3,AM (B)) or from the area of fluorescence per cell for anti-NPC1 (C), filipin (D) and lysotracker (E). N=3, scale bar = 10 μ m. Representative picture shown. Statistical analyses were calculated using one-way anova; * $p \leq 0.05$; ** $p \leq 0.01$; *** $p \leq 0.001$; **** $p \leq 0.0001$. Data are shown as mean \pm SD.

7.2.4 Reducing cholesterol storage normalises NPC phenotypes.

So far, I have demonstrated that TRPML1 is not involved in physiological lysosomal Zn^{2+} transport and that secondary glycolipid accumulation does not alter cellular Zn^{2+} whilst lysosomal pH changes can induce lysosomal Zn^{2+} accumulation. To better understand the effect of the accumulated substrates on NPC1 function, I grew the cells in lipoprotein-deficient serum (LPDS), which reduces cellular cholesterol. Growth of LSD cells in LPDS has been shown to reduce cholesterol (Kruth et al. 1986) and also been shown to normalise the localisation of NPC1 (Puri et al. 1999). I wanted to see whether this cholesterol depletion would normalise the Zn^{2+} and NPC1 expression phenotypes. Control and LSD fibroblasts were grown in culture medium supplemented with either FBS or LPDS for 7 days. LSD fibroblasts grown in FBS showed increased lysosomal cholesterol by Filipin imaging (~3-fold in NPC1 and ~1.5-fold in Fabry). Filipin staining of cholesterol appeared increased in CLN5, but this was not significant (Figure 7.5 A & D). In contrast, LSD fibroblasts grown in LPDS had approximately normal cholesterol levels (Figure 7.5 A & D). In addition, LPDS significantly reduced lysosomal Zn^{2+} levels in Fabry and CLN5, although there were no significant changes in lysosomal Zn^{2+} or NPC1 expression in NPC fibroblasts (Figure 7.5 B & E). NPC1 expression was significantly increased in Fabry and CLN5 grown in FCS, which was normalised by growth in LPDS (Figure 7.5 D & F). This finding highlights the fact that lysosomal Zn^{2+} accumulation is predominantly NPC1-protein-dependent and is regulated by endosomal lipid levels that may themselves interact with and reduce the efficiency of residual NPC1 function (e.g. sterols).

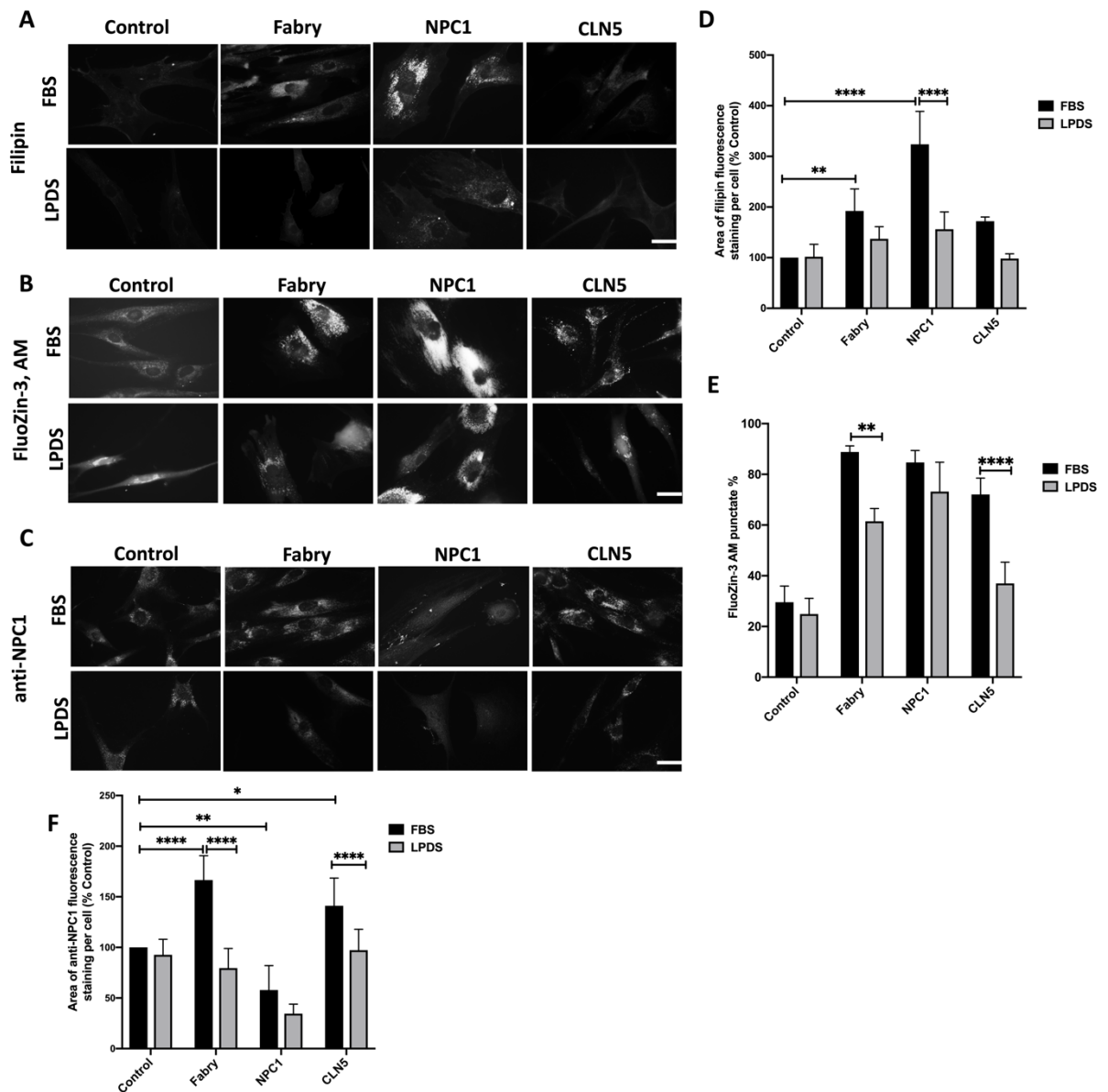


Figure 7.5 Cholesterol depletion reduces Zn^{2+} levels in LSDs human fibroblasts.

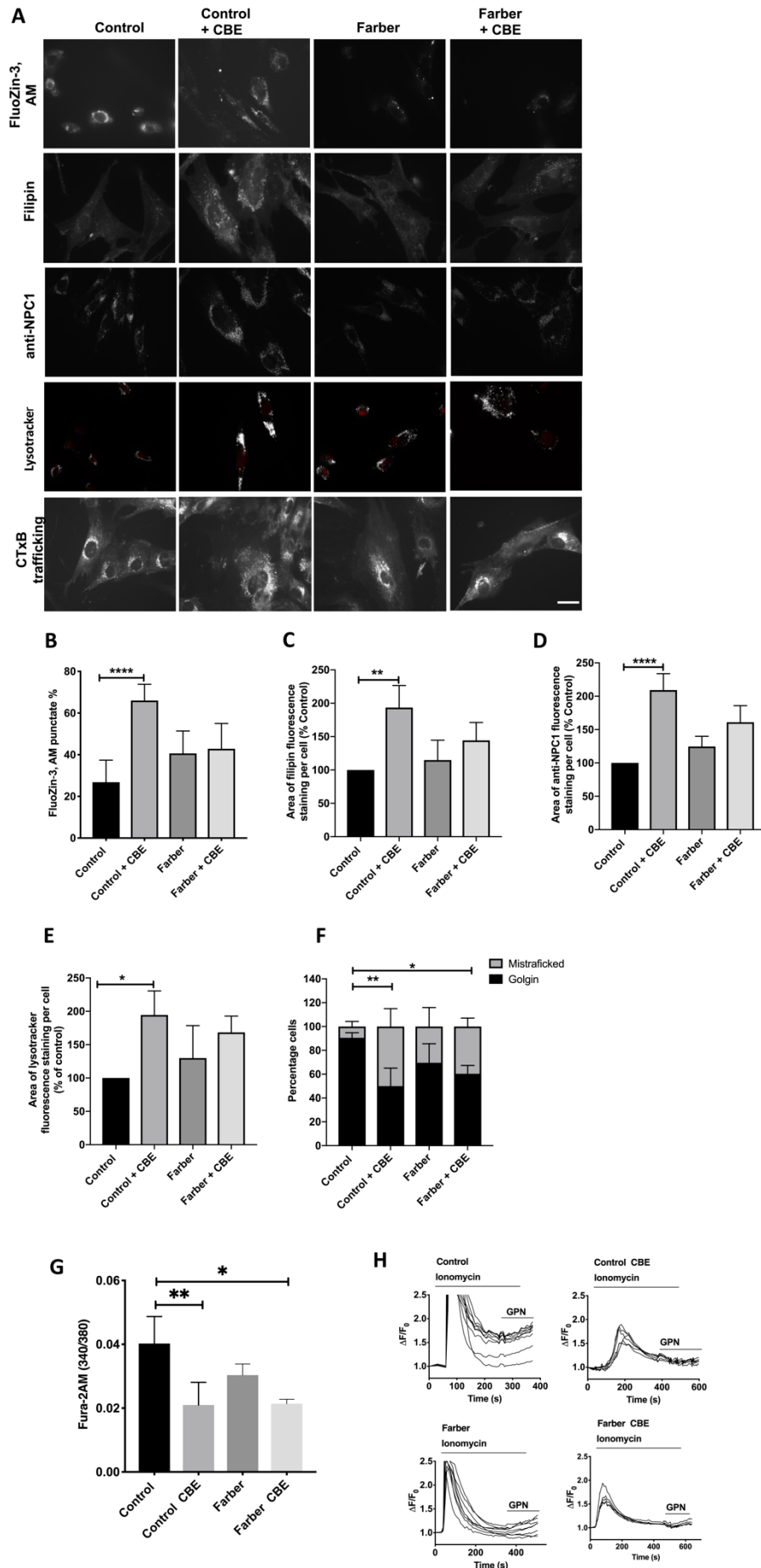
Control (GM05399), Fabry (GM00881), NPC1 (GM03123) and CLN5 fibroblasts were grown in a complete medium containing either FBS or LPDS for 7 days and stained with Filipin (A), FluoZin-3, AM (B) and anti-NPC1 (C). The graphs (D and F) were generated by measuring the area of fluorescence per cell, and graph (E) was generated by counting the percentage of cells with punctate FluoZin-3,AM distribution. N=3, scale bar = 10 μ m. Representative pictures shown. The significance was calculated using a two way ANOVA anova; * $p \leq 0.05$, ** $p \leq 0.01$, *** $p \leq 0.001$, **** $p \leq 0.0001$. Data are shown as mean \pm SD.

7.2.5 Inhibition of GCCase modulates cellular lipid storage and induces an NPC-like phenotype in control, but not Farber, fibroblasts.

In order to investigate the mechanism by which NPC1 function is altered among LSDs, I decided to investigate whether sphingolipids, or their lyso-derivative, are responsible for the appearance of NPC phenotypes in other LSDs. To achieve this, I used conduritol B epoxide (CBE) to inhibit GCCase. I hypothesized that CBE treatment would increase GlcCer and GlcSph levels in control fibroblasts whilst only GlcCer would be increased in Farber disease cells due to the genetic lack of acid ceramidase enzyme needed to generate the GlcSph. CBE treatment significantly increased by 2.5 fold the lysosomal Zn^{2+} levels in control fibroblasts, but not in Farber fibroblasts where there was no change (Figure 7.6 A & B). There was a ~3-fold increase in filipin staining in the CBE-treated control, but only a slight, not significant, increase of filipin compared to control in Farber, whether CBE treated or untreated (Figure 7.6 A & C). NPC1 antibody staining showed a significant increase in control fibroblasts treated with CBE (Figure 7.6 A & D). LysoTracker staining showed a significant increase in lysosomal volume in the CBE-treated control, in comparison to the untreated, and there was a marginal, but not significant, increase in both CBE-treated and untreated Farber fibroblasts (Figure 7.6 A & E). To follow the endocytic trafficking of ganglioside GM1, I utilized a live cell CtxB trafficking assay (see chapter 2, section 2.6.8) and analysed the cellular distribution of GM1 according to either Golgi localisation (correct trafficking) or punctate lysosomal localisation (mistrafficked). CBE-treated cells showed reductions in correct trafficking of ~60% in control fibroblasts, and ~40% in Farber (Figure 7.6 A & F) with no worsening of the endocytic trafficking defect following CBE treatment. Finally, I looked at lysosomal Ca^{2+} content by using ionomycin to clamp the non-lysosomal intracellular Ca^{2+} stores, followed by GPN to release lysosomal Ca^{2+} . Lysosomal Ca^{2+} levels were reduced to the same level in control and Farber fibroblasts following CBE treatment. However, as lysosomal Ca^{2+} levels are already reduced in untreated Farber, CBE induced an overall greater change in reducing lysosomal Ca^{2+} levels by 50% in control fibroblasts (Figure 7.6 G & H) compared to a further reduction of only 30% in the Farber cells.

Figure 7.6 Inhibition of GCase with CBE modulates cellular lipid storage, which induces NPC-like phenotypes in control, but not Farber, fibroblasts.

Control (GM05399) and Farber (GM05752) fibroblasts were treated with 500 μ M CBE for 5 days prior to staining with FluoZin-3,AM (Zn^{2+} probe), filipin, anti-NPC1, LysoTracker (lysosomal marker) or live assessment of transport of ganglioside GM1 trafficking (via cellular uptake and following of CtxB trafficking), Images (A) were quantified by counting the percentage of cells with punctate FluoZin-3,AM staining (B), or the area of fluorescence per cell for filipin (C), anti-NPC1 (D), and LysoTracker (E). CtxB trafficking was quantified by counting crescent shaped Golgi staining versus mistrafficked lysosomal puncta (F). Elevations in cytosolic Ca^{2+} following GPN induced lysosomal release, detected using Fura-2,AM (G), and representative Ca^{2+} traces (H). N = 3, scale bar = 10 μ m. Representative pictures shown. Statistical analyses were calculated using one-way anova; * $p \leq 0.05$, ** $p \leq 0.01$, *** $p \leq 0.001$, **** $p \leq 0.0001$. Data are shown as mean \pm SD.

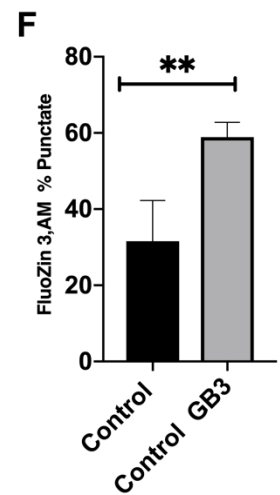
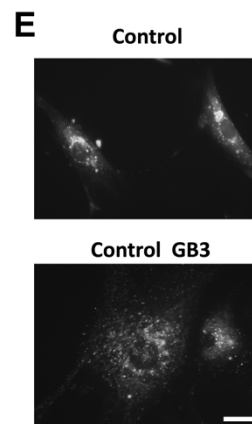
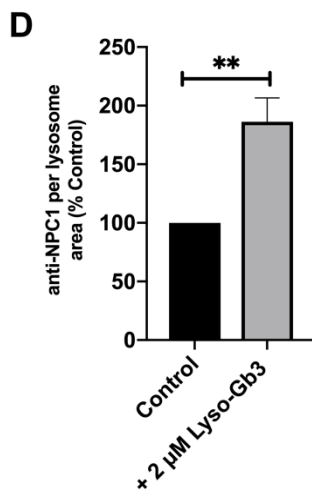
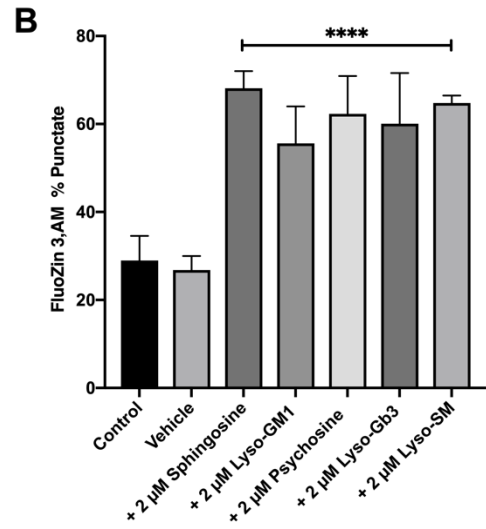
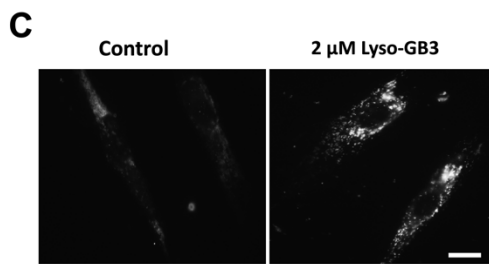
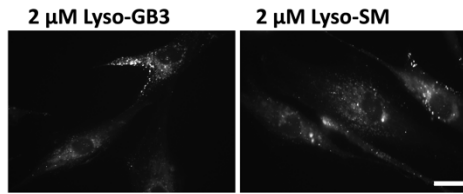
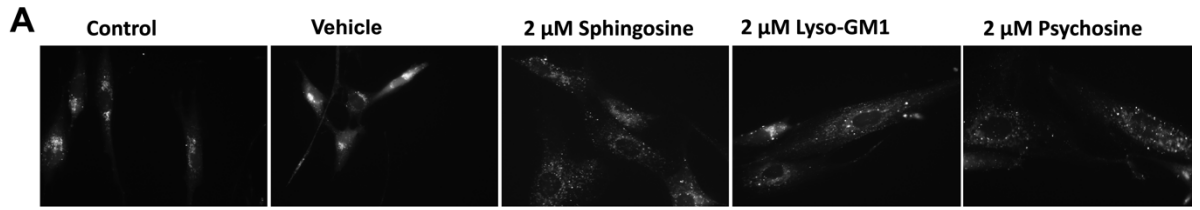


7.2.6 The effects of exogenous Lyso-SLs on lysosomal Zn²⁺ levels in control fibroblasts

Our previous findings suggest that the action of acid ceramidase in generating lyso-SLs may ultimately impair NPC1 function (Figure 7.6). Therefore, I further investigated the effect of various lyso-SLs on Zn²⁺ homeostasis. Control fibroblasts were incubated in culture medium containing 2 μM sphingosine for 24 hours, or 2 μM of either Lyso-GM1, Lyso-Gb3, psychosine or lyso-SM for 48 hours (longer incubation time owing to their more hydrophobic properties compared to sphingosine), followed by staining with FluoZin3,AM to localize intracellular Zn²⁺. Zn²⁺ staining was clearly redistributed and was more punctate in control cells treated with sphingosine and lyso-SLs in comparison to Golgi localization in the untreated controls. In order to eliminate the effect of the solvents used to solubilize the hydrophobic lyso-SLs, which are known to modulate cellular and tissue levels of Zn²⁺ (Brzoska et al. 2000), I treated cells with ethanol (all sphingosine and lyso-SL stocks were made in ethanol) as a vehicle control (Figure 7.7 A & B) and did not observe any discernable effects on lysosomal Zn²⁺. Furthermore, Lyso-Gb3 significantly increased NPC1 expression (Figure 7.7 C & D). The addition of the parental globoside Gb3 also led to a Zn²⁺ accumulation when used at a high 40 μM concentration which would saturate lysosomal αGal A during 48 hours incubation and lead to lyso-Gb3 storage (Figure 7.7 E & F). Therefore, lyso-SLs as suspected (Hannun and Bell 1987) might indeed be more pathogenic than the primary lipid (a non-degradable lipid) and appear to be the cause of inhibition of NPC1 function.

Figure 7.7 Exogenous lyso-SLs elevate lysosomal Zn²⁺ levels in control fibroblasts.

(A) Control HFs were grown in culture medium containing 2 μ M of either lyso-GM1, lyso-Gb3, psychosine, lyso-SM (for 48 hours) or 2 μ M sphingosine (for 24 hours) prior to the live staining with FluoZin3, AM. Graph (B) was generated from counting the percentage of cells with punctate staining. (C) Control fibroblasts were treated with 2 μ M lyso-Gb3 for 48 hours, and stained with an anti-NPC1 antibody. Graph (D) was generated by measuring the area of fluorescence per cell. (E) Control fibroblasts were treated with 40 μ M globoside Gb3 for 48 hours prior to staining with FluoZin3,AM. Graph (F) was generated from counting the percentage of cells with punctate staining. N = 3. Scale bar = 10 μ m. Representative pictures shown. Statistical analyses were calculated using either one-way anova (B) or using a t test (D&F); *** p \leq 0.001, ****p \leq 0.0001. Data are shown as mean \pm SD.



7.2.7 Both inhibiting NPC1 function, or adding psychosine leads to Zn²⁺ and lipid accumulation in Krabbe

No significant increase in lysosomal Zn²⁺ accumulation was seen in Krabbe fibroblasts, however this is not surprising as Krabbe cells are known not to accumulate lysosomal storage material owing to very low levels of GalCer in human fibroblasts (Takuro et al. 1985; Tanaka and Suzuki 1978). To determine whether this lack of lysosomal Zn²⁺ storage occurs because of a lack of NPC1 protein inhibition in Krabbe cells, U18666A was added to inhibit NPC1 (Lloyd-Evans et al. 2008; Lu et al. 2015). U18666A significantly increased punctate Zn²⁺ staining in both control and Krabbe fibroblasts (Figure 7.8 A & B), indicating that NPC1 can be inhibited in these cells. NPC1 staining also increased significantly, with an approximate 2-fold elevation in the area of anti-NPC1 staining (Figure 7.8 A & C). Filipin also accumulated in control and Krabbe fibroblasts treated with U18666A (Figure 7.8 A & D). LysoTracker fluorescence also increased ~ 4 fold in control and krabbe (Figure 7.8 A & E).

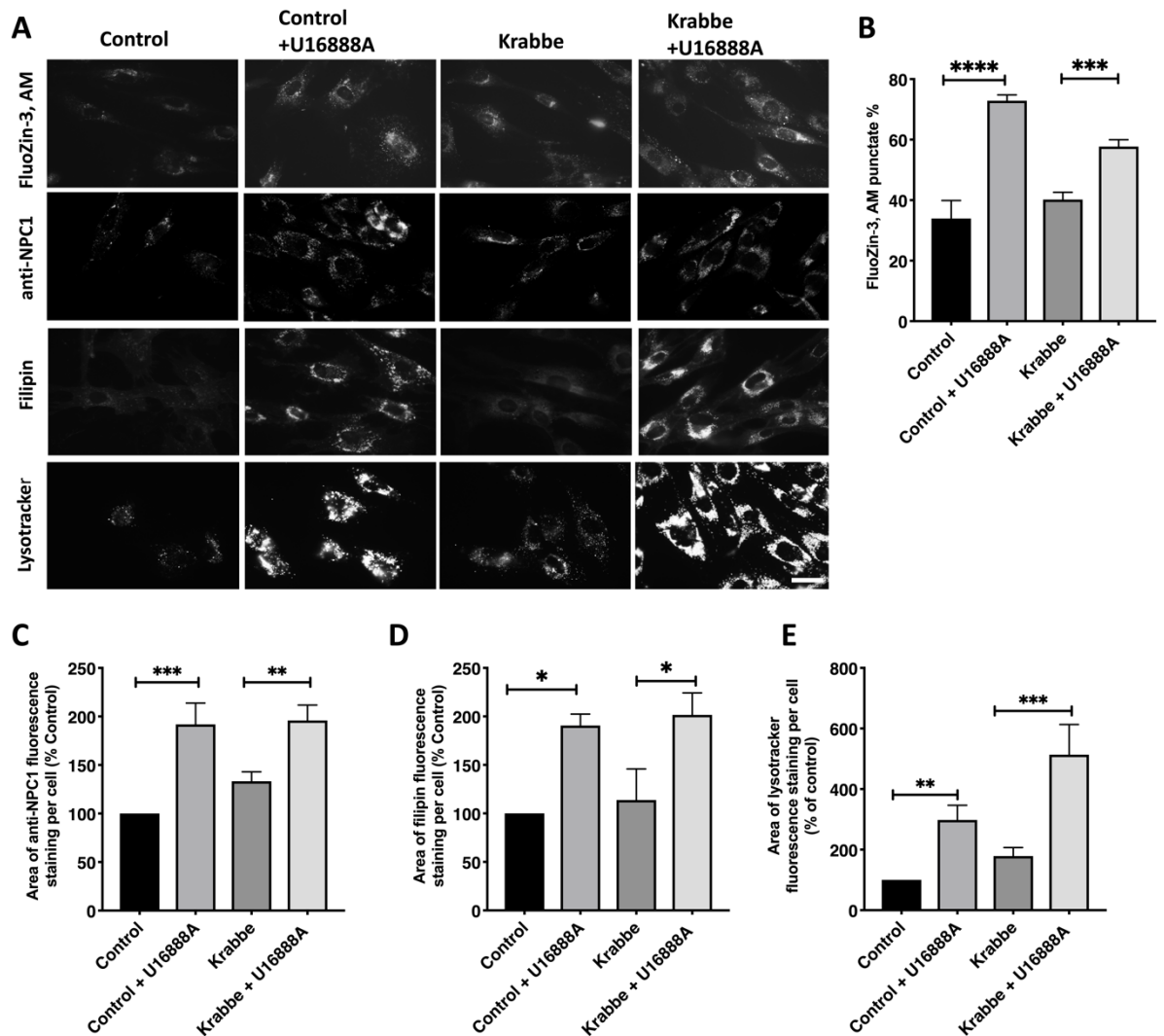


Figure 7.8 U18666A treatment induces lysosomal Zn²⁺ accumulation in control and Krabbe fibroblasts.

Control (GM05399) and Krabbe (GM06805) fibroblasts were treated with U18666A for 16 hours, and stained with the indicated probes (FluoZin,3 AM, anti-NPC1, Filipin and LysoTracker). Images (A) were quantified by either counting FluoZin-3,AM distribution (B) or by measuring the area of fluorescent signal per cell for anti-NPC1 (C), filipin (D) and lysoTracker (E). N = 3. Scale bar = 10 μ m. Representative pictures shown. Statistical analyses were calculated using one-way anova; * $p \leq 0.05$, ** $p \leq 0.01$, *** $p \leq 0.001$, **** $p \leq 0.0001$. Data are shown as mean \pm SD.

Krabbe fibroblasts do not store galactosylceramide, the primary storage material that is elevated within lysosomes following genetic mutation in α Gal A (Takuro et al. 1985; Tanaka and Suzuki 1978). To determine whether the deacylated form of GalCer, galactosylsphingosine which is known as psychosine, induces lysosomal Zn^{2+} accumulation in Krabbe, I treated control and Krabbe fibroblasts with psychosine (galactosylsphingosine, or lyso-GalCer. At a concentration of 2 μ M, psychosine treatment for 48 hours significantly increased the numbers of punctate lysosomal Zn^{2+} structures by \sim 60% in both control and Krabbe fibroblasts (Figure 7.9).

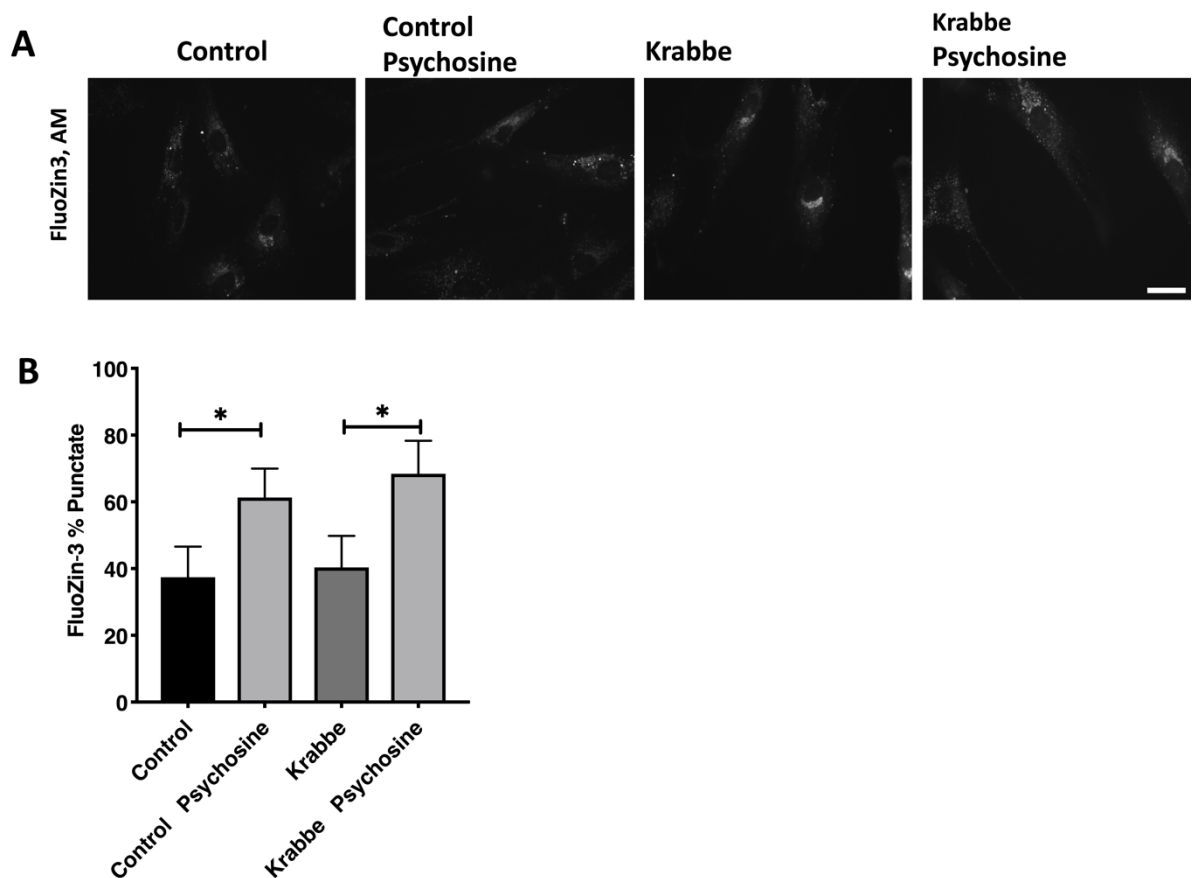


Figure 7.9 Psychosine induces lysosomal Zn^{2+} accumulation in control and Krabbe fibroblasts.

Control (GM05399) and Krabbe (GM06805) fibroblasts were treated with 2 μ M psychosine for 24 hours and stained with the Zn^{2+} probe FluoZin-3,AM. Images (A) were quantified by counting the percentage of cells with Zn^{2+} puncta (B). N = 3. Scale bar = 10 μ m. Representative pictures shown. Statistical analyses were calculated using one-way anova; * $p \leq 0.05$. Data are shown as mean \pm SD.

7.2.8 Inhibition of lyso-SL formation reduced lysosomal Zn²⁺ accumulation

By further investigating the effect of lyso-SLs on lysosomal Zn²⁺ storage, I demonstrated that Fabry disease, where globoside Gb3 is the primary storage material, has high levels of Zn²⁺ storage. I hypothesize that blocking the access of acid ceramidase to Gb3 will prevent the formation of lyso-Gb3, which is possibly more pathogenic and which our data indicates may be the cause of the lysosomal Zn²⁺ accumulation in Fabry patient cells. Shiga toxin (StxB), produced by some strains of *E. coli*, specifically binds to globosides Gb3 and Gb4, and has been found to bind weakly to Lyso-Gb3 (Gallegos et al. 2012). I grew control and Fabry HFs in the presence of 10 µg/ml Stx for 72 hours, to mask Gb3 and block the action of acid ceramidase on this lipid, prior to staining with FluoZin-3,AM. Stx treatment significantly reduced the Zn²⁺ levels back to control and normalized Zn²⁺ localisation in the Fabry patient cells (Figure 7.10).

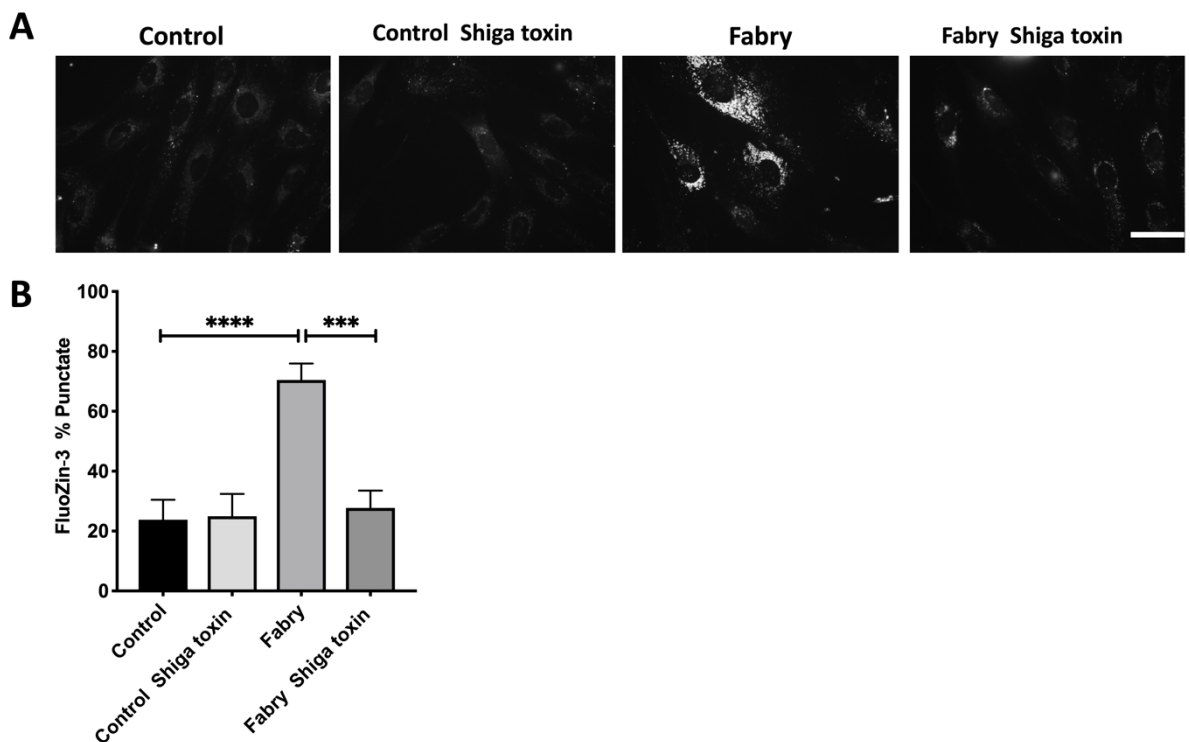


Figure 7.10 Inhibition of lyso-Gb3 formation rescues lysosomal Zn²⁺ accumulation.

Control (GM05399) and Fabry (GM00881) fibroblast were treated with 10 µg/ml Shiga Toxin for 72 hours prior to staining with FluoZin-3,AM. Images (A) were quantified by counting the percentage of cells with Zn²⁺ puncta (B). N = 3. Scale bar = 10 µm. Representative pictures shown. Statistical analyses were calculated using one-way anova; ***p ≤ 0.001; ****p ≤ 0.0001. Data are shown as mean ± SD

Moreover, having shown that lyso-SLs are the main cause of the lysosomal Zn^{2+} accumulation I next decided to confirm the role of acid ceramidase in this process. To do this I treated cells with the strong acid ceramidase inhibitor D-NMAPPD, which leads to an accumulation of ceramide within the cells (Raisova et al. 2002). I used $5\mu\text{M}$ D-NMAPPD, a high concentration of D-NMAPPD, and it led to a cessation of proliferation but no obvious cell death. Treatment of MLIV fibroblasts with $5\mu\text{M}$ D-NMAPPD for 48 hours was able to reduce the level of lysosomal Zn^{2+} accumulation, but not return it back to control levels (Figure 7.11).

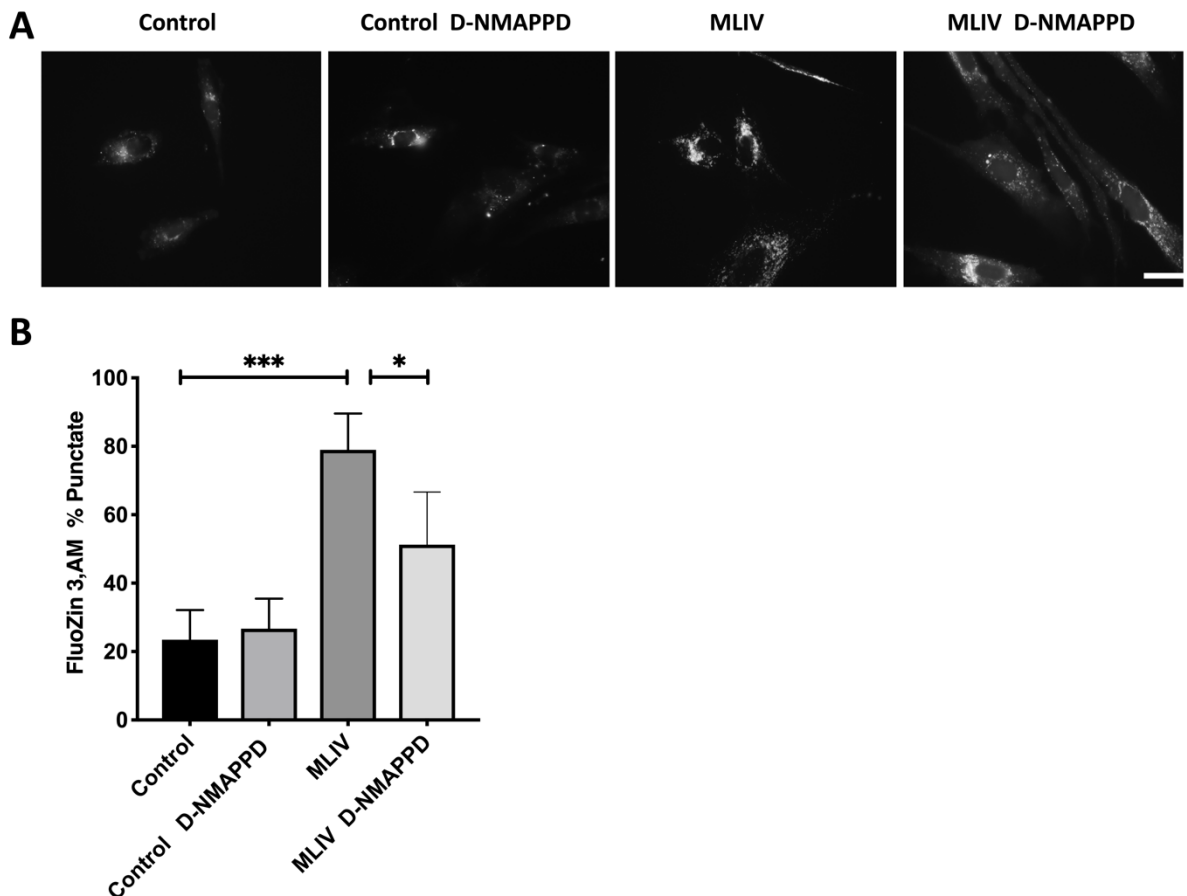


Figure 7.11 Inhibition of acid ceramidase reduces lysosomal Zn^{2+} storage.

Control (GM05399) and MLIV (GM02527) human fibroblast were treated with $5\mu\text{M}$ D-NMAPPD for 48 hours prior to staining with FluoZin-3,AM. Images (A) were quantified by counting the percentage of cells with Zn^{2+} puncta (B). N = 3. Scale bar = $10\mu\text{m}$. Representative pictures shown. Statistical analyses were calculated using one-way anova; *p ≤ 0.05 ; ***p ≤ 0.001 . Data are shown as mean \pm SD.

7.2.9 Miglustat treatment corrects lysosomal Zn²⁺ storage and NPC1 levels.

Previous results (Figure 7.3) have shown that miglustat was unable to correct lysosomal Zn²⁺ storage in NPC1, which I believe to be the lysosomal Zn²⁺ efflux transporter. However, subsequent data demonstrated that storage of sphingolipids, in particular their lyso-derivatives, induce lysosomal Zn²⁺ accumulation, presumably by inhibiting the NPC1 protein. To determine whether reduction of SL and lyso-SL levels could reverse this inhibition and normalize Zn²⁺ distribution, I treated control and Fabry fibroblasts with 50µM miglustat for 5 days. Miglustat treatment significantly reduces lysosomal Zn²⁺ storage in Fabry fibroblasts and normalises its distribution (Figure 7.12 A & B). Endocytic trafficking defects, measured using the CtxB trafficking assay (CtxB) (Chapter 2, Section 2.6.8) are also corrected in Fabry fibroblasts following miglustat treatment (Figure 7.12 A & C). NPC1 levels are significantly reduced and lysotracker fluorescence is decreased in response to miglustat treatment (Figure 7.12 A & D & E). Miglustat is, therefore, capable of improving all NPC-like phenotypes measured in Fabry fibroblasts indicating that a reduction in globoside or lyso-globoside is sufficient to normalise NPC1 function.

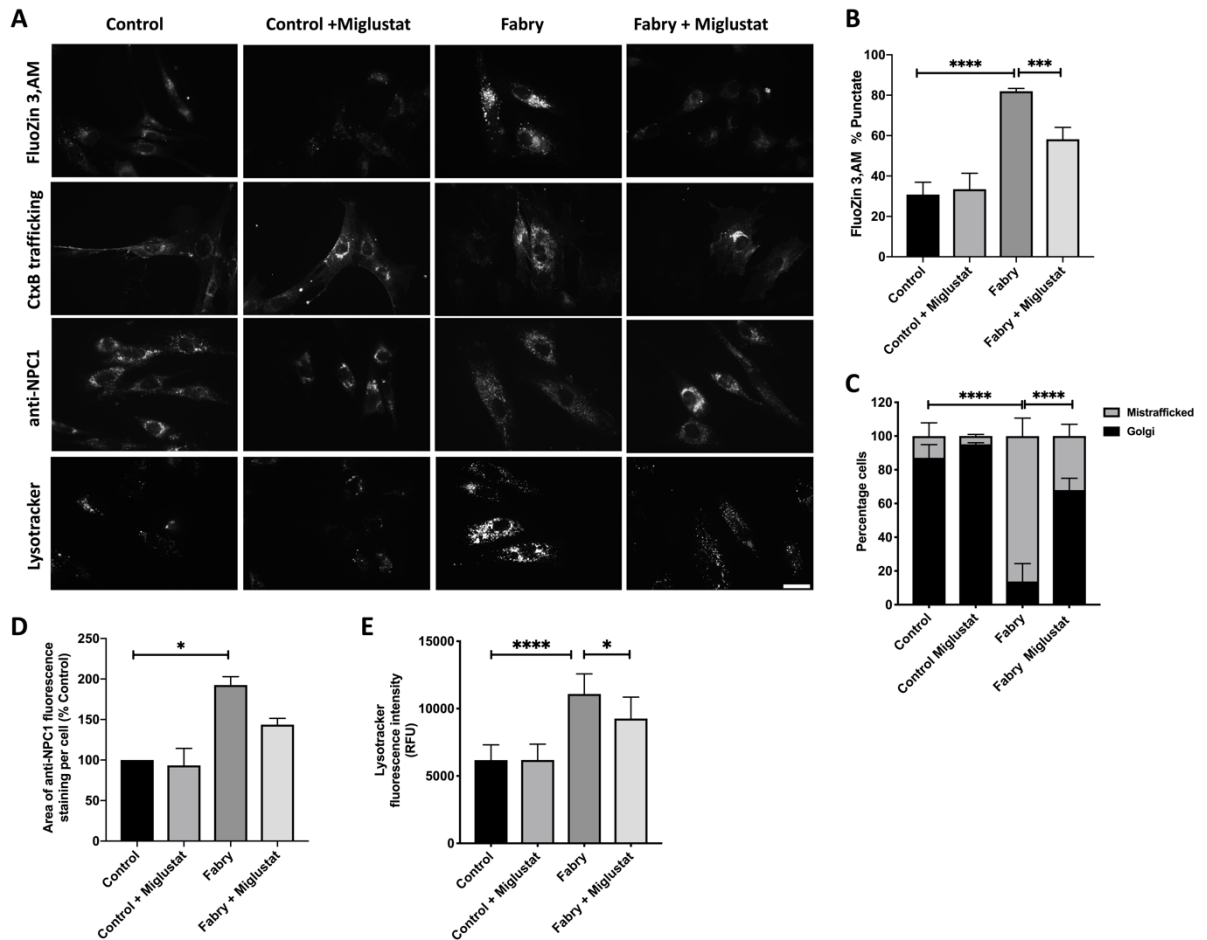


Figure 7.12 Miglustat treatment improves NPC disease-like phenotypes in Fabry fibroblasts.

Control (GM05399) and Fabry (GM00881) fibroblasts were grown in medium containing 50 μ M miglustat for five days prior to staining with FluoZin-3,AM (Zn²⁺ probe), undergoing an assessment of ganglioside GM1 trafficking (CtxB trafficking), anti-NPC1 or LysoTracker (lysosomal marker), Images (A) were quantified by counting the percentage of cells with punctate FluoZin-3,AM staining (B), counting Golgi staining versus mistrafficked puncta for CtxB trafficking (C) or the area of fluorescence per cell for anti-NPC1 (D). (E) Control (GM05399) and Fabry (GM00881) cells were grown in medium containing 50 μ M Miglustat for five days before staining with lysotracker prior and quantification of lysotracker fluorescence intensity using a fluorescent plate reader plate reader. N = 3. Scale bar = 10 μ m. Representative pictures shown. Statistical analyses were calculated using one-way anova; * p \leq 0.05, **** p \leq 0.0001. Data are shown as mean \pm SD

7.3 Discussion

I investigated lysosomal storage of Zn^{2+} across the majority of LSDs in Chapter 6. Due to previous findings; 1) indicating that the NPC1 protein can bind Zn^{2+} (Watari et al. 2000), 2) evidence suggesting that NPC1 is the mammalian lysosomal Zn^{2+} transporter as it shares close homology to a Zn^{2+} transporting bacterial RND permease (Maguire 2017), 3) evidence that NPC1 and the yeast homologue are simple sphingolipid transporters (Lloyd-Evans et al. 2008; Malathi et al. 2004; Wheeler et al. 2019), and 4) that NPC1 is a general amine transporter (Kaufmann and Krise 2008; Lloyd-Evans and Platt 2010), I investigated whether this lysosomal Zn^{2+} accumulation is caused by altered NPC1 function in other LSDs. I found evidence of disrupted NPC1 function in almost all LSDs and propose a mechanism whereby lyso-sphingolipids, all of which are secondary amines, and accumulate in most LSDs are disrupting NPC1 function.

7.3.1 Lysosomal Zn^{2+} accumulation is mainly NPC1 dependent

The aim was to investigate the reason behind the lysosomal accumulation of Zn^{2+} among several LSDs. I knew from previous research in the Lloyd-Evans lab that the NPC1 protein was likely to be the transporter for pumping Zn^{2+} out of lysosomes (Maguire 2017). LSDs accumulate secondary metabolites, such as SLs and cholesterol that are unlinked to the primary genetic defect (Lloyd-Evans and Platt 2010; Vitner et al. 2010). It was therefore consistent that I found a similarity in free cholesterol and GM1 ganglioside storage in NPC, GM1 gangliosidosis, NPA, I cell and Wolman, although only mild ganglioside GM1 storage is present in Wolman. Interestingly, Farber disease fibroblasts, deficient in acid ceramidase activity, had normal levels of free cholesterol and GM1 ganglioside (Figure 7.1). The interaction and interplay between combined cholesterol and GSL storage in LSDs has been widely discussed in previous research (Pagano et al. 2000; Te Vruchte et al. 2010). Furthermore, the accumulation of sphingosine in NPC causes a reduction in lysosomal Ca^{2+} content that in turn disrupts lipid endocytosis and results in the secondary accumulation of cholesterol and GSLs (Lloyd-Evans et al. 2008). In Chapter 3, I found that this reduction in lysosomal Ca^{2+} was not only present in NPC, but is found in several LSDs. In this chapter, I have also found that most NPC disease phenotypes (lysosomal accumulation of cholesterol, ganglioside GM1 and Zn^{2+} , and endocytic mistrafficking) are present in several LSDs. Therefore, due to this high degree of similarity across the LSDs, I hypothesized that the NPC1 protein may lose function through either a single or multiple mechanisms in LSDs.

In terms of Zn^{2+} accumulation, a previous study has suggested that TRPML1 is a lysosomal Zn^{2+} channel as Zn^{2+} accumulates in MLIV (Eichelsdoerfer et al. 2010). This was followed up by another study using an siRNA TRPML1 knockdown in HeLa cells; however, in both studies the cells were treated with 100 μ M extracellular Zn^{2+} to enable the Zn^{2+} accumulation to be observed (Kukic et al. 2013). This is far in excess of physiological extracellular Zn^{2+} , disputing the relevance of this finding *in vivo*. In contrast to these previous findings, our results, using MLSA1 to activate TRPML1, showed no significant reduction in Zn^{2+} within the lysosomes of control or NPC1 fibroblasts (Figure 7.2). This would suggest that TRPML1 may not be the main lysosomal Zn^{2+} channel. Other possibilities, however, cannot be excluded, for example perhaps TRPML1 is utilised under conditions of extreme stress (Wang et al. 2015). To build up our evidence about the involvement of NPC1 in Zn^{2+} transportation, I used miglustat, which depletes GSL in NPC cells. However, it was unable to correct lysosomal Zn^{2+} accumulation (Figure 7.3). This finding is in agreement with a previous report that showed miglustat was not able to correct metal homeostasis alteration in NPC patients (Hung et al. 2014). Therefore, I have to some extent reinforced our finding that NPC1 is highly likely to be the Zn^{2+} transporter from lysosomes to the cytosol.

I then decided to investigate whether Zn^{2+} accumulates due to the accumulation of lipids across LSDs. Baf A1 causes alkalisation of the lysosome by inhibition of the vATPase proton pump (Yoshimori et al. 1991). This leads to the accumulation of different lipids in the lysosome, as lysosomal pH is elevated above the optimum pH of lysosomal enzymes. Baf A1 treatment leads to an accumulation of Zn^{2+} and cholesterol and to increased expression of NPC1 in control fibroblasts. However, as NPC1 relies upon a proton motive force to function (Davies et al. 2000), it seems likely that the change in pH may also be a factor here in causing the Zn^{2+} accumulation.

LPDS is able to deplete the cholesterol level in cells. It has also been shown to normalise the localisation of NPC1 (Puri et al. 1999) and to reduce secondary lipid storage in NPC1 patient cells (Salvioli et al. 2004). I have also found that LPDS is capable of rescuing lysosomal Zn^{2+} storage in Fabry and in CLN5 by presumably reducing lipid levels and normalising NPC1 function and ultimately protein levels (Figure 7.5). However, LPDS was unable to correct lysosomal Zn^{2+} storage in NPC fibroblasts, although it did reduce cholesterol storage in NPC (Figure 7.5), indicating that the presence of functioning NPC1 is critical to normalise the Zn^{2+} defect across the LSDs. This strongly suggests that lysosomal Zn^{2+} levels are most dependent on NPC1 function, may also require lysosomal pH and are affected by the presence of lipid storage in the other LSDs.

7.3.2 Accumulating lyso-SLs have a greater effect on NPC function than SLs

Interestingly, Farber disease demonstrated normal levels of lysosomal cholesterol, Zn^{2+} and GM1 ganglioside (Figure 7.1). In Farber disease, ceramide accumulates due to a lack of acid ceramidase activity. Acid ceramidase is an enzyme that degrades ceramide into sphingosine and a free fatty acid. It is a candidate enzyme in the catabolism of GSLs to generate lyso-SLs (Ferraz et al. 2016). This raised the possibility that lyso-SLs, which have sphingosine, rather than ceramide, bases and which are known to accumulate across several LSDs (Hannun and Bell 1987), affect NPC1 function. It has also previously been claimed that NPC1 is highly likely to be the sphingoid base transporter due to the accumulation of sphingosine in NPC1 (Lloyd-Evans and Platt 2010) and a role for SL recycling in yeast (Malathi et al. 2004). I also found that I cell is another disease that has a lack of acid ceramidase. However, lysosomal cholesterol and Zn^{2+} accumulate in I cell. The lack of GlcNAc-1-phosphotransferase results in a failure to add mannose 6-phosphate residues on proteins destined for the lysosome in I cell tissues and cells leading to the loss, amongst other, of lysosomal NPC2. This results in cholesterol accumulation (Kollmann et al. 2012) and would ultimately disturb NPC1 function, as the two act in the same pathway (Friedland et al. 2003). Furthermore, I cell fibroblasts are highly autofluorescent, presumably due to the loss of NCL related enzymes that are involved in degradation of autofluorescent SCMAS containing lipofuscin. This makes further investigation of I cell material difficult, as this autofluorescence precludes the use of several fluorescent probes (Supplementary figure 30). Therefore, to investigate the role of acid ceramidase in the Zn^{2+} phenotype across the LSDs, I used the small molecule CBE to fully inhibit GCCase (a Gaucher disease model), causing an accumulation of GlcCer and GlcSph in control fibroblasts, but of only GlcCer in Farber fibroblasts due to lack of the acid ceramidase enzyme. Lysosomal Zn^{2+} levels was significantly increased in control cells, but only slightly increased in Farber (Figure 7.6). Endocytic trafficking was also more severely affected in control cells. Lysosomal lipid storage assessed using filipin (for cholesterol) also accumulated to a greater degree in CBE treated control cells than in CBE treated Farber patient cells. Finally, NPC1 levels were elevated more in the CBE treated control cells than the CBE treated Farber cells. This data allowed us to establish a correlation between the accumulation of sphingoid base molecules (lyso-SLs, in this instance of GlcSph) and NPC1 function.

I also speculated that inhibition of acid ceramidase might help to reduce lysosomal Zn^{2+} storage. To test this, I first prevented acid ceramide from reaching lysosomal SLs by using Stx to bind globoside Gb3. Treatment with Stx, endocytosed into lysosomes, reduced lysosomal Zn^{2+} storage in Fabry disease, where globoside Gb3 is the primary storage material (Figure 7.10), suggesting that hydrolysis of Gb3 into lyso-Gb3 is indeed a critical component of

inhibiting NPC1 function. Secondly, I inhibited acid ceramidase using a small molecule inhibitor, DNMAPPD, in MLIV fibroblasts, and were able to reduce lysosomal Zn^{2+} storage (Figure 7.11). Further testing is required in Fabry disease cells. Collectively, the lyso-SLs may disturb NPC1 function, and consequences of this are the accumulation of Zn^{2+} and other lipids in lysosomes (Figure 7.13).

Furthermore, treatment of control cells with a low concentration (2 μM) of exogenous lyso-SLs, including lyso-Gb3 that accumulates in Fabry disease, also increased NPC1 expression and induced lysosomal Zn^{2+} . In contrast, only a high concentration (40 μM) of exogenous primary lipid, such as globoside Gb3, resulted in lysosomal Zn^{2+} accumulation (Figure 7.7). This most likely means that it is the sphingoid bases that primarily affect NPC1 function and that a high concentration of the parent lipid is required to induce the same effect as it must first be acted upon by acid ceramidase to release the lyso-lipid derivative. Experiments combining the parent lipid with the acid ceramidase inhibitor should confirm this requirement and strengthen the hypothesis. Lyso-SLs accumulate in the majority of LSDs, which raises the genuine possibility that these lyso-derivative molecules have an impact on NPC1 function, thus generating NPC-like phenotypes and contributing to disease pathology across most of the LSDs where secondary ganglioside storage for example has been reported (Walkley and Vanier 2009b).

Krabbe disease is one of the sphingolipidoses that did not accumulate lysosomal Zn^{2+} . This may be as a consequence of a lack of storage in the Krabbe patient cells (there is very little GalCer in human fibroblasts) or as a result of a change in lysosomal pH, although that would be expected to inhibit NPC1 based on our bafilomycin A1 experiment outcome. I therefore tested whether inhibition of NPC1 could induce the Zn^{2+} phenotype in Krabbe cells. U18666A causes lysosomal storage of sphingosine which inhibits expulsion of cholesterol from lysosomes by binding, and inhibiting, NPC1 (Lloyd-Evans et al. 2008; Lu et al. 2015). The use of U18666A induced NPC phenotypes in control and Krabbe fibroblasts, including elevated lysosomal levels of Zn^{2+} and cholesterol alongside increased lysotracker fluorescence and NPC1 protein expression (Figure 7.8), suggesting that the absence of phenotypes in the Krabbe cells is a result of either lack of GalCer or mildness of the disease causing mutation rather than a loss of lysosomal pH regulation. The lack of GalCer accumulation in the Krabbe patient fibroblast might be due to residual activity of the GALC enzyme (Tanaka and Suzuki 1978). Without GalCer accumulation, Krabbe cells would not generate the lyso-SL psychosine (galactosylsphingosine), which I would expect to inhibit NPC1. Treatment with exogenous psychosine induced lysosomal Zn^{2+} accumulation in Krabbe fibroblasts (Figure 7.9), supporting this theory. It seems that lyso-SLs are the primary lipids affecting NPC1 function.

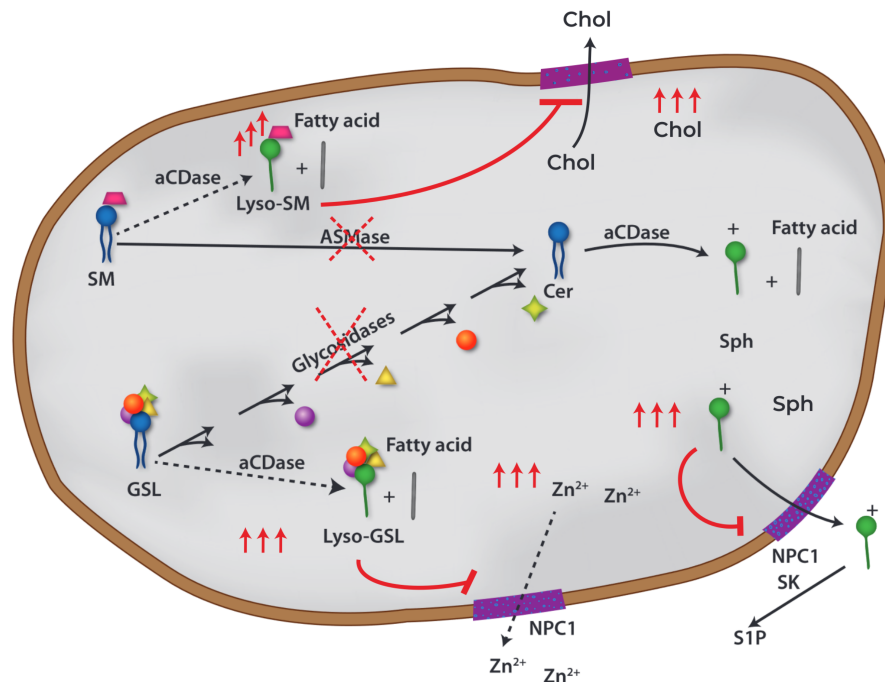


Figure 7.13 Diagram illustrating prospective disruption to NPC1 function and subsequent lysosomal Zn²⁺ storage in LSDs.

An increase in lyso-SLs (lyso-GSL and lyso-SM) may lead to disruption in NPC1 function. The defect in enzymes such as ASMase and Glycosidases (GCase, β -gal, α Gal A, HexA, HexB, Total Hex etc) leads to the accumulation of SLs. Lyso-SLs are generated from the degradation of SLs via the action of acid ceramidase (aCDase), which also degrades ceramide to generate sphingosine, which is protonated and positively charged at acidic pH. NPC1 potentially transports sphingoid bases out of lysosomes, and is regulated by them. Inhibition of NPC1 by high levels of lyso-SL would lead to NPC-like phenotypes, including accumulation of Zn²⁺ and secondary cholesterol storage in lysosomes. Cholesterol (Chol), Ceramide (Cer), Sphingosine (Sph), Sphingosine kinase (SK), Sphingosine-1-phosphate (S1P), Acid ceramidase (aCDase). Adapted from (Aureli et al. 2016; Lloyd-Evans and Platt 2010).

7.3.3 Blocking GSL biosynthesis is beneficial to Fabry disease

It has come to our attention that the use of miglustat as substrate reduction therapy may be useful in several LSDs, as this would reduce the lysosomal accumulation of GSLs and therefore reduce the pool of substrate for acid ceramidase which would in turn reduce the presence of lyso-SLs within the lysosome and ultimately reduce the resulting inhibition of

NPC1 function. Treatment of Fabry disease fibroblasts with miglustat demonstrated that the phenotypes, including lysosomal Zn^{2+} accumulation, endocytic trafficking defects and increased lysotracker fluorescence were rescued (Figure 7.12). This might be due to the reduced accumulation of globoside Gb3 mediated by miglustat. This finding raises the possibility of using miglustat across the LSDs.

I also have to think about gene therapy to overexpress NPC1 in other LSDs, which may help to reduce secondary lipid storage. Gene therapy treatment for NPC1 has become promising with the use of adeno-associated viral vectors (AAV). The efficacy of gene therapy for NPC1 has been reported in *Npc1*^{-/-} mice, with gene therapy correcting cholesterol storage and reducing Purkinje cell loss (Xie et al. 2017). It is possible that overexpression of the *NPC1* gene in other LSDs would stimulate Zn^{2+} and sphingosine egress from lysosomes and thereby potentially overcome secondary lipid storage. Currently, in collaboration with Dr. Ahad Rahim, we are looking into overexpression of NPC1 using AAV9-delivered gene therapy in a *Cln5* mouse model. These experiments are currently underway but are too early stage and preliminary to include in this thesis.

Finally, small molecule modulators of NPC1 function have been reported. NPC1 inhibitors including U18666a and the recently identified naphthylmethylpiperazines, which were developed as inhibitors of NPC1 function in order to treat Ebola virus infection (which infects cells via a direct interaction with NPC1), exist but are not useful as potential NPC1 stimulators. A study by Kaufmann and Krise (Kaufmann and Krise 2008). Indicated that small molecules including neutral red, morpholine and imidazole were capable of enhancing the ability of NPC1 to remove amines from lysosomes. This provides a possibility that small molecule modulators may also be found, based on neutral red, morpholine or imidazole that could in future stimulate NPC1 function and act as a broad LSD therapy.

7.4 Conclusion

To conclude, considerable evidence highlights that NPC1 function is highly likely to be altered across the LSDs, thereby explaining the presence of secondary lipid storage and Zn^{2+} accumulation in lysosomes, and the reduction in lysosomal Ca^{2+} content. Further work is needed to continue the current gene therapy treatment on CLN5 disease and to investigate the outcomes which may have relevance across the LSDs. Further work is also needed to test the utility of Zn^{2+} chelators or small molecule activators of NPC1 as potential therapeutics for NPC1 and other LSDs.

Chapter 8: General Discussion

8.1 Summary

There is a lack of suitable biomarkers for the majority of LSDs. This thesis aimed to investigate potential novel biomarkers for LSDs. The findings from Chapter 3 showed the possibility of using a simple fluorimetric test utilizing lysotracker for identifying and monitoring lysosomal swelling to identify LSDs. The results revealed that it is, in fact, a highly sensitive and suitable biomarker for diagnosis, drug screening and also for the monitoring of new therapies for the majority of LSDs. Chapter 4 investigated alterations in multiple lysosomal enzyme activities in the LSDs, and the possibility of using them for diagnosis, treatment monitoring and uncovering hitherto unidentified mechanisms of disease and potential drug targets. Chapter 5 demonstrated the power of electron microscopy for lipid characterisation in the majority of LSDs and confirmed in many cases that defective enzyme activities in chapter 4 did indeed lead to subsequent secondary lipid storage. Ca^{2+} and TEs were investigated in Chapter 6, and our results from these investigations highlighted the possibility of using ICP-MS for monitoring LSD treatment and the presence of a common abnormality in Zn^{2+} homeostasis across the LSDs. Finally, in Chapter 7 I was able to produce more evidence concerning the involvement of the NPC1 protein in Zn^{2+} transportation, and found evidence suggesting a loss of NPC1 function in the majority of LSDs.

8.2 Investigating the optimum conditions of lysotracker becoming a suitable biomarker for majority of LSDs

In this project, I had the opportunity to work on a broad range of LSDs to study whether it was possible to detect common phenotypes across the LSDs and, as a result, find suitable LSD biomarkers. Working on such large cohort of control and LSD cells was challenging but ultimately a very useful way to study the fundamental commonalities between the LSDs. I investigated whether it was possible to use a novel and simple fluorescence assay for detecting the majority of LSDs. I determined the most suitable conditions for loading cells with lysotracker for monitoring lysosomal expansion. Fixation was unsuitable as it leads to the loss of lysotracker fluorescence (Figure 3.2). Using a low concentration and a short incubation time for lysotracker should avoid lysosomal deacidification (Figure 3.4), which is known to induce abnormalities in lysosomal Ca^{2+} , endocytosis and lipid storage (Yoshimori et al. 1991). I discovered that lysotracker fluorescence correlates with lysosome expansion and substrate accumulation in the majority of LSDs (Figure 3.5) and now provides a clear methodology for the field so that artefactual results from lysotracker staining can be avoided. I have adapted

this method to ensure a high-throughput on LSDs' fibroblasts to detect the majority of diseases (Figure 3.7). I have also developed a potential magnetic capture assay that could be used in a clinical environment to monitor LSDs via patient blood samples. This assay requires further proof of concept work using a wide range of LSD blood samples, which may be available in future via a collaboration with the Metabolic clinic at the University Hospital Wales.

There are some LSDs that cannot be detected by lysotracker due to there being either a pH alteration in these diseases or a lack of accumulated storage within the lysosomes in fibroblasts (e.g. Gaucher). An ultrastructural examination of LSDs by electron microscopy showed the correlation between lysotracker signals and the level of storage substrates in LE/Lys. However, the exception was CLN10, which showed an accumulation of ganglioside and globoside by electron microscopy (Figure 5.6 O-S), but no increase in lysotracker, which was reduced compared to the control signal (Figure 3.10). From this it would be expected that there could be an elevation in intralysosomal pH in CLN10 disease. That could be proven by using exas Red-Dextran and FITC-Dextran for the pH measurement (see chapter 2, section 2.6.3).

In summary, lysotracker is a highly useful method for detecting lysosomal dysfunction in the majority of LSDs, and drug screening, superior to the current gold standard methods, such as elevation in levels of LAMPs (Figure 3.16). By looking at the potential for the clinical use of lysotracker, I discovered that detection of lysotracker by FACS analysis could be suitable for monitoring LSD treatment in the clinic. There are, however, limitations on the use of lysotracker on isolated B cells as first the cells must be stained and maintained as living cells, which restricts the usefulness of the assay in samples which are beyond 48h from original blood draw, also FACS requires expensive equipment and training while the high-throughput assay involves the use of a magnetic capture method where there is currently a lack of good standardization methods.

8.3 Secondary lysosomal enzyme alterations are a common feature of LSDs

Investigating multiple lysosomal activities across LSDs is crucial when trying to find a new approach to LSD biomarkers. I discovered that the activities of several enzymes are altered within each LSD (Figure 4.1). The data obtained from this large study on enzyme activity across LSDs has two major applications. In terms of LSD diagnosis, it could be used to generate a unique pattern of enzyme activities for either each disease or group of LSDs. That would be useful to design a multiplex assay that can diagnose each group of LSDs using characteristic patterns of changes in enzyme activity, and that would be useful for newborn

screening. There were some groups of LSDs that showed a consistent pattern of altered enzyme activities in all the diseases included in the group (Figure 4.1 B & C & D & F). For example, HexA and HexB activity are clearly and consistently elevated in the mucopolysaccharidoses in cells and tissues. HexA/B assays may therefore constitute a new clinical biomarker for the MPS group of diseases, where currently no broad biomarker exists for this family of diseases, discussed in more detail below. Further work is required, potentially in collaboration with a biostatistician, to determine the best 6 enzymes based on our studies to take forward for potential use in diagnostic multiplex assays.

The second main application of these findings is in understanding the underlying mechanisms of pathogenesis in these diseases. I was able to confirm some of our findings from patient fibroblasts in tissues from *Idua*^{-/-}, *Sgsh*^{-/-}, *Naglu*^{-/-} and *Npc1*^{-/-} mouse models (Figures 4.2 & 4.3). The HexA, HexB enzymes and Total Hex activity could be useful biochemical markers for monitoring treatment in the mucopolysaccharidoses. As I discussed in chapter 4, this upregulation of HexA, HexB and Total Hex enzymes might be due to these enzymes being affected by the accumulated GAGs in the mucopolysaccharidoses; a previous study on the *Hexa*^{-/-} *Hexb*^{-/-} double knockout mouse found a mucopolysaccharidoses-like phenotype (Sango et al. 1996). However, no increased GAGs storage is observed in *Hexb*^{-/-} mice; this could be due to the remaining isoenzyme activity of HexS is in the mutant mice (Neufeld 2001), which has been shown to degrade dermatan sulphate (Hepbildikler et al. 2002). This finding could be interesting when investigating the inhibition of the HexB enzyme in the mucopolysaccharidoses, to discover if this results in upregulation of HexS, thereby reducing storage and potentially explaining elevated values of HexA and HexB in the MPS cells. The different *Npc1*^{-/-} mouse tissues and fibroblasts from NPC patients with different mutations exhibited different patterns of enzyme activities, apart from the TPP1 enzyme, which was high across all *Npc1*^{-/-} mouse tissues and different NPC1 mutations (Figures 4.3 & 4.5). As TPP1 has recently been identified as an enzyme that cleaves lysosomal amyloid, this may be a mechanism for why Alzheimer like phenotypes and accumulation of amyloid fragments are observed in the NPC brain. Further testing of our major enzyme changes in multiple patients, tissues or biological samples would clearly be useful to increase the reliability and impact of the enzyme activity findings.

Previously, some genes with a direct cause of LSDs (e.g., *GBA1* mutations), have been identified as risk factors for Parkinson's disease. Here, I have found more evidence of the similarities between LSDs and diseases of ageing and other neurodegenerative disease, which would be due to the lysosome which are of fundamental importance in the pathophysiology of these diseases. The TPP1 lysosomal protease, which is involved in the

degradation of fibrillar A β , was upregulated not only in NPC1, but also across several LSDs (Supplementary figure 22) (Solé-Domènech et al. 2018). Loss of TPP1 activity leads to accumulation of SCMAS. The lipofuscin is observed not only in the NCLs but also in aged cells (Jolly et al. 1993). Therefore, the TPP1 enzyme upregulation may be the metabolic response to the accumulation of TPP1 substrates. The LAL enzymes were also defective across the majority of LSDs, and also in Alzheimer's and Huntington's diseases (Supplementary figure 24) where secondary storage of cholesterol and gangliosides have been reported (Trushina et al. 2006). Recent emerging data indicates the involvement of cholesterol metabolism in the pathogenesis of Alzheimer's disease (Kivipelto et al. 2001; Lütjohann and Von Bergmann 2003).

Finally, our preliminary data showed that correction of a secondary defect in enzyme activity can improve lysosomal storage so that, for example, LAL could indeed be useful for treatment purposes, thus opening up a potential new therapeutic avenue. I obtained a reduction in lysotracker (storage materials) in Wolman, NPC1 and CLN5 by using rhLAL (Figure 4.8). This proof of principle experiment indicates that there is scope for utilizing ERT, or small molecule enzyme chaperones, developed for primary defects of metabolism to potentially treat other LSDs where the enzymes are secondarily affected. This would constitute a new therapeutic avenue of research for the LSDs and could be more easily translated as in most cases already approved therapies would be repurposed.

8.4 Electron microscopy is one of the most useful tools for identifying secondary storage materials among LSDs

Using electron microscopy, I was able to investigate the storage of specific lipids among some LSDs. I identified the nature of the primary storage lipid in the majority of LSDs studied (Figure 5.2). This is the first study showing an accumulation of sphingosine-containing structures in NPC1 (Figure 5.3 V&X) and is the first study to identify the nature of lipid and polysaccharide storage bodies using primary storage diseases. Furthermore, I was then able to identify which lipid/sugar structures accumulated secondarily across LSD fibroblasts. The presences of ganglioside (in NPC1) and globoside (in CLN5) were identified by using the electro-immunolabelling method on the ultrathin section of NPC1 and CLN5 fibroblasts. The secondary storage materials I have seen in the electron microscope ultrastructure among several LSDs were mostly explained by deficiencies in the activities of lysosomal enzymes that break down that storage material (Table 5.3). However, some storage materials in LSDs were identified by electron microscopy, with no corresponding reduction in enzyme activity and even some elevations in activity. This can be explained by the possibility that an enzyme

is mislocalized, resulting in normal or even higher activity in the enzyme assay but an inability to degrade the substrate *in vivo*. A more detailed analysis will ultimately be required to compare the enzyme activities to the EM storage in order to target LSDs in which enzyme localization should be studied. These defects may benefit the most from small molecule chaperone therapy.

8.5 Trace elements are promising, but untested, biomarkers for LSDs.

Alterations in Ca^{2+} homeostasis have been reported among some LSDs (Lloyd-Evans 2016a; Lloyd-Evans et al. 2010). According to Lloyd-Evans *et al.*'s 2008 report, lysosomal Ca^{2+} reduction has been reported in NPC1 following sphingosine accumulation. In this study I expanded on this finding, which was restricted to only NPC1, by discovering a reduction in the lysosomal Ca^{2+} level in several LSDs (Figure 6.1). I also identified that Zn^{2+} storage is common within lysosomes across almost all LSDs, including NPC1 (Figure 6.2).

In addition to the upregulation in the TPP1 enzyme across all NPC1 mutations (Figure 4.4), our findings showed that Zn^{2+} storage is the second cellular phenotype present across all NPC1 mutations (Figure 6.7). This raises the possibility that Zn^{2+} may regulate the activity of TPP1, as this enzyme activity was also elevated across most of the other LSDs tested (apart from the NCLs). However, no information currently exists on the heavy metal dependence of this enzyme whilst dipeptidyl peptidases are known to be Zn^{2+} dependent (Baral et al. 2008; FUKASAWA et al. 1998). The lysotracker, filipin and other lysosomal enzymes were not identical across all NPC1 mutations. That finding of Zn^{2+} storage across NPC1 mutations; common or variant was supported by low Zn^{2+} levels in CSF samples obtained from NPC1 patients (Figure 6.12), indicating storage of Zn^{2+} within cells of the brain. There is, however, an exception of one patient, potentially being treated with miglustat, who has shown a normal level of Zn^{2+} . Of interest were the changes in selenium, which was high in cells but low in the medium and also non-existent in patient CSF. What role this plays in disease pathogenesis is unknown but the relationship between cellular and CSF data suggests an important function that needs following up. More access to more clinical samples would be useful to study the potential usefulness of ICP-MS to measure the TEs in LSDs for the diagnosis and treatment monitoring as I have done with CLN5 in the next section.

Alterations in other TEs, namely Cu^+ and Fe^{2+} , were detected in other LSDs using live probes (Figure 6.5 & Figure 6.6). Comparison of cellular and secreted TE levels in NPC fibroblasts suggested the possibility that LSD cells have a defect in TE secretion from lysosomes, and not in the filling of lysosomes with TEs (Figure 6.9 & Figure 6.10).

8.6 Combination of biomarkers showed the success of miglustat therapy on CLN5 patients

Our investigation of the common phenotypes across LSDs led to identification of a possible bioassay for following miglustat treatment of CLN5 patients. By EM I was able to detect the presence of secondary gangliosides and globoside structures in CLN5 patient fibroblasts and I confirmed the presence of Gb3 by using cryo-immunolabelling (Figure 5.7 A-C). Following miglustat treatment of CLN5 patient cells, the presence of large empty vacuoles and the elimination of storage material with the lysosomes was observed (Figure 5.7 D-G), confirming the reduction in lysotracker fluorescence (storage materials) observed following miglustat treatments (Supplementary 27). As part of a small off label safety study of miglustat in CLN5 patients I was able to use and validate a few enzymes that had been altered in CLN5 fibroblasts (Figure 4.1), to monitor changes in enzyme activities during the course of miglustat treatment in patient DBS samples. This clearly showed that GCCase activity, which is reduced in CLN5 disease, was responsive to the treatment and returned to normal reference range after 9 months of miglustat treatment (Figure 4.7). I also demonstrated the potential use of TE analysis by ICP-MS using patients' serum/blood to monitor the effects of miglustat on CLN5 disease progression. In particular, it showed that miglustat normalized Mn levels in the blood of CLN5 patients within 9 months of treatment (Figure 6.13). These findings raise the exciting possibility of the existence of a link between mutations in *GBA1*, which is the gene that encodes GCCase and is a genetic risk factor for developing Parkinson's disease, and Mn being elevated in Parkinson's disease (Neudorfer et al. 1996), particularly Mn induced Parkinson's. There are several other genes associated with an increased risk of Parkinson's disease; these include the *ATP13A2* gene (Bras et al. 2012), which regulates Mn homeostasis and contributes to NCLs, further suggesting links between NCLs, Mn, GCCase and Parkinson's. However, further study is required to gain a deeper understanding of the mechanisms behind these potential links. This finding is particularly encouraging for the treatment of other forms of NCLs with miglustat as, according to our knowledge, this is possibly the first viable small molecule treatment for all NCLs in which I have observed GSL accumulation (CLN3, CLN5 and CLN10 tested in this thesis).

From the biomarker development view, the key finding is that a combination of biomarkers, lysotracker, enzyme activity, TEs and electron microscope ultrastructure were capable of monitoring phenotypic improvement following miglustat treatment in CLN5 patients. This is a good example of how the combination of biomarkers could be useful in treatment monitoring and is a validation of our decision to focus on these assays.

8.7 NPC1 protein defect is associated with the presence of secondary Zn²⁺ and storage phenotypes across the majority of LSDs and may constitute a common therapeutic target for the LSD family.

Loss of function of the NPC1 protein leads to low lysosomal Ca²⁺ content due to a failure to fill the lysosome with Ca²⁺, resulting in defects in Ca²⁺ release. This results in a defect in LE/Lys fusion and, consequently, to multiple lipid storage (Lloyd-Evans et al. 2008). NPC1 is also suggested to be involved in the transport of sphingosine from the lysosome (Lloyd-Evans et al. 2008; Lloyd-Evans and Platt 2010). New findings have shown that NPC1 binds to Zn²⁺ and may directly pump Zn²⁺ out of lysosomes to the cytosol (Maguire 2017). Lysosomal Ca²⁺ defects and Zn²⁺ storage have been discovered among several LSDs (Figure 6.1 & 6.3). The accumulation of SLs is common in several LSDs, which I have confirmed by electron microscopy, where I see the accumulation of multilamellar-like whorl structures in the majority of LSDs (Table 5.2). Imaging of fixed cells revealed intralysosomal accumulation of ganglioside GM1 (indicated by elevated CtxB staining) and unesterified cholesterol (indicated by elevated filipin staining) in several LSDs, including NPC (Figure 7.1). Therefore, the NPC cellular phenotype (uniquely characterized by presence of sphingosine, cholesterol, GSLs, sphingomyelin and low lysosomal Ca²⁺) is common across several LSDs, suggesting a reduction in NPC1 function in these diseases. This is supported by the overexpression of NPC1 in several LSDs, possibly due to cells attempting to overcome its reduced activity (Figure 7.5). Further investigation showed that normalization of cholesterol accumulation, by depleting cellular cholesterol levels via growth in LPDS, leads to the correction of NPC1 localisation and reduction of lysosomal Zn²⁺ storage in all LSDs tested bar NPC1 deficiency itself. There are a few diseases such as Farber, Krabbe, MPS I and MPS IIIA that have shown a normal Zn²⁺ distribution (Figure 6.3). Inhibition of NPC1 function by U18666A leads to Zn²⁺, cholesterol accumulation and lysosome expansion in Krabbe disease demonstrating that NPC phenotypes can be induced in Krabbe (Figure 7.8). The addition of psychosine to Krabbe fibroblasts also leads to Zn²⁺ storage (Figure 7.9), indicating that it is the absence of storage that results in no phenotype being observed in Krabbe patient fibroblasts. Addition of lyso-SLs to control fibroblasts also induced lysosomal Zn²⁺ storage and increased levels of anti-NPC1 (Figure 7.7 A-D). That would suggest those diseases with normal Zn²⁺ and Ca²⁺ presumably do not accumulate high enough level of lyso-lipids in the fibroblast cell lines in order to be able to interfere/bind with NPC1. These findings strongly indicate that NPC1 is involved in the efflux of Zn²⁺ and sphingoid bases from the lysosome, and that it is inhibited by storage material in the majority of LSDs. Indeed, a recent paper has modelled the NPC1 protein binding to sphingosine within the hydrophobic transport cavity of NPC1 (Wheeler et al. 2019). This has obvious implications for therapy, with treatments that increase NPC1 activity likely to be

beneficial across the majority of LSDs. I suggested using miglustat, which is indeed useful for decreasing the SL biosynthesis and therefore reducing the lyso-SLs generation and subsequent inhibition of the NPC1 protein, which may correct some LSD phenotypes in the same way as the Fabry and CLN5 treatment with miglustat has been shown to do in this study (Figure 7.12).

Interestingly, the TRPML1 channel has been suggested to be the lysosomal Zn^{2+} channel (Eichelsdoerfer et al. 2010). However, increasing TRPML1 activity using MLSA1 does not correct lysosomal Zn^{2+} storage in NPC1 (Figure 7.2). The findings from our study of MLIV, which is the LSD caused by genetic loss of TRPML1 function, have, however, shown that there is a noticeable decrease in lysosomal Zn^{2+} levels in MLIV cells treated with D-NMAPPD (inhibitor of acid ceramidase function), thereby reducing the accumulation of sphingoid bases (Figure 7.11) that most likely emerge from ganglioside storage reported in these cells (Bach et al. 1975). This presumably means the Zn^{2+} storage in MLIV is not just TRPML1 function dependent, but also depends upon the function of NPC1. Therefore, both findings suggested the TRPML 1 is possibly not the primary Zn^{2+} channel in LE/Lys.

8.8 Concluding remarks

To conclude this thesis, I have developed and fully characterized a simple fluorimetric test for LE/Lys swelling to identify, monitor and develop therapies for the majority of LSDs. I also present the first in depth analysis of secondary alterations in the activities of lysosomal enzymes across a panel of cells covering the majority of LSDs, and the use of electron microscopy led to the discovery that secondary storage material in LSDs is correlated with the secondary changes in lysosomal enzymes. Changes in TEs were also detected in several LSDs, and could indeed be suitable biomarkers for monitoring treatment, as demonstrated by the reduction in Mn in CLN5 patients following miglustat treatment. The NPC1 protein defect in LSDs may explain the Zn^{2+} and other secondary storage materials in LSDs, and constitutes a novel pan-LSD therapeutic target. Future work will involve greater access to clinical samples to validate the new biomarkers and electron microscopy findings, and designing more experiments to understand the mechanisms behind the secondary lysosomal enzyme alterations in LSDs. Further investigation into the NPC1 defect in LSDs, using LSD animal models, is also required.

Chapter 9: References

- Aerts, J. et al. 2005. Identification and use of biomarkers in Gaucher disease and other lysosomal storage diseases. *Acta Paediatrica* 94, pp. 43-46.
- Aerts, J. M. et al. 2008. Elevated globotriaosylsphingosine is a hallmark of Fabry disease. *Proceedings of the National Academy of Sciences* 105(8), pp. 2812-2817.
- Aerts, J. M. et al. 2011. Biomarkers in the diagnosis of lysosomal storage disorders: proteins, lipids, and inhibodies. *Journal of inherited metabolic disease* 34(3), pp. 605-619.
- Aguisanda, F. et al. 2017. Neural stem cells for disease modeling of Wolman disease and evaluation of therapeutics. *Orphanet journal of rare diseases* 12(1), p. 120.
- Alattia, J.-R. et al. 2006. Direct visualization of saposin remodelling of lipid bilayers. *Journal of molecular biology* 362(5), pp. 943-953.
- Alattia, J.-R. et al. 2007. Molecular imaging of membrane interfaces reveals mode of β -glucosidase activation by saposin C. *Proceedings of the National Academy of Sciences* 104(44), pp. 17394-17399.
- Alberts, B. 2017. *Molecular Biology of the Cell*. Garland Science, p. 1 online resource (1464 pages).
- Alberts, B. et al. 2002. Transport from the trans Golgi network to lysosomes. *Molecular Biology of the Cell*. 4th edition. Garland Science.
- Alfonso, P. et al. 2005. Miglustat (NB-DNJ) works as a chaperone for mutated acid β -glucosidase in cells transfected with several Gaucher disease mutations. *Blood Cells, Molecules, and Diseases* 35(2), pp. 268-276.
- Alroy, J. et al. 2013. Electron microscopy as a useful tool in the diagnosis of lysosomal storage diseases. *Diagnostic Electron Microscopy: A Practical Guide to Interpretation and Technique*. West Sussex, UK: Wiley, pp. 237-267.
- Alroy, J. and Ucci, A. A. 2006. Skin biopsy: a useful tool in the diagnosis of lysosomal storage diseases. *Ultrastructural pathology* 30(6), pp. 489-503.
- Amaral, O. et al. 1994. Molecular characterisation of type 1 Gaucher disease families and patients: intrafamilial heterogeneity at the clinical level. *Journal of medical genetics* 31(5), pp. 401-404.
- Amritraj, A. et al. 2009. Increased activity and altered subcellular distribution of lysosomal enzymes determine neuronal vulnerability in Niemann-Pick type C1-deficient mice. *The American journal of pathology* 175(6), pp. 2540-2556.
- An, Y. et al. 2005. Glucose tetrasaccharide as a biomarker for monitoring the therapeutic response to enzyme replacement therapy for Pompe disease. *Molecular genetics and metabolism* 85(4), pp. 247-254.
- Aschner, J. L. and Aschner, M. 2005. Nutritional aspects of manganese homeostasis. *Molecular aspects of medicine* 26(4-5), pp. 353-362.

- Aslanidis, C. et al. 1994. Genomic organization of the human lysosomal acid lipase gene (LIPA). *Genomics* 20(2), pp. 329-331.
- Atakpa, P. et al. 2019. GPN does not release lysosomal Ca²⁺ but evokes Ca²⁺ release from the ER by increasing the cytosolic pH independently of cathepsin C. *J Cell Sci* 132(3), p. jcs223883.
- Au, C. et al. 2008. Manganese transport in eukaryotes: the role of DMT1. *Neurotoxicology* 29(4), pp. 569-576.
- Auburger, G. et al. 2012. Primary skin fibroblasts as a model of Parkinson's disease. *Molecular neurobiology* 46(1), pp. 20-27.
- Aula, P. et al. 1979. 'Salla Disease': A New Lysosomal Storage Disorder. *Archives of Neurology* 36(2), pp. 88-94.
- Aureli, M. et al. 2016. Unravelling the role of sphingolipids in cystic fibrosis lung disease. *Chemistry and physics of lipids* 200, pp. 94-103.
- Avila, J. and Convit, J. 1975. Inhibition of leucocytic lysosomal enzymes by glycosaminoglycans in vitro. *Biochemical Journal* 152(1), pp. 57-64.
- Avrahami, L. et al. 2013. Inhibition of Glycogen Synthase Kinase-3 Ameliorates β -Amyloid Pathology and Restores Lysosomal Acidification and Mammalian Target of Rapamycin Activity in the Alzheimer Disease Mouse Model IN VIVO AND IN VITRO STUDIES. *Journal of Biological Chemistry* 288(2), pp. 1295-1306.
- Aydemir, T. B. et al. 2009. Zinc transporter ZIP8 (SLC39A8) and zinc influence IFN- γ expression in activated human T cells. *Journal of leukocyte biology* 86(2), pp. 337-348.
- Bach, G. et al. 1999. Elevated lysosomal pH in Mucopolidosis type IV cells. *Clinica Chimica Acta* 280(1-2), pp. 173-179.
- Bach, G. et al. 1975. Abnormal ganglioside accumulation in cultured fibroblasts from patients with mucopolidosis IV. *Biochemical and biophysical research communications* 66(4), pp. 1483-1490.
- Bagshaw, R. D. et al. 2005. Lysosomal membrane proteomics and biogenesis of lysosomes. *Molecular neurobiology* 32(1), pp. 27-41.
- Ballabio, A. 2016. The awesome lysosome. *EMBO molecular medicine* 8(2), pp. 73-76.
- Ballabio, A. and Gieselmann, V. 2009. Lysosomal disorders: from storage to cellular damage. *Biochimica et Biophysica Acta (BBA)-Molecular Cell Research* 1793(4), pp. 684-696.
- Bar-Peled, L. and Sabatini, D. M. 2014. Regulation of mTORC1 by amino acids. *Trends in cell biology* 24(7), pp. 400-406.
- Baral, P. K. et al. 2008. The first structure of dipeptidyl-peptidase III provides insight into the catalytic mechanism and mode of substrate binding. *Journal of Biological Chemistry* 283(32), pp. 22316-22324.
- Bargal, R. and Bach, G. 1997. Mucopolidosis type IV: abnormal transport of lipids to lysosomes. *Journal of inherited metabolic disease* 20(5), pp. 625-632.

- Bartke, N. and Hannun, Y. A. 2009. Bioactive sphingolipids: metabolism and function. *Journal of lipid research* 50(Supplement), pp. S91-S96.
- Barton, N. W. et al. 1991. Replacement therapy for inherited enzyme deficiency—macrophage-targeted glucocerebrosidase for Gaucher's disease. *New England Journal of Medicine* 324(21), pp. 1464-1470.
- Barton, N. W. et al. 1990. Therapeutic response to intravenous infusions of glucocerebrosidase in a patient with Gaucher disease. *Proceedings of the National Academy of Sciences* 87(5), pp. 1913-1916.
- Baumkötter, J. and Michael, C. 1983. Decreased ganglioside neuraminidase activity in fibroblasts from mucopolysaccharidosis patients Inhibition of the activity in vitro by sulfated glycosaminoglycans and other compounds. *Biochimica et Biophysica Acta (BBA)-General Subjects* 761(2), pp. 163-170.
- Bayleran, J. et al. 1987. Tay-Sachs disease with hexosaminidase A: characterization of the defective enzyme in two patients. *American journal of human genetics* 41(4), p. 532.
- Beckenkamp, A. et al. 2015. Differential expression and enzymatic activity of DPPIV/CD26 affects migration ability of cervical carcinoma cells. *PloS one* 10(7), p. e0134305.
- Becker, E. 1999. *Magnetic isolation of lysosomes from human fibroblasts: characterization of the lipid pattern*. Rheinische Friedrich-Wilhelms-Universität zu Bonn.
- Belcher, R. 1972. Ultrastructure and cytochemistry of lymphocytes in the genetic mucopolysaccharidoses. *Archives of pathology* 93(1), p. 1.
- Beltroy, E. P. et al. 2005. Cholesterol accumulation and liver cell death in mice with Niemann-Pick type C disease. *Hepatology* 42(4), pp. 886-893.
- Bembi, B. et al. 2008. Diagnosis of glycogenosis type II. *Neurology* 71(23 suppl 2), pp. S4-S11.
- Bergy, M. E. and Eble, T. E. 1968. Filipin complex. *Biochemistry* 7(2), pp. 653-659.
- Berridge, M. J. et al. 2000. The versatility and universality of calcium signalling. *Nature reviews Molecular cell biology* 1(1), p. 11.
- Bhaumik, M. et al. 1999. A mouse model for mucopolysaccharidosis type III A (Sanfilippo syndrome). *Glycobiology* 9(12), pp. 1389-1396.
- Biffi, A. et al. 2013. Lentiviral hematopoietic stem cell gene therapy benefits metachromatic leukodystrophy. *Science* 341(6148), p. 1233158.
- Blaby-Haas, C. E. and Merchant, S. S. 2014. Lysosome-related organelles as mediators of metal homeostasis. *Journal of Biological Chemistry* 289(41), pp. 28129-28136.
- Blanz, J. et al. 2015. Mannose 6-phosphate-independent Lysosomal Sorting of LIMP-2. *Traffic* 16(10), pp. 1127-1136.
- Bobillo Lobato, J. et al. 2016. Biomarkers in lysosomal storage diseases. *Diseases* 4(4), p. 40.

- Bolognin, S. et al. 2009. Metal ion physiopathology in neurodegenerative disorders. *Neuromolecular medicine* 11(4), pp. 223-238.
- Boot, R. G. et al. 1998. The human chitotriosidase gene nature of inherited enzyme deficiency. *Journal of Biological Chemistry* 273(40), pp. 25680-25685.
- Boot, R. G. et al. 2004. Marked elevation of the chemokine CCL18/PARC in Gaucher disease: a novel surrogate marker for assessing therapeutic intervention. *Blood* 103(1), pp. 33-39.
- Bounford, K. M. and Gissen, P. 2014. Genetic and laboratory diagnostic approach in Niemann Pick disease type C. *Journal of neurology* 261(2), pp. 569-575.
- Boustany, R.-M. N. et al. 1990. Ultrastructural findings in skin from patients with Niemann-Pick disease, type C. *Pediatric neurology* 6(3), pp. 177-183.
- Bradbury, A. et al. 2016. Cerebrospinal fluid calbindin D concentration as a biomarker of cerebellar disease progression in Niemann-Pick type C1 disease. *Journal of Pharmacology and Experimental Therapeutics* 358(2), pp. 254-261.
- Brailoiu, E. et al. 2009. Essential requirement for two-pore channel 1 in NAADP-mediated calcium signaling. *The Journal of cell biology* 186(2), pp. 201-209.
- Bramwell, K. K. et al. 2014. Lysosomal β -glucuronidase regulates Lyme and rheumatoid arthritis severity. *The Journal of clinical investigation* 124(1), pp. 311-320.
- Brandt, A. M. 1978. Racism and research: the case of the Tuskegee Syphilis Study. *Hastings center report* 8(6), pp. 21-29.
- Bras, J. et al. 2012. Mutation of the parkinsonism gene ATP13A2 causes neuronal ceroid-lipofuscinosis. *Human molecular genetics* 21(12), pp. 2646-2650.
- Braulke, T. and Bonifacino, J. S. 2009. Sorting of lysosomal proteins. *Biochimica et Biophysica Acta (BBA)-Molecular Cell Research* 1793(4), pp. 605-614.
- Bright, N. A. et al. 2016. Endolysosomes are the principal intracellular sites of acid hydrolase activity. *Current Biology* 26(17), pp. 2233-2245.
- Broadhead, D. and Butterworth, J. 1977. The diagnosis of Gaucher's disease in liver using 4-methylumbelliferyl-beta-D-glucopyranoside. *Clinica chimica acta; international journal of clinical chemistry* 75(1), pp. 155-161.
- Broadhead, D. and Butterworth, J. 1978. Pompe's disease: Diagnosis in kidney and leucocytes using 4-methylumbelliferyl- α -D-glucopyranoside. *Clinical genetics* 13(6), pp. 504-510.
- Brooks, D. et al. 2007. I-cell disease. *Lysosomal Storage Disorders*. Springer, pp. 529-537.
- Brooks, D. A. 1997. Protein processing: a role in the pathophysiology of genetic disease. *FEBS letters* 409(2), pp. 115-120.
- Brown, M. S. and Goldstein, J. L. 1997. The SREBP pathway: regulation of cholesterol metabolism by proteolysis of a membrane-bound transcription factor. *Cell* 89(3), pp. 331-340.

- Brunngraber, E. G. et al. 1973. Altered levels of tissue glycoproteins, gangliosides, glycosaminoglycans and lipids in Niemann-Pick's disease. *Clinica Chimica Acta* 48(2), pp. 173-181.
- Brzoska, M. et al. 2000. Effect of short-term ethanol administration on cadmium retention and bioelement metabolism in rats continuously exposed to cadmium. *Alcohol and Alcoholism* 35(5), pp. 439-445.
- Bush, A. I. et al. 1994. Modulation of A beta adhesiveness and secretase site cleavage by zinc. *Journal of Biological Chemistry* 269(16), pp. 12152-12158.
- Bygrave, F. L. and Benedetti, A. 1996. What is the concentration of calcium ions in the endoplasmic reticulum? *Cell calcium* 19(6), pp. 547-551.
- Calcraft, P. J. et al. 2009. NAADP mobilizes calcium from acidic organelles through two-pore channels. *Nature* 459(7246), p. 596.
- Camargo, F. et al. 2001. Cyclodextrins in the treatment of a mouse model of Niemann-Pick C disease. *Life sciences* 70(2), pp. 131-142.
- Cantz, M. and Ulrich-Bott, B. 1990. Disorders of glycoprotein degradation. *Journal of inherited metabolic disease* 13(4), pp. 523-537.
- Canuel, M. et al. 2008. Sortilin mediates the lysosomal targeting of cathepsins D and H. *Biochemical and biophysical research communications* 373(2), pp. 292-297.
- Cao, Q. et al. 2015. BK channels alleviate lysosomal storage diseases by providing positive feedback regulation of lysosomal Ca²⁺ release. *Developmental cell* 33(4), pp. 427-441.
- Cao, Y. et al. 2006. Autophagy is disrupted in a knock-in mouse model of juvenile neuronal ceroid lipofuscinosis. *Journal of Biological Chemistry* 281(29), pp. 20483-20493.
- Carstea, E. D. et al. 1997. Niemann-Pick C1 disease gene: homology to mediators of cholesterol homeostasis. *Science* 277(5323), pp. 228-231.
- Carstea, E. D. et al. 1993. Linkage of Niemann-Pick disease type C to human chromosome 18. *Proceedings of the National Academy of Sciences* 90(5), pp. 2002-2004.
- Caspersson, T. et al. 1970. Analysis of human metaphase chromosome set by aid of DNA-binding fluorescent agents. *Experimental cell research* 62(2-3), pp. 490-492.
- Caudron, E. et al. 2015. Enzymatic diagnosis of Fabry disease using a fluorometric assay on dried blood spots: an alternative methodology. *European journal of medical genetics* 58(12), pp. 681-684.
- Cermak, S. et al. 2016. Loss of Cathepsin B and L leads to lysosomal dysfunction, NPC-Like cholesterol sequestration and accumulation of the key Alzheimer's proteins. *PloS one* 11(11), p. e0167428.
- Chamoles, N. A. et al. 2001a. Diagnosis of α -L-iduronidase deficiency in dried blood spots on filter paper: the possibility of newborn diagnosis. *Clinical chemistry* 47(4), pp. 780-781.
- Chamoles, N. A. et al. 2002a. Gaucher and Niemann-Pick diseases—enzymatic diagnosis in dried blood spots on filter paper: retrospective diagnoses in newborn-screening cards. *Clinica chimica acta* 317(1-2), pp. 191-197.

- Chamoles, N. A. et al. 2002b. Tay-Sachs and Sandhoff diseases: enzymatic diagnosis in dried blood spots on filter paper: retrospective diagnoses in newborn-screening cards. *Clinica chimica acta* 318(1-2), pp. 133-137.
- Chamoles, N. A. et al. 2001b. Retrospective diagnosis of GM1 gangliosidosis by use of a newborn-screening card. *Clinical chemistry* 47(11), pp. 2068-2068.
- Chandler, R. J. et al. 2016. Systemic AAV9 gene therapy improves the lifespan of mice with Niemann-Pick disease, type C1. *Human molecular genetics* 26(1), pp. 52-64.
- Chandrachud, U. et al. 2015. Unbiased cell-based screening in a neuronal cell model of Batten disease highlights an interaction between Ca²⁺ homeostasis, autophagy, and CLN3 protein function. *Journal of Biological Chemistry* 290(23), pp. 14361-14380.
- Chang, M. H. et al. 2000. Saposins A, B, C, and D in plasma of patients with lysosomal storage disorders. *Clinical chemistry* 46(2), pp. 167-174.
- Chang, T. et al. 1997. Acyl-coenzyme A: cholesterol acyltransferase. *Annual review of biochemistry* 66(1), pp. 613-638.
- Chapel, A. et al. 2013. An extended proteome map of the lysosomal membrane reveals novel potential transporters. *Molecular & Cellular Proteomics* 12(6), pp. 1572-1588.
- Chartier-Harlin, M.-C. et al. 1991. Early-onset Alzheimer's disease caused by mutations at codon 717 of the β -amyloid precursor protein gene. *Nature* 353(6347), p. 844.
- Chavez-Crooker, P. et al. 2001. Copper transport by lobster hepatopancreatic epithelial cells separated by centrifugal elutriation: measurements with the fluorescent dye Phen Green. *Journal of Experimental Biology* 204(8), pp. 1433-1444.
- Chen, C.-S. et al. 2000. Probing the cathepsin D using a BODIPY FL-pepstatin A: applications in fluorescence polarization and microscopy. *Journal of biochemical and biophysical methods* 42(3), pp. 137-151.
- Chen, C.-S. et al. 1999. Broad screening test for sphingolipid-storage diseases. *The Lancet* 354(9182), pp. 901-905.
- Chen, R. et al. 2014. The general amino acid control pathway regulates mTOR and autophagy during serum/glutamine starvation. *J Cell Biol* 206(2), pp. 173-182.
- Chen, X. et al. 2015. Lysosomal targeting with stable and sensitive fluorescent probes (Superior LysoProbes): applications for lysosome labeling and tracking during apoptosis. *Scientific reports* 5, p. 9004.
- Cheng, X. et al. 2010. Mucolipins: intracellular TRPML1-3 channels. *FEBS letters* 584(10), pp. 2013-2021.
- Chiang, S.-C. et al. 2012. Algorithm for Pompe disease newborn screening: results from the Taiwan screening program. *Molecular genetics and metabolism* 106(3), pp. 281-286.
- Chien, Y.-H. et al. 2013. Pompe disease: early diagnosis and early treatment make a difference. *Pediatrics & Neonatology* 54(4), pp. 219-227.

- Chikte, S. et al. 2014. Use of LysoTracker dyes: a flow cytometric study of autophagy. *Cytometry Part A* 85(2), pp. 169-178.
- Choudhury, A. et al. 2002. Rab proteins mediate Golgi transport of caveola-internalized glycosphingolipids and correct lipid trafficking in Niemann-Pick C cells. *The Journal of clinical investigation* 109(12), pp. 1541-1550.
- Christensen, K. A. et al. 2002. pH-dependent regulation of lysosomal calcium in macrophages. *Journal of cell science* 115(3), pp. 599-607.
- Christine, V. and Ponchel, G. 2017. Polymer nanoparticles for nanomedicines. A guide for their design. *Anticancer Res* 37, p. 1544.
- Chuang, W.-L. et al. 2014. Lyso-sphingomyelin is elevated in dried blood spots of Niemann-Pick B patients. *Molecular genetics and metabolism* 111(2), pp. 209-211.
- Chuang, W.-L. et al. 2013. Determination of psychosine concentration in dried blood spots from newborns that were identified via newborn screening to be at risk for Krabbe disease. *Clinica chimica acta* 419, pp. 73-76.
- Churchill, G. C. et al. 2002. NAADP mobilizes Ca²⁺ from reserve granules, lysosome-related organelles, in sea urchin eggs. *Cell* 111(5), pp. 703-708.
- Claus, V. et al. 1998. Lysosomal enzyme trafficking between phagosomes, endosomes, and lysosomes in J774 macrophages enrichment of cathepsin H in early endosomes. *Journal of Biological Chemistry* 273(16), pp. 9842-9851.
- Colacurcio, D. J. and Nixon, R. A. 2016. Disorders of lysosomal acidification—The emerging role of v-ATPase in aging and neurodegenerative disease. *Ageing research reviews* 32, pp. 75-88.
- Comings, D. E. et al. 1975. Mechanisms of chromosome banding. *Chromosoma* 50(2), pp. 111-145.
- Connolly, G. P. 1998. Fibroblast models of neurological disorders: fluorescence measurement studies. *Trends in pharmacological sciences* 19(5), pp. 171-177.
- Constantopoulos, G. and Dekaban, A. S. 1978. Neurochemistry of the mucopolysaccharidoses: brain lipids and lysosomal enzymes in patients with four types of mucopolysaccharidosis and in normal controls. *Journal of neurochemistry* 30(5), pp. 965-973.
- Cooper, G. M. et al. 2000. *The cell: a molecular approach*. ASM press Washington, DC.
- Coutinho, M. et al. 2016. Less is more: substrate reduction therapy for lysosomal storage disorders. *International journal of molecular sciences* 17(7), p. 1065.
- Coutinho, M. F. et al. 2012. Mannose-6-phosphate pathway: a review on its role in lysosomal function and dysfunction. *Molecular genetics and metabolism* 105(4), pp. 542-550.
- Coward, J. et al. 2009. Safingol (L-threo-sphinganine) induces autophagy in solid tumor cells through inhibition of PKC and the PI3-kinase pathway. *Autophagy* 5(2), pp. 184-193.
- Cox, T. et al. 2000. Novel oral treatment of Gaucher's disease with N-butyldeoxynojirimycin (OGT 918) to decrease substrate biosynthesis. *The Lancet* 355(9214), pp. 1481-1485.

- Cox, T. M. and Cachón-González, M. B. 2012. The cellular pathology of lysosomal diseases. *The Journal of pathology* 226(2), pp. 241-254.
- Creasy, B. M. et al. 2007. New assay using fluorogenic substrates and immunofluorescence staining to measure cysteine cathepsin activity in live cell subpopulations. *Cytometry Part A: the journal of the International Society for Analytical Cytology* 71(2), pp. 114-123.
- Crumling, M. A. et al. 2012. Hearing loss and hair cell death in mice given the cholesterol-chelating agent hydroxypropyl- β -cyclodextrin. *PloS one* 7(12), p. e53280.
- Cuajungco, M. P. et al. 2014. Cellular zinc levels are modulated by TRPML1–TMEM163 interaction. *Traffic* 15(11), pp. 1247-1265.
- Czartoryska, B. et al. 1998. Serum chitotriosidase activity in Gaucher patients on enzyme replacement therapy (ERT). *Clinical biochemistry* 31(5), pp. 417-420.
- d'Azzo, A. et al. 1982. Molecular defect in combined beta-galactosidase and neuraminidase deficiency in man. *Proceedings of the National Academy of Sciences* 79(15), pp. 4535-4539.
- Darzynkiewicz, Z. and Kapuscinski, J. 1990. Acridine orange: a versatile probe of nucleic acids and other cell constituents. *Flow cytometry and sorting* 2, pp. 291-314.
- Davidson, C. D. et al. 2009. Chronic cyclodextrin treatment of murine Niemann-Pick C disease ameliorates neuronal cholesterol and glycosphingolipid storage and disease progression. *PloS one* 4(9), p. e6951.
- Davies, J. P. et al. 2000. Transmembrane molecular pump activity of Niemann-Pick C1 protein. *Science* 290(5500), pp. 2295-2298.
- Davies, J. P. and Ioannou, Y. A. 2000. Topological analysis of Niemann-Pick C1 protein reveals that the membrane orientation of the putative sterol-sensing domain is identical to those of 3-hydroxy-3-methylglutaryl-CoA reductase and sterol regulatory element binding protein cleavage-activating protein. *Journal of Biological Chemistry* 275(32), pp. 24367-24374.
- De Bruijn, W. and Den Breejen, P. 1974. Selective glycogen contrast by hexavalent osmium oxide compounds. *Histochem J* 6, pp. 61-62.
- de Duve, C. 1959. Lysosomes, a new group of cytoplasmic particles. *Subcellular particles* 60, pp. 128-159.
- De Duve, C. ed. 1963. *The lysosome concept*. Ciba Foundation Symposium-Anterior Pituitary Secretion (Book I of Colloquia on Endocrinology). Wiley Online Library.
- De Jong, J. et al. 1989. Dimethylmethylene blue-based spectrophotometry of glycosaminoglycans in untreated urine: a rapid screening procedure for mucopolysaccharidoses. *Clinical chemistry* 35(7), pp. 1472-1477.
- de Mello, A. et al. 2011. Effect of one year of cryopreservation on the activity of lysosomal hydrolases from EBV-transformed lymphocytes. *BioMed Research International* 2011.
- De Mello, A. et al. 2010. Feasibility of using cryopreserved lymphoblastoid cells to diagnose some lysosomal storage diseases. *Cell proliferation* 43(2), pp. 164-169.

- de Ruijter, J. et al. 2012a. Heparan sulfate and dermatan sulfate derived disaccharides are sensitive markers for newborn screening for mucopolysaccharidoses types I, II and III. *Molecular genetics and metabolism* 107(4), pp. 705-710.
- de Ruijter, J. et al. 2012b. Genistein in Sanfilippo disease: a randomized controlled crossover trial. *Annals of neurology* 71(1), pp. 110-120.
- Dean, K. M. et al. 2012. Visualizing metal ions in cells: an overview of analytical techniques, approaches, and probes. *Biochimica et Biophysica Acta (BBA)-Molecular Cell Research* 1823(9), pp. 1406-1415.
- Deegan, P. B. et al. 2005. Clinical evaluation of chemokine and enzymatic biomarkers of Gaucher disease. *Blood Cells, Molecules, and Diseases* 35(2), pp. 259-267.
- Desnick, R. et al. 2001. The metabolic and molecular bases of inherited disease. by Scriver CR, Beaudet AL, Sly WS, Valle D., McGraw-Hill, New York, pp. 3733-3774.
- Devlin, C. et al. 2010. Improvement in lipid and protein trafficking in Niemann-Pick C1 cells by correction of a secondary enzyme defect. *Traffic* 11(5), pp. 601-615.
- Di Giacomo, R. et al. 2015. Protracted late infantile ceroid lipofuscinosis due to TPP1 mutations: Clinical, molecular and biochemical characterization in three sibs. *Journal of the neurological sciences* 356(1-2), pp. 65-71.
- di Ronza, A. et al. 2018. CLN8 is an endoplasmic reticulum cargo receptor that regulates lysosome biogenesis. *Nature cell biology* 20(12), p. 1370.
- Dittmer, F. et al. 1999. Alternative mechanisms for trafficking of lysosomal enzymes in mannose 6-phosphate receptor-deficient mice are cell type-specific. *Journal of cell science* 112(10), pp. 1591-1597.
- Dong, X.-P. et al. 2008. The type IV mucopolysaccharidosis-associated protein TRPML1 is an endolysosomal iron release channel. *Nature* 455(7215), p. 992.
- Dong, X.-p. et al. 2010. PI (3, 5) P 2 controls membrane trafficking by direct activation of mucopolin Ca²⁺ release channels in the endolysosome. *Nature communications* 1, p. 38.
- Donida, B. et al. 2017. Oxidative damage and redox in lysosomal storage disorders: Biochemical markers. *Clinica Chimica Acta* 466, pp. 46-53.
- Duvvuri, M. et al. 2004. Weak base permeability characteristics influence the intracellular sequestration site in the multidrug-resistant human leukemic cell line HL-60. *Journal of Biological Chemistry* 279(31), pp. 32367-32372.
- Eichelsdoerfer, J. L. et al. 2010. Zinc dyshomeostasis is linked with the loss of mucopolysaccharidosis IV-associated TRPML1 ion channel. *Journal of Biological Chemistry* 285(45), pp. 34304-34308.
- Eskelinen, E.-L. 2006. Roles of LAMP-1 and LAMP-2 in lysosome biogenesis and autophagy. *Molecular aspects of medicine* 27(5-6), pp. 495-502.
- Falcón-Pérez, J. M. and Dell'Angelica, E. C. 2007. Zinc transporter 2 (SLC30A2) can suppress the vesicular zinc defect of adaptor protein 3-depleted fibroblasts by promoting zinc accumulation in lysosomes. *Experimental cell research* 313(7), pp. 1473-1483.

- Fan, J.-Q. et al. 1999. Accelerated transport and maturation of lysosomal α -galactosidase A in Fabry lymphoblasts by an enzyme inhibitor. *Nature medicine* 5(1), p. 112.
- Fan, M. et al. 2013. Identification of Niemann-Pick C1 disease biomarkers through sphingolipid profiling. *Journal of lipid research* 54(10), pp. 2800-2814.
- Fernández-Marmiesse, A. et al. 2014. Assessment of a targeted resequencing assay as a support tool in the diagnosis of lysosomal storage disorders. *Orphanet journal of rare diseases* 9(1), p. 59.
- Ferraz, M. J. et al. 2016. Lysosomal glycosphingolipid catabolism by acid ceramidase: formation of glycosphingoid bases during deficiency of glycosidases. *FEBS letters* 590(6), pp. 716-725.
- Ferreira, C. R. and Gahl, W. A. 2017. Lysosomal storage diseases. *Translational science of rare diseases* 2(1-2), pp. 1-71.
- Filocamo, M. and Morrone, A. 2011. Lysosomal storage disorders: molecular basis and laboratory testing. *Human genomics* 5(3), p. 156.
- Finbow, M. E. and Harrison, M. A. 1997. The vacuolar H⁺-ATPase: a universal proton pump of eukaryotes. *Biochemical Journal* 324(3), pp. 697-712.
- Fiore, M. et al. 2002. Reversible G1 arrest by dimethyl sulfoxide as a new method to synchronize Chinese hamster cells. *Mutagenesis* 17(5), pp. 419-424.
- Folts, C. J. et al. 2016. Lysosomal re-acidification prevents lysosphingolipid-induced lysosomal impairment and cellular toxicity. *PLoS biology* 14(12), p. e1002583.
- Fossale, E. et al. 2004. Membrane trafficking and mitochondrial abnormalities precede subunit c deposition in a cerebellar cell model of juvenile neuronal ceroid lipofuscinosis. *BMC neuroscience* 5(1), p. 57.
- Frankfurt, O. S. 1983. Increased uptake of vital dye Hoechst 33342 during S phase in synchronized HeLa S3 cells. *Cytometry: The Journal of the International Society for Analytical Cytology* 4(3), pp. 216-221.
- Frese, M.-A. et al. 2008. Arylsulfatase G, a novel lysosomal sulfatase. *Journal of Biological Chemistry* 283(17), pp. 11388-11395.
- Freundt, E. C. et al. 2007. Photoconversion of LysoTracker Red to a green fluorescent molecule. *Cell Res* 17(11), pp. 956-958.
- Friedland, N. et al. 2003. Structure of a cholesterol-binding protein deficient in Niemann-Pick type C2 disease. *Proceedings of the National Academy of Sciences* 100(5), pp. 2512-2517.
- Fu, R. et al. 2010. Oxidative stress in Niemann-Pick disease, type C. *Molecular genetics and metabolism* 101(2-3), pp. 214-218.
- FUKASAWA, K. et al. 1998. Dipeptidyl peptidase III is a zinc metallo-exopeptidase: molecular cloning and expression. *Biochemical Journal* 329(2), pp. 275-282.
- Fukuda, M. 1991. Lysosomal membrane glycoproteins. Structure, biosynthesis, and intracellular trafficking. *Journal of Biological Chemistry* 266(32), pp. 21327-21330.

- Fukuda, M. et al. 1988. Cloning of cDNAs encoding human lysosomal membrane glycoproteins, h-lamp-1 and h-lamp-2. Comparison of their deduced amino acid sequences. *Journal of Biological Chemistry* 263(35), pp. 18920-18928.
- Fuller, M. et al. 2006. Epidemiology of lysosomal storage diseases: an overview.
- Funakoshi, T. et al. 2000. Reconstitution of ATP- and cytosol-dependent transport of de novo synthesized ceramide to the site of sphingomyelin synthesis in semi-intact cells. *Journal of Biological Chemistry* 275(39), pp. 29938-29945.
- Furuchi, T. et al. 1993. Bafilomycin A1, a specific inhibitor of vacuolar-type H (+)-ATPase, blocks lysosomal cholesterol trafficking in macrophages. *Journal of Biological Chemistry* 268(36), pp. 27345-27348.
- Futerman, A. H. and Van Meer, G. 2004. The cell biology of lysosomal storage disorders. *Nature reviews Molecular cell biology* 5(7), p. 554.
- Fyrst, H. and Saba, J. D. 2010. An update on sphingosine-1-phosphate and other sphingolipid mediators. *Nature chemical biology* 6(7), p. 489.
- Galbiati, F. et al. 2007. Autonomic denervation of lymphoid organs leads to epigenetic immune atrophy in a mouse model of Krabbe disease. *Journal of Neuroscience* 27(50), pp. 13730-13738.
- Gallegos, K. M. et al. 2012. Shiga toxin binding to glycolipids and glycans. *PloS one* 7(2), p. e30368.
- Garrity, A. G. et al. 2016. The endoplasmic reticulum, not the pH gradient, drives calcium refilling of lysosomes. *Elife* 5, p. e15887.
- Garver, W. S. et al. 2007a. The National Niemann–Pick C1 disease database: report of clinical features and health problems. *American Journal of Medical Genetics Part A* 143(11), pp. 1204-1211.
- Garver, W. S. et al. 2000. Localization of the murine Niemann-Pick C1 protein to two distinct intracellular compartments. *Journal of lipid research* 41(5), pp. 673-687.
- Garver, W. S. et al. 2007b. Characterization of liver disease and lipid metabolism in the Niemann-Pick C1 mouse. *Journal of cellular biochemistry* 101(2), pp. 498-516.
- Garver, W. S. et al. 2005. Niemann-Pick C1 expression is not regulated by the amount of cholesterol flowing through cells in the mouse. *Journal of lipid research* 46(8), pp. 1745-1754.
- Gault, C. R. et al. 2010. An overview of sphingolipid metabolism: from synthesis to breakdown. *Sphingolipids as Signaling and Regulatory Molecules*. Springer, pp. 1-23.
- Geisler, M. et al. 2000. The ACA4 gene of Arabidopsis encodes a vacuolar membrane calcium pump that improves salt tolerance in yeast. *Plant physiology* 124(4), pp. 1814-1827.
- Geisow, M. J. et al. 1981. Temporal changes of lysosome and phagosome pH during phagolysosome formation in macrophages: studies by fluorescence spectroscopy. *The Journal of cell biology* 89(3), pp. 645-652.
- Gelb, M. H. et al. 2015. Newborn screening for lysosomal storage diseases. *Clinical chemistry* 61(2), pp. 335-346.

- Gelb, M. H. et al. 2006. Direct multiplex assay of enzymes in dried blood spots by tandem mass spectrometry for the newborn screening of lysosomal storage disorders. *Journal of inherited metabolic disease* 29(2-3), pp. 397-404.
- Giese, A.-K. et al. 2015. A novel, highly sensitive and specific biomarker for Niemann-Pick type C1 disease. *Orphanet journal of rare diseases* 10(1), p. 78.
- Ginzburg, L. and Futerman, A. H. 2005. Defective calcium homeostasis in the cerebellum in a mouse model of Niemann–Pick A disease. *Journal of neurochemistry* 95(6), pp. 1619-1628.
- Gitzelmann, R. et al. 1994. Feline mucopolysaccharidosis VII due to β -glucuronidase deficiency. *Veterinary pathology* 31(4), pp. 435-443.
- Golabek, A. A. et al. 2000. CLN3 protein regulates lysosomal pH and alters intracellular processing of Alzheimer's amyloid- β protein precursor and cathepsin D in human cells. *Molecular genetics and metabolism* 70(3), pp. 203-213.
- Golabek, A. A. et al. 2005. Glycosaminoglycans modulate activation, activity, and stability of tripeptidyl-peptidase I in vitro and in vivo. *Journal of Biological Chemistry* 280(9), pp. 7550-7561.
- Goldin, E. et al. 1995. Cultured skin fibroblasts derived from patients with mucopolidosis 4 are auto-fluorescent. *Pediatric research* 37(6), p. 687.
- Goldstein, J. L. and Brown, M. S. 2009. The LDL receptor. *Arteriosclerosis, thrombosis, and vascular biology* 29(4), pp. 431-438.
- Goldstein, J. L. et al. 2006. Protein sensors for membrane sterols. *Cell* 124(1), pp. 35-46.
- Goñi, F. M. and Alonso, A. 2006. Biophysics of sphingolipids I. Membrane properties of sphingosine, ceramides and other simple sphingolipids. *Biochimica et Biophysica Acta (BBA)-Biomembranes* 1758(12), pp. 1902-1921.
- Gonzalez, A. et al. 2014. Lysosomal integral membrane protein-2: a new player in lysosome-related pathology. *Molecular genetics and metabolism* 111(2), pp. 84-91.
- Gotoda, Y. et al. 1998. Missense and nonsense mutations in the lysosomal α -mannosidase gene (MANB) in severe and mild forms of α -mannosidosis. *The American Journal of Human Genetics* 63(4), pp. 1015-1024.
- Grabowski, G. A. et al. 1995. Enzyme therapy in type 1 Gaucher disease: comparative efficacy of mannose-terminated glucocerebrosidase from natural and recombinant sources. *Annals of internal medicine* 122(1), pp. 33-39.
- Grant, B. D. and Donaldson, J. G. 2009. Pathways and mechanisms of endocytic recycling. *Nature reviews Molecular cell biology* 10(9), p. 597.
- Gravel, R. A. 1995. The GM2 gangliosidoses. *The metabolic and molecular basis of inherited disease*, pp. 2839-2879.
- Graves, A. R. et al. 2008. The Cl⁻/H⁺ antiporter ClC-7 is the primary chloride permeation pathway in lysosomes. *Nature* 453(7196), p. 788.

- Graziano, A. C. E. and Cardile, V. 2015. History, genetic, and recent advances on Krabbe disease. *Gene* 555(1), pp. 2-13.
- Greiner-Tollersrud, O. K. and Berg, T. 2005. Lysosomal storage disorders. *Lysosomes*. Springer, pp. 60-73.
- Griffiths, G. et al. 1988. The mannose 6-phosphate receptor and the biogenesis of lysosomes. *Cell* 52(3), pp. 329-341.
- Griffiths, G. et al. 1990. Characterization of the cation-independent mannose 6-phosphate receptor-enriched prelysosomal compartment in NRK cells. *Journal of Cell Science* 95(3), pp. 441-461.
- Grimm, C. et al. 2010. Small molecule activators of TRPML3. *Chemistry & biology* 17(2), pp. 135-148.
- Grubb, J. H. et al. 2010. New strategies for enzyme replacement therapy for lysosomal storage diseases. *Rejuvenation research* 13(2-3), pp. 229-236.
- Grubman, A. et al. 2014a. Deregulation of subcellular biometal homeostasis through loss of the metal transporter, Zip7, in a childhood neurodegenerative disorder. *Acta neuropathologica communications* 2(1), p. 25.
- Grubman, A. et al. 2014b. Deregulation of biometal homeostasis: the missing link for neuronal ceroid lipofuscinoses? *Metallomics* 6(4), pp. 932-943.
- Gruenheid, S. et al. 1999. The iron transport protein NRAMP2 is an integral membrane glycoprotein that colocalizes with transferrin in recycling endosomes. *Journal of Experimental Medicine* 189(5), pp. 831-841.
- Guerra, F. et al. 2019. Synergistic Effect of Mitochondrial and Lysosomal Dysfunction in Parkinson's Disease. *Cells* 8(5), p. 452.
- Guha, S. et al. 2014. Approaches for detecting lysosomal alkalinization and impaired degradation in fresh and cultured RPE cells: evidence for a role in retinal degenerations. *Experimental eye research* 126, pp. 68-76.
- Guhaniyogi, J. et al. 2009. Crystal structure and autoactivation pathway of the precursor form of human tripeptidyl-peptidase 1, the enzyme deficient in late infantile ceroid lipofuscinosis. *Journal of Biological Chemistry* 284(6), pp. 3985-3997.
- Hakomori, S.-i. et al. 1998. New insights in glycosphingolipid function: "glycosignaling domain," a cell surface assembly of glycosphingolipids with signal transducer molecules, involved in cell adhesion coupled with signaling. Oxford University Press.
- Haltia, M. 2006. The neuronal ceroid-lipofuscinoses: from past to present. *Biochimica Et Biophysica Acta (BBA)-Molecular Basis of Disease* 1762(10), pp. 850-856.
- Hammel, I. and Alroy, J. 1995. The effect of lysosomal storage diseases on secretory cells: an ultrastructural study of pancreas as an example. *Journal of submicroscopic cytology and pathology* 27(2), pp. 143-160.
- Hanada, K. et al. 2003. Molecular machinery for non-vesicular trafficking of ceramide. *Nature* 426(6968), p. 803.

- Hannun, Y. A. and Bell, R. M. 1987. Lysosphingolipids inhibit protein kinase C: implications for the sphingolipidoses. *Science* 235(4789), pp. 670-674.
- Hannun, Y. A. and Bell, R. M. 1989. Functions of sphingolipids and sphingolipid breakdown products in cellular regulation. *Science* 243(4890), pp. 500-507.
- Hannun, Y. A. and Obeid, L. M. 2008. Principles of bioactive lipid signalling: lessons from sphingolipids. *Nature reviews Molecular cell biology* 9(2), p. 139.
- Hansson, H.-A. et al. 1977. Ultrastructural localization of cell membrane GM1 ganglioside by cholera toxin. *Proceedings of the National Academy of Sciences* 74(9), pp. 3782-3786.
- Hao, M. et al. 2002. Vesicular and non-vesicular sterol transport in living cells The endocytic recycling compartment is a major sterol storage organelle. *Journal of Biological Chemistry* 277(1), pp. 609-617.
- Harada, M. et al. 1997. Bafilomycin A1, a specific inhibitor of V-type H⁺-ATPases, inhibits the acidification of endocytic structures and inhibits horseradish peroxidase uptake in isolated rat sinusoidal endothelial cells. *Liver* 17(5), pp. 244-250.
- Harzer, K. et al. 2002. Residual galactosylsphingosine (psychosine) β -galactosidase activities and associated GALC mutations in late and very late onset Krabbe disease. *Clinica Chimica Acta* 317(1-2), pp. 77-84.
- Harzer, K. et al. 2003. Concurrent increase of cholesterol, sphingomyelin and glucosylceramide in the spleen from non-neurologic Niemann–Pick type C patients but also patients possibly affected with other lipid trafficking disorders. *FEBS letters* 537(1-3), pp. 177-181.
- Haugland, R. and Spence, M. 2002. Indicators for Ca²⁺, Mg²⁺, Zn²⁺ and other metal ions. *Handbook of fluorescent probes and research products*. ed. Gregory, J, pp. 771-826.
- Hayre, J. K. et al. 2012. Optimization of a direct spectrophotometric method to investigate the kinetics and inhibition of sialidases. *BMC biochemistry* 13(1), p. 19.
- He, X. et al. 2001. An enzymatic assay for quantifying sphingomyelin in tissues and plasma from humans and mice with Niemann–Pick disease. *Analytical biochemistry* 293(2), pp. 204-211.
- He, X. et al. 2002. A fluorescence-based, high-throughput sphingomyelin assay for the analysis of Niemann–Pick disease and other disorders of sphingomyelin metabolism. *Analytical biochemistry* 306(1), pp. 115-123.
- Headlam, H. A. et al. 2006. Inhibition of cathepsins and related proteases by amino acid, peptide, and protein hydroperoxides. *Free Radical Biology and Medicine* 40(9), pp. 1539-1548.
- Hechtman, P. 1977. Characterization of an activating factor required for hydrolysis of GM2 ganglioside catalyzed by hexosaminidase A. *Canadian journal of biochemistry* 55(4), pp. 315-324.
- Heitner, R. et al. 2002. Low-dose N-butyldeoxynojirimycin (OGT 918) for type I Gaucher disease. *Blood Cells, Molecules, and Diseases* 28(2), pp. 127-133.

- Helmy, M. H. et al. 2000. Effect of selenium supplementation on the activities of glutathione metabolizing enzymes in human hepatoma Hep G2 cell line. *Toxicology* 144(1-3), pp. 57-61.
- Hepbildikler, S. T. et al. 2002. Physiological substrates for human lysosomal β -hexosaminidase S. *Journal of Biological Chemistry* 277(4), pp. 2562-2572.
- Hetmańczyk, K. et al. 2016. Monitoring of dipeptidyl peptidase-IV (DPP-IV) activity in patients with mucopolysaccharidoses types I and II on enzyme replacement therapy—Results of a pilot study. *Clinical biochemistry* 49(6), pp. 458-462.
- Heybrock, S. et al. 2019. Lysosomal integral membrane protein-2 (LIMP-2/SCARB2) is involved in lysosomal cholesterol export. *Nature communications* 10(1), pp. 1-12.
- Heywood, W. E. et al. 2015. Proteomic discovery and development of a multiplexed targeted mrm-lc-ms/ms assay for urine biomarkers of extracellular matrix disruption in mucopolysaccharidoses I, II, and VI. *Analytical chemistry* 87(24), pp. 12238-12244.
- Higaki, K. and Ohno, K. 1998. Niemann-Pick disease [type A and B](acid sphingomyelinase deficiencies). *Ryoikibetsu shokogun shirizu* (19 Pt 2), p. 360.
- Higgins, M. E. et al. 1999. Niemann-Pick C1 is a late endosome-resident protein that transiently associates with lysosomes and the trans-Golgi network. *Molecular genetics and metabolism* 68(1), pp. 1-13.
- Hirayama, T. et al. 2013. A highly selective turn-on fluorescent probe for iron (II) to visualize labile iron in living cells. *Chemical Science* 4(3), pp. 1250-1256.
- Hobro, A. J. and Smith, N. I. 2017. An evaluation of fixation methods: Spatial and compositional cellular changes observed by Raman imaging. *Vibrational Spectroscopy* 91, pp. 31-45.
- Hoffman, J. D. et al. 2013. Next-generation DNA sequencing of HEXA: a step in the right direction for carrier screening. *Molecular genetics & genomic medicine* 1(4), pp. 260-268.
- Höglinger, D. et al. 2015. Intracellular sphingosine releases calcium from lysosomes. *Elife* 4, p. e10616.
- Höhn, A. et al. 2010. Lipofuscin-bound iron is a major intracellular source of oxidants: role in senescent cells. *Free Radical Biology and Medicine* 48(8), pp. 1100-1108.
- Hollak, C. et al. 1994. Marked elevation of plasma chitotriosidase activity. A novel hallmark of Gaucher disease. *The Journal of clinical investigation* 93(3), pp. 1288-1292.
- Hollister, D. et al. 1975. The Morquio syndrome (mucopolysaccharidosis IV): Morphologic and biochemical studies. *The Johns Hopkins Medical Journal* 137(4), pp. 176-183.
- Holopainen, J. M. et al. 2001. Elevated lysosomal pH in neuronal ceroid lipofuscinoses (NCLs). *European Journal of Biochemistry* 268(22), pp. 5851-5856.
- Holthuis, J. C. et al. 2001. The organizing potential of sphingolipids in intracellular membrane transport. *Physiological reviews* 81(4), pp. 1689-1723.
- Hopwood, J. J. et al. 1979. A fluorometric assay using 4-methylumbelliferyl α -L-iduronide for the estimation of α -L-iduronidase activity and the detection of Hurler and Scheie syndromes. *Clinica chimica acta* 92(2), pp. 257-265.

- Howard, C. and Reed, M. 2005. *Unbiased Stereology* (Garland Science/BIOS Scientific, New York).
- Hua, C. T. et al. 1998. Evaluation of the lysosome-associated membrane protein LAMP-2 as a marker for lysosomal storage disorders. *Clinical chemistry* 44(10), pp. 2094-2102.
- Huang, L. and Gitschier, J. 1997. A novel gene involved in zinc transport is deficient in the lethal milk mouse. *Nature genetics* 17(3), p. 292.
- Hughes, M. P. et al. 2018. AAV9 intracerebroventricular gene therapy improves lifespan, locomotor function and pathology in a mouse model of Niemann–Pick type C1 disease. *Human molecular genetics* 27(17), pp. 3079-3098.
- Huizing, M. et al. 2008. Disorders of lysosome-related organelle biogenesis: clinical and molecular genetics. *Annu. Rev. Genomics Hum. Genet.* 9, pp. 359-386.
- Hung, Y. H. et al. 2014. Altered transition metal homeostasis in Niemann–Pick disease, type C1. *Metallomics* 6(3), pp. 542-553.
- Huotari, J. and Helenius, A. 2011. Endosome maturation. *The EMBO journal* 30(17), pp. 3481-3500.
- Ikonen, E. 2008. Cellular cholesterol trafficking and compartmentalization. *Nature reviews Molecular cell biology* 9(2), p. 125.
- Infante, R. E. et al. 2008. NPC2 facilitates bidirectional transfer of cholesterol between NPC1 and lipid bilayers, a step in cholesterol egress from lysosomes. *Proceedings of the National Academy of Sciences* 105(40), pp. 15287-15292.
- Ioannou, Y. A. 2000. The structure and function of the Niemann–Pick C1 protein. *Molecular genetics and metabolism* 71(1-2), pp. 175-181.
- Ismael, F. O. et al. 2016. Role of Myeloperoxidase oxidants in the modulation of cellular Lysosomal enzyme function: a contributing factor to macrophage dysfunction in atherosclerosis? *PloS one* 11(12), p. e0168844.
- Ito, M. et al. 2000. [32] Enzymatic N-deacylation of sphingolipids. *Methods in enzymology*. Vol. 311. Elsevier, pp. 297-303.
- Jack, R. M. et al. 2006. The use of acarbose inhibition in the measurement of acid alpha-glucosidase activity in blood lymphocytes for the diagnosis of Pompe disease. *Genetics in Medicine* 8(5), p. 307.
- Jackson, R. L. et al. 1991. Glycosaminoglycans: molecular properties, protein interactions, and role in physiological processes. *Physiological reviews* 71(2), pp. 481-539.
- Jiang, X. et al. 2009. Direct quantitation of psychosine from alkaline-treated lipid extracts with a semi-synthetic internal standard. *Journal of lipid research* 50(1), pp. 162-172.
- Jolly, R. et al. 1993. Ceroid, lipofuscin and the ceroid-lipofuscinoses (Batten Disease). *Journal of inherited metabolic disease* 16(2), pp. 280-283.

- Jones, L. J. et al. 1997. Quenched BODIPY dye-labeled casein substrates for the assay of protease activity by direct fluorescence measurement. *Analytical biochemistry* 251(2), pp. 144-152.
- Jovic, M. et al. 2010. The early endosome: a busy sorting station for proteins at the crossroads. *Histology and histopathology* 25(1), p. 99.
- Kaksonen, M. and Roux, A. 2018. Mechanisms of clathrin-mediated endocytosis. *Nature Reviews Molecular Cell Biology* 19(5), p. 313.
- Kálmán, S. et al. 2016. Human dermal fibroblasts in psychiatry research. *Neuroscience* 320, pp. 105-121.
- Kaltenberg, J. et al. 2010. Zinc signals promote IL-2-dependent proliferation of T cells. *European journal of immunology* 40(5), pp. 1496-1503.
- Kamensky, E. et al. 1973. Cultured skin fibroblasts in storage disorders: an analysis of ultrastructural features. *The American journal of pathology* 73(1), p. 59.
- Kanazawa, T. et al. 2000. Inhibition of cytokinesis by a lipid metabolite, psychosine. *The Journal of cell biology* 149(4), pp. 943-950.
- Kanninen, K. M. et al. 2013a. Altered biometal homeostasis is associated with CLN6 mRNA loss in mouse neuronal ceroid lipofuscinosis. *Biology open* 2(6), pp. 635-646.
- Kanninen, K. M. et al. 2013b. Increased zinc and manganese in parallel with neurodegeneration, synaptic protein changes and activation of Akt/GSK3 signaling in ovine CLN6 neuronal ceroid lipofuscinosis. *PLoS One* 8(3), p. e58644.
- Kannurpatti, S. S. et al. 2000. Calcium sequestering ability of mitochondria modulates influx of calcium through glutamate receptor channel. *Neurochemical research* 25(12), pp. 1527-1536.
- Kapuscinski, J. and Darzynkiewicz, Z. 1987. Interactions of acridine orange with double stranded nucleic acids. Spectral and affinity studies. *Journal of Biomolecular Structure and Dynamics* 5(1), pp. 127-143.
- Karageorgos, L. et al. 2004. Mutational analysis of mucopolysaccharidosis type VI patients undergoing a trial of enzyme replacement therapy. *Human mutation* 23(3), pp. 229-233.
- Karageorgos, L. E. et al. 1997. Lysosomal biogenesis in lysosomal storage disorders. *Experimental cell research* 234(1), pp. 85-97.
- Karovic, O. et al. 2007. Toxic effects of cobalt in primary cultures of mouse astrocytes: similarities with hypoxia and role of HIF-1 α . *Biochemical pharmacology* 73(5), pp. 694-708.
- Karpova, E. et al. 1996. A fluorimetric enzyme assay for the diagnosis of Sanfilippo disease type A (MPS IIIA). *Journal of inherited metabolic disease* 19(3), pp. 278-285.
- Kaufmann, A. M. and Krise, J. P. 2008. Niemann-Pick C1 functions in regulating lysosomal amine content. *Journal of Biological Chemistry* 283(36), pp. 24584-24593.
- Kilpatrick, B. S. et al. 2013. Direct mobilisation of lysosomal Ca²⁺ triggers complex Ca²⁺ signals. *J Cell Sci* 126(1), pp. 60-66.

- Kilpatrick, B. S. et al. 2016. Endoplasmic reticulum and lysosomal Ca²⁺ stores are remodelled in GBA1-linked Parkinson disease patient fibroblasts. *Cell Calcium* 59(1), pp. 12-20.
- Kim, J. H. et al. 2016. Long-term enzyme replacement therapy for Fabry disease: efficacy and unmet needs in cardiac and renal outcomes. *Journal of human genetics* 61(11), p. 923.
- Kingma, S. D. et al. 2013. An algorithm to predict phenotypic severity in mucopolysaccharidosis type I in the first month of life. *Orphanet journal of rare diseases* 8(1), p. 99.
- Kint, J. et al. 1973. Mucopolysaccharidosis: secondarily induced abnormal distribution of lysosomal isoenzymes. *Science* 181(4097), pp. 352-354.
- Kiss, A. L. and Botos, E. 2009. Endocytosis via caveolae: alternative pathway with distinct cellular compartments to avoid lysosomal degradation? *Journal of cellular and molecular medicine* 13(7), pp. 1228-1237.
- Kivipelto, M. et al. 2001. Midlife vascular risk factors and Alzheimer's disease in later life: longitudinal, population based study. *Bmj* 322(7300), pp. 1447-1451.
- Klein, D. et al. 1998. Association of copper to metallothionein in hepatic lysosomes of Long-Evans cinnamon (LEC) rats during the development of hepatitis [see e comments]. *European journal of clinical investigation* 28(4), pp. 302-310.
- Klumperman, J. and Raposo, G. 2014. The complex ultrastructure of the endolysosomal system. *Cold Spring Harbor perspectives in biology* 6(10), p. a016857.
- Knöpfel, M. et al. 2005. Transport of divalent transition-metal ions is lost in small-intestinal tissue of b/b Belgrade rats. *Biochemistry* 44(9), pp. 3454-3465.
- Ko, D. C. et al. 2003. The integrity of a cholesterol-binding pocket in Niemann–Pick C2 protein is necessary to control lysosome cholesterol levels. *Proceedings of the National Academy of Sciences* 100(5), pp. 2518-2525.
- Kobayashi, T. et al. 1999. Late endosomal membranes rich in lysobisphosphatidic acid regulate cholesterol transport. *Nature cell biology* 1(2), p. 113.
- Kobayashi, T. et al. 1992. Accumulation of lysosphingolipids in tissues from patients with GM1 and GM2 gangliosidoses. *Journal of neurochemistry* 59(4), pp. 1452-1458.
- Kobayashi, T. et al. 1988. Infantile and fetal globoid cell leukodystrophy: analysis of galactosylceramide and galactosylsphingosine. *Annals of Neurology: Official Journal of the American Neurological Association and the Child Neurology Society* 24(4), pp. 517-522.
- Kobayashi, T. et al. 2000. The tetraspanin CD63/lamp3 cycles between endocytic and secretory compartments in human endothelial cells. *Molecular biology of the cell* 11(5), pp. 1829-1843.
- Kodam, A. et al. 2010. Altered levels and distribution of amyloid precursor protein and its processing enzymes in Niemann-Pick type C1-deficient mouse brains. *Glia* 58(11), pp. 1267-1281.
- Kollmann, K. et al. 2012. Lysosomal dysfunction causes neurodegeneration in mucopolipidosis II 'knock-in'mice. *Brain* 135(9), pp. 2661-2675.

- Kolter, T. and Sandhoff, K. 2006. Sphingolipid metabolism diseases. *Biochimica et Biophysica Acta (BBA)-Biomembranes* 1758(12), pp. 2057-2079.
- Korkotian, E. et al. 1999. Elevation of intracellular glucosylceramide levels results in an increase in endoplasmic reticulum density and in functional calcium stores in cultured neurons. *Journal of Biological Chemistry* 274(31), pp. 21673-21678.
- Kornfeld, S. 1987. Trafficking of lysosomal enzymes. *The FASEB Journal* 1(6), pp. 462-468.
- Kornfeld, S. 2001. I-cell disease and pseudo-Hurler polydystrophy: disorders of lysosomal enzyme phosphorylation and localization. *The metabolic and molecular bases of inherited disease*, pp. 3469-3482.
- Kruth, H. S. et al. 1986. Type C Niemann-Pick disease. Abnormal metabolism of low density lipoprotein in homozygous and heterozygous fibroblasts. *Journal of Biological Chemistry* 261(35), pp. 16769-16774.
- Kuizon, S. et al. 2010. A critical tryptophan and Ca²⁺ in activation and catalysis of TPPI, the enzyme deficient in classic late-infantile neuronal ceroid lipofuscinosis. *PLoS One* 5(8), p. e11929.
- Kukic, I. et al. 2014. Zn²⁺ efflux through lysosomal exocytosis prevents Zn²⁺-induced toxicity. *J Cell Sci* 127(14), pp. 3094-3103.
- Kukic, I. et al. 2013. Zinc-dependent lysosomal enlargement in TRPML1-deficient cells involves MTF-1 transcription factor and ZnT4 (Slc30a4) transporter. *Biochemical Journal* 451(2), pp. 155-163.
- Kumagai, T. et al. 2010. Involvement of murine β -1, 4-galactosyltransferase V in lactosylceramide biosynthesis. *Glycoconjugate journal* 27(7-9), pp. 685-695.
- Kuriwaki, K. and Yoshida, H. 1999. Morphological characteristics of lipid accumulation in liver-constituting cells of acid lipase deficiency rats (Wolman's disease model rats). *Pathology international* 49(4), pp. 291-297.
- Kurz, T. et al. 2011. The role of lysosomes in iron metabolism and recycling. *The international journal of biochemistry & cell biology* 43(12), pp. 1686-1697.
- Kuter, D. J. et al. 2013. Miglustat therapy in type 1 Gaucher disease: clinical and safety outcomes in a multicenter retrospective cohort study. *Blood Cells, Molecules, and Diseases* 51(2), pp. 116-124.
- Kwakye, G. et al. 2015. Manganese-induced parkinsonism and Parkinson's disease: shared and distinguishable features. *International journal of environmental research and public health* 12(7), pp. 7519-7540.
- Kwon, H. J. et al. 2009. Structure of N-terminal domain of NPC1 reveals distinct subdomains for binding and transfer of cholesterol. *Cell* 137(7), pp. 1213-1224.
- Lachmann, R. et al. 2004a. Twin pairs showing discordance of phenotype in adult Gaucher's disease. *Qjm* 97(4), pp. 199-204.
- Lachmann, R. H. 2005. Miglustat: substrate reduction therapy for glycosphingolipid storage disorders. *Clinical Practice* 2(4), p. 569.

- Lachmann, R. H. et al. 2004b. Treatment with miglustat reverses the lipid-trafficking defect in Niemann–Pick disease type C. *Neurobiology of disease* 16(3), pp. 654-658.
- Lambeir, A.-M. et al. 2003. Dipeptidyl-peptidase IV from bench to bedside: an update on structural properties, functions, and clinical aspects of the enzyme DPP IV. *Critical reviews in clinical laboratory sciences* 40(3), pp. 209-294.
- Langereis, E. J. et al. 2015. A multiplex assay for the diagnosis of mucopolysaccharidoses and mucopolipidoses. *PLoS One* 10(9), p. e0138622.
- LaPlante, J. M. et al. 2002. Identification and characterization of the single channel function of human mucolipin-1 implicated in mucopolipidosis type IV, a disorder affecting the lysosomal pathway. *FEBS letters* 532(1-2), pp. 183-187.
- LaPlante, J. M. et al. 2004. Functional links between mucolipin-1 and Ca²⁺-dependent membrane trafficking in mucopolipidosis IV. *Biochemical and biophysical research communications* 322(4), pp. 1384-1391.
- Lawrence, S. P. et al. 2010. The sodium/proton exchanger NHE8 regulates late endosomal morphology and function. *Molecular biology of the cell* 21(20), pp. 3540-3551.
- LEAKE, D. S. et al. 1982. Properties and subcellular localization of acid phosphatase activity in cultured arterial smooth muscle cells. *European journal of biochemistry* 128(2-3), pp. 557-563.
- Lee, D.-w. et al. 2006. Recruitment dynamics of GAK and auxilin to clathrin-coated pits during endocytosis. *J Cell Sci* 119(17), pp. 3502-3512.
- Lee, J.-H. et al. 2015. Presenilin 1 maintains lysosomal Ca²⁺ homeostasis via TRPML1 by regulating vATPase-mediated lysosome acidification. *Cell reports* 12(9), pp. 1430-1444.
- Lee, J.-H. et al. 2010. Lysosomal proteolysis and autophagy require presenilin 1 and are disrupted by Alzheimer-related PS1 mutations. *Cell* 141(7), pp. 1146-1158.
- Lefrancois, S. et al. 2003. The lysosomal trafficking of sphingolipid activator proteins (SAPs) is mediated by sortilin. *The EMBO journal* 22(24), pp. 6430-6437.
- Lehman, T. J. et al. 2011. Diagnosis of the mucopolysaccharidoses. *Rheumatology* 50(suppl_5), pp. v41-v48.
- Levade, T. et al. 1985. New tools for the study of Niemann-Pick disease: analogues of natural substrate and Epstein-Barr virus-transformed lymphoid cell lines. *Pediatric research* 19(1), p. 153.
- Levičar, N. et al. 2002. Lysosomal enzymes, cathepsins in brain tumour invasion. *Journal of neuro-oncology* 58(1), pp. 21-32.
- Li, J. and Pfeffer, S. R. 2016. Lysosomal membrane glycoproteins bind cholesterol and contribute to lysosomal cholesterol export. *Elife* 5, p. e21635.
- Li, Y. et al. 2004. Direct multiplex assay of lysosomal enzymes in dried blood spots for newborn screening. *Clinical chemistry* 50(10), pp. 1785-1796.
- Lin, H. J. et al. 2003. Fluorescence lifetime-resolved pH imaging of living cells. *Cytometry Part A: the journal of the International Society for Analytical Cytology* 52(2), pp. 77-89.

- Liu, B. et al. 2009. Reversal of defective lysosomal transport in NPC disease ameliorates liver dysfunction and neurodegeneration in the npc1^{-/-} mouse. *Proceedings of the National Academy of Sciences* 106(7), pp. 2377-2382.
- Liu, J. et al. 2007. Regulation of copper-dependent endocytosis and vacuolar degradation of the yeast copper transporter, Ctr1p, by the Rsp5 ubiquitin ligase. *Traffic* 8(10), pp. 1375-1384.
- Lloyd-Evans, E. 2016a. Acidic Ca²⁺ stores in neurodegeneration. *Messenger* 5(1-2), pp. 37-55.
- Lloyd-Evans, E. 2016b. On the move, lysosomal CAX drives Ca²⁺ transport and motility. *J Cell Biol* 212(7), pp. 755-757.
- Lloyd-Evans, E. and Haslett, L. J. 2016. The lysosomal storage disease continuum with ageing-related neurodegenerative disease. *Ageing research reviews* 32, pp. 104-121.
- Lloyd-Evans, E. et al. 2008. Niemann-Pick disease type C1 is a sphingosine storage disease that causes deregulation of lysosomal calcium. *Nat Med* 14(11), pp. 1247-1255.
- Lloyd-Evans, E. et al. 2003a. Glucosylceramide and glucosylsphingosine modulate calcium mobilization from brain microsomes via different mechanisms. *Journal of Biological Chemistry* 278(26), pp. 23594-23599.
- Lloyd-Evans, E. et al. 2003b. Lyso-glycosphingolipids mobilize calcium from brain microsomes via multiple mechanisms. *Biochemical Journal* 375(3), pp. 561-565.
- Lloyd-Evans, E. and Platt, F. M. 2011. Lysosomal Ca²⁺ homeostasis: role in pathogenesis of lysosomal storage diseases. *Cell calcium* 50(2), pp. 200-205.
- Lloyd-Evans, E. et al. 2010. Endolysosomal calcium regulation and disease. Portland Press Limited.
- Lloyd-Evans, E. and Platt, F. M. 2010. Lipids on trial: the search for the offending metabolite in Niemann-Pick type C disease. *Traffic* 11(4), pp. 419-428.
- Lobato, J. B. et al. 2015. Cathepsin K as a biomarker of bone involvement in type 1 Gaucher disease. *Medicina Clínica (English Edition)* 145(7), pp. 281-287.
- Locatelli-Hoops, S. et al. 2006. Saposin A Mobilizes Lipids from Low Cholesterol and High Bis (monoacylglycerol) phosphate-containing Membranes PATIENT VARIANT SAPOSIN A LACKS LIPID EXTRACTION CAPACITY. *Journal of Biological Chemistry* 281(43), pp. 32451-32460.
- Lonnerdal, B. 2000. Dietary factors influencing zinc absorption. *The Journal of nutrition* 130(5), pp. 1378S-1383S.
- Lovell, M. et al. 1998. Copper, iron and zinc in Alzheimer's disease senile plaques. *Journal of the neurological sciences* 158(1), pp. 47-52.
- Lu, F. et al. 2015. Identification of NPC1 as the target of U18666A, an inhibitor of lysosomal cholesterol export and Ebola infection. *Elife* 4, p. e12177.
- Lu, Q. et al. 2016. Intracellular zinc distribution in mitochondria, ER and the Golgi apparatus. *International journal of physiology, pathophysiology and pharmacology* 8(1), p. 35.

- Lübke, T. et al. 2009. Proteomics of the lysosome. *Biochimica et Biophysica Acta (BBA)-Molecular Cell Research* 1793(4), pp. 625-635.
- Lucocq, J. 2012. Can data provenance go the full monty? *Trends in cell biology* 22(5), p. 229.
- Lüllmann, H. et al. 1978. Lipidosis induced by amphiphilic cationic drugs. *Biochemical pharmacology* 27(8), pp. 1103-1108.
- Lüllmann-Rauch, R. 2005. History and morphology of the lysosome. *Lysosomes*. Springer, pp. 1-16.
- Lütjohann, D. and Von Bergmann, K. 2003. 24S-hydroxycholesterol: a marker of brain cholesterol metabolism. *Pharmacopsychiatry* 36(S 2), pp. 102-106.
- Luzio, J. P. et al. 2007. Lysosomes: fusion and function. *Nature reviews Molecular cell biology* 8(8), p. 622.
- Ma, L. et al. 2017. Live-cell Microscopy and Fluorescence-based Measurement of Luminal pH in Intracellular Organelles. *Frontiers in cell and developmental biology* 5, p. 71.
- Magnusson, G. 1994. Synthesis of glycosphingolipids and corresponding neoglycolipids. *Advanced drug delivery reviews* 13(3), pp. 267-284.
- Maguire, E. 2017. *Investigating ion dyshomeostasis in Niemann-Pick disease type C, both in vitro and in vivo*. Cardiff University.
- Malathi, K. et al. 2004. Mutagenesis of the putative sterol-sensing domain of yeast Niemann Pick C-related protein reveals a primordial role in subcellular sphingolipid distribution. *J Cell Biol* 164(4), pp. 547-556.
- Malnar, M. et al. 2014. Bidirectional links between Alzheimer's disease and Niemann-Pick type C disease. *Neurobiology of disease* 72, pp. 37-47.
- Mamo, A. et al. 2012. The role of ceroid lipofuscinosis neuronal protein 5 (CLN5) in endosomal sorting. *Molecular and cellular biology* 32(10), pp. 1855-1866.
- Mancias, J. D. et al. 2014. Quantitative proteomics identifies NCOA4 as the cargo receptor mediating ferritinophagy. *Nature* 509(7498), p. 105.
- Mane, S. M. et al. 1989. Purification and characterization of human lysosomal membrane glycoproteins. *Archives of biochemistry and biophysics* 268(1), pp. 360-378.
- Manwaring, V. et al. 2012. Urine analysis of glucose tetrasaccharide by HPLC; a useful marker for the investigation of patients with Pompe and other glycogen storage diseases. *Journal of Inherited Metabolic Disease: Official Journal of the Society for the Study of Inborn Errors of Metabolism* 35(2), pp. 311-316.
- Marcó, S. et al. 2016. Progressive neurologic and somatic disease in a novel mouse model of human mucopolysaccharidosis type III C. *Disease models & mechanisms* 9(9), pp. 999-1013.
- Maret, A. et al. 1985. Epstein-Barr virus transformed lymphoid cell lines as a new model system in culture for the study of GM2-gangliosidosis: Tay-Sachs and Sandhoff diseases. *Biology of the Cell* 53(3), pp. 293-296.

- Maret, W. 2015. Analyzing free zinc (II) ion concentrations in cell biology with fluorescent chelating molecules. *Metallomics* 7(2), pp. 202-211.
- Martin, J. L. et al. 2006. Determining zinc with commonly used calcium and zinc fluorescent indicators, a question on calcium signals. *Cell calcium* 40(4), pp. 393-402.
- Matern, D. et al. eds. 2015. *Newborn screening for lysosomal storage disorders*. Seminars in perinatology. Elsevier.
- Maulucci, G. et al. 2015. Quantitative analysis of autophagic flux by confocal pH-imaging of autophagic intermediates. *Autophagy* 11(10), pp. 1905-1916.
- Mauri, V. et al. 2013. A rapid and sensitive method for measuring N-acetylglucosaminidase activity in cultured cells. *PLOS one* 8(6), p. e68060.
- Mayes, J. S. et al. 1981. Differential assay for lysosomal alpha-galactosidases in human tissues and its application to Fabry's disease. *Clinica Chimica Acta* 112(2), pp. 247-251.
- Mayeux, R. 2004. Biomarkers: potential uses and limitations. *NeuroRx* 1(2), pp. 182-188.
- Mayor, S. and Pagano, R. E. 2007. Pathways of clathrin-independent endocytosis. *Nature reviews Molecular cell biology* 8(8), p. 603.
- Mayran, N. et al. 2003. Annexin II regulates multivesicular endosome biogenesis in the degradation pathway of animal cells. *The EMBO journal* 22(13), pp. 3242-3253.
- Maziere, J. et al. 1981. Inhibition of human fibroblasts sphingomyelinase by cholesterol and 7-dehydrocholesterol. *Biochemical and biophysical research communications* 100(3), pp. 1299-1304.
- Mazzacuva, F. et al. 2016. Identification of novel bile acids as biomarkers for the early diagnosis of Niemann-Pick C disease. *FEBS letters* 590(11), pp. 1651-1662.
- McCormick, N. H. and Kelleher, S. L. 2012. ZnT4 provides zinc to zinc-dependent proteins in the trans-Golgi network critical for cell function and Zn export in mammary epithelial cells. *American Journal of Physiology-Cell Physiology* 303(3), pp. C291-C297.
- McGlynn, R. et al. 2004. Differential subcellular localization of cholesterol, gangliosides, and glycosaminoglycans in murine models of mucopolysaccharide storage disorders. *Journal of Comparative Neurology* 480(4), pp. 415-426.
- Medina, D. L. et al. 2015. Lysosomal calcium signalling regulates autophagy through calcineurin and TFEB. *Nature cell biology* 17(3), p. 288.
- Medina, D. L. et al. 2011. Transcriptional activation of lysosomal exocytosis promotes cellular clearance. *Developmental cell* 21(3), pp. 421-430.
- Mehta, A. B. and Winchester, B. 2012. *Lysosomal storage disorders : a practical guide*. Oxford: Wiley-Blackwell, pp. x, 197 p.
- Meikle, P. J. et al. 1997. Diagnosis of lysosomal storage disorders: evaluation of lysosome-associated membrane protein LAMP-1 as a diagnostic marker. *Clinical chemistry* 43(8), pp. 1325-1335.

- Meikle, P. J. et al. 2006. Newborn screening for lysosomal storage disorders. *Molecular genetics and metabolism* 88(4), pp. 307-314.
- Meikle, P. J. et al. 1999. Prevalence of lysosomal storage disorders. *Jama* 281(3), pp. 249-254.
- Mellman, I. et al. 1986. Acidification of the endocytic and exocytic pathways. *Annual review of biochemistry* 55(1), pp. 663-700.
- Mello, A. et al. 2006. Epstein–Barr virus-induced transformation of B cells for the diagnosis of genetic metabolic disorders—enumerative conditions for cryopreservation. *Cell proliferation* 39(1), pp. 29-36.
- Merrill Jr, A. H. 2011. Sphingolipid and glycosphingolipid metabolic pathways in the era of sphingolipidomics. *Chemical reviews* 111(10), pp. 6387-6422.
- Michalski, J.-C. and Klein, A. 1999. Glycoprotein lysosomal storage disorders: α - and β -mannosidosis, fucosidosis and α -N-acetylgalactosaminidase deficiency. *Biochimica et Biophysica Acta (BBA)-Molecular Basis of Disease* 1455(2-3), pp. 69-84.
- Millat, G. et al. 2005. Niemann–Pick C disease: use of denaturing high performance liquid chromatography for the detection of NPC1 and NPC2 genetic variations and impact on management of patients and families. *Molecular genetics and metabolism* 86(1-2), pp. 220-232.
- Millat, G. et al. 2001. Niemann-Pick C1 disease: correlations between NPC1 mutations, levels of NPC1 protein, and phenotypes emphasize the functional significance of the putative sterol-sensing domain and of the cysteine-rich luminal loop. *The American Journal of Human Genetics* 68(6), pp. 1373-1385.
- Minami, R. et al. 1977. α -L-Iduronidase activity in established lymphoblastoid cells from patients with Hurler and Scheie syndromes transformed by Epstein-Barr virus. *The Tohoku journal of experimental medicine* 122(4), pp. 393-396.
- Mindell, J. A. 2012. Lysosomal acidification mechanisms. *Annual review of physiology* 74, pp. 69-86.
- Mitsche, M. A. et al. 2015. Flux analysis of cholesterol biosynthesis in vivo reveals multiple tissue and cell-type specific pathways. *Elife* 4, p. e07999.
- Miura, N. et al. 1996. Human UDP-galactose translocator: molecular cloning of a complementary DNA that complements the genetic defect of a mutant cell line deficient in UDP-galactose translocator. *The Journal of Biochemistry* 120(2), pp. 236-241.
- Miyagawa, K. et al. 2016. Lipid-induced endoplasmic reticulum stress impairs selective autophagy at the step of autophagosome-lysosome fusion in hepatocytes. *The American journal of pathology* 186(7), pp. 1861-1873.
- Moheimani, F. et al. 2012. Inhibition of lysosomal function in macrophages incubated with elevated glucose concentrations: a potential contributory factor in diabetes-associated atherosclerosis. *Atherosclerosis* 223(1), pp. 144-151.
- Mokhtariye, A. et al. 2019. Diagnostic methods for Lysosomal storage disease. *Reports of biochemistry & molecular biology* 7(2), p. 119.

- Mole, S. E. et al. 2018. Clinical challenges and future therapeutic approaches for neuronal ceroid lipofuscinosis. *The Lancet Neurology*.
- Mole, S. E. et al. 2005. Correlations between genotype, ultrastructural morphology and clinical phenotype in the neuronal ceroid lipofuscinoses. *Neurogenetics* 6(3), pp. 107-126.
- Mole, S. E. et al. 2011. *The neuronal ceroid lipofuscinoses (Batten disease)*. 2nd ed. Oxford: Oxford University Press, pp. xxx, 444 p.
- Morgan, A. J. et al. 2013. Bidirectional Ca²⁺ signaling occurs between the endoplasmic reticulum and acidic organelles. *J Cell Biol* 200(6), pp. 789-805.
- Morgan, A. J. and Galione, A. 2007. NAADP induces pH changes in the lumen of acidic Ca²⁺ stores. *Biochemical Journal* 402(2), pp. 301-310.
- Morgan, A. J. et al. 2011. Molecular mechanisms of endolysosomal Ca²⁺ signalling in health and disease. *Biochemical Journal* 439(3), pp. 349-378.
- Motabar, O. et al. 2009. A new resorufin-based α -glucosidase assay for high-throughput screening. *Analytical biochemistry* 390(1), pp. 79-84.
- Motyl, J. and Strosznajder, J. B. 2018. Sphingosine kinase 1/sphingosine-1-phosphate receptors dependent signalling in neurodegenerative diseases. The promising target for neuroprotection in Parkinson's disease. *Pharmacological Reports* 70(5), pp. 1010-1014.
- Muenzer, J. 2011. Overview of the mucopolysaccharidoses. *Rheumatology* 50(suppl_5), pp. v4-v12.
- Murphy, D. J. 2012. The dynamic roles of intracellular lipid droplets: from archaea to mammals. *Protoplasma* 249(3), pp. 541-585.
- Napolitano, G. et al. 2015. Impairment of chaperone-mediated autophagy leads to selective lysosomal degradation defects in the lysosomal storage disease cystinosis. *EMBO molecular medicine* 7(2), pp. 158-174.
- Naureckiene, S. et al. 2000. Identification of HE1 as the second gene of Niemann-Pick C disease. *Science* 290(5500), pp. 2298-2301.
- Neises, G. R. et al. 1997. Ultrastructural changes in the Golgi apparatus and secretory granules of HL-60 cells treated with the imino sugar N-butyldeoxynojirimycin. *Biology of the Cell* 89(2), pp. 123-131.
- Neiss, W. 1984. A coat of glycoconjugates on the inner surface of the lysosomal membrane in the rat kidney. *Histochemistry* 80(6), pp. 603-608.
- Neiss, W. F. 2013. *Ultracytochemistry of intracellular membrane glycoconjugates*. Springer Science & Business Media.
- Neitzel, H. 1986. A routine method for the establishment of permanent growing lymphoblastoid cell lines. *Human genetics* 73(4), pp. 320-326.
- Neudorfer, O. et al. 1996. Occurrence of Parkinson's syndrome in type 1 Gaucher disease. *QJM: An International Journal of Medicine* 89(9), pp. 691-694.

- Neufeld, E. F. 2001. The mucopolysaccharidoses. *The metabolic and molecular bases of inherited disease*, pp. 3421-3452.
- Ni, X. and Morales, C. R. 2006. The lysosomal trafficking of acid sphingomyelinase is mediated by sortilin and mannose 6-phosphate receptor. *Traffic* 7(7), pp. 889-902.
- Nicoli, E.-R. et al. 2019. Lysosomal Storage and Albinism Due to Effects of a De Novo CLCN7 Variant on Lysosomal Acidification. *The American Journal of Human Genetics*.
- Nijssen, P. C. et al. 2003. Autosomal dominant adult neuronal ceroid lipofuscinosis: a novel form of NCL with granular osmiophilic deposits without palmitoyl protein thioesterase 1 deficiency. *Brain pathology* 13(4), pp. 574-581.
- Nishie, T. et al. 2010. β 4-Galactosyltransferase-5 is a lactosylceramide synthase essential for mouse extra-embryonic development. *Glycobiology* 20(10), pp. 1311-1322.
- Nordestgaard, B. G. et al. 2007. Nonfasting triglycerides and risk of myocardial infarction, ischemic heart disease, and death in men and women. *Jama* 298(3), pp. 299-308.
- Nowakowski, R. et al. 1988. Diagnosis of feline GM1 gangliosidosis by enzyme assay of cultured conjunctival cells. *Investigative ophthalmology & visual science* 29(3), pp. 487-490.
- Nowroozi, N. et al. 2001. High β -galactosidase and ganglioside GM1 levels in the human parotid gland. *Archives of Otolaryngology–Head & Neck Surgery* 127(11), pp. 1381-1384.
- Obermeyer, Z. and Emanuel, E. J. 2016. Predicting the future—big data, machine learning, and clinical medicine. *The New England journal of medicine* 375(13), p. 1216.
- Oheda, Y. et al. 2005. Elimination of abnormal sialylglycoproteins in fibroblasts with sialidosis and galactosialidosis by normal gene transfer and enzyme replacement. *Glycobiology* 16(4), pp. 271-280.
- Ohm, T. et al. 2003. Cholesterol and tau protein-findings in Alzheimer's and Niemann Pick C's disease. *Pharmacopsychiatry* 36(S 2), pp. 120-126.
- Öhrvik, H. and Thiele, D. J. 2015. The role of Ctr1 and Ctr2 in mammalian copper homeostasis and platinum-based chemotherapy. *Journal of Trace Elements in Medicine and Biology* 31, pp. 178-182.
- Olivova, P. et al. 2009. Effect of sample collection on α -galactosidase A enzyme activity measurements in dried blood spots on filter paper. *Clinica Chimica Acta* 403(1-2), pp. 159-162.
- Ollig, J. et al. 2016. Parameters influencing zinc in experimental systems in vivo and in vitro. *Metals* 6(3), p. 71.
- Ong, W.-Y. et al. 2001. Neurodegeneration in Niemann-Pick type C disease mice. *Experimental brain research* 141(2), pp. 218-231.
- Orsini, J. J. et al. 2016. Newborn screening for Krabbe disease in New York State: the first eight years' experience. *Genetics in Medicine* 18(3), p. 239.
- Orsini, J. J. et al. 2012. Lysosomal storage disorder 4+ 1 multiplex assay for newborn screening using tandem mass spectrometry: application to a small-scale population study for five lysosomal storage disorders. *Clinica Chimica Acta* 413(15-16), pp. 1270-1273.

- Orsini, J. J. et al. 2009. Implementation of newborn screening for Krabbe disease: population study and cutoff determination. *Clinical biochemistry* 42(9), pp. 877-884.
- Ory, D. S. et al. 2017. Intrathecal 2-hydroxypropyl- β -cyclodextrin decreases neurological disease progression in Niemann-Pick disease, type C1: a non-randomised, open-label, phase 1–2 trial. *The Lancet* 390(10104), pp. 1758-1768.
- Ostrowski, P. P. et al. 2016. Cresyl violet: a superior fluorescent lysosomal marker. *Traffic* 17(12), pp. 1313-1321.
- Otomo, T. et al. 2011. Lysosomal storage causes cellular dysfunction in mucopolidosis II skin fibroblasts. *Journal of Biological Chemistry* 286(40), pp. 35283-35290.
- Oussoren, E. et al. 2011. Bone, joint and tooth development in mucopolysaccharidoses: relevance to therapeutic options. *Biochimica et Biophysica Acta (BBA)-Molecular Basis of Disease* 1812(11), pp. 1542-1556.
- Pagano, R. E. et al. 2000. Membrane traffic in sphingolipid storage diseases. *Traffic* 1(11), pp. 807-815.
- Palade, G. E. 1955. A small particulate component of the cytoplasm. *The Journal of biophysical and biochemical cytology* 1(1), p. 59.
- Palmer, D. et al. 1997. Accumulation of sphingolipid activator proteins (SAPs) A and D in granular osmiophilic deposits in miniature Schnauzer dogs with ceroid-lipofuscinosis. *Journal of inherited metabolic disease* 20(1), pp. 74-84.
- Palmer, D. N. 2015. The relevance of the storage of subunit c of ATP synthase in different forms and models of Batten disease (NCLs). *Biochimica et Biophysica Acta (BBA)-Molecular Basis of Disease* 1852(10), pp. 2287-2291.
- Palmer, D. N. et al. 1992. Mitochondrial ATP synthase subunit c storage in the ceroid-lipofuscinoses (Batten disease). *American journal of medical genetics* 42(4), pp. 561-567.
- Palmieri, M. et al. 2011. Characterization of the CLEAR network reveals an integrated control of cellular clearance pathways. *Human molecular genetics* 20(19), pp. 3852-3866.
- Palmiter, R. D. et al. 1996. ZnT-2, a mammalian protein that confers resistance to zinc by facilitating vesicular sequestration. *The EMBO journal* 15(8), pp. 1784-1791.
- Parenti, G. 2009. Treating lysosomal storage diseases with pharmacological chaperones: from concept to clinics. *EMBO molecular medicine* 1(5), pp. 268-279.
- Parkinson-Lawrence, E. et al. 2006. Immunocytochemistry of lysosomal storage disorders. *Clinical chemistry* 52(9), pp. 1660-1668.
- Parkinson-Lawrence, E. J. et al. 2010. Lysosomal storage disease: revealing lysosomal function and physiology. *Physiology* 25(2), pp. 102-115.
- Paschal, D. and Bailey, G. 1988. Determination of manganese in serum with zeeman effect graphite-furnace atomic-absorption. *JOURNAL OF RESEARCH OF THE NATIONAL BUREAU OF STANDARDS* 93(3), pp. 323-326.

- Pastores, G. M. and Barnett, N. L. 2003. Substrate reduction therapy: miglustat as a remedy for symptomatic patients with Gaucher disease type 1. *Expert opinion on investigational drugs* 12(2), pp. 273-281.
- Pastores, G. M. and Maegawa, G. H. 2013. Clinical neurogenetics: neuropathic lysosomal storage disorders. *Neurologic clinics* 31(4), pp. 1051-1071.
- Patel, S. and Cai, X. 2015. Evolution of acidic Ca²⁺ stores and their resident Ca²⁺-permeable channels. *Cell calcium* 57(3), pp. 222-230.
- Patel, S. C. et al. 1999. Localization of Niemann–Pick C1 protein in astrocytes: implications for neuronal degeneration in Niemann–Pick type C disease. *Proceedings of the National Academy of Sciences* 96(4), pp. 1657-1662.
- Patterson, M. C. et al. 2007. Miglustat for treatment of Niemann-Pick C disease: a randomised controlled study. *The Lancet Neurology* 6(9), pp. 765-772.
- Pelled, D. et al. 2003. Inhibition of calcium uptake via the sarco/endoplasmic reticulum Ca²⁺-ATPase in a mouse model of Sandhoff disease and prevention by treatment with N-butyldeoxynojirimycin. *Journal of Biological Chemistry* 278(32), pp. 29496-29501.
- Pentchev, P. et al. 1987. Group C Niemann-Pick disease: faulty regulation of low-density lipoprotein uptake and cholesterol storage in cultured fibroblasts. *The FASEB Journal* 1(1), pp. 40-45.
- Pentchev, P. et al. 1980. A lysosomal storage disorder in mice characterized by a dual deficiency of sphingomyelinase and glucocerebrosidase. *Biochimica et Biophysica Acta (BBA)-Lipids and Lipid Metabolism* 619(3), pp. 669-679.
- Pentchev, P. G. et al. 1985. A defect in cholesterol esterification in Niemann-Pick disease (type C) patients. *Proceedings of the National Academy of Sciences* 82(23), pp. 8247-8251.
- Pereira, V. G. et al. 2010. Evidence of lysosomal membrane permeabilization in mucopolysaccharidosis type I: rupture of calcium and proton homeostasis. *Journal of cellular physiology* 223(2), pp. 335-342.
- Persaud-Sawin, D.-A. et al. 2004. A galactosylceramide binding domain is involved in trafficking of CLN3 from Golgi to rafts via recycling endosomes. *Pediatric research* 56(3), p. 449.
- Petrat, F. et al. 1999. Determination of the chelatable iron pool of isolated rat hepatocytes by digital fluorescence microscopy using the fluorescent probe, phen green SK. *Hepatology* 29(4), pp. 1171-1179.
- Petrov, A. et al. 2016. Brain cholesterol metabolism and its defects: linkage to neurodegenerative diseases and synaptic dysfunction. *Acta Naturae (англоязычная версия)* 8(1 (28)).
- Pierzyńska-Mach, A. et al. 2014. Evaluation of acridine orange, LysoTracker Red, and quinacrine as fluorescent probes for long-term tracking of acidic vesicles. *Cytometry Part A* 85(8), pp. 729-737.
- Pipalia, N. H. et al. 2006. Automated microscopy screening for compounds that partially revert cholesterol accumulation in Niemann-Pick C cells. *Journal of lipid research* 47(2), pp. 284-301.

- Piper, R. C. and Katzmann, D. J. 2007. Biogenesis and function of multivesicular bodies. *Annu. Rev. Cell Dev. Biol.* 23, pp. 519-547.
- Piper, R. C. and Luzio, J. P. 2001. Late endosomes: sorting and partitioning in multivesicular bodies. *Traffic* 2(9), pp. 612-621.
- Platt, F. M. et al. 2012. Lysosomal storage disorders: The cellular impact of lysosomal dysfunction. *J Cell Biol* 199(5), pp. 723-734.
- Platt, F. M. et al. 2018. Lysosomal storage diseases. *Nature Reviews Disease Primers* 4(1), p. 27.
- Platt, F. M. et al. 1994. N-butyldeoxynojirimycin is a novel inhibitor of glycolipid biosynthesis. *Journal of Biological Chemistry* 269(11), pp. 8362-8365.
- Polishchuk, E. V. and Polishchuk, R. S. 2016. The emerging role of lysosomes in copper homeostasis. *Metallomics* 8(9), pp. 853-862.
- Polo, G. et al. 2017. Diagnosis of sphingolipidoses: a new simultaneous measurement of lysosphingolipids by LC-MS/MS. *Clinical Chemistry and Laboratory Medicine (CCLM)* 55(3), pp. 403-414.
- Pols, M. S. and Klumperman, J. 2009. Trafficking and function of the tetraspanin CD63. *Experimental cell research* 315(9), pp. 1584-1592.
- Popova, M. and Popov, C. S. 1998. Effect of heavy metal salts on the activity of rat liver and kidney catalase and lysosomal hydrolases. *Journal of Veterinary Medicine Series A* 45(1-10), pp. 343-351.
- Porter, F. D. et al. 2010. Cholesterol oxidation products are sensitive and specific blood-based biomarkers for Niemann-Pick C1 disease. *Science translational medicine* 2(56), pp. 56ra81-56ra81.
- Prasad, A. et al. 1996. Electron microscopic examination of skin biopsy as a cost-effective tool in the diagnosis of lysosomal storage diseases. *Journal of child neurology* 11(4), pp. 301-308.
- Prence, E. M. and Natowicz, M. 1992. Diagnosis of alpha-mannosidosis by measuring alpha-mannosidase in plasma. *Clinical chemistry* 38(4), pp. 501-503.
- Priestman, D. et al. 2000. Imino sugar therapy for type 1 Gaucher disease. *Glycobiology* 10(11), p. iv.
- Pryor, P. R. 2012. Analyzing lysosomes in live cells. *Methods in enzymology*. Vol. 505. Elsevier, pp. 145-157.
- Pryor, P. R. et al. 2000. The role of intraorganellar Ca²⁺ in late endosome–lysosome heterotypic fusion and in the reformation of lysosomes from hybrid organelles. *The Journal of cell biology* 149(5), pp. 1053-1062.
- Pryor, P. R. et al. 2006. Mucolipin-1 is a lysosomal membrane protein required for intracellular lactosylceramide traffic. *Traffic* 7(10), pp. 1388-1398.
- Pu, J. et al. 2016. Mechanisms and functions of lysosome positioning. *J Cell Sci* 129(23), pp. 4329-4339.

- Puri, V. et al. 1999. Cholesterol modulates membrane traffic along the endocytic pathway in sphingolipid-storage diseases. *Nature cell biology* 1(6), p. 386.
- Radhakrishnan, A. et al. 2008. Switch-like control of SREBP-2 transport triggered by small changes in ER cholesterol: a delicate balance. *Cell metabolism* 8(6), pp. 512-521.
- Raffaniello, R. D. and Wapnir, R. A. 1989. Zinc uptake by isolated rat enterocytes: effect of low molecular weight ligands. *Proceedings of the Society for Experimental Biology and Medicine* 192(3), pp. 219-224.
- Rahman, N. et al. 2016. Soluble adenylyl cyclase is essential for proper lysosomal acidification. *The Journal of general physiology* 148(4), pp. 325-339.
- Raisova, M. et al. 2002. Bcl-2 overexpression prevents apoptosis induced by ceramidase inhibitors in malignant melanoma and HaCaT keratinocytes. *FEBS letters* 516(1-3), pp. 47-52.
- Rakheja, D. and Bennett, M. J. 2018. Neuronal ceroid-lipofuscinoses. *Translational Science of Rare Diseases* 3(2), pp. 83-95.
- Ramirez, A. et al. 2006. Hereditary parkinsonism with dementia is caused by mutations in ATP13A2, encoding a lysosomal type 5 P-type ATPase. *Nature genetics* 38(10), p. 1184.
- Rappaport, J. et al. 2016. A comparative study on the alterations of endocytic pathways in multiple lysosomal storage disorders. *Molecular pharmaceuticals* 13(2), pp. 357-368.
- Rebsamen, M. et al. 2015. SLC38A9 is a component of the lysosomal amino acid sensing machinery that controls mTORC1. *Nature* 519(7544), p. 477.
- Reczek, D. et al. 2007. LIMP-2 is a receptor for lysosomal mannose-6-phosphate-independent targeting of β -glucocerebrosidase. *Cell* 131(4), pp. 770-783.
- Reddy, A. et al. 2001. Plasma membrane repair is mediated by Ca²⁺-regulated exocytosis of lysosomes. *Cell* 106(2), pp. 157-169.
- Reddy, J. V. et al. 2006. Clues to neuro-degeneration in Niemann-Pick type C disease from global gene expression profiling. *PLoS one* 1(1), p. e19.
- Reitman, M. L. et al. 1981. Fibroblasts from patients with I-cell disease and pseudo-Hurler polydystrophy are deficient in uridine 5'-diphosphate-N-acetylglucosamine: glycoprotein N-acetylglucosaminylphosphotransferase activity. *The Journal of clinical investigation* 67(5), pp. 1574-1579.
- Rommel, N. et al. 2007. Saposin B mobilizes lipids from cholesterol-poor and bis (monoacylglycero) phosphate-rich membranes at acidic pH: Unglycosylated patient variant saposin B lacks lipid-extraction capacity. *The FEBS journal* 274(13), pp. 3405-3420.
- Repetto, G. et al. 2008. Neutral red uptake assay for the estimation of cell viability/cytotoxicity. *Nature protocols* 3(7), p. 1125.
- Ribas, G. S. et al. 2017. Validation of a multiplex tandem mass spectrometry method for the detection of selected lysosomal storage diseases in dried blood spots. *Journal of Inborn Errors of Metabolism and Screening* 5, p. 2326409817692360.

- Rice, G. C. et al. 1985. FACS analysis of a hyperthermia-induced alteration in Hoechst 33342 permeability and direct measurement of its relationship to cell survival. *Journal of cellular physiology* 122(3), pp. 387-396.
- Rink, J. et al. 2005. Rab conversion as a mechanism of progression from early to late endosomes. *Cell* 122(5), pp. 735-749.
- Rodriguez-Gil, J. L. et al. 2013. A somatic cell defect is associated with the onset of neurological symptoms in a lysosomal storage disease. *Molecular genetics and metabolism* 110(1-2), pp. 188-190.
- RODRIGUEZ-LAFRASSE, C. et al. 1997. Modulation of protein kinase C by endogenous sphingosine: inhibition of phorbol dibutyrate binding in Niemann–Pick C fibroblasts. *Biochemical Journal* 325(3), pp. 787-791.
- Rodriguez-Lafresse, C. and Vanier, M. T. 1999. Sphingosylphosphorylcholine in Niemann-Pick disease brain: accumulation in type A but not in type B. *Neurochemical research* 24(2), pp. 199-205.
- Rolfs, A. et al. 2013. Glucosylsphingosine is a highly sensitive and specific biomarker for primary diagnostic and follow-up monitoring in Gaucher disease in a non-Jewish, Caucasian cohort of Gaucher disease patients. *PloS one* 8(11), p. e79732.
- Rombach, S. M. et al. 2010. Plasma globotriaosylsphingosine: diagnostic value and relation to clinical manifestations of Fabry disease. *Biochimica et Biophysica Acta (BBA)-Molecular Basis of Disease* 1802(9), pp. 741-748.
- Roth, J. A. 2006. Homeostatic and toxic mechanisms regulating manganese uptake, retention, and elimination. *Biological research* 39(1), pp. 45-57.
- Rozenberg, R. and Pereira, L. d. V. 2001. The frequency of Tay-Sachs disease causing mutations in the Brazilian Jewish population justifies a carrier screening program. *Sao Paulo Medical Journal* 119(4), pp. 146-149.
- Ruas, M. et al. 2015. Expression of Ca²⁺-permeable two-pore channels rescues NAADP signalling in TPC-deficient cells. *The EMBO journal* 34(13), pp. 1743-1758.
- Rusyn, E. et al. 2008. CLN3p impacts galactosylceramide transport, raft morphology, and lipid content. *Pediatric research* 63(6), p. 625.
- Ryazantsev, S. et al. 2007. Lysosomal accumulation of SCMAS (subunit c of mitochondrial ATP synthase) in neurons of the mouse model of mucopolysaccharidosis III B. *Molecular genetics and metabolism* 90(4), pp. 393-401.
- Saito, Y. et al. 2002. Niemann–Pick type C disease: Accelerated neurofibrillary tangle formation and amyloid β deposition associated with apolipoprotein E ϵ 4 homozygosity. *Annals of neurology* 52(3), pp. 351-355.
- Sakashita, N. et al. 2000. Localization of human acyl-coenzyme A: cholesterol acyltransferase-1 (ACAT-1) in macrophages and in various tissues. *The American journal of pathology* 156(1), pp. 227-236.
- Sakiyama, T. et al. 1987. Subcellular localization of acid sphingomyelinase and lipid in Niemann-Pick mice. *Journal of inherited metabolic disease* 10(3), pp. 301-304.

- Salvioli, R. et al. 2004. Glucosylceramidase mass and subcellular localization are modulated by cholesterol in Niemann-Pick disease type C. *Journal of Biological Chemistry* 279(17), pp. 17674-17680.
- Sampson, B. 2004. Clinical applications of inductively coupled plasma mass spectrometry. *CPD Bulletin Clinical Biochemistry* 6(1), pp. 24-31.
- Sandhoff, K. 2013. Metabolic and cellular bases of sphingolipidoses. Portland Press Limited.
- Sango, K. et al. 1996. Mice lacking both subunits of lysosomal β -hexosaminidase display gangliosidosis and mucopolysaccharidosis. *Nature genetics* 14(3), p. 348.
- Santana-Codina, N. and Mancias, J. 2018. The role of NCOA4-mediated ferritinophagy in health and disease. *Pharmaceuticals* 11(4), p. 114.
- Sardiello, M. et al. 2009. A gene network regulating lysosomal biogenesis and function. *Science* 325(5939), pp. 473-477.
- Sawkar, A. R. et al. 2002. Chemical chaperones increase the cellular activity of N370S β -glucosidase: a therapeutic strategy for Gaucher disease. *Proceedings of the National Academy of Sciences* 99(24), pp. 15428-15433.
- Schielen, P. et al. 2017. Newborn screening for lysosomal storage diseases: a concise review of the literature on screening methods, therapeutic possibilities and regional programs. *International journal of neonatal screening* 3(2), p. 6.
- Schneede, A. et al. 2011. Role for LAMP-2 in endosomal cholesterol transport. *Journal of cellular and molecular medicine* 15(2), pp. 280-295.
- Schneider, C. A. et al. 2012. NIH Image to ImageJ: 25 years of image analysis. *Nature methods* 9(7), p. 671.
- Schultz, M. L. et al. 2018. Coordinate regulation of mutant NPC1 degradation by selective ER autophagy and MARCH6-dependent ERAD. *Nature communications* 9.
- Schulz, A. et al. 2013. NCL diseases—clinical perspectives. *Biochimica et Biophysica Acta (BBA)-Molecular Basis of Disease* 1832(11), pp. 1801-1806.
- Schumacher, A. et al. 2005. Effect of 1-(1-naphthylmethyl)-piperazine, a novel putative efflux pump inhibitor, on antimicrobial drug susceptibility in clinical isolates of Enterobacteriaceae other than Escherichia coli. *Journal of Antimicrobial Chemotherapy* 57(2), pp. 344-348.
- Schwake, M. et al. 2013. Lysosomal membrane proteins and their central role in physiology. *Traffic* 14(7), pp. 739-748.
- Scott, C. and Ioannou, Y. 2004. The NPC1 protein: structure implies function. *Biochimica et Biophysica Acta (BBA)-Molecular and Cell Biology of Lipids* 1685(1-3), pp. 8-13.
- Settembre, C. et al. 2007. Systemic inflammation and neurodegeneration in a mouse model of multiple sulfatase deficiency. *Proceedings of the National Academy of Sciences* 104(11), pp. 4506-4511.
- Settembre, C. et al. 2011. TFEB links autophagy to lysosomal biogenesis. *science* 332(6036), pp. 1429-1433.

- Settembre, C. and Medina, D. L. 2015. TFEB and the CLEAR network. *Methods in cell biology*. Vol. 126. Elsevier, pp. 45-62.
- Settembre, C. et al. 2012. A lysosome-to-nucleus signalling mechanism senses and regulates the lysosome via mTOR and TFEB. *The EMBO journal* 31(5), pp. 1095-1108.
- Shen, D. et al. 2012. Lipid storage disorders block lysosomal trafficking by inhibiting a TRP channel and lysosomal calcium release. *Nature communications* 3, p. 731.
- Shetty, S. P. et al. 2014. Regulation of selenocysteine incorporation into the selenium transport protein, selenoprotein P. *Journal of Biological Chemistry* 289(36), pp. 25317-25326.
- Shigeto, S. et al. 2011. Improved assay for differential diagnosis between Pompe disease and acid α -glucosidase pseudodeficiency on dried blood spots. *Molecular genetics and metabolism* 103(1), pp. 12-17.
- Shirai, T. et al. 2000. Atypical Fabry's disease presenting with cholesterol crystal embolization. *Internal medicine* 39(8), pp. 646-649.
- Siintola, E. et al. 2006. Cathepsin D deficiency underlies congenital human neuronal ceroid-lipofuscinosis. *Brain* 129(6), pp. 1438-1445.
- Sillence, D. J. 2013. Glucosylceramide modulates endolysosomal pH in Gaucher disease. *Molecular genetics and metabolism* 109(2), pp. 194-200.
- Sillence, D. J. et al. 2002. Glucosylceramide modulates membrane traffic along the endocytic pathway. *Journal of lipid research* 43(11), pp. 1837-1845.
- Sleat, D. E. et al. 2012. Proteomic analysis of mouse models of Niemann-Pick C disease reveals alterations in the steady-state levels of lysosomal proteins within the brain. *Proteomics* 12(23-24), pp. 3499-3509.
- Smart, E. J. et al. 1999. Caveolins, liquid-ordered domains, and signal transduction. *Molecular and cellular biology* 19(11), pp. 7289-7304.
- Snitsarev, V. et al. 2001. Fluorescent detection of Zn²⁺-rich vesicles with Zinquin: mechanism of action in lipid environments. *Biophysical Journal* 80(3), pp. 1538-1546.
- Solé-Domènech, S. et al. 2018. Lysosomal enzyme tripeptidyl peptidase 1 destabilizes fibrillar A β by multiple endoproteolytic cleavages within the β -sheet domain. *Proceedings of the National Academy of Sciences* 115(7), pp. 1493-1498.
- Somogyi, A. et al. 2018. Altered expression of ganglioside metabolizing enzymes results in GM3 ganglioside accumulation in cerebellar cells of a mouse model of juvenile neuronal ceroid lipofuscinosis. *International journal of molecular sciences* 19(2), p. 625.
- Soyombo, A. A. et al. 2006. TRP-ML1 regulates lysosomal pH and acidic lysosomal lipid hydrolytic activity. *Journal of Biological Chemistry* 281(11), pp. 7294-7301.
- Steinman, R. M. et al. 1976. Membrane flow during pinocytosis. A stereologic analysis. *The Journal of cell biology* 68(3), pp. 665-687.
- Stoka, V. et al. 2016. Lysosomal cathepsins and their regulation in aging and neurodegeneration. *Ageing research reviews* 32, pp. 22-37.

- Storch, J. and Xu, Z. 2009. Niemann–Pick C2 (NPC2) and intracellular cholesterol trafficking. *Biochimica et Biophysica Acta (BBA)-Molecular and Cell Biology of Lipids* 1791(7), pp. 671-678.
- Sugimoto, Y. et al. 2001. Accumulation of cholera toxin and GM1 ganglioside in the early endosome of Niemann–Pick C1-deficient cells. *Proceedings of the National Academy of Sciences* 98(22), pp. 12391-12396.
- Sun, X. et al. 2001. Niemann-Pick C variant detection by altered sphingolipid trafficking and correlation with mutations within a specific domain of NPC1. *The American Journal of Human Genetics* 68(6), pp. 1361-1372.
- Svennerholm, L. et al. 1980. Krabbe disease: a galactosylsphingosine (psychosine) lipidosis. *Journal of lipid research* 21(1), pp. 53-64.
- Sweeley, C. C. and Klionsky, B. 1963. Fabry's disease: classification as a sphingolipidosis and partial characterization of a novel glycolipid. *Journal of Biological Chemistry* 238(9), pp. PC3148-PC3150.
- Szewczyk, B. 2013. Zinc homeostasis and neurodegenerative disorders. *Frontiers in aging neuroscience* 5, p. 33.
- Tabuchi, M. et al. 2000. Human NRAMP2/DMT1, which mediates iron transport across endosomal membranes, is localized to late endosomes and lysosomes in HEp-2 cells. *Journal of Biological Chemistry* 275(29), pp. 22220-22228.
- Taki, M. et al. 2010. Development of highly sensitive fluorescent probes for detection of intracellular copper (I) in living systems. *Journal of the American Chemical Society* 132(17), pp. 5938-5939.
- Takuro, K. et al. 1985. Galactosylceramide-and lactosylceramide-loading studies in cultured fibroblasts from normal individuals and patients with globoid cell leukodystrophy (Krabbe's disease) and GM1-gangliosidosis. *Biochimica et Biophysica Acta (BBA)-Lipids and Lipid Metabolism* 835(3), pp. 456-464.
- Tamura, H. et al. 2006. Niemann–Pick type C disease: novel NPC1 mutations and characterization of the concomitant acid sphingomyelinase deficiency. *Molecular genetics and metabolism* 87(2), pp. 113-121.
- Tan, J. et al. 2011. Regulation of intracellular manganese homeostasis by Kufor-Rakeb syndrome-associated ATP13A2 protein. *Journal of Biological Chemistry* 286(34), pp. 29654-29662.
- Tanaka, H. and Suzuki, K. 1978. Globoid cell leukodystrophy (Krabbe's disease): Metabolic studies with cultured fibroblasts. *Journal of the neurological sciences* 38(3), pp. 409-419.
- Tardieu, M. et al. 2014. Intracerebral administration of adeno-associated viral vector serotype rh. 10 carrying human SGSH and SUMF1 cDNAs in children with mucopolysaccharidosis type IIIA disease: results of a phase I/II trial. *Human gene therapy* 25(6), pp. 506-516.
- Te Vrugte, D. et al. 2010. Glycosphingolipid storage leads to the enhanced degradation of the B cell receptor in Sandhoff disease mice. *Journal of inherited metabolic disease* 33(3), pp. 261-270.

- te Vruchte, D. et al. 2004. Accumulation of glycosphingolipids in Niemann-Pick C disease disrupts endosomal transport. *Journal of Biological Chemistry* 279(25), pp. 26167-26175.
- te Vruchte, D. et al. 2014. Relative acidic compartment volume as a lysosomal storage disorder-associated biomarker. *The Journal of clinical investigation* 124(3), pp. 1320-1328.
- te Vruchte, D. et al. 2015. Measuring relative lysosomal volume for monitoring lysosomal storage diseases. *Methods Cell Biol* 126, pp. 331-347.
- Tellez-Nagel, I. et al. 1976. Mucopolidosis IV: clinical, ultrastructural, histochemical, and chemical studies of a case, including a brain biopsy. *Archives of neurology* 33(12), pp. 828-835.
- Tettamanti, G. et al. 2003. Salvage pathways in glycosphingolipid metabolism. *Biochimie* 85(3-4), pp. 423-437.
- Thomas, G. et al. 1989. Correction of sphingomyelinase deficiency in Niemann-Pick type C fibroblasts by removal of lipoprotein fraction from culture media. *Journal of inherited metabolic disease* 12(2), pp. 139-151.
- Thurberg, B. L. et al. 2004. Monitoring the 3-year efficacy of enzyme replacement therapy in Fabry disease by repeated skin biopsies. *Journal of investigative dermatology* 122(4), pp. 900-908.
- Thurberg, B. L. and Politei, J. M. 2012. Histologic abnormalities of placental tissues in Fabry disease: a case report and review of the literature. *Human pathology* 43(4), pp. 610-614.
- Thurberg, B. L. et al. 2012. Liver and skin histopathology in adults with acid sphingomyelinase deficiency (Niemann-Pick disease type B). *The American journal of surgical pathology* 36(8), p. 1234.
- Tian, X. et al. 2015. A voltage-gated calcium channel regulates lysosomal fusion with endosomes and autophagosomes and is required for neuronal homeostasis. *PLoS biology* 13(3), p. e1002103.
- Tokuyasu, K. 1980. Immunocytochemistry on ultrathin frozen sections. *The Histochemical journal* 12(4), pp. 381-403.
- Tomatsu, S. et al. 2013. Newborn screening and diagnosis of mucopolysaccharidoses. *Molecular genetics and metabolism* 110(1-2), pp. 42-53.
- Torres, J. B. et al. 2019. Imaging of changes in copper trafficking and redistribution in a mouse model of Niemann-Pick C disease using positron emission tomography. *BioMetals* 32(2), pp. 293-306.
- Tortelli, B. et al. 2014. Cholesterol homeostatic responses provide biomarkers for monitoring treatment for the neurodegenerative disease Niemann-Pick C1 (NPC1). *Human molecular genetics* 23(22), pp. 6022-6033.
- Tortorelli, S. et al. 2016. Simultaneous testing for 6 lysosomal storage disorders and X-adrenoleukodystrophy in dried blood spots by tandem mass spectrometry. *Clinical chemistry* 62(9), pp. 1248-1254.

- Tropak, M. B. et al. 2004. Pharmacological enhancement of β -hexosaminidase activity in fibroblasts from adult Tay-Sachs and Sandhoff patients. *Journal of Biological Chemistry* 279(14), pp. 13478-13487.
- Trushina, E. et al. 2006. Mutant huntingtin inhibits clathrin-independent endocytosis and causes accumulation of cholesterol in vitro and in vivo. *Human molecular genetics* 15(24), pp. 3578-3591.
- Tseng, T.-T. et al. 1999. The RND permease superfamily: an ancient, ubiquitous and diverse family that includes human disease and development proteins. *Journal of molecular microbiology and biotechnology* 1(1), pp. 107-125.
- Tsuboyama, K. et al. 2016. The ATG conjugation systems are important for degradation of the inner autophagosomal membrane. *Science* 354(6315), pp. 1036-1041.
- Turgeon, C. T. et al. 2015. Measurement of psychosine in dried blood spots—a possible improvement to newborn screening programs for Krabbe disease. *Journal of Inherited Metabolic Disease: Official Journal of the Society for the Study of Inborn Errors of Metabolism* 38(5), pp. 923-929.
- Twining, S. S. 1984. Fluorescein isothiocyanate-labeled casein assay for proteolytic enzymes. *Analytical biochemistry* 143(1), pp. 30-34.
- Tyynelä, J. et al. 1995. Sphingolipid activator proteins in the neuronal ceroid-lipofuscinoses: an immunological study. *Acta neuropathologica* 89(5), pp. 391-398.
- Tyynelä, J. et al. 1993. Storage of saposins A and D in infantile neuronal ceroid-lipofuscinosis. *FEBS letters* 330(1), pp. 8-12.
- Ucar, S. K. et al. 2010. An association among iron, copper, zinc, and selenium, and antioxidative status in dyslipidemic pediatric patients with glycogen storage disease types IA and III. *Journal of Trace Elements in Medicine and Biology* 24(1), pp. 42-45.
- Urbanowski, J. L. and Piper, R. C. 2001. Ubiquitin sorts proteins into the intraluminal degradative compartment of the late-endosome/vacuole. *Traffic* 2(9), pp. 622-630.
- Vairo, F. et al. 2015. Osteopontin: a potential biomarker of Gaucher disease. *Annals of hematology* 94(7), pp. 1119-1125.
- Van Breemen, M. J. et al. 2007. Increased plasma macrophage inflammatory protein (MIP)-1 α and MIP-1 β levels in type 1 Gaucher disease. *Biochimica et Biophysica Acta (BBA)-Molecular Basis of Disease* 1772(7), pp. 788-796.
- Van den Berghe, P. V. et al. 2007. Human copper transporter 2 is localized in late endosomes and lysosomes and facilitates cellular copper uptake. *Biochemical Journal* 407(1), pp. 49-59.
- Van der Valk, J. et al. 2010. Optimization of chemically defined cell culture media—replacing fetal bovine serum in mammalian in vitro methods. *Toxicology in vitro* 24(4), pp. 1053-1063.
- Van Diggelen, O. et al. 1999. A rapid fluorogenic palmitoyl-protein thioesterase assay: pre- and postnatal diagnosis of INCL. *Molecular genetics and metabolism* 66(4), pp. 240-244.
- Van Diggelen, O. et al. 2005. A new fluorimetric enzyme assay for the diagnosis of Niemann–Pick A/B, with specificity of natural sphingomyelinase substrate. *Journal of inherited metabolic disease* 28(5), pp. 733-741.

- Van Dussen, L. et al. 2014. Value of plasma chitotriosidase to assess non-neuronopathic Gaucher disease severity and progression in the era of enzyme replacement therapy. *Journal of inherited metabolic disease* 37(6), pp. 991-1001.
- Van Meer, G. et al. 2008. Membrane lipids: where they are and how they behave. *Nature reviews Molecular cell biology* 9(2), p. 112.
- van Veen, S. et al. 2014. Cellular function and pathological role of ATP13A2 and related P-type transport ATPases in Parkinson's disease and other neurological disorders. *Frontiers in molecular neuroscience* 7, p. 48.
- Vance, J. E. et al. eds. 2005. *Cholesterol homeostasis in neurons and glial cells*. Seminars in cell & developmental biology. Elsevier.
- Vanier, M. et al. 1996. Genetic heterogeneity in Niemann-Pick C disease: a study using somatic cell hybridization and linkage analysis. *American journal of human genetics* 58(1), p. 118.
- Vanier, M. T. 1983. Biochemical studies in Niemann-Pick disease I. Major sphingolipids of liver and spleen. *Biochimica Et Biophysica Acta (BBA)-Lipids and Lipid Metabolism* 750(1), pp. 178-184.
- Vanier, M. T. 1999. Lipid changes in Niemann-Pick disease type C brain: personal experience and review of the literature. *Neurochemical research* 24(4), pp. 481-489.
- Vanier, M. T. 2010. Niemann-Pick disease type C. *Orphanet journal of rare diseases* 5(1), p. 16.
- Vanier, M. T. 2015. Complex lipid trafficking in Niemann-Pick disease type C. *Journal of inherited metabolic disease* 38(1), pp. 187-199.
- Vanier, M. T. et al. 2016. Diagnostic tests for Niemann-Pick disease type C (NP-C): A critical review. *Molecular genetics and metabolism* 118(4), pp. 244-254.
- Vanier, M. T. and Latour, P. 2015. Laboratory diagnosis of Niemann-Pick disease type C: The filipin staining test. *Methods in cell biology*. Vol. 126. Elsevier, pp. 357-375.
- Vanier, M. T. and Millat, G. 2003. Niemann-Pick disease type C. *Clinical genetics* 64(4), pp. 269-281.
- Vanier, M. T. et al. 1991. Type C Niemann-Pick disease: spectrum of phenotypic variation in disruption of intracellular LDL-derived cholesterol processing. *Biochimica et Biophysica Acta (BBA)-Molecular Basis of Disease* 1096(4), pp. 328-337.
- Vanier, M. T. et al. 1988. Niemann-Pick disease group C: clinical variability and diagnosis based on defective cholesterol esterification: A collaborative study on 70 patients. *Clinical genetics* 33(5), pp. 331-348.
- Vanlandingham, P. A. and Ceresa, B. P. 2009. Rab7 regulates late endocytic trafficking downstream of multivesicular body biogenesis and cargo sequestration. *Journal of Biological Chemistry* 284(18), pp. 12110-12124.
- Vellodi, A. 2005. Lysosomal storage disorders. *British journal of haematology* 128(4), pp. 413-431.

- Vienken, H. et al. 2017. Characterization of cholesterol homeostasis in sphingosine-1-phosphate lyase-deficient fibroblasts reveals a Niemann-Pick disease type C-like phenotype with enhanced lysosomal Ca²⁺ storage. *Scientific reports* 7, p. 43575.
- Viswanathan, K. et al. 2012. Nonpeptidic lysosomal modulators derived from Z-Phe-Ala-diazomethylketone for treating protein accumulation diseases. *ACS Medicinal Chemistry Letters* 3(11), pp. 920-924.
- Vite, C. H. et al. 2015. Intracisternal cyclodextrin prevents cerebellar dysfunction and Purkinje cell death in feline Niemann-Pick type C1 disease. *Science translational medicine* 7(276), pp. 276ra226-276ra226.
- Vitner, E. B. et al. 2010. Common and uncommon pathogenic cascades in lysosomal storage diseases. *Journal of Biological Chemistry*, p. jbc. R110. 134452.
- Vogler, C. et al. 2005. Overcoming the blood-brain barrier with high-dose enzyme replacement therapy in murine mucopolysaccharidosis VII. *Proceedings of the National Academy of Sciences* 102(41), pp. 14777-14782.
- Vogler, C. et al. 1987. Electron microscopy in the diagnosis of lysosomal storage diseases. *American Journal of Medical Genetics* 28(S3), pp. 243-255.
- von Trotha, K.-T. et al. 2006. Influence of lysosomal acid lipase polymorphisms on chromosome 10 on the risk of Alzheimer's disease and cholesterol metabolism. *Neuroscience letters* 402(3), pp. 262-266.
- Vozyi, Y. V. et al. 1993. Applications of a new fluorimetric enzyme assay for the diagnosis of aspartylglucosaminuria. *Journal of inherited metabolic disease* 16(6), pp. 929-934.
- Vult von Steyern, F. et al. 1996. Rhodamine B, a fluorescent probe for acidic organelles in denervated skeletal muscle. *Journal of Histochemistry & Cytochemistry* 44(3), pp. 267-274.
- Wakida, K. et al. 2004. Diagnosis of adult type of Niemann-Pick disease (type C) in two brothers by filipin staining of bone marrow smears. *No to shinkei= Brain and nerve* 56(12), pp. 1047-1053.
- Walker, J. M. 2009. The bicinchoninic acid (BCA) assay for protein quantitation. *The protein protocols handbook*. Springer, pp. 11-15.
- Walkley, S. U. and Vanier, M. T. 2009a. Pathomechanisms in lysosomal storage disorders. *Biochimica et biophysica acta* 1793(4), p. 726.
- Walkley, S. U. and Vanier, M. T. 2009b. Secondary lipid accumulation in lysosomal disease. *Biochimica et Biophysica Acta (BBA)-Molecular Cell Research* 1793(4), pp. 726-736.
- Wang, G. et al. 2000. Mitochondrial DNA damage and a hypoxic response are induced by CoCl₂ in rat neuronal PC12 cells. *Nucleic acids research* 28(10), pp. 2135-2140.
- Wang, P. et al. 2018. A GNPTAB nonsense variant is associated with feline mucopolipidosis II (I-cell disease). *BMC veterinary research* 14(1), p. 416.
- Wang, W. et al. 2015. Up-regulation of lysosomal TRPML1 channels is essential for lysosomal adaptation to nutrient starvation. *Proceedings of the National Academy of Sciences* 112(11), pp. E1373-E1381.

- Wang, Y. et al. 2011. Advances in the understanding of mammalian copper transporters. *Advances in nutrition* 2(2), pp. 129-137.
- Wassif, C. A. et al. 2016. High incidence of unrecognized visceral/neurological late-onset Niemann-Pick disease, type C1, predicted by analysis of massively parallel sequencing data sets. *Genetics in Medicine* 18(1), p. 41.
- Watari, H. et al. 2000. Determinants of NPC1 expression and action: key promoter regions, posttranscriptional control, and the importance of a "cysteine-rich" loop. *Experimental cell research* 259(1), pp. 247-256.
- Weidemann, F. et al. 2013. Long-term outcome of enzyme-replacement therapy in advanced F abry disease: evidence for disease progression towards serious complications. *Journal of internal medicine* 274(4), pp. 331-341.
- Weinreb, N. J. et al. 2002. Effectiveness of enzyme replacement therapy in 1028 patients with type 1 Gaucher disease after 2 to 5 years of treatment: a report from the Gaucher Registry. *The American journal of medicine* 113(2), pp. 112-119.
- Wenger, D. A. et al. 2002. Lysosomal storage disorders: diagnostic dilemmas and prospects for therapy. *Genetics in Medicine* 4(6), p. 412.
- Wenger, D. A. et al. 2003. Insights into the diagnosis and treatment of lysosomal storage diseases. *Archives of neurology* 60(3), pp. 322-328.
- Wheeler, S. et al. 2019. Lipid-Protein Interactions in Niemann-Pick Type C Disease: Insights from Molecular Modeling. *International journal of molecular sciences* 20(3), p. 717.
- Whitfield, P. D. et al. 2001. Quantification of galactosylsphingosine in the twitcher mouse using electrospray ionization-tandem mass spectrometry. *Journal of lipid research* 42(12), pp. 2092-2095.
- Wiesmann, U. et al. 1971. Multiple lysosomal enzyme deficiency due to enzyme leakage? *The New England journal of medicine* 284(2), pp. 109-110.
- Wilcox, W. R. 2004. Lysosomal storage disorders: the need for better pediatric recognition and comprehensive care. *The Journal of pediatrics* 144(5), pp. S3-S14.
- Wilke, S. et al. 2012. Crystal structure of the conserved domain of the DC lysosomal associated membrane protein: implications for the lysosomal glyocalyx. *BMC biology* 10(1), p. 62.
- Willén, K. et al. 2017. A β accumulation causes MVB enlargement and is modelled by dominant negative VPS4A. *Molecular neurodegeneration* 12(1), p. 61.
- Williams, R. E. et al. 2006. Diagnosis of the neuronal ceroid lipofuscinoses: an update. *Biochimica et Biophysica Acta (BBA)-Molecular Basis of Disease* 1762(10), pp. 865-872.
- Winchester, B. et al. 1990. Inhibition of α -L-fucosidase by derivatives of deoxyfuconojirimycin and deoxymannojirimycin. *Biochemical Journal* 265(1), pp. 277-282.
- Winter, R. et al. 1980. Sialidosis type 2 (acid neuraminidase deficiency): clinical and biochemical features of a further case. *Clinical genetics* 18(3), pp. 203-210.

- Wiseman, H. and Halliwell, B. 1996. Damage to DNA by reactive oxygen and nitrogen species: role in inflammatory disease and progression to cancer. *Biochemical Journal* 313(Pt 1), p. 17.
- Wolf, H. et al. 2016. A mouse model for fucosidosis recapitulates storage pathology and neurological features of the milder form of the human disease. *Disease models & mechanisms* 9(9), pp. 1015-1028.
- Xie, C. et al. 2017. AAV9-NPC1 significantly ameliorates Purkinje cell death and behavioral abnormalities in mouse NPC disease. *Journal of lipid research* 58(3), pp. 512-518.
- Xiong, J. and Zhu, M. X. 2016. Regulation of lysosomal ion homeostasis by channels and transporters. *Science China Life Sciences* 59(8), pp. 777-791.
- Xu, H. and Ren, D. 2015. Lysosomal physiology. *Annual review of physiology* 77, pp. 57-80.
- Xu, M. et al. 2012a. A high-throughput sphingomyelinase assay using natural substrate. *Analytical and bioanalytical chemistry* 404(2), pp. 407-414.
- Xu, M. et al. 2012b. δ -Tocopherol reduces lipid accumulation in Niemann-Pick type C1 and Wolman cholesterol storage disorders. *Journal of Biological Chemistry* 287(47), pp. 39349-39360.
- Xu, M. et al. 2014. A phenotypic compound screening assay for lysosomal storage diseases. *Journal of biomolecular screening* 19(1), pp. 168-175.
- Xu, S. et al. 2007. Structural basis of sterol binding by NPC2, a lysosomal protein deficient in Niemann-Pick type C2 disease. *Journal of Biological Chemistry* 282(32), pp. 23525-23531.
- Yam, G. H.-F. et al. 2006. Pharmacological chaperone corrects lysosomal storage in Fabry disease caused by trafficking-incompetent variants. *American Journal of Physiology-Cell Physiology* 290(4), pp. C1076-C1082.
- Yamada, T. et al. 1983. Lysosomal sialidase deficiency in sialidosis with partial β -galactosidase deficiency. *Biochimica et Biophysica Acta (BBA)-General Subjects* 755(1), pp. 106-111.
- Yamazaki, T. et al. 2001. Accumulation and aggregation of amyloid β -protein in late endosomes of Niemann-pick type C cells. *Journal of Biological Chemistry* 276(6), pp. 4454-4460.
- Yanagimoto, C. et al. 2009. Niemann-Pick C1 protein transports copper to the secretory compartment from late endosomes where ATP7B resides. *Experimental cell research* 315(2), pp. 119-126.
- Yang, N.-D. et al. 2014. Artesunate induces cell death in human cancer cells via enhancing lysosomal function and lysosomal degradation of ferritin. *Journal of Biological Chemistry* 289(48), pp. 33425-33441.
- Yapici, N. B. et al. 2015. Highly stable and sensitive fluorescent probes (LysoProbes) for lysosomal labeling and tracking. *Scientific reports* 5, p. 8576.
- Yogalingam, G. et al. 2008. Neuraminidase 1 is a negative regulator of lysosomal exocytosis. *Developmental cell* 15(1), pp. 74-86.

- Yoshida, S. et al. 2016. Prenatal diagnosis of Gaucher disease using next-generation sequencing. *Pediatrics International* 58(9), pp. 946-949.
- Yoshii, S. R. and Mizushima, N. 2017. Monitoring and measuring autophagy. *International journal of molecular sciences* 18(9), p. 1865.
- Yoshimori, T. et al. 1991. Bafilomycin A1, a specific inhibitor of vacuolar-type H (+)-ATPase, inhibits acidification and protein degradation in lysosomes of cultured cells. *Journal of Biological Chemistry* 266(26), pp. 17707-17712.
- Young, E. et al. 1997. Plasma chitotriosidase activity in Gaucher disease patients who have been treated either by bone marrow transplantation or by enzyme replacement therapy with alglucerase. *Journal of inherited metabolic disease* 20(4), pp. 595-602.
- Young, E. et al. 2005. Is globotriaosylceramide a useful biomarker in Fabry disease? *Acta Paediatrica* 94, pp. 51-54.
- Young, S. P. et al. 2009. Long-term monitoring of patients with infantile-onset Pompe disease on enzyme replacement therapy using a urinary glucose tetrasaccharide biomarker. *Genetics in Medicine* 11(7), p. 536.
- Yu, C. et al. 2013. Enzymatic screening and diagnosis of lysosomal storage diseases. *North American journal of medicine & science* 6(4), p. 186.
- Yu, W. et al. 2005. Neurodegeneration in heterozygous Niemann-Pick type C1 (NPC1) mouse: implication of heterozygous npc1 mutations being a risk for tauopathy. *Journal of Biological Chemistry* 280(29), pp. 27296-27302.
- Zahran, A. M. et al. 2015. Oxidative stress, trace elements, and circulating microparticles in patients with Gaucher disease before and after enzyme replacement therapy. *Clinical and Applied Thrombosis/Hemostasis* 21(1), pp. 58-65.
- Zalewski, P. D. et al. 1993. Correlation of apoptosis with change in intracellular labile Zn (II) using zinquin [(2-methyl-8-p-toluenesulphonamido-6-quinolyloxy) acetic acid], a new specific fluorescent probe for Zn (II). *Biochemical Journal* 296(2), pp. 403-408.
- Zervas, M. et al. 2001. Critical role for glycosphingolipids in Niemann-Pick disease type C. *Current Biology* 11(16), pp. 1283-1287.
- Zhang, L. 2010. Glycosaminoglycan (GAG) biosynthesis and GAG-binding proteins. *Progress in molecular biology and translational science*. Vol. 93. Elsevier, pp. 1-17.
- Zhang, X. K. et al. 2008. Multiplex enzyme assay screening of dried blood spots for lysosomal storage disorders by using tandem mass spectrometry. *Clinical chemistry* 54(10), pp. 1725-1728.
- Zhang, Y. et al. 2003. Cholesterol is superior to 7-ketocholesterol or 7 α -hydroxycholesterol as an allosteric activator for acyl-coenzyme A: cholesterol acyltransferase 1. *Journal of Biological Chemistry* 278(13), pp. 11642-11647.
- Zhitomirsky, B. et al. 2018. LysoTracker and MitoTracker Red are transport substrates of P-glycoprotein: implications for anticancer drug design evading multidrug resistance. *Journal of cellular and molecular medicine* 22(4), pp. 2131-2141.

- Zhong, X. Z. et al. 2016. BK channel agonist represents a potential therapeutic approach for lysosomal storage diseases. *Scientific reports* 6, p. 33684.
- Zhong, X. Z. et al. 2017. Methods for monitoring Ca²⁺ and ion channels in the lysosome. *Cell Calcium* 64, pp. 20-28.
- Zhou, H. et al. 2011. Newborn bloodspot screening for lysosomal storage disorders. *The Journal of pediatrics* 159(1), pp. 7-13. e11.
- Zhou, X. Y. et al. 1995. Mouse model for the lysosomal disorder galactosialidosis and correction of the phenotype with overexpressing erythroid precursor cells. *Genes & development* 9(21), pp. 2623-2634.
- Zhou, Y.-j. et al. 2009. The protection of selenium on ROS mediated-apoptosis by mitochondria dysfunction in cadmium-induced LLC-PK1 cells. *Toxicology in Vitro* 23(2), pp. 288-294.
- Zlomy, M. et al. 2019. The value of axillary skin electron microscopic analysis in the diagnosis of lysosomal storage disorders. *Modern Pathology*, p. 1.
- Zunke, F. et al. 2016. Characterization of the complex formed by β -glucocerebrosidase and the lysosomal integral membrane protein type-2. *Proceedings of the National Academy of Sciences* 113(14), pp. 3791-3796.

Chapter 10: Supplementary

Supplementary Table 1.

List of cell lines, their types, the ages of the sample collection and the provider of the cell lines.

	Name	Type	Age	Code	Code in figures
1.	APPARENTLY HEALTHY	Fibroblast	1 YR	GM05399	Control 1yr
2.	APPARENTLY HEALTHY	Fibroblast	6 YR	GM05400	Control 6yr
3.	APPARENTLY HEALTHY	Fibroblast	13 YR	GM01651	Control 13yr
4.	APPARENTLY HEALTHY	Fibroblast	26 YR	GM02912	Control 26yr
5.	APPARENTLY HEALTHY	Fibroblast	45 YR	GM00730	Control 45yr
6.	APPARENTLY HEALTHY	Fibroblast	54 YR	GM04787	Control 54yr
7.	GANGLIOSIDOSIS, GM1, TYPE I	Fibroblast	7 MO	GM03589	GM1 gangliosidosis
8.	TAY-SACHS DISEASE	Fibroblast	8 MO	GM00502	Tay Sachs/ Tay Sachs patient 1
9.	TAY-SACHS DISEASE	Fibroblast	45 YR	GM13204	Tay Sachs patient 2
10.	TAY-SACHS DISEASE, AB VARIANT	Fibroblast	1 YR	GM01675	Tay Sachs AB variant
11.	SANDHOFF DISEASE	Fibroblast	1 YR	GM00317	Sandhoff
12.	GAUCHER DISEASE, TYPE I	Fibroblast	20 YR	GM00852	GDI/ GDI patient 1
13.	GAUCHER DISEASE, TYPE I	Fibroblast	30 YR	GM01607	GDI patient 2
14.	GAUCHER DISEASE, TYPE II	Fibroblast	1 YR	GM08760	GDII
15.	KRABBE DISEASE	Fibroblast	2 YR	GM06806	Krabbe
16.	FABRY DISEASE	Fibroblast	10 YR	GM00107	Fabry/ Fabry patient 1
17.	FABRY DISEASE	Fibroblast	17 YR	GM00881	Fabry patient 2
18.	METACHROMATIC LEUKODYSTROPHY	Fibroblast	3 YR	GM00243	MLD
19.	NIEMANN-PICK DISEASE, TYPE A	Fibroblast	10 MO	GM00112	NPA/ NPA patient 1
20.	NIEMANN-PICK DISEASE, TYPE A	Fibroblast	1 YR	GM00370	NPA patient 2
21.	FARBER LIPOGRANULOMATOSIS	Fibroblast	1 DAY	GM05752	Farber
22.	HURLER SYNDROME MPS I	Fibroblast	1 YR	GM00798	MPS I
23.	MUCOPOLYSACCHARIDOSIS TYPE II	Fibroblast	5 YR	GM02268	MPS II/ MPS II patient 1
24.	MUCOPOLYSACCHARIDOSIS TYPE II	Fibroblast	2 YR	GM00298	MPS II patient 2
25.	MUCOPOLYSACCHARIDOSIS TYPE IIIA	Fibroblast	3 YR	GM01881	MPS IIIA
26.	MUCOPOLYSACCHARIDOSIS TYPE IIIB	Fibroblast	7 YR	GM00156	MPS IIIB
27.	MUCOPOLYSACCHARIDOSIS TYPE IIID	Fibroblast	7 YR	GM05093	MPS IIID
28.	MORQUIO DISEASE, TYPE B, MPS IVB	Fibroblast	2 YR	GM05335	MPS IVB
29.	MUCOPOLYSACCHARIDOSIS TYPE VII	Fibroblast	4 YR	GM00151	MPS VII
30.	CLN1	Fibroblast	19 YR	GM20389	CLN1
31.	CLN2	Fibroblast	No Data	GM16485	CLN2
32.	CLN3 1KB	Fibroblast	No Data	Prof. Sara Mole	CLN3/ CLN3 patient 1
33.	CLN3 Point mutation	Fibroblast	No Data	Prof. Sara Mole	CLN3 patient 2
34.	CLN5 P1 (HFG84a)	Fibroblast	No Data	Prof. Sara Mole	CLN5 patient 1

35.	CLN5 P2 (HFG84b)	Fibroblast	No Data	Prof. Sara Mole	CLN5 patient 2
36.	CLN5 P3 (HFG90)	Fibroblast	No Data	Prof. Sara Mole	CLN5 patient 3
37.	CLN6	Fibroblast	No Data	Prof. Sara Mole	CLN6
38.	CLN7	Fibroblast	No Data	Prof. Sara Mole	CLN7
39.	CLN8	Fibroblast	No Data	Prof. Sara Mole	CLN8
40.	CLN10 (473)	Fibroblast	No Data	Prof. Sara Mole	CLN10 /CLN10 patient 1
41.	CLN10 (597)	Fibroblast	No Data	Prof. Sara Mole	CLN10 patient 2
42.	FUCOSIDOSIS	Fibroblast	9 YR	GM00291	Fucosidosis
43.	NEURAMINIDASE DEFICIENCY	Fibroblast	2 MO	GM01718	Sialidosis
44.	MANNOSIDOSIS	Fibroblast	7 YR	GM00654	α-mannosidosis
45.	GLYCOGEN STORAGE DISEASE II	Fibroblast	5 MO	GM00248	Pompe disease
46.	WOLMAN	Fibroblast	7 MO	GM01606	Wolman disease
47.	MULTIPLE SULFATASE DEFICIENCY	Fibroblast	9 YR	GM03245	MSD/ MSD patient 1
48.	MULTIPLE SULFATASE DEFICIENCY	Fibroblast		Sheffield	MSD patient 2
49.	MUCOLIPIDOSIS II; ML2; ML II	Fibroblast	2 WK	GM02013	I Cell
50.	GALACTOSIALIDOSIS	Fibroblast	9 MO	GM02438	Galactosialidosis
51.	NIEMANN-PICK DISEASE, TYPE C1; NPC1	Fibroblast	9 YR	GM03123	NPC1
52.	NIEMANN-PICK DISEASE, TYPE C2 NPC2	Fibroblast	No data	GM18455	NPC2
53.	NIEMANN-PICK DISEASE, TYPE C1; NPC1	Fibroblast	39 YR	GM23151	NPC1 ^{+/-}
54.	Salla	Fibroblast	No data	Prof. Sara Mole	Salla
55.	MUCOLIPIDOSIS IV	Fibroblast	2 YR	GM02527	MLIV
56.	CYSTINOSIS	Fibroblast	5 YR	GM00008	Cystinosis
57.	APPARENTLY HEALTHY	B-Lymphocyte	4 YR	GM13072	Control 4yr
58.	APPARENTLY HEALTHY	B-Lymphocyte	14 YR	GM03797	Control 14yr
59.	APPARENTLY HEALTHY	B-Lymphocyte	26 YR	GM06051	Control 26yr
60.	TAY-SACHS DISEASE; TSD HEXOSAMINIDASE A; HEXA	B-Lymphocyte	1 YR	GM03585	Tay Sachs
61.	GAUCHER DISEASE, TYPE I	B-Lymphocyte	11 YR	GM10874	GDI
62.	GAUCHER DISEASE, TYPE II	B-Lymphocyte	1 YR	GM08752	GDII
63.	KRABBE DISEASE	B-Lymphocyte	2 YR	GM06805	Krabbe
64.	FABRY DISEASE	B-Lymphocyte	41 YR	GM04391	Fabry
65.	GALACTOSIALIDOSIS	B-Lymphocyte	8 YR	GM04305	Galactosialidosis

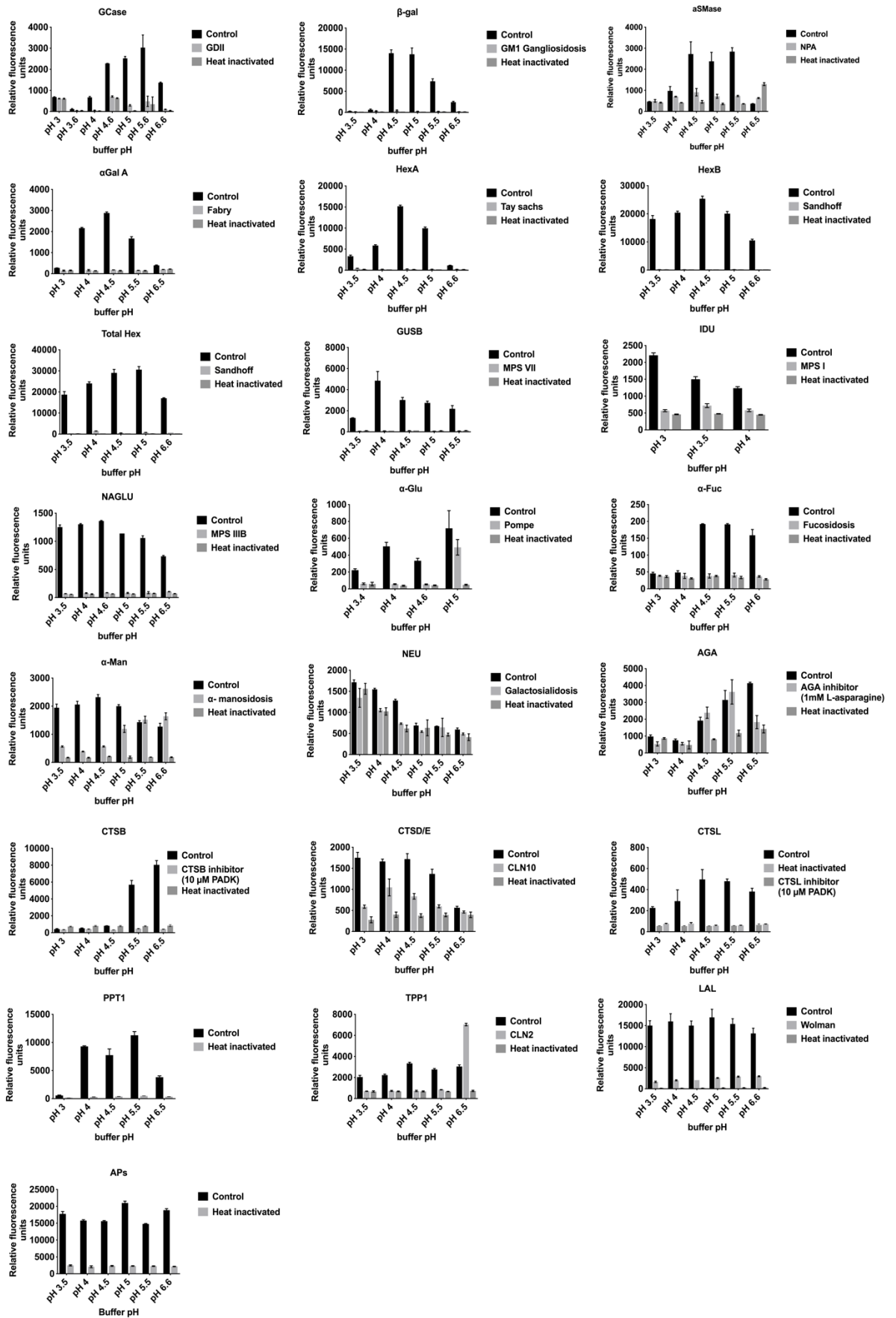
66.	MUCOPOLYSACCHARIDOSIS TYPE II	B-Lymphocyte	11 YR	GM10866	MPS II
67.	NIEMANN-PICK DISEASE, TYPE C1; NPC1	B-Lymphocyte	9 YR	GM03124	NPC1
68.	BSNPC (G46V/P691L)	Fibroblast	No data	Dr. C. Wassif, NIH	BSNPC (G46V/P691L)
69.	KWNPC (I061T/P1007A)	Fibroblast	No data	Dr. C. Wassif, NIH	KWNPC (I061T/P1007A)
70.	MONPC (I0161T/D948N)	Fibroblast	No data	Dr. C. Wassif, NIH	MONPC (I0161T/D948N)
71.	Huntington disease	Fibroblast	6 YR	GM09197	Huntington disease
72.	APP (Familial AD)	Fibroblast	No data		APP (Familial AD)
73.	PSEN 1 (Familial AD)	Fibroblast	No data		PSEN 1 (Familial AD)
74.	ATP6AP2-deficient	Fibroblast	No data		ATP6AP2-deficient
75.	CYSTIC FIBROSIS	Fibroblast	4 YR	GM03466	Cystic fibrosis

Optimum conditions for the enzyme assays

In order to find out the optimum conditions for the enzymes assay, I have modified the methods (As in chapter 2 table 2.2) to obtain the most suitable accurate method. I have used the homogenised fibroblast to find out the optimum pH conditions of the lysosomal enzymes.

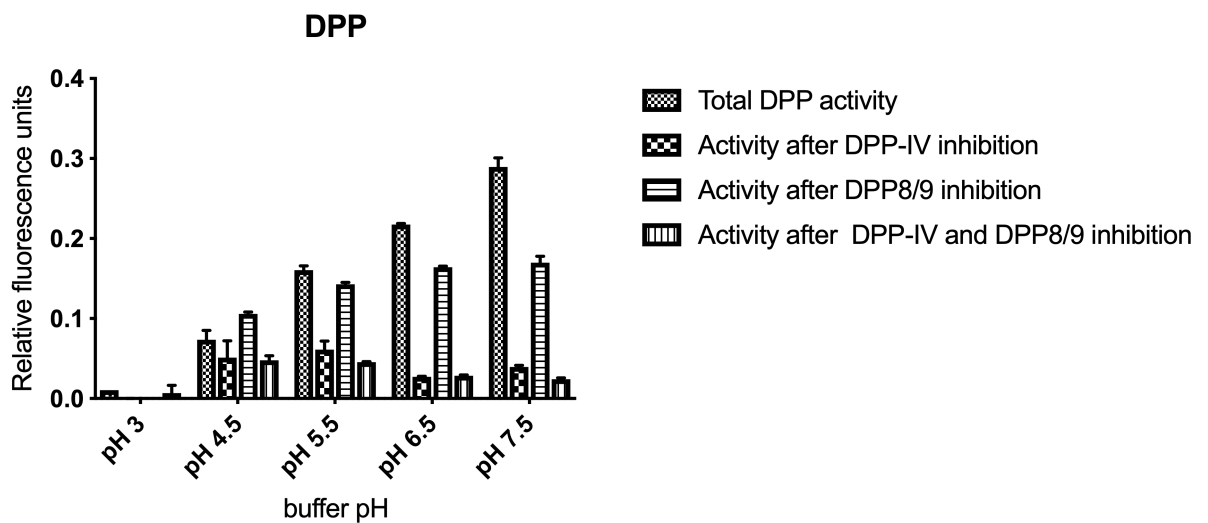
Supplementary Figure 1. The pH dependence of lysosomal enzymes activity in fibroblasts.

The enzyme results were achieved with a varying working buffer pH. I tested the buffer pH to find the highest control enzyme activity was recorded comparing to either specific disease, enzyme inhibitor and heat-inactivated. The optimum pH obtained from these graphs is in (Chapter 2.3).



Suitable conditions to measure the dipeptidyl-peptidase (DPP) enzymes

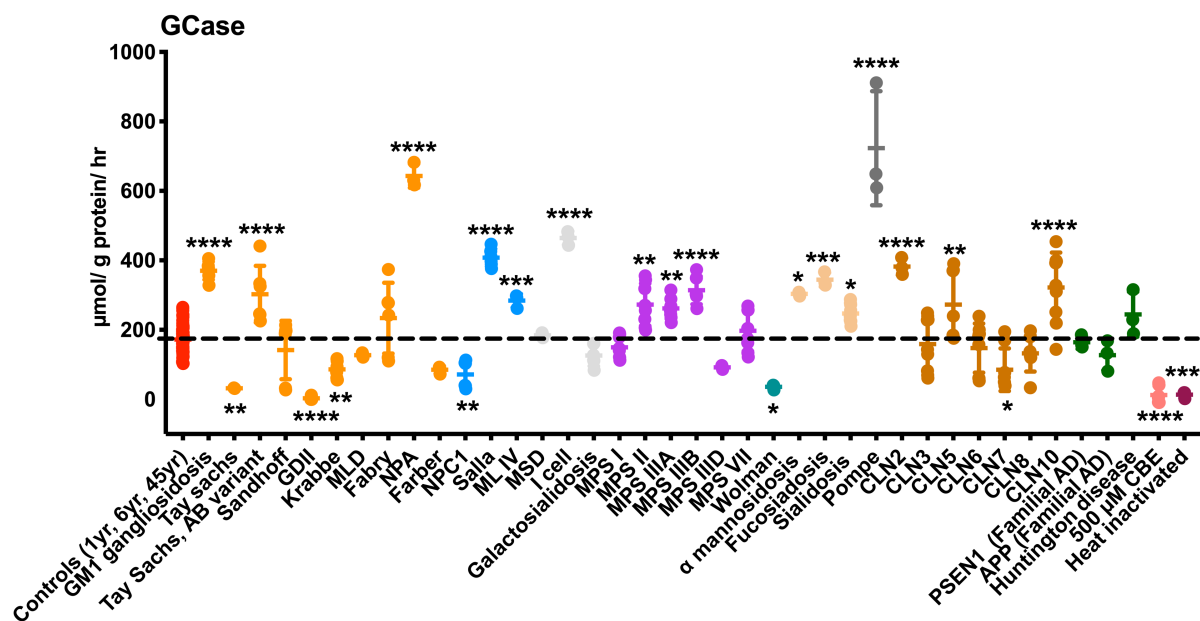
In this study I was able to identify the suitable conditions to measure the dipeptidyl-peptidase (DPP) enzymes. The substrate Gly-Pro-p-nitroanilide was used as it is not only specific to DPPIV, it is also cleaved by other DPP enzymes activities. By using different inhibitors (DPPIV inhibitor, sitagliptin 2mM, and N-Ethylmaleimide (NEM) 5mM to inhibit DP-8/9) and pH conditions I was able to discriminate the DPPIV, DPPII, DPP7 and DDP8. At 37°C, all the DPP proteins were active, including DPP-IV, DPP8/9 and DPP2. The total DPP protein starts to be active in pH 4.5 and the activity increases when the pH increases. With the DPPIV protein inhibitor sitagliptin present, there was an increased reduction of activity from pH 4.5 to 7.5, starting from about a 30% inhibition in pH 4.5 to an over 80% inhibition in pH 7.5 compared to the total DPP protein activity. On the other hand, with the addition of the DPP8/9 inhibitor, the activity started to decrease from pH 5.5, with a reduction of about 10% to about 40% in pH 7.5. This indicates that DPP8/9 is active above pH 5.5 and is even more active in higher pHs. It was noted that when both DPP-IV and DPP8/9 inhibitors were used, the reduction activity started from 35% of inhibition at pH 4.5 to 70% at pH 5.5 and over 90% at pH 7.5. This means that the DPP2 enzymes are only active at pH 4.5–5.5. It was to use pH 7.5 in the assay as it had the highest DPP activity which is possibly only DPP-IV and DPP8/9.



Supplementary Figure 2. The activity of Gly-pro-p-nitroanilide substrate hydrolysis. Control fibroblast (GM05399) were untreated or treated either with sitagliptin 2 mM as the DPPIV inhibitor or NEM 5 mM as the DP-8/9 inhibitor or with a combination of both inhibitors. The results showed that after the subtraction of the enzyme activity due to heat inactivation, the Gly-pro-p-nitroanilide hydrolysis could be carried out with a different buffer pH. N=2 for all assays. The data are shown as mean \pm SD. The experiments were performed as teamwork with Ms. Hiu Tung Shek.

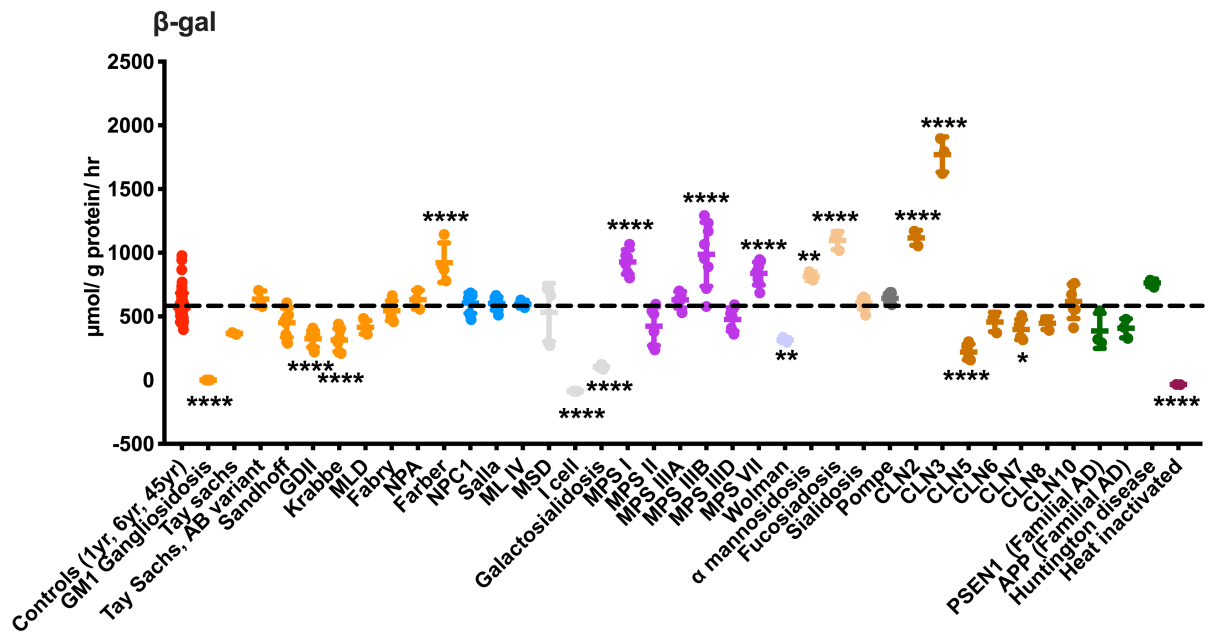
Enzyme activity among lysosomal storage disease fibroblast and statistical analysis

The activities of 23 lysosomal enzymes among LSDs and neurodegenerative disease are shown in (Supplementary Figures 3–25). Each graph shows single lysosomal enzyme activity among all diseases. The dashed line is the mean of the controls (1 year, 6 years, 45 years). Each group of LSDs is represented by different colour; sphingolipidoses, transmembrane protein defect, multiple enzyme deficiency, mucopolysaccharidoses, cholesteryl esters and triglycerides storage disease, Oligosaccharidoses, Glycogenoses, NCLs, and other neurovegetative diseases. One-way ANOVA and Bonferroni's multiple comparisons tests were carried out on. Statistical significance was determined at * $P \leq 0.05$; ** $P \leq 0.01$; *** $P \leq 0.001$; **** $P \leq 0.0001$. Data are shown as mean \pm SD.



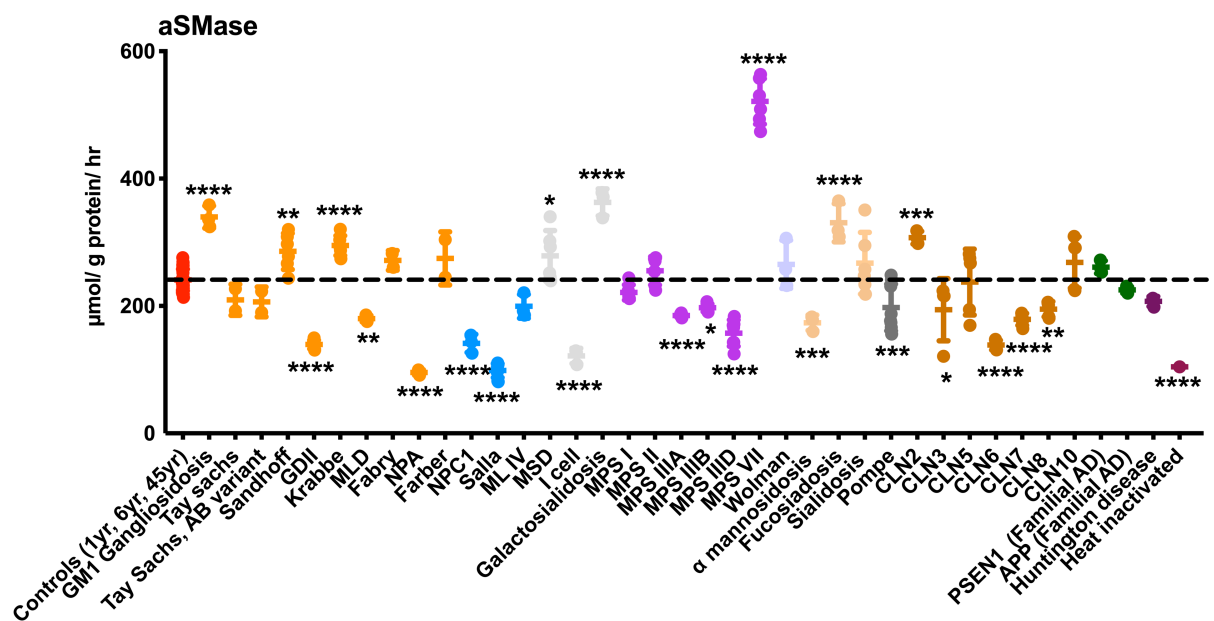
Supplementary Figure 3. GCase activity in controls vs. LSDs and other neurovegetative disease patient fibroblasts.

Compared to controls, the GCase activity increased in Sphingolipidoses; GM1 gangliosidosis, Tay-Sachs, AB variant, NPA ($p \leq 0.0001$). By contrast, it decreased in Tay-Sachs ($p \leq 0.01$), and Krabbe ($p \leq 0.01$), with more reduction in GDII ($p \leq 0.0001$). There was a reduction in NPC1 ($p \leq 0.01$), and, by contrast, a significant increase in activity in Salla ($p \leq 0.0001$) and MLIV ($p \leq 0.001$). There was a significant increase only in MPS II ($p \leq 0.01$), MPS IIIA ($p \leq 0.01$) and MPS IIIB ($p \leq 0.0001$) among MPSs. The GCase activity was a defect in Wolman ($p \leq 0.01$). α mannosidosis and Sialidosis exhibited an increase in GCase activity ($p \leq 0.05$), and more increased in GCase activity in Fucosidosis ($p \leq 0.0001$). The enzyme activity was also upregulated in Pompe ($p \leq 0.0001$). The CLN2 and CLN5 showed an increase in GCase activity of ($p \leq 0.0001$) and ($p \leq 0.01$), respectively. In CLN0, GCase activity increased, with $p \leq 0.0001$. The decreased in GCase activity was detected in CLN7 ($p \leq 0.01$). The CBE, as a known inhibitor, was used here alongside the heat inactivated been added to confirm the specificity of the assay.



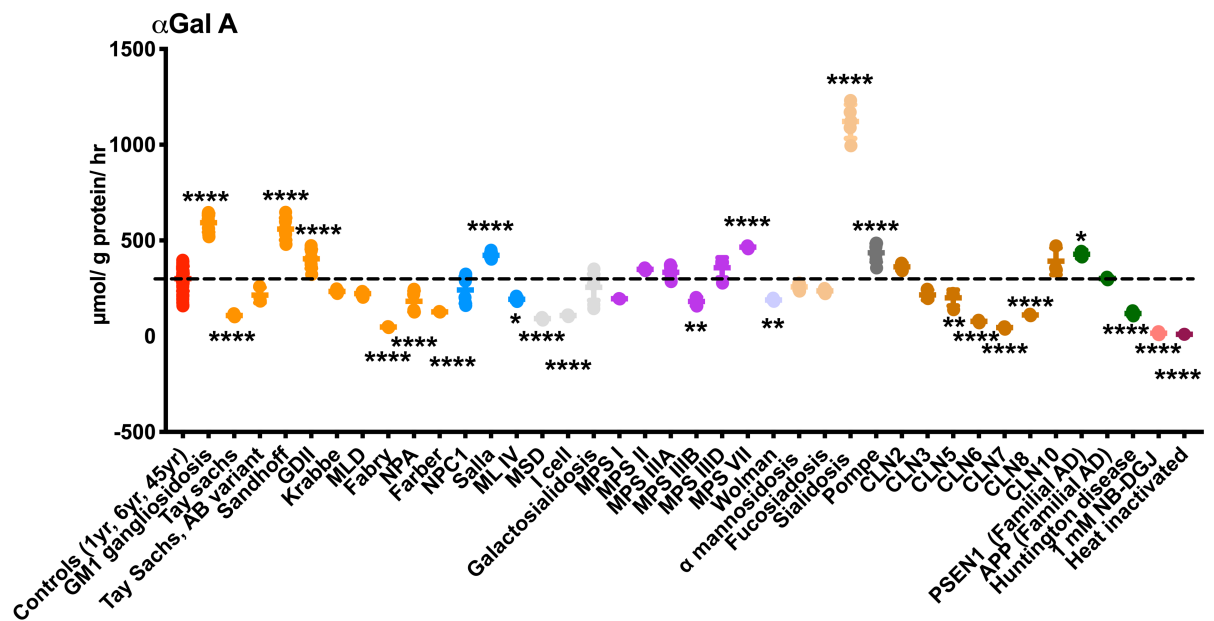
Supplementary Figure 4. β-gal activity in controls vs. LSDs and other neurovegetative disease patient fibroblasts.

The β-gal activity decreased in GM1 gangliosidosis ($p \leq 0.0001$), GDII ($p \leq 0.0001$), Krabbe ($p \leq 0.0001$). The enzyme activity increased in NPA ($p \leq 0.0001$). The I cell and Galactosialidosis showed a reduction in β-gal activity ($p \leq 0.0001$). The MPS I, MPS IIIB, and MPS VII showed an increased in β-gal activity ($p \leq 0.0001$). The β-gal activity was slightly decreased in Wolman ($p \leq 0.01$), whereas it increased in α mannosidosis ($p \leq 0.01$) and Fucosidosis ($p \leq 0.0001$). In NCLs the β-gal activity increased in CLN2 and CLN3 ($p \leq 0.0001$). By contrast, there was a reduction in CLN5 ($p \leq 0.0001$) and CLN7 ($p \leq 0.05$). There was no detectable activity in heat-inactivated.



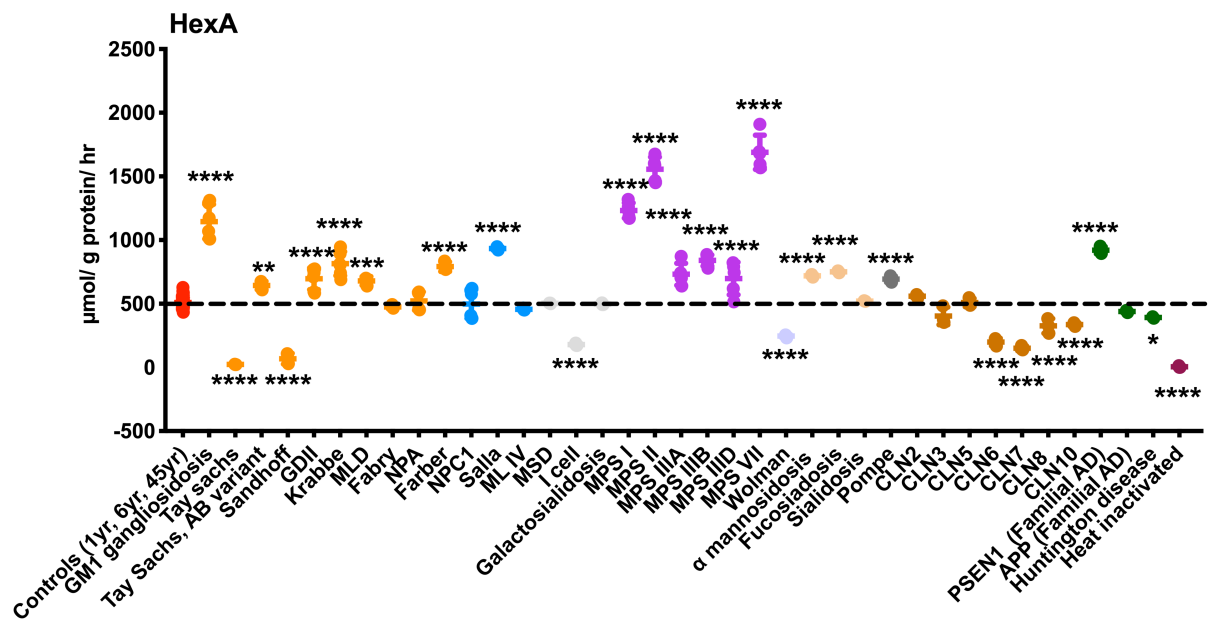
Supplementary Figure 5. aSMase activity in controls vs. LSDs and other neurovegetative disease patient fibroblasts.

The aSMase activity increased in GM1 gangliosidosis ($p \leq 0.0001$), Sandhoff ($p \leq 0.01$) and in Krabbe ($p \leq 0.0001$). There was a reduction in aSMase activity in GDII ($p \leq 0.0001$), MLD ($p \leq 0.01$) and NPA ($p \leq 0.0001$). NPC1 ($p \leq 0.0001$) and Salla ($p \leq 0.0001$), showed a reduction in activity compared to the controls. There was only a slight increase in MSD ($p \leq 0.05$) and a significant decrease in I cell ($p \leq 0.0001$). The aSMase activity increased in Galactosialidosis ($p \leq 0.0001$). The aSMase activity decreased in MPS IIIA ($p \leq 0.0001$), MPS IIIB ($p \leq 0.05$) and MPS IIID ($p \leq 0.0001$). There was a significant increase in MPS VII ($p \leq 0.0001$). aSMase activity decreased in α mannosidosis ($p \leq 0.0001$) and increased in Fucosidosis ($p \leq 0.001$). Pompe disease saw a reduction in aSMase activity ($p \leq 0.0001$). In NCLs, there was increased activity only in CLN2 ($p \leq 0.001$). By contrast, there was a decrease in CLN3 ($p \leq 0.05$), CLN6, CLN7 ($p \leq 0.0001$) and CLN8 ($p \leq 0.01$). The aSMase enzyme showed low activity in a heat-inactivated sample



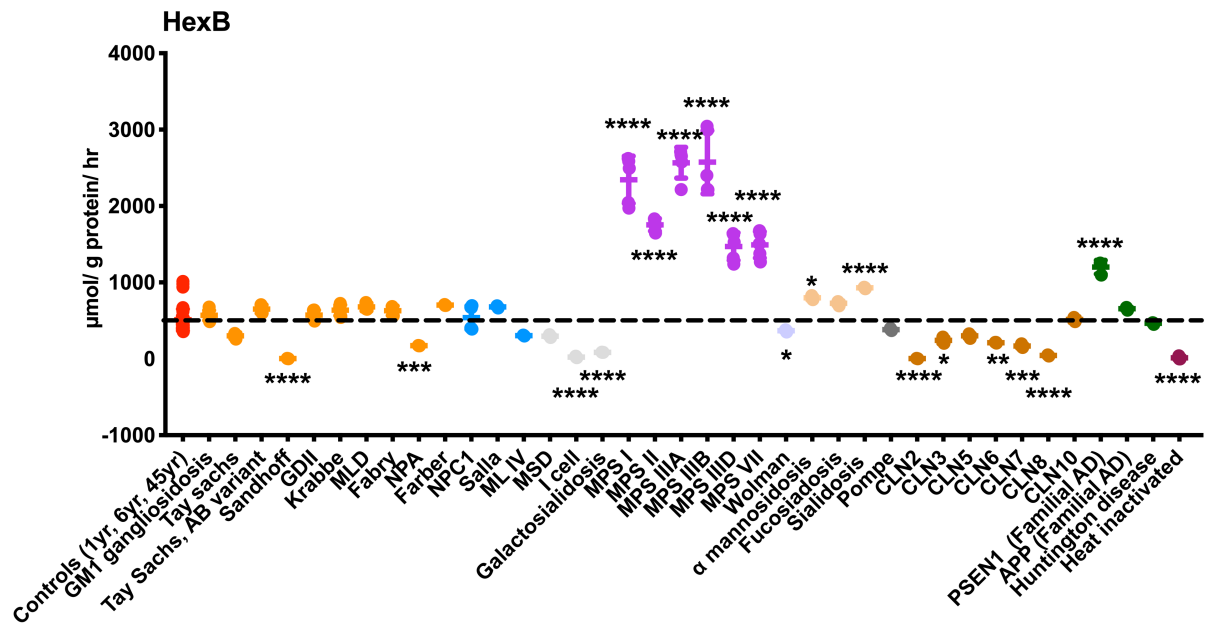
Supplementary Figure 6. αGal A activity in controls vs. LSDs and other neurovegetative disease patient fibroblasts.

αGal A activity was altered in several of the LSDs diseases compared to the control activity. The enzyme activity increased in GM1 gangliosidosis, Sandhoff, and GDII ($p \leq 0.0001$). The αGal A activity, by contrast, decreased in Tay-Sachs, Fabry, NPA, and Farber ($p \leq 0.0001$). Salla showed an increase in αGal A activity ($p \leq 0.0001$). The MLIV ($p \leq 0.05$), compared to the control, showed a decrease in αGal A. αGal A activity decreased in MSD and I cell ($p \leq 0.0001$). αGal A activity decreased in MPS IIIB ($p \leq 0.01$) and increased in MPS VII ($p \leq 0.0001$). Wolman disease showed a reduction in αGal A activity ($p \leq 0.05$). In contrast αGal A activity increased in Sialidosis and Pompe ($p \leq 0.0001$). There was a reduction in αGal A activity in CLN5 ($p \leq 0.01$), CLN6 ($p \leq 0.0001$), CLN7 ($p \leq 0.0001$), and CLN8 ($p \leq 0.0001$). PSEN1 had an increase in αGal activity ($p \leq 0.05$). By contrast, Huntington's showed a decrease in αGal A activity ($p \leq 0.0001$). The αGal A enzyme showed low activity in NB-DGJ inhibitor and a heat-inactivated samples.



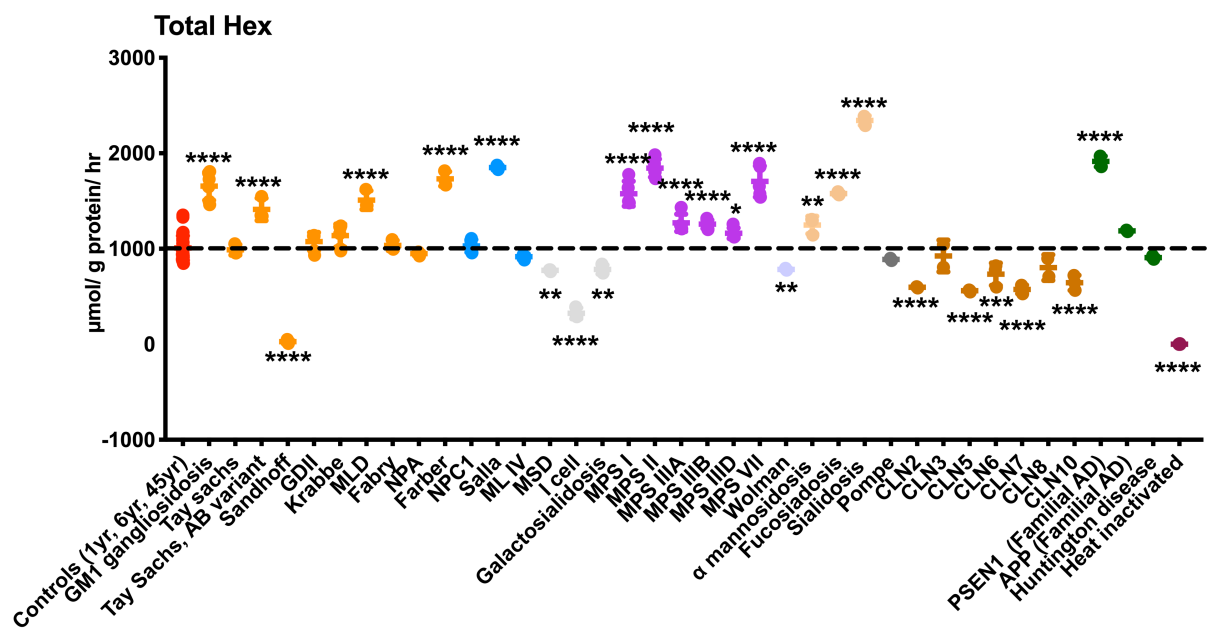
Supplementary Figure 7. HexA activity in controls vs. LSDs and other neurovegetative disease patient fibroblasts.

Compared to the controls, HexA activity increased in the majority of LSDs included in this study. The enzyme increased in GM1 gangliosidosis ($p \leq 0.0001$), Tay-Sachs, AB variant ($p \leq 0.01$), GDII, Krabbe, and Farber ($p \leq 0.0001$), and MLD ($p \leq 0.001$). There was a reduction in enzyme activity in Tay-Sachs and Sandhoff ($p \leq 0.0001$). HexA activity increased in Salla ($p \leq 0.0001$). There was a significant reduction in I cell ($p \leq 0.0001$). All MPSs had an increase in HexA activity ($p \leq 0.0001$). HexA activity decreased in Wolman ($p \leq 0.0001$). There was an increase in the enzyme activity in α mannosidosis, Fucosidosis, and Pompe ($p \leq 0.0001$). HexA activity reduced in CLN6, CLN7, CLN8, and CLN10 ($p \leq 0.0001$). There was an increase in activity in PSEN1 ($p \leq 0.0001$) and a slight reduction in Huntington's disease ($p \leq 0.05$). HexA had no activity in a heat-inactivated sample.



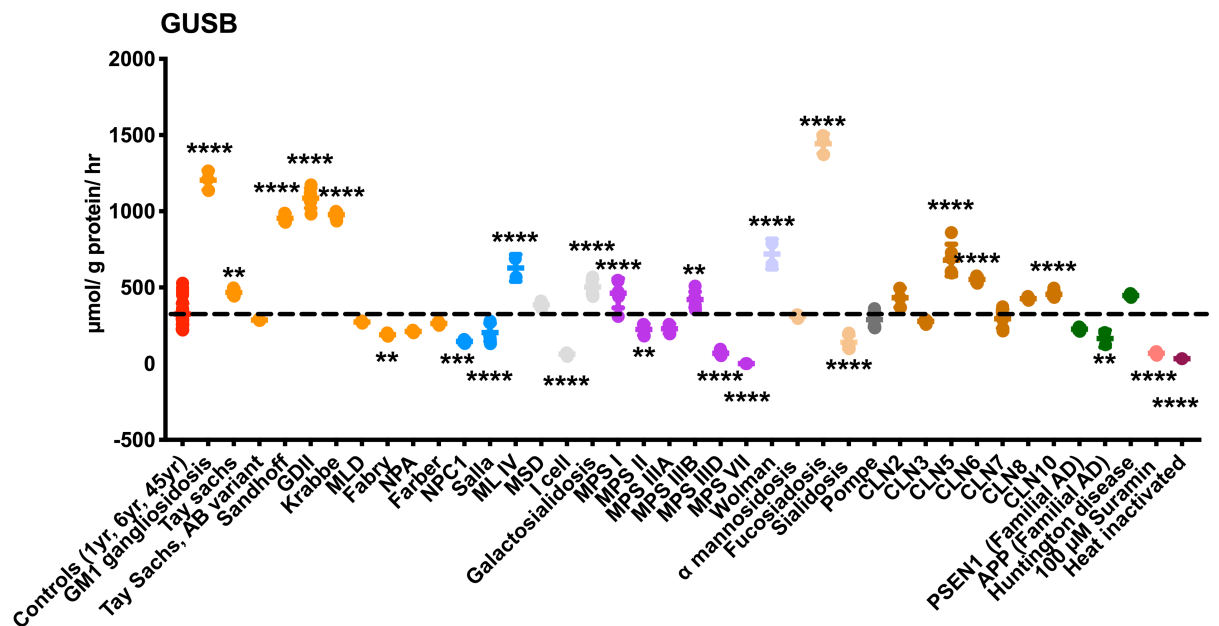
Supplementary Figure 8. HexB activity in controls vs. LSDs and other neurovegetative disease patient fibroblasts.

Compared to the controls, the HexB enzyme decreased in Sandhoff ($p \leq 0.0001$) and NPA ($p \leq 0.001$). There was a decreased in HexB enzyme activity in I cell and Galactosialidosis ($p \leq 0.0001$). There was an increase in HexB enzyme activity across all MPSs ($p \leq 0.0001$). There was only a slight decrease in the enzyme in Wolman ($p \leq 0.05$) and an increase in α mannosidosis ($p \leq 0.05$). In Sialidosis, the enzyme also increased ($p \leq 0.0001$). There was a reduction in HexB activity in the majority of NCLs; CLN2 ($p \leq 0.0001$), CLN3 ($p \leq 0.05$), CLN6 ($p \leq 0.01$), CLN7 ($p \leq 0.001$), and CLN8 ($p \leq 0.0001$). There was increased activity in PSEN1 ($p \leq 0.0001$). There was no detectable activity of HexA in a heat-inactivated sample



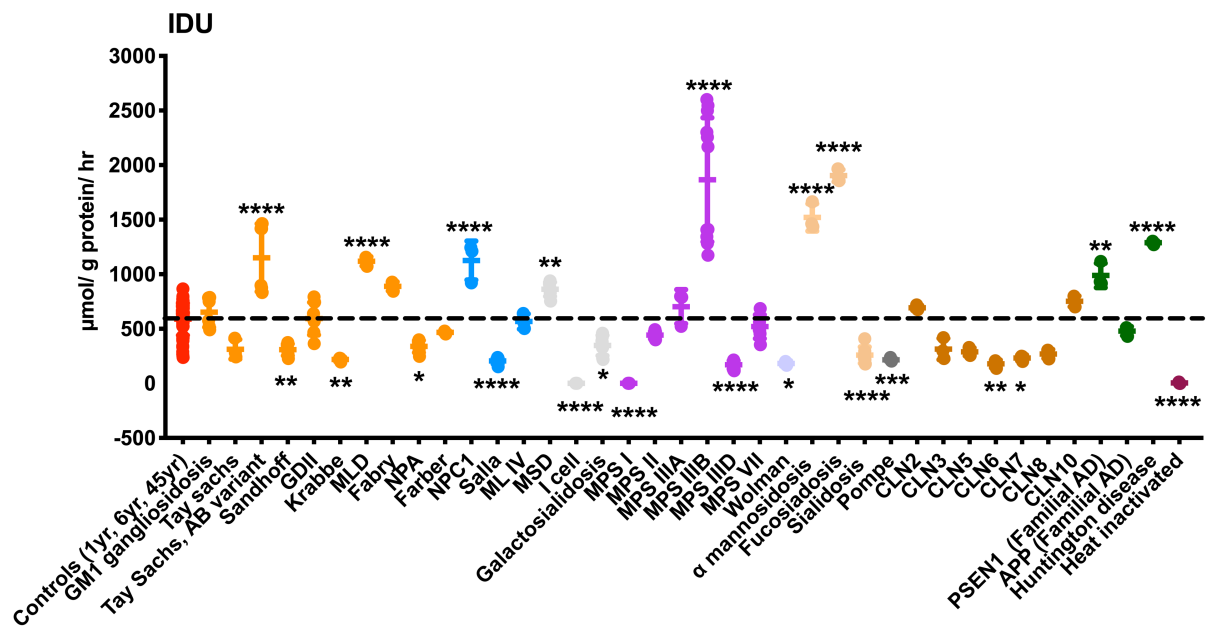
Supplementary Figure 9. Total Hex activity in controls vs. LSDs and other neurovegetative disease patient fibroblasts.

Total Hex activity increased in GM1 gangliosidosis, Tay-Sachs, AB variant, MLD, Farber, and NPC1 ($p \leq 0.0001$). Sandhoff demonstrated a reduction in Total Hex activity ($p \leq 0.0001$). Total Hex activity decreased in all multiple enzyme deficiency diseases; MSD, Galactosidosis ($p \leq 0.001$) and I cell ($p \leq 0.0001$). All MPSs showed an increase in Total Hex activity; MPS I, MPS II, MPS IIIA, MPS III B, and MPS VII ($p \leq 0.0001$). There was only a slight increase in MPS III D ($p \leq 0.05$). Total Hex activity was reduced in Wolman ($p \leq 0.01$). By contrast, the enzyme activity decreased in α mannosidosis ($p \leq 0.01$) and increased in Fucosialidosis ($p \leq 0.0001$) and Sialidosis ($p \leq 0.0001$). The reduction in Total Hex activity was seen across the majority of NCLs: CLN2, CLN5, CLN7, CLN10 ($p \leq 0.0001$) and CLN6 ($p \leq 0.001$). Finally, there was increased activity in PSEN1 ($p \leq 0.0001$). There was no enzyme activity in a heat-inactivated sample.



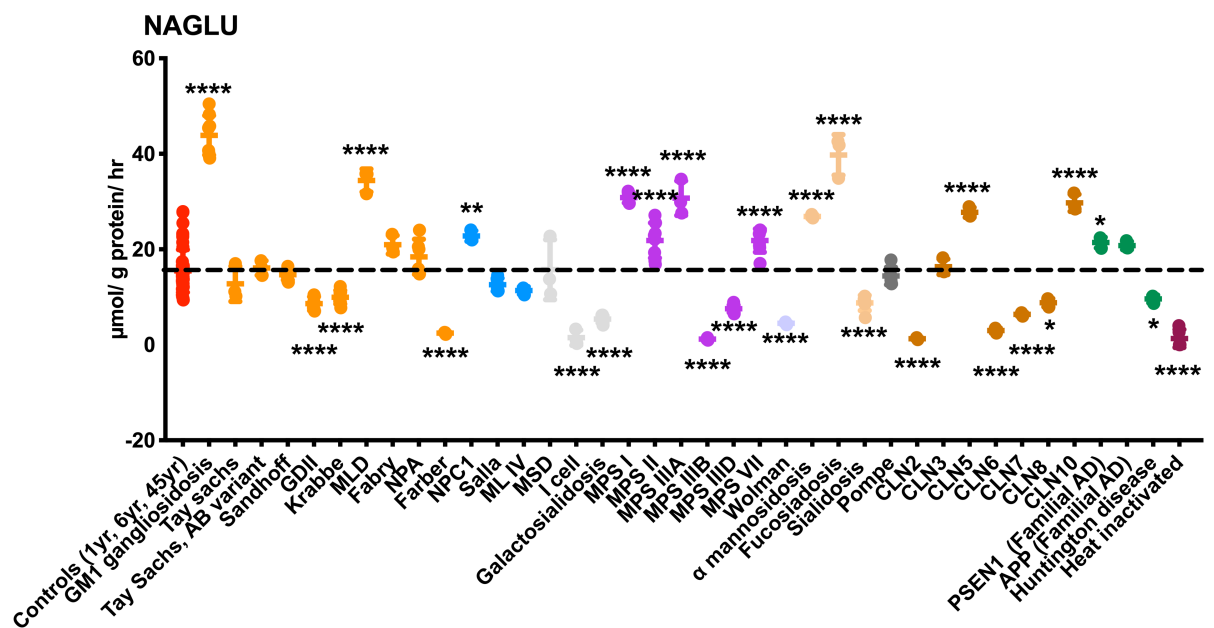
Supplementary Figure 10. GUSB activity in controls vs. LSDs and other neurovegetative disease patient fibroblasts.

GUSB activity increased in GM1 gangliosidosis, Sandhoff, GDII, and Krabbe ($p \leq 0.0001$). There was only a slightly increase in Tay-Sachs ($p \leq 0.01$). There was also a reduction in GUSB activity in Fabry ($p \leq 0.01$). The reduction in GUSB activity was also present in NPC1 ($p \leq 0.001$) and Salla ($p \leq 0.0001$). GUSB activity increased in MLIV ($p \leq 0.0001$). The I cell showed a reduction in enzyme activity ($p \leq 0.0001$). By contrast, there was an increase in GUSB activity in Galactosialidosis ($p \leq 0.0001$). GUSB activity also increased in MPS I ($p \leq 0.0001$) and MPS IIIB ($p \leq 0.01$). Meanwhile, MPS II ($p \leq 0.01$), MPS IIID ($p \leq 0.0001$) and MPS VII ($p \leq 0.0001$) demonstrated a reduction in GUSB activity. There was an increase in enzyme activity in Wolman and Fucosidosis ($p \leq 0.0001$). The reduction in enzymes was significant in Sialidosis ($p \leq 0.0001$). CLN5, CLN6, CLN10 ($p \leq 0.0001$) increased the GUSB activity. There was a reduction in GUSB activity in APP ($p \leq 0.01$). The control sample in the presence of 100µM Suramin showed no enzyme activity similar to that of the heat-inactivated sample.



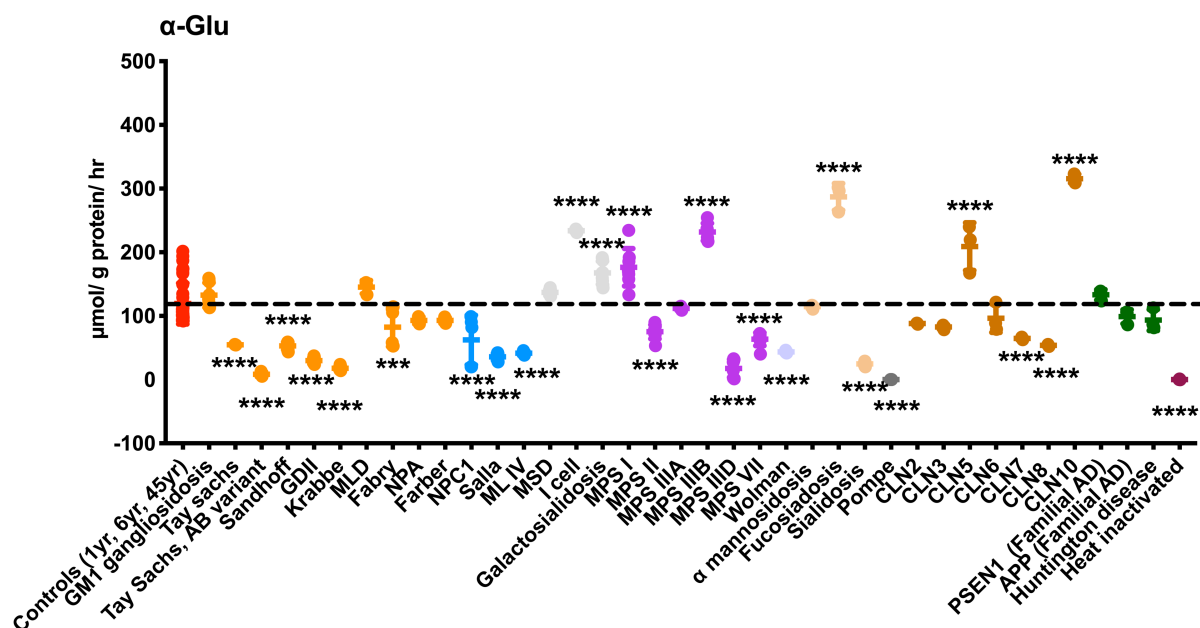
Supplementary Figure 11. IDU activity in controls vs. LSDs and other neurovegetative disease patient fibroblasts.

There was an increase in IDU activity in Tay-Sachs, AB variant, and MLD ($p \leq 0.0001$). There was a reduction in enzyme activity in Sandhoff and Krabbe ($p \leq 0.01$) and in NPA ($p \leq 0.05$). NPC1 showed an increase in IDU activity ($p \leq 0.0001$) while Salla, by contrast, showed a reduction in enzyme activity ($p \leq 0.0001$). In MSD, there was only a slight increase in IDU activity ($p \leq 0.01$). By contrast, there was a reduction in I cell ($p \leq 0.0001$) and in Galactosialidosis ($p \leq 0.05$). IDU activity was low in MPS I and MPS IIID ($p \leq 0.0001$). There was a big increase in the activity of MPS IIIB ($p \leq 0.0001$). There was only a slight reduction in enzyme activity in Wolman ($p \leq 0.05$). IDU activity increased in α mannosidosis and Fucosialidosis ($p \leq 0.0001$). The reduction in IDU activity was in Sialidosis ($p \leq 0.0001$) and Pompe ($p \leq 0.001$). There was a noticeable reduction in CLN6 ($p \leq 0.01$) and CLN7 ($p \leq 0.05$). The increase in IDU activity was in PSEN1 ($p \leq 0.01$) and Huntington ($p \leq 0.0001$). There was no enzyme activity in the heat-inactivated sample



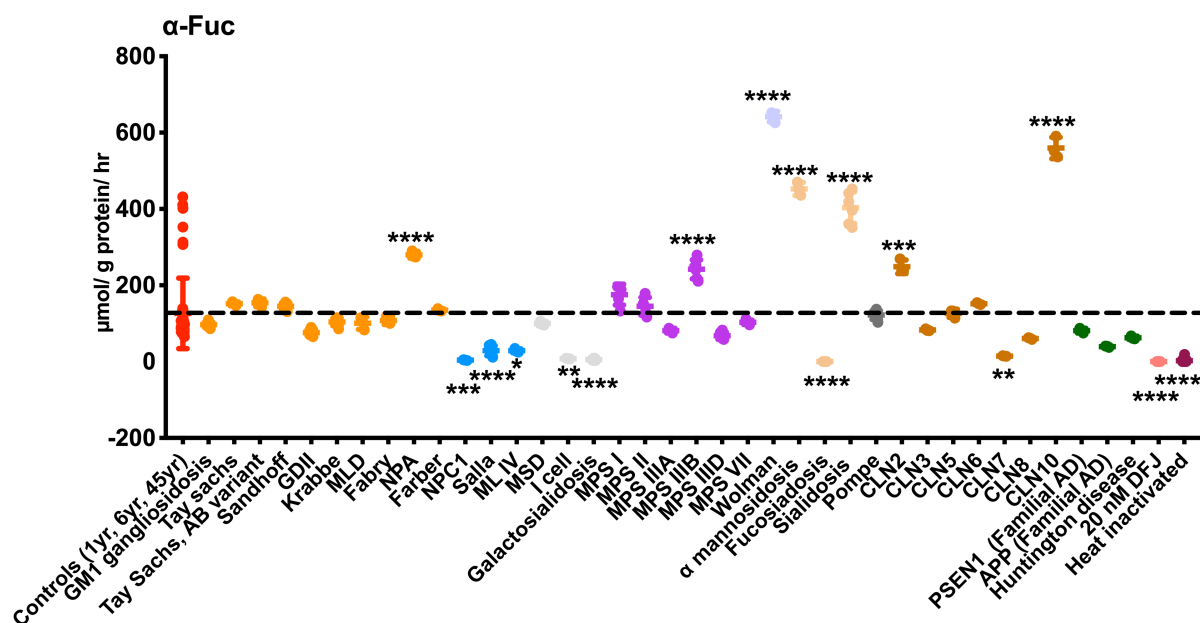
Supplementary Figure 12. NAGLU activity in controls vs. LSDs and other neurovegetative disease patient fibroblasts.

NAGLU activity increased in GM1 gangliosidosis and MLD ($p \leq 0.0001$). The reduction in NAGLU activity was significant in GDII, Krabbe, and Farber ($p \leq 0.0001$). Also, there was an increase in NPC1 ($p \leq 0.01$). In contrast the reduction was in I cell and Galactosialidosis ($p \leq 0.0001$). NAGLU activity increased in MPS I, MPS II, MPS IIIA, and MPS VII ($p \leq 0.0001$). MPS IIIB and MPS IIID NAGLU activity was low ($p \leq 0.0001$). Wolman ($p \leq 0.0001$) showed a decrease in activity, whereas there was an increase in α mannosidosis and Fucosidosis ($p \leq 0.0001$) and a reduction in NAGLU activity in Sialidosis ($p \leq 0.0001$). There was also a reduction in NAGLU activity in CLN2, CLN6, and CLN7 ($p \leq 0.0001$) and only a slight reduction in CLN8 ($p \leq 0.05$). NAGLU activity increased in CLN5 and CLN10 ($p \leq 0.0001$). PSEN1 ($p \leq 0.05$) showed an increase in NAGLU activity. By contrast, Huntington ($p \leq 0.05$) showed a slight reduction in activity. The heat-inactivated sample showed no enzyme activity.



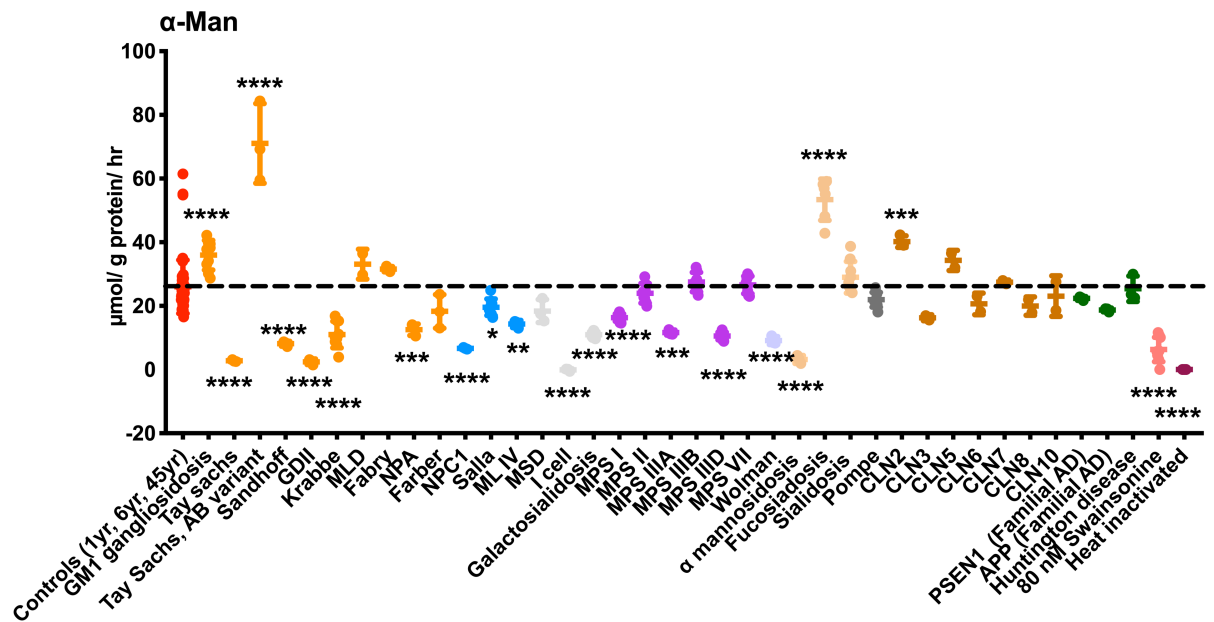
Supplementary Figure 13. α -Glu activity in controls vs. LSDs and other neurovegetative disease patient fibroblasts.

In comparison to the control level of α -Glu activity, there was a reduction in Tay Sachs, Tay Sachs, AB variant, Sandhoff, GDII, and Krabbe ($p \leq 0.0001$) and in Fabry ($p \leq 0.001$). There was also a reduction in α -Glu activity in NPC1, Salla and MLIV ($p \leq 0.0001$). The α -Glu activity increased in I cell and Galactosialidosis ($p \leq 0.0001$). The MPS I and MPS IIIB showed an increase in α -Glu activity ($p \leq 0.0001$). There was a reduction in α -Glu activity in MPS II, MPS IIID, MPS VII, and Wolman ($p \leq 0.0001$). There was an increase in α -Glu activity in Fucosidosis ($p \leq 0.0001$). Sialidosis and Pompe showed a reduction in α -Glu activity ($p \leq 0.0001$). Meanwhile, CLN5 and CLN10 showed an increase in α -Glu activity ($p \leq 0.0001$). By contrast, α -Glu activity was low in CLN7 and CLN8 ($p \leq 0.0001$). There was a lack of enzyme activity in the heat-inactivated sample.



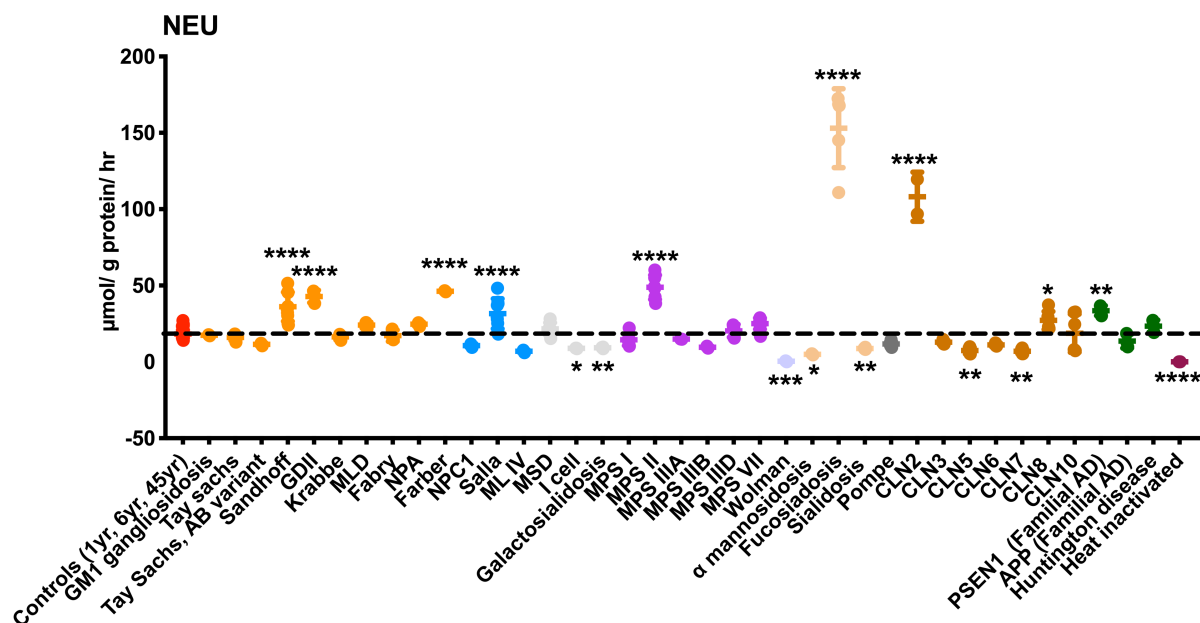
Supplementary Figure 14. α-Fuc activity in controls vs. LSDs and other neurovegetative disease patient fibroblasts.

α-Fuc activity varied across the controls. In Sphingolipidoses disease only NPA showed an increase in α-Fuc activity ($p \leq 0.0001$). There was α-Fuc reduction in NPC1 ($p \leq 0.001$), Salla ($p \leq 0.0001$), and MLIV ($p \leq 0.05$). α-Fuc also had low activity in I cell ($p \leq 0.01$) and Galactosialidosis ($p \leq 0.0001$). The MPS IIIB showed an increase in on enzyme activity ($p \leq 0.0001$). There was an increase in α-Fuc activity in Wolman, α mannosidosis, and Sialidosis ($p \leq 0.0001$). A reduction in activity was demonstrated in Fucosidosis ($p \leq 0.0001$). There was an increase in CLN2 ($p \leq 0.01$), and in CLN10 ($p \leq 0.0001$). There was a decrease of α-Fuc activity in CLN7 ($p \leq 0.01$). The presence of DFJ inhibitor produced a reduction in α-Fuc activity similar to that of the heat-inactivated sample.



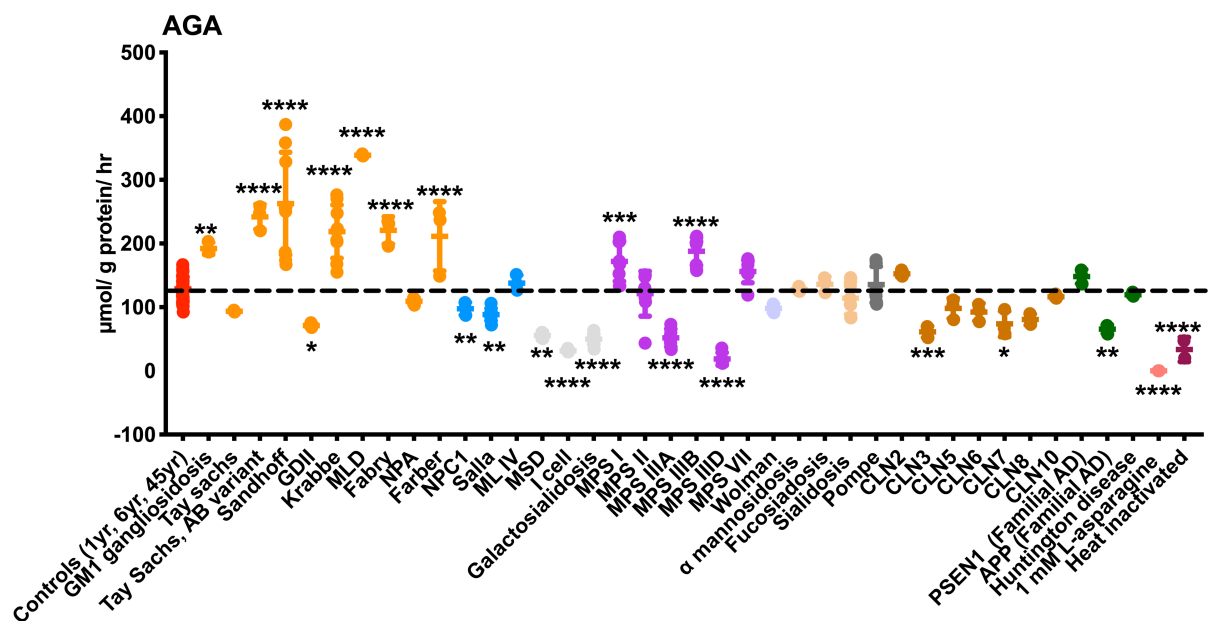
Supplementary Figure 15. α-Man activity in controls vs. LSDs and other neurovegetative disease patient fibroblasts.

α-Man activity increased in GM1 gangliosidosis and Tay-Sachs, AB variant ($p \leq 0.0001$). A reduction in enzyme activity was demonstrated in Tay-Sachs, Sandhoff, GDII and Krabbe ($p \leq 0.0001$) and NPA ($p \leq 0.001$). The α-Man activity decreased in NPC1 ($p \leq 0.0001$), Salla ($p \leq 0.05$), and MLIV ($p \leq 0.01$). There was a reduction in I cell, Galactosialidosis ($p \leq 0.0001$). The α-Man enzyme was low in MPSI ($p \leq 0.0001$) and MPS IIIA ($p \leq 0.001$) and in MPS IIID ($p \leq 0.0001$). In Wolman and α mannosidosis, the enzyme was clearly low ($p \leq 0.0001$). There was a noticeable increase in Fucosidosis ($p \leq 0.0001$) and CLN2 ($p \leq 0.001$). Either the heat-inactivated sample or the presence of 80 nM Swainsonine inhibited the total enzyme activity.



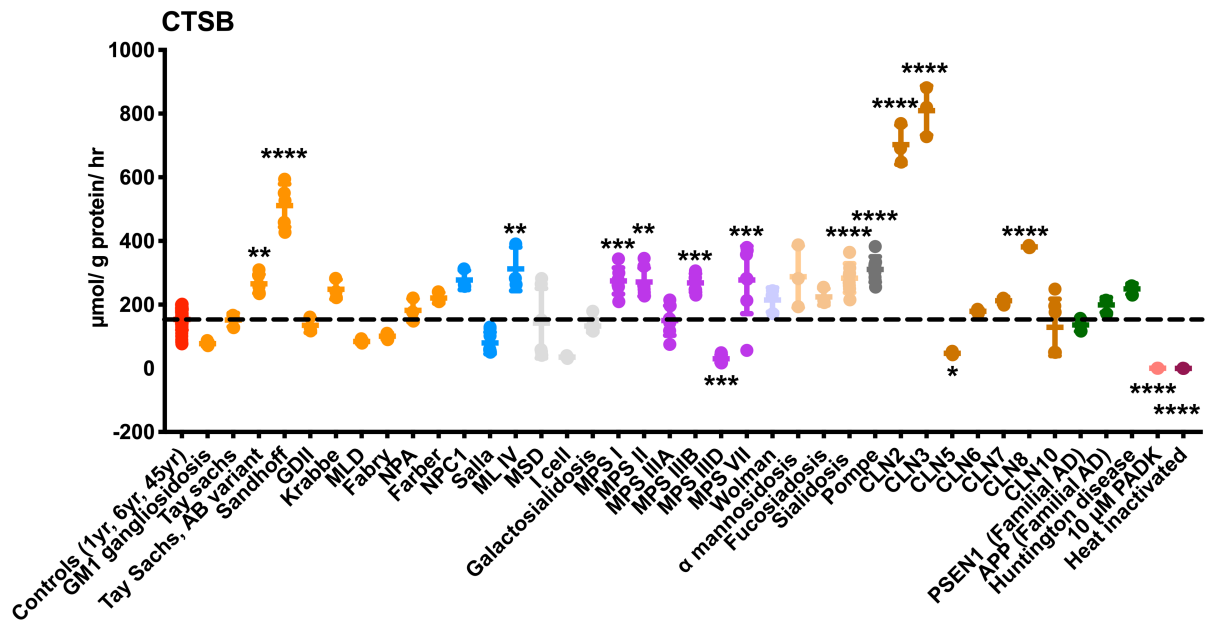
Supplementary Figure 16. NEU activity in controls vs. LSDs and other neurovegetative disease patient fibroblasts.

NEU activity increased in Sandhoff, GDII, and Farber ($p \leq 0.0001$). There was also an increase in Salla ($p \leq 0.0001$). A reduction in NEU activity was present in I cell ($p \leq 0.05$) and Galactosialidosis ($p \leq 0.001$). There was an increase only in MPS II ($p \leq 0.0001$) among MPSs. Wolman showed a reduction in NEU activity ($p \leq 0.001$). Low NEU activity was seen in α mannosidosis ($p \leq 0.05$) and Sialidosis ($p \leq 0.001$). There was an increase in enzyme activity in Fucosidosis ($p \leq 0.0001$). There was also an increase in CLN2 ($p \leq 0.0001$) and CLN8 ($p \leq 0.05$). By contrast, low enzyme activity was seen in CLN5 and CLN7 ($p \leq 0.01$). There was an increase in NEU activity in PSEN1 ($p \leq 0.01$). The heat-inactivated sample showed no enzyme activity.



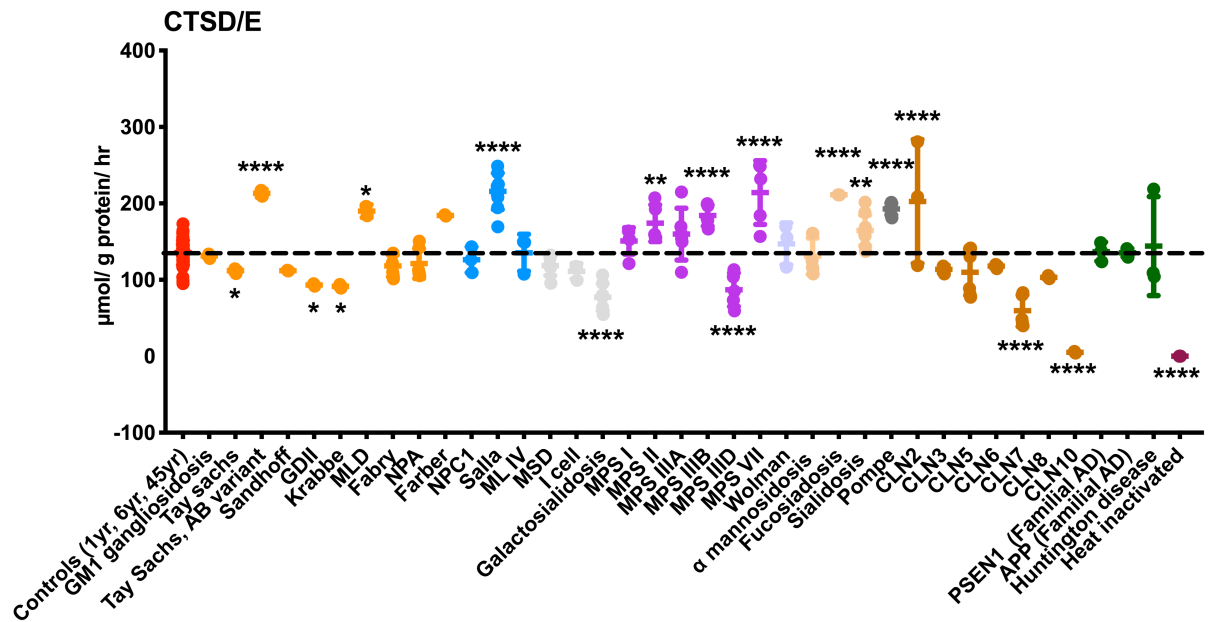
Supplementary Figure 17. AGA activity in controls vs. LSDs and other neurovegetative disease patient fibroblasts.

There was an increase in AGA activity among Sphingolipidoses and GM1 gangliosidosis ($p \leq 0.01$), and in Tay-Sachs, AB variant, Sandhoff, Krabbe, MLD, Fabry, and Farber ($p \leq 0.0001$). Low AGA activity was found in GD II ($p \leq 0.05$). There was a reduction in enzyme activity in NPC1 and Salla ($p \leq 0.01$). All multiple enzyme deficiency diseases showed a reduction in AGA activity, MSD ($p \leq 0.01$), and I cell and Galactosialidosis ($p \leq 0.0001$). There was an increase in AGA activity in MPS I ($p \leq 0.001$) and MPS IIIB ($p \leq 0.0001$). There was a reduction in MPS IIIA and MPS IIID ($p \leq 0.0001$). CLN3 showed a reduction in AGA activity ($p \leq 0.001$). Also, a reduction was present in CLN7 ($p \leq 0.05$). APP ($p \leq 0.01$) showed a reduction in AGA activity. There was no detectable enzyme in the presence of L-asparagine and only slightly of residual in AGA activity heat-inactivity.



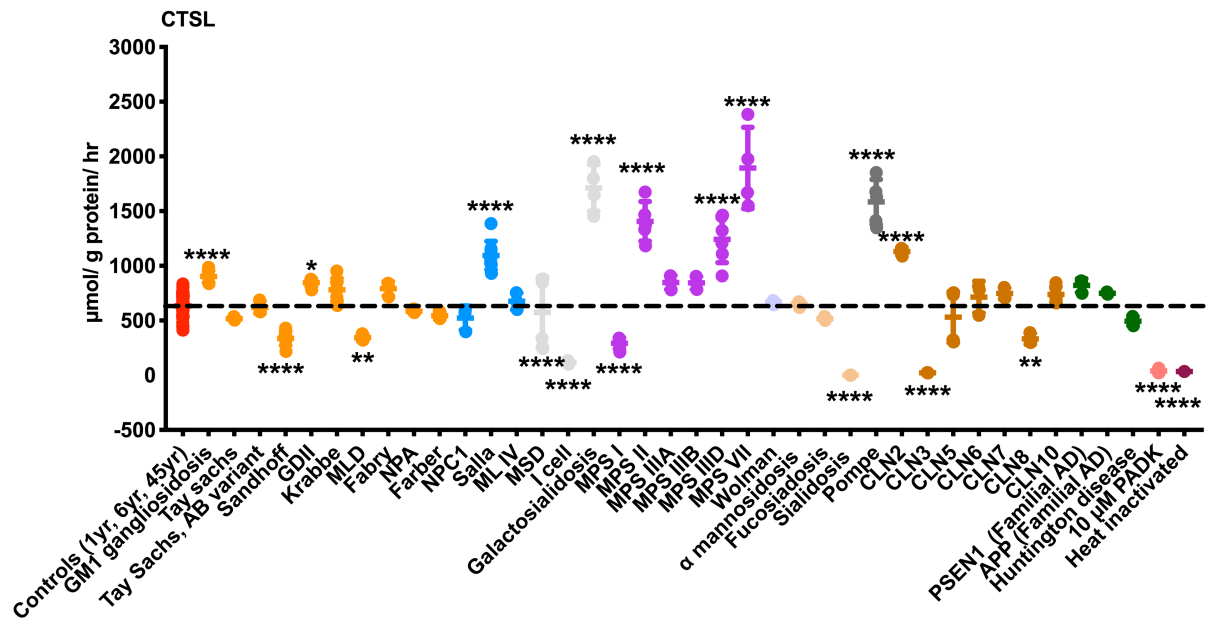
Supplementary Figure 18. CTSSB activity in controls vs. LSDs and other neurovegetative disease patient fibroblasts.

There was an increase in CTSSB activity among the majority of LSDs. There was an increase in CTSSB activity in Tay-Sachs, AB variant ($p \leq 0.01$) and Sandhoff ($p \leq 0.0001$). There was an increase in MLIV ($p \leq 0.01$). There was upregulation in enzyme activity in MPS I ($p \leq 0.001$), MPSII ($p \leq 0.01$), MPS IIIB ($p \leq 0.001$), and MPS VII ($p \leq 0.001$). There was a reduction only in MPS IIID ($p \leq 0.001$). Sialidosis and Pompe showed an increase in CTSSB activity ($p \leq 0.0001$). There was also an increase in CLN2, CLN3, and CLN7 ($p \leq 0.0001$). By contrast, there was a reduction in CTSSB activity in CLN5 ($p \leq 0.05$). The heat-inactivated sample and the presence of the enzyme inhibitor; PADK were able to eliminate the enzyme activity.



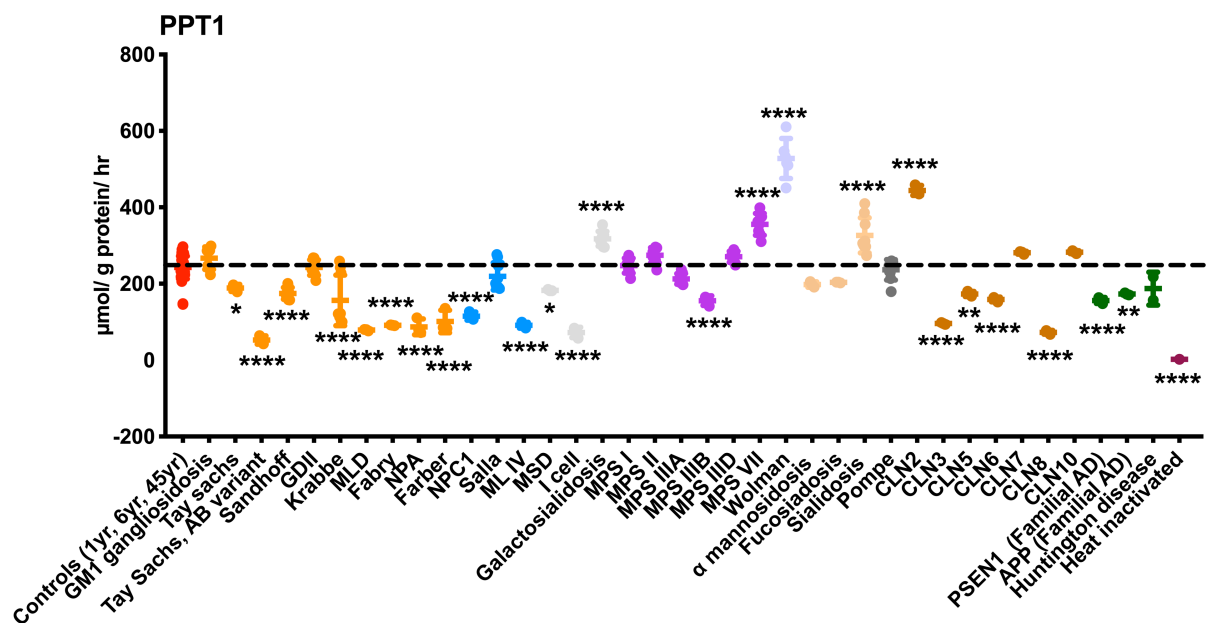
Supplementary Figure 19. CTSD/E activity in controls vs. LSDs and other neurovegetative disease patient HFs.

CTSD/E activity slightly decreased in Tay-Sachs, GDII, and Krabbe ($p \leq 0.05$). There was more of an increase in CTSD/E activity in Tay-Sachs, AB variant ($p \leq 0.0001$). There was also an increase in enzyme activity in MLD ($p \leq 0.05$) and Salla ($p \leq 0.0001$). Galactosialidosis showed a reduction in CTSD/E activity ($p \leq 0.0001$). There was upregulation in CTSD/E activity in MPS II ($p \leq 0.001$), and in MPS IIIB and MPS VII ($p \leq 0.0001$). Low CTSD/E activity was detected in MPS IIID ($p \leq 0.0001$). CTSD/E was upregulated in Fucosidosis ($p \leq 0.0001$), Sialidosis ($p \leq 0.01$), and Pompe ($p \leq 0.0001$). Among the NCLs, there was an increase in only CLN2 ($p \leq 0.0001$). By contrast, there was a noticeable reduction in CLN7 and CLN10 ($p \leq 0.0001$). There was no CTSD/E activity in the heat-inactivated sample.



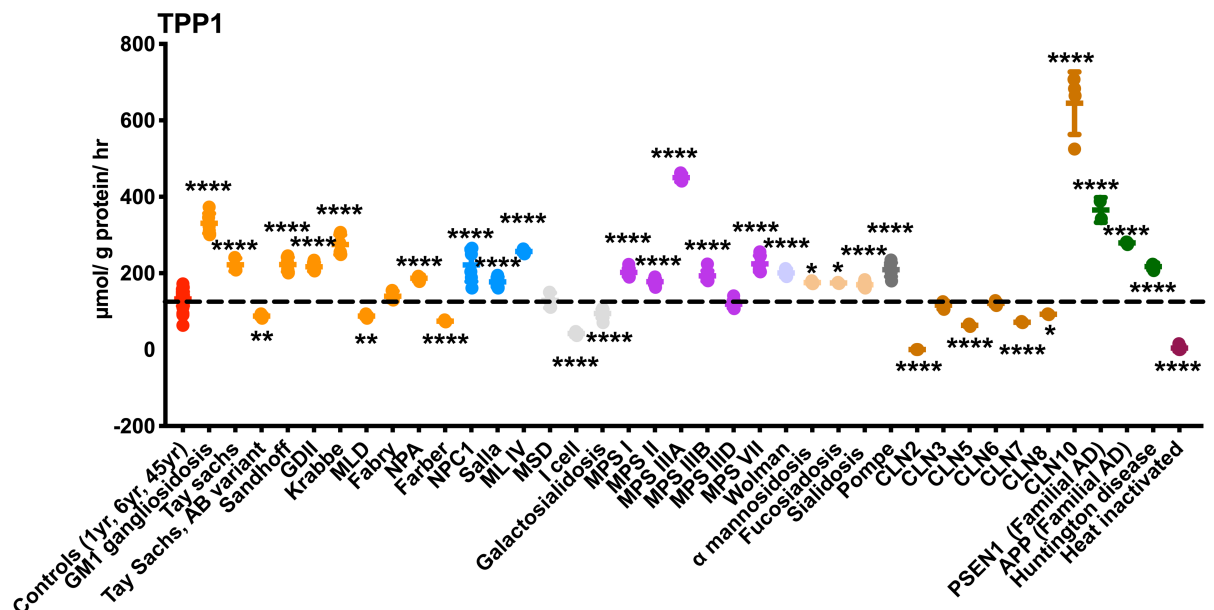
Supplementary Figure 20. CTSL activity in controls vs. LSDs and other neurovegetative disease patient fibroblasts.

CTSL activity increased in GM1 gangliosidosis ($p \leq 0.0001$) and GD II ($p \leq 0.05$). There was a reduction in CTSL activity in Sandhoff ($p \leq 0.0001$) and MLD ($p \leq 0.01$). Salla showed an increase in enzyme activity ($p \leq 0.0001$). There was a significant reduction in MSD and I cell ($p \leq 0.0001$) and an increase in enzyme activity in Galactosialidosis ($p \leq 0.0001$). Among the MPSs, there was a reduction only in MPS I ($p \leq 0.0001$) while there were increases in MPS II, MPS IIIA, and MPS VII ($p \leq 0.0001$). Sialidosis ($p \leq 0.0001$) and Pompe ($p \leq 0.0001$) showed a reduction and an increase in CTSL activity, respectively. CLN2 showed an increase in CTSL activity ($p \leq 0.0001$) while a reduction was detected in CLN3 ($p \leq 0.0001$) and CLN8 ($p \leq 0.01$). The presence of PADK inhibitor and a heat-inactivated sample reduced the enzyme activity.



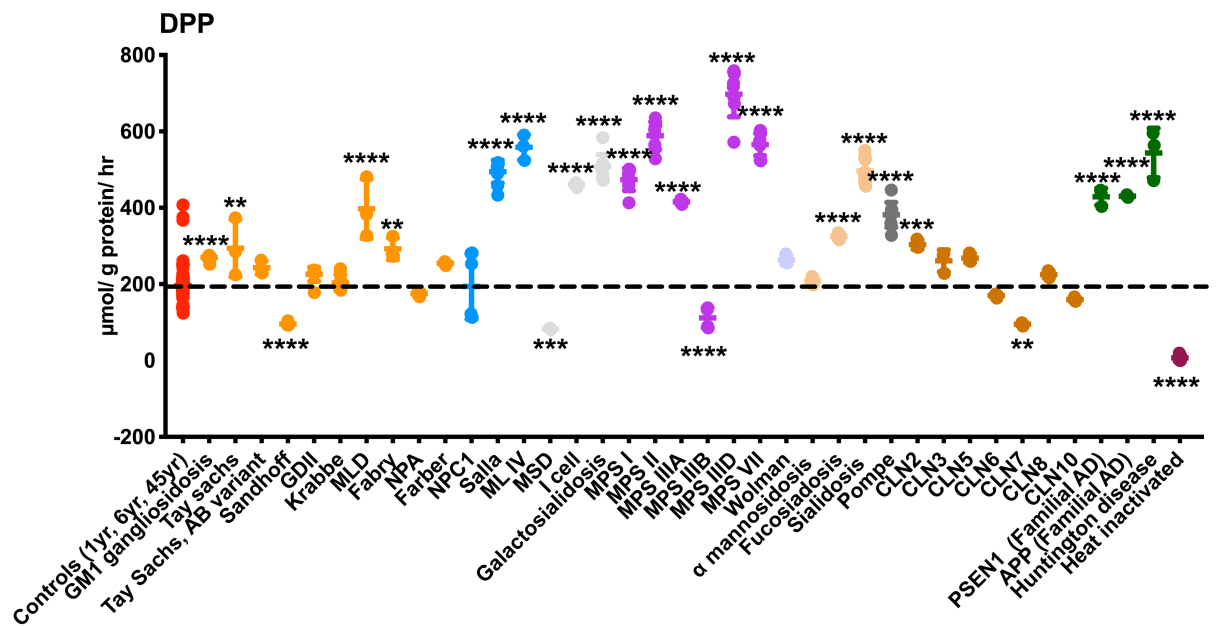
Supplementary Figure 21. PPT1 activity in controls vs. LSDs and other neurovegetative disease patient fibroblasts.

PPT1 activity decreased among the majority of LSDs. There was a decrease in Tay-Sachs ($p \leq 0.05$), Tay-Sachs, AB variant, Sandhoff, Krabbe, MLD, Fabry, NPA, and Farber ($p \leq 0.0001$). Low enzyme activity was also found in NPC1 and MLIV; $p \leq 0.0001$. There was a PPT1 enzyme reduction in MSD ($p \leq 0.05$) and I cell ($p \leq 0.0001$). There was an upregulation in PPT1 activity in Galactosialidosis ($p \leq 0.0001$). MPS IIIB ($p \leq 0.0001$) showed a reduction in PPT1 activity, while there was an increase in MPS VII ($p \leq 0.0001$). Wolman ($p \leq 0.0001$) and Sialidosis ($p \leq 0.0001$) exhibited an increase in PPT1 activity. Among the NCLs, there was an increase only in CLN2 ($p \leq 0.0001$), while, in contrast, there was a reduction in CLN3 ($p \leq 0.0001$), CLN5 ($p \leq 0.01$), CLN6 ($p \leq 0.0001$), and CLN8 ($p \leq 0.0001$). PPT1 was reduced in PSEN1 ($p \leq 0.0001$) and APP ($p \leq 0.01$). The heat-inactivated sample showed no enzyme activity.



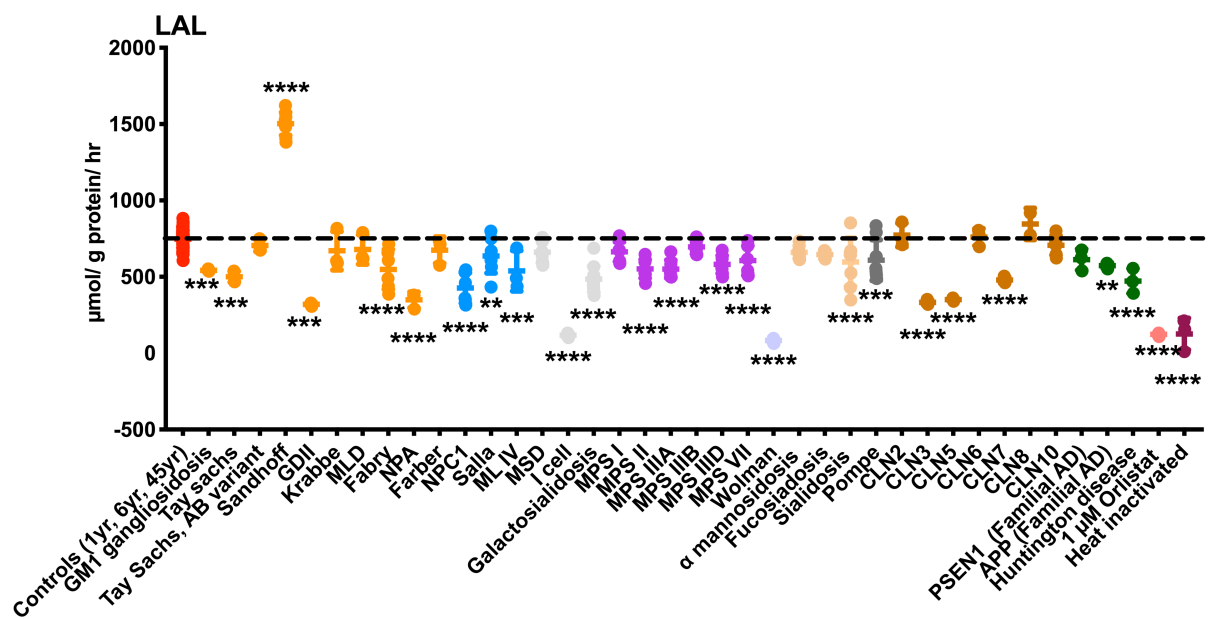
Supplementary Figure 22. TPP1 activity in controls vs. LSDs and other neurovegetative disease patient fibroblasts.

TPP1 enzyme activity was upregulated among the majority of LSDs. There was an increase in GM1 gangliosidosis ($p \leq 0.0001$), Tay-Sachs ($p \leq 0.0001$), Sandhoff ($p \leq 0.0001$), GDII ($p \leq 0.0001$), Krabbe ($p \leq 0.0001$), and NPA ($p \leq 0.0001$). There was a reduction in Tay-Sachs AB variant ($p \leq 0.01$), MLD ($p \leq 0.01$) and Farber ($p \leq 0.0001$). TPP1 enzyme activity was also increased ($p \leq 0.0001$) in NPC1, Salla, and MLIV. There was a reduction ($p \leq 0.0001$) in MSD and I cell. All the MPSs exhibited an increase ($p \leq 0.0001$) apart from MPS IIID. There was an increase with different levels in Wolman ($p \leq 0.01$), α mannosidosis ($p \leq 0.05$), Fucosidosis ($p \leq 0.05$), Sialidosis, and Pompe ($p \leq 0.0001$). Reductions were detected in CLN2 ($p \leq 0.0001$), CLN5 ($p \leq 0.0001$), CLN7 ($p \leq 0.0001$), and CLN8 ($p \leq 0.05$). CLN10 showed an increase in TPP1 ($p \leq 0.0001$) enzyme activity. All the neurodegenerative diseases in this study showed an upregulation in TPP1 PSEN1 ($p \leq 0.0001$), APP ($p \leq 0.0001$) and Huntington ($p \leq 0.0001$). The heat-inactivated sample exhibited no activity of the TPP1 enzyme.



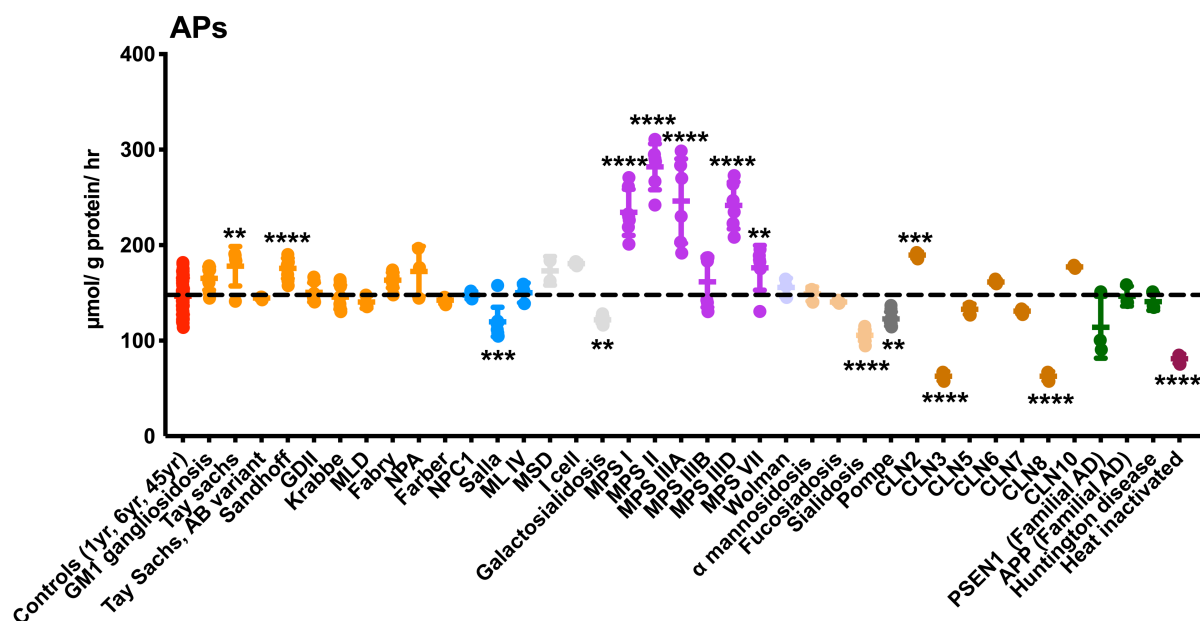
Supplementary Figure 23. DPP activity in controls vs. LSDs and other neurovegetative disease patient fibroblasts.

In general, DPP activity increased in the majority of LSDs. Compared to the control, the activity increased in GM1 gangliosidosis ($p \leq 0.0001$), Tay-Sachs ($p \leq 0.01$), MLD ($p \leq 0.0001$), and Fabry ($p \leq 0.01$). There was a reduction in enzyme activity in Sandhoff ($p \leq 0.0001$). Also, there was an increase in activity in Salla ($p \leq 0.0001$) and MLIV ($p \leq 0.0001$). By contrast, there was a reduction in MSD ($p \leq 0.001$). There was an increase in enzyme activity compared to the controls in I cell ($p \leq 0.0001$), Galactosialidosis ($p \leq 0.0001$). The majority of MPs and Olygosaccharidoses showed an increase in DPP activity; MPS I ($p \leq 0.0001$), MPS II ($p \leq 0.0001$), MPS IIIA ($p \leq 0.0001$), MPS IIID ($p \leq 0.0001$), MPS VII ($p \leq 0.0001$), Fucosidosis ($p \leq 0.0001$), Sialidosis ($p \leq 0.0001$), and Pompe ($p \leq 0.0001$). CLN2 ($p \leq 0.001$) demonstrated an increase in DPP activity. However, MPS IIIB ($p \leq 0.0001$) and CLN7 ($p \leq 0.01$) showed a reduction in DPP activity. PSEN1 ($p \leq 0.0001$), APP ($p \leq 0.0001$), and Huntington's disease ($p \leq 0.0001$) showed an increase in DPP activity comparing to the controls. There was no DPP activity in the heat-inactivated sample.



Supplementary Figure 24. LAL activity in controls vs. LSDs and other neurovegetative disease patient fibroblasts.

The majority of LSDs showed a reduction in LAL activity. In Sphingolipidoses diseases The only noticeable increase was in Sandhoff ($p \leq 0.0001$). There was low LAL activity in GM1 gangliosidosis ($p \leq 0.001$), Tay-Sachs ($p \leq 0.001$), GD II ($p \leq 0.001$), Fabry ($p \leq 0.0001$), and NPA ($p \leq 0.0001$). The transmembrane defect protein showed low LAL activity; NPC1 ($p \leq 0.0001$), Salla ($p \leq 0.01$), MLIV ($p \leq 0.0001$). Meanwhile, I cell ($p \leq 0.0001$) and Galactosialidosis ($p \leq 0.0001$) showed a reduction in LAL activity. LAL activity was also low across LSDs: MPS II ($p \leq 0.0001$), MPSIIIA ($p \leq 0.0001$), MPS IIID ($p \leq 0.0001$), and MPS VII ($p \leq 0.0001$). There was also a reduction in Wolman ($p \leq 0.0001$), Sialidosis ($p \leq 0.0001$), and Pompe ($p \leq 0.001$). CLN3 ($p \leq 0.001$), CLN5 ($p \leq 0.001$), and CLN7 ($p \leq 0.001$) showed a significant reduction in LAL activity. Low enzyme activity was also present in APP ($p \leq 0.01$) and Huntington's disease ($p \leq 0.0001$). The presence of 1 μ M Orlistat inhibited LAL activity and there was only small residual activity in the heat-inactivated sample.

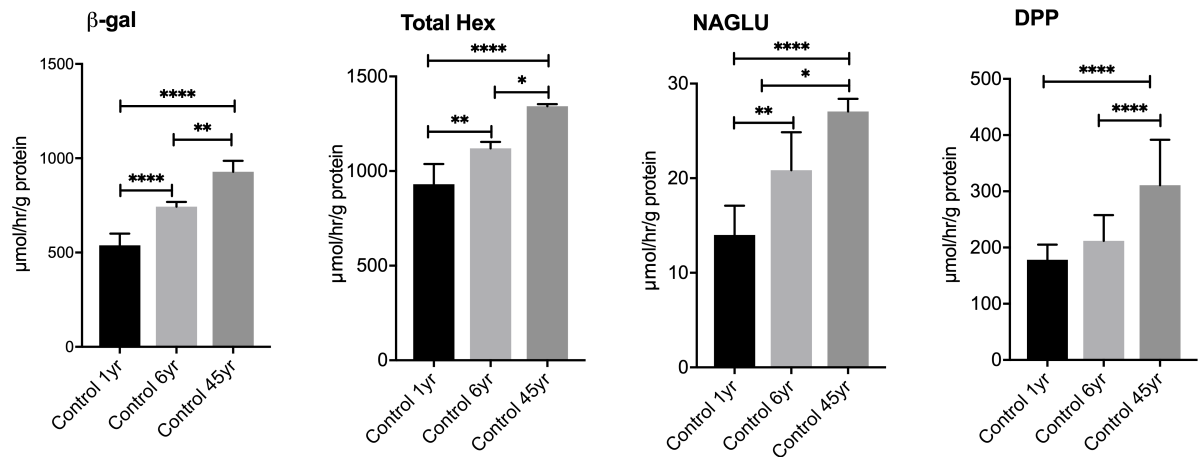


Supplementary Figure 25. Aps activity in controls vs. LSDs and other neurovegetative disease patient HF.

There was an increase in Aps activity in Tay-Sachs ($p \leq 0.01$) and Sandhoff ($p \leq 0.0001$) compared to the controls. There was a noticeable reduction in APs activity in Salla ($p \leq 0.001$) and Galactosialidosis ($p \leq 0.01$). Increased Aps activity was seen in MPS I ($p \leq 0.0001$), MPS II ($p \leq 0.0001$), MPS IIIA ($p \leq 0.0001$), MPS IIID ($p \leq 0.0001$), and MPS VII ($p \leq 0.01$). Meanwhile, Sialidosis ($p \leq 0.0001$) and Pompe ($p \leq 0.01$) showed a reduction in Aps activity. CLN2 ($p \leq 0.01$) showed upregulation in APs activity while, by contrast, CLN3 ($p \leq 0.0001$) and CLN8 ($p \leq 0.0001$) showed a reduction in enzyme activity. The heat-inactivated sample demonstrated no detectable Aps activity.

Enzymes altered in age-dependent manner

Some lysosomal enzymes were found to increase activity with influence of ageing. β -gal, Total Hex, NAGLU and DPP levels were increased statistically significantly during this study. Further studies can be carried out to investigate the importance of age matched controls for comparisons and mechanism behind such changes in enzymes activity.

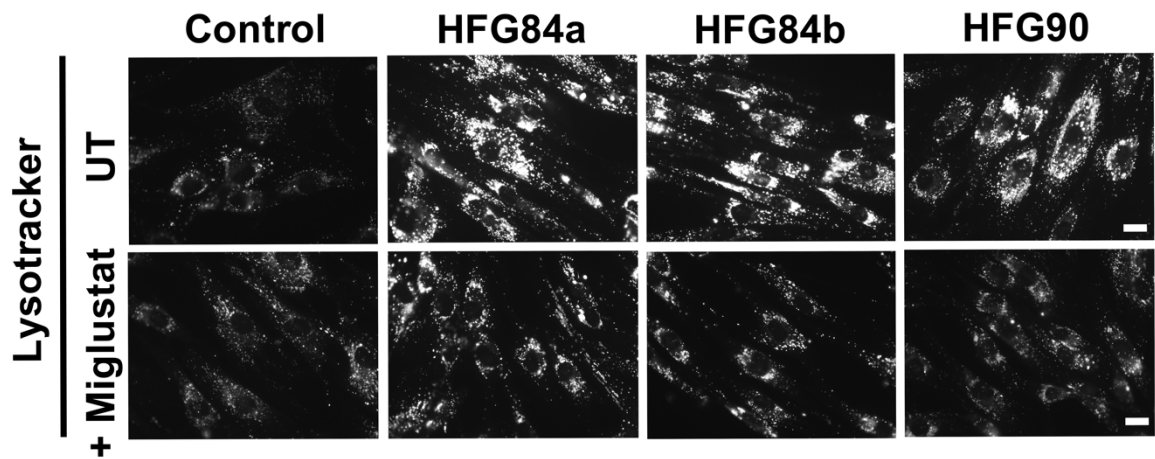


Supplementary Figure 26 The enzyme activity in different age controls.

B-gal, Total Hex, NAGLU and DPP enzymes among control fibroblast. N=3 for all assays. * $p \leq 0.05$; ** $p \leq 0.01$, *** $p \leq 0.001$; **** $p \leq 0.0001$. Data are shown as mean \pm SD. The experiments were performed as teamwork with Ms. Hiu Tung.

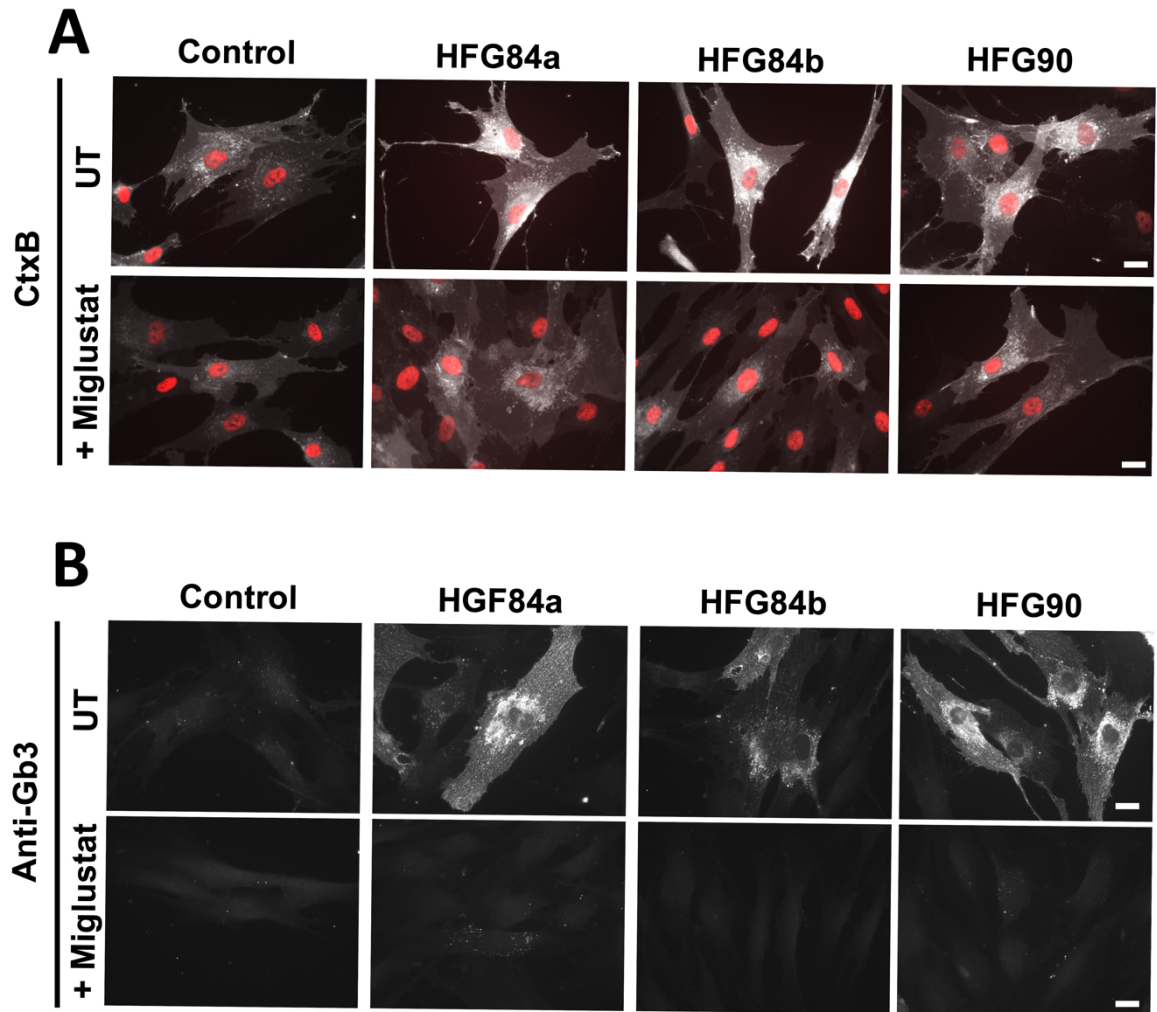
The miglustat treatment capable to rescue the lipid storage in CLN5

The cellular phenotyping of CLN5 patients' fibroblasts showed increased lysotracker staining and lysosomal accumulation of GM1 ganglioside and GB3. The miglustat have been shown decreased lysotracker (lysosome swelling) in treated CLN5 fibroblast. It was also reduce the accumulated lipids. The treatment showed successful clearance of lysosomal Gb3 and GM1 ganglioside storage.



Supplementary Figure 27. Reduction in storage material in CLN5 post miglustat treatment.

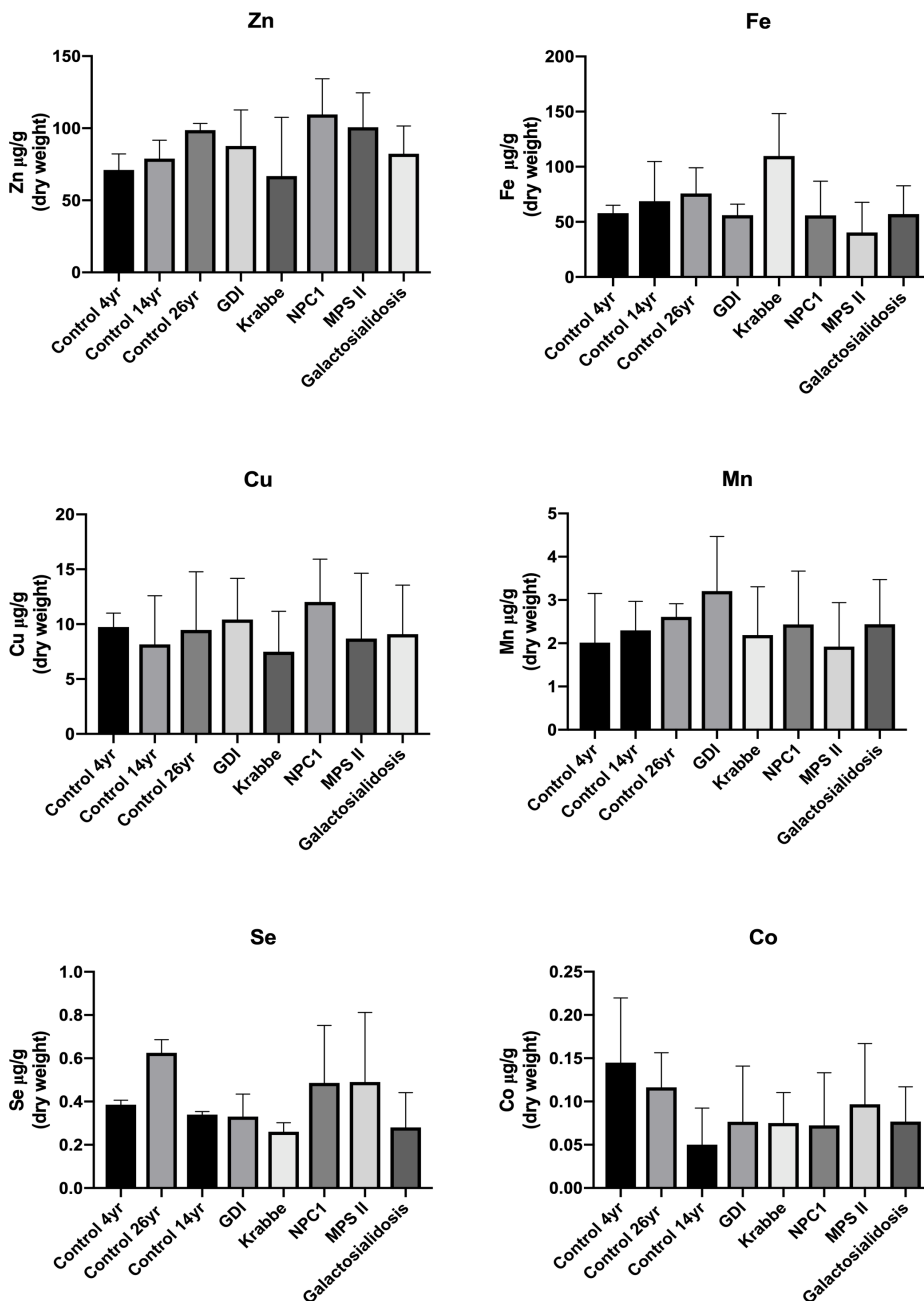
The control (GM05399), CLN5 P1 (HG84a), CLN5 P2 (HFG85b) and CLN5 P3 (HFG90) fibroblasts were either untreated or treated with 50 μ M miglustat for 5 days prior to staining with lysotracker. This data was generated by Katie Shipley and I have her permission to show it in my thesis.



Supplementary Figure 28. Storage Lipids in CLN5 corrected by the miglustat treatment. The control (GM05399), CLN5 P1 (HG84a), CLN5 P2 (HFG85b) and CLN5 P3 (HFG90) fibroblasts were either untreated or treated with 50 μ M miglustat for 5 days prior to staining with (A) CtxB (GM1 gangliosides), (B) anti-GB3 (Gglobotriaosylceramide). The miglustat treatment showed a reduction in both GM1 gangliosides and Globotriaosylceramide lipids. This data was generated by Katie Shipley and I have her permission to show it in my thesis.

Trace elements measurement among several lysosomal storage disease

ICP-MS has been used to measure Zn, Fe, Cu, Se, Mn and Co during metal analysis in controls and LSDs B-LCL. The ICP-MS findings showed a level of variability which causes the lack statistical significance across LSDs compared to the control B-LCL.

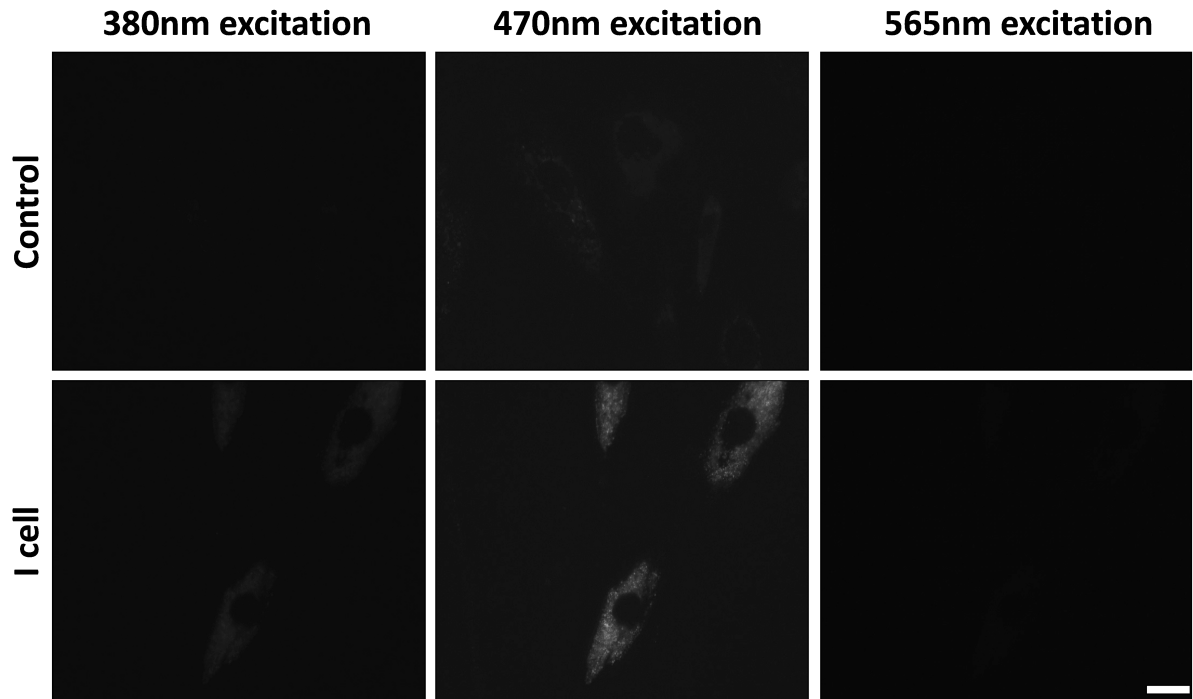


Supplementary Figure 29. Altered metal homeostasis in the LSDs patient LCL.

Zn, Fe, Cu, Se, Mn and Co metal analysis of controls and LSD patient (see supplementary Table 1). LCL were pelleted out and the measurements were determined by ICPMS. n=2-3. Data are shown as mean \pm SD. The data were obtained from the ICP-MS facilities in collaboration with Cardiff University Hospital

I cell exhibited high level of autofluorescence

The assessment of autofluorescence was observed at 380nm, 470nm and 565nm excitation in the I cell compared to control.



Supplementary Figure 30. The autofluorescence assessment in I cell fibroblasts.

The control (GM05399) and I cell (GM02013) patient fibroblasts were excited with a 380nm, 470nm, and 565nm LED with images on a Colibri LED fluorescence microscope; this was done by using an excitation LED light source set to 100% and 100ms of exposure time. The scale bar =10 μ m. N=3.